THE INTERNATIONAL INTRAVAL PROJECT

TO STUDY VALIDATION OF GEOSPHERE
TRANSPORT MODELS FOR PERFORMANCE ASSESSMENT
OF NUCLEAR WASTE DISPOSAL

PHASE 1, TEST CASES 10, 11 and 12

Flow and Tracer Experiments in Unsaturated Tuff and Soil

APPENDICES

The Coordinating Group of the INTRAVAL Project
Swedish Nuclear Power Inspectorate (SKI)

NUCLEAR ENERGY AGENCY
ORGANISATION FOR ECONOMIC CO-OPERATION AND DEVELOPMENT

NEA SKi

THE INTERNATIONAL INTRAVAL PROJECT

TO STUDY VALIDATION OF GEOSPHERE
TRANSPORT MODELS FOR PERFORMANCE ASSESSMENT
OF NUCLEAR WASTE DISPOSAL

PHASE 1, TEST CASES 10, 11 and 12

Flow and Tracer Experiments in Unsaturated Tuff and Soil

APPENDICES

The Coordinating Group of the INTRAVAL Project
Swedish Nuclear Power Inspectorate (SKI)

NUCLEAR ENERGY AGENCY
ORGANISATION FOR ECONOMIC CO-OPERATION AND DEVELOPMENT

NEA SKi

Table of contents

APPENDIX A1

Prototype evaluation of the effects of wet and dry drilling fluids on the in situ hydrologic conditions of tuffaceous rocks in support of exploratory shaft hydrologic testing

NNWSI PROJECT

UNITED STATES GEOLOGICAL SURVEY

DENVER, COLORADO

USGS DETAILED TEST PLAN

PROTOTYPE EVALUATION OF THE EFFECTS OF WET AND DRY DRILLING FLUIDS ON THE IN SITU HYDROLOGIC CONDITIONS OF TUFFACEOUS ROCKS IN SUPPORT OF EXPLORATORY SHAFT HYDROLOGIC TESTING

WBS 1.2.6.9.4.2.1

Principal Investigator - Alan L. Flint

Co-Investigator - Dwight T. Hoxie
Michael P. Chornack

Alan L. Flint 3/7/85
Principal Investigator Date
Alan L. Flint

Dwight T. Hoxie 3.6.85
Co-Investigator Date
Dwight T. Hoxie

Michael P. Chornack 3/13/85
Co-Investigator Date
Michael P. Chornack

Robert C. Trautz 3/7/85
Technical Reviewer Date
Robert C. Trautz

Larry R. Hayes 3/8/85
Chief, Branch of NNWSI Date
Larry R. Hayes

Table of contents

Figures

Figure

Tables

Table

1.0 INTRODUCTION

The Nevada Nuclear Waste Storage Investigations (NNWSI) project was established to evaluate Yucca Mountain, Nevada, as a potential site for the storage of high-level radioactive waste in a mined geologic repository. To better characterize the geology and hydrology of the Yucca Mountain site, an Exploratory Shaft Facility (ESF) will be constructed at Yucca Mountain. Hydrologic tests, many requiring instrumented boreholes, will be conducted in the ESF. Some of these ESF hydrologic tests require that the in situ hydrologic conditions of the rock be preserved to insure that experimental results reflect the in situ conditions at Yucca Mountain. The type of drilling fluid used during the drilling of boreholes could directly influence the in situ hydrologic conditions prevailing in the tuffaceous rocks surrounding the boreholes (Kwicklis and Hoxie, written commun., 1987). The in situ hydrologic conditions within core samples collected from the boreholes could also be influenced by the drilling fluids. Dry drilling, using air as the drilling fluid, may be an effective way to minimize changes in the in situ hydrologic conditions of the tuffaceous rock.

1.1 PURPOSE

The purpose of this prototype test is to determine how air and water, when used as drilling fluids in tuffaceous rock, affect the in situ hydrologic conditions of the surrounding rock matrix and core samples taken from the boreholes. The effects that any drilling-induced changes in the in situ hydrologic conditions have on geophysical logs and borehole instrumentation will also be tested.

Data from this test will be used to calibrate and validate a set of numerical hydrologic models that will be constructed to simulate and predict quantitatively both short-term and long-term results of the test. A set of models will be required because of the differing hydrologic properties of the tuff units in which the test is being conducted as well as to allow for different physical process and system geometries associated with each borehole or borehole pair. All hydrologic modeling will be performed using the computer code TOUGH (Pruess, 1987), which allows for simultaneous flow and storage of liquid-water, air, water-vapor, and heat in hydrogeologic systems. These hydrologic models are intended to be transferable to similar tests and situations in the ESF. This will allow for the proper siting of experiments which require minimally disturbed in situ hydrologic properties. The test will also determine whether air or water can or should be used as the drilling fluid for boreholes used in the unsaturated-zone hydrologic ESF tests.

This prototype test will be conducted in the G-Tunnel Underground Facility (GTUF). Tuffaceous rocks exposed in this portion of G-Tunnel have matrix properties and fracture densities similar to those of the tuffs that the ESF will penetrate at Yucca Mountain. The results from the G-Tunnel prototype test and the hydrologic models should, therefore, be useful in predicting how the two different drilling fluids would effect the rocks in the ESF.

1.2 SCOPE

This prototype test is designed to be conducted in the GTUF and the U.S. Geological Survey (USGS) Unsaturated Zone Testing Laboratory. Hydrologic modeling will be conducted by the USGS. The Detailed Test Plan activities include the preparation, execution, and documentation of the work. Work will include sample collection, sample testing, data analysis, and hydrologic modeling.

The activities which will be conducted in the GTUF include:

1) borehole coring by wet and dry methods
2) core sample collection
3) borehole geophysical and TV camera logging
4) borehole instrumentation and data collection

The laboratory activities will include measurements of:

1) imbibition,
2) bulk-density,
3) grain-density,
4) porosity,
5) volumetric water-content,
6) water potential,
7) thermal conductivity,
8) moisture retention curves,
9) relative permeability curves,
10) saturated hydraulic conductivities and
11) analysis and interpretation of laboratory test data and borehole instrumentation measurements

The hydrologic modeling activities will include:

1) model design
2) model calibration
3) model validation

1.3 OBJECTIVES

The objectives of this test are as follows:

(a) Measure the rock matrix and hydrologic properties of core samples collected from wet and dry drilled boreholes.
(b) Determine the amount of imbibition of water, from wet drilling fluid, into the rock matrix and the extent of the movement of wet drilling fluid along fractures which intersect the borehole.
(c) Determine the effect of drilling fluids on borehole instrumentation and borehole geophysical logs.
(d) Compare the results obtained from wet and dry drilled boreholes to determine how the drilling fluids effect the ambient hydrologic conditions of the formation.
(e) Provide empirical data that can be used to calibrate and validate the hydrologic models.
(f) Evaluate quantitatively the expected limits of uncertainties of hydrologic-model predictions based on statistical characterization of the input hydrologic-property dataset.

(g) Use the results from the hydrologic models to assess the transfer value to the drilling and coring of boreholes to be used in the ESF for tests which must have minimally disturbed in situ hydrologic properties.

1.4 RATIONALE

The effects of drilling fluids on the in situ hydrologic conditions of the formation in the unsaturated zone at Yucca Mountain must be known before any boreholes are drilled in the ESF. Alteration of in situ hydrologic conditions of the rock matrix surrounding boreholes could have a significant impact on hydrologic experiments performed in or near boreholes, instrumentation installed in boreholes, and geophysical logging. To minimize the possibility of contaminating an area where an unsaturated zone hydrologic tests is to be conducted, the extent of drilling fluid penetration in the rock matrix and fractures must be accurately estimated. This can be accomplished in part by providing data to be used in structuring appropriate unsaturated-zone hydrologic models.

2.0 DESCRIPTION OF WORK

This prototype test entails a sequence of field, laboratory, and hydrologic-modeling activities. The field activities require the coring of two pairs of horizontal boreholes in the G-Tunnel Underground Facility (GTUF). One pair of boreholes will be drilled into a fractured, welded tuff, and the second pair will be drilled into a nonwelded tuff. Of each pair of boreholes, one will be cored using a dry method (air) and the second will be cored using a wet method (water). After each borehole is cored to its total depth, it will be logged using television (TV) and standard geophysical techniques. Following completion of the logging, sets of moisture, temperature, and air-pressure sensors will be installed at selected locations within each borehole. These sensors will be located within each borehole in order (1) to monitor the change with time of environmental conditions near each borehole and (2) to establish ambient background moisture and temperature conditions appropriate to each tuff unit.

Laboratory activities consist of the measurement of rock-sample properties and of experiments performed on these rock samples. Laboratory measurements of in situ water-saturation and moisture-potential conditions will be made on samples taken from selected intervals of the core recovered from each borehole. In addition, the material and hydrologic properties of these samples will be measured. A sufficient number of samples from each borehole will be analyzed to estimate statistical parameters and to develop appropriate statistical characterization for the hydrologic properties of each of the two tuff units penetrated by the boreholes. A sequence of imbibition and moisture-release experiments also will be performed on selected core samples. This full suite of laboratory data are required in order to analyze and interpret the test results as well as to construct numerical hydrologic models to simulate the test results.

Numerical hydrologic models will be used to simulate quantitatively both the ambient background hydrologic conditions in the tuff units penetrated by the boreholes as well as the effects of disturbance and recovery due to the coring of the boreholes. Consequently, the models will be designed to predict the simultaneous storage and flow of liquid water, water vapor, pore gas, and heat within the near-field environment of each borehole. The models will also be designed to simulate cross-hole effects between each pair of wet- and dry-cored boreholes should such effects be observed. The laboratory material-property and hydrologic-property data are requisite input data for the models. The models will be calibrated with respect to the rock-matrix properties by using the measured in situ saturation and moisture-potential data and the results of the laboratory imbibition and moisture release experiments. Observed fracture properties in the fractured welded tuff unit together with the amounts and rates of water lost to the fractures during the wet-coring operations in this unit will be used to calibrate the models with respect to the fracture hydrologic properties. The models will have been validated if their predictions of the test results agree with the observed results to within acceptable limits of error. An analysis of expected model accuracy will be performed using the statistical distribution functions developed from the laboratory measurements and analysis of the core-sample hydrologic-property data.

2.1 Field Data Acquisition

The prototype test will be conducted in two areas of the GTUF. One pair of boreholes will be drilled in the U12g.12 Drift Extension, where the nonwelded Tunnel Bed 5 member of the Belted Range Tuff is exposed. The other pair will be located in either the Laser Drift or the Experiment Drift, where the fractured, moderately to densely welded Grouse Canyon Member of the Belted Range Tuff is exposed. These areas were chosen to provide a wide range of data which can be used in the hydrologic models and will be most readily transferable to the ESF site at Yucca Mountain.

2.1.1 Drilling and Sampling

The exact configuration of the paired boreholes will be determined by the Principal Investigator or his representative prior to the start of drilling. The two boreholes in each pair will be approximately 10 feet apart and will be centered on a level line which is approximately 5 feet above the invert (Figure 2.1-1). The boreholes will be approximately 30 feet in length. The boreholes will be continuously cored and will be approximately 3.790 inches in diameter (HQ3). The core samples obtained from the boreholes will have an outside diameter of approximately 2.4 inches.

Each pair of boreholes will consist of a dry-cored and a wet-cored borehole. Air will be the circulating fluid used to drill the dry-cored borehole. The air-coring technology developed in the Los Alamos National Laboratory (LANL) Prototype Air-Coring test (WBS 1.2.6.9.4.6.1.A) will be used for the dry-cored boreholes. The wet-cored boreholes will use straight water as the circulating fluid.

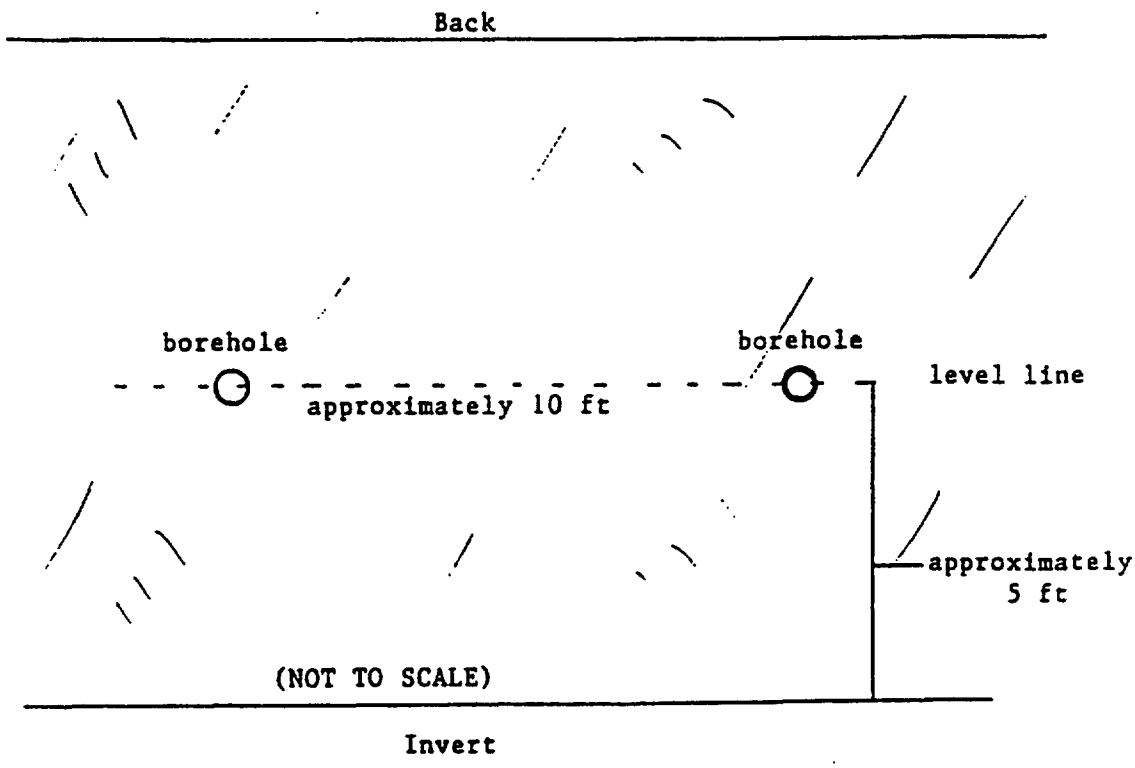

Figure 2.1-1. Layout of Boreholes

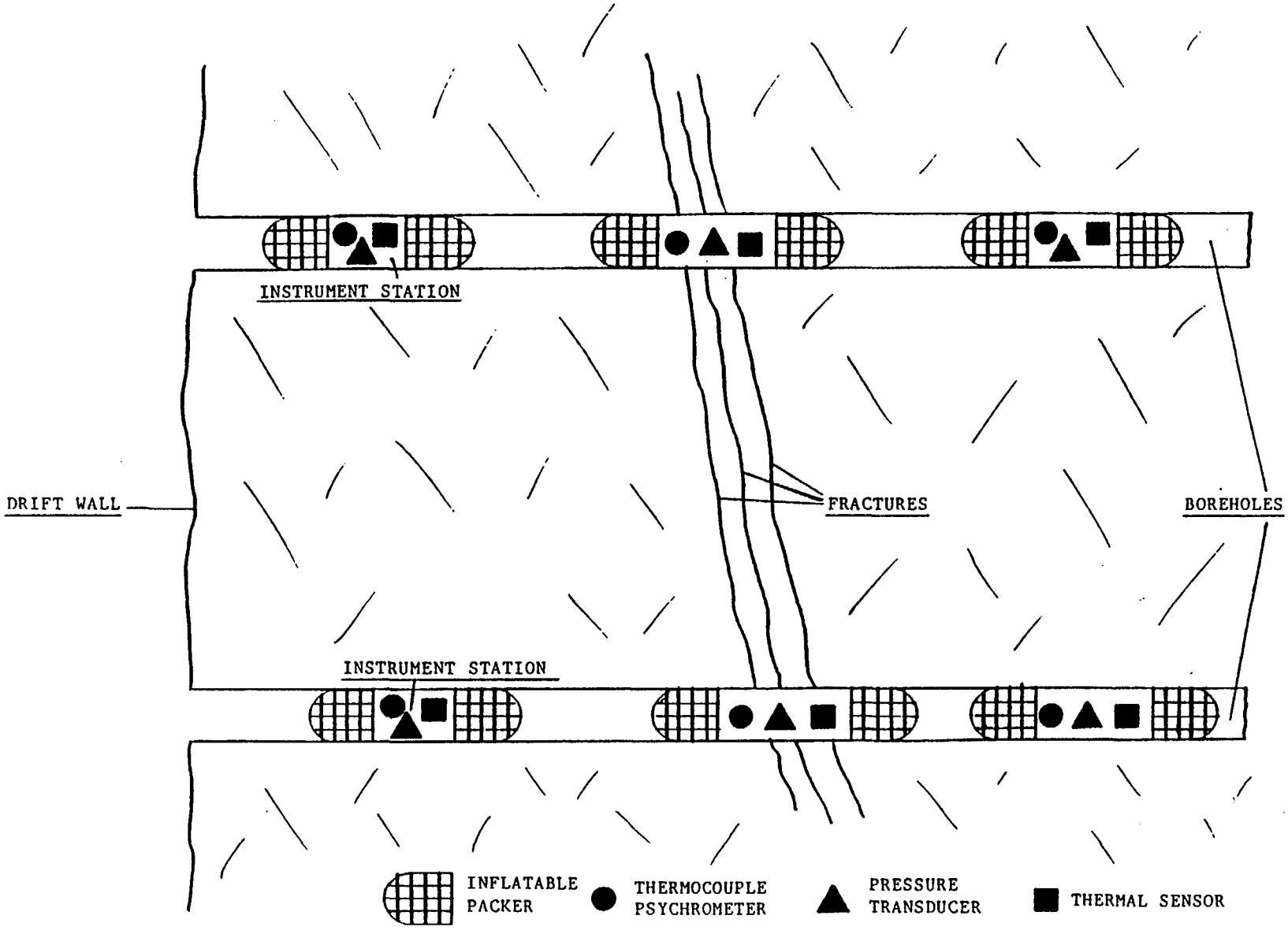

SCHEMATIC PLAN VIEW OF LAYOUT OF HORIZONTAL BOREHOLES/NOT TO SCALE

Standard underground drilling procedures will be followed during the drilling of these boreholes. A lithium tracer will be added to the water during the drilling of the wet-cored boreholes.

The four boreholes will be drilled in the following order: 1) the dry-cored borehole in the U12g.12 Drift Extension (nonwelded tuff), 2) the dry-cored borehole in the welded, fractured Grouse Canyon Member, 3) the wet-cored borehole in the U12g.12 Drift Extension, and 4) the wet-cored borehole in the welded, fractured Grouse Canyon Member.

Drilling data, penetration rates, and drilling fluid data will be collected and recorded in accordance with the LANL Prototype Air-Coring test during the drilling of the dry-cored boreholes. Both dry-cored boreholes will be drilled to total depth, sampled, logged, and instrumented before the wet-cored boreholes are drilled. Drilling data, penetration rates, and drilling fluid balance measurements will be collected and recorded while drilling the wet-cored boreholes.

When a borehole is completed to total depth, the drilling rig can be moved to the location of the next borehole to be drilled. Drilling can be started on the next borehole while the previously completed borehole is being logged and instrumented.

Core samples will be collected from the boreholes using a lexan liner inner-sleeve in the core barrel or a split core barrel. The core samples will be processed in accordance with NNWSI Technical Procedure NWM-USGS-HP-12, R3. Core samples will tentatively be collected and tested as shown in Table 2.1-1

Results from the laboratory testing of core samples will provide empirical data to be used in hydrologic modeling. The hydrologic data obtained from the core samples can also be used to determine how the different drilling fluids have affected the hydrologic conditions of the rock matrix.

2.1.2 Borehole Logging

When a borehole has been completed to total depth, a suite of downhole logs will be run in the borehole. A neutron moisture meter, which measures volumetric water content of the surrounding rock, will be run in the borehole at the end and beginning of each drilling shift or whenever the borehole is accessible. By doing this, the change in the volumetric water-content of the surrounding rock matrix can be monitored throughout the drilling operation. This will provide data on how the rock matrix equilibrates after drilling has stopped. The results obtained from the laboratory analysis of samples and the first neutron logs can be used to calibrate the neutron moisture meter.

A down-hole TV camera will be used to visually inspect the borehole for fractures and other rock-property features. This log can be used to determine possible areas of drilling fluid loss to fractures and the rock matrix. The TV camera log will be used to help

Table 2.1-1. Collection and Testing of Core Samples

Test	Sample Frequency[1]
Porosity*	15 samples at 2 ft spacing
Bulk Density*	15 samples at 2 ft spacing
Grain Density*	15 samples at 2 ft spacing
Volumetric Water-Content*	15 samples at 2 ft spacing
Ambient Moisture Potential*	15 samples at 2 ft spacing
Moisture Retention Curves**	6 samples at 5 ft spacing
Relative Permeability Curves**	6 samples at 5 ft spacing
Saturated Hydraulic Conductivities**	6 samples at 5 ft spacing
Thermal Conductivity	3 samples at 10 ft spacing
Prototype Rubble-Coring Test***	1 sample at 2 ft spacing

(All remaining core samples will be processed in accordance with NWM-USGS-HP-12, R2 for additional testing)

* Same sample is used for all five tests
** Same sample is used for all three tests
*** Sample will be collected to support Prototype Rubble-Coring test (WBS 1.2.6.9.4.2.14).
1 Number of samples and sampling frequency are approximations and may change due to borehole conditions

locate the borehole instrument stations. A caliper log will also be run in the borehole to determine the rugosity of the borehole to help select packer seats for the installation of the borehole instrument packages.

2.1.3 Borehole Instrumentation

The borehole instrumentation package will be emplaced in the borehole at the completion of all borehole logging activities. The design and emplacement of the borehole instruments will be in accordance with the Prototype Drill Hole Instrumentation test (WBS 1.2.6.9.4.2.2). Data taken from the caliper, neutron moisture meter, and TV camera logs will be used to determine the exact location of the instruments and inflatable packers in the borehole. Each borehole will have three instrument stations which are isolated by the inflatable packers. The instruments will remain in the borehole until the instrument readings indicate that the isolated areas of the borehole have equilibrated or the PI directs that the instrumentation be removed from the borehole.

Each instrument station will consist of a pressure transducer, a thermal sensor, and a thermocouple psychrometer. A Campbell Scientific CR-7 data logger will be used to monitor and record instrument output. One data logger will be required for each pair of boreholes.

2.2 Laboratory Analysis

There are specific laboratory analysis of core required for the hydrologic models (Table 2.1-1). The boreholes will, however, be continuously cored providing many extra samples. These additional core samples will be analyzed as needed to fill in any missing information that may arise during the hydrologic modeling or interpretation of borehole instrumentation data. Although it is unlikely that all of the test mentions in Table 2.1-1 will be run on all the cores, it is expect that at least one core from each foot of borehole will be tested for volumetric water content, porosity and bulk density.

2.2.1 Analysis of Core Samples for Ambient Conditions

Core samples collected to determine ambient water conditions will be analyzed in the USGS UZ Hydrology Laboratory. Water potentials will be measured using thermocouple psychrometer and tensiometer methods currently being developed under USGS-SIP-3343G-02, R0. Those cores will then be oven dried to determine gravimetric water content. Once the ambient conditions are known those same samples will be analyzed to determine particle density, bulk density and porosity. Volumetric water content and percent saturation will be calculated from these data.

2.2.2 Experimental Analysis of Core

The USGS UZ Hydrology Laboratory will conduct several experimental analyses on core samples. Imbibition experiments, similar to that of Peters et al. (1987) and Handy (1959), will be conducted to provide basic data for comparisons between laboratory samples and geophysical logs and borehole instrumentation data for both the welded and nonwelded units. Moisture retention characteristic curves will be measure to provide information for the hydrologic models as well as determining the accuracy of the water potential water content measurement take from cores at ambient conditions. Contract laboratories will be use to determine saturated and unsaturated hydraulic conductivities using centrifuge techniques. Although thermal conductivities and heat capacities are needed for the hydrologic models, previous reports (Lappin and Nimick, 1985) provided sufficient data for initial modeling efforts. If thermal conductivity and heat capacity are found to be to sensitive in the hydrologic modeling, then core samples will be tested by contract laboratories to give site specific values.

2.2.3 Interpretation of Logs

Caliper logs and TV logs are straightforward and will be used to help locate the borehole instrumentation package. These logs will also provide data as to fracture or fault locations within the units. The neutron moisture-meter log will need to be field calibrated. Although neutron calibration data exists for welded and nonwelded tuff (Blout et al., 1988) core data will be used to help determine the proper application of those calibrations.

2.3 Synthesis and Analysis of Field and Laboratory Data

The data generated from field and laboratory analysis will be evaluated to determine the hydrologic nature of the two units. This analysis will include an examination of ambient conditions and changes that occurred as a result of using the different drilling fluids. Although both air and water will effect the in situ conditions, it will be assumed that changes in the measured conditions in the boreholes will be in the direction of the actual initial conditions. It is expected that dry-cored boreholes will become wetter with time as water returns to the system and the wet-cored borehole will dry with time as the excess water moves away from the boreholes or dries from the fractures. It is the rate of change over time, differences between the wet- and dry-cored boreholes, and the final values at the end of the experiment that will provide the most information about the actual ambient conditions.

2.4 Hydrologic Modeling

An important aspect of this experiment is the acquisition of sufficient empirical data to construct appropriate numerical hydrologic models in order to simulate and interpret the test results. The purpose of the hydrologic modeling is to improve understanding of the test results and to demonstrate the capability of simulating

hydrologic processes occurring at the scale of the test. This latter exercise provides an opportunity to validate the hydrologic models through direct comparison of model predictions with the empirical data collected during the test. Successful model validation under these test conditions will increase the credibility of applying hydrologic models to analogous problems during site-characterization as well as to the hydrologic tests to be performed within the ESF.

In order that this experiment provide adequate data to accomplish the hydrologic modeling, the following data are to be collected from core samples, borehole logging, and the drilling operations:

1. Rock matrix porosities, ambient saturations, ambient matric potentials, moisture retention functions, relative permeability functions, saturated hydraulic conductivities, and thermal conductivities.
2. Approximate fracture densities, orientations, and apertures within the boreholes.
3. A quantitative determination of fluid losses to the formation during coring.

The rock-matrix hydrologic properties are to be measured on a sufficient number of independent samples so that the statistical properties as well as any systematic spatial variation of any of these properties within or between the boreholes can be determined. It is estimated that approximately 15 to 20 samples per borehole will be required for statistical characterization for the modeling efforts. However, a complete suite of properties may not be needed for each sample, depending on the inherent homogeneity of the units from which the samples are taken. The statistical data will be used to assess model accuracy and validity. The occurrence of observed systematic variation of hydrologic properties within or between the boreholes will permit the effects of rock heterogeneities and spatial correlations to be evaluated by the hydrologic model.

The boreholes cored by using air as a drilling fluid will be used in the modeling (1) to assess the expected short-term effects of heat and airflow on the immediate borehole environment and (2) to provide a long-term control against which to compare the expected changing moisture conditions in those boreholes cored by using water as the drilling fluid. It is expected that each pair of boreholes will remain hydrologically isolated from each other throughout the duration of the test. However, in case continuous fractures systems exist between the locations selected for the wet or dry cored boreholes, the dry-cored boreholes will be drilled first. This will allow the dry hole to reach equilibrium after the effects of drilling so that ambient conditions within the welded and nonwelded units can be determined.

The pair of boreholes within the fractured welded unit present specific problems because of the likely presence of fracture systems that may act as conduits for fluid movement. Not only may a large quantity of fluid be lost to fractures during drilling operations, but the fluid may be easily transmitted within the fractures over

distances equal to or greater than the separation between the pair of boreholes. Consequently, the wet borehole should be located to minimize the possibility of liquid-water invasion of the dry borehole during or following drilling of the wet borehole. Direct air communication between the wet and dry boreholes by fractures or fracture systems may be detected by the instruments within the dry borehole. Such communication may be indicated either by an air-pressure front or humidity pulse moving past the dry borehole as a result of drilling the wet borehole. Air-flow communication probably would be the results of a continuous fracture system being intersected by the two boreholes. Quantitative measurement of air flow communication would provide indirect estimates of the fracture transmissive properties. It is important, therefore, that a instrument station in each borehole in the welded unit be installed in a fracture zone oriented to favor the detection of fracture communication between the wet and dry boreholes.

Although the matrix hydrologic properties for both the welded and nonwelded unit can be measured or estimated in the laboratory, such will not be the case for the fracture systems encountered in the welded tuff unit. The hydrologic properties of the fractures will have to be inferred from the empirical fracture data, which include fracture apertures, densities, orientations, and the measured quantities of drilling fluid lost to these fractures during the drilling operations. To model the fractured welded tuff unit, the fractures and the rock-matrix will be treated as separate hydrogeologic systems. Because the modeling of fluid movement in complex fracture systems remains poorly developed, the fracture system will be treated as an equivalent porous medium whose hydrologic properties, in general, will reflect a large saturated hydraulic conductivity coupled with a low capacity for fluid storage. The remaining fracture hydrologic properties will have to be estimated from the data obtained early in the test; that is, these test data will be used to calibrate the hydrologic model for subsequent application to the system. The model will be calibrated with respect to the rock-matrix hydrologic properties for both the welded and nonwelded units by using the hydrologic simulator to replicate the results of a set of imbibition and moisture release experiments to be performed in the laboratory on core samples recovered from the boreholes. Field validation of the model will be achieved if it predicts to within acceptable limits of uncertainty the change with time of the moisture conditions within the near environment of the boreholes during the duration of the test as recorded by the monitoring instruments installed within the borehole.

The statistical data accumulated for the rock-matrix hydrologic-property data set and estimated for the fracture properties will be used as input data to assess quantitatively the accuracy of model predictions. These assessments will be performed both for the steady-state situation as presumably monitored by the dry-cored boreholes as well as for the transient effects observed in the wet-cored boreholes. These modeling efforts will provide a prototype test for applying hydrologic models both to nonwelded and to fractured

welded tuff units under steady-state and transient conditions as well as to test methods for assessing model accuracy and, hence, validity.

It is expected that the construction calibration, and validation of at least two and perhaps four distinct hydrologic models will be required as part of the overall hydrologic modeling program for the test. A minimum of two independent models will be needed for the borehole pairs in the nonwelded tuff and the fractured welded tuff. If no cross-hole effects between the wet-cored and the dry-cored boreholes of a given pair of boreholes are observed during the test, then each borehole and its environment will be regarded as an isolated hydrologic system that will be modeled separately. If cross-hole effects occur, then the borehole pair in which these effects are observed together with the enclosing and intervening rock unit will be regarded as a single, complex hydrologic system. Consequently, the geometry and boundary conditions for the hydrologic models will depend on both the immediate and long-term responses observed in the boreholes. Initially, in order to simplify system geometry, preliminary model construction and calibration will be performed under the assumption that each member of a pair of boreholes is an independent system. The validity of this initially simplifying assumption will depend on the mechanism and rate of propagation of possible cross-hole effects. The occurrence of and the need to include cross-hole effects in a model will complicate the system configuration and process but would clearly enhance the credibility of the model following successful model validation. In all cases of model construction, the calculation efficiency and the numerical accuracy of the model predictions will be optimized with respect to the governing hydrologic processes, system complexity, and the inherent error bounds and uncertainties of the input hydrologic-property data set.

It is planned to use the numerical simulator TOUGH (Pruess, 1987) to perform all of the hydrologic modeling tasks. This computer code is capable of treating the storage and flow of liquid water, water vapor, gas, and heat in three-dimensional systems of arbitrary geometry. The details of code implementation for this experiment will depend on drilling fluid flux measurements, on the system geometry as inferred from the borehole locations in G-Tunnel and the borehole logging operations, and on the locations of the instrument stations within the boreholes.

2.5 Experimental Parameters

This test is dependent upon the successful development and implementation of air-coring techniques for horizontal boreholes in an underground environment. The volume of air used while dry-coring will be closely monitored and recorded in accordance with the LANL Prototype Air-Coring test (WBS 1.2.6.9.4.6.1.A). The volume of water used while wet-coring will also be closely monitored and recorded. The volume and concentrations of any tracers added to the drilling fluids will be recorded.

The core samples collected for laboratory testing must be processed in accordance with technical procedure NWM-USGS-HP-12, R3.

Procedures detailing how tests are to be conducted must be strictly adhered to at all times.

Borehole geophysical logging will be conducted according to USGS technical procedures, manufacturer's procedures, developed industry standards, or contractor's procedures.

2.6 Operational and Measurement Equipment

All equipment needed to collect, process, and test samples for this prototype test are described in the technical procedures which are being used as guidelines for conducting this test. Drilling equipment which has been modified for underground air coring will be developed by LANL in the Prototype Air-Coring test. All other materials used in this test are commercially available.

2.6.1 Since the prototype test have been classified as Quality Assurance (QA) Level III, calibration requirements listed in Chapter 12 of the Quality Assurance Manual (NNWSI-USGS-QMP-12.01, R1) do not apply. Guidelines listed in Chapter 12 apply only to QA Level I and II activities. Instead, acceptable industry standards or procedures will be adopted and used to calibrate prototype test instrumentation.

2.7 Field Operations

Field operations for this test will be conducted in two areas of the GTUF, the U12g.12 Drift Extension and either the Laser Drift or the Experiment Drift. The boreholes will be cored, samples, logged, and instrumented. The instruments will be monitored for an appropriate length of time. At the conclusion of this prototype test, these boreholes will be made available to other investigators for their use.

2.8 Related Analysis and Experiments

Sample testing will be conducted in the laboratory by the USGS or their contractors. Table 2.1-1 lists the types of samples that will be collected and the tests that will be conducted with them. Analysis of the borehole logs will be conducted by the USGS. Interpretation of the data from the borehole instrumentation will be conducted by the USGS.

Statistical analysis of the data from the sample testing and borehole logging will be conducted by the USGS to determine if the two types of drilling fluids used while coring cause statistically significant differences in the hydrologic properties of the formation in regions of fractures and unfractured rock.

3.0 QA LEVEL

This work has been approved as Quality Assurance (QA) Level III in accordance with NNWSI-USGS-QMP-3.02, R1.

4.0 OPERATIONS

4.1 Sequence of Activities

Activities planned for FY 88 are as follows:

Field Data Acquisition

a) Develop dry-coring technology
b) Core and sample horizontal boreholes in the GTUF
c) Log completed horizontal boreholes
d) Instrument horizontal boreholes
e) Monitor borehole instrumentation for an appropriate length of time
f) Prepare preliminary report on field operations

Laboratory Analysis

a) Analyze core samples from horizontal boreholes for ambient conditions
b) Conduct imbibition and moisture release experiments on core samples from horizontal boreholes
c) Provide data for the calibration of the hydrologic models
d) Analyze and interpret the results of the borehole logs
e) Analyze and interpret the results collected by the borehole instrumentation
f) Synthesize and analyze the field and laboratory data
g) Provide data for the validation of the hydrologic models
h) Prepare preliminary report on laboratory analysis
i) Prepare preliminary report on borehole instrumentation
j) Prepare final report on influence of wet and dry drilling fluids on the ambient conditions

Hydrologic Modeling

a) Use initial laboratory data to calibrate the hydrologic models.
b) Prepare report on the calibration of the hydrologic models.
c) Use laboratory data, logging data, and borehole instrumentation data to validate the hydrologic models.
d) Prepare final report on the validation of the hydrologic models and their transfer value.

Prerequisites

a) Dry-coring technology must be developed before the test can begin. The dust-collection system for the underground dry-coring must be developed.
b) All materials for processing core samples must be available. The USGS field laboratory trailer must be located near the G-Tunnel portal and must be fully operational.
c) Monitoring, sampling, and logging personnel must be available whenever drilling operations begin.
d) Borehole instrumentation and data logging equipment must be available before drilling operations begin.
e) Laboratory personnel must be available to conduct the tests on the core samples.
f) Necessary laboratory equipment must be available for testing

the core samples.

Postrequisites

The prototype test will be completed when:

a) The boreholes have been completed to total depth and all associated borehole logging has been completed.
b) Core samples have been tested in the laboratory, statistical analysis has been completed, and this data has been used to calibrate the hydrological models.
c) Results from the borehole instrumentation have been provided, along with laboratory and field data, to the hydrologic models for their validation.
d) All reports and other post-completion data analysis are completed.

4.2 Technical Procedures

Formal technical procedures are not required for QA Level III work, but due to the nature of this test, certain technical procedures will be used. Safe Operating Procedures (SOPs) are separate and are defined in Section 9.0. The following technical procedures are to be used:

NWM-USGS-HP-12	Methods for Collection, Processing, and Handling of Drill Cuttings and Core from Unsaturated-Zone Boreholes at the Well Site

Procedures developed under the Prototype Air-Coring test (WBS 1.2.6.9.4.6.1.A) will be used while coring the boreholes.

4.3 Changes in Experimental Procedures

The initial issue of this procedure was Revision 0. This is Revision 2. The approval sheet identifies those who reviewed and approved Revision 2. Should it become necessary to change this document, the Principal Investigator will draft the necessary changes and follow the same approval process, and a revised document will be issued and distributed.

4.4 Management

Prototype evaluation of the effect of drilling fluid on the hydrologic conditions within tuffaceous rocks consists of three major components: field data acquisition, laboratory analysis, and hydrologic modeling. Field data acquisition consists of borehole drilling and sampling, borehole logging, borehole instrumentation, data-system operation and management, and experiment evaluation. Laboratory testing involves conducting measurements on core samples collected during borehole drilling. Analysis of borehole logs and borehole instrumentation data is a laboratory activity. Instrument

preparation and calibration, equipment preparation, and diagnostic testing, as well as actual sample testing are laboratory activities. Application of the results from the field and the laboratory phase of the test to the hydrologic models is a significant goal of this prototype test. An analytical component of prototype testing is iteratively related to each phase of this test.

These activities are to be performed by a team of USGS personnel and USGS subcontractors. Figure 2.1-2 shows the man power organization for this prototype testing. The work is performed under the general direction of the Principal Investigator and specific direction of the USGS Investigator, who has overall responsibility for the experimental effort. The field testing component of the test involved G-Tunnel support. Current USGS personnel assignments and contracts are shown for these activities.

5.0 DATA ACQUISITION SYSTEM

Two Campbell Scientific CR-7 data loggers will be used for the data collection in this prototype test in the GTUF.

6.0 PERSONNEL QUALIFICATIONS

Quality Level III work does not require formal certification of project personnel; nevertheless, the personnel involved in this testing could be shown to have the appropriate technical experience necessary for the tasks planned.

7.0 NONCONFORMANCE ACTIONS

Nonconformance of Quality Level III items or processes will be documented per the requirements of NNWSI-USGS-QMP-10.01, R1. Corrective action will be documented per the requirements of NNWSI-USGS-QMP-16.01, R1.

8.0 DOCUMENTATION

Coring information will be documented in a manner similar to that used by LANL in the Prototype Air-Coring test (WBS 1.2.6.9.4.6.1.A). Data forms and log books will be used to document sample collections, test results, and daily drilling operations connected with this test. Hard copies of borehole logs will be documentation of the logging operations.

As described in NNWSI-USGS-QMP-3.02, R1, existing USGS good scientific practice requirements shall apply to Quality Level III work. Therefore, field notes, log books, and data records (computer or otherwise) will be maintained with the utmost of care and precision. All manual data entries are to be recorded in black permanent ink, and are to be signed and dated by the person responsible for that data collection. Computer-stored data are to be tagged, as described in NNWSI-USGS-QMP-5.1.4, R1 and NNWSI-USGS-QMP-5.2.2, R1. All log books and records are to be permanently maintained and archived in the USGS Denver offices. A

MANPOWER ORGANIZATION

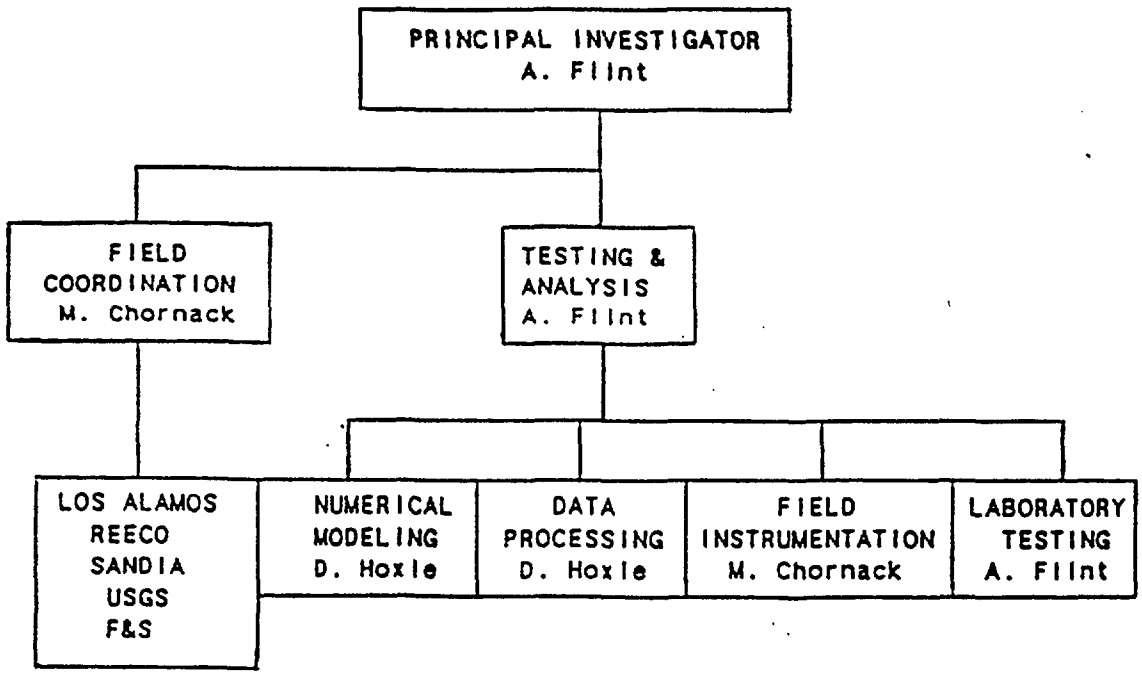

Figure 2.1-2. Manpower Organization Chart.

USGS data-records management system will be maintained in Denver for support of all data-collection activities associated with the USGS prototype testing program.

9.0 SAFETY

All Reynolds Electrical and Engineering Company (REECo) and Sandia National Laboratory (SNL) G-Tunnel safety procedures will be adhered to during this test. Manufacturer's instructions and industrial hygiene safety procedures will be followed when handling any tracer materials.

10.0 REPORTS

10.1 Preliminary Reports

A series of preliminary and progress reports will be prepared as principal tasks of the field, laboratory, and hydrologic modeling are completed. These reports will be provided to the Department of Energy as well as to other Principal Investigators involved with similar or related studies. Specific activities that will generate preliminary reports are as follows:

10.1.1 Field Operations

A preliminary report will be prepared describing the emplacement and logging of the boreholes in the GTUF upon completion of this activity. This report will provide detailed information on borehole configurations, the coring methods and history, and the results obtained from the TV and geophysical logging operations.

10.1.2 Laboratory Analyses

This report will summarize the data obtained from measurements of material and hydrologic properties on core samples, in situ measurements of moisture content and potentials made on these samples, and the statistical characterization of the hydrologic properties as determined from the measured sample values. In addition, the report will describe the results of the imbibition and moisture-release experiments performed on core samples. Fracture properties in the welded tuff unit as well as the rock-matrix petrology of the core samples will be described in this report.

10.1.3 Construction and Calibration of Preliminary Hydrologic Models

The construction of the numerical hydrologic models will proceed stepwise by increasing the degree of complexity as the field and laboratory data become available and as the need to incorporate specific hydrologic processes warrants. Initial calibration of the models, based in part on the laboratory imbibition and moisture release experiments and in part on the initial borehole field conditions, will be described in this report. Preliminary model

geometry and boundary conditions will be discussed in the context of optimizing model accuracy and efficiency.

10.1.4 Field Instrumentation

Details of the instrument packages, the locations of the instrument stations within the boreholes, and the data-collecting system will be described in this report. Data collection frequencies will be described both for initial short-term monitoring of the immediate system disturbance and response to coring as well as for longer-term monitoring of system recovery and equilibration.

10.2 Final Reports

Two final reports will be prepared and published to describe the overall results of this prototype test. The first of these reports will describe the field and laboratory procedures, summarize the quantitative data in terms of the identifiable and quantifiable impacts of wet and dry drilling methods on welded and nonwelded tuffs. Both the magnitude of the initial drilling-induced disturbance on ambient hydrologic conditions as well as the rates of recovery and the degree of equilibration within each tuff unit at the termination of the test will be assessed. From these assessments, specific drilling procedures to be used in drilling exploratory boreholes within the Exploratory Shaft Facility will be recommended.

The second final report will describe the construction, calibration, and validation of the numerical hydrologic models for the system. It is presumed that at least a separate model will be constructed for each tuff unit. If no cross-hole effects are observed during the test, then it will be assumed that each borehole is hydrologically isolated from the others. In this case the environment surrounding each borehole would be viewed as a separate hydrologic system that would lead to the construction, calibration, and validation of four individual models. The principal subject of this final report will deal with model construction and model validation. Model validation involves the assessment of the degree to which the model predicts the observed response of the modeled system. The issue of model accuracy will be addressed in this report in terms of input-data uncertainty by using the statistical characterization of the hydrologic-property data developed from the laboratory and field measurements of these properties.

11.0 DEFINITIONS

All necessary definitions are included in the technical procedures which are being used to support this test.

12.0 REFERENCES

Blout, D. O., Hammermeister, D. P., Johnson, M. F. and A. L. Flint. 1988. Neutron moisture logging data, Yucca Mountain area, Nye County, Nevada. U. S. Geological Survey, Open File Report 88__. (Manuscript in Review).

Lappin, A. R., and F. B. Nimick. 1985. Thermal properties of the Grouse Canyon member of the Belted Range Tuff and of Tunnel Bed 5, G-Tunnel, Nevada Test Site. SAND82-2203, Sandia National Laboratories, Albuquerque, NM.

Handy, L. L. 1959. Determination of effective capillary pressures for porous media from imbibition data. Petroleum Transactions, AIME 219:75-80.

NWM-USGS-HP-12, R3. NNWSI Project Technical Procedure, Methods for Collection, Processing, and Handling of Drill Cuttings and Core from Unsaturated-Zone Boreholes at the Well Site, USGS, Denver, Colorado.

NWM-USGS-QAPP-01, R1. Quality Assurance Program Plan for Nuclear Waste Storage Investigations, USGS, Denver, Colorado.

Peters, R. R., E. A. Klavetter, J. T. George, and J. J. Gauthier. 1987. Measuring and modeling water imbibition into tuff. IN: Flow and Transport Through Unsaturated Fractured Rock. D. D. Evans and T J. Nicholson, Eds. Geophysical Monograph 42, AGU, Washington, D.C.

Pruess, K., 1987. TOUGH User's Code, LBL-20700, Lawrence Berkeley Laboratory, Berkeley, California.

APPENDIX A2

Summary drilling report for the wet versus dry drilling experiment

Table of contents

SUMMARY DRILLING REPORT FOR THE WET VERSUS DRY DRILLING EXPERIMENT

by
Michael P. Chornack and Alan L. Flint, USGS

Introduction

The "Prototype Evaluation of the Effects of Wet and Dry Drilling Fluids on the in situ Hydrologic Conditions of Tuffaceous Rocks in Support of Exploratory Shaft Hydrologic Testing" (hereafter called the "Wet and Dry Drilling test") was conducted by the U. S. Geological Survey to provide comparative data on what effects drilling fluids have on core samples from and the rock matrix surrounding boreholes drilled in pyroclastic rocks in the unsaturated zone. This prototype test is part of the Yucca Mountain Project investigations being undertaken by the U. S. Geological Survey in cooperation with the U. S. Department of Energy, Yucca Mountain Project Office, under Interagency Agreement DE-AI08-78ET44802.

Location

The Wet and Dry Drilling test was conducted in the G-Tunnel complex at the Nevada Test Site (NTS). The G-Tunnel portal is located near the southeast corner of Rainier Mesa at Nevada State Central Zone Coordinates N. 881,026.26, E. 637,707.81 (Fig. 1). The elevation of the portal is 1863.9 meters above sea level. An area in the G-Tunnel complex, designated the G-Tunnel Underground Facility (GTUF), was chosen for ESF prototype testing (Fig. 2). This area of the G-Tunnel complex provides access to nonwelded tuff and fractured, welded tuff. These rock types are similar to those that will be encountered in the ESF at Yucca Mountain.

Two areas in the GTUF were selected for the Wet and Dry Drilling test. One site is located in the U12g.12 Drift (Fig. 2). This area provides access to bedded, nonwelded tuff of Tunnel Bed 5 of the Belted Range Tuff. The other site is in the Laser Drift (Fig. 2), an area located in the highly fractured, densely welded tuff of the Grouse Canyon Member of the Belted Range Tuff.

Borehole Configuration

A pair of horizontal boreholes was continuously cored at each location. Each pair of boreholes consisted of one borehole cored with air as the circulating fluid and one borehole cored with water as the circulating fluid. The arrangement of the pairs of boreholes was designed to provide the maximum amount of information on the influence that the circulating fluids have on the surrounding rock matrix. The boreholes in the nonwelded tuff provided data on the wetting and drying effects that the circulating fluids have on a porous rock matrix. The boreholes in the fractured, welded tuff provided data on the influence that the wet and dry circulating fluids have on a low porosity matrix. The pair of boreholes in the welded tuff also investigated the effect that the circulating fluids have on the fractures in the welded tuff.

The pair of boreholes in the U12g.12 Drift are designated U12g.12 DD-1 (dry cored) and U12g.12 WD-1 (wet cored). The two boreholes are approximately 2.4 meters apart and aligned parallel to each other. Borehole U12g.12 DD-1 is 1.6 meters above the invert and borehole U12g.12 WD-1 is 1.8 meters above the invert This pair of boreholes was oriented to penetrate differing lithologic units in the bedded nonwelded tuff and to intersect a major fracture trend.

The two boreholes in the Laser Drift are U12g DD-2 (dry cored) and U12g WD-2 (wet cored). U12g DD-2 is 1.3 meters above the invert and U12g WD-2 is 1.5 meters above the invert. These boreholes are approximately 1.7 meters apart. The boreholes are oriented perpendicular to a major fracture trend observed in the Laser Drift. To further investigate the effect of the wet drilling fluid on fractures, borehole U12g WD-2 was angled slightly toward borehole U12g DD-2. The decrease in distance between the two boreholes with depth could provide data on the radius of influence of wet drilling fluids in fractures. Deviation during drilling of the two boreholes was such that when borehole U12g WD-2 reached a depth of 7.9 meters, it intersected borehole U12g DD-2. The core bit in borehole U12g WD-2 cut through the packer-instrument string in borehole U12g DD-2 at a depth of 7.6 meters. A hole approximately 0.4 meters long was created between the two boreholes. Drilling of borehole U12g WD-2 was terminated due to the intersection of the boreholes.

Borehole Drilling

The drilling of boreholes for the Wet and Dry Drilling test began on November 14, 1988, with borehole U12g.12 DD-1. The boreholes were drilled in the following sequence: U12g.12 DD-1, U12g DD-2, U12g.12 WD-1, and then U12g WD-2. The dry-drilled boreholes were completed first so that the borehole instrumentation packages would be in place during the wet-drilling phase of the test. The borehole instrumentation in the dry-drilled boreholes could potentially detect any cross-hole contamination that might occur. The time between the drilling of the dry-cored boreholes and the wet-cored boreholes allowed the instrumentation in the dry-cored boreholes to reequilibrate, providing data on the in situ conditions in the boreholes. Changes in these conditions caused by the drilling of the wet-cored boreholes could be detected and monitored by the borehole instrumentation.

The boreholes were drilled with a Longyear LY-38 Electric/Hydrostatic drilling rig[1]. A 1.5-meter long, split inner tube with polycarbonate (Lexan) liners was used in conjunction with a standard outer core barrel assembly. Core samples were retrieved using wireline coring techniques. Standard coring bits were used to drill the boreholes. A tungsten-carbide (Geoset) chisel tooth core bit was used to drill the boreholes in the nonwelded tuff. Diamond impregnated core bits were used when drilling in the fractured, welded tuff. Methods developed during the "Prototype Air-Coring Test" (Ray and Newsom, LANL, written commun., 1989) were used when dry coring. When air was used as the circulating fluid, an Atlas-Copco DCT-90/9504 dust collector[1] was utilized

[1]Any use of trade names is for identification only and does not constitute endorsement by the U. S. Geological Survey.

to contain the dust generated during coring. Standard underground coring procedures were followed when using water as the circulating fluid.

A record of drilling parameters was kept for each borehole. Information that could be used to help interpret data gathered from the boreholes or that could be used to evaluate the two drilling processes was recorded on the drilling parameters form. The combination of drilling parameters used while coring can influence the penetration rate and the condition of the core samples recovered from the borehole. The drilling parameters that can be easily varied during coring operations are the weight on bit, the revolutions per minute, and the amount of circulating fluid passing through the bit (either in liters of air per minute or liters of water per minute). The type of core bit can also be changed, but this is normally only done to replace a worn core bit. Tables containing the drilling parameter data are presented later.

The weight on bit, revolutions per minute, and amount of circulating fluid used were visually monitored and recorded on site during drilling operations. A gage on the drilling rig indicates the weight on the bit. The gage was monitored during each core run and the average weight on bit to the nearest 100 kilograms was recorded. If the weight on bit was changed during a core run, the extremes to the nearest 100 kilograms were recorded. Revolutions per minute were determined by counting the revolutions the chuck on the drilling rig made in one minute. The rpm's were normally rounded to the nearest 5 rpm's and represent averages for a core run. Extremes were recorded for core runs where the revolutions per minute were significantly changed. Air flow, in liters per minute, was measured using a flow meter connected to the air inflow line. The air inflow was set by the driller at the start of each core run and this number was recorded. If the air flow had to be changed during a core run, the extremes were recorded. The liters per minute of water circulated during a core run were determined by counting the number of pump strokes per minute and, using the capacity of the pump, calculating the liters per minutes. This method gives the approximate liters of water circulated through the bit in one minute.

When drilling with air as the circulating fluid, the use of the dust collection system made it impossible to monitor how much air was returned to the surface. Thus, the amount of air lost to the formation (matrix and fractures) could not be determined. When water was used as the circulating fluid, a circular tank with an open top was used to monitor the fluid loss. The tank was filled with water before the start of drilling and the volume of water in the tank was calculated. The water used to cool the bit and to circulate the cuttings out of the borehole was pumped from the circular tank. The returning circulating fluid from the borehole was pumped from a sump pit at the well head back to the circular tank. Water depth measurements were taken in the tank at the start and finish of each core run, and the amount of water lost per core run was calculated from these measurements.

Borehole U12g.12 DD-1 was started on November 14, 1988 and reached total depth (TD) of 9.7 meters on November 16, 1988. Air was used as the circulating fluid during the drilling of this borehole. A total of seven core runs were made to complete the borehole to total depth. Total core recovery

for the borehole amounted to 9.4 meters or 97 percent of the total amount of core drilled. It required approximately 133 minutes of actual drilling time to complete the borehole to TD, averaging 4.3 meters per hour (14 minutes to core one meter). Approximately 636,000 liters of air were used to cool the core bit and to circulate cuttings during the drilling of U12g.12 DD-1. Table 1 gives the amount of air used during each core run and the cummulative total for all the core runs. The drilling parameters for this borehole are listed in table 2.

At the completion of U12g.12 DD-1, the drilling rig, dust collector, and support equipment were moved to the Laser Drift in preparation for drilling borehole U12g DD-2. The drilling of this borehole commenced on December 5, 1988 and finished on December 7, 1988. Air was used as the circulating fluid during the drilling of U12g DD-2. Eight core runs were required to complete the borehole to a total depth of 9.1 meters. The core recovery for the borehole was 93 percent for a total of 8.5 meters of core recovered. The total time needed to complete the borehole was 397 minutes, that included time taken to add drill rods during two core runs. Using this total time estimate, the average drilling rate for the borehole was 1.4 meters per hour (44 minutes to core one meter). During the drilling of U12g DD-2, approximately 1.4 million liters of air were circulated through the borehole. Table 3 shows the cummulative air use for borehole U12g DD-2. The drilling parameters for this borehole are shown in table 4.

The wet-drilling phase of the test began on December 12, 1988, with the start of borehole U12g.12 WD-1. Water, with a lithium bromide tracer, was used as the circulating fluid during all wet-drilling operations. As stated previously, the circulating fluid was recirculated during wet drilling, providing data on fluid loss to the formation. The method for recirculating was improved upon during the drilling; reaching a point where most fluid loss could be attributed to loss to the formation.

Borehole U12g.12 WD-1 was completed in three days, starting on December 12, 1988 and ending on December 14, 1988. A total of seven core runs were made during the drilling of the borehole. The total depth reached was 9.0 meters. A total of 8.9 meters of core was recovered from U12g.12 WD-1, representing a 99 percent recovery rate. It took 109 minutes of drilling time to complete the borehole. The average penetration rate for the borehole was 5 meters per hour (12 minutes to core one meter). During the drilling of U12g.12 WD-1 a total of 424.7 liters of water were lost. Over 390 liters of water were lost during the first three core runs. Some of this water was lost from the sump pit, and some of the water was lost from the end of the drill rods when the inner core barrel was being retrieved. Loss of water from the sump pit was controlled by lining the pit with plastic sheeting. The water lost from the open drill rods while retrieving the inner core barrel was controlled by catching it in a container and returning it to the circular water tank. After these modifications were made, the majority of water lost can be attributed to loss to the formation. The water loss per core run for the borehole is shown in table 5. The drilling parameters for this borehole are given in table 6.

The final borehole drilled for the Wet and Dry Drilling test was the

wet-drilled borehole in the Laser Drift. This borehole, designated U12g WD-2, was started on December 19, 1988 and was terminated on December 20, 1988. Drilling was terminated when this borehole inadvertently intersected borehole U12g DD-2 at 7.6 meters. The depth of U12g WD-2 was 7.9 meters when it intersected the dry-drilled borehole. Six core runs, including the core run that intersected the other borehole, were made during the drilling of U12g WD-2 to a total depth of 7.9 meters. The core recovery for the borehole was 7.7 meters, a recovery rate of 97 percent. It required 185 minutes of drilling time to complete the borehole to TD. The average penetration rate for the borehole was 23 minutes per meter drilled. Water loss during the first five core runs totaled 2005 liters. This figure reflects some water lost at the sump during the first two core runs. The actual water lost to the formation is probably closer to 1350 liters. When the two boreholes in the Laser Drift intersected, a large quantity of water was lost through the inside of the packer-instrument string in U12g DD-2. The water loss data for U12g WD-2 is given in Table 7. Drilling parameters for borehole U12g WD-2 are presented in table 8.

General Geology

Rainier Mesa is composed of a thick sequence of Tertiary pyroclastic rocks (Gibbons et al, 1963) ranging from vitric ash- fall to devitrified ash-flow tuffs (Fig. 3). Tunnel Bed 1 is the lowest pyroclastic unit in the vicinity of the G-Tunnel portal. It was deposited on a paleotopographic surface developed in upper
Precambrian and lower Paleozoic sedimentary rocks. Dips measured in Tunnel Bed 1 reflect the attitude of the paleotopography that it was deposited on. Deposition of Tunnel Beds 2 through 5 resulted in the smoothing or flattening of the Tertiary landscape that was being developed, as indicated by a progressive decrease in the dips of these units when moving up through the stratigraphic section (Thordarson, 1965). The deposition of the overlying Grouse Canyon
ash flow and the emplacement of a thick bedded tuff sequence completed the process of leveling the Tertiary landscape. The uppermost pyroclastic unit in the vicinity of G-Tunnel, the Rainier Mesa Member of the Timber Mountain Tuff, was deposited on a fairly level surface. This is indicated by it's uniform thickness at Rainier Mesa.

Tunnel Beds 1, 2, 3 and 4 are a sequence of bedded tuffs, ash falls and tuffaceous sediments, in which the volcanic glass has been diagenetically altered to zeolites and clays by the interaction with ground water. At G-Tunnel, the combined thickness of Tunnel Beds 1 through 4 is approximately 305 meters.

Tunnel Bed 5 and the Grouse Canyon Member of the Belted Range Tuff are stratigraphly above the Tunnel Beds. Tunnel Bed 5 is the bedded, nonwelded base of the Grouse Canyon Member. It consists of a series of predominantly normally graded, ash-fall deposits. The original pyroclastic components of Tunnel Bed 5 have been strongly affected by diagenetic alteration. The coarser, more pumiceous, beds have been altered to zeolites by the interaction with ground water (S. Diehl, USGS, written commun., 1990). The finer, volcanic ash layers show evidence of secondary silicification. The average

thickness of Tunnel Bed 5 at the G-Tunnel Underground Facility (GTUF) is 30 meters. Boreholes U12g.12 DD-1 and U12g.12 WD-1 are located in this unit.

The Grouse Canyon Member of the Belted Range Tuff is an ash-flow tuff consisting, in ascending order, of: a basal vitrophyre; a lower rubble zone; a middle moderately to densely welded, devitrified unit; an upper rubble zone; and, an upper partially to moderately welded, devitrified unit (Connolly, et al., 1983). The lower and upper rubble zones consist of volcanic clasts contained within a glass shard or diagenetic clay matrix. The middle devitrified unit contains isolated rubble zones and large argillized pumice fragments. The Grouse Canyon Member is approximately 14 meters thick at the GTUF. This is the unit in which boreholes U12g DD-2 and U12g WD-2 are located.

Overlying the Grouse Canyon Member are the tuffs of Area 20 and the nonwelded Paintbrush Tuffs. These two units are a sequence of bedded, ash-fall tuffs up to 305 meters thick. With the exception of the lower 30 meters which are locally zeolitized, these units are vitric. In the southwest portion of Rainier Mesa, the Stockade Wash Tuff is stratigraphically between the tuffs of Area 20 and the nonwelded Paintbrush Tuff, and the Tiva Canyon Member of the Paintbrush Tuff is interfingered within the nonwelded Paintbrush Tuff.

The Rainier Mesa Member of the Timber Mountain Tuff is the upper pyroclastic unit in the vicinity of G-Tunnel and is stratigraphically above the nonwelded Paintbrush Tuff. It is an ash-flow tuff that grades from a nonwelded base upwards to a densely welded, devitrified middle zone, and then to a moderately to densely welded quartz latitic caprock. The average thickness of the Rainier Mesa Member in the vicinity of G-Tunnel is 108 meters.

Hydrology

The static water level beneath Rainier Mesa is approximately 1300 meters above sea level, at an average depth of 550 meters below the drifts of the G-Tunnel complex. Recharge occurs on the upland surface of Rainier Mesa where precipitation, in the form of rain and snow, falling on the top of the mesa infiltrates into the fractured caprock (Thordarson, 1965). A portion of this water percolates downward either by fracture flow or a combination of matrix and fracture flow to a depth where it can no longer be removed by evapotranspiration. If unimpeded, this water may continue to migrate downward under the influence of gravity and reach the regional water table. Where the downward movement of water is interrupted, perched-water zones may form (Thordarson, 1965).

Perched-water zones may occur where fracture permeability is impeded by the secondary filling of fractures or where fractures terminate at lithologic contacts. In the case of matrix dominated flow, perched-water zones can form at lithologic contacts where permeability barriers impede the downward movement of water. If there is a component of dip to a lithologic contact where perched water is accumulating, downdip movement of the perched water may occur. Perched-water zones can be created where the downdip movement of water

at lithologic contacts is interrupted by offset in permeable beds due to faulting. When fractures intersect or terminate in units that have high matrix permeability, water may be imbibed into the pore space in the high permeability matrix creating zones of saturation adjacent to the fractures. At the G-Tunnel complex, water has been observed in fractures and at lithologic contacts.

Borehole Lithology

The boreholes for the "Wet and Dry Drilling" test are located in the G-Tunnel Underground Facility area in G-Tunnel. This area was chosen because the pyroclastic rocks exposed in this area are similar to the pyroclastic rocks at Yucca Mountain. Connolly et al (1983) give a summary and comparison of the Grouse Canyon Member of the Belted Range Tuff and Topopah Spring Member of the Paintbrush Tuff. The Topopah Spring Member will be the principle unit penetrated by the Exploratory Shaft Facility (ESF) and the majority of boreholes drilled in the unsaturated zone will be in this unit. Tunnel Bed 5 is representative of the nonwelded ash-fall and ash-flow tuffs which will be encountered in the unsaturated zone in the ESF. A comparison between Tunnel Bed 5 and the tuffaceous beds of Calico Hills is given in Connolly et al (1984).

Boreholes U12g.12 DD-1 and U12g.12 WD-1 were cored into Tunnel Bed 5. Both boreholes were spud into a zeolitized ash-fall tuff exposed in the wall of the U12g.12 Drift. The lithologic sequence exposed in the drift wall above the boreholes consisted of: the zeolitized ash-fall tuff mentioned above; a silicified ash fall; a zeolitized ash fall; a silicified ash fall; and, a zeolitized ash fall. The apparent dip of the beds in the boreholes varied from 5 to 7 degrees towards the bottom of the boreholes. The dip of the beds resulted in the boreholes penetrating the alternating sequence of zeolitized and silicified ash-fall tuffs exposed in the drift wall.

Lithologies for boreholes U12g.12 DD-1 and U12g.12 WD-1 were determined by examining core from the two boreholes. The apparent dip of the units resulted in lithologic contacts that intersect the top of the boreholes, angle through the boreholes, and then exit the bottom of the boreholes at a greater depth (Fig. 4). The lithologies for boreholes U12g.12 DD-1 and U12g.12 WD-1 are given in table 9.

The Laser Drift was the area in the GTUF selected to investigate the effects of the drilling fluids on a fractured, densely welded, ash-flow tuff. Boreholes U12g DD-2 and U12g WD-2 were cored into the middle moderately to densely welded unit of the Grouse Canyon Member which is exposed in the Laser Drift. The boreholes were spud into the northwest rib of the Laser Drift and were cored in a northwesterly direction. Only minor changes in lithology occurred from the collar to total depth in both boreholes. A rubble zone was encountered in U12g DD-2 at the depth interval from 7.4 m to 8.6 m. The rubble zone consisted of welded Grouse Canyon lithic fragments in a clayey matrix. Another exception was the occurrence of large, argillized pumice or lithic fragments in both of the boreholes (Fig. 5). An argillized fragment was encountered at 1.5 m in U12g DD-2. It was approximately 0.1 m in length,

phenocryst-rich, with possible vapor phase mineralization. Borehole U12g WD-2 intersected two argillized pumice or lithic fragments. The first was at a depth of 1.5 m and the second was a depth of 5.6 m. The fragments were 0.1 m and 0.2 m in length respectively.

Borehole Fractures

Core logs and borehole video survey tape recordings were used to compile fracture data from the boreholes. Borehole fracture data was used to help interpret borehole geophysical logs. The geophysical logs provided data on the *in situ* moisture re-equilibration times in the boreholes. The relationship between fracture frequency and degree of welding or induration was also examined.

A total of 27 fractures were logged in borehole U12g.12 DD-1 (Fig. 4). All but two fractures occurred where the lithology was entirely silicified or was in a silicified-zeolitized contact area. The stikes of the majority of the fractures were approximately parallel to the U12g.12 drift and to a fault to the southwest of
the borehole. Twenty-one of the measured fractures had strike directions between N. 50° W. and N. 65° W. The remaining fractures had strikes of N.70° E. and N. 55° E. Dips were generally steep, between 80 to 90 degrees, and to the southwest. Twelve of the fractures had manganese oxide deposits on the fracture faces. A change in the lithology at 2.5 meters may indicate a fault. Another lithologic change at a depth of 8.35 meters from a silicified bed to a zeolitized bed may indicate movement along a fault at that depth.

Borehole U12g.12 WD-1 had 19 fractures measured in recovered core samples (Fig. 4). All of the fractures occurred in silicified or silicified-zeolitized contact areas. The strike of the fractures in U12g.12 WD-1 ranged from N. 50° W. to N. 65° W. and dipped steeply to the northeast or the southwest. Two faults were tentatively identified in this borehole. The first occurred at a depth of 2.4 meters where a possible breccia zone was encountered. The second was at a depth of 3.8 meters where there was possible offset of beds.

The fracture logs for the two boreholes that were cored in Tunnel Bed 5 indicate that there is a direct correlation between the degree of induration and fracture frequency. The more indurated and brittle silicified units were highly fractured whereas the zeolitized units were not. The number of fractures encountered in the vicinity of the silicified-zeolitized contacts indicates that fractures in the silicified beds can propagate into the zeolitized beds, but probably pinch-out within a short distance.

The two boreholes cored into the moderately to densely welded Grouse Canyon Member from the Laser Drift were oriented to intersect a major fracture trend exposed in the Laser Drift. Core fracture logs provided much of the fracture orientation data, but the TV camera logs were used where intact core samples were not available.

Borehole U12g DD-2 intersected 50 fractures that could be identified and oriented using the core log and the TV log (Fig. 5). The majority of the

fractures encountered had strike directions between N. 20° E. and N. 40° E. (27 fractures) with the remaining fractures distributed from N. 10° E. to N. 85° E. and N. 5° W. to N. 60° W. The dip angles on the fractures ranged from 45° to 90° to the northwest and the southeast. Most fractures (77 percent) had dips from 81° to 90°.

The combined fracture log for U12g WD-2 had a total of 71 fractures. The major strike directions for fractures intersected by this borehole were from N 20° E. to N. 45° E. with a total of 23 fractures in this range. Eight fractures had strike directions between N. 85° E. and N 10° W.; the remaining fractures had strikes from N. 5° E. to N. 75° E. and N. 20° W. to N. 25° W. Seventy-eight percent of the fractures had dip angles between 81° and 90° with all dips being greater than 45°.

The large number of fractures intersected by the boreholes cored in the welded Grouse Canyon demonstrate the correlation between degree of welding and fracture frequency. Water loss data for borehole U12g WD-2 indicates that many of the fractures intersected by the borehole were capable of conducting water away from the borehole.

References

Connolly, J.R., Keil, K, Mansker, W.L., Allen, C.C., Husler, J., Lowy, R., Fortney, D.R., and Lappin, A.R., 1984, "Petrology and Geochemistry of Samples From Bed-Contact Zones in Tunnel Bed 5, U12g-Tunnel, Nevada Test Site," Sandia National Laboratories, SAND84-1060, Albuquerque, NM.

Connolly, J.R., Mansker, W.L., Hicks, R., Allen, C.C., Husler, J.,Keil, K., and Lappin, A.R., 1983, "Petrology and Geochemistry of the Grouse Canyon Member of the Belted Range Tuff, Rock Mechanics Drift, U12g Tunnel, Nevada Test Site," Sandia National Laboratories, SAND81-1970, Albuquerque, NM.

Gibbons, A.B., Hinrichs, E.N., Hansen, W.R., and Lemke, R.W., 1963, Geology of the Rainier Mesa Quadrangle, Nye County, Nevada: U.S. Geological Survey Geologic Quadrangle Map GQ-215.

Smith, C., Vollendorf, W.C., and Warren, W.E., 1981 "In-situ Stress From Hydraulic Fracture Measurements in G-Tunnel, NTS," Sandia National Laboratory, SAND80-1138, Albuquerque, NM.

Thordarson, William, 1965, Perched ground water in zeolitized-bedded tuff, Rainier Mesa and vicinity, Nevada Test Site, Nevada: U.S. Geological Survey Trace Element Investigative Report TEI-862, 90 p.

Table 1. AIR CIRCULATED WHILE DRILLING BOREHOLE U12g.12 DD-1

CORE RUN NUMBER	INTERVAL (meters)	FLUID USED PER CORE RUN (liters)	CUMULATIVE FLUID USAGE[1] (liters)
1	0.0 - 0.3	18400	635650
2	0.3 - 2.1	79300	617250
3	2.1 - 3.6	120360	537950
4	3.6 - 5.1	90620	417590
5	5.1 - 6.6	104220	326970
6	6.6 - 8.1	133650	222750
7	8.1 - 9.7	89100	89100

[1] Total amount of air circulated past starting footage in this interval during drilling.

Table 2. DRILLING PARAMETERS FOR BOREHOLE U12g.12 DD-1

CORE RUN NO.	DRILLED INTERVAL (meters)	REC'D (m)	BIT TYPE	FLUID	TIME START/STOP	WT. ON BIT (kg)	RPM'S	AIR FLOW (liters/min)
1	0.0 - 0.3	0.1	*	AIR	1455/1500			3680
2	0.3 -2.1	1.6	*	AIR	0844/0900	1800		3680 - 5660
3	2.1 - 3.6	1.4	*	AIR	1045/1110	1800	120	4240 - 5660
4	3.6 - 5.1	1.5	*	AIR	1315/1335	1800	120	4240 - 5660
5	5.1 - 6.6	1.6	*	AIR	1355/1418	1800	60-100	4240 - 4950
6	6.6 - 8.1	1.6	*	AIR	0815/0842	2200	65	4950
7	8.1 - 9.7	1.6	*	AIR	0917/0935	1800	75	4950

* Longyear HQ size Geoset bit with Syndax matrix[1]

Table 3. ***AIR CIRCULATED WHILE DRILLING BOREHOLE U12g.12 DD-2***

CORE RUN NUMBER	INTERVAL (meters)	FLUID USED PER CORE RUN (liters)	CUMULATIVE FLUID USAGE (liters)
1	0.0 - 1.4	221078	1419178
2	1.4 - 2.4	158400	1198100
3	2.4 - 3.5	293250	1039700
4	3.5 - 4.8	170000	746450
5	4.8 - 5.5	170000	576450
6	5.5 - 5.9	56600	406450
7	5.9 - 7.5	184100	349850
8	7.5 - 9.1	165750	165750

[1] Total amount of air circulated past starting footage in this interval during drilling.

Table 4. DRILLING PARAMETERS FOR BOREHOLE U12g DD-2

CORE RUN NO.	DRILLED INTERVAL (meters)	RED'D (m)	BIT TYPE	DRILLING FLUID	TIME START/STOP	WT. ON BIT (kg)	RPM'S	AIR FLOW (liters/min)
1	0.0 - 0.3		*	AIR	1002/1023	2900-3600	59 - 102 120	2270
1	0.3 1.4	1.4	*	AIR	1259/1407	3600-4000	95 - 128	2550
2	1.4 - 2.4	1.0	*	AIR	1430/1510	3600-4000	90 - 120	3960
3	2.4 - 3.5	1.0	*	AIR	0835/0944	3200-4000	90 - 120	4250
4	3.5 - 4.8	1.2	*	AIR	1025/1105	3200-4000	90 - 150	4250
5	4.8 - 5.5	0.8	*	AIR	1250/1330	3200-3600	150	4250
6	5.5 - 5.9	0.4	*	AIR	1347/1407	2700-3200	100	2830
7	5.9 - 6.0		*	AIR	1425/1445	4500	80	2830
7	6.0 - 7.5	1.4	*	AIR	0820/0850	4500	120	4250
8	7.5 - 9.1	1.3	*	AIR	0908/0947	3200	54	4250

*Longyear HQ3WL size Diamond Impregnated with Series-1 matrix[1]
**Longyear HQ3WL size Diamond Impregnated with Series-1 matrix[1]

Table 5. **WATER LOSS WHILE DRILLING U12g.12 WD-1**

CORE RUN NUMBER	INTERVAL (meters)	WATER LEVEL START/STOP (meters)	WATER LOSS PER CORE RUN (liters)
1	0.0 - 1.4	0.399/0.378	88.6[1]
2	1.4 - 2.9	0.378/0.320	244.3[2]
3	2.9 - 4.4	0.320/0.302	75.8[2]
4	4.4 - 5.9	0.302/0.293	37.9
5	5.9 - 6.9	0.293/0.289	16.8
6	6.9 - 7.5	0.289/0.296	+29.5
7	7.5 - 9.0	0.296/0.296	0.0

[1] Some water loss at sump pit and when pulling inner core barrel.
[2] Some water loss when pulling inner core barrel. Water loss from sump pit corrected.

Table 6. DRILLING PARAMETERS FOR BOREHOLE U12g.12 WD-1

CORE RUN NO.	DRILLED INTERVAL (meters)	REC'D (m)	BIT TYPE	FLUID	TIME START/STOP	WT. ON BIT (kg)	RPM'S	WATER FLOW (approx. liters/min)
1	0.0 - 1.4	1.3	*	Water	1425/1440	1800	120	37
2	1.4 - 2.9	1.5	*	Water	0930/0952	2000	120-150	37
3	2.9 - 4.4	1.6	*	Water	1015/1037	2000	120-150	37
4	4.4 - 5.9	1.5	*	Water	1245/1302	2000	120-150	37
5	5.9 - 6.9	1.0	*	Water	1320/1335	2000-2300	120-150	37
6	6.9 - 7.5	0.5	*	Water	1425/1435	2000-2300	120-150	37
7	7.5 - 9.0	1.5	*	Water	1455/1503	2000-2300	120-150	37

* Longyear HQ size Geoset bit with Syndax matrix

Table 7. WATER LOSS WHILE DRILLING U12g WD-2

CORE RUN NUMBER	INTERVAL (meters)	WATER LEVEL START/STOP (meters)	WATER LOSS PER CORE RUN (liters)
1	0.0 - 1.6	0.497/0.375	513.9[2]
2	1.6 - 3.2	0.375/0.247	539.2[3]
3	3.2 - 4.7	0.427[1]/0.381	193.8
4	4.7 - 6.2	0.381/0.320	257
5	6.2 - 7.6	0.320/0.202	497.1
6	7.6 - 7.9	0.202/[4]	

1 Added water to tank before starting core run.
2 Loss of water at sump pit increased total water loss.
3 Water flowing from fracture in drift wall approximately 0.9 meters from borehole. Still losing some water from sump pit.
4 No final water level reading due to intersection of boreholes and loss of water through borehole U12g DD-2.

Table 8. DRILLING PARAMETERS FOR BOREHOLE U12g WD-2

CORE RUN NO.	DRILLED INTERVAL (meters)	REC'D (m)	BIT TYPE	FLUID	TIME START/STOP	WT. ON BIT (kg)	RPM'S	WATER FLOW (liters/min)
1	0.0 - 1.6	1.6	*	WATER	1310/1345	2300 - 2700	120-150	37 - 57
2	1.6 - 3.2	1.5	*	WATER	1410/1435	2700 - 3200	150	37 - 57
3	3.2 - 4.7	1.4	*	WATER	0850/0935	2700 - 3200	150	37 - 57
4	4.7 - 6.2	1.6	*	WATER	0955/1035	2700 - 3200	150-180	37 - 57
5	6.2 - 7.6	1.4	*	WATER	1055/1115 1250/1305	2700 - 3200	150	37 - 57
6[2]	7.6 - 7.9	0.2	*	WATER	1325/1330	2700 - 3200	120-150	37 - 57

* Longyear HQ3WL size Diamond Impregnated with Series-1 matrix[1]

2 Core run 6 terminated due to intersection with borehole U12g DD-2.

Table 9. Borehole Lithology for U12g.12 DD-1 and U12g.12 WD-1.

U12g.12 DD-1 *Contact At Top Of Borehole/Contact At Bottom Of Borehole (meters)	U12g.12 WD-1 *Contact At Top Of Borehole/Contact At Bottom Of Borehole (meters)	Lithology
0.0/2.4	0.0/3.1	Zeolitized ash-fall tuff
1.7/5.0	2.0/4.7	Silicified ash-fall tuff with lithic fragments
3.2/6.4	3.5/5.6	Zeolitized ash-fall tuff
5.2/8.4	4.9/7.7	Silicified ash-fall tuff with small lithic fragments and manganese staining
8.1/TD	6.7/TD	Zeolitized ash-fall tuff

* Indicates depth in borehole (from collar) where units is first and last encountered in the borehole.

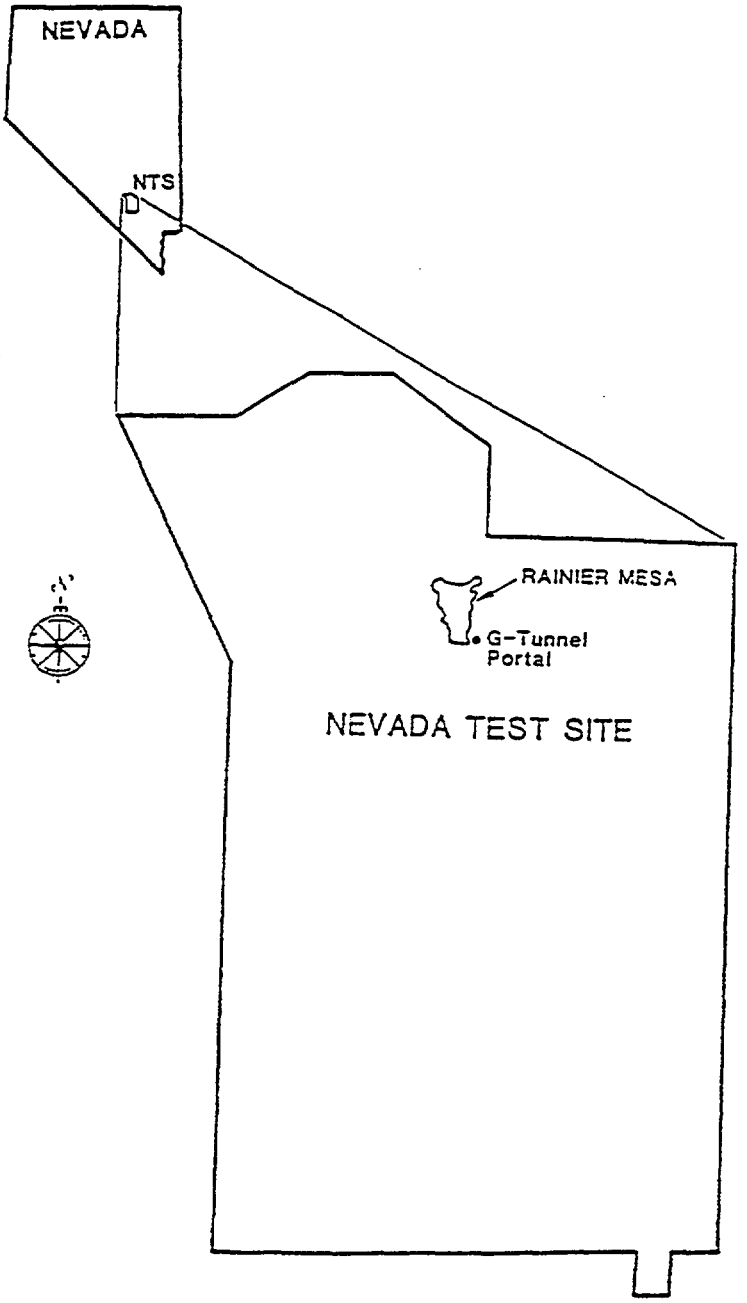

Figure 1. Location map for the Nevada Test Site, Rainier Mesa, and the G-Tunnel portal.

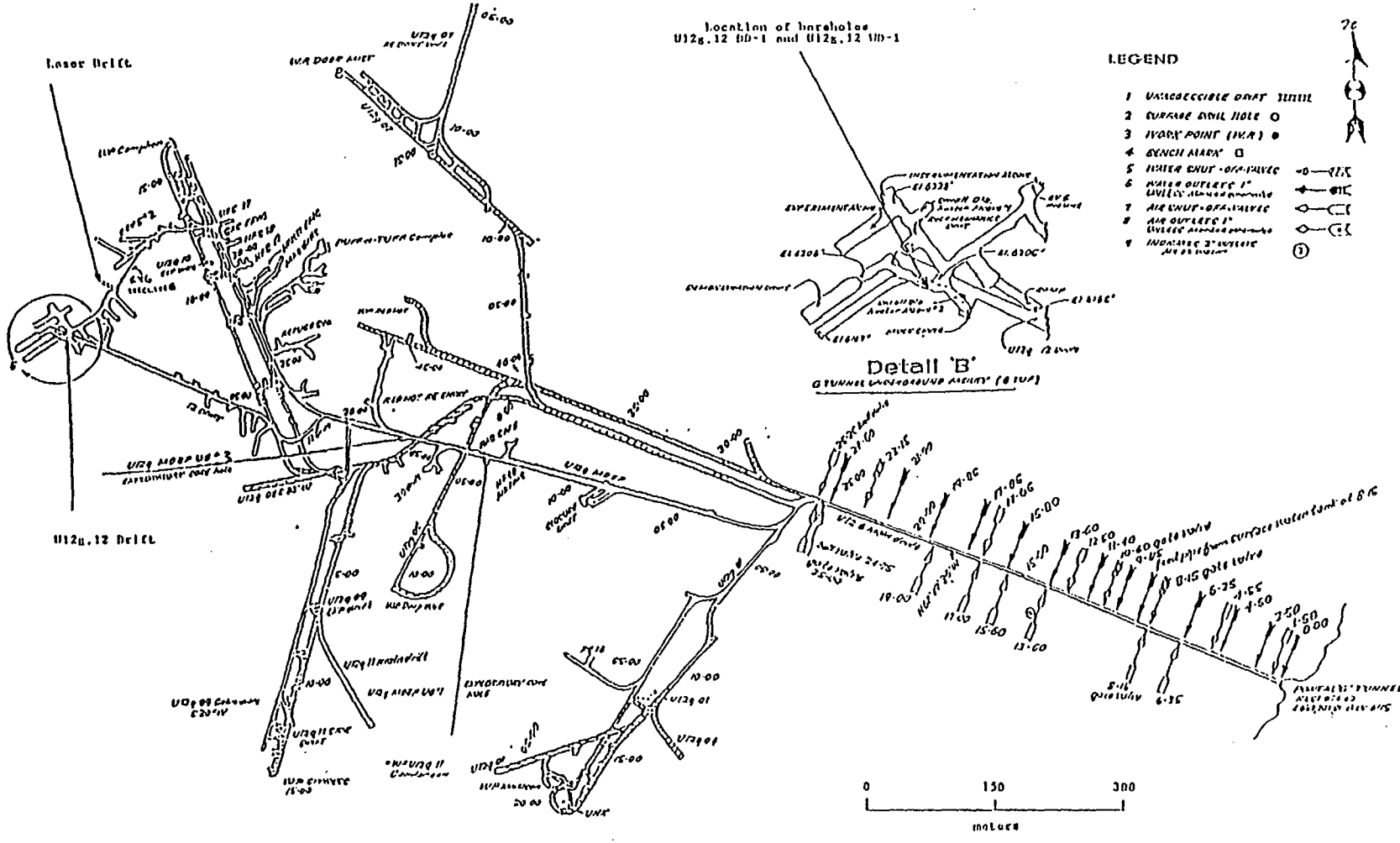

Figure 2. Map of G-Tunnel with a detailed enlargement of the G-Tunnel Underground Facility.

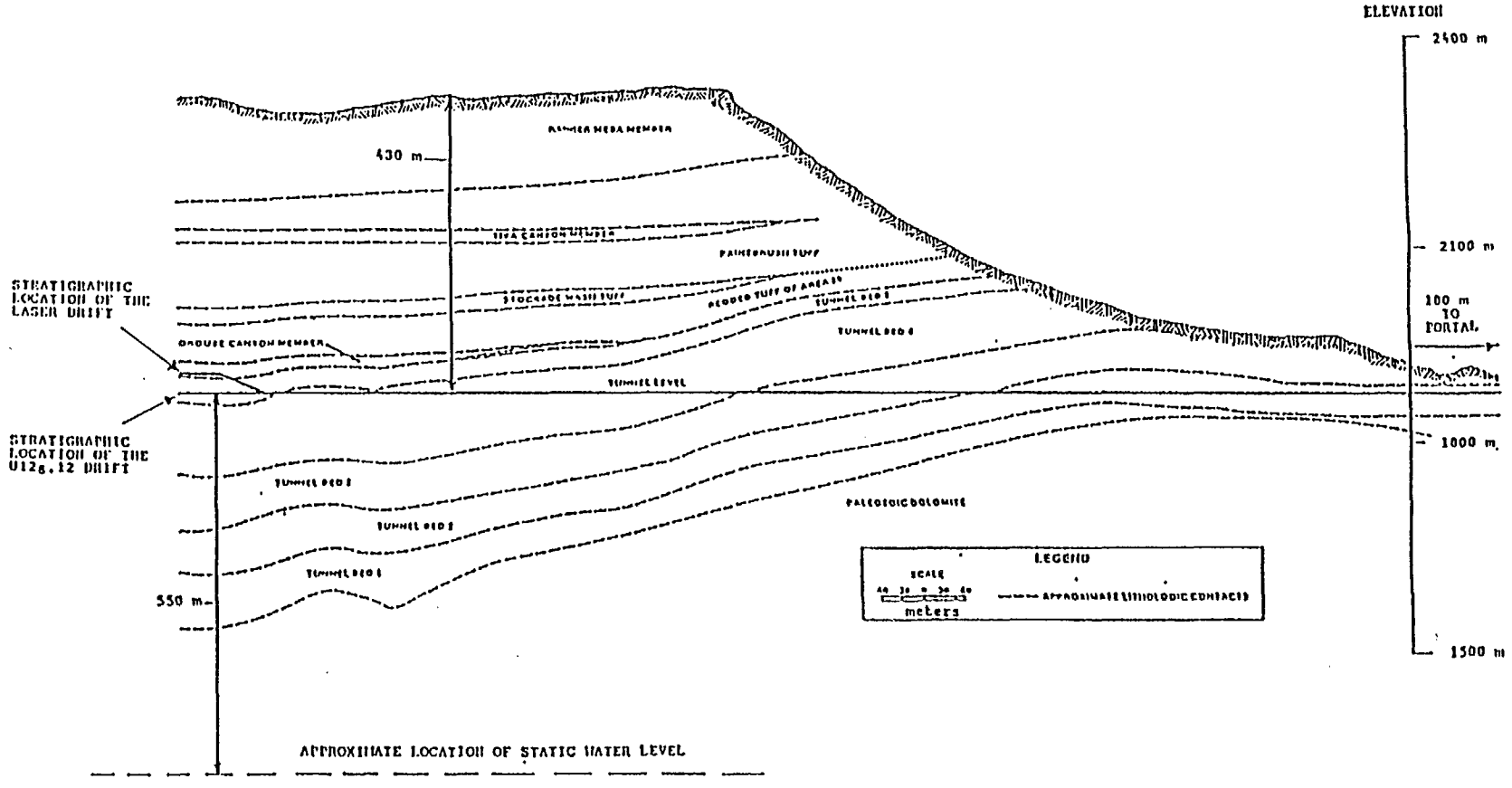

Figure 3 . Partial cross-section of Rainier Mesa modified from Smith and others, 1981.

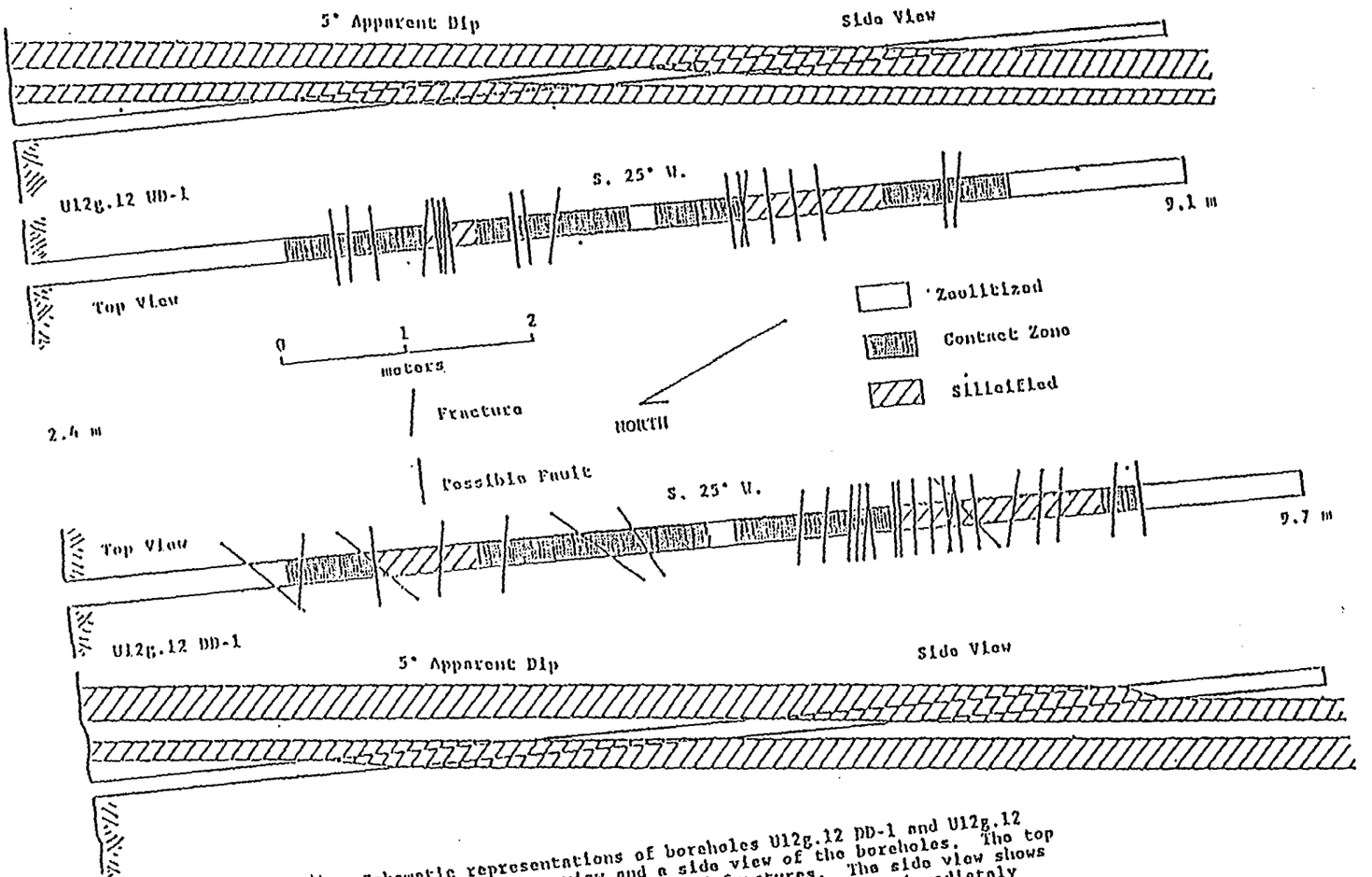

Figure 4. Schematic representations of boreholes U12g.12 DD-1 and U12g.12 DD-1 showing a top view and a side view of the boreholes. The top view shows borehole lithology and fractures. The side view shows the borehole lithology and the projected lithology immediately above and below the boreholes.

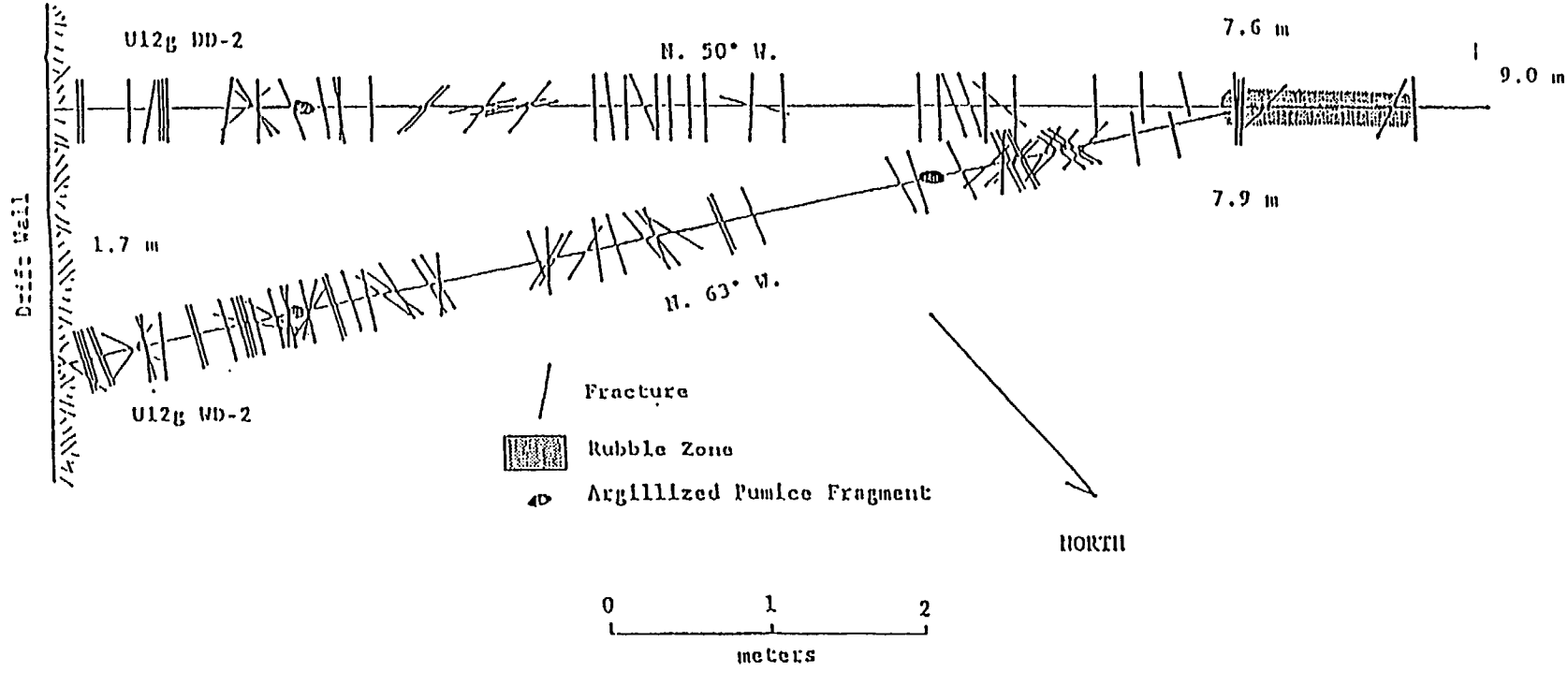

Figure 5. Schematic representation of boreholes U12g DD-2 and U12g WD-2 showing borehole orientations, fractures, and lithologic features.

APPENDIX A3

Yucca Mountain project
wet and dry drilling
rock core densities, water contents
and Lithium Bromide analysis
WBS 1.2.3.3.6.1

UNITED STATES DEPARTMENT OF ENERGY
NEVADA TEST SITE

YUCCA MOUNTAIN PROJECT
WET AND DRY DRILLING
ROCK CORE DENSITIES, WATER CONTENTS
AND LITHIUM BROMIDE ANALYSIS
WBS 1.2.3.3.6.1

PREPARED FOR U.S.G.S, AREA 25
NTS,NV

HOLMES & NARVER, INC.
MATERIALS TESTING LABORATORY
MERCURY, NV

DECEMBER 1989

Table of contents

List of Figures

List of Tables

I INTRODUCTION

A. PROJECT OVERVIEW

This work was performed at the request of Alan Flint, Michael Chornack and Lorrie Flint of United States Geological Survey (U.S.G.S) Nevada Test Site (NTS), Area 25 for the Yucca Mountain Project (YMP). The work consists of various rock properties testing and is part of the Wet and Dry Drilling Project being conducted by the USGS on the YMP. The requested rock properties include bulk and grain densities, water contents and saturations, porosities, permeabilities, capillary pressures and lithium bromide concentrations.

This is the second report issued by Holmes & Narver, Materials Testing Laboratory (MTL) and the report consists of the test data and results on the rock samples bulk and grain densities , water contents and lithium bromide analysis. This work was performed by J.N. Walker, R.K. Singal, J.G. Moore and N. Bailey at the MTL. The saturation studies, porosities, and and data analysis were reported in the MTL's report #89-111, dated June 21, 1989 and titled " Wet and Dry Drilling Comparison of Porosity Determination Methods.

The remaining test work on the this project includes obtaining permeability data using centrifuge, mercury porosimeter and permeameters and data analysis. The work on this project was stopped in December, 1989 due to the YMP budgetary and scheduling priorities. The above remaining test work have to be completed at a future date.

B. SAMPLE DETAILS

Holmes & Narver (H&N) Materials Testing Laboratory (MTL), NTS, received forty rock samples from the United States Geological Survey (USGS) for testing. The samples came from four core holes, with ten samples taken from each hole. Also provided for testing were three water samples used as the drilling fluid in two of the holes.

The sample traceability information for this project is given in the appendix A.

C. LABORATORY TESTS

1. PROCEDURES

The work is being conducted as per the Quality Assurance Level III guidelines. All the testing was performed in accordance with procedures recommended by the American Society for Testing and Materials (ASTM) or the American Petroleum Institute (API).

2. COMPLETED TESTS

The samples were first tested to obtain the as received physical properties. The samples were removed from the sealed lexan liners and immediately tested for natural bulk density and water content values Pieces approximately 1 inch long were then cut from the samples and 1.5 inch diameter cores undercut from the larger diameter piece. The fragments remaining after the undercoring were used to determine the grain densities of the samples. The cores were saturated and the dry

bulk densities and the effective non-effective, and total porosities determined. Due to the irregular pore structures inherent in volcanic tuffs, the saturation test methods were studied. Eight cores samples were tested using three saturation methods.

3. Lithium Bromide Analysis

In order to measure the amount of infiltration of drilling fluid into the samples lithium bromide (LiBr) was added to the drilling fluid as a tracer. The MTL tested three samples of the drilling fluid and six samples of water removed from rock samples for LiBr content. The six rock samples from which the water was removed had a small section removed before any tests were performed. A core was cut out of the section and rotated in the centrifuge to remove the water for testing. The remaining sample was then used in previously discussed test sequence.

4. Remaining Test Work Sequence

The prepared core samples have to be tested in a permeameter and saturated water permeabilities will be measured. Following the permeability tests cores will be again saturated and tested in an ultracentrifuge and the capillary pressure curves will be developed from the centrifuge data. Fragments of the core and cores will then be tested using a mercury porosimeter and capillary pressure curves will be constructed. Also from the mercury porosimeter data, the pore size distribution within the fragments were determined.

II. ROCK SAMPLES PHYSICAL PROPERTIES

A. BULK DENSITY

The bulk density of a sample was calculated after determining the weight and volume of the sample. Each sample was removed from its sealed container and weighed. It was then coated with beeswax and a composite weight determined. Following that it was submerged in distilled water and weighed. From the bouyant force of the water a volume was calculated from the wax coated core, from which the wax volume was subtracted to yield a core volume. The measurements and results are shown for the samples from eahc borehole in Tables 1 through 4.

B. WATER CONTENT

Following the bulk density tests, the wax was removed and the cores reweighed to account for any minor alterations in the weight of the sample. The cores were dried in a convection oven set at 110 degrees Celsius for approximately 36 hours. Upon removal from the oven, the cores were cooled in a descicator and weighed. The water contents were calculated as percent of wet and dry weights and the core volume. The water content results for the samples from each borehole are given in Tables 5 through 8.

Where possible the entire sample was used for the bulk density and water content procedures. By using the largest sample possible, errors in measurements have a

smaller effect on the final calculations. It also helps to ensure that a representative sample is tested. In a few instances it was discovered that the samples were in two or more pieces. For those samples the largest piece was used. For the samples selected for the lithium bromide analysis it was necessary to remove a section of the sample for use in those tests. The remaining portion of the sample was used for the bulk density and water content procedures.

C. DATA ANALYSIS

The primary data from Tables 1 through 8 are presented graphically in Figures 1 through 4. The figures show the bulk density and volumetric water content values versus the depth of the boreholes. Linear extrapolation is used between the measured data points. The properties show a wide range of values in the non-welded tuffs from U12g.12 DD1 and U12g.12 WD1. The welded tuffs from U12g DD2 and U12g WD2 exhibit a much narrower range of values. For all four boreholes an inverse relationship between bulk density and volumetric water content can be observed. This indicates that increases (decreases) in the volumetric water content correlate with increases (decreases) in porosity.

HOLMES & NARVER, INC.

MATERIALS TESTING LABORATORY

NEVADA TEST SITE

TABLE 1

BULK DENSITY DATA SHEET FOR U12g.12 DD-1

Project: Wet & Dry Drilling
Requestor: Dr. Alan L. Flint
Organization: USGS
Address: Box 327, M/S 721, Mercury, NV
Phone: 5-5805
Tested by: Jerry N. Walker
Test date: 2-15-89 through 2-18-89

Checked by: John G. Moore John G. Moore
Check date: 12/5/89
MTL Lab #: 2779 through 2788
Request #: GT-38
H&N ID #: 50036C
WBS #: 1.2.3.3.6.1
WIN #: YMP:NTS:WI:89-006
QA level: III

MTL Sample Number	Depth Interval (ft)	Uncoated Weight (g)	Coated Weight (g)	Wax Volume (cc)	Submerged Weight (g)	Water Temp. (Celsius)	Water Density (g/cc)	Core Volume (cc)	Bulk Density (g/cc)
2779	1.7-2.2	752.10	798.01	47.71	282.23	18.2	0.9986	468.8	1.604
2780	6.8-7.3	460.26	484.10	24.77	200.91	18.3	0.9985	258.8	1.778
2781	8.0-8.4	697.82	727.51	30.85	352.89	18.3	0.9985	344.3	2.027
2782	12.4-12.8	617.72	649.31	32.83	294.29	18.4	0.9985	322.7	1.914
2783	15.7-16.1	516.01	541.49	26.48	218.63	18.5	0.9985	296.9	1.738
2784	16.4-16.7	647.42	688.42	42.61	255.27	18.6	0.9985	391.2	1.655
2785	21.3-21.6	183.80	198.83	15.62	82.89	18.6	0.9985	100.5	1.829
2786	23.6-24.0	573.48	614.15	42.26	255.34	18.6	0.9985	317.1	1.809
2787	28.8-29.2	537.09	575.67	40.09	189.57	18.7	0.9985	346.6	1.550
2788	30.3-30.7	528.65	565.62	38.42	186.44	18.8	0.9984	341.4	1.549

Minimum In Situ Bulk Density (g/cc)	1.549
Maximum In Situ Bulk Density (g/cc)	2.027
Average In Situ Bulk Density (g/cc)	1.745
Standard Deviation in Measurements of Bulk Density (g/cc)	0.150

EQUIPMENT USED	CALIBRATION DUE DATE
Mettler PK 4800 Digital Balance, PTL 4513	6-22-89
Omega 871A Digital Thermometer, PTL 6976	3-8-89

REMARKS: None

HOLMES & NARVER, INC.

MATERIALS TESTING LABORATORY

NEVADA TEST SITE

TABLE 2

BULK DENSITY DATA SHEET FOR U12g.12 WD-1

Project: Wet & Dry Drilling
Requestor: Dr. Alan L. Flint/M.Chornack
Organization: USGS
Address: Box 327, M/S 721, Mercury, NV
Phone: 5-5805
Tested by: Jerry N. Walker
Test date: 2-15-89 through 2-18-89
* 3-21-89

Checked by: John G. Moore John G. Moore
Check date: 12/5/89
MTL Lab #: 2789 through 2798
Request #: GT-38
H&N ID #: 50036C
WBS #: 1.2.3.3.6.1
WIN #: YMP:NTS:WI:89-006
QA level: III

MTL Sample Number	Depth Interval (ft)	Uncoated Weight (g)	Coated Weight (g)	Wax Volume (cc)	Submerged Weight (g)	Water Temp. (Celsius)	Water Density (g/cc)	Core Volume (cc)	Bulk Density (g/cc)
2789	1.8-2.3	704.51	758.39	55.99	269.05	19.3	0.9983	434.2	1.623
2790	7.6-7.9	280.56	301.55	21.81	119.78	19.3	0.9983	160.3	1.751
*2791	8.7-9.0	243.42	266.85	24.35	108.78	19.6	0.9983	134.0	1.817
2792	12.4-12.8	593.87	623.37	30.66	296.69	19.3	0.9983	296.6	2.002
*2793	14.0-14.5	614.42	648.77	35.70	287.98	19.6	0.9983	325.7	1.886
2794	16.1-16.5	466.84	502.80	37.37	196.41	19.4	0.9983	269.5	1.732
2795	19.1-19.5	829.40	877.00	49.46	395.31	19.4	0.9983	433.0	1.915
2796	24.5-24.9	539.60	579.11	41.06	217.88	19.4	0.9983	320.8	1.682
*2797	27.4-27.8	388.29	421.98	35.01	157.33	19.6	0.9983	230.1	1.688
2798	29.2-29.5	326.23	347.97	22.59	136.86	19.5	0.9983	188.9	1.727

Minimum In Situ Bulk Density (g/cc)	1.623
Maximum In Situ Bulk Density (g/cc)	2.002
Average In Situ Bulk Density (g/cc)	1.782
Standard Deviation in Measurements of Bulk Density (g/cc)	0.114

EQUIPMENT USED	CALIBRATION DUE DATE
Mettler PK 4800 Digital Balance, PTL 4513	6-22-89
Omega 871A Digital Thermometer, PTL 6976	3-8-89
Omega 871A Digital Thermometer, PTL 6976	9-13-89

REMARKS: *Lithium bromide content analysis performed on water centrifuged from these cores.

HOLMES & NARVER, INC.

MATERIALS TESTING LABORATORY

NEVADA TEST SITE

TABLE 3

BULK DENSITY DATA SHEET FOR U12g DD-2

Project: Wet & Dry Drilling
Requestor: Dr. Alan L. Flint/M.Chornack
Organization: USGS
Address: Box 327, M/S 721, Mercury, NV
Phone: 5-5805
Tested by: Jerry N. Walker
Test date: 2-15-89 through 2-18-89

Checked by: John G. Moore John G. Moore
Check date: 12/5/89
MTL Lab #: 2799 through 2808
Request #: GT-38
H&N ID #: 50036C
WBS #: 1.2.3.3.6.1
WIN #: YMP:NTS:WI:89-006
QA level: III

MTL Sample Number	Depth Interval (ft)	Uncoated Weight (g)	Coated Weight (g)	Wax Volume (cc)	Submerged Weight (g)	Water Temp. (Celsius)	Water Density (g/cc)	Core Volume (cc)	Bulk Density (g/cc)
2799	0.7-1.0	670.35	697.97	28.70	378.87	19.7	0.9983	291.0	2.304
2800	3.6-4.0	840.30	889.50	51.13	475.50	19.7	0.9983	363.6	2.311
2801	6.3-6.7	639.09	675.31	37.64	350.96	19.7	0.9983	287.3	2.225
2802	8.0-8.4	866.50	915.00	50.40	488.10	19.6	0.9983	377.2	2.297
2803	12.4-12.7	636.56	663.04	27.52	362.81	19.6	0.9983	273.2	2.330
2804	18.5-18.8	531.43	565.67	35.58	300.79	19.6	0.9983	229.8	2.313
2805	19.5-20.0	481.19	503.38	23.06	267.54	19.6	0.9983	213.2	2.257
2806	20.7-21.0	460.38	480.02	20.41	257.64	19.6	0.9983	202.4	2.275
2807	23.3-23.6	616.93	644.76	28.92	347.83	19.6	0.9983	268.5	2.298
2808	27.5-27.8	304.06	324.68	21.43	173.34	19.6	0.9983	130.2	2.336

Minimum In Situ Bulk Density (g/cc)..... 2.225
Maximum In Situ Bulk Density (g/cc)..... 2.336
Average In Situ Bulk Density (g/cc)..... 2.295
Standard Deviation in Measurements of Bulk Density (g/cc)..... 0.032

EQUIPMENT USED	CALIBRATION DUE DATE
Mettler PK 4800 Digital Balance, PTL 4513	6-22-89
Omega 871A Digital Thermometer, PTL 6976	3-8-89

REMARKS: None

HOLMES & NARVER, INC.

MATERIALS TESTING LABORATORY

NEVADA TEST SITE

TABLE 4

BULK DENSITY DATA SHEET FOR U12g WD-2

Project: Wet & Dry Drilling
Requestor: Dr. Alan L. Flint
Organization: USGS
Address: Box 327, M/S 721, Mercury, NV
Phone: 5-5805
Tested by: Jerry N. Walker
Test date: 2-15-89 through 2-18-89
*3-21-89

Checked by: John G. Moore John G. Moore
Check date: 12/5/89
MTL Lab #: 2809 through 2818
Request #: GT-38
H&N ID #: 50036C
WBS #: 1.2.3.3.6.1
WIN #: YMP:NTS:WI:89-006
QA level: III

MTL Sample Number	Depth Interval (ft)	Uncoated Weight (g)	Coated Weight (g)	Wax Volume (cc)	Submerged Weight (g)	Water Temp. (Celsius)	Water Density (g/cc)	Core Volume (cc)	Bulk Density (g/cc)
2809	1.0-1.4	548.43	582.25	35.14	310.01	17.7	0.9987	237.5	2.310
2810	4.0-4.3	655.30	683.70	29.51	374.91	17.4	0.9987	279.7	2.343
*2811	5.5-5.9	643.02	679.37	37.77	365.82	19.5	0.9983	276.3	2.327
2812	11.7-12.1	517.93	543.75	26.83	291.68	17.5	0.9987	225.6	2.296
2813	14.0-14.3	795.04	834.10	40.59	459.15	17.5	0.9987	334.9	2.374
*2814	16.1-16.4	392.83	417.66	25.80	223.85	19.4	0.9983	168.3	2.334
2815	17.7-18.0	729.49	768.15	40.17	416.23	17.6	0.9987	312.2	2.337
2816	19.4-19.7	571.73	602.07	31.53	323.11	17.7	0.9987	247.8	2.307
*2817	21.1-21.4	280.19	300.24	20.84	159.60	19.5	0.9983	120.0	2.334
2818	22.2-22.6	829.30	882.60	55.39	472.00	17.7	0.9987	355.8	2.331

Minimum In Situ Bulk Density (g/cc)	2.296
Maximum In Situ Bulk Density (g/cc)	2.374
Average In Situ Bulk Density (g/cc)	2.329
Standard Deviation in Measurements of Bulk Density (g/cc)	0.021

EQUIPMENT USED	CALIBRATION DUE DATE
Mettler PK 4800 Digital Balance, PTL 4513	6-22-89
Omega 871A Digital Thermometer, PTL 6976	3-8-89
Omega 871A Digital Thermometer, PTL 6976	9-13-89

REMARKS: *Lithium bromide content analysis performed on water centrifuged from these cores.

HOLMES & NARVER, INC.

MATERIALS TESTING LABORATORY

NEVADA TEST SITE

TABLE 5

WATER CONTENT DATA SHEET FOR U12g.12 DD-1

Project: Wet & Dry Drilling
Requestor: Dr. Alan L. Flint
Organization: USGS
Address: Box 327, M/S 721, Mercury, NV
Phone: 5-5805
Tested by: Jerry N. Walker
Test date: 2-15-89 through 2-18-89

Checked by: John G. Moore John G. Moore
Check date: 12/5/89
MTL Lab #: 2779 through 2788
Request #: GT-38
H&N ID #: 50036C
WBS #: 1.2.3.3.6.1
WIN #: YMP:NTS:WI:89-006
QA level: III

MTL Sample Number	Depth Interval (ft)	Wet Weight (g)	Dry Weight (g)	*Water Content (g or cc)	Core Volume (cc)	Dry Bulk Density (g/cc)	% Water of Wet Weight	% Water of Dry Weight	Volumetric Water Content (%)
2779	1.7-2.2	750.88	613.16	137.72	468.8	1.308	18.3	22.5	29.4
2780	6.8-7.3	461.12	387.00	74.12	258.8	1.495	16.1	19.2	28.6
2781	8.0-8.4	697.33	627.59	69.74	344.3	1.823	10.0	11.1	20.3
2782	12.4-12.8	617.99	543.97	74.02	322.7	1.686	12.0	13.6	22.9
2783	15.7-16.1	514.49	423.41	91.08	296.9	1.426	17.7	21.5	30.7
2784	16.4-16.7	646.27	511.98	134.29	391.2	1.309	20.8	26.2	34.3
2785	21.3-21.6	183.46	154.39	29.07	100.5	1.536	15.8	18.8	28.9
2786	23.6-24.0	573.96	491.03	82.93	317.1	1.549	14.4	16.9	26.2
2787	28.8-29.2	539.21	414.36	124.85	346.6	1.195	23.2	30.1	36.0
2788	30.3-30.7	527.10	409.74	117.36	341.6	1.199	22.3	28.6	34.4

Minimum Volumetric Water Content (%)	20.3
Maximum Volumetric Water Content (%)	36.0
Average Volumetric Water Content (%)	29.2
Standard Deviation in Measurements of Volumetric Water Content (%)	4.8

EQUIPMENT USED	CALIBRATION DUE DATE
Mettler PK 4800 Digital Balance, PTL 4513	6-22-89
Despatch Oven V-31-2, PTL 8784	6-28-89

REMARKS: *Density of pore water assumed to be 1.00 g/cc.

HOLMES & NARVER, INC.

MATERIALS TESTING LABORATORY

NEVADA TEST SITE

TABLE 6

WATER CONTENT DATA SHEET FOR U12g.12 WD-1

Project: Wet & Dry Drilling
Requestor: Dr. Alan L. Flint
Organization: USGS
Address: Box 327, M/S 721, Mercury, NV
Phone: 5-5805
Tested by: Jerry N. Walker
Test date: 2-15-89 through 2-18-89
*3-21-89 through 3-22-89

Checked by: John G. Moore John G. Moore
Check date: 12/5/89
MTL Lab #: 2789 through 2798
Request #: GT-38
H&N ID #: 50036C
WBS #: 1.2.3.3.6.1
WIN #: YMP:NTS:WI:89-006
QA level: III

MTL Sample Number	Depth Interval (ft)	Wet Weight (g)	Dry Weight (g)	**Water Content (g or cc)	Core Volume (cc)	Dry Bulk Density (g/cc)	% Water of Wet Weight	% Water of Dry Weight	Volumetric Water Content (%)
2789	1.8-2.3	703.03	555.04	147.99	434.2	1.278	21.1	26.7	34.1
2790	7.6-7.9	280.00	221.18	58.82	160.3	1.380	21.0	26.6	36.7
*2791	8.7-9.0	242.91	201.25	41.66	134.0	1.502	17.2	20.7	31.1
2792	12.4-12.8	593.11	524.80	68.31	296.6	1.769	11.5	13.0	23.0
*2793	14.0-14.5	613.41	521.70	91.71	325.7	1.602	15.0	17.6	28.2
2794	16.1-16.5	465.82	360.76	105.06	269.5	1.339	22.6	29.1	39.0
2795	19.1-19.5	828.90	713.43	115.47	433.0	1.648	13.9	16.2	26.7
2796	24.5-24.9	538.53	419.03	119.50	320.8	1.306	22.2	28.5	37.3
*2797	27.4-27.8	387.55	300.91	86.64	230.1	1.308	22.4	28.8	37.7
2798	29.2-29.5	325.22	254.25	70.97	188.9	1.346	21.8	27.9	37.6

Minimum Volumetric Water Content (%)	23.0
Maximum Volumetric Water Content (%)	39.0
Average Volumetric Water Content (%)	33.1
Standard Deviation in Measurements of Volumetric Water Content (%)	5.3

EQUIPMENT USED	CALIBRATION DUE DATE
Mettler PK 4800 Digital Balance, PTL 4513	6-22-89
Despatch Oven V-31-2, PTL 8784	6-28-89

REMARKS: *Lithium bromide content analysis performed on water centrifuged from these cores.
** Density of pore water assumed to be 1.00 g/cc.

HOLMES & NARVER, INC.

MATERIALS TESTING LABORATORY

NEVADA TEST SITE

TABLE 7

WATER CONTENT DATA SHEET FOR U12g DD-2

Project: Wet & Dry Drilling
Requestor: Dr. Alan L. Flint
Organization: USGS
Address: Box 327, M/S 721, Mercury, NV
Phone: 5-5805
Tested by: Jerry N. Walker
Test date: 2-15-89 through 2-18-89

Checked by: John G. Moore John G. Moore
Check date: 12/5/89
MTL Lab #: 2799 through 2808
Request #: GT-38
H&N ID #: 50036C
WBS #: 1.2.3.3.6.1
WIN #: YMP:NTS:WI:89-006
QA level: III

MTL Sample Number	Depth Interval (ft)	Wet Weight (g)	Dry Weight (g)	*Water Content (g or cc)	Core Volume (cc)	Dry Bulk Density (g/cc)	% Water of Wet Weight	% Water of Dry Weight	Volumetric Water Content (%)
2799	0.7-1.0	669.86	635.81	34.05	291.0	2.185	5.1	5.4	11.7
2800	3.6-4.0	839.85	788.70	51.15	363.6	2.169	6.1	6.5	14.1
2801	6.3-6.7	637.99	598.48	39.51	287.3	2.083	6.2	6.6	13.8
2802	8.0-8.4	866.57	818.17	48.40	377.2	2.169	5.6	5.9	12.8
2803	12.4-12.7	636.08	598.73	37.35	273.2	2.192	5.9	6.2	13.7
2804	18.5-18.8	530.75	502.01	28.74	229.8	2.185	5.4	5.7	12.5
2805	19.5-20.0	480.83	454.72	26.11	213.2	2.133	5.4	5.7	12.2
2806	20.7-21.0	459.89	428.79	31.10	202.4	2.119	6.8	7.3	15.4
2807	23.3-23.6	616.39	574.68	41.71	268.5	2.140	6.8	7.3	15.5
2808	27.5-27.8	302.30	288.46	13.84	130.2	2.216	4.6	4.8	10.6

Minimum Volumetric Water Content (%)	10.6
Maximum Volumetric Water Content (%)	15.5
Average Volumetric Water Content (%)	13.2
Standard Deviation in Measurements of Volumetric Water Content (%)	1.5

EQUIPMENT USED	CALIBRATION DUE DATE
Mettler PK 4800 Digital Balance, PTL 4513	6-22-89
Despatch Oven V-31-2, PTL 8784	6-28-89

REMARKS: *Density of pore water assumed to be 1.00 g/cc.

HOLMES & NARVER, INC.

MATERIALS TESTING LABORATORY

NEVADA TEST SITE

TABLE 8

WATER CONTENT DATA SHEET FOR U12g WD-2

Project: Wet & Dry Drilling
Requestor: Dr. Alan L. Flint
Organization: USGS
Address: Box 327, M/S 721, Mercury, NV
Phone: 5-5805
Tested by: Jerry N. Walker
Test date: 2-15-89 through 2-18-89
*3-22-89 through 3-23-89

Checked by: John G. Moore
Check date: 12/5/89
MTL Lab #: 2809 through 2818
Request #: GT-38
H&N ID #: 50036C
WBS #: 1.2.3.3.6.1
WIN #: YMP:NTS:WI:89-006
QA level: III

MTL Sample Number	Depth Interval (ft)	Wet Weight (g)	Dry Weight (g)	**Water Content (g or cc)	Core Volume (cc)	Dry Bulk Density (g/cc)	% Water of Wet Weight	% Water of Dry Weight	Volumetric Water Content (%)
2809	1.0-1.4	548.32	513.40	34.92	237.5	2.162	6.4	6.8	14.7
2810	4.0-4.3	654.99	613.15	41.84	279.7	2.192	6.4	6.8	15.0
*2811	5.5-5.9	642.48	602.10	40.38	276.3	2.179	6.3	6.7	14.6
2812	11.7-12.1	518.33	485.23	33.10	225.6	2.151	6.4	6.8	14.7
2813	14.0-14.3	794.63	752.59	42.04	334.9	2.247	5.3	5.6	12.6
*2814	16.1-16.4	392.27	367.91	24.36	168.3	2.186	6.2	6.6	14.5
2815	17.7-18.0	729.49	683.15	46.34	312.2	2.188	6.4	6.8	14.8
2816	19.4-19.7	571.37	531.13	40.24	247.8	2.143	7.0	7.6	16.2
*2817	21.1-21.4	279.90	261.05	18.85	120.0	2.175	6.7	7.2	15.7
2818	22.2-22.6	828.71	772.96	55.75	355.8	2.172	6.7	7.2	15.7

Minimum Volumetric Water Content (%)	12.6
Maximum Volumetric Water Content (%)	16.2
Average Volumetric Water Content (%)	14.8
Standard Deviation in Measurements of Volumetric Water Content (%)	0.9

EQUIPMENT USED	CALIBRATION DUE DATE
Mettler PK 4800 Digital Balance, PTL 4513	6-22-89
Despatch Oven V-31-2, PTL 8784	6-28-89

REMARKS: *Lithium bromide content analysis performed on water centrifuged from these cores.
**Density of pore water assumed to be 1.00 g/cc.

FIGURE 1

Core Properties

Holmes & Narver Materials Test Lab (JNW)

3–1–89

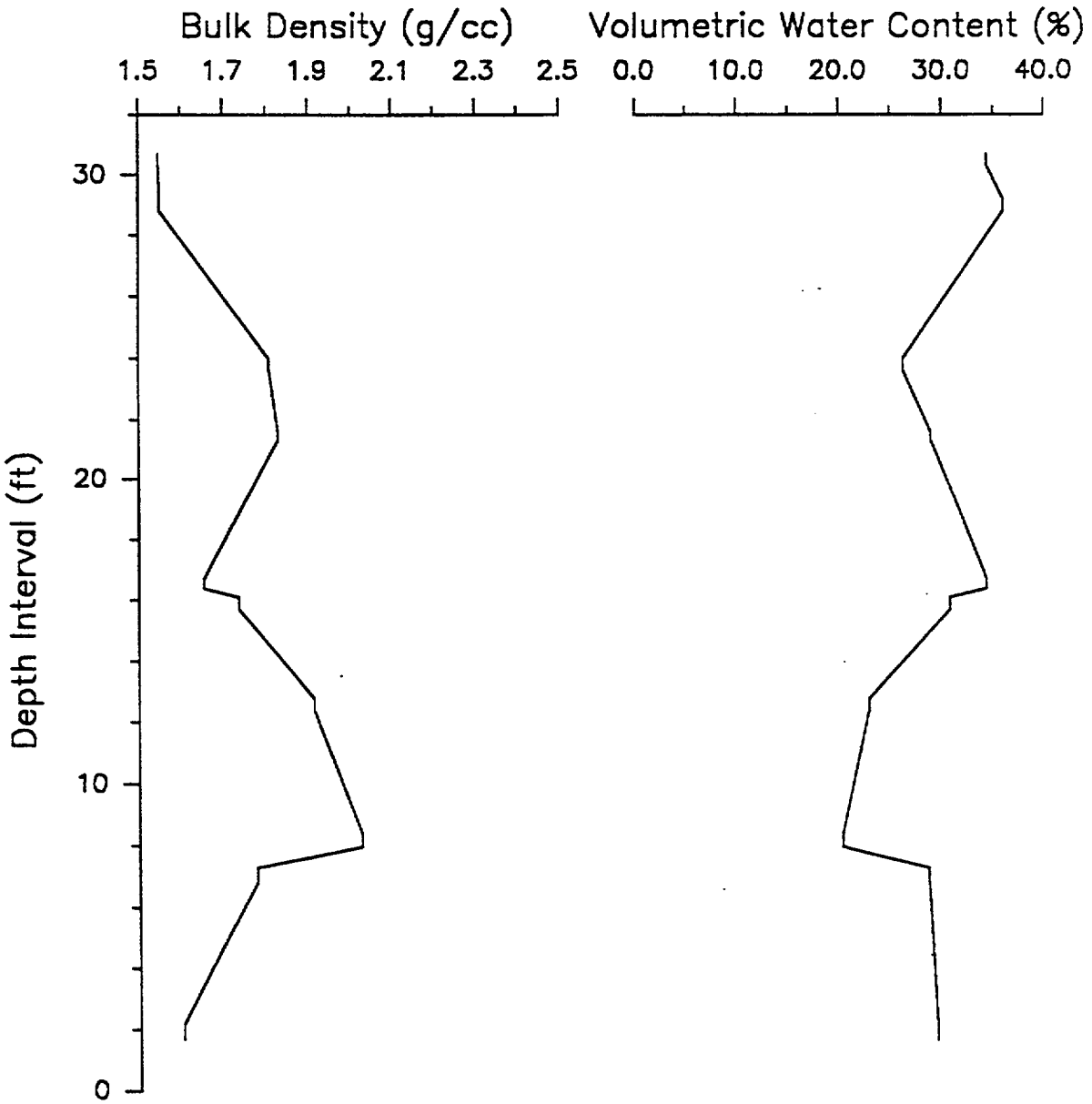

USGS Wet & Dry Drilling
U12g.12 DD1
WBS # 1.2.3.3.6.1
QA Level III
MTL Lab #'s 2779 through 2788

FIGURE 2

Core Properties

Holmes & Narver Materials Test Lab (JNW)

3-1-89

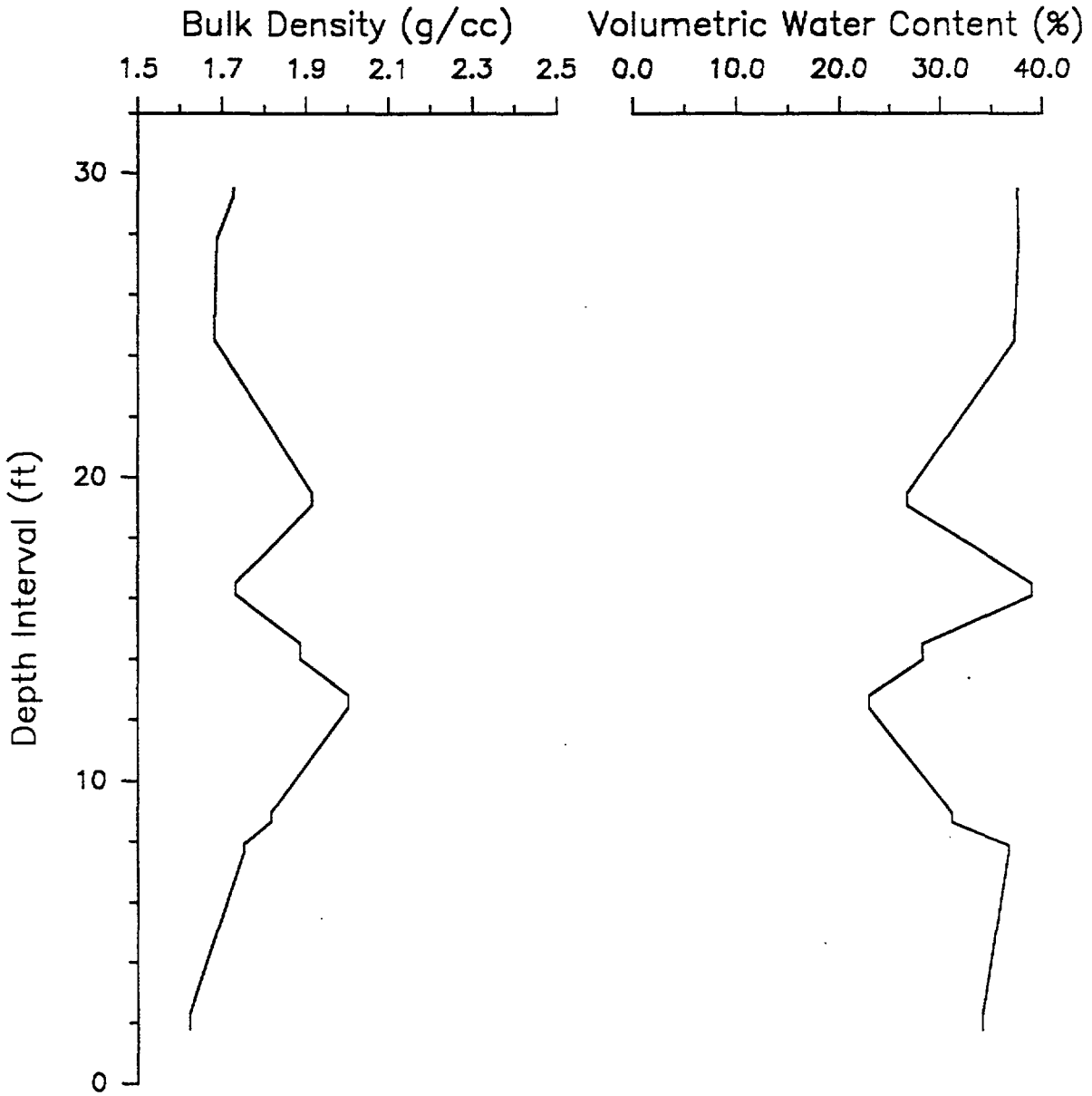

USGS Wet & Dry Drilling
U12g.12 WD1
WBS # 1.2.3.3.6.1
QA Level III
MTL Lab #'s 2789 through 2798

FIGURE 3

Core Properties

Holmes & Narver Materials Test Lab (JNW)

3–1–89

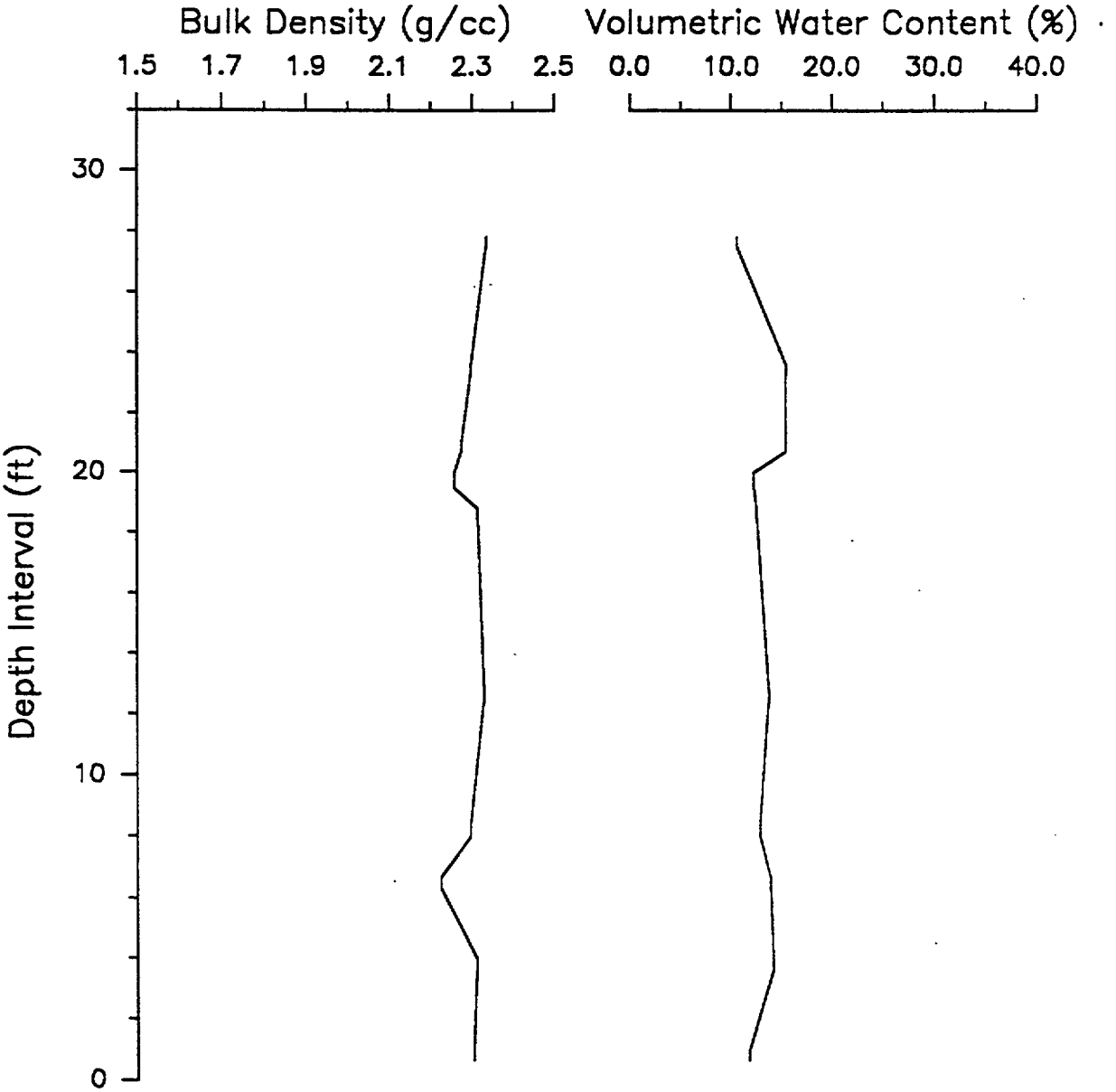

USGS Wet & Dry Drilling
U12g DD2
WBS # 1.2.3.3.6.1
QA Level III
MTL Lab #'s 2799 through 2808

FIGURE 4

Core Properties

Holmes & Narver Materials Test Lab (JNW)

3–1–89

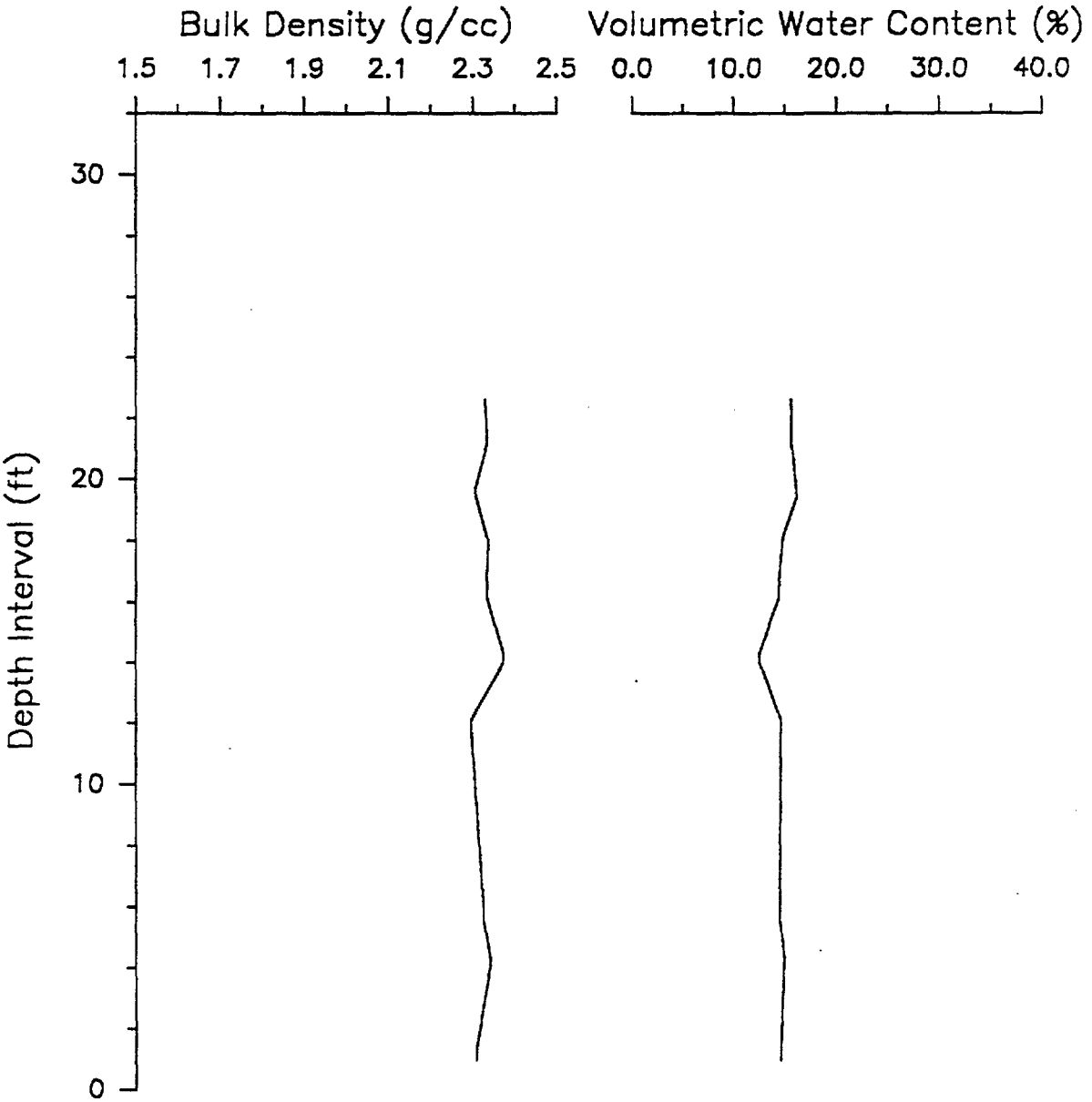

USGS Wet & Dry Drilling

U12g WD2

WBS # 1.2.3.3.6.1

QA Level III

MTL Lab #'s 2809 through 2818

III. GRAIN DENSITIES

A. DENSITY TESTS

Due to the differences in saturation for various liquids, results reported in the previous report on this project MTL report # 89 - 111, the grain density tests (particle specific gravity) were also done using helium, water and toluene. The grain densities were tested using a helium porosimeter and glass pycnometers were used for water and toluene determined densities.

B. HELIUM POROSIMETER

The helium porosimeter calibration data was developed by using different size steel samples and the results are given in figure 5 and table 9.

C. REFERENCE MATERIAL TESTS

The densities were also measured on the nonreactive silica reference samples by using helium, water and toluene. The data presented in tables 10 to 12 indicates that the all three test methods are consistent and the values can be reproduced by using either test method on nonreactive materials. The density results for the silica samples using three methods are comparable and given in tables 10 to 12.

D. NONWELDED TUFF SAMPLE TESTS

The welded tuff samples from the holes DD-1 and WD-1 were tested using helium, water and toluene. As shown in

figures 6 and 7, water determined densities are about 5 to 10 % higher than the helium and toluene determined values. The higher water determined densities indicate that the water is reacting with the test samples. Actual type causes of the water reaction with the nonwelded test samples may have to be further investigated. The results and data for all the nonwelded samples are given in the tables 13 to 17 and figures 6 and 7.

E. WELDED TUFF SAMPLE TESTS

The welded tuff samples density tests were also tested using helium, toluene and water. The results of the welded samples from the holes DD-2 and WD-2 are given in figures 8 and 9 and tables from 18 to 21. The data indicates that the density values determined by the three methods overlapped each other (figures 8 and 9) and the welded tuff samples are nonreactive to the water.

FIGURE 5
Helium Porosimeter Calibration Curve
Holmes & Narver Materials Test Lab (JNW)
7-31-89

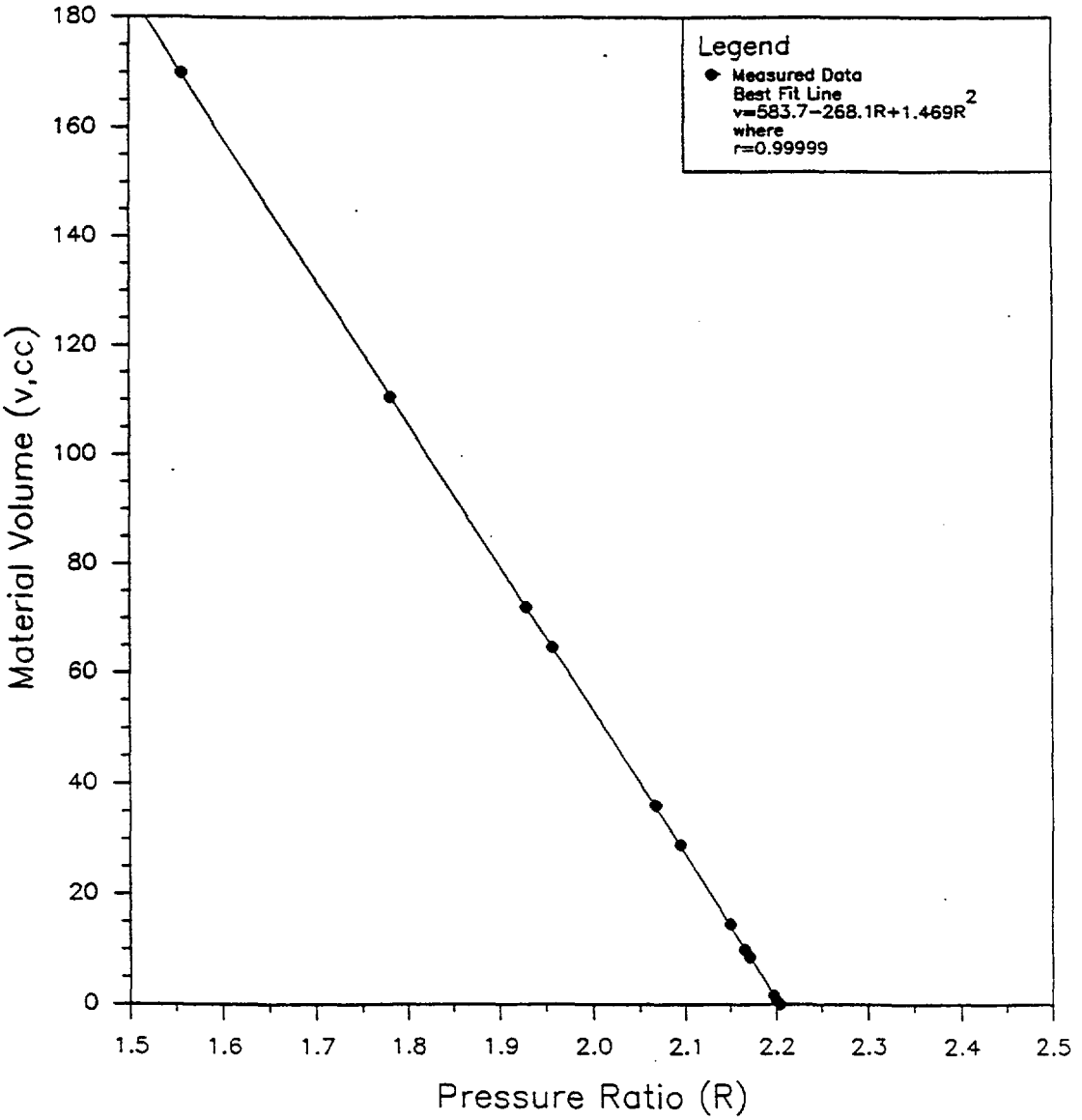

USGS Wet & Dry Drilling
WBS #1.2.3.3.6.1
QA Level III

HOLMES & NARVER, INC.

MATERIALS TESTING LABORATORY

NEVADA TEST SITE

TABLE 9

CALIBRATION SHEET FOR HELIUM POROSIMETER

Project: Wet & Dry Drilling
Requestor: Dr. Alan L. Flint
Organization: USGS
Address: Box 327, M/S 721, Mercury, NV
Phone: 5-5805
Tested by: Jerry N. Walker
Test date: 7-31-89

Checked by: John G. Moore
Check date: 12/5/89
MTL Lab #: N/A
Request #: GT-38
H&N ID #: 50036C
WBS #: 1.2.3.3.6.1
WIN #: YMP:NTS:WI:89-006
QA level: III

MTL Sample Number	Uncoated Weight (g)	Submerged Weight (g)	Water Temp. (Celsius)	Water Density (g/cc)	Core Volume (cc)	Bulk Density (g/cc)	Initial Pressure (I,psia)	Final Pressure (F,psia)	Pressure Ratio (I/F)
1	1343.80	1174.20	20.8	0.9980	169.93	7.91	99.58	63.97	1.557
2	869.00	758.68	20.8	0.9980	110.54	7.86	99.92	56.09	1.781
3	506.35	441.84	20.8	0.9980	64.64	7.83	99.87	51.04	1.957
4	563.75	491.90	20.8	0.9980	71.99	7.83	99.86	51.76	1.929
5	282.18	246.23	20.9	0.9980	36.02	7.83	99.92	48.35	2.067
6	112.58	98.22	20.9	0.9980	14.39	7.82	99.76	46.41	2.150
7	222.25	193.40	20.9	0.9980	28.91	7.69	99.69	47.61	2.094
8	65.66	57.12	20.9	0.9980	8.56	7.67	99.71	45.92	2.171
9	76.99	67.17	20.9	0.9980	9.84	7.82	99.72	46.06	2.165
10	12.58	10.98	20.9	0.9980	1.60	7.85	99.82	45.43	2.197
11	6.29	5.49	20.9	0.9980	0.80	7.85	99.57	45.26	2.200
12	0.00	0.00	N/A	N/A	0.00	N/A	99.72	45.25	2.204

EQUIPMENT USED	CALIBRATION DUE DATE
Mettler PK 4800 Digital Balance, PTL 4513	1-5-90
Omega 871A Digital Thermometer, PTL 6976	9-13-89
Heise Digital Absolute Pressure Gauge, PTL 8784	8-18-89

REMARKS: None

HOLMES & NARVER, INC.

MATERIALS TESTING LABORATORY

NEVADA TEST SITE

TABLE 10

WATER DETERMINED GRAIN DENSITY DATA SHEET FOR GROUND SILICA

Project: Wet & Dry Drilling
Requestor: Dr. Alan L. Flint
Organization: USGS
Address: Box 327, M/S 721, Mercury, NV
Phone: 5-5805
Tested by: Jerry N. Walker
Test date: 8-9-89 through 8-10-89

Checked by: John G. Moore John G Moore
Check date: 12/5/89
MTL Lab #: N/A
Request #: GT-38
H&N ID #: 50036C
WBS #: 1.2.3.3.6.1
WIN #: YMP:NTS:WI:89-006
QA level: III

Sample Test Number	Depth Interval (ft)	MTL Pycnometer Number	Total Weight Dry (g)	Sample Weight Dry (g)	Total Weight Wet (g)	Water Temp. (C)	Water Density (g/cc)	Sample Volume (cc)	Grain Density (g/cc)
1	N/A	247	109.372	46.370	191.578	22.4	0.9977	17.55	2.642
2	N/A	248	108.461	44.943	191.080	22.5	0.9977	17.07	2.634
3	N/A	249	111.144	47.851	192.712	22.5	0.9977	18.12	2.640
4	N/A	250	110.524	47.731	192.149	22.4	0.9977	18.07	2.641
5	N/A	251	107.027	44.647	189.880	22.3	0.9977	16.89	2.644
6	N/A	252	107.351	44.759	190.124	22.3	0.9977	16.94	2.642
7	N/A	254	106.582	43.582	189.775	22.3	0.9977	16.56	2.632
8	N/A	255	107.274	45.351	189.783	22.4	0.9977	17.21	2.635
9	N/A	256	109.805	46.885	191.789	22.4	0.9977	17.74	2.643
10	N/A	257	106.461	44.061	189.466	22.6	0.9976	16.71	2.637

Minimum Grain Density (g/cc)..... 2.632
Maximum Grain Density (g/cc)..... 2.644
Average Grain Density (g/cc)..... 2.639
Standard Deviation in Measurements of Grain Density (g/cc)..... 0.004

EQUIPMENT USED	CALIBRATION DUE DATE
Mettler PK 4800 Digital Balance, PTL 4513	1-5-90
Omega 871A Digital Thermometer, PTL 6976	9-13-89

REMARKS: If the data spread is assumed representive for a correctly performed test, than results for individual samples will have 95% confidence intervals of + 0.006 g/cc using this procedure.

HOLMES & NARVER, INC.

MATERIALS TESTING LABORATORY

NEVADA TEST SITE

TABLE 11

HELIUM DETERMINED GRAIN DENSITY DATA SHEET FOR GROUND SILICA

Project: Wet & Dry Drilling
Requestor: Dr. Alan L. Flint
Organization: USGS
Address: Box 327, M/S 721, Mercury, NV
Phone: 5-5805
Tested by: Jerry N. Walker
Test date: 8-8-89 through 8-9-89

Checked by: John G. Moore
Check date: 12/5/89
MTL Lab #: N/A
Request #: GT-38
H&N ID #: 50036C
WBS #: 1.2.3.3.6.1
WIN #: YMP:NTS:WI:89-006
QA level: III

Sample Test Number	Depth Interval (ft)	Cup Volume (cc)	Dry Weight (g)	Initial Pressure (I,psia)	Final Pressure (F,psia)	Pressure Ratio (I/F)	Total Volume (cc)	Grain Volume (cc)	Grain Density (g/cc)
1	N/A	34.425	47.155	99.76	49.76	2.005	52.111	17.69	2.666
2	N/A	34.425	45.858	99.77	49.84	2.002	52.902	18.48	2.482
3	N/A	34.425	49.163	99.88	49.92	2.001	53.166	18.74	2.623
4	N/A	34.425	49.078	100.05	49.98	2.002	52.904	18.48	2.656
5	N/A	34.425	47.254	99.86	49.84	2.004	52.429	18.00	2.625
6	N/A	34.425	46.657	99.71	49.74	2.005	52.163	17.74	2.630
7	N/A	34.425	50.104	99.92	49.95	2.000	53.271	18.85	2.659
8	N/A	34.425	48.186	100.26	50.06	2.003	52.643	18.22	2.645
9	N/A	34.425	48.823	99.73	49.82	2.002	52.902	18.48	2.642
10	N/A	34.425	50.350	99.90	49.95	2.000	53.376	18.95	2.657

Minimum Grain Density (g/cc)	2.482
Maximum Grain Density (g/cc)	2.666
Average Grain Density (g/cc)	2.628
Standard Deviation in Measurements of Grain Density (g/cc)	0.051

EQUIPMENT USED	CALIBRATION DUE DATE
Fisher Scientific Top Loading Balance, PTL 2678	9-3-89
Heise Digital Absolute Pressure Gauge, PTL 8784	8-18-89

REMARKS: If the data spread is assumed representative for a correctly performed test, then results for individual samples will have 95% confidence intervals of + 0.029 g/cc using this procedure.

HOLMES & NARVER, INC.

MATERIALS TESTING LABORATORY

NEVADA TEST SITE

TABLE 12

TOLUENE DETERMINED GRAIN DENSITY DATA SHEET FOR GROUND SILICA

Project: Wet & Dry Drilling
Requestor: Dr. Alan L. Flint
Organization: USGS
Address: Box 327, M/S 721, Mercury, NV
Phone: 5-5805
Tested by: Jerry N. Walker
Test date: 8-21-89 through 8-22-89

Checked by: John G. Moore
Check date: 12/5/89
MTL Lab #: N/A
Request #: GT-38
H&N ID #: 50036C
WBS #: 1.2.3.3.6.1
WIN #: YMP:NTS:WI:89-006
QA level: III

Sample Test Number	Depth Interval (ft)	MTL Pycnometer Number	Total Weight Dry (g)	Sample Weight Dry (g)	Total Weight Wet (g)	Toluene Temp. (C)	Toluene Density (g/cc)	Sample Volume (cc)	Grain Density (g/cc)
1	N/A	247	100.696	37.694	174.716	N/A	0.8641	14.29	2.638
2	N/A	248	110.977	47.459	181.773	N/A	0.8641	17.95	2.644
3	N/A	249	101.053	37.760	175.032	N/A	0.8641	14.27	2.646
4	N/A	250	95.153	32.360	170.867	N/A	0.8641	12.26	2.639
5	N/A	251	93.876	31.496	169.903	N/A	0.8641	11.95	2.636
6	N/A	252	95.851	33.259	171.287	N/A	0.8641	12.61	2.638
7	N/A	254	106.908	43.908	178.935	N/A	0.8641	16.59	2.647
8	N/A	255	102.733	40.810	175.734	N/A	0.8641	15.43	2.645
9	N/A	256	102.381	39.461	175.829	N/A	0.8641	14.91	2.646
10	N/A	257	103.276	40.876	176.219	N/A	0.8641	15.49	2.638

Minimum Grain Density (g/cc)..... 2.636
Maximum Grain Density (g/cc)..... 2.647
Average Grain Density (g/cc)..... 2.642
Standard Deviation in Measurements of Grain Density (g/cc)..... 0.004

EQUIPMENT USED	CALIBRATION DUE DATE
Mettler PK 4800 Digital Balance, PTL 4513	1-5-90
Omega 871A Digital Thermometer, PTL 6976	9-13-89

REMARKS: If the data spread is assumed representive for a correctly performed test, than results for individual samples will have 95% confidence intervals of + 0.008 g/cc using this procedure.

FIGURE 6
Grain Density Results, U12g.12 DD–1
Holmes & Narver Materials Test Lab (JNW)
9–2–89

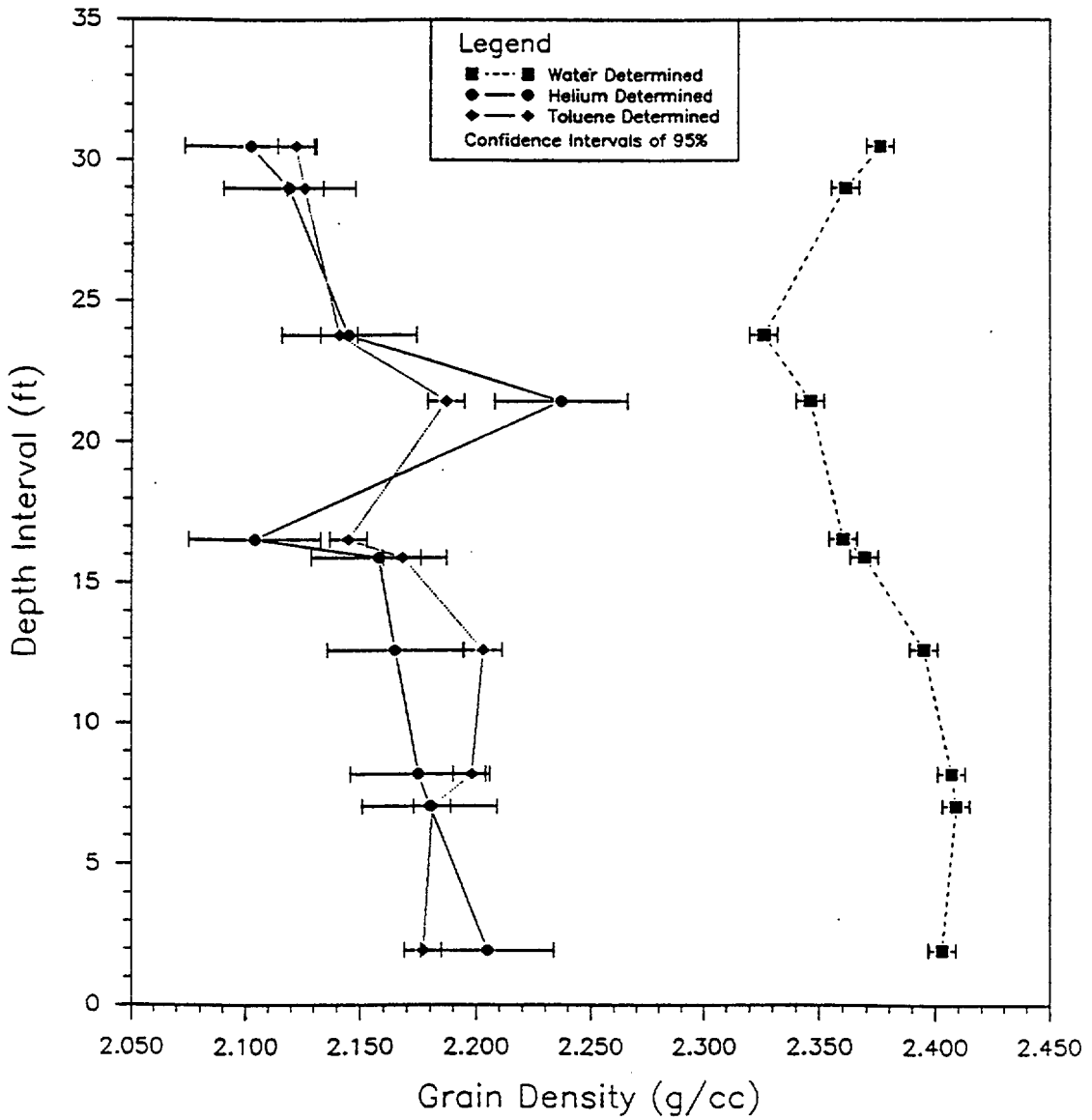

USGS Wet & Dry Drilling
WBS #1.2.3.3.6.1
QA Level III

HOLMES & NARVER, INC.

MATERIALS TESTING LABORATORY

NEVADA TEST SITE

TABLE 13

WATER DETERMINED GRAIN DENSITY DATA SHEET FOR U12g.12 DD-1

Project: Wet & Dry Drilling
Requestor: Dr. Alan L. Flint
Organization: USGS
Address: Box 327, M/S 721, Mercury, NV
Phone: 5-5805
Tested by: Jerry N. Walker
Test date: 8-2-89 through 8-3-89

Checked by: John G. Moore John S. Moore
Check date: 12/5/89
MTL Lab #: 2779 through 2788
Request #: GT-38
H&N ID #: 50036C
WBS #: 1.2.3.3.6.1
WIN #: YMP:NTS:WI:89-006
QA level: III

MTL Sample Number	Depth Interval (ft)	MTL Pycnometer Number	Total Weight Dry (g)	Sample Weight Dry (g)	Total Weight Wet (g)	Water Temp. (C)	Water Density (g/cc)	Sample Volume (cc)	Grain Density (g/cc)
2779	1.7-2.2	247	93.577	30.575	180.604	22.4	0.9977	12.72	2.403
2780	6.8-7.3	248	91.956	28.438	179.831	22.1	0.9977	11.81	2.409
2781	8.0-8.4	249	94.620	31.327	181.288	22.2	0.9977	13.02	2.407
2782	12.4-12.8	250	90.516	27.723	178.627	22.2	0.9977	11.57	2.395
2783	15.7-16.1	251	93.166	30.786	179.906	22.1	0.9977	13.00	2.369
2784	16.4-16.7	252	89.992	27.400	178.090	22.1	0.9977	11.61	2.360
2785	21.3-21.6	254	102.058	39.058	185.164	22.1	0.9977	16.65	2.346
2786	23.6-24.0	255	88.125	26.202	176.569	22.1	0.9977	11.27	2.326
2787	28.8-29.2	256	91.274	28.354	178.977	22.2	0.9977	12.01	2.361
2788	30.3-30.7	257	87.788	25.388	176.809	22.2	0.9977	10.69	2.376

Minimum Grain Density (g/cc)	2.326
Maximum Grain Density (g/cc)	2.409
Average Grain Density (g/cc)	2.375
Standard Deviation in Measurements of Grain Density (g/cc)	0.027

EQUIPMENT USED	CALIBRATION DUE DATE
Mettler PM 400 Digital Balance, PTL 1255	9-14-89
Omega 871A Digital Thermometer, PTL 6976	9-1389

REMARKS: None

HOLMES & NARVER, INC.

MATERIALS TESTING LABORATORY

NEVADA TEST SITE

TABLE 14

HELIUM DETERMINED GRAIN DENSITY DATA SHEET FOR U12g.12 DD-1

Project: Wet & Dry Drilling
Requestor: Dr. Alan L. Flint
Organization: USGS
Address: Box 327, M/S 721, Mercury, NV
Phone: 5-5805
Tested by: Jerry N. Walker
Test date: 7-31-89 through 8-1-89

Checked by: John G. Moore
Check date: 12/5/89
MTL Lab #: 2779 through 2788
Request #: GT-38
H&N ID #: 50036C
WBS #: 1.2.3.3.6.1
WIN #: YMP:NTS:WI:89-006
QA level: III

MTL Sample Number	Depth Interval (ft)	Cup Volume (cc)	Dry Weight (g)	Initial Pressure (I,psia)	Final Pressure (F,psia)	Pressure Ratio (I/F)	Total Volume (cc)	Grain Volume (cc)	Grain Density (g/cc)
2779	1.7-2.2	34.036	31.553	99.99	49.52	2.019	48.346	14.31	2.205
2780	6.8-7.3	34.036	35.985	100.42	49.94	2.011	50.541	16.50	2.180
2781	8.0-8.4	34.036	34.699	99.72	49.54	2.013	49.989	15.95	2.175
2782	12.4-12.8	34.036	36.498	99.89	49.71	2.009	50.897	16.86	2.165
2783	15.7-16.1	34.036	34.804	100.27	49.83	2.012	50.166	16.13	2.158
2784	16.4-16.7	34.036	28.299	99.89	49.39	2.022	47.483	13.45	2.104
2785	21.3-21.6	34.036	44.316	99.73	49.91	1.998	53.849	19.81	2.237
2786	23.6-24.0	34.036	26.555	100.01	49.35	2.027	46.416	12.38	2.145
2787	28.8-29.2	34.036	29.038	99.68	49.31	2.021	47.740	13.70	2.119
2788	30.3-30.7	34.036	26.179	100.26	49.48	2.026	46.488	12.45	2.102

Minimum Grain Density (g/cc)	2.102
Maximum Grain Density (g/cc)	2.237
Average Grain Density (g/cc)	2.159
Standard Deviation in Measurements of Grain Density (g/cc)	0.041

EQUIPMENT USED	CALIBRATION DUE DATE
Fisher Scientific Top Loading Balance, PTL 2678	9-3-89
Heise Digital Absolute Pressure Gauge, PTL 8784	8-18-89

REMARKS: None

HOLMES & NARVER, INC.

MATERIALS TESTING LABORATORY

NEVADA TEST SITE

TABLE 15

TOLUENE DETERMINED GRAIN DENSITY DATA SHEET FOR U12g.12 DD-1

Project: Wet & Dry Drilling
Requestor: Dr. Alan L. Flint
Organization: USGS
Address: Box 327, M/S 721, Mercury, NV
Phone: 5-5805
Tested by: Jerry N. Walker
Test date: 8-3-89 through 8-4-89

Checked by: John G. Moore
Check date: 12/5/89
MTL Lab #: 2779 through 2788
Request #: GT-38
H&N ID #: 50036C
WBS #: 1.2.3.3.6.1
WIN #: YMP:NTS:WI:89-006
QA level: III

MTL Sample Number	Depth Interval (ft)	MTL Pycnometer Number	Total Weight Dry (g)	Sample Weight Dry (g)	Total Weight Wet (g)	Toluene Temp. (C)	Toluene Density (g/cc)	Sample Volume (cc)	Grain Density (g/cc)
2779	1.7-2.2	247	85.602	22.600	163.025	N/A	0.8644	10.38	2.177
2780	6.8-7.3	248	90.340	26.822	166.044	N/A	0.8644	12.30	2.181
2781	8.0-8.4	249	90.352	27.059	166.050	N/A	0.8644	12.31	2.198
2782	12.4-12.8	250	93.503	30.710	167.795	N/A	0.8644	13.94	2.203
2783	15.7-16.1	251	89.820	27.440	165.260	N/A	0.8644	12.66	2.168
2784	16.4-16.7	252	80.388	17.796	159.575	N/A	0.8644	8.30	2.145
2785	21.3-21.6	254	76.509	13.509	157.561	N/A	0.8644	6.18	2.187
2786	23.6-24.0	255	83.789	21.866	161.325	N/A	0.8644	10.21	2.141
2787	28.8-29.2	256	87.227	24.307	163.708	N/A	0.8644	11.43	2.126
2788	30.3-30.7	257	81.634	19.234	160.161	N/A	0.8644	9.06	2.122

Minimum Grain Density (g/cc)..... 2.122
Maximum Grain Density (g/cc)..... 2.203
Average Grain Density (g/cc)..... 2.165
Standard Deviation in Measurements of Grain Density (g/cc)..... 0.028

EQUIPMENT USED	CALIBRATION DUE DATE
Mettler PM 400 Digital Balance, PTL 1255	9-14-89
Omega 871A Digital Thermometer, PTL 6976	9-13-89

REMARKS: None

FIGURE 7

Grain Density Results, U12g.12 WD−1

Holmes & Narver Materials Test Lab (JNW)

9−2−89

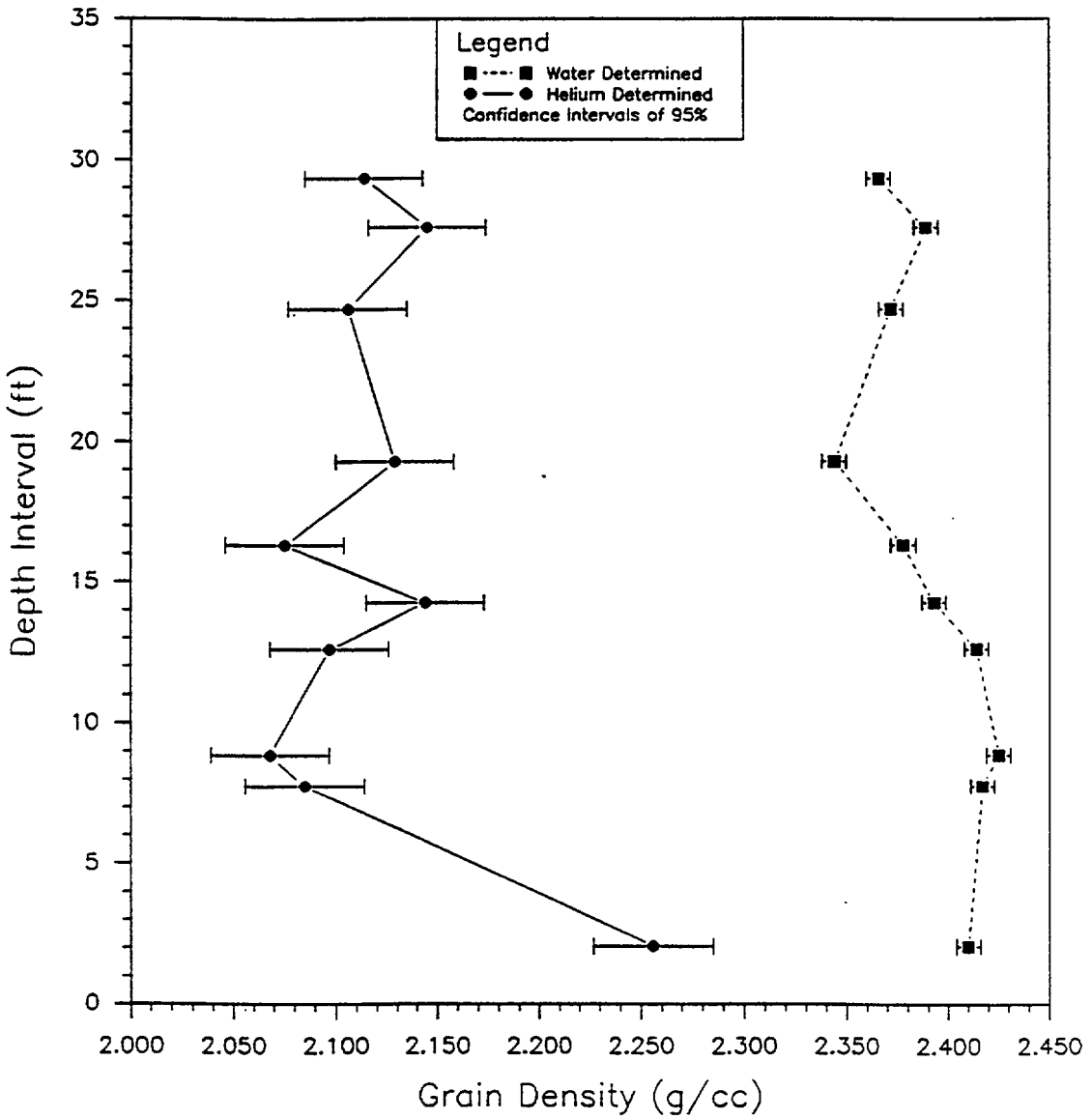

USGS Wet & Dry Drilling
WBS #1.2.3.3.6.1
QA Level III

HOLMES & NARVER, INC.

MATERIALS TESTING LABORATORY

NEVADA TEST SITE

TABLE 16

WATER DETERMINED GRAIN DENSITY DATA SHEET FOR U12g.12 WD-1

Project: Wet & Dry Drilling
Requestor: Dr. Alan L. Flint
Organization: USGS
Address: Box 327, M/S 721, Mercury, NV
Phone: 5-5805
Tested by: Jerry N. Walker
Test date: 8-7-89 through 8-8-89

Checked by: John G. Moore John G. Moore
Check date: 12/5/89
MTL Lab #: 2789 through 2798
Request #: GT-38
H&N ID #: 50036C
WBS #: 1.2.3.3.6.1
WIN #: YMP:NTS:WI:89-006
QA level: III

MTL Sample Number	Depth Interval (ft)	MTL Pycnometer Number	Total Weight Dry (g)	Sample Weight Dry (g)	Total Weight Wet (g)	Water Temp. (C)	Water Density (g/cc)	Sample Volume (cc)	Grain Density (g/cc)
2789	1.8-2.3	247	81.495	18.493	173.570	21.8	0.9978	7.674	2.410
2790	7.6-7.9	248	82.227	18.709	174.167	21.6	0.9979	7.742	2.417
2791	8.7-9.0	249	84.829	21.536	175.629	22.0	0.9978	8.879	2.425
2792	12.4-12.8	250	86.867	24.074	176.586	21.7	0.9978	9.973	2.414
2793	14.0-14.5	251	100.367	37.987	184.242	21.9	0.9978	15.87	2.393
2794	16.1-16.5	252	81.835	19.243	173.450	21.8	0.9978	8.090	2.378
2795	19.1-19.5	254	88.254	25.254	177.228	21.9	0.9978	10.77	2.344
2796	24.5-24.9	255	80.014	18.091	172.094	21.8	0.9978	7.628	2.372
2797	27.4-27.8	256	81.442	18.522	173.397	22.0	0.9978	7.752	2.389
2798	29.2-29.5	257	82.200	19.800	173.535	22.0	0.9978	8.370	2.366

Minimum Grain Density (g/cc)	2.344
Maximum Grain Density (g/cc)	2.425
Average Grain Density (g/cc)	2.391
Standard Deviation in Measurements of Grain Density (g/cc)	0.025

EQUIPMENT USED	CALIBRATION DUE DATE
Mettler PK 4800 Digital Balance, PTL 4513	1-5-90
Omega 871A Digital Thermometer, PTL 6976	9-13-89

REMARKS: None

HOLMES & NARVER, INC.

MATERIALS TESTING LABORATORY

NEVADA TEST SITE

TABLE 17

HELIUM DETERMINED GRAIN DENSITY DATA SHEET FOR U12g.12 WD-1

Project: Wet & Dry Drilling
Requestor: Dr. Alan L. Flint
Organization: USGS
Address: Box 327, M/S 721, Mercury, NV
Phone: 5-5805
Tested by: Jerry N. Walker
Test date: 8-8-89 through 8-9-89

Checked by: John G. Moore
Check date: 12/5/89
MTL Lab #: 2789 through 2798
Request #: GT-38
H&N ID #: 50036C
WBS #: 1.2.3.3.6.1
WIN #: YMP:NTS:WI:89-006
QA level: III

MTL Sample Number	Depth Interval (ft)	Cup Volume (cc)	Dry Weight (g)	Initial Pressure (I,psia)	Final Pressure (F,psia)	Pressure Ratio (I/F)	Total Volume (cc)	Grain Volume (cc)	Grain Density (g/cc)
2789	1.8-2.3	34.366	18.784	100.14	49.07	2.041	42.691	8.32	2.256
2790	7.6-7.9	34.366	19.249	99.97	49.07	2.037	43.599	9.23	2.085
2791	8.7-9.0	34.366	21.764	99.83	49.12	2.032	44.889	10.52	2.068
2792	12.4-12.8	34.366	24.462	99.92	49.27	2.028	46.033	11.67	2.097
2793	14.0-14.5	34.366	38.510	100.06	49.93	2.004	52.326	17.96	2.144
2794	16.1-16.5	34.366	19.665	100.25	49.23	2.036	43.843	9.48	2.075
2795	19.1-19.5	34.366	25.868	99.89	49.30	2.026	46.516	12.15	2.129
2796	24.5-24.9	34.366	18.462	99.67	48.88	2.039	43.132	8.77	2.106
2797	27.4-27.8	34.366	19.171	99.74	48.93	2.038	43.303	8.94	2.145
2798	29.2-29.5	34.366	20.236	99.56	48.90	2.036	43.940	9.57	2.114

Minimum Grain Density (g/cc)	2.068
Maximum Grain Density (g/cc)	2.256
Average Grain Density (g/cc)	2.122
Standard Deviation in Measurements of Grain Density (g/cc)	0.052

EQUIPMENT USED	CALIBRATION DUE DATE
Fisher Scientific Top Loading Balance, PTL 2678	9-3-89
Heise Digital Absolute Pressure Gauge, PTL 8784	8-18-89

REMARKS: None

FIGURE 8

Grain Density Results, U12g DD-2

Holmes & Narver Materials Test Lab (JNW)

9-2-89

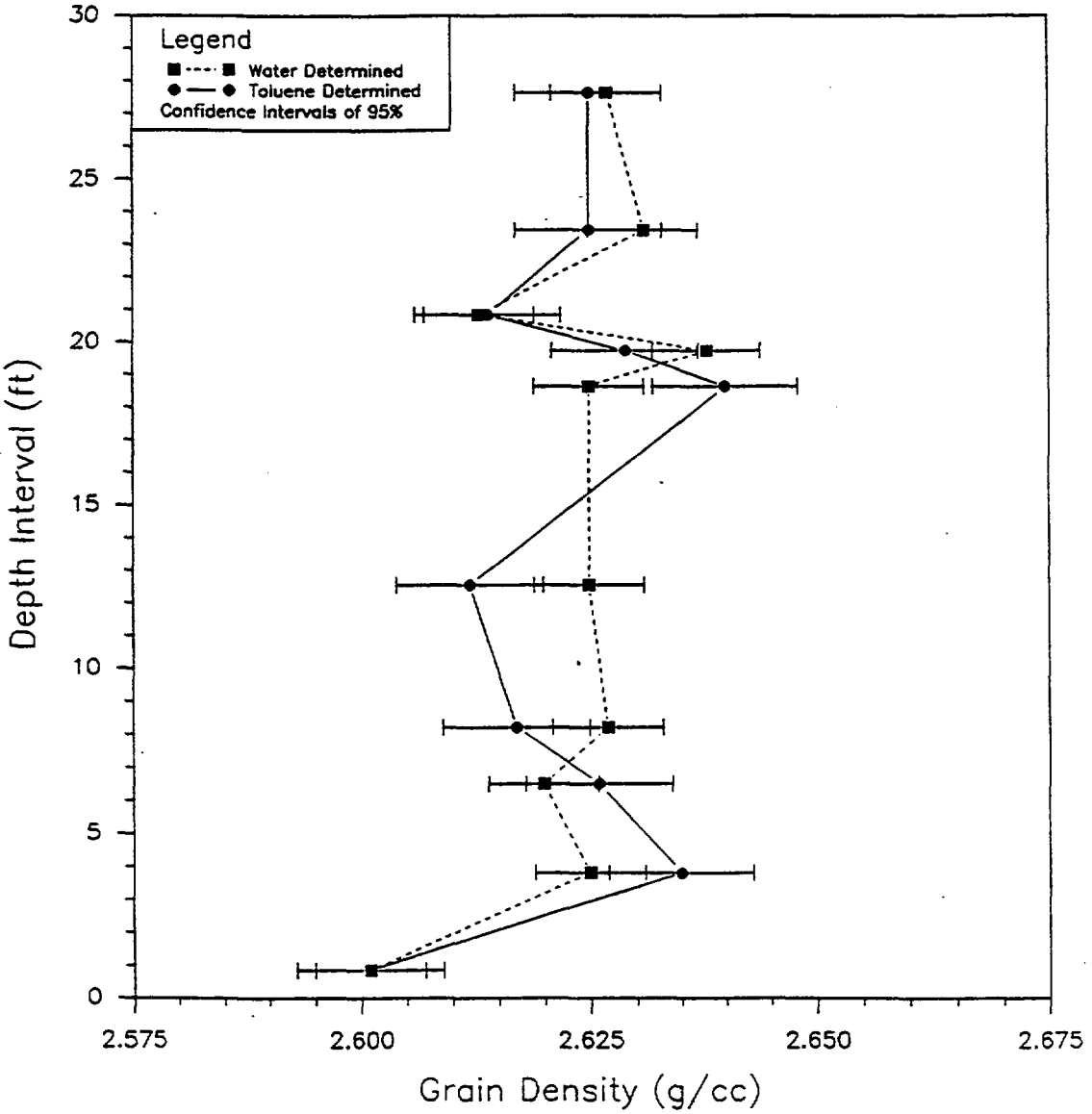

USGS Wet & Dry Drilling

WBS #1.2.3.3.6.1

QA Level III

HOLMES & NARVER, INC.

MATERIALS TESTING LABORATORY

NEVADA TEST SITE

TABLE 18

WATER DETERMINED GRAIN DENSITY DATA SHEET FOR U12g DD-2

Project: Wet & Dry Drilling
Requestor: Dr. Alan L. Flint
Organization: USGS
Address: Box 327, M/S 721, Mercury, NV
Phone: 5-5805
Tested by: Jerry N. Walker
Test date: 8-14-89 through 8-15-89

Checked by: John G. Moore
Check date: 12/5/89
MTL Lab #: 2799 through 2808
Request #: GT-38
H&N ID #: 50036C
WBS #: 1.2.3.3.6.1
WIN #: YMP:NTS:WI:89-006
QA level: III

MTL Sample Number	Depth Interval (ft)	MTL Pycnometer Number	Total Weight Dry (g)	Sample Weight Dry (g)	Total Weight Wet (g)	Water Temp. (C)	Water Density (g/cc)	Sample Volume (cc)	Grain Density (g/cc)
2799	0.7-1.0	247	91.479	28.477	180.265	22.8	0.9976	10.95	2.601
2800	3.6-4.0	248	87.426	23.908	177.988	22.4	0.9977	9.11	2.625
2801	6.3-6.7	249	93.979	30.686	181.942	22.6	0.9976	11.71	2.620
2802	8.0-8.4	250	95.021	32.228	182.428	22.7	0.9976	12.27	2.627
2803	12.4-12.7	251	95.612	33.232	182.676	22.8	0.9976	12.66	2.625
2804	18.5-18.8	252	91.659	29.067	180.274	23.0	0.9975	11.07	2.625
2805	19.5-20.0	254	99.343	36.343	185.308	22.6	0.9976	13.78	2.638
2806	20.7-21.0	255	97.550	35.627	183.616	22.8	0.9976	13.64	2.613
2807	23.3-23.6	256	99.825	36.905	185.505	22.8	0.9976	14.02	2.631
2808	27.5-27.8	257	102.059	39.659	186.666	22.9	0.9976	15.10	2.627

Minimum Grain Density (g/cc)	2.601
Maximum Grain Density (g/cc)	2.638
Average Grain Density (g/cc)	2.623
Standard Deviation in Measurements of Grain Density (g/cc)	0.010

EQUIPMENT USED	CALIBRATION DUE DATE
Mettler PM 400 Digital Balance, PTL 1255	1-5-90
Omega 871A Digital Thermometer, PTL 6976	9-13-89

REMARKS: None

HOLMES & NARVER, INC.

MATERIALS TESTING LABORATORY

NEVADA TEST SITE

TABLE 19

TOLUENE DETERMINED GRAIN DENSITY DATA SHEET FOR U12g DD-2

Project: Wet & Dry Drilling
Requestor: Dr. Alan L. Flint
Organization: USGS
Address: Box 327, M/S 721, Mercury, NV
Phone: 5-5805
Tested by: Jerry N. Walker
Test date: 8-10-89 through 8-11-89

Checked by: John G. Moore John G. Moore
Check date: 12/5/89
MTL Lab #: 2799 through 2808
Request #: GT-38
H&N ID #: 50036C
WBS #: 1.2.3.3.6.1
WIN #: YMP:NTS:WI:89-006
QA level: III

MTL Sample Number	Depth Interval (ft)	MTL Pycnometer Number	Total Weight Dry (g)	Sample Weight Dry (g)	Total Weight Wet (g)	Toluene Temp. (C)	Toluene Density (g/cc)	Sample Volume (cc)	Grain Density (g/cc)
2799	0.7-1.0	247	91.539	28.537	168.416	N/A	0.8640	10.97	2.601
2800	3.6-4.0	248	87.526	24.008	165.950	N/A	0.8640	9.11	2.635
2801	6.3-6.7	249	94.192	30.899	170.324	N/A	0.8640	11.77	2.626
2802	8.0-8.4	250	95.283	32.490	170.859	N/A	0.8640	12.41	2.617
2803	12.4-12.7	251	95.933	33.553	171.175	N/A	0.8640	12.85	2.612
2804	18.5-18.8	252	91.927	29.335	168.644	N/A	0.8640	11.11	2.640
2805	19.5-20.0	254	99.608	36.608	173.929	N/A	0.8640	13.93	2.629
2806	20.7-21.0	255	97.884	35.961	172.321	N/A	0.8640	13.76	2.614
2807	23.3-23.6	256	100.026	37.106	174.137	N/A	0.8640	14.14	2.625
2808	27.5-27.8	257	102.096	39.696	175.353	N/A	0.8640	15.12	2.625

Minimum Grain Density (g/cc)	2.601
Maximum Grain Density (g/cc)	2.640
Average Grain Density (g/cc)	2.622
Standard Deviation in Measurements of Grain Density (g/cc)	0.011

EQUIPMENT USED	CALIBRATION DUE DATE
Mettler PM 400 Digital Balance, PTL 1255	1-5-90
Omega 871A Digital Thermometer, PTL 6976	9-13-89

REMARKS: None

FIGURE 9
Grain Density Results, U12g WD-2
Holmes & Narver Materials Test Lab (JNW)
9-2-89

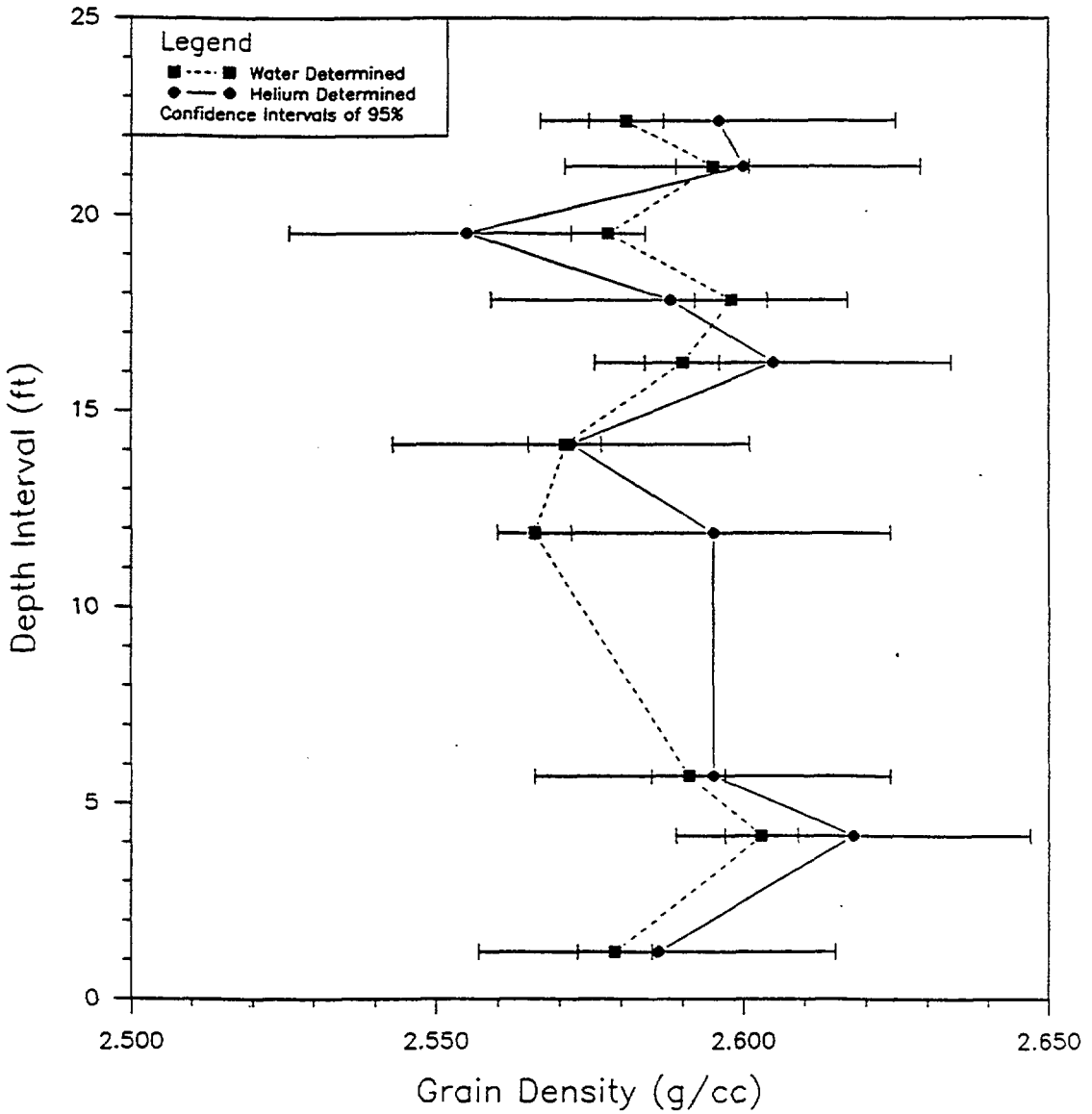

USGS Wet & Dry Drilling
WBS #1.2.3.3.6.1
QA Level III

HOLMES & NARVER, INC.

MATERIALS TESTING LABORATORY

NEVADA TEST SITE

TABLE 20

WATER DETERMINED GRAIN DENSITY DATA SHEET FOR U12g WD-2

Project: Wet & Dry Drilling
Requestor: Dr. Alan L. Flint
Organization: USGS
Address: Box 327, M/S 721, Mercury, NV
Phone: 5-5805
Tested by: Jerry N. Walker
Test date: 8-9-89 through 8-10-89

Checked by: John G. Moore
Check date: 12/5/89
MTL Lab #: 2779 through 2788
Request #: GT-38
H&N ID #: 50036C
WBS #: 1.2.3.3.6.1
WIN #: YMP:NTS:WI:89-006
QA level: III

MTL Sample Number	Depth Interval (ft)	MTL Pycnometer Number	Total Weight Dry (g)	Sample Weight Dry (g)	Total Weight Wet (g)	Water Temp. (C)	Water Density (g/cc)	Sample Volume (cc)	Grain Density (g/cc)
2809	1.0-1.4	247	110.382	47.380	191.781	22.1	0.9977	18.37	2.579
2810	4.0-4.3	248	101.688	38.170	186.709	22.3	0.9977	14.66	2.603
2811	5.5-5.9	249	112.349	49.056	193.113	22.2	0.9977	18.93	2.591
2812	11.7-12.1	250	105.721	42.928	188.687	22.3	0.9977	16.73	2.566
2813	14.0-14.3	251	112.228	49.848	192.586	22.3	0.9977	19.39	2.571
2814	16.1-16.4	252	102.889	40.297	187.043	22.4	0.9977	15.56	2.590
2815	17.7-18.0	254	100.725	37.725	185.954	22.3	0.9977	14.52	2.598
2816	19.4-19.7	255	114.658	52.735	193.931	22.4	0.9977	20.45	2.578
2817	21.1-21.4	256	109.411	46.491	191.212	22.5	0.9977	17.92	2.595
2818	22.2-22.6	257	97.820	35.420	183.801	22.5	0.9977	13.73	2.581

Minimum Grain Density (g/cc)..... 2.566
Maximum Grain Density (g/cc)..... 2.603
Average Grain Density (g/cc)..... 2.585
Standard Deviation in Measurements of Grain Density (g/cc)..... 0.011

EQUIPMENT USED	CALIBRATION DUE DATE
Mettler PK 4800 Digital Balance, PTL 4513	1-5-90
Omega 871A Digital Thermometer, PTL 6976	9-13-89

REMARKS: None

HOLMES & NARVER, INC.

MATERIALS TESTING LABORATORY

NEVADA TEST SITE

TABLE 21

HELIUM DETERMINED GRAIN DENSITY DATA SHEET FOR U12g WD-2

Project: Wet & Dry Drilling
Requestor: Dr. Alan L. Flint
Organization: USGS
Address: Box 327, M/S 721, Mercury, NV
Phone: 5-5805
Tested by: Jerry N. Walker
Test date: 8-8-89 through 8-9-89

Checked by: John G. Moore John G. Moore
Check date: 12/5/89
MTL Lab #: 2809 through 2818
Request #: GT-38
H&N ID #: 50036C
WBS #: 1.2.3.3.6.1
WIN #: YMP:NTS:WI:89-006
QA level: III

MTL Sample Number	Depth Interval (ft)	Cup Volume (cc)	Dry Weight (g)	Initial Pressure (I,psia)	Final Pressure (F,psia)	Pressure Ratio (I/F)	Total Volume (cc)	Grain Volume (cc)	Grain Density (g/cc)
2809	1.0-1.4	34.21	48.352	100.33	50.12	2.002	52.905	18.70	2.586
2810	4.0-4.3	34.21	39.120	100.10	49.65	2.016	49.151	14.94	2.618
2811	5.5-5.9	34.21	49.735	99.66	49.83	2.000	53.376	19.17	2.595
2812	11.7-12.1	34.21	43.842	99.67	49.62	2.009	51.104	16.89	2.595
2813	14.0-14.3	34.21	50.777	100.09	50.10	1.998	53.952	19.74	2.572
2814	16.1-16.4	34.21	40.569	100.00	49.66	2.014	49.786	15.58	2.605
2815	17.7-18.0	34.21	38.358	99.80	49.49	2.017	49.032	14.82	2.588
2816	19.4-19.7	34.21	52.858	99.77	50.03	1.994	54.896	20.69	2.555
2817	21.1-21.4	34.21	47.383	100.12	49.97	2.004	52.431	18.22	2.600
2818	22.2-22.6	34.21	37.101	99.86	49.47	2.019	48.500	14.29	2.596

Minimum Grain Density (g/cc)	2.555
Maximum Grain Density (g/cc)	2.618
Average Grain Density (g/cc)	2.591
Standard Deviation in Measurements of Grain Density (g/cc)	0.017

EQUIPMENT USED	CALIBRATION DUE DATE
Mettler PJ 3000 Digital Balance, PTL 2677	9-3-89
Heise Digital Absolute Pressure Gauge, PTL 8784	8-18-89

REMARKS: None

IV. LITHIUM BROMIDE TESTS AND ANALYSIS

A. TEST SAMPLES

Lithium Bromide content tests were conducted on the three liquid (trace samples) and on the water extracted from the six rock core samples. Six sections of core, ranging from 3.5 to 6 inches long, were taken from the two core holes WD-1 and WD-2. A 1-inch long piece was dry cut from each core and a 1.1 inch diameter core undercut (dry) from the larger core. The undercut cores were placed in an ultracentrifuge and rotated at speeds of 10,000 and 16,000 RPM's, for a minimum of one hour at each speed. The water forced out of the cores was collected and tested for lithium bromide concentrations. Centrifuge yielded 0.3cc of water from #2791, 2.5 cc from #2793, 1.5cc from #2797, 0.2cc from #2811, 0.2cc from #2814, and 0.4cc from #2817.

B. LITHIUM BROMIDE TESTS

The chemical analysis was conducted as per ASTM E663-78 procedures and using Atomic Absorption Spectrophotometer. The lithium and calculated lithium bromide contents are given in table 22.

The lithium bromide contents in the rock samples show higher values than the trace solution (for sample # 2819 to 2821 , table 22). The higher lithium bromide values in rock samples might be due to the loss of water during the core preparation at MTL leaving higher lithium concentration in the extracted water samples from the cores.

C. LITHIUM BROMIDE CONTENT ANALYSIS

The actual lithium bromide % in the rock samples were estimated under the following assumptions and the movable water, actual lithium bromide, intruded and original water values are given in table 23. Figure 10 shows the volume of natural water and intruded drilling fluid in each core before any water was lost. Figure 11 shows the same data only with each plotted as a percentage of the total fluid content.

Assumptions

1. Properties remain constant in the individual six sections of core.

2. During the heating of the cores caused by dry cutting, the LiBr in solution precipitated out as the water evaporated off.

3. During the subsequent centrifuge runs, the LiBr which had precipitated out was dissolved back into solution in the water being removed from the cores.

4. The irreducible water saturations which remained in the cores after the centrifuge runs had the same LiBr concentrations as when they were removed from the lexan liners.

5. The original water in the core had no lithium bromide in solution.

6. The irreducible water saturations, at the pressures induced by 16,000 RPM's in the unltracentrifuge are 40% of saturation for the nonwelded tuffs and 50% for the welded tuffs.

Calculations

Calculations of the movable, intruded and original water and lithium bromide are as follows.

Movable water: The movable water that could have been removed by the centrifuge at 16000 rpm given in table 23 was calculated as per the following:

MW = VWC * BV * (1-Swi)
MW = Volume of movable water initially in core (cc)
VWC = Volumetric water content of core
BV = Bulk volume of core (cc)
SWI = Irreducible water content of core, as given in the above Assumption #6.

Lithium Bromide: The corrected concentration of LiBr in the water given in table 23 in each core before the heat of dry cutting removed some of the water and altered the concentration based on Assumptions #2, #3, and #4 and the following calculations:

AC = MC* (VR/MW)
AC = Actual LiBr concentration (ppm)
MC = Measured LiBr concentration (ppm)
VR = Volume of water removed from core (cc)

Intruded fluid: Determine amount of drilling fluid intruded into core based on Assumption #5

IW = (AC * VWC * BV)/DFC
IW = Amount of water intruded into core (cc)
DFC = Concentration of LiBr in drilling fluid

Original Water: Determine amount of water left in core that was there before drilling.

OW = (VWC * BV) - IW
OW: Original water left in core after drilling

Comments

1. The precipitation of lithium bromide during cutting was unforeseen. It is recommended that during future similar testing, a large piece be broken from the core end placed in the centrifuge for removal of the water. This will prevent precipitation of lithium bromide and make Assumptions 2 and 3 unnecessary. In order to measure the volume of an irregular piece it will be necessary to pack the sample in the centrifuge sample chamber to prevent breakage. Following the centrifuge run the bulk volume and the pore volume of the sample should be measured using the Archimedes method.

2. Porosities will be measured on cores from the same section intervals in upcoming tests. The measured values should be used to evaluate the amount of intrusion on a saturation basis.

3. Irreducible water saturations will also be measured on the same samples using the centrifuge. When possible the measured values should be used rather than the ones in Assumption #5. The measured irreducible water saturations should also be considered when analyzing the intrusion data.

HOLMES & NARVER, INC.
MATERIALS TESTING LABORATORY

TABLE-22. CHEMICAL ANALYSIS (ASTM E 663)-ATOMIC ABSORPTION SPECTROPHOTOMETER (AA)

Requested by:MICHAEL P. CHORNACK
User/Agency: U S G S
Project: WBS#1.2.3.3.6.1 QA LEVEL III
Location: WET AND DRY DRILLING, U12g
Sampled by: REQUESTOR
Material: LIQUID SAMPLES AND CORE SAMPLES

Request #: GT 38
Lab #: 2791 THRU 2821
I.D #: 50036C
Date: 3/23/89
Tested by: R.K.SINGAL
Checked by: V.THUMMALA V. Thummala

Lab #	HOLE	Hole Depth For Core Sample (ft.)	Sample Dilution Factor	LI Metal In Standard** PPM	AA Reading* In Standard	AA Reading* In Sample	LI Metal In Sample PPM	LiBr(PPM) (Lix12.43)
2819	U12g.12 WD-1	N/A	1	0.2	0.160	0.235	0.29	3.7
2820	U12g. WD-2	N/A	1	0.2	0.160	0.195	0.24	3.0
2821	U12g. WD-2	N/A	1	0.2	0.160	0.139	0.17	2.2
2791	U12g.12 WD-1	8.7-9.0	2	0.5	0.405	0.280	0.69	8.6
2793	U12g.12 WD-1	14.0-14.5	1	0.2	0.160	0.065	0.08	1.0
2797	U12g.12 WD-1	27.4-27.8	1	0.5	0.405	0.310	0.38	4.8
2811	U12g. WD-2	5.5-5.9	1	0.5	0.405	0.236	0.29	3.6
2814	U12g. WD-2	16.1-16.4	2	0.5	0.405	0.290	0.72	8.9
2817	U12g. WD-2	21.1-21.4	2	0.5	0.405	0.235	0.58	7.2

Equipment used:
Balance AE-240, M-455
AA Perkin-Elmer 3030

Control #:
PTL 2683
DOE 185368

Calibration Due:
9/3/89
Not Required

* EMISSION MODE
** NIST LITHIUM STANDARD #3129

HOLMES & NARVER, INC.

MATERIALS TESTING LABORATORY

NEVADA TEST SITE

TABLE 23

LITHIUM BROMIDE CONTENT DATA SHEET

Project: Wet & Dry Drilling
Requestor: Dr. Alan L. Flint
Organization: USGS
Address: Box 327, M/S 721, Mercury, NV
Phone: 5-5805
Tested by: Rajendar K. Singal
Test date: 3/24/89
Calculations by: Jerry N. Walker

Checked by: V. Hennigwate
Check date: 12/8/89
MTL Lab #: 2819,2820,2821,2791,2793, 2797,2811,2814,2817
Request #: GT-38
H&N ID #: 50036C
WBS #: 1.2.3.3.6.1
WIN #: YMP:NTS:WI:89-006
QA level: III

Lithium bromide content of water used as drilling fluid in core hole U12g.12 WD-1, as determined from MTL sample #2819 (taken 12-11-89), was 3.7 ppm. Lithium bromide content of the water used in core hole U12g WD-2 was determined to be 3.1 ppm on 12-19-89 (MTL sample #2820), and 2.2 ppm on 12-20-89 (MTL sample #2821). An average of 2.7 ppm will be used for hole U12g WD-2.

MTL Sample Number	Measured LiBr (ppm)	Core Radius (cm)	Core Length (cm)	Volumetric Water Content(%)	Bulk Volume (cc)	Moveable Water (cc)	Actual Estimated: LiBr(ppm):	Intruded Water (cc)	Original Water (cc)
*2791	8.6	1.92	2.98	31.1	34.5	6.4	0.40	1.2	9.6
*2793	1.0	1.91	2.89	28.2	33.1	5.6	0.45	1.1	8.2
*2797	4.7	1.92	3.21	37.7	37.2	8.4	0.84	3.2	10.8
**2811	3.6	1.91	3.79	14.6	43.4	3.2	0.23	0.5	5.8
**2814	8.9	1.91	3.91	14.5	44.8	3.2	0.55	1.3	5.2
**2817	7.2	1.90	3.13	15.7	35.5	2.8	1.03	2.1	3.4

EQUIPMENT USED	CALIBRATION DUE DATE
Atomic Absorption Unit	
Digital Caliper, PTL 6786	7-13-89
Ultracentrifuge	
Diamond coring unit and saw	

REMARKS: *Samples 2791, 2793, and 2797 are non-welded tuffs taken from core hole U12g.12 WD-1, at depths of 8.7' to 9.0', 14.0' to 14.5', and 27.4' to 27.8' respectively. Sample 2791 yielded 0.3 cc of water after rotating at 16,000 rpm in the ultracentrifuge; sample 2793 produced 2.5 cc of water and sample 2797 1.5 cc of water.

**Samples 2811, 2814, and 2817 are welded tuffs taken from core hole U12g WD-2 at depths of 5.5' to 5.9', 16.1' to 16.4', and 21.1' to 21.4' respectively. Sample 2811 yielded 0.2 cc of water after rotating at 16,000 rpm in the ultracentrifuge; sample 2814 also produced 0.2 cc of water and sample 2817 0.4 cc of water.

FIGURE 10

Water Volume Distributions in Infiltration Test Samples

Holmes & Narver Materials Test Lab (JNW)

4–4–89

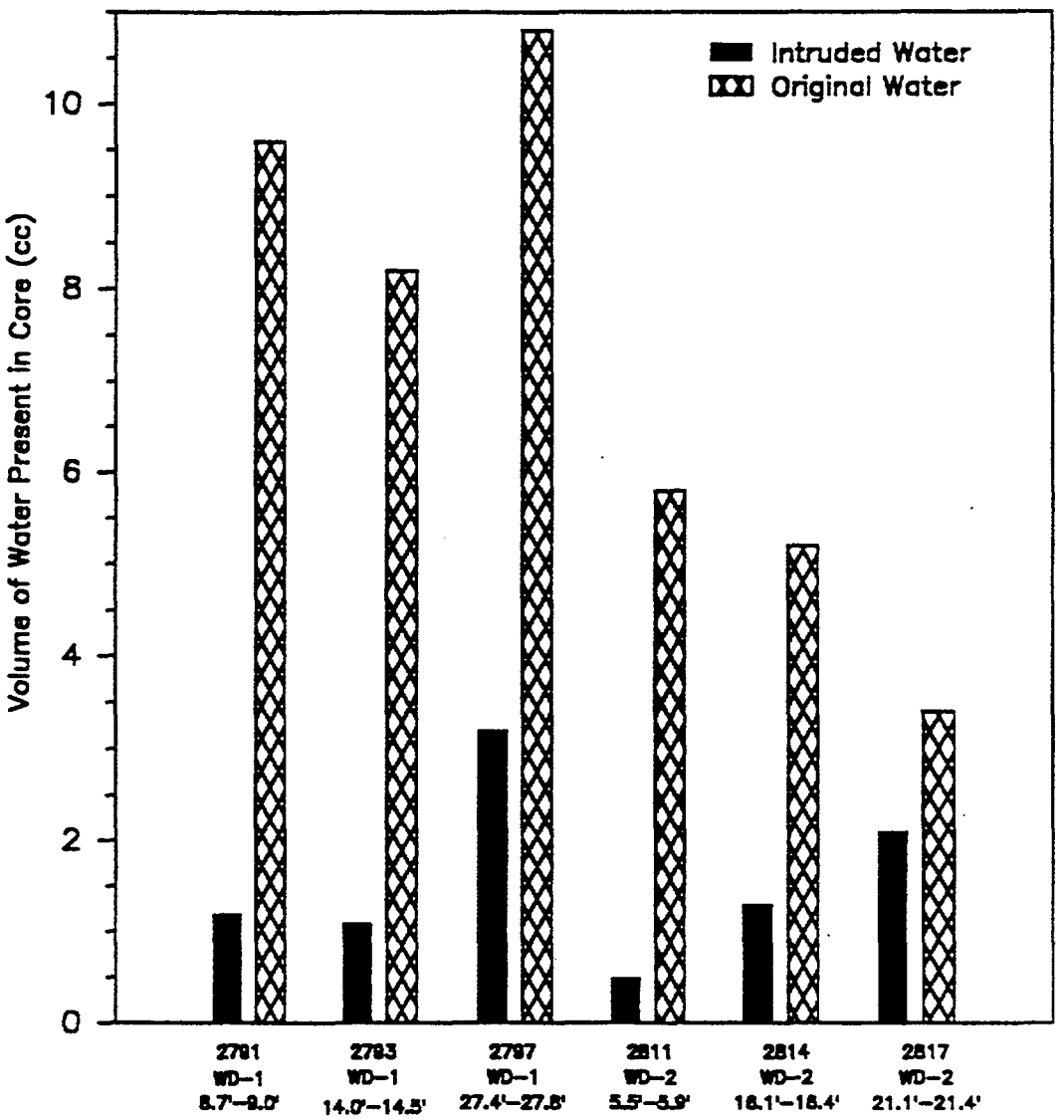

USGS Wet & Dry Drilling
WBS #1.2.3.3.6.1
QA Level III

FIGURE 11

General Fluid Distributions in Infiltration Test Samples

Holmes & Narver Materials Test Lab (JNW)

4–4–89

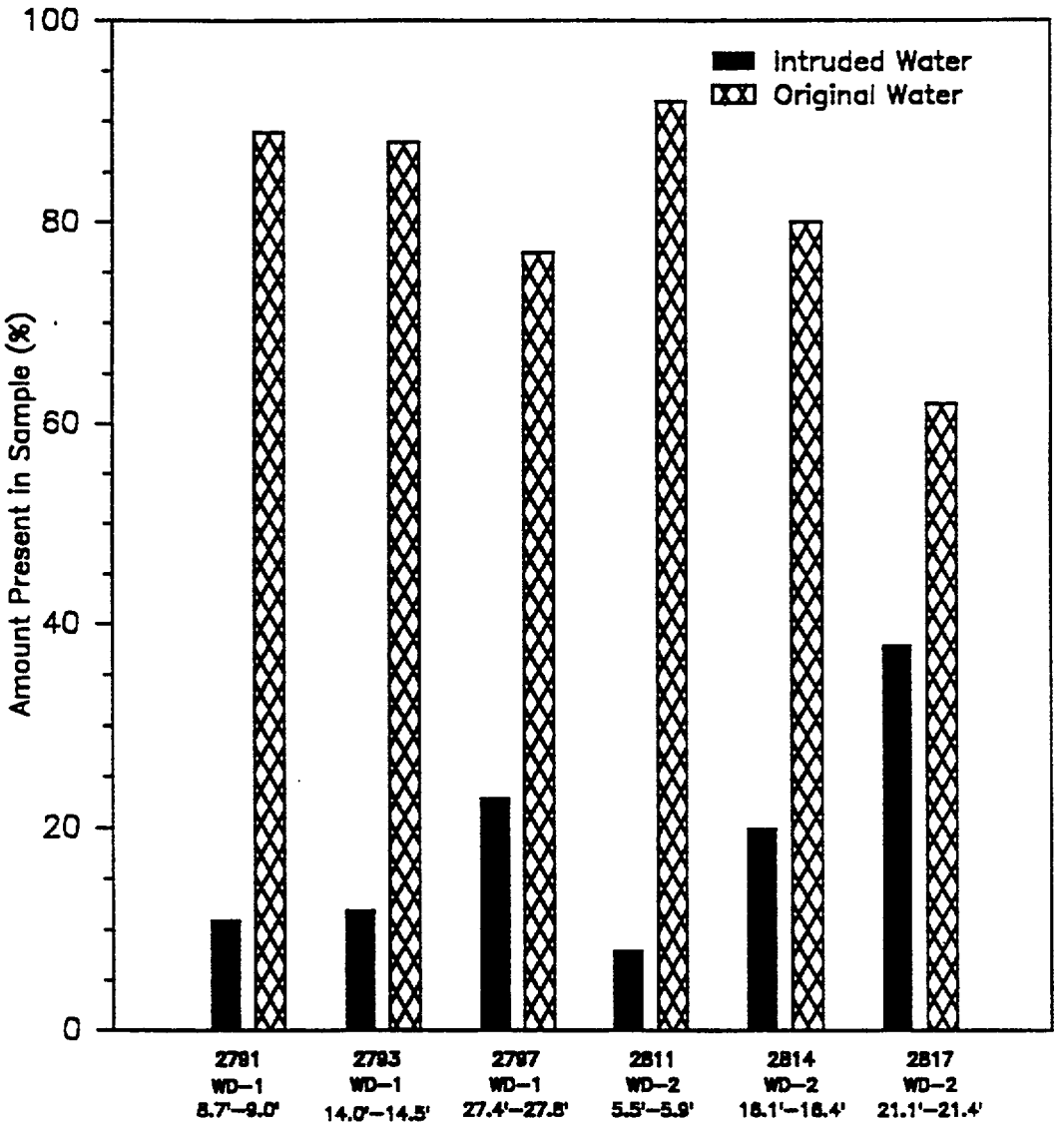

USGS Wet & Dry Drilling

WBS #1.2.3.3.6.1

QA Level III

V. APPENDIX A. SAMPLE TRACEABILITY DETAILS

The sample source and traceability details are given in this appendix.

YUCCA MOUNTAIN PROJECT
SAMPLES TRACEABILITY INFORMATION

HOLMES & NARVER, INC.
MATERIALS TESTING LABORATORY, NTS
PREPARED BY GEOTECHNICAL SECTION
MERCURY, NV 89023
(702) 295 6669
FTS 575 6669

WBS 1.2.3.3.1
QA: N/A

DATE: NOVEMBER, 1989

PROJECT NAME: PROTOTYPE TESTING – WET & DRY DRILLING

TEST WORK REQUESTED BY: MICHAEL P. CHORNACK, A. FLINT AND LORRIE FLINT U.S.G.S, NTS , AREA 25

SAMPLE SOURCE: G–TUNNEL

SAMPLE TYPE: ROCK CORE AND LIQUID SAMPLES

SAMPLE SUPPLIED BY: DELIVERED TO MTL BY DELIVERED TO MTL BY M.P. CHORNACK OF U.S.G.S

SAMPLES RECEIVED DATE AT MTL: 1/18/89

SAMPLES USED BY AT MTL: CURRENTLY BEING TESTED BY MTL

SAMPLE TRACEABILITY DETAILS: SEE ATTACHED LETTERS AND SAMPLE USE LOGS

PROJECT WORK STATUS: TEST WORK IN PROGRESS

MTL TEST RESULTS REPORT REFERENCE: 89–111, DATED JUNE 21, 1989

REMARKS: NONE

NNWSI

HOLMES & NARVER, INC.
MATERIALS TESTING LABORATORY
NEVADA TEST SITE

WORK REQUEST FOR GEOTECHNICAL, GROUT, CHEMICAL & SPECIAL TESTS

Project: WET & DRY DRILLING I. D. No: 500366 Requested By: MICHAEL P. CHORNAK

Phone: 5-5805 Date Received: 11/18/89 Completion Date: NOT GIVEN WORK WITH A. FLINT AND PROVIDE DATA AS TESTED

Material Type: ROCK CORES & 3 LIQUID SAMPLES Return Material After Testing? (Y) N

Work Request #: GT-38 Sample Lab #: 2749 TO 2821

Work Request Filled By: V. THUNNALA (SEE ATTACHED LETTER. Samples Received By: V. THUNNALA ON 11/18/8

TPO's Work Initiation #: _____ Q.A. Level: III

WBS #: 1.2.3.3.6.1

Test Procedures: ASTM, API

GEOTECHNICAL

- ☐ COMPRESSIVE STRENGTH:
  - ☐ Uniaxial ☐ Triaxial
- ☐ YOUNG'S MODULUS
- ☐ BULK MODULUS
- ☐ SHEAR MODULUS
- ☐ POISSON'S RATION
- ☐ TENSILE STRENGTH:
  - ☐ Direct
  - ☐ Indirect
  - ☐ Split
- ☐ SONIC VELOCITY
- ☒ SPECIFIC GRAVITY
- ☒ GRAIN DENSITY
- ☒ PERCENT MOISTURE VOLUME
- ☐ PERMEABILITY:
  - ☐ Gas ☐ Water
- ☒ POROSITY:
  - ☐ Gas
  - ☒ Calculated ☒ POROSIMETER
- ☐ PERCENT SATURATION
- ☒ ULTRACENTRIFUGE:
  - ☒ Capillary Pressure Curve
  - ☒ Liquid Extraction 6 SAMPLES
- ☐ THERMAL CONDUCTIVITY
- ☐ ELECTRICAL RESISTIVITY
- ☐ DIRECT SHEAR/COHESION
- ☐ CONSOLIDATION

GROUT/SHOTCRETE

- ☐ COMPRESSIVE STRENGTH:
  - ☐ Uniaxial ☐ Triaxial
- ☐ FLEXURAL STRENGTH
- ☐ EXOTHERM
- ☐ VICAT NEEDLE
- ☐ SLURRY DENSITY
- ☐ MARSH FUNNEL VISCOSITY
- ☐ SAND CONTENT
- ☐ SONIC VELOCITY

CHEMICAL

- ☐ MgC 2 CONTENT
- ☐ METAL ANALYSIS
- ☐ IRON CONTENT
- ☐ STEEL CARBON/SULFUR
- ☐ DRILLING FLUID ANALYSIS

OTHER

- ☐ SEISMIC SURVEY
- ☐ STYROFOAM STRENGTH
- ☐ BANDING MATERIAL
- ☐ VLAVE HYDROSTATIC TEST
- ☐ WIRE ROPE PULL
- ☐ WELD PULL
- ☐ HARDNESS
- ☐ CHARPY IMPACT
- ☐ BROOKFIELD VISCOSITY
- ☒ SPECIAL PROJECTS (Complete REMARKS)

REMARKS: SEE ATTACHED LETTER FOR TEST DETAILS.
See ATTACHED Table For Sample Source.

United States Department of the Interior

GEOLOGICAL SURVEY

P. O. Box 327
Mercury, NV 89023

TAKE PRIDE IN AMERICA

WBS #1.2.3.3.6.1.G
QA: "N/A"

January 18, 1989

TO: Venkatrao Thummala
Senior Engineer II
Holmes & Narver, Inc.
P. O. Box 1, M/S 607
Mercury, NV 89023

FROM: Michael P. Chornack
U. S. Geological Survey
P. O. Box 327, M/S 721
Mercury, NV 89023

SUBJECT: Transmittal of core samples from prototype test WBS 1.2.6.9.4.2.1 to the Holmes & Narver Materials Testing Laboratory (HNMTL) for testing.

Forty (40) core samples contained in lexan liners are being delivered to the Holmes & Narver MTL. The core samples are all labeled to include the borehole from which the core samples were taken and the depth interval of the core samples to the nearest tenth of a foot. In addition to the core samples, three (3) samples of drilling fluid are being submitted for lithium bromide (LiBr) analysis. This analysis is needed to determine the extent of drilling fluid imbibition into the core samples in the boreholes cored using water as the circulating fluid.

Enclosed under this cover letter is a listing of the core samples and the measurements and calculations we are requesting be conducted.

Questions regarding the testing of the core samples should be directed to Alan L. Flint, Principle Investigator, at (FTS) 575-5805.

Michael P. Chornack

U. S. Geological Survey

The following measurements and calculations should be made on the core samples listed below:

Bulk Density
Grain Density (Particle Density)
~~Porosity~~ - Centrifuge and Mercury Porosimetry
Volumetric Water Content
Water Release Curves
Saturated Hydraulic Conductivities

U12g.12 DD-1 KTL #	U12g.12 WD-1	U12g DD-2	U12g WD-2
1.7-2.2-2779	1.8-2.3-2789	0.7-1.0-2799	1.0-1.4-2809
6.8-7.3-2780	7.6-7.9-2790	3.6-4.0-2800	4.0-4.3-2810
8.0-8.4-2781	8.7-9.0-2791	6.3-6.7-2801	5.5-5.9-2811
12.4-12.8-2782	12.4-12.8-2792	8.0-8.4-2802	11.7-12.1-2812
15.7-16.1-2783	14.0-14.5-2793	12.4-12.7-2803	14.0-14.3-2813
16.4-16.7-2784	16.1-16.5-2794	18.5-18.8-2804	16.1-16.4-2814
21.3-21.6-2785	19.1-19.5-2795	19.5-20.0-2805	17.7-18.0-2815
23.6-24.0-2786	24.5-24.9-2796	20.7-21.0-2806	19.4-19.7-2816
28.8-29.2-2787	27.4-27.8-2797	23.3-23.6-2807	21.1-21.4-2817
30.3-30.7-2788	29.2-29.5-2798	27.5-27.8-2808	22.2-22.6-2818

Additionally, lithium bromide (LiBr) analysis should be conducted on water samples centrifuged from the following core samples:

U12g.12 WD-1	U12g WD-2
8.7-9.0	5.5-5.9
14.0-14.5	16.1-16.4
27.4-27.8	21.1-21.4

The volumes of these core samples should be measured.

The concentration of lithium bromide in the following samples should be measured:

U12g.12 WD-1 Sample 12/11/88 — 2819

U12g WD-2 Sample 12/19/88 — 2820

U12g WD-2 Sample 12/20/88 — 2821

United States Department of the Interior

GEOLOGICAL SURVEY

P. O. Box 327
Mercury, NV 89023

WBS 1.2.3.3.4.7.G
QA: "N/A"

January 24, 1989

TO: Venkatrao Thummala
Senior Engineer II
Holmes & Narver, Inc.
P. O. Box 1, M/S 607
Mercury, NV 89023

FROM: Lorrie Flint
USGS/NHP
P. O. Box 327, M/S 721
Mercury, NV 89023

SUBJECT: Laboratory measurements of core samples from prototype test WBS 1.2.6.9.4.2.1 by Holmes & Narver Materials Testing Laboratory (HNMTL).

Forty core samples were delivered to HNMTL according to correspondence to you from Mike Chornack dated 1/18/89. Among other tests, these core are to undergo testing for water release curve determination. Alan Flint has agreed that several additional tests be made on 4 of the core samples. I would like to choose 4 suitable core samples (samples with integrity that would not be likely to fracture during high speed centrifugation), to have run through Greg Moore's procedure for determination of water retention using the gas-drive method. When undercoring is done for the centrifuge samples, I would like the remains of the 2 1/2" core to be used to generate the fragment pieces for the mercury porosimetry test. In addition, the core from the centrifuge test would also be used in the porosimeter. In a conversation I had with Dale Daffern, he seemed to think this was possible. The outcome of these procedures would allow for the comparison of three methods of water retention determination: gas-drive, centrifuge and mercury porosimetry. In addition, there would be a comparison of the porosimetry methodology using fragments and intact core from one original core sample. Let me know if this is all feasible, and if so, I would like to visit the laboratory to choose the appropriate samples. Thanks, TV.

Lorrie Flint

USGS Hydrology Lab, 5-5998

HOLMES & NARVER
MATERIALS TESTING LABORATORY
YUCCA MOUNTAIN PROJECT

SAMPLE USE LOG SHEET Y

PROJECT NAME: *WET & DRY DRILLING*

REQUESTOR'S NAME: *MICHAEL P.CHORNACK*

MTL WORK REQ# *GT-38*

MTL SAMPLE LAB#(s): *2779 TO 2821*

WBS#: *1.2.3.3.6.1*

SAMPLE SOURCE: *U12g.12 – DD-1, DD-2, WD-1, & WD2*

Q.A.LEVEL: *III*

A3:57

MTL SAMPLE #	DATE	SAMPLED USE	SAMPLES RETURNED#	REMARKS	USED BY	dat
2779 thru 2790,	2-15-87	determine bulk densities	same	use of log sheet	JO	
2792, 2794	thru	& water saturations		initiated 3-25-87		3-25-87
thru 2796,	2-18-89					
2798 thru						
2810, 2812,						
2813, 2815,						
2816, 2818						
2791, 2793,	3-21-89	dry cut core from core	same		Hw	3-25-89
2797, 2811,	thru	part of sample &				
2814, 2817	3-23-89	centrifuse to remove				
		water, determine bulk				
		densities & water				
		saturations on other				
		sections of cores				

HOLMES & NARVER
MATERIALS TESTING LABORATORY
YUCCA MOUNTAIN PROJECT

SAMPLE USE LOG SHEET 2/

PROJECT NAME: *WET & DRY DRILLING*

REQUESTOR'S NAME: *MICHAEL P.CHORNACK*

MTL WORK REQ# *GT-38*

MTL SAMPLE LAB#(s): *2779 TO 2821*

WBS#: *1.2.3.3.6.1*

SAMPLE SOURCE: *U12g.12 – DD-1, DD-2, WD-1, & WD2*

Q.A.LEVEL: *III*

MTL SAMPLE #	DATE	SAMPLED USE	SAMPLES RETURNED#	REMARKS	USED BY	Date
2819, 2824	3-22-89	tested samples USED	samples used	recorded by J. Walker	Rai Singh	3-25-89
2821		water previously	during tested &			
		centrifuged from 6	hence couldn't			
		cores for lithium	be returned			
		bromide content				
2783, 2789	3-25-89	Cut cores for	same			3-25-89
2795, 2800		~~compression testing~~				
2818		water retention				
		Comprisen testing				

A3:58

HOLMES & NARVER
MATERIALS TESTING LABORATORY
YUCCA MOUNTAIN PROJECT

SAMPLE USE LOG SHEET

PROJECT NAME: *WET & DRY DRILLING*

REQUESTOR'S NAME: *MICHAEL P.CHORNACK*

MTL WORK REQ# *GT-38*

MTL SAMPLE LAB#(s): *2779 TO 2821*

WBS#: *1.2.3.3.6.1*

SAMPLE SOURCE: *U12g.12 – DD-1, DD-2, WD-1, & WD2*

Q.A.LEVEL: *III*

A3:59

MTL SAMPLE #	DATE	SAMPLED USE	SAMPLES RETURNED#	REMARKS	USED BY
2781, 2788,	3-28-84	cut off sections	all	put removed sections	J.
2789, 2795,		for use in CO_2		in oven	
2802, 2808,		saturation analysis			
2815, 2817					
2779 through	5-31-84	Cut off sections	all	returned when finished	
2788		for grain densities			
		+ wireless for			
		saturated permeabilities			

HOLMES & NARVER
MATERIALS TESTING LABORATORY
YUCCA MOUNTAIN PROJECT

SAMPLE USE LOG SHEET

PROJECT NAME: *WET & DRY DRILLING*

REQUESTOR'S NAME: *MICHAEL P.CHORNACK*

MTL WORK REQ# *GT-38*

MTL SAMPLE LAB#(s): *2779 TO 2821*

WBS#: *1.2.3.3.6.1*

SAMPLE SOURCE: *U12g.12 – DD-1, DD-2, WD-1, & WD2*

Q.A.LEVEL: *III*

A3:60

MTL SAMPLE #	DATE	SAMPLED USE	SAMPLES RETURNED#	REMARKS	USED BY
2779 thru 2788	7-26-89	grain densities		pieces used will be discarded when finished	
2780 thru 2788	7-26-89	helium permeameter			
2779, 2787, 2809, 2814	7-26-89	water retension			
2799 thru 2808	7-31-89	grain densities		pieces used will be discarded when finished	
2787 thru 2798	8-1-89	grain densities		Same	
2809 thru 2818	8-3-89	grain densities		Same	

HOLMES & NARVER
MATERIALS TESTING LABORATORY
YUCCA MOUNTAIN PROJECT

SAMPLE USE LOG SHEET

PROJECT NAME: *WET & DRY DRILLING*

REQUESTOR'S NAME: *MICHAEL P.CHORNACK*

MTL WORK REQ# *GT-38*

MTL SAMPLE LAB#(s): *2779 TO 2821*

WBS#: *1.2.3.3.6.1*

SAMPLE SOURCE: *U12g.12 - DD-1, DD-2, WD-1, & WD2*

Q.A.LEVEL: *III*

A3:61

MTL SAMPLE #	DATE	SAMPLED USE	SAMPLES RETURNED#	REMARKS	USED BY
2779	7/27/89	Water & gas permeability	None	To be undercored later	
2789	7/27/89	Water & gas permeability	None	To be undercored later	
2800	7/27/89	Water & gas permeability	None	To be undercored later	
2818	7/27/89	Water & gas permeability	None	To be undercored later	

APPENDIX A4

Yucca Mountain Project
wet and dry drilling
comparison of porosity determination methods
WBS 1.2.3.3.6.1

UNITED STATES DEPARTMENT OF ENERGY
NEVADA TEST SITE

YUCCA MOUNTAIN PROJECT
WET AND DRY DRILLING
COMPARISON OF POROSITY DETERMINATION METHODS
WBS 1.2.3.3.6.1

HOLMES & NARVER
MATERIALS TESTING LABORATORY
MERCURY NV

JUNE 1989

Table of contents

WET AND DRY DRILLING PROJECT

Introduction

The Holmes & Narver Materials Testing Laboratory (MTL) has recently completed a series of tests comparing different porosity measurement methods. The testing is part of a continuing work request to determine various properties of a set of cores from the United States Geological Survey's (USGS) Wet and Dry Drilling Project. The testing was initiated after USGS personnel expressed concerns over whether incomplete saturation of cores during the normal MTL porosity measurement method was yielding low porosity values. Initial results indicated that problems due to incomplete saturations were insignificant. Following those results MTL personnel also tested to see if reactivity between the distilled water used as the saturating fluid, and minerals in the core samples, contributed to incorrect porosity values. Initial results showed that reactivity between the cores and the water led to erroneously high estimates for all the non-welded tuff cores tested. The USGS investigators were then consulted and is was decided to further expand the testing so that the initial results could either be confirmed or repudiated. Further testing both confirmed and expanded upon the initial results.

Definitions

In order to clarify the upcoming discussion of test methods and results, definitions of the relevant terminology are offered. The effective porosity of a sample is defined as the ratio of the volume of interconnected void space within the sample matrix to the bulk volume of the sample. The non-effective porosity of a sample is defined as the ratio of the volume of isolated void space within the sample to the bulk volume of the sample. The total porosity of a sample is defined as the ratio of the volume of total void space within the sample to the bulk volume of the sample. The total porosity is equivalent to the sum of the effective and the non-effective porosities. The absolute effective porosity is hereby defined as the effective porosity of a sample to a non-reactive fluid. Porosity is usually expressed in total percent of the sample, or in porosity units. A porosity unit (pu) is equivalent to one percent porosity.

A hydratable mineral is a mineral which will, in the presence of water, adsorb and/or absorb water molecules into the molecular structure, thereby chemically bonding the water to the mineral. The inclusion of the water will result in an increase in the mass and the volume of the mineral. If temperatures are increased sufficiently the mineral will dehydrate resulting in a decrease of the mass and volume of the mineral. Two hydratable mineral groups are known to be present in some of the formations

encountered at the Nevada Test Site. The two mineral groups present are the zeolite and smectite groups. Both groups are composed of oxygen, silica, and aluminum molecules within tetrahedral frameworks, which provide locations for the retention of large cations. Water molecules are attracted and held due to the polarity of the molecule.

The fluid storage capacity of a sample is hereby defined as the ratio of the volume of fluid which can be contained in an initially dry sample to the bulk volume of the sample. The non-effective porosity will not contribute to the storage capacity. In a sample with hydratable minerals the water storage capacity will be different than the storage capacity to an inert fluid. Since an inert fluid will not chemically bond with the sample the storage capacity to the inert fluid is equivalent to the absolute effective porosity. If water is added to the hydratable sample, the intrusion of water into the chemical structure will add a new storage location to the storage capacity. However this will be offset by a decrease in the effective pore volume due to the expansion of the hydratable mineral. Whether the sample has a larger or smaller storage capacity for the water than for an inert fluid will depend on whether the volume of water chemically bound is greater or less than the amount of effective pore volume lost to the expansion of the hydratable minerals.

Test Procedures

Tests on ten samples from each of four separate core holes have been requested by USGS. For the comparison of porosity measurement methods, sections of two samples were selected from each set. The samples selected were the highest and lowest density samples in a set, which had a sufficient volume of core intact. This was done in order to provide the widest range of sample porosities. Cylindrical sections approximately 2.7 centimeters long were cut from each sample, yielding samples which had approximately equivalent bulk densities of around 80 cubic centimeters. Two of the sample sets were cored from welded volcanic tuffs and the other two from non-welded volcanic tuffs. the effective porosities of the eight samples were measured nine times using seven different procedures. The tests performed, and the order they were performed in, are:

First Test	Normal Water Saturation
Second Test	Carbon Dioxide/Water Saturation
Third Test	Toluene Saturation
Forth Test	Normal Water Saturation
Fifth Test	Helium Porosimeter
Sixth Test	2,500 ppm KCl
Seventh Test	20,000 ppm KCl
Eighth Test	Benzyl Alcohol
Ninth Test	Normal Water Saturation

All the tests, except the helium porosimeter test, were based upon the Archimedes Method, also known as the Hydrocarbon Resturation Method. The helium porosimeter test was based upon the Boyle's Law Double Cell Method. The Archimedes Method, although time consuming, is considered to be the most accurate method for determining effective porosities. When performed properly it is considered accurate to ±0.5 porosity units. The tests were all performed in accordance with the American Petroleum Institute's Recommended Practice for Core-Analysis Procedure (API RP 40).

The normal water saturation method is the procedure usually performed at the MTL. It was performed three times to insure that no irreversible mechanical or chemical alterations were occurring in the samples. It consists of first drying the samples in a convection oven at a temperature of 110 degrees Celsius for 24 to 48 hours. The samples were removed from the oven and their dry weights measured, then allowed to cool in a dessicator containing dessicant. The samples were then placed in an empty dessicator and subjected to a maximum obtainable vacuum for 24 to 48 hours. At that time deaerated distilled water was added to the dessicator until the cores were submerged. The cores were allowed to stabilize 12 to 24 hours then atmospheric pressure was applied to the submerged cores and they were allowed to stabilize another 12 to 24 hours. Following the final stabilization period a core would be removed, all surface liquid

carefully removed by hand, and the saturated weight measured. The core was then submerged in a container filled with distilled water and the submerged weight measured. From the dry weight, saturated weight and calculated saturation water density the pore volume of the sample was calculated. From the saturated weight, submerged weight, and calculated immersion water density the bulk volume of the sample was calculated. The effective porosity was then calculated from the pore volume and the bulk volume.

The second test performed was the one initially requested by USGS. It is similar to the normal saturation test, the only difference being that following the initial vacuum period carbon dioxide was injected into the dessicator. The cores were left in the carbon dioxide for 24 hours, then placed under another vacuum for 24 hours and the test completed as before. The test was performed since it was believed that due to the small pore channels inherent in the tuffs residual air could be trapped, subsequently resulting in incomplete saturation by the water and low porosity estimates. The reasoning behind the carbon dioxide is that it would replace any residual air left behind, and since it is soluble in water would allow complete saturation by the water.

The third test was performed using toluene as the saturation fluid. The test was done using the same procedure as with the water with two exceptions. First, due to the expense and

disposal problem of using a large amount of toluene in an immersion bath, the sample bulk volumes were taken as the averages of the values determined in the three normal water saturation tests. Second, the density of the toluene was determined using a calibrated pycnometer rather than a empirical correlation. The test was undertaken since it was felt possible that hydratable minerals could be present in the sample which could be causing the normal water saturation method to yield incorrect results. The Toluene was used since it is inert with hydratable minerals, has good wetting properties, and has a low vapor pressure. Toluene is also recommended in the API RP 40 for this test.

After discrepancies between the results from the water and toluene tests were noted another water saturation test was conducted to insure that irreversible alterations had not occurred in the samples. After the results from the second water saturation tests were shown to be in agreement with the initial results, the data was discussed with USGS personnel. At that time it was agreed that due to the magnitude of the discrepancies more testing should be conducted to further explore the problem.

In order to measure the effective porosities by a totally different method a Boyle's Law Double Cell Helium Porosimeter was constructed. In order to simplify the procedure a general modification recommended in API RP 40 was used. The modification

bases the calculations on an empirical correlation rather than on the theoretical Boyles Law. The empirical correlation compensates for deviations from the idealized Boyle's Law and for transient temperature changes due to gas expansion. The equipment consists of two chambers, a core chamber and a gas chamber, a compressed helium source, a digital absolute pressure gauge, a vacuum pump and gauge, and connecting tubing and valves. The equipment was connected and checked for leaks then the volume of several metal cylinders determined from their buoyancy. Before the samples could be tested a calibration curve was calculated using the known volumes of the metal cylinders. The calibration procedure consists of first placing one of the cylinders in the sample chamber then pulling a vacuum on both chambers. The pressure inlet to the sample chamber is closed and helium admitted into the gas chamber until a pressure of 100 psi ± 0.5 psig registers on the digital absolute pressure gauge. The gas is allowed to stabilize for 2 minutes then the initial pressure is recorded. The sample chamber is opened to the gas and the system allowed to stabilize for 10 minutes after which the final pressure is recorded. The volume of the samples is plotted against the ratio of the inlet and outlet pressure and a quantitative correlation developed. The calibration data for the helium porosimeter is shown in Table 1. The graph and quantitative correlation are shown in Figure 1. The correlation coefficient indicates that the volume - pressure ratio relationship is quite well defined.

To determine the effective porosity of a sample, the oven dried sample was put through the same procedure. When the initial and final pressures had been determined the correlation presented in Figure 1 was used to determine a sample volume. The sample volume is the sum of the grain volume and the non-effective pore volume; when subtracted from the bulk volume the difference is the effective pore volume. The bulk volumes were taken as the averages of the volumes determined in the three normal water saturations.

Following the helium porosimeter tests, the cores are tested with two concentrations of potassium chloride (KCI) brines. They were first saturated with distilled water which had 2,500 parts per million (ppm) KCl dissolved in it. The same methodology used for the toluene saturation was followed. After the test was completed the cores were placed in a modified triaxial soil permeameter and flushed with three to five pore volumes of distilled water. The cores were then tested with 20,000 ppm KCl and again flushed. Potassium chloride brines were used since they have been shown to reduce and even reverse hydration in the smectite group.

The next test was conducted using benzyl alcohol. It was used so that the results from another inert liquid test could be compared with the toluene results to insure that variations in fluid

wettablilities were not influencing the results. The tests were conducted using the toluene saturation methodology. following the tests it was necessary to put the cores through a water saturation and several days in the oven to remove minor amounts of residual benzyl alcohol.

A final normal water saturation test was performed to conclude the testing. The final test was done in order to check that the final properties of the cores were the same as when the testing began. The samples have been saved and stored in case further testing or mineralogical analysis of the samples is desired.

Results

The measured and calculated data from the nine tests are presented in Tables 2 through 10. As part of the tests the cores were oven dried and weighed before each test. A comparison of the initial dry weights, for the non-welded and the welded tuff samples, are shown in Figures 2 and 3 respectively. As can be seen from the Figures, the initial dry weights for all the samples remained consistent throughout the testing. This indicates that the integrity of the samples was maintained, and that the drying process was yielding constant results. It is assumed that the drying process used removed approximately 100 % of the water from the samples.

The results for each of the samples are compared in Tables 11 through 18. The results of each test are shown relative to the average effective porosities determined from the three normal water saturations. The results are also compared to the average effective porosities determined from the three inert fluids; that is the toluene, helium, and benzyl alcohol tests. the results for the individual samples are compared graphically in Figures 4 through 11.

Non-Welded Tuffs

Comparison of the non-welded tuff results are shown in Tables 11 through 14 and Figures 4 through 7. From the results it is obvious two different values are being measured. The tests based on water are yielding the water storage capacities of the samples. The tests performed with inert fluids, that is the helium, toluene, and benzyl alcohol tests, are yielding the absolute effective porosities of the samples. Since hydratable minerals are present the two values are not equivalent. The inclusion of the water into the chemical structures of the hydratable minerals is related to the size and polarity of the water molecules. The larger toluene and benzyl alcohol molecules, and the nonpolar helium molecules, are excluded from the hydratable minerals. The fact that the water storage capacities are greater than the absolute effective porosities indicates that a greater volume of water is being stored in the

hydratable minerals than is being lost to mineral expansion. This is apparently an effect of the zeolites as smectites are believed to have the opposite effect.

The slight increase in the storage capacities when a 20,000 ppm KCl brine was used were probably due to the dehydration of small amounts of smectite present in the samples. The lack of significant and consistent changes following the carbon dioxide preflush indicates that incomplete saturation is not a problem in the welded tuff samples. The good correlation of the normal water saturation tests indicates that a minimal amount of irreversible damage is being done during the drying process.

It is interesting to note that the differences between the water storage capacities and the absolute effective porosities from the four non-welded tuff samples are all approximately seven porosity units. since the samples are approximately the same size and were closely situated in the formation, it is reasonable to assume that they contain similar amounts of zeolite. It then appears that the amount of zeolite, and hence the absorptive capacity of the sample to water and ions in solution, is related to the difference between the water storage capacity and the absolute effective porosity of the sample.

Welded Tuffs

Comparison of the welded tuff results are shown in Tables 15 through 18 and Figures 8 through 11. The outstanding agreement between the various test procedures indicates that any of the methods will provide accurate porosity results for future welded tuff samples. The agreement also indicates that problems in measuring porosities are unique to the non-welded tuffs, and are due to the mineralogical composition of the non-welded tuffs rather than errors in the various procedures.

As can be seen from the results, the carbon dioxide preflush increased the measured porosities in all the welded tuffs slightly. However, since the increases were less than the error range of the measurement method the results are inconclusive. Even if it is assumed the increases were due solely to increased saturations resulting from the carbon dioxide preflush, the discrepancies can be considered negligible.

Implications and Recommendations

The presence of hydratable minerals will cause problems for any test performed using water. One possible solution is to change the drying process. Currently samples are dried in a convection oven at 110 degrees Celcius for 24 to 48 hours. This procedure should lead to almost complete removal of all the water in a

sample, with a minimal amount of irreversible damage to the sample. If a humidity controlled oven, or a vacuum oven, were used it might be possible to remove all the pore water while leaving all the chemically bound water. If all samples could be dried to that state, further amounts of water would not be reactive and all tests could be performed relative to that starting point. However, due to the strong pore water retention qualities exhibited by the tuffs, it could be difficult to reach an equilibrium where the pore water is totally removed while the zeolites and smectites remain completely hydrated. If the pore water is only partly removed, or if the hydratable minerals are partly dehydrated, than the problem will be further complicated. In addition, the MTL does not currently have the necessary equipment to perform that type of limited drying. The following discussion will be based on the assumption that the samples will be completely dried using the convection oven before testing, and concerns only samples with hydratable minerals.

As shown in this report the porosity of a sample will vary with the method by which it is determined. Since it will be necessary to saturate the cores with water for other testing the MTL recommends that the samples be first tested using a helium porosimeter followed by the normal water saturation procedure. As previously defined, the results would be referred to as the absolute effective porosity and the water storage capacity. In addition it is felt that the discrepancy between the two values

may relate to the ability of the rock to absorb ions in solution.

Grain densities have previously been determined at the MTL using water. A sample is crushed to a fine powder, oven dried in the convection oven, weighed and added to a calibrated pycnometer, then distilled water is added to pycnometer and the volume of the grain sample determined, from which the grain density is calculated. If zeolites are present the volume of water added to the pycnometer will be greater, resulting in a lower estimate of the sample volume and a erroneously high calculated grain density. The MTL recommends modifying the helium porosimeter to accurately measure the volume of a crushed grain sample rather than using water in a calibrated pycnometer. It should be noted that this will provide the dehydrated grain density. If hydrated grain densities are desired it will be necessary to use a humidity controlled or vacuum oven to equilibrate the crushed grain sample at the correct saturation.

The presence of hydratable minerals will result in the alteration of the pore structure of a sample when water is used as the test fluid in a permeability test. The expansion of the minerals due to hydration will cause a decrease in the effective flow channel radii and an increase in the flow channel tortuosity, both of which lead to reduced permeability. Consequently water determined permeabilities will be lower than those determined using inert liquids or equivalent liquid permeabilities

extrapolated from gas permeability tests. The MTL recommends that when only saturated permeabilities are required, that both water and equivalent liquid permeabilities from gas tests be determined and compared.

The MTL constructs capillary pressure curves using both the centrifuge and the mercury porosimeter methods. Although the curves should correlate the MTL has previously noted significant discrepancies between the results from the two methods. It now appears that part of the problem is due to the presence of hydratable minerals. The measured capillary pressures are plotted as a function of the percent of the pore volume which remains saturated. The mercury porosimeter curve is based on the absolute effective porosity since mercury is an inert fluid in this situation. However the centrifuge curve, since water is used, is based on the larger water storage capacity volume. The result is that the mercury porosimeter curve plots to the left of the centrifuge curve. This also helps account for previous discrepancies between the grain densities and bulk densities calculated from the mercury porosimeter data and those determined using water based methods. The MTL recommends plotting the centrifuge capillary pressure curves relative to both the water storage capacity and the absolute effective porosity. It is further recommended that the mercury porosimeter and centrifuge determined curves be compared on the mutual basis of the absolute effective porosities.

Conclusions

A variety of tests have been performed to determine the effective porosities of four welded and four non-welded tuff samples. The good correlation between the results for the welded tuff samples indicates that water is nonreactive with the samples. Therefore normal testing procedures followed at the MTL are acceptable for use in any future testing of welded tuff samples. The results for the non-welded tuff samples indicate the water based test methods will yield consistently higher estimates of porosity than will tests performed using inert fluids. The discrepancy between the results is believed to be due to the presence of hydratable minerals in the non-welded tuff samples. The presence of the hydratable minerals will also affect other water based tests performed at the MTL.

Work Performed By:

Jerry N. Walker
Engineer

Holmes & Narver, Inc.
Materials Testing Laboratory
June 21, 1989

HOLMES & NARVER, INC.

MATERIALS TESTING LABORATORY

NEVADA TEST SITE

TABLE 1

CALIBRATION SHEET FOR HELIUM POROSIMETER

Project: Wet & Dry Drilling
Requestor: Dr. Alan L. Flint
Organization: USGS
Address: Box 327, M/S 721, Mercury, NV
Phone: 5-5805
Tested by: Jerry W. Walker
Test date: 4-25-89 through 4-26-89

Checked by: John G. Moore
Check date: 6/14/89
NTL Lab #: N/A
Request #: GT-38
H&N ID #: 50036C
WBS #: 1.2.3.3.6.1
WIN #: YMP:NTS:WI:89-006
QA level: III

NTL Sample Number	Uncoated Weight (g)	Submerged Weight (g)	Water Temp. (Celsius)	Water Density (g/cc)	Core Volume (cc)	Bulk Density (g/cc)	Initial Pressure (I,psia)	Final Pressure (F,psia)	Pressure Ratio (I/F)
1	1343.80	1174.20	20.8	0.9980	169.93	7.91	99.76	63.60	1.569
2	869.00	758.68	20.8	0.9980	110.54	7.86	99.86	55.44	1.801
3	506.35	441.84	20.8	0.9980	64.64	7.83	100.07	50.47	1.983
4	563.75	491.90	20.8	0.9980	71.99	7.83	99.78	51.07	1.954
5	282.18	246.23	20.9	0.9980	36.02	7.83	100.05	47.72	2.097
6	112.58	98.22	20.9	0.9980	14.39	7.82	100.39	46.03	2.181
7	222.25	193.40	20.9	0.9980	28.91	7.69	99.63	46.91	2.124
8	65.66	57.12	20.9	0.9980	8.56	7.67	99.64	45.21	2.204
9	76.99	67.17	20.9	0.9980	9.84	7.82	100.25	45.56	2.200
10	12.58	10.98	20.9	0.9980	1.60	7.85	99.63	44.63	2.232
11	6.29	5.49	20.9	0.9980	0.80	7.85	100.19	44.83	2.235
12	0.00	0.00	N/A	N/A	0.00	N/A	99.93	44.64	2.239

EQUIPMENT USED	CALIBRATION DUE DATE
Mettler PK 4800 Digital Balance, PTL 4513	6-22-89
Omega 871A Digital Thermometer, PTL 6976	9-13-89
Despatch Oven V-31-2, PTL 87984	6-28-89
Heise Digital Absolute Pressure Gauge, PTL 8784	8-18-89

REMARKS: None

HOLMES & NARVER, INC.

MATERIALS TESTING LABORATORY

NEVADA TEST SITE

TABLE 2

FIRST NORMAL WATER SATURATION DATA SHEET FOR SAMPLE CORES

Project: Wet & Dry Drilling
Requestor: Dr. Alan L. Flint
Organization: USGS
Address: Box 327, M/S 721, Mercury, NV
Phone: 5-5805
Tested by: Jerry R. Walker
Test date: 3-28-89 through 4-1-89
QA level: III

Checked by: John C. Moore
Check date: 6/30/89
MTL Lab #: 2781,2788,2789,2795,2800, 2802,2813,2815
Request #: GT-38
H&N ID #: 50036C
WBS #: 1.2.3.3.6.1
WIN #: YMP:NTS:WI:89-806

Saturation Water Temperature (C):	20.1	Saturation Water Density (g/cc):	0.9982
Immersion Water Temperature (C):	20.6	Immersion Water Density (g/cc):	0.9981

MTL Sample Number	Core Hole Number	Depth Interval (ft)	Dry Weight (g)	Saturated Weight (g)	Pore Volume (cc)	Submerged Weight (g)	Bulk Volume (cc)	Effective Porosity (%)
*2781	U12g.12 DD-1	8.0-8.4	152.82	172.73	19.95	89.63	83.26	24.0
*2788	U12g.12 DD-1	30.3-30.7	92.88	131.12	38.31	54.64	76.63	50.0
*2789	U12g.12 WD-1	1.8-2.3	100.59	138.67	38.15	59.73	79.09	48.2
*2795	U12g.12 WD-1	19.1-19.5	128.59	151.18	22.63	73.57	77.76	29.1
**2800	U12g DD-2	3.6-4.0	168.31	179.52	11.23	104.01	75.66	14.8
**2802	U12g DD-2	8.0-8.4	175.65	190.65	15.03	108.55	82.26	18.3
**2813	U12g WD-2	14.0-14.3	183.92	194.37	10.47	113.71	80.82	13.0
**2815	U12g WD-2	17.7-18.0	175.59	187.57	12.00	108.52	79.14	15.2

EQUIPMENT USED	CALIBRATION DUE DATE
Mettler PK 4800 Digital Balance, PTL 4513	6-22-89
Omega 871A Digital Thermometer, PTL 6976	9-13-89
Despatch Oven V-31-2, PTL 8784	6-28-89

REMARKS: *Non-welded tuff cores
**Welded tuff cores

HOLMES & NARVER, INC.

MATERIALS TESTING LABORATORY

NEVADA TEST SITE

TABLE 3

CARBON DIOXIDE/WATER SATURATION DATA SHEET FOR SAMPLE CORES

Project: Wet & Dry Drilling
Requestor: Dr. Alan L. Flint
Organization: USGS
Address: Box 327, M/S 721, Mercury, NV
Phone: 5-5805
Tested by: Jerry R. Walker
Test date: 4-2-89 through 4-8-89
QA level: III

Checked by: John G. Moore
Check date: 9/20/89
NTL Lab #: 2781,2788,2789,2795,2800, 2802,2813,2815
Request #: GT-38
N&N ID #: 50036C
WBS #: 1.2.3.3.6.1
WIN #: YMP:NTS:WI:89-006

Saturation Water Temperature (C): 20.9
Immersion Water Temperature (C): 20.7

Saturation Water Density (g/cc): 0.9980
Immersion Water Density (g/cc): 0.9981

NTL Sample Number	Core Hole Number	Depth Interval (ft)	Dry Weight (g)	Saturated Weight (g)	Pore Volume (cc)	Submerged Weight (g)	Bulk Volume (cc)	Effective Porosity (%)
*2781	U12g.12 DD-1	8.0-8.4	152.90	172.80	19.94	89.57	83.39	23.9
*2788	U12g.12 DD-1	30.3-30.7	93.02	131.16	38.22	54.54	76.77	49.8
*2789	U12g.12 WD-1	1.8-2.3	100.63	138.79	38.24	59.73	79.21	48.3
*2795	U12g.12 WD-1	19.1-19.5	128.11	151.31	23.25	73.52	77.94	29.8
**2800	U12g DD-2	3.6-4.0	168.09	179.67	11.60	103.92	75.90	15.3
**2802	U12g DD-2	8.0-8.4	175.42	190.78	15.39	108.49	82.45	18.7
**2813	U12g WD-2	14.0-14.3	183.70	194.42	10.74	113.65	80.93	13.3
**2815	U12g WD-2	17.7-18.0	175.38	187.68	12.32	108.53	79.30	15.5

EQUIPMENT USED	CALIBRATION DUE DATE
Mettler PK 4800 Digital Balance, PTL 4513	6-22-89
Omega 871A Digital Thermometer, PTL 6976	9-13-89
Despatch Oven V-31-2, PTL 8784	6-28-89

REMARKS: *Non-welded tuff cores
**Welded tuff cores

HOLMES & NARVER, INC.

MATERIALS TESTING LABORATORY

NEVADA TEST SITE

TABLE 4

TOLUENE SATURATION DATA SHEET FOR SAMPLE CORES

Project: Wet & Dry Drilling
Requestor: Dr. Alan L. Flint
Organization: USGS
Address: Box 327, M/S 721, Mercury, NV
Phone: 5-5805
Tested by: Jerry M. Walker
Test date: 4-9-89 through 4-14-89
QA level: III

Checked by: John C. Moore
Check date: 4/20/89
MTL Lab #: 2781,2788,2789,2795,2800, 2802,2813,2815
Request #: GT-38
H&N ID #: 50036C
WBS #: 1.2.3.3.6.1
WIN #: YMP:NTS:WI:89-006

Saturation Fluid Temperature (C): 21.3
Immersion Water Temperature (C): N/A

Toluene Density (g/cc): 0.8643
Immersion Water Density (g/cc): N/A

MTL Sample Number	Core Hole Number	Depth Interval (ft)	Dry Weight (g)	Saturated Weight (g)	Pore Volume (cc)	Submerged Weight (g)	Bulk Volume (cc)	Effective Porosity (%)
*2781	U12g.12 DD-1	8.0-8.4	152.91	165.11	14.12	N/A	83.31	16.9
*2788	U12g.12 DD-1	30.3-30.7	93.08	121.30	32.65	N/A	76.72	42.6
*2789	U12g.12 WD-1	1.8-2.3	100.73	128.81	32.49	N/A	79.24	41.0
*2795	U12g.12 WD-1	19.1-19.5	128.33	143.64	17.71	N/A	77.87	22.7
**2800	U12g DD-2	3.6-4.0	168.10	177.78	11.20	N/A	75.66	14.8
**2802	U12g DD-2	8.0-8.4	175.42	188.34	14.95	N/A	82.27	18.2
**2813	U12g WD-2	14.0-14.3	183.71	192.61	10.30	N/A	80.82	12.7
**2815	U12g WD-2	17.7-18.0	175.38	185.70	11.94	N/A	79.14	15.1

EQUIPMENT USED	CALIBRATION DUE DATE
Mettler PK 4800 Digital Balance, PTL 4513	6-22-89
Omega 871A Digital Thermometer, PTL 6976	9-13-89
Fisher Scientific Top Loading Balance, PTL 2678	9-3-89
Despatch Oven V-31-2, PTL 8784	6-28-89

REMARKS: *Non-welded tuff cores
**Welded tuff cores
Toluene density determined using calibrated pycnometer.

HOLMES & NARVER, INC.

MATERIALS TESTING LABORATORY

NEVADA TEST SITE

TABLE 5

SECOND NORMAL WATER SATURATION DATA SHEET FOR SAMPLE CORES

Project: Wet & Dry Drilling
Requestor: Dr. Alan L. Flint
Organization: USGS
Address: Box 327, M/S 721, Mercury, NV
Phone: 5-5805
Tested by: Jerry K. Walker
Test date: 4-16-89 through 4-20-89
QA level: III

Checked by: John G. Moore
Check date: 4/20/89
MTL Lab #: 2781,2788,2789,2795,2800, 2802,2813,2815
Request #: GT-38
H&N ID #: 50036C
WBS #: 1.2.3.3.6.1
WIN #: YMP:NTS:WI:89-006

Saturation Water Temperature (C): 21.8
Immersion Water Temperature (C): 19.9

Saturation Water Density (g/cc): 0.9978
Immersion Water Density (g/cc): 0.9982

MTL Sample Number	Core Hole Number	Depth Interval (ft)	Dry Weight (g)	Saturated Weight (g)	Pore Volume (cc)	Submerged Weight (g)	Bulk Volume (cc)	Effective Porosity (%)
*2781	U12g.12 DD-1	8.0-8.4	152.28	172.70	20.46	89.46	83.39	24.5
*2788	U12g.12 DD-1	30.3-30.7	93.18	131.15	38.05	54.56	76.73	49.6
*2789	U12g.12 WD-1	1.8-2.3	100.64	138.68	38.12	59.65	79.17	48.2
*2795	U12g.12 WD-1	19.1-19.5	128.04	151.25	23.26	73.52	77.87	29.9
**2800	U12g DD-2	3.6-4.0	168.11	179.51	11.42	103.98	75.66	15.1
**2802	U12g DD-2	8.0-8.4	175.44	190.64	15.23	108.51	82.28	18.5
**2813	U12g WD-2	14.0-14.3	183.71	194.36	10.67	113.69	80.81	13.2
**2815	U12g WD-2	17.7-18.0	175.40	187.55	12.18	108.57	79.12	15.4

EQUIPMENT USED	CALIBRATION DUE DATE
Mettler PK 4800 Digital Balance, PTL 4513	6-22-89
Omega 871A Digital Thermometer, PTL 6976	9-13-89
Despatch Oven V-31-2, PTL 8784	6-28-89

REMARKS: *Non-welded tuff cores
**Welded tuff cores

HOLMES & NARVER, INC.

MATERIALS TESTING LABORATORY

NEVADA TEST SITE

TABLE 6

HELIUM POROSIMETER DATA SHEET FOR SAMPLE CORES

Project: Wet & Dry Drilling
Requestor: Dr. Alan L. Flint
Organization: USGS
Address: Box 327, M/S 721, Mercury, NV
Phone: 5-5805
Tested by: Jeffy N. Walker
Test date: 4-25-89 through 4-26-89
QA level: III

Checked by: John G. Moore
Check date: 6/30/89
NTL Lab #: 2781,2788,2789,2795,2800, 2802,2813,2815
Request #: GT-38
M&N ID #: 50036C
WBS #: 1.2.3.3.6.1
WIN #: YMP:NTS:WI:89-006

NTL Sample Number	Core Hole Number	Depth Interval (ft)	Dry Weight (g)	Initial Pressure (psia)	Final Pressure (psia)	Grain Volume (cc)	Bulk Volume (cc)	Effective Porosity (%)
*2781	U12g.12 DD-1	8.0-8.4	153.08	99.92	50.89	69.60	83.31	16.5
*2788	U12g.12 DD-1	30.3-30.7	93.32	99.90	48.36	43.70	76.72	43.0
*2789	U12g.12 WD-1	1.8-2.3	100.80	99.72	48.56	46.79	79.24	41.0
*2795	U12g.12 WD-1	19.1-19.5	128.56	100.05	49.95	59.58	77.87	23.5
**2800	U12g DD-2	3.6-4.0	168.12	100.33	50.56	64.30	75.66	15.0
**2802	U12g DD-2	8.0-8.4	175.44	99.84	50.59	67.05	82.27	18.5
**2813	U12g WD-2	14.0-14.3	183.74	100.07	51.10	70.90	80.82	12.3
**2815	U12g WD-2	17.7-18.0	175.40	100.31	50.85	67.27	79.14	15.0

EQUIPMENT USED	CALIBRATION DUE DATE
Mettler PK 4800 Digital Balance, PTL 4513	6-22-89
Omega 871A Digital Thermometer, PTL 6976	9-13-89
Despatch Oven V-31-2, PTL 8784	6-28-89
Heise Digital Absolute Pressure Gauge, PTL 1985	8-18-89

REMARKS: *Non-welded tuff cores
**Welded tuff cores

HOLMES & NARVER, INC.

MATERIALS TESTING LABORATORY

NEVADA TEST SITE

TABLE 7

2,500 PPM KCl SATURATION DATA SHEET FOR SAMPLE CORES

Project: Wet & Dry Drilling
Requestor: Dr. Alan L. Flint
Organization: USGS
Address: Box 327, M/S 721, Mercury, NV
Phone: 5-5805
Tested by: Jerry N. Walker
Test date: 4-9-89 through 4-14-89
QA level: III

Checked by: John E. Moore
Check date: 4/20/89
NTL Lab #: 2781,2788,2789,2795,2800, 2802,2813,2815
Request #: GT-38
H&N ID #: 50036C
WBS #: 1.2.3.3.6.1
WIN #: YMP:NTS:W:89-006

Saturation Fluid Temperature (C): 21.2
Immersion Water Temperature (C): N/A

2,500 PPM KCl Density (g/cc): 0.9990
Immersion Water Density (g/cc): N/A

NTL Sample Number	Core Hole Number	Depth Interval (ft)	Dry Weight (g)	Saturated Weight (g)	Pore Volume (cc)	Submerged Weight (g)	Bulk Volume (cc)	Effective Porosity (%)
*2781	U12g.12 DD-1	8.0-8.4	152.40	172.74	20.36	N/A	83.31	24.4
*2788	U12g.12 DD-1	30.3-30.7	92.85	131.07	38.26	N/A	76.72	49.9
*2789	U12g.12 WD-1	1.8-2.3	100.51	138.75	38.28	N/A	79.24	48.3
*2795	U12g.12 WD-1	19.1-19.5	127.88	151.11	23.25	N/A	77.87	29.9
**2800	U12g DD-2	3.6-4.0	168.12	179.52	11.41	N/A	75.66	15.1
**2802	U12g DD-2	8.0-8.4	175.42	190.59	15.19	N/A	82.27	18.5
**2813	U12g WD-2	14.0-14.3	183.71	194.31	10.61	N/A	80.82	13.1
**2815	U12g WD-2	17.7-18.0	175.39	187.52	12.14	N/A	79.14	15.3

EQUIPMENT USED	CALIBRATION DUE DATE
Mettler PK 4800 Digital Balance, PTL 4513	6-22-89
Omega 871A Digital Thermometer, PTL 6976	9-13-89
Fisher Scientific Top Loading Balance, PTL 2678	9-3-89
Despatch Oven V-31-2, PTL 8784	6-28-89

REMARKS: *Non-welded tuff cores
**Welded tuff cores
KCl brine density determined using calibrated pycnometer.

HOLMES & NARVER, INC.

MATERIALS TESTING LABORATORY

NEVADA TEST SITE

TABLE 8

20,000 PPM KCl SATURATION DATA SHEET FOR SAMPLE CORES

Project: Wet & Dry Drilling
Requestor: Dr. Alan L. Flint
Organization: USGS
Address: Box 327, M/S 721, Mercury, NV
Phone: 5-5805
Tested by: Betty M. Walker
Test date: 5-7-89 through 5-10-89
QA level: III

Checked by: John G. Moore
Check date: 6/20/89
NTL Lab #: 2781,2788,2789,2795,2800, 2802,2813,2815
Request #: GT-38
M&N ID #: 50036C
WBS #: 1.2.3.3.6.1
WIN #: YMP:NTS:WI:89-006

Saturation Fluid Temperature (C): 20.7
Immersion Water Temperature (C): N/A

20,000 PPM KCl Density (g/cc): 1.0107
Immersion Water Density (g/cc): N/A

NTL Sample Number	Core Hole Number	Depth Interval (ft)	Dry Weight (g)	Saturated Weight (g)	Pore Volume (cc)	Submerged Weight (g)	Bulk Volume (cc)	Effective Porosity (%)
*2781	U12g.12 DD-1	8.0-8.4	152.26	172.76	20.28	N/A	83.31	24.3
*2788	U12g.12 DD-1	30.3-30.7	92.61	131.79	38.77	N/A	76.72	50.5
*2789	U12g.12 WD-1	1.8-2.3	100.35	139.46	38.70	N/A	79.24	48.8
*2795	U12g.12 WD-1	19.1-19.5	127.69	151.54	23.60	N/A	77.87	30.3
**2800	U12g DD-2	3.6-4.0	168.02	179.57	11.43	N/A	75.66	15.1
**2802	U12g DD-2	8.0-8.4	175.39	190.77	15.22	N/A	82.27	18.5
**2813	U12g WD-2	14.0-14.3	183.69	194.43	10.63	N/A	80.82	13.1
**2815	U12g WD-2	17.7-18.0	175.36	187.64	12.15	N/A	79.14	15.4

EQUIPMENT USED	CALIBRATION DUE DATE
Mettler PK 4800 Digital Balance, PTL 4513	6-22-89
Omega 871A Digital Thermometer, PTL 6976	9-13-89
Fisher Scientific Top Loading Balance, PTL 2678	9-3-89
Despatch Oven V-31-2, PTL 8784	6-28-89

REMARKS: *Non-welded tuff cores
**Welded tuff cores
KCl brine density determined using calibrated pycnometer.

HOLMES & NARVER, INC.

MATERIALS TESTING LABORATORY

NEVADA TEST SITE

TABLE 9

BENZYL ALCOHOL SATURATION DATA SHEET FOR SAMPLE CORES

Project: Wet & Dry Drilling
Requestor: Dr. Alan L. Flint
Organization: USGS
Address: Box 327, M/S 721, Mercury, NV
Phone: 5-5805
Tested by: Jerry N. Walker
Test date: 5-16-89 through 5-18-89
QA level: III

Checked by: John G. Moore
Check date: 6/22/89
MTL Lab #: 2781,2788,2789,2795,2800, 2802,2813,2815
Request #: GT-38
H&N ID #: 50036C
WBS #: 1.2.3.3.6.1
WIN #: YMP:NTS:WI:89-006

Saturation Fluid Temperature (C): 21.4
Immersion Water Temperature (C): N/A

Benzyl Alcohol Density (g/cc): 1.0428
Immersion Water Density (g/cc): N/A

MTL Sample Number	Core Hole Number	Depth Interval (ft)	Dry Weight (g)	Saturated Weight (g)	Pore Volume (cc)	Submerged Weight (g)	Bulk Volume (cc)	Effective Porosity (%)
*2781	U12g.12 DD-1	8.0-8.4	153.18	168.05	14.26	N/A	83.31	17.1
*2788	U12g.12 DD-1	30.3-30.7	93.25	127.41	32.76	N/A	76.72	42.7
*2789	U12g.12 WD-1	1.8-2.3	100.95	135.05	32.70	N/A	79.24	41.3
*2795	U12g.12 WD-1	19.1-19.5	128.51	147.21	17.93	N/A	77.87	23.0
**2800	U12g DD-2	3.6-4.0	168.05	179.64	11.11	N/A	75.66	14.7
**2802	U12g DD-2	8.0-8.4	175.43	190.90	14.84	N/A	82.27	18.0
**2813	U12g WD-2	14.0-14.3	183.74	194.32	10.15	N/A	80.82	12.6
**2815	U12g WD-2	17.7-18.0	175.40	187.71	11.80	N/A	79.14	14.9

EQUIPMENT USED	CALIBRATION DUE DATE
Mettler PK 4800 Digital Balance, PTL 4513	6-22-89
Omega 871A Digital Thermometer, PTL 6976	9-13-89
Fisher Scientific Top Loading Balance, PTL 2678	9-3-89
Despatch Oven V-31-2, PTL 8784	6-28-89

REMARKS: *Non-welded tuff cores
**Welded tuff cores
Benzyl alcohol density determined using calibrated pycnometer.

HOLMES & NARVER, INC.

MATERIALS TESTING LABORATORY

NEVADA TEST SITE

TABLE 10

THIRD NORMAL WATER SATURATION DATA SHEET FOR SAMPLE CORES

Project: Wet & Dry Drilling
Requestor: Dr. Alan L. Flint
Organization: USGS
Address: Box 327, M/S 721, Mercury, NV
Phone: 5-5805
Tested by: Jerry P. Walker
Test date: 5-22-89 through 5-26-89
QA level: III

Checked by: John G. Moore
Check date: 6/22/89
NTL Lab #: 2781,2788,2789,2795,2800, 2802,2813,2815
Request #: GT-38
H&N ID #: 50036C
WBS #: 1.2.3.3.6.1
WIN #: YMP:NTS:WI:89-006

Saturation Water Temperature (C):	21.2	Saturation Water Density (g/cc):	0.9979
Immersion Water Temperature (C):	19.5	Immersion Water Density (g/cc):	0.9983

NTL Sample Number	Core Hole Number	Depth Interval (ft)	Dry Weight (g)	Saturated Weight (g)	Pore Volume (cc)	Submerged Weight (g)	Bulk Volume (cc)	Effective Porosity (%)
*2781	U12g.12 DD-1	8.0-8.4	152.86	172.52	19.70	89.37	83.29	23.7
*2788	U12g.12 DD-1	30.3-30.7	93.22	131.43	38.29	54.75	76.81	49.8
*2789	U12g.12 WD-1	1.8-2.3	101.46	139.20	37.82	59.87	79.46	47.6
*2795	U12g.12 WD-1	19.1-19.5	128.89	151.56	22.72	73.71	77.98	29.1
**2800	U12g DD-2	3.6-4.0	168.61	179.61	11.02	104.08	75.66	14.6
**2802	U12g DD-2	8.0-8.4	175.83	190.82	15.02	108.69	82.27	18.3
**2813	U12g WD-2	14.0-14.3	184.01	194.43	10.44	113.74	80.83	12.9
**2815	U12g WD-2	17.7-18.0	175.69	187.62	11.95	108.58	79.17	15.1

EQUIPMENT USED	CALIBRATION DUE DATE
Mettler PK 4800 Digital Balance, PTL 4513	6-22-89
Omega 871A Digital Thermometer, PTL 6976	9-13-89
Despatch Oven V-31-2, PTL 8784	6-28-89

REMARKS: *Non-welded tuff cores
**Welded tuff cores

HOLMES & NARVER, INC.

MATERIALS TESTING LABORATORY

NEVADA TEST SITE

TABLE 11

COMPARISON OF RESULTS FOR SAMPLE NUMBER 2781

Project: Wet & Dry Drilling
Requestor: Dr. Alan L. Flint
Organization: USGS
Address: Box 327, M/S 721, Mercury, NV
Phone: 5-5805
Tested by: Jerry N. Walker
Test date: 3-28-89 through 4-1-89
QA level: III

Checked by: John E. Moore
Check date: June 20, 1989
NTL Lab #: 2781
Request #: GT-38
H&N ID #: 50036C
WBS #: 1.2.3.3.6.1
WIN #: YMP:NTS:UI:89-006

Non-welded tuff sample from core hole U12g.12 DD-1 at depth interval of 8.0 to 8.4 feet.
Average effective porosity from water saturations, in porosity units, is 24.1
Average effective porosity from inert fluid tests, in porosity units, is 16.8

Test Number	Test Type Performed	Measured Effective Porosity (pu)	Difference From Avg. Water (pu)	Error to Avg. Water (%)	Difference From Avg. Inert (pu)	Error to Avg. Inert (%)
One	Normal Water	24.0	-0.1	-0.4	7.2	42.9
Two	Carbon Dioxide	23.9	-0.2	-0.8	7.1	42.3
Three	*Toluene	16.9	-7.2	-29.9	0.1	0.6
Four	Normal Water	24.5	0.4	1.7	7.7	45.8
Five	*Helium	16.5	-7.6	-31.5	-0.3	-1.8
Six	2,500 ppm KCl	24.4	0.3	1.2	7.6	45.2
Seven	20,000 ppm KCl	24.3	0.2	0.8	7.5	44.6
Eight	*Benzyl Alcohol	17.1	-7.0	-29.0	0.3	1.8
Nine	Normal Water	23.7	-0.4	-1.7	6.9	41.1

REMARKS: * Inert fluid tests

HOLMES & NARVER, INC.

MATERIALS TESTING LABORATORY

NEVADA TEST SITE

TABLE 12

COMPARISON OF RESULTS FOR SAMPLE NUMBER Z788

Project: Wet & Dry Drilling
Requestor: Dr. Alan L. Flint
Organization: USGS
Address: Box 327, M/S 721, Mercury, NV
Phone: 5-5805
Tested by: Betty N. Walker
Test date: 3-28-89 through 4-1-89
QA level: III

Checked by: John G. Moore
Check date: June 20, 1989
NTL Lab #: Z788
Request #: GT-38
H&N ID #: 58036C
WBS #: 1.2.3.3.6.1
WIN #: WMP-NTS:WI:89-006

Non-welded tuff sample from core hole U12g.12 DD-1 at depth interval of 30.3 to 30.7 feet.
Average effective porosity from water saturations, in porosity units, is 49.8
Average effective porosity from inert fluid tests, in porosity units, is 42.8

Test Number	Test Type Performed	Measured Effective Porosity (pu)	Difference From Avg. Water (pu)	Error to Avg. Water (%)	Difference From Avg. Inert (pu)	Error to Avg. Inert (%)
One	Normal Water	50.0	0.2	0.4	7.2	16.8
Two	Carbon Dioxide	49.8	0.0	0.0	7.0	16.4
Three	*Toluene	42.6	-7.2	-14.5	-0.2	-0.5
Four	Normal Water	49.6	-0.2	-0.4	6.8	15.9
Five	*Helium	43.0	-6.8	-13.7	0.2	0.5
Six	2,500 ppm KCl	49.9	0.1	0.2	7.1	16.6
Seven	20,000 ppm KCl	50.5	0.7	1.4	7.7	18.0
Eight	*Benzyl Alcohol	42.7	-7.1	-14.3	-0.1	-0.2
Nine	Normal Water	49.8	0.0	0.0	7.0	16.4

REMARKS: * Inert fluid tests

HOLMES & NARVER, INC.

MATERIALS TESTING LABORATORY

NEVADA TEST SITE

TABLE 13

COMPARISON OF RESULTS FOR SAMPLE NUMBER 2789

Project: Wet & Dry Drilling
Requestor: Dr. Alan L. Flint
Organization: USGS
Address: Box 327, M/S 721, Mercury, NV
Phone: 5-5805
Tested by: Jeffry M. Walker
Test date: 3-28-89 through 4-1-89
QA level: III

Checked by: John G. Moore
Check date: June 20, 1989
NTL Lab #: 2789
Request #: GT-38
NRN ID #: 50036C
WBS #: 1.2.3.3.6.1
WIN #: YMP:NTS:WI:89-006

Non-welded tuff sample from core hole U12g.12 WD-1 at depth interval of 1.8 to 2.3 feet.
Average effective porosity from water saturations, in porosity units, is 48.0
Average effective porosity from inert fluid tests, in porosity units, is 41.1

Test Number	Test Type Performed	Measured Effective Porosity (pu)	Difference From Avg. Water (pu)	Error to Avg. Water (%)	Difference From Avg. Inert (pu)	Error to Avg. Inert (%)
One	Normal Water	48.2	0.2	0.4	7.1	17.3
Two	Carbon Dioxide	48.3	0.3	0.6	7.2	17.5
Three	*Toluene	41.0	-7.0	-14.6	-0.1	-0.2
Four	Normal Water	48.2	0.2	0.4	7.1	17.3
Five	*Helium	41.0	-7.0	-14.6	-0.1	-0.2
Six	2,500 ppm KCl	48.3	0.3	0.6	7.2	17.5
Seven	20,000 ppm KCl	48.8	0.8	1.7	7.7	18.7
Eight	*Benzyl Alcohol	41.3	-6.7	-14.0	0.2	0.5
Nine	Normal Water	47.6	-0.4	-0.8	6.5	15.8

REMARKS: * Inert fluid tests

HOLMES & NARVER, INC.

MATERIALS TESTING LABORATORY

NEVADA TEST SITE

TABLE 14

COMPARISON OF RESULTS FOR SAMPLE NUMBER 2795

Project: Wet & Dry Drilling
Requestor: Dr. Alan L. Flint
Organization: USGS
Address: Box 327, M/S 721, Mercury, NV
Phone: 5-5805
Tested by: Jeffrey L. Walker
Test date: 3-28-89 through 4-1-89
QA level: III

Checked by: John G. Moore
Check date: June 5, 1989
NTL Lab #: 2795
Request #: GT-38
H&N ID #: 50036C
WBS #: 1.2.3.3.6.1
WIN #: WMP:NTS:W1:89-006

Non-welded tuff sample from core hole U12g.12 WD-1 at depth interval of 19.1 to 19.5 feet.
Average effective porosity from water saturations, in porosity units, is 29.4
Average effective porosity from inert fluid tests, in porosity units, is 23.1

Test Number	Test Type Performed	Measured Effective Porosity (pu)	Difference From Avg. Water (pu)	Error to Avg. Water (%)	Difference From Avg. Inert (pu)	Error to Avg. Inert (%)
One	Normal Water	29.1	-0.3	-1.0	6.0	26.0
Two	Carbon Dioxide	29.8	0.4	1.4	6.7	29.0
Three	*Toluene	22.7	-6.7	-22.8	-0.4	-1.7
Four	Normal Water	29.9	0.5	1.7	6.8	29.4
Five	*Helium	23.5	-5.9	-20.1	0.4	1.7
Six	2,500 ppm KCl	29.9	0.5	1.7	6.8	29.4
Seven	20,000 ppm KCl	30.3	0.9	3.1	7.2	31.2
Eight	*Benzyl Alcohol	23.0	-6.4	-21.8	-0.1	-0.4
Nine	Normal Water	29.1	-0.3	-1.0	6.0	26.0

REMARKS: * Inert fluid tests

HOLMES & NARVER, INC.

MATERIALS TESTING LABORATORY

NEVADA TEST SITE

TABLE T5

COMPARISON OF RESULTS FOR SAMPLE NUMBER 2800

Project: Wet & Dry Drilling
Requestor: Dr. Alan L. Flint
Organization: USGS
Address: Box 327, M/S 721, Mercury, NV
Phone: 5-5805
Tested by: Betty D. Walker
Test date: 3-28-89 through 4-1-89
QA level: III

Checked by: John G. Moore
Check date: June 20, 1989
NTL Lab #: 2800
Request #: GT-38
M&N ID #: 50036C
WBS #: 1.2.3.3.6.1
WIN #: YMP:NTS:WI:89-006

Non-welded tuff sample from core hole U12g DD-2 at depth interval of 3.6 to 4.0 feet.
Average effective porosity from water saturations, in porosity units, is 14.8
Average effective porosity from inert fluid tests, in porosity units, is 14.8

Test Number	Test Type Performed	Measured Effective Porosity (pu)	Difference From Avg. Water (pu)	Error to Avg. Water (%)	Difference From Avg. Inert (pu)	Error to Avg. Inert (%)
One	Normal Water	14.8	0.0	0.0	0.0	0.0
Two	Carbon Dioxide	15.3	0.5	3.4	0.5	3.4
Three	*Toluene	14.8	0.0	0.0	0.0	0.0
Four	Normal Water	15.1	0.3	2.0	0.3	2.0
Five	*Helium	15.0	0.2	1.4	0.2	1.4
Six	2,500 ppm KCl	15.1	0.3	2.0	0.3	2.0
Seven	20,000 ppm KCl	15.1	0.3	2.0	0.3	2.0
Eight	*Benzyl Alcohol	14.7	-0.1	-0.7	-0.1	-0.7
Nine	Normal Water	14.6	-0.2	-1.4	-0.2	-1.4

REMARKS: * Inert fluid tests

HOLMES & NARVER, INC.

MATERIALS TESTING LABORATORY

NEVADA TEST SITE

TABLE 16

COMPARISON OF RESULTS FOR SAMPLE NUMBER 2802

Project: Wet & Dry Drilling
Requestor: Dr. Alan L. Flint
Organization: USGS
Address: Box 327, M/S 721, Mercury, NV
Phone: 5-5805
Tested by: Jerry D. Walker
Test date: 3-28-89 through 4-1-89
QA level: III

Checked by: John E. Moore
Check date: June 20, 1989
NTL Lab #: 2802
Request #: GT-38
NEN ID #: 50036C
WBS #: 1.2.3.3.6.1
WIN #: YMP:NTS:WI:89-006

Non-welded tuff sample from core hole U12g DD-2 at depth interval of 8.0 to 8.4 feet.
Average effective porosity from water saturations, in porosity units, is 18.4
Average effective porosity from inert fluid tests, in porosity units, is 18.2

Test Number	Test Type Performed	Measured Effective Porosity (pu)	Difference From Avg. Water (pu)	Error to Avg. Water (%)	Difference From Avg. Inert (pu)	Error to Avg. Inert (%)
One	Normal Water	18.3	-0.1	-0.5	0.1	0.5
Two	Carbon Dioxide	18.7	0.3	1.6	0.5	2.7
Three	*Toluene	18.2	-0.2	-1.1	0.0	0.0
Four	Normal Water	18.5	0.1	0.5	0.3	1.6
Five	*Helium	18.5	0.1	0.5	0.3	1.6
Six	2,500 ppm KCl	18.5	0.1	0.5	0.3	1.6
Seven	20,000 ppm KCl	18.5	0.1	0.5	0.3	1.6
Eight	*Benzyl Alcohol	18.0	-0.4	-2.2	-0.2	-1.1
Nine	Normal Water	18.3	-0.1	-0.5	0.1	0.5

REMARKS: * Inert fluid tests

HOLMES & NARVER, INC.

MATERIALS TESTING LABORATORY

NEVADA TEST SITE

TABLE 17

COMPARISON OF RESULTS FOR SAMPLE NUMBER 2813

Project: Wet & Dry Drilling
Requestor: Dr. Alan L. Flint
Organization: USGS
Address: Box 327, M/S 721, Mercury, NV
Phone: 5-5805
Tested by: Jerry N. Walker
Test date: 3-28-89 through 4-1-89
QA level: III

Checked by: John G. Moore
Check date: June 20, 1989
HTL Lab #: 2813
Request #: GT-38
HSN ID #: 50036C
WBS #: 1.2.3.3.6.1
WIN #: YMP:HTS:WI:89-006

Non-welded tuff sample from core hole U12g WD-2 at depth interval of 14.0 to 14.3 feet.
Average effective porosity from water saturations, in porosity units, is 13.0
Average effective porosity from inert fluid tests, in porosity units, is 12.5

Test Number	Test Type Performed	Measured Effective Porosity (pu)	Difference From Avg. Water (pu)	Error to Avg. Water (%)	Difference From Avg. Inert (pu)	Error to Avg. Inert (%)
One	Normal Water	13.0	0.0	0.0	0.5	4.0
Two	Carbon Dioxide	13.3	0.3	2.3	0.8	6.4
Three	*Toluene	12.7	-0.3	-2.3	0.2	1.6
Four	Normal Water	13.2	0.2	1.5	0.7	5.6
Five	*Helium	12.3	-0.7	-5.4	-0.2	-1.6
Six	2,500 ppm KCl	13.1	0.1	0.8	0.6	4.8
Seven	20,000 ppm KCl	13.1	0.1	0.8	0.6	4.8
Eight	*Benzyl Alcohol	12.6	-0.4	-3.1	0.1	0.8
Nine	Normal Water	12.9	-0.1	-0.8	0.4	3.2

REMARKS: * Inert fluid tests

HOLMES & NARVER, INC.

MATERIALS TESTING LABORATORY

NEVADA TEST SITE

TABLE 18

COMPARISON OF RESULTS FOR SAMPLE NUMBER 2815

Project: Wet & Dry Drilling
Requestor: Dr. Alan L. Flint
Organization: USGS
Address: Box 327, M/S 721, Mercury, NV
Phone: 5-5805
Tested by: Betty H. Walker
Test date: 3-28-89 through 4-1-89
QA level: III

Checked by: John E. Moore
Check date: June 20, 1989
NTL Lab #: 2815
Request #: GT-38
NEN ID #: 50036C
WBS #: 1.2.3.3.6.1
WIN #: YMP:NTS:WI:89-006

Non-welded tuff sample from core hole U12g UD-2 at depth interval of 17.7 to 18.0 feet.
Average effective porosity from water saturations, in porosity units, is 15.2
Average effective porosity from inert fluid tests, in porosity units, is 15.0

Test Number	Test Type Performed	Measured Effective Porosity (pu)	Difference From Avg. Water (pu)	Error to Avg. Water (%)	Difference From Avg. Inert (pu)	Error to Avg. Inert (%)
One	Normal Water	15.2	0.0	0.0	0.2	1.3
Two	Carbon Dioxide	15.5	0.3	2.0	0.5	3.3
Three	*Toluene	15.1	-0.1	-0.7	0.1	0.7
Four	Normal Water	15.4	0.2	1.3	0.4	2.7
Five	*Helium	15.0	-0.2	-1.3	0.0	0.0
Six	2,500 ppm KCl	15.3	0.1	0.7	0.3	2.0
Seven	20,000 ppm KCl	15.4	0.2	1.3	0.4	2.7
Eight	*Benzyl Alcohol	14.9	-0.3	-2.0	-0.1	-0.7
Nine	Normal Water	15.1	-0.1	-0.7	0.1	0.7

REMARKS: * Inert fluid tests

FIGURE 1
Helium Porosimeter
Calibration Curve

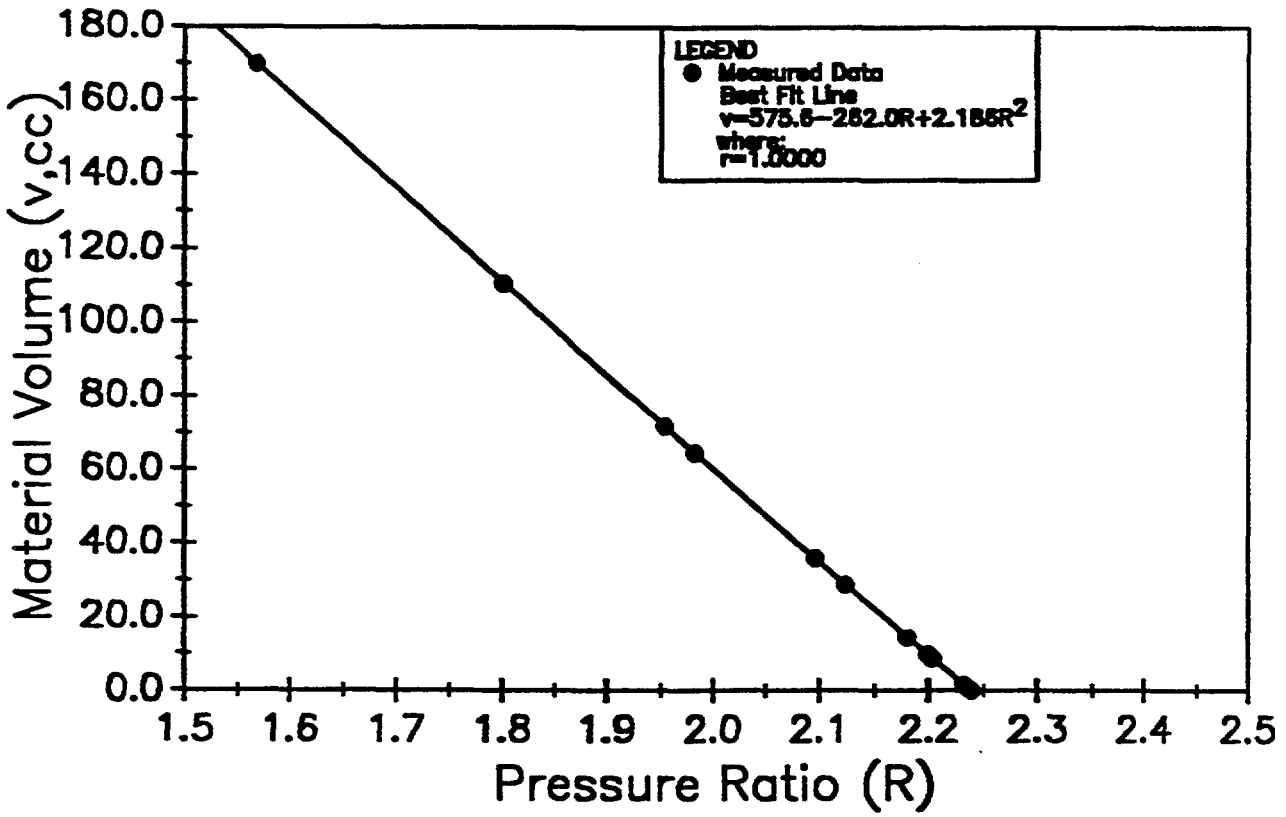

Wet & Dry Drilling
Holmes & Narver Materials Test Lab (JNW)
4–26–89

FIGURE 2

Comparison of Initial Dry Weights, Non–Welded Tuff Samples

Holmes & Narver Materials Test Lab (JNW)

6–7–89

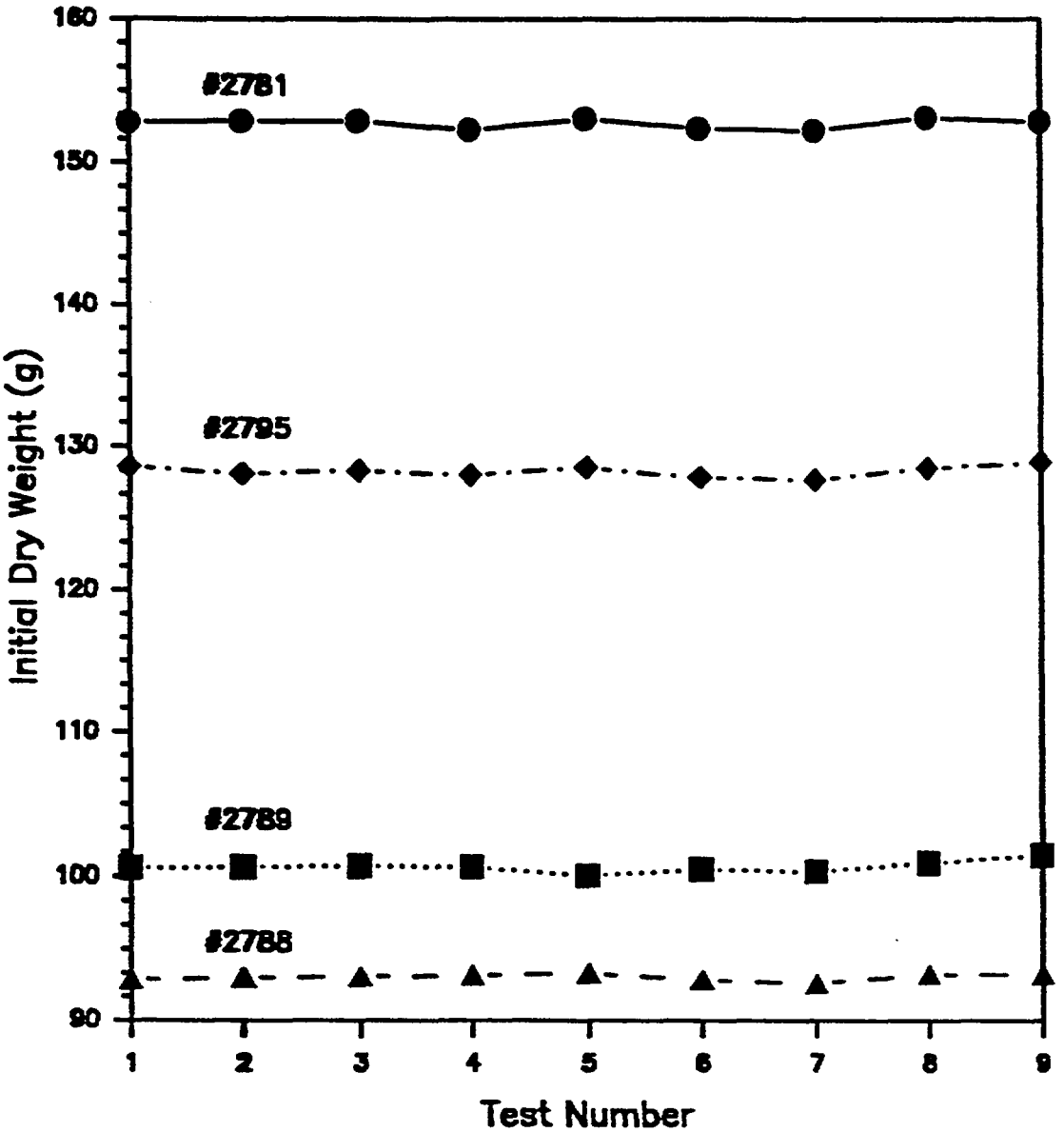

USGS Wet & Dry Drilling

WBS #1.2.3.3.8.1

QA Level III

FIGURE 3

Comparison of Initial Dry Weights, Welded Tuff Samples

Holmes & Narver Materials Test Lab (JNW)

6-7-89

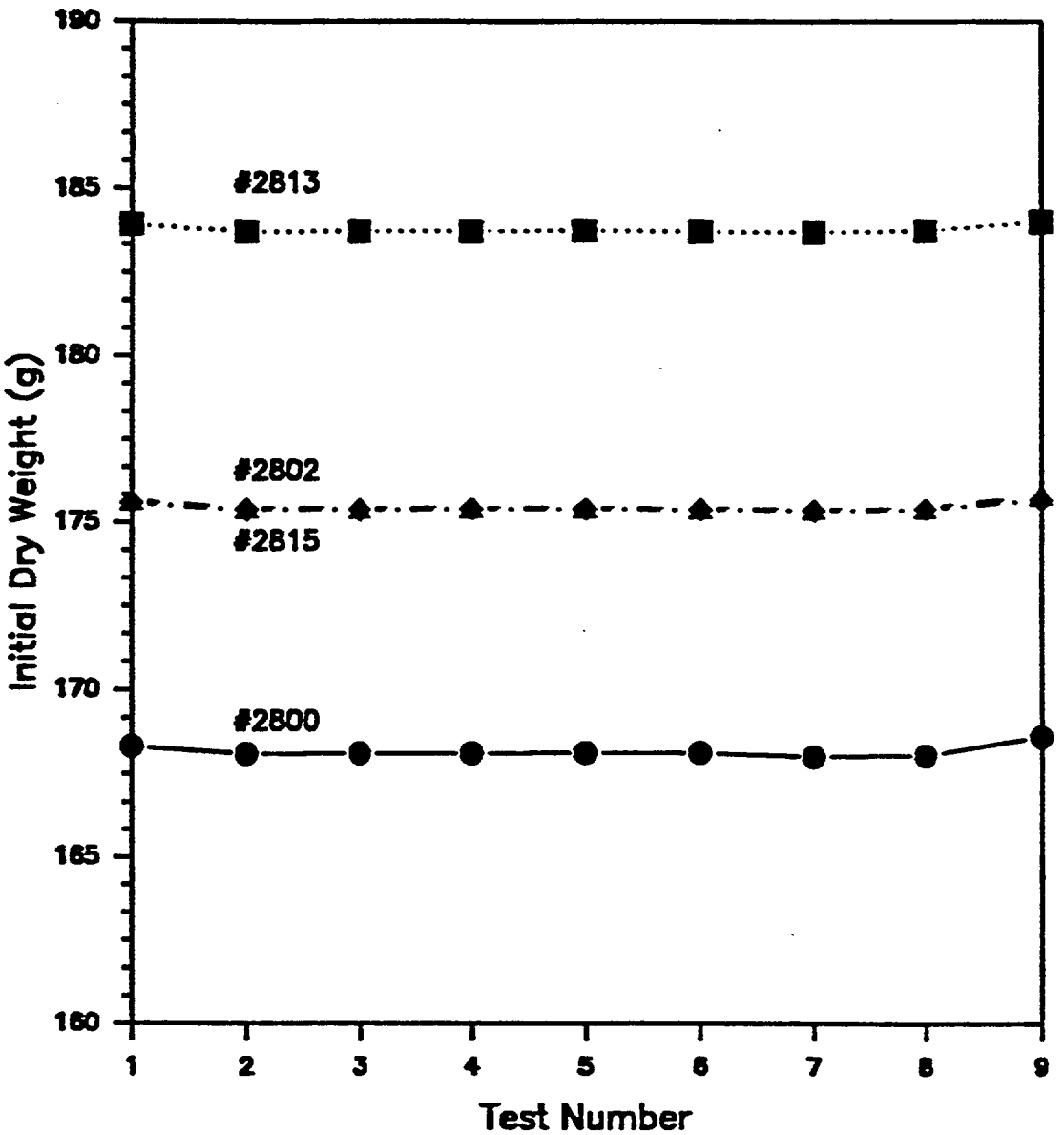

USGS Wet & Dry Drilling
WBS #1.2.3.3.6.1
QA Level III

FIGURE 4

Comparison of Porosity Measurement Methods

Non–Welded Tuff Sample #2781

Holmes & Narver Materials Test Lab (JNW)

6–7–89

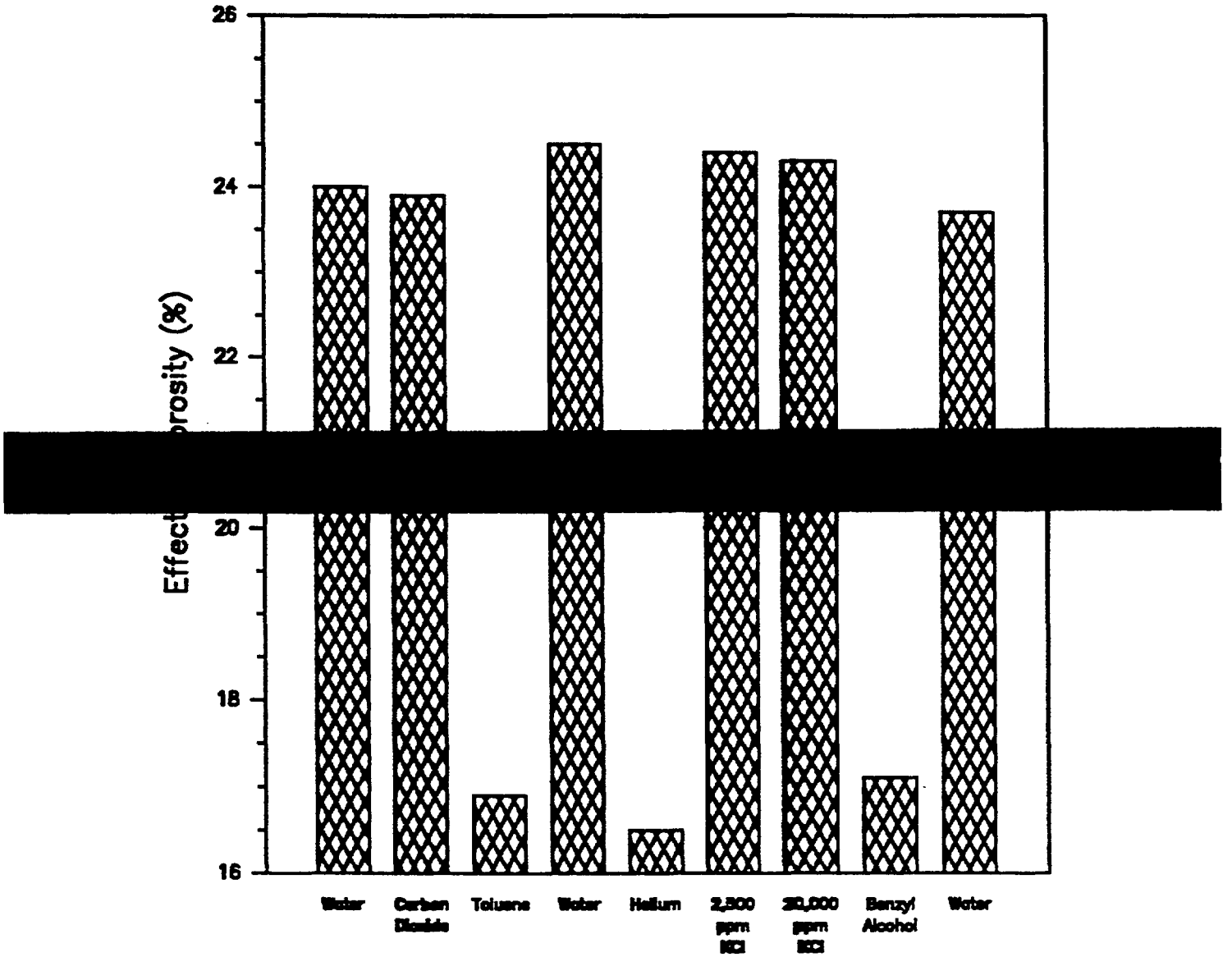

USGS Wet & Dry Drilling

WBS #1.2.3.3.6.1

QA Level III

FIGURE 5

Comparison of Porosity Measurement Methods

Non-Welded Tuff Sample #2788

Holmes & Narver Materials Test Lab (JNW)

6-7-89

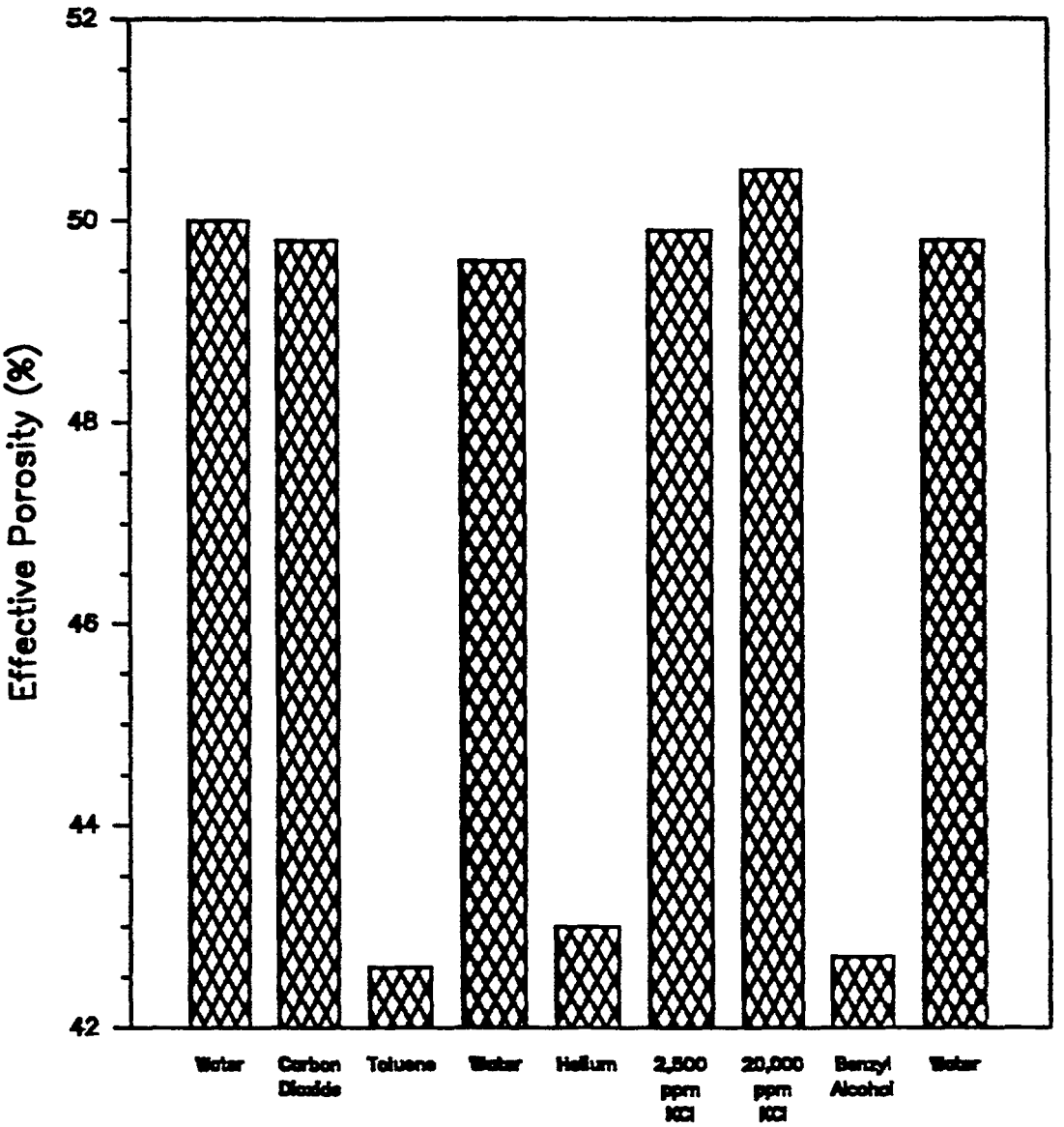

USGS Wet & Dry Drilling

WBS #1.2.3.3.6.1

QA Level III

FIGURE 6

Comparison of Porosity Measurement Methods

Non-Welded Tuff Sample #2769

Holmes & Narver Materials Test Lab (JNW)

6-7-89

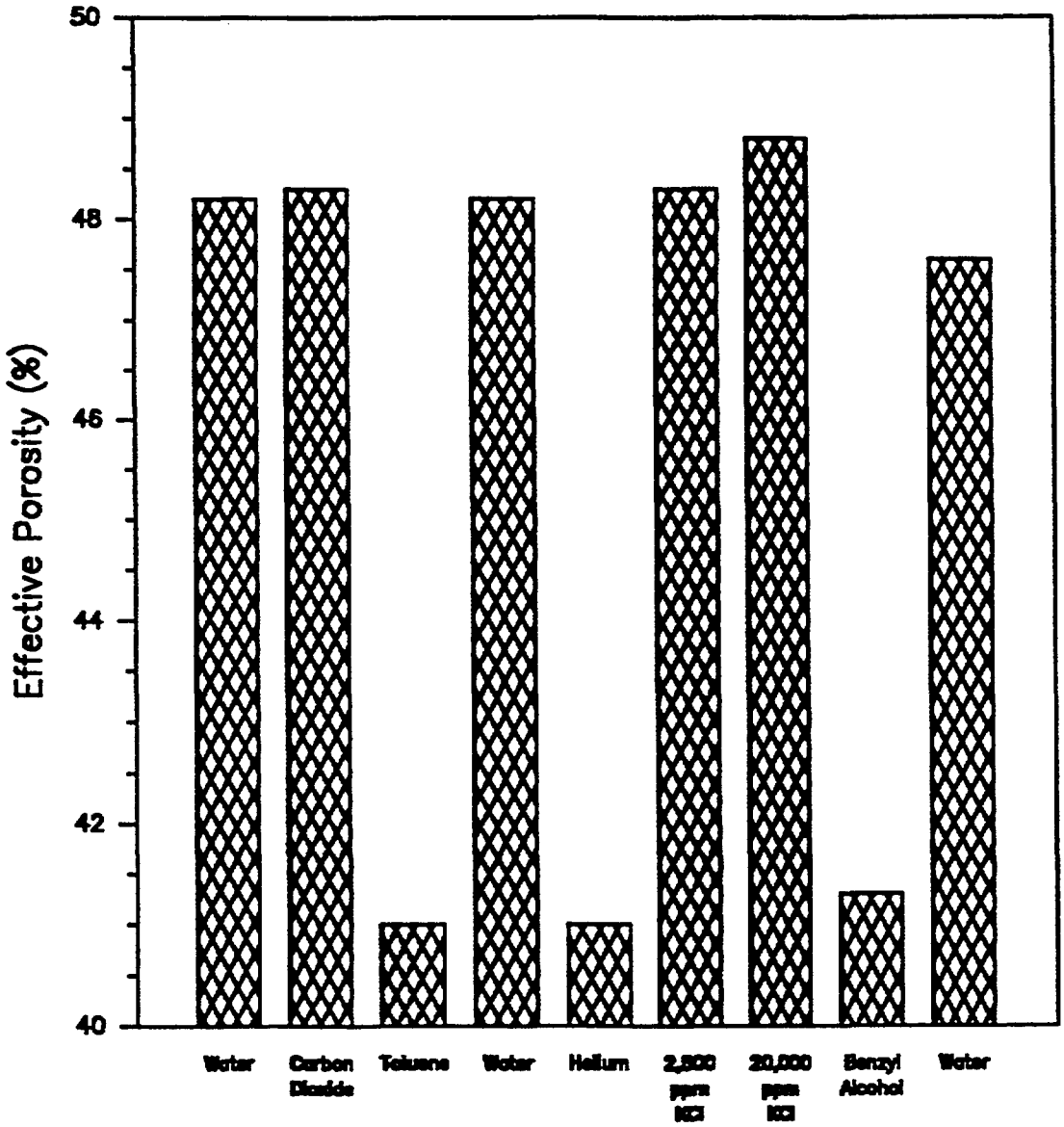

USGS Wet & Dry Drilling

WBS #1.2.3.3.6.1

QA Level III

FIGURE 7

Comparison of Porosity Measurement Methods

Non-Welded Tuff Sample #2795

Holmes & Narver Materials Test Lab (JNW)

6-7-89

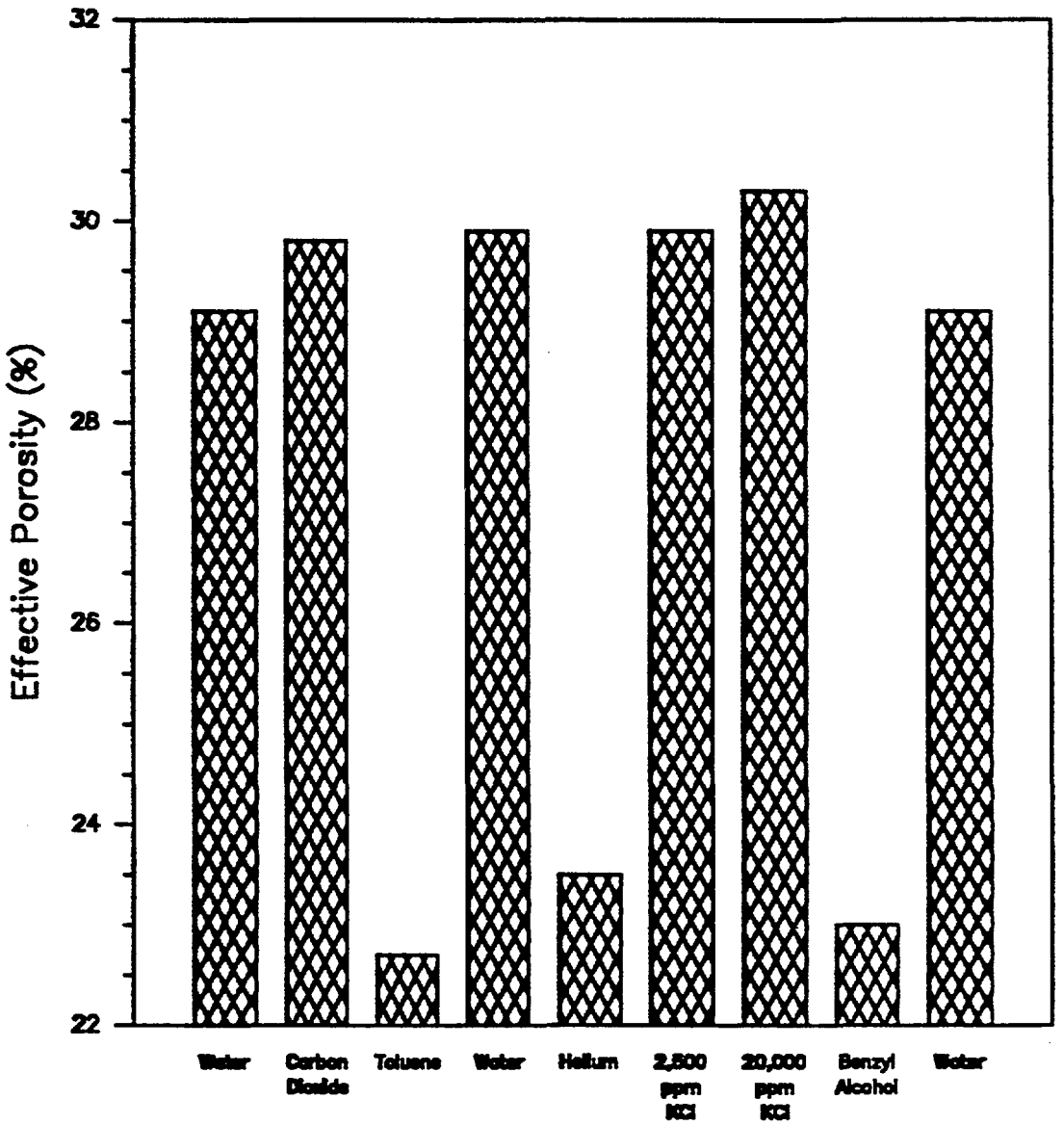

USGS Wet & Dry Drilling
WBS #1.2.3.3.6.1
QA Level III

FIGURE 8

Comparison of Porosity Measurement Methods

Welded Tuff Sample #2800

Holmes & Narver Materials Test Lab (JNW)

8-7-89

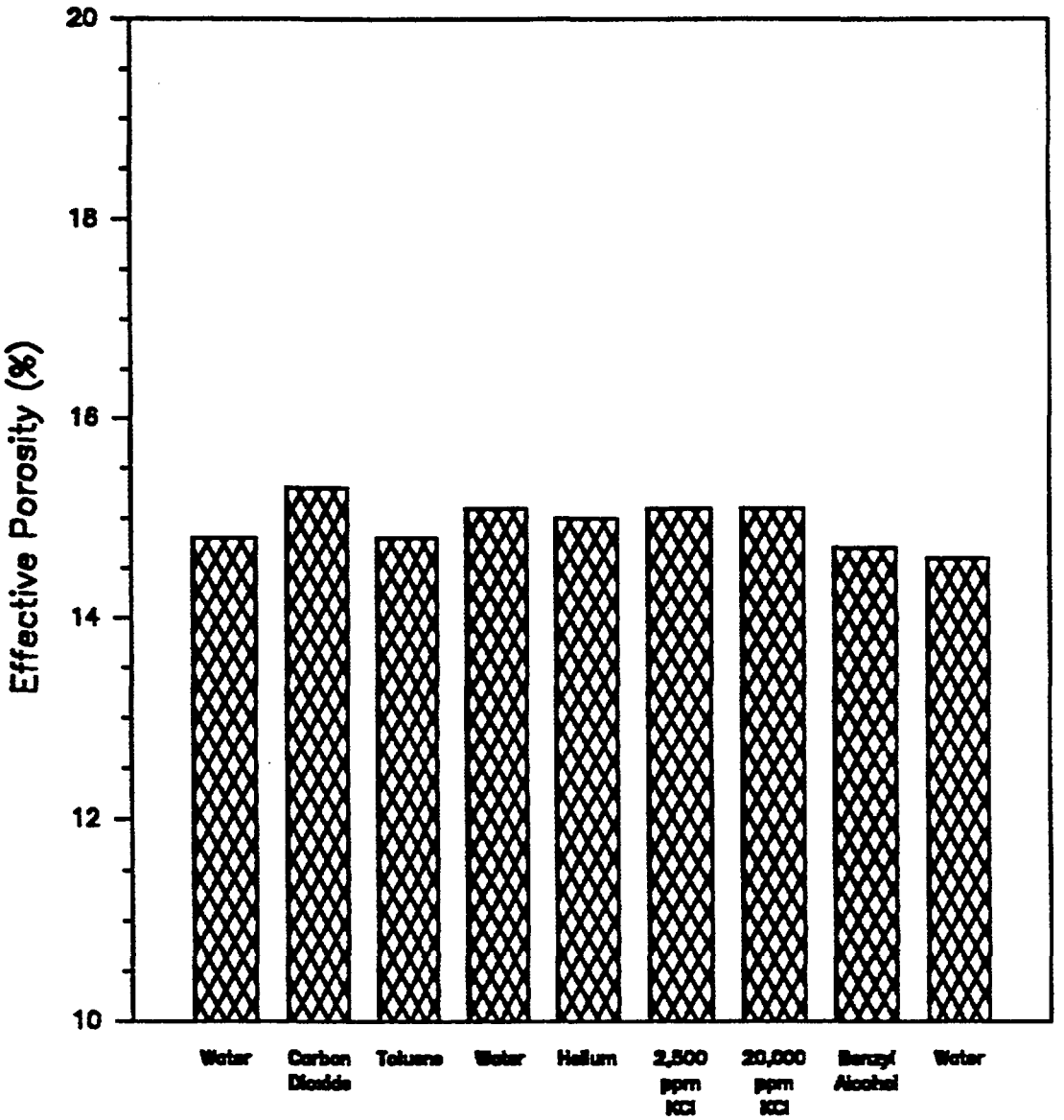

USGS Wet & Dry Drilling

WBS #1.2.3.3.6.1

QA Level III

FIGURE 9

Comparison of Porosity Measurement Methods

Welded Tuff Sample #2802

Holmes & Narver Materials Test Lab (JNW)

6-7-89

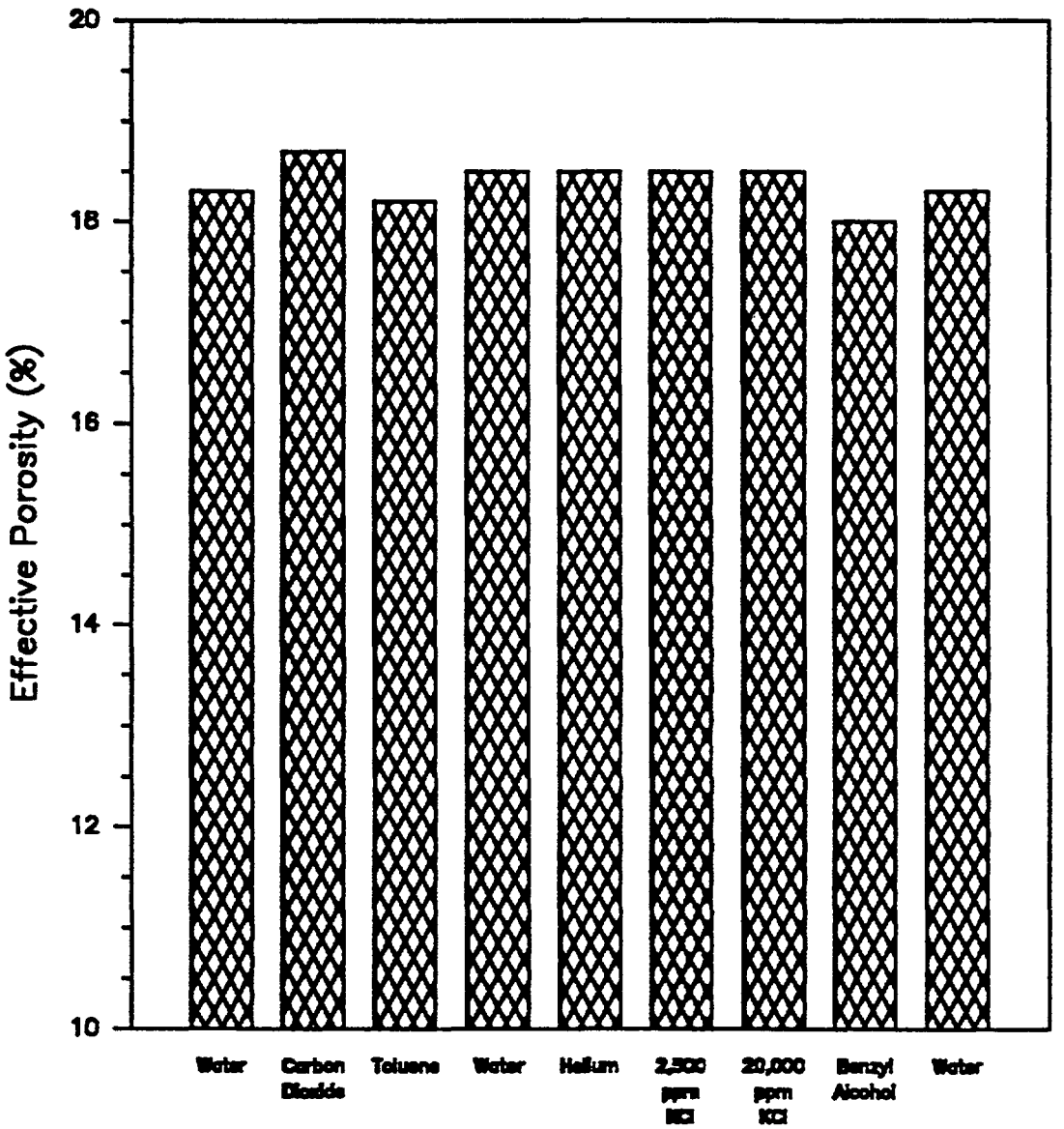

USGS Wet & Dry Drilling

WBS #1.2.3.3.6.1

QA Level III

FIGURE 10

Comparison of Porosity Measurement Methods

Welded Tuff Sample #2B13

Holmes & Narver Materials Test Lab (JNW)

6-7-89

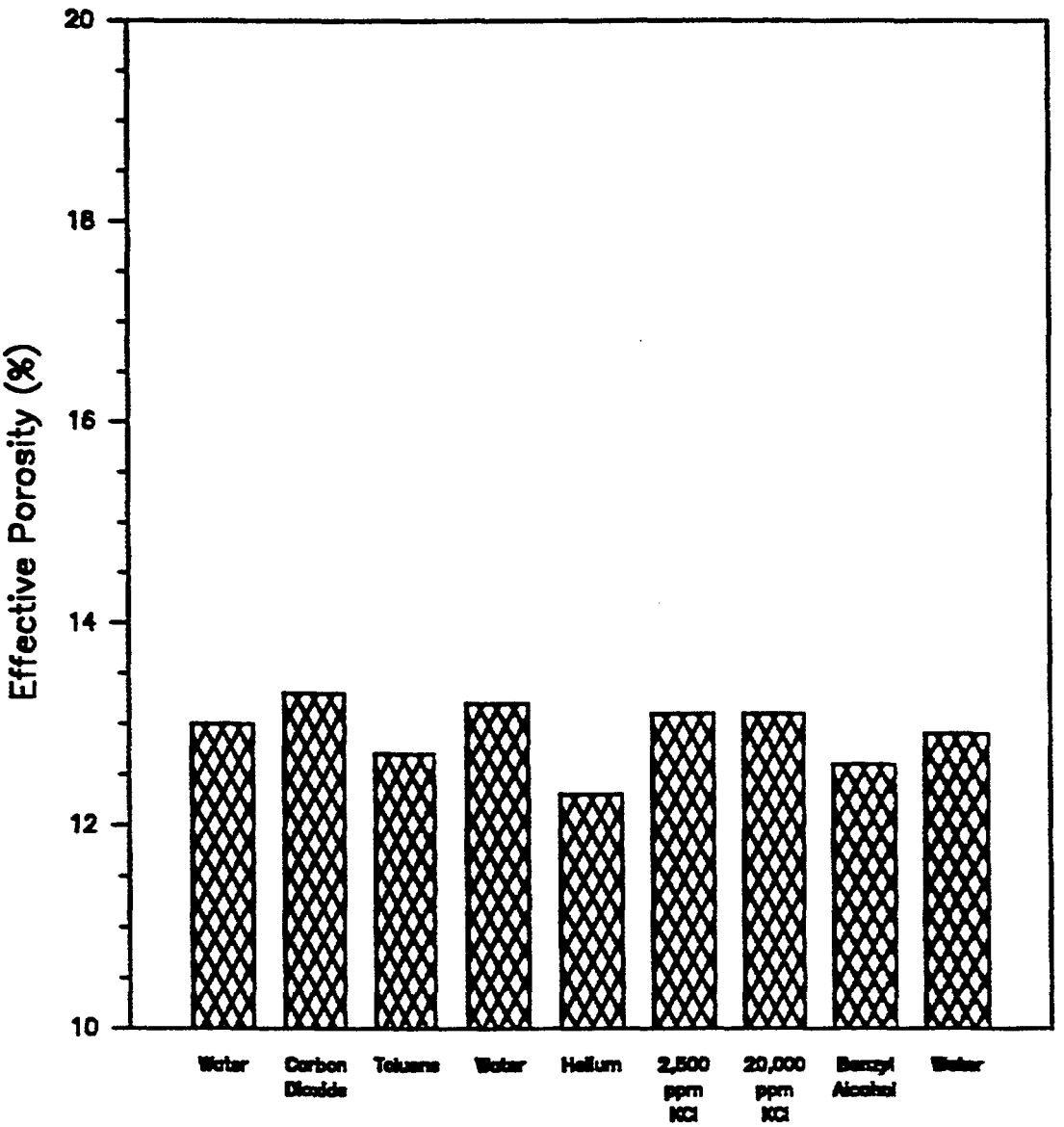

USGS Wet & Dry Drilling

WBS #1.2.3.3.6.1

QA Level III

FIGURE 11

Comparison of Porosity Measurement Methods

Welded Tuff Sample #2815

Holmes & Narver Materials Test Lab (JNW)

6-7-89

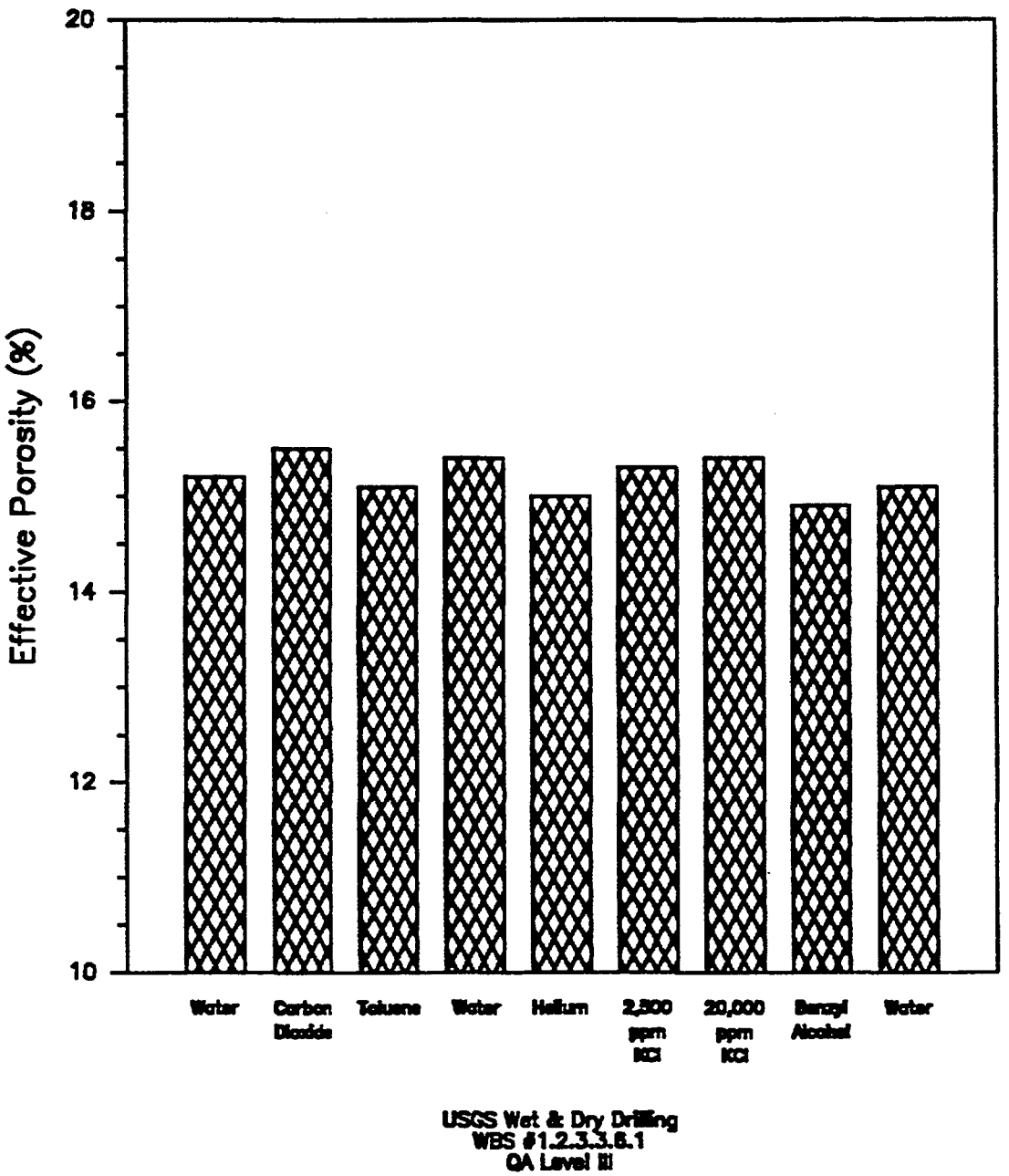

USGS Wet & Dry Drilling

WBS #1.2.3.3.6.1

QA Level III

APPENDIX A5

Preliminary results of permeability tests
performed for the YMP wet and dry drilling project
WBS # 1.2.3.3.6.1

Table of contents

TABLE 1. NITROGEN GAS PERMEABILITY (API RP27)

Project: YMP Wet & Dry Drilling	Print date: January 10, 1990	664.0 = atmospheric pressure (mm Hg)
Requestor: Dr. Alan L. Flint	Request #: GT-38	6.081 = diameter (cm)
Organization: USGS	H&N ID #: 50036 C	29.043 = cross-sectional area (cm2)
Address: Box 327, M/S 721, Mercury, Nv	WBS #: 1.2.3.3.6.1	2.992 = length (cm)
Phone: 5-5805	WIN #: YMP:NTS:WI:89-006	113.59 = weight (g)
Tested by: J. Moore	SCN: Not established	1.307 = density (g/cc)
Test date: 8/7/89	QA level: III	0.0 = moisture (%)
Checked by:	Lab #: 2779	
Check date:	Hole & depth: U12G.12 DD-1, 1.7-2.2'	

Inlet pressure (psig)	Outlet pressure (psig)	Meter code	Meter type	(For Actual dT/dF	rotameters) Lookup dT/dF	Flow rate (std. cc/sec)	Nitrogen temp (C)	Nitrogen vis-cosity (cp)	(P1^2-P2^2)/2L (atm^2/cm)	(QbPb)/A (cm atm/sec)	1/((P1+P2)/2) (1/atm)	Permeability (millidarcys)
5.00	0.00	pip	Pipette & stopwatch		NA	2.264	21.80	0.01759	0.1187	0.078	0.958	11.578
10.00	0.00	pip	Pipette & stopwatch		NA	4.852	21.80	0.01759	0.2761	0.167	0.824	10.669
15.00	0.00	pip	Pipette & stopwatch		NA	7.494	21.80	0.01759	0.4721	0.259	0.723	9.636
20.00	0.00	pip	Pipette & stopwatch		NA	10.426	21.90	0.01759	0.7069	0.360	0.643	8.959
25.00	0.00	pip	Pipette & stopwatch		NA	13.550	21.90	0.01759	0.9803	0.468	0.580	8.396
30.00	0.00	pip	Pipette & stopwatch		NA	16.945	22.00	0.01760	1.2925	0.585	0.528	7.969
40.00	0.00	pip	Pipette & stopwatch		NA	23.891	22.10	0.01760	2.0328	0.825	0.448	7.147
50.00	0.00	pip	Pipette & stopwatch		NA	31.696	22.10	0.01760	2.9279	1.095	0.388	6.583
60.00	0.00	pip	Pipette & stopwatch		NA	40.356	22.10	0.01760	3.9777	1.394	0.343	6.170
80.00	0.00	pip	Pipette & stopwatch		NA	57.020	22.20	0.01761	6.5416	1.971	0.278	5.304
100.00	0.00	pip	Pipette & stopwatch		NA	74.649	22.20	0.01761	9.7246	2.580	0.234	4.671
120.00	0.00	pip	Pipette & stopwatch		NA	94.990	22.30	0.01761	13.5265	3.284	0.202	4.276

Equipment used:	Control No.:	Calibration due date:
Mettler PM6100 balance	PTL-2684	9/3/89
Brown & Sharpe Digit-Cal II micrometer	PTL-6786	1/17/90
Omega Model 871 digital thermometer	PTL-6976	9/13/89
Heise digital barometer	PTL-5296	6/19/90
Heise CMM 61186 0-200 psi gauge	PTL-4481	8/16/89
Wallace & Tiernan FA145 0-30 psi gauge	PTL-388	8/18/89
Markson Science #16573 digital stopwatch	S/N 006543	Manufacturer's undated certificate
SKC soap film flowmeters	None	Not calibrated

Permeability from Base Flow vs. Pressure Gradient. Lab #: 2779

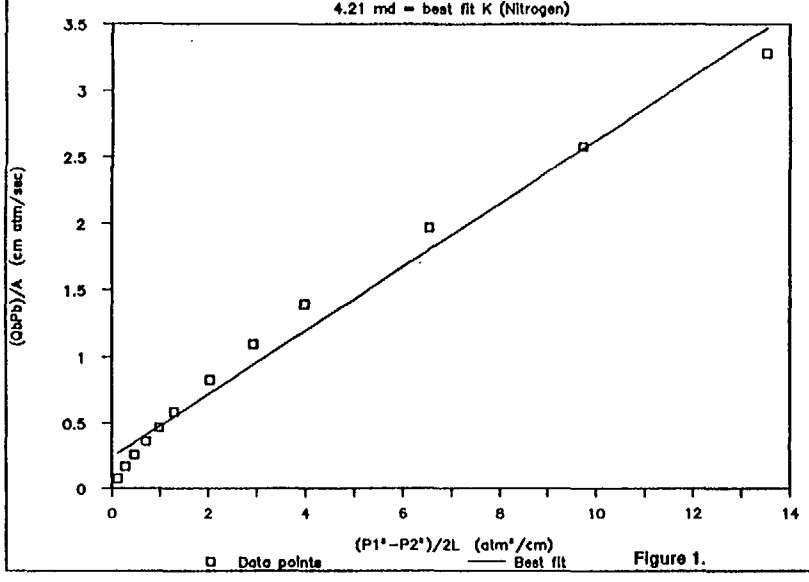

Figure 1.

Klinkenberg Extrapolation from Nitrogen Gas Data, Lab #: 2779

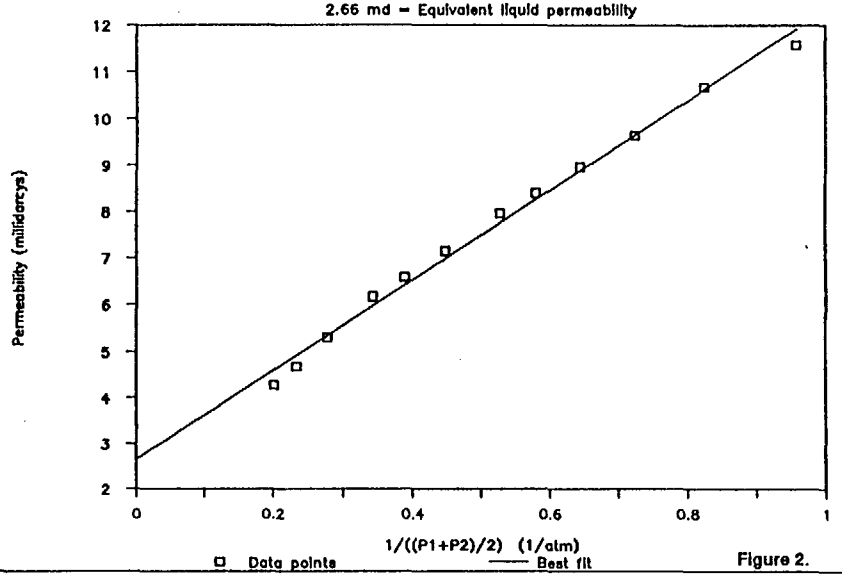

Figure 2.

TABLE 2. WATER PERMEABILITY (API RP27)

Project: YMP Wet & Dry Drilling	Print date: January 8, 1990	6.081	= diameter (cm)
Requestor: Dr. Alan L. Flint	Request #: GT-38	29.041	= cross-sectional area (cm2)
Organization: USGS	H&N ID #: 50036C	2.992	= length (cm)
Address: Box 327, M/S 721, Mercury, Nv	WBS #: 1.2.3.3.6.1	113.59	= dry wt. (g)
Phone: 5-5805	WIN #: YMP:NTS:WI:89-006	3639.49	= dry potted wt. (g)
Tested by: J. Moore	SCN: Not established	3679.06	= wet potted wt. (g)
Test date: 11/22/89	QA level: III	1.763	= density (g/cc)
Checked by:	Lab #: 2779	25.8	= moisture (%)
Check date:	Hole & depth (ft): U12G.12, DD-1, 1.7-2.2'	psi	= pressure unit: cm = cm of water; psi = psig

Pressures, psi		Temp.,	Differential pressure		Q,	Q/A,	P/L,	Water viscosity,	Permeability,
Inlet	Outlet	deg. C	psi	atm	cc/sec	cm/sec	atm/cm	cP	millidarcys
5.00	0.00	26.00	5.00	0.3402	0.001168	4.02E-05	0.1137	0.870	0.308
10.00	0.00	26.00	10.00	0.6805	0.002415	8.32E-05	0.2274	0.870	0.318
15.00	0.00	26.00	15.00	1.0207	0.003626	1.25E-04	0.3411	0.870	0.319
20.00	0.00	26.00	20.00	1.3609	0.004812	1.66E-04	0.4548	0.870	0.317
25.00	0.00	26.00	25.00	1.7011	0.005999	2.07E-04	0.5685	0.870	0.316
30.00	0.00	26.00	30.00	2.0414	0.007183	2.47E-04	0.6823	0.870	0.316
40.00	0.00	26.00	40.00	2.7218	0.009369	3.23E-04	0.9097	0.870	0.309
50.00	0.00	26.00	50.00	3.4023	0.011836	4.08E-04	1.1371	0.870	0.312
60.00	0.00	26.00	60.00	4.0828	0.013921	4.79E-04	1.3645	0.870	0.306
80.00	0.00	26.00	80.00	5.4437	0.018342	6.32E-04	1.8193	0.870	0.302
100.00	0.00	26.00	100.00	6.8046	0.022969	7.91E-04	2.2742	0.870	0.303
120.00	0.00	26.00	120.00	8.1655	0.026962	9.28E-04	2.7290	0.870	0.296

Equipment used:	Control No.:	Calibration due date:
Mettler PM6100 balance	PTL-2684	3/21/90
Brown & Sharpe Digit-Cal II micrometer	PTL-6786	1/17/90
Omega Model 871 digital thermometer	PTL-6976	3/27/90
Heise digital barometer	PTL-5296	6/19/90
Heise CMM 61186 0-200 psi gauge	PTL-4481	1/10/90
Wallace & Tiernan FA145 0-30 psi gauge	PTL-388	2/24/90
Markson Science #16573 digital stopwatch	S/N 006543	Manufacturer's undated certificate
Corning pipettes	None	Not calibrated
Kimble pipettes	None	Not calibrated

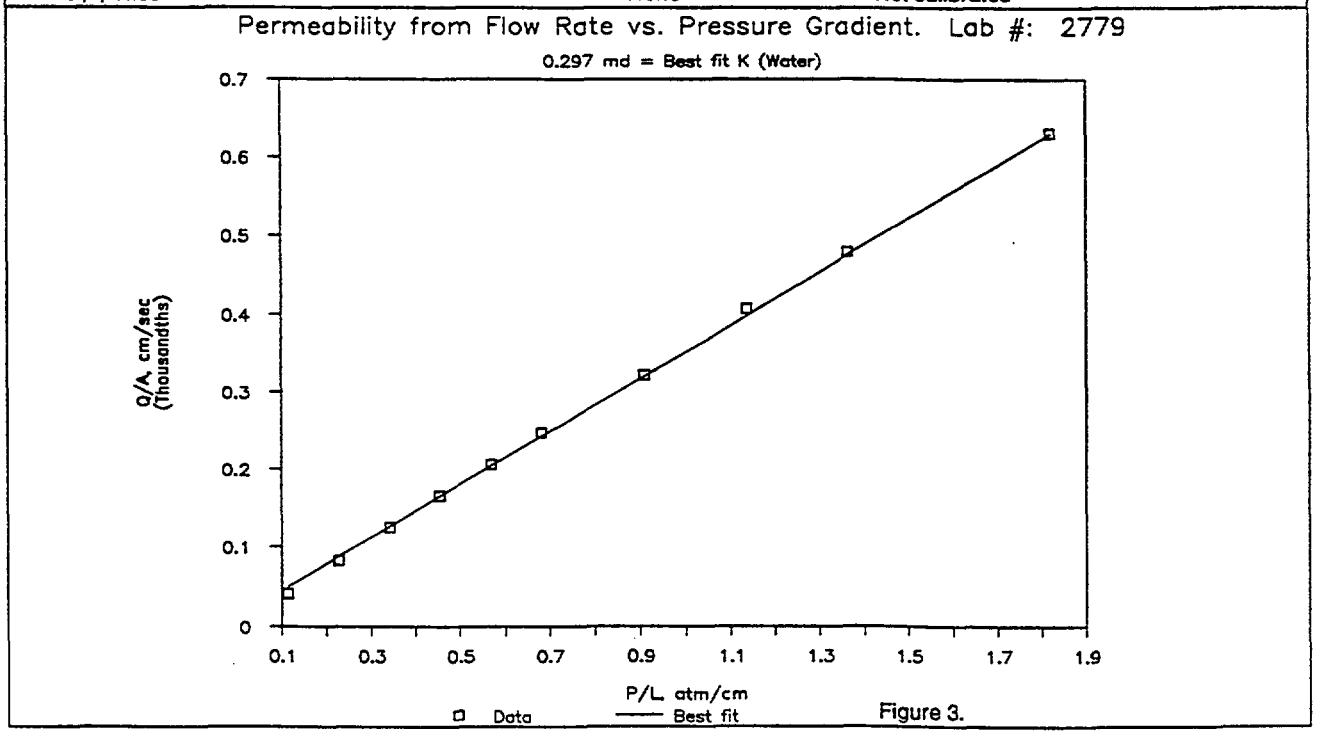

Figure 3.

TABLE 3. NITROGEN GAS PERMEABILITY AT VARIOUS DEGREES OF SATURATION (API RP27)

Project: YMP Wet & Dry Drilling	Test date: 11/28-11/30/89	WBS #: 1.2.3.3.6.1	672.6	= atmospheric pressure (m	113.59 = dry sample wt. (g)
Requestor: Dr. Alan L. Flint	Checked by:	WIN #: YMP:NTS:WI:89-006	6.081	= diameter (cm)	3639.49 = dry potted wt. (g)
Organization: USGS	Check date:	SCN: Not established	29.043	= cross-sectional area (cm	3679.06 = saturated potted wt. (g)
Address: Box 327, M/S 721, Mercury, Nv	Print date: January 10, 1990	QA level: III	2.992	= length (cm)	223.42 = empty water jar wt. (g)
Phone: 5-5805	Request #: GT-38	Lab #: 2779	1.763	= saturated density (g/cc)	153.16 = saturated sample wt. (g)
Tested by: J. Moore	H&N ID #: 50036C	Hole & depth: U12G.12 DD-1, 1.7-2.2'	25.8	= moisture (% by wt.)	45.5 = moisture (% by volume)

Inlet pressure (psig)	Outlet pressure (psig)	Meter code	Meter type	Actual dT/dF	Lookup dT/dF	Flow rate (std. cc/sec)	Nitrogen temp (C)	Nitrogen viscosity (cp)	P1^2-P2^2)/2L (atm^2/cm)	(QbPb)/A (cm atm/sec)	As-tested permeability (millidarcys)	Water jar + water wt. (g)	Saturation (%)	Dry-core permeability (millidarcys)	Relative permeability to nitrogen (ratio)
5.00	0.00	pip	Pipette & stopwatch	NA	0.000	26.20	0.01778	0.1200	0.000	0.000	223.42	100	11.578	0.000
10.00	0.00	pip	Pipette & stopwatch	NA	0.004	25.90	0.01777	0.2786	0.000	0.009	224.17	98	10.669	0.001
15.00	0.00	pip	Pipette & stopwatch	NA	0.048	25.70	0.01776	0.4760	0.002	0.063	226.33	93	9.636	0.007
20.00	0.00	pip	Pipette & stopwatch	NA	0.151	28.30	0.01787	0.7120	0.005	0.134	228.11	88	8.959	0.015
25.00	0.00	pip	Pipette & stopwatch	NA	0.296	28.00	0.01786	0.9868	0.010	0.189	228.93	86	8.396	0.022
30.00	0.00	pip	Pipette & stopwatch	NA	0.569	26.90	0.01781	1.3002	0.020	0.273	230.17	83	7.969	0.034
40.00	0.00	pip	Pipette & stopwatch	NA	1.203	26.40	0.01779	2.0431	0.042	0.367	231.20	80	7.147	0.051
50.00	0.00	pip	Pipette & stopwatch	NA	2.048	26.10	0.01778	2.9408	0.072	0.433	232.07	78	6.583	0.066
60.00	0.00	pip	Pipette & stopwatch	NA	3.201	25.80	0.01776	3.9932	0.112	0.498	232.81	76	6.170	0.081
80.00	0.00	pip	Pipette & stopwatch	NA	6.085	25.60	0.01775	6.5623	0.213	0.576	233.64	74	5.304	0.109
100.00	0.00	pip	Pipette & stopwatch	NA	10.034	25.30	0.01774	9.7504	0.350	0.638	234.45	72	4.671	0.136
120.00	0.00	pip	Pipette & stopwatch	NA	14.819	25.00	0.01773	13.5576	0.517	0.676	235.18	70	4.276	0.158

Equipment used:	Control No.:	Calibration due date:
Mettler PM6100 balance	PTL-2684	3/21/90
Brown & Sharpe Digit-Cal II micrometer	PTL-6786	1/17/90
Omega Model 871 digital thermometer	PTL-6976	3/27/90
Heise digital barometer	PTL-5296	6/19/90
Heise CMM 61186 0-200 psi gauge	PTL-4481	1/10/90
Wallace & Tiernan FA145 0-30 psi gauge	PTL-388	2/24/90
Markson Science #16573 digital stopwatch	S/N 006543	Manufacturer's undated certificate
Corning and Kimble pipettes	None	Not calibrated
SKC soap film flowmeters	None	Not calibrated

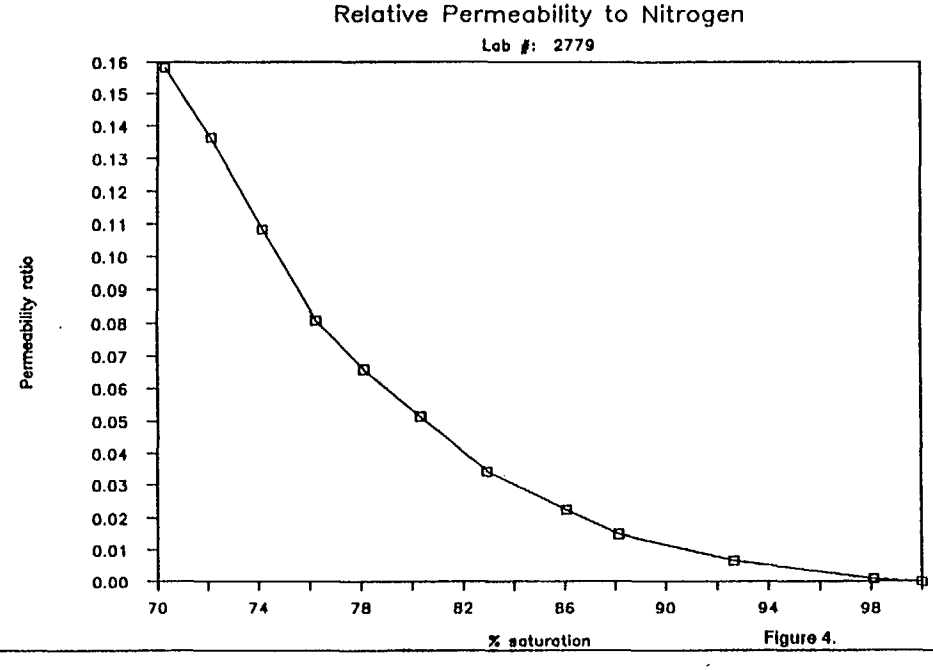

Figure 4.

TABLE 4. NITROGEN GAS PERMEABILITY (API RP27)

Project: YMP Wet & Dry Drilling	Print date: January 10, 1990	664.0	= atmospheric pressure (mm Hg)
Requestor: Dr. Alan L. Flint	Request #: GT-38	6.081	= diameter (cm)
Organization: USGS	H&N ID #: 50036 C	29.043	= cross-sectional area (cm2)
Address: Box 327, M/S 721, Mercury, Nv	WBS #: 1.2.3.3.6.1	3.084	= length (cm)
Phone: 5-5805	WIN #: YMP:NTS:WI:89-006	114.37	= weight (g)
Tested by: J. Moore	SCN: Not established	1.277	= density (g/cc)
Test date: 8/7/89	QA level: III	0.0	= moisture (%)
Checked by:	Lab #: 2789		
Check date:	Hole & depth: U12G.12 WD-1, 1.8-2.3'		

Inlet pressure (psig)	Outlet pressure (psig)	Meter code	Meter type	(For rotameters) Actual dT/dF	Lookup dT/dF	Flow rate (std. cc/sec)	Nitrogen temp (C)	Nitrogen vis-cosity (cp)	(P1^2-P2^2)/2L (atm^2/cm)	(QbPb)/A (cm atm/sec)	1/((P1+P2)/2) (1/atm)	Permeability (millidarcys)
5.00	0.00	pip	Pipette & stopwatch		NA	1.152	22.80	0.01763	0.1151	0.040	0.958	6.107
10.00	0.00	pip	Pipette & stopwatch		NA	2.559	22.80	0.01763	0.2678	0.089	0.824	5.834
15.00	0.00	pip	Pipette & stopwatch		NA	4.218	22.80	0.01763	0.4580	0.146	0.723	5.622
20.00	0.00	pip	Pipette & stopwatch		NA	5.968	22.80	0.01763	0.6858	0.207	0.643	5.313
25.00	0.00	pip	Pipette & stopwatch		NA	8.066	22.80	0.01763	0.9511	0.279	0.580	5.179
30.00	0.00	pip	Pipette & stopwatch		NA	10.459	22.80	0.01763	1.2539	0.362	0.528	5.093
40.00	0.00	pip	Pipette & stopwatch		NA	15.506	22.80	0.01763	1.9721	0.537	0.448	4.801
50.00	0.00	pip	Pipette & stopwatch		NA	21.122	22.80	0.01763	2.8405	0.731	0.388	4.541
60.00	0.00	pip	Pipette & stopwatch		NA	27.537	22.80	0.01763	3.8590	0.954	0.343	4.357
80.00	0.00	pip	Pipette & stopwatch		NA	42.126	22.80	0.01763	6.3465	1.459	0.278	4.053
100.00	0.00	pip	Pipette & stopwatch		NA	57.851	22.90	0.01764	9.4345	2.004	0.234	3.746
120.00	0.00	pip	Pipette & stopwatch		NA	75.607	22.90	0.01764	13.1230	2.619	0.202	3.520

Equipment used:	Control No.:	Calibration due date:
Mettler PM6100 balance	PTL-2684	9/3/89
Brown & Sharpe Digit-Cal II micrometer	PTL-6786	1/17/90
Omega Model 871 digital thermometer	PTL-6976	9/13/89
Heise digital barometer	PTL-5296	6/19/90
Heise CMM 61186 0-200 psi gauge	PTL-4481	8/16/89
Wallace & Tiernan FA145 0-30 psi gauge	PTL-388	8/18/89
Markson Science #16573 digital stopwatch	S/N 006543	Manufacturer's undated certificate
SKC soap film flowmeters	None	Not calibrated

Permeability from Base Flow vs. Pressure Gradient. Lab #: 2789

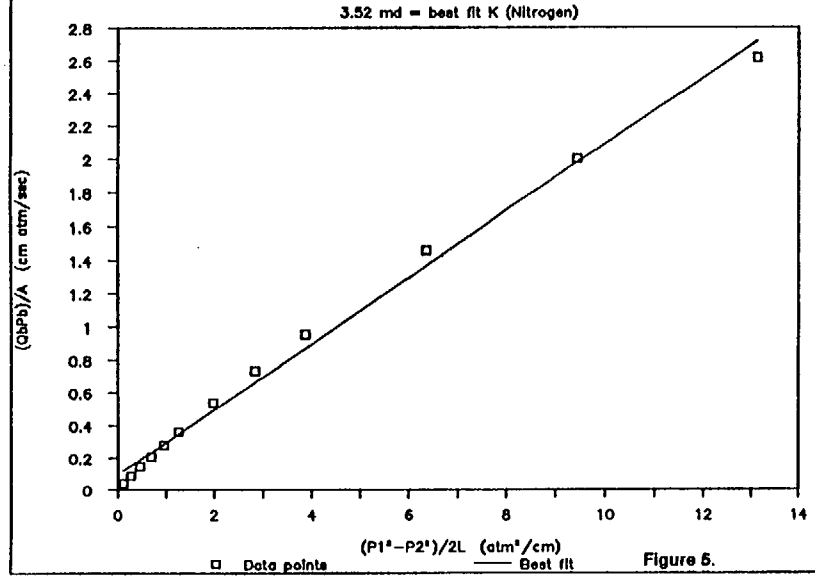

Figure 5.

Klinkenberg Extrapolation from Nitrogen Gas Data, Lab #: 2789

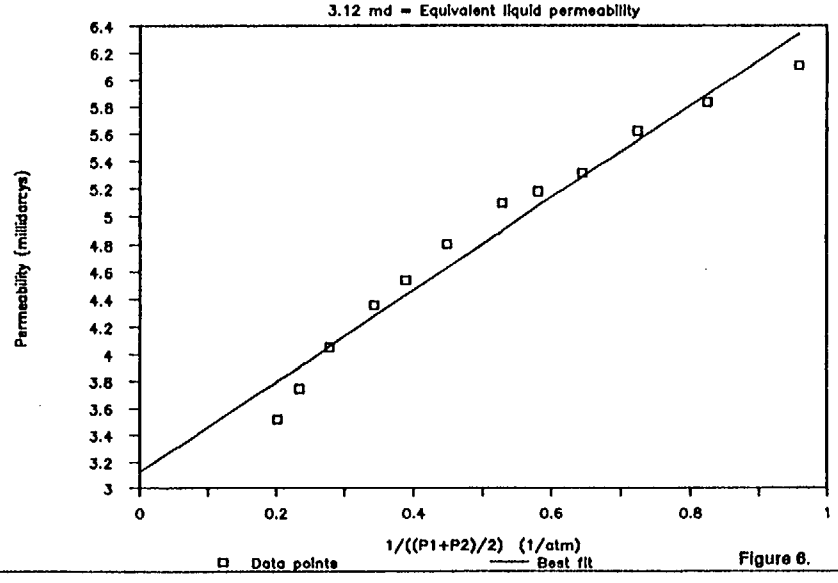

Figure 6.

TABLE 5. WATER PERMEABILITY (API RP27)

Project: YMP Wet & Dry Drilling	Print date: January 8, 1990	6.081	= diameter (cm)
Requestor: Dr. Alan L. Flint	Request #: GT-38	29.043	= cross-sectional area (cm2)
Organization: USGS	H&N ID #: 50036C	3.084	= length (cm)
Address: Box 327, M/S 721, Mercury, Nv	WBS #: 1.2.3.3.6.1	114.37	= dry wt. (g)
Phone: 5-5805	WIN #: YMP:NTS:WI:89-006	3641.54	= dry potted wt. (g)
Tested by: J. Moore	SCN: Not established	3682.20	= wet potted wt. (g)
Test date: December 4, 1989	QA level: III	1.731	= density (g/cc)
Checked by:	Lab #: 2789	26.2	= moisture (%)
Check date:	Hole & depth (ft): U12G.12, WD-1, 1.8-2.3	psi	= pressure unit: cm = cm of water; psi = psig

Pressures, psi			Differential pressure						
Inlet	Outlet	Temp., deg. C	psi	atm	Q, cc/sec	Q/A, cm/sec	P/L, atm/cm	Water viscosity, cP	Permeability, millidarcys
5.00	0.00	25.90	5.00	0.3402	0.001832	6.31E-05	0.1103	0.872	0.499
10.00	0.00	25.80	10.00	0.6805	0.003765	1.30E-04	0.2206	0.874	0.514
15.00	0.00	25.80	15.00	1.0207	0.005597	1.93E-04	0.3310	0.874	0.509
20.00	0.00	25.80	20.00	1.3609	0.007371	2.54E-04	0.4413	0.874	0.503
25.00	0.00	25.80	25.00	1.7011	0.009219	3.17E-04	0.5516	0.874	0.503
30.00	0.00	25.80	30.00	2.0414	0.010824	3.73E-04	0.6619	0.874	0.492
40.00	0.00	25.70	40.00	2.7218	0.014335	4.94E-04	0.8826	0.876	0.490
50.00	0.00	25.70	50.00	3.4023	0.017908	6.17E-04	1.1032	0.876	0.490
60.00	0.00	25.70	60.00	4.0828	0.021477	7.40E-04	1.3239	0.876	0.489
80.00	0.00	25.70	80.00	5.4437	0.027942	9.62E-04	1.7651	0.876	0.478
100.00	0.00	25.70	100.00	6.8046	0.035095	1.21E-03	2.2064	0.876	0.480
120.00	0.00	25.60	120.00	8.1655	0.040782	1.40E-03	2.6477	0.878	0.466

Equipment used:	Control No.:	Calibration due date:
Mettler PM6100 balance	PTL-2684	9/3/89
Brown & Sharpe Digit-Cal II micrometer	PTL-6786	1/17/90
Omega Model 871 digital thermometer	PTL-6976	9/13/89
Heise digital barometer	PTL-5296	6/19/90
Heise CMM 61186 0-200 psi gauge	PTL-4481	8/16/89
Wallace & Tiernan FA145 0-30 psi gauge	PTL-388	8/18/89
Markson Science #16573 digital stopwatch	S/N 006543	Manufacturer's undated certificate
Corning pipettes	None	Not calibrated
Kimble pipettes	None	Not calibrated

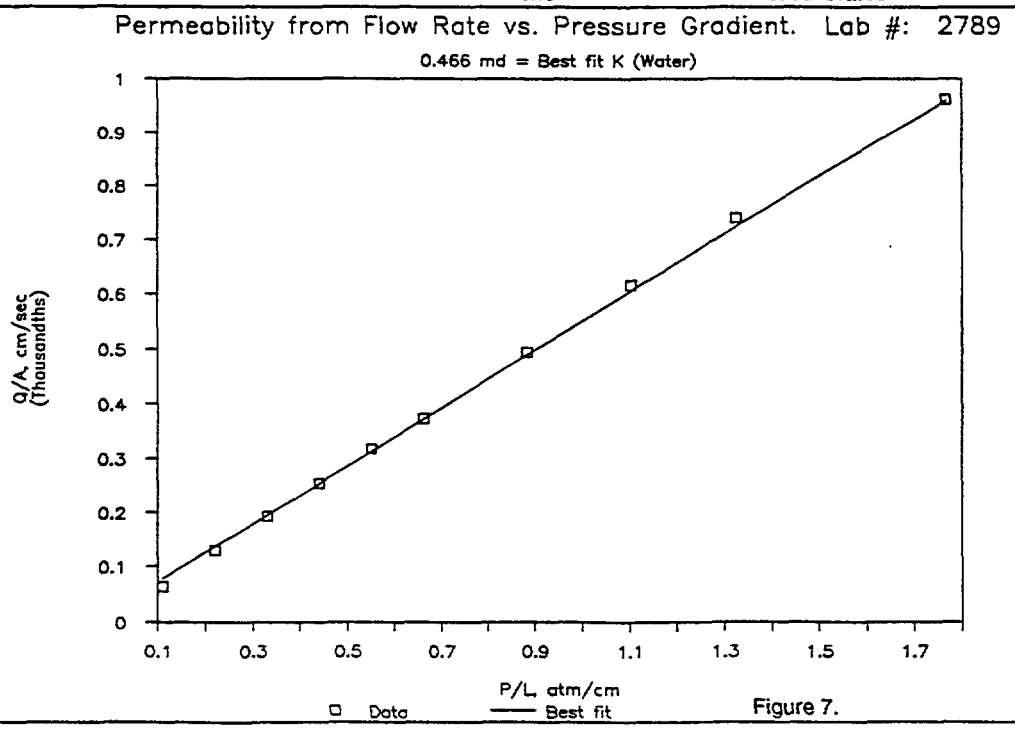

Figure 7.

TABLE 6. NITROGEN GAS PERMEABILITY AT VARIOUS DEGREES OF SATURATION (API RP27)

Project: YMP Wet & Dry Drilling	Test date: 12/5-12/7/89	WBS #: 1.2.3.3.6.1	666.0 = atmospheric pressure (m	114.37 = dry sample wt. (g)
Requestor: Dr. Alan L. Flint	Checked by:	WIN #: YMP:NTS:WI:89-006	6.081 = diameter (cm)	3641.54 = dry potted wt. (g)
Organization: USGS	Check date:	SCN: Not established	29.043 = cross-sectional area (cm	3682.20 = saturated potted wt. (g)
Address: Box 327, M/S 721, Mercury, Nv	Print date: January 9, 1990	QA level: III	3.084 = length (cm)	222.55 = empty water jar wt. (g)
Phone: 5-5805	Request #: GT-38	Lab #: 2789	1.731 = saturated density (g/cc)	155.03 = saturated sample wt. (g)
Tested by: J. Moore	H&N ID#: 50036C	Hole & depth: U12G.12 WD-1, 1.8-2.3	26.2 = moisture (% by wt.)	45.4 = moisture (% by volume)

Inlet pressure (psig)	Outlet pressure (psig)	Meter code	Meter type	Actual dT/dF	Lookup dT/dF	Flow rate (std. cc/sec)	Nitrogen temp (C)	Nitrogen vis-cosity (cp)	P1^2-P2^2)/2L (atm^2/cm)	(QbPb)/A (cm atm/sec)	As-tested permeability (millidarcys)	Water jar + water wt. (g)	Saturation (%)	Dry-core permeability (millidarcys)	Relative permeability to nitrogen (ratio)
5.00	0.00	none	No gas flow		NA	0.000	26.10	0.01778	0.1154	0.000	0.000	222.55	100	6.107	0.000
10.00	0.00	none	No gas flow		NA	0.000	25.70	0.01776	0.2684	0.000	0.000	224.78	95	5.834	0.000
15.00	0.00	pip	Pipette & stopwatch		NA	0.027	27.70	0.01784	0.4589	0.001	0.037	226.88	89	5.622	0.007
20.00	0.00	pip	Pipette & stopwatch		NA	0.099	26.80	0.01781	0.6870	0.003	0.090	228.58	85	5.313	0.017
25.00	0.00	pip	Pipette & stopwatch		NA	0.218	26.50	0.01779	0.9526	0.008	0.143	229.70	82	5.179	0.028
30.00	0.00	pip	Pipette & stopwatch		NA	0.382	26.40	0.01779	1.2557	0.013	0.190	230.40	81	5.093	0.037
40.00	0.00	pip	Pipette & stopwatch		NA	0.896	26.30	0.01778	1.9745	0.031	0.283	231.89	77	4.801	0.059
50.00	0.00	pip	Pipette & stopwatch		NA	1.686	27.60	0.01784	2.8435	0.059	0.372	233.13	74	4.541	0.082
60.00	0.00	pip	Pipette & stopwatch		NA	2.600	27.10	0.01782	3.8626	0.091	0.421	233.83	72	4.357	0.097
80.00	0.00	pip	Pipette & stopwatch		NA	4.767	26.60	0.01780	6.3512	0.167	0.468	234.58	70	4.053	0.116
100.00	0.00	pip	Pipette & stopwatch		NA	8.068	25.90	0.01777	9.4404	0.282	0.531	235.33	69	3.746	0.142
120.00	0.00	pip	Pipette & stopwatch		NA	13.607	25.10	0.01773	13.1301	0.475	0.641	237.08	64	3.520	0.182

Equipment used:	Control No.:	Calibration due date:
Mettler PM6100 balance	PTL-2684	3/21/90
Brown & Sharpe Digit-Cal II micrometer	PTL-6786	1/17/90
Omega Model 871 digital thermometer	PTL-6976	3/27/90
Heise digital barometer	PTL-5296	6/19/90
Heise CMM 61186 0-200 psi gauge	PTL-4481	1/10/90
Wallace & Tiernan FA145 0-30 psi gauge	PTL-388	2/24/90
Markson Science #16573 digital stopwatch	S/N 006543	Manufacturer's undated certificate
Corning and Kimble pipettes	None	Not calibrated
SKC soap film flowmeters	None	Not calibrated

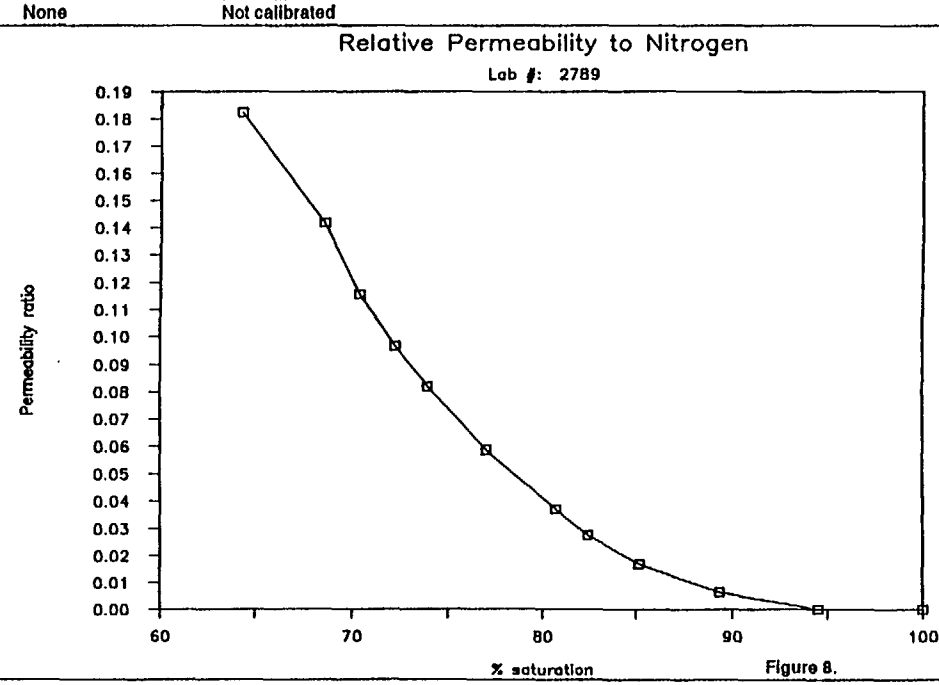

Figure 8.

TABLE 7. NITROGEN GAS PERMEABILITY (API RP27)

Project: YMP Wet & Dry Drilling	Print date: January 8, 1990	663.2	= atmospheric pressure (mm Hg)
Requestor: Dr. Alan L. Flint	Request #: GT-38	6.025	= diameter (cm)
Organization: USGS	H&N ID #: 50036 C	28.510	= cross-sectional area (cm2)
Address: Box 327, M/S 721, Mercury, Nv	WBS #: 1.2.3.3.6.1	3.848	= length (cm)
Phone: 5-5805	WIN #: YMP:NTS:WI:89-006	237.93	= weight (g)
Tested by: J. Moore	SCN: Not established	2.169	= density (g/cc)
Test date: 8/4/89	QA level: III	0.0	= moisture (%)
Checked by:	Lab #: 2800		
Check date:	Hole & depth: U12G.12 DD-2, 3.6-4.0'		

Inlet pressure (psig)	Outlet pressure (psig)	Meter code	Meter type	(For rotameters) Actual dT/dF	Lookup dT/dF	Flow rate (std. cc/sec)	Nitrogen temp (C)	Nitrogen vis-cosity (cp)	(P1^2-P2^2)/2L (atm^2/cm)	(QbPb)/A (cm atm/sec)	1/((P1+P2)/2) (1/atm)	Permeability (millidarcys)
5.00	0.00	pip	Pipette & stopwatch		NA	0.136	23.10	0.01765	0.0922	0.005	0.959	0.919
10.00	0.00	pip	Pipette & stopwatch		NA	0.302	23.10	0.01765	0.2145	0.011	0.825	0.877
15.00	0.00	pip	Pipette & stopwatch		NA	0.502	23.20	0.01765	0.3668	0.018	0.723	0.854
20.00	0.00	pip	Pipette & stopwatch		NA	0.732	23.20	0.01765	0.5493	0.026	0.644	0.831
25.00	0.00	pip	Pipette & stopwatch		NA	0.988	23.20	0.01765	0.7618	0.035	0.580	0.809
30.00	0.00	pip	Pipette & stopwatch		NA	1.289	23.20	0.01765	1.0044	0.046	0.528	0.800
40.00	0.00	pip	Pipette & stopwatch		NA	1.990	23.20	0.01765	1.5799	0.070	0.448	0.785
50.00	0.00	pip	Pipette & stopwatch		NA	2.750	23.20	0.01765	2.2757	0.097	0.389	0.753
60.00	0.00	pip	Pipette & stopwatch		NA	3.542	23.20	0.01765	3.0918	0.125	0.343	0.714
80.00	0.00	pip	Pipette & stopwatch		NA	5.469	23.20	0.01765	5.0850	0.193	0.278	0.671
100.00	0.00	pip	Pipette & stopwatch		NA	7.662	23.20	0.01765	7.5595	0.271	0.234	0.632
120.00	0.00	pip	Pipette & stopwatch		NA	10.103	23.20	0.01765	10.5154	0.357	0.202	0.599

Equipment used:	Control No.:	Calibration due date:
Mettler PM6100 balance	PTL-2684	9/3/89
Brown & Sharpe Digit-Cal II micrometer	PTL-6786	1/17/90
Omega Model 871 digital thermometer	PTL-6976	9/13/89
Heise digital barometer	PTL-5296	6/19/90
Heise CMM 61186 0-200 psi gauge	PTL-4481	8/16/89
Wallace & Tiernan FA145 0-30 psi gauge	PTL-388	8/18/89
Markson Science #16573 digital stopwatch	S/N 006543	Manufacturer's undated certificate
SKC soap film flowmeters	None	Not calibrated

Permeability from Base Flow vs. Pressure Gradient. Lab #: 2800

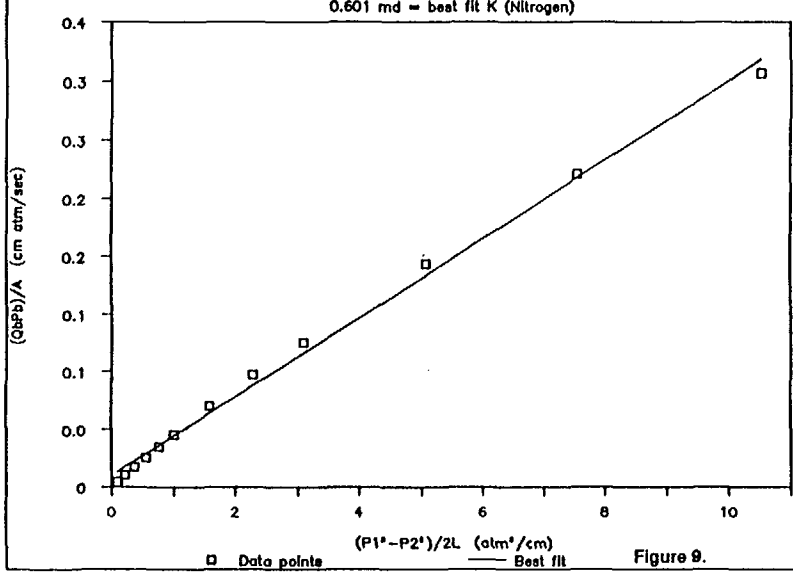

Figure 9.

Klinkenberg Extrapolation from Nitrogen Gas Data, Lab #: 2800

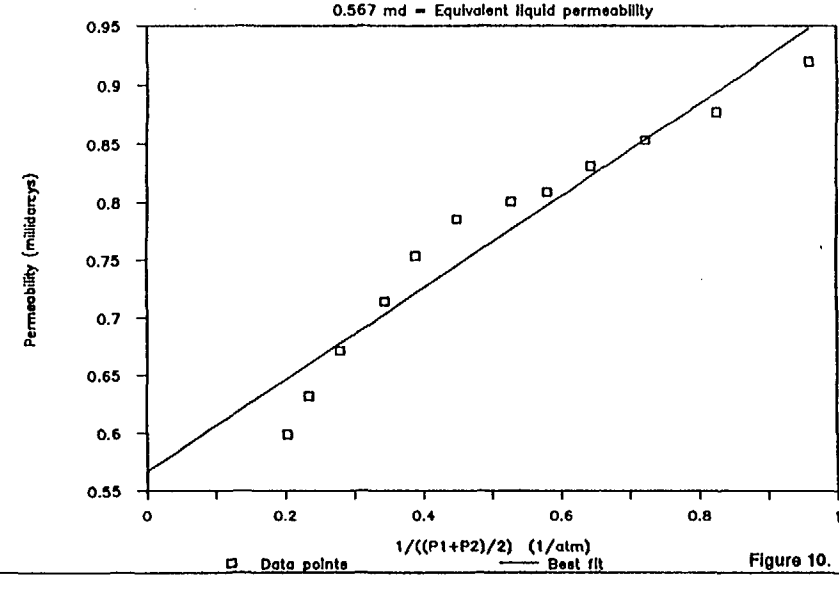

Figure 10.

TABLE 8. WATER PERMEABILITY (API RP27)

Project: YMP Wet & Dry Drilling	Print date: January 8, 1990	6.025	= diameter (cm)
Requestor: Dr. Alan L. Flint	Request #: GT-38	28.510	= cross-sectional area (cm2)
Organization: USGS	H&N ID #: 50036C	3.848	= length (cm)
Address: Box 327, M/S 721, Mercury, Nv	WBS #: 1.2.3.3.6.1	237.93	= dry wt. (g)
Phone: 5-5805	WIN #: YMP:NTS:WI:89-006	3736.96	= dry potted wt. (g)
Tested by: J. Moore	SCN: Not established	3756.04	= wet potted wt. (g)
Test date: 12/8/89	QA level: III	2.343	= density (g/cc)
Checked by:	Lab #: 2800	7.4	= moisture (%)
Check date:	Hole & depth (ft): U12G.12, DD-2, 3.6-4.0'	psi	= pressure unit: cm = cm of water; psi = psig

Pressures, psi			Differential pressure						
Inlet	Outlet	Temp., deg. C	psi	atm	Q, cc/sec	Q/A, cm/sec	P/L, atm/cm	Water viscosity, cP	Permeability, millidarcys
5.00	0.00	25.00	5.00	0.3402	0.000632	2.22E-05	0.0884	0.890	0.223
10.00	0.00	25.10	10.00	0.6805	0.001246	4.37E-05	0.1768	0.888	0.220
15.00	0.00	25.10	15.00	1.0207	0.001860	6.52E-05	0.2653	0.888	0.218
20.00	0.00	25.10	20.00	1.3609	0.002602	9.13E-05	0.3537	0.888	0.229
25.00	0.00	25.10	25.00	1.7011	0.003230	1.13E-04	0.4421	0.888	0.228
30.00	0.00	25.20	30.00	2.0414	0.003797	1.33E-04	0.5305	0.886	0.222
40.00	0.00	25.20	40.00	2.7218	0.005327	1.87E-04	0.7073	0.886	0.234
50.00	0.00	25.20	50.00	3.4023	0.007040	2.47E-04	0.8842	0.886	0.247
60.00	0.00	25.20	60.00	4.0828	0.008490	2.98E-04	1.0610	0.886	0.249
80.00	0.00	25.20	80.00	5.4437	0.012007	4.21E-04	1.4147	0.886	0.264
100.00	0.00	25.20	100.00	6.8046	0.015322	5.37E-04	1.7683	0.886	0.269
120.00	0.00	25.20	120.00	8.1655	0.018742	6.57E-04	2.1220	0.886	0.275

Equipment used:	Control No.:	Calibration due date:
Mettler PM6100 balance	PTL-2684	9/3/89
Brown & Sharpe Digit-Cal II micrometer	PTL-6786	1/17/90
Omega Model 871 digital thermometer	PTL-6976	9/13/89
Heise digital barometer	PTL-5296	6/19/90
Heise CMM 61186 0-200 psi gauge	PTL-4481	8/16/89
Wallace & Tiernan FA145 0-30 psi gauge	PTL-388	8/18/89
Markson Science #16573 digital stopwatch	S/N 006543	Manufacturer's undated certificate
Corning pipettes	None	Not calibrated
Kimble pipettes	None	Not calibrated

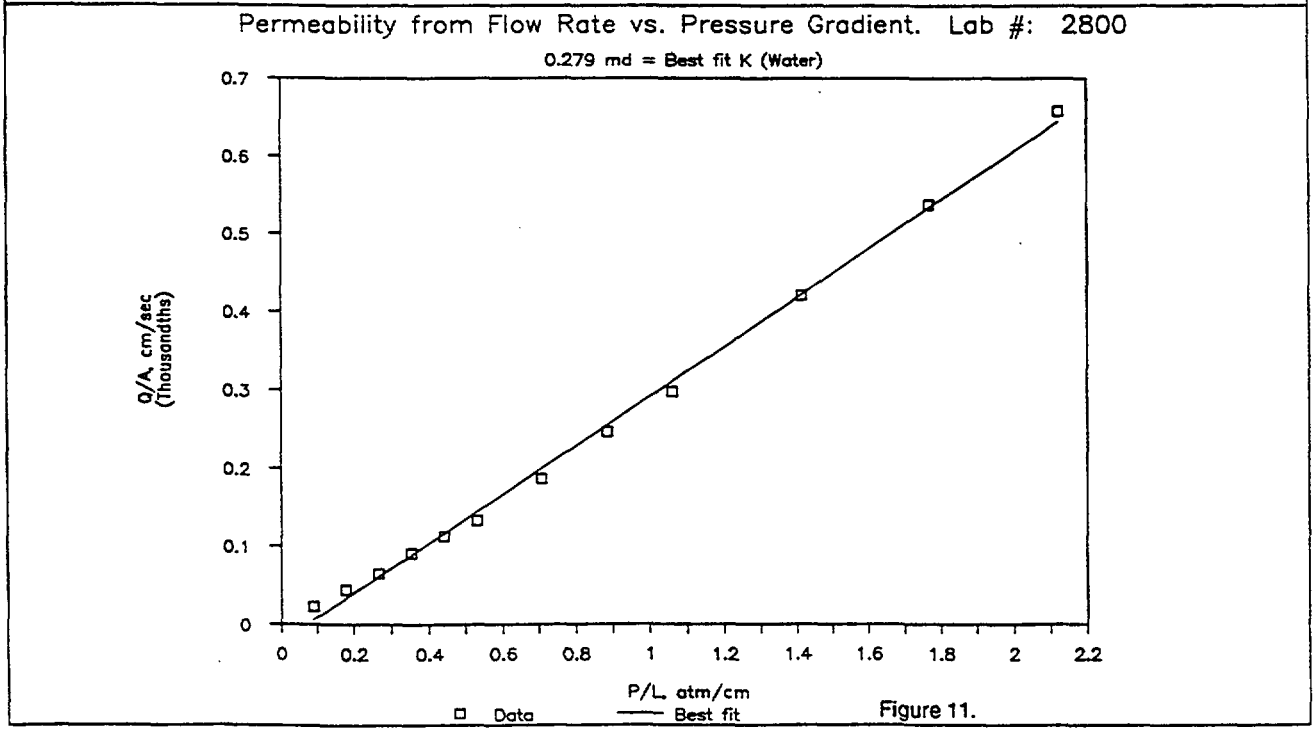

Figure 11.

TABLE 9. NITROGEN GAS PERMEABILITY AT VARIOUS DEGREES OF SATURATION (API RP27)

Project: YMP Wet & Dry Drilling	Test date: 12/11/89	WBS #: 1.2.3.3.6.1	672.8	= atmospheric pressure (m	237.93 = dry sample wt. (g)
Requestor: Dr. Alan L. Flint	Checked by:	WIN #: YMP:NTS:WI:89-006	6.025	= diameter (cm)	3736.98 = dry potted wt. (g)
Organization: USGS	Check date:	SCN: Not established	28.510	= cross-sectional area (cm	3756.04 = saturated potted wt. (g)
Address: Box 327, M/S 721, Mercury, Nv	Print date: January 9, 1990	QA level: III	3.848	= length (cm)	221.21 = empty water jar wt. (g)
Phone: 5-5805	Request #: GT-38	Lab #: 2800	2.343	= saturated density (g/cc)	257.01 = saturated sample wt. (g)
Tested by: J. Moore	H&N ID #: 50036C	Hole & depth: U12G.12 DD-2, 3.6-4.0	7.4	= moisture (% by wt.)	17.4 = moisture (% by volume)

Inlet pressure (psig)	Outlet pressure (psig)	Meter code	Meter type	Actual dT/dF	Lookup dT/dF	Flow rate (std. cc/sec)	Nitrogen temp (C)	Nitrogen viscosity (cp)	P1^2-P2^2)/2L (atm^2/cm)	(QbPb)/A (cm atm/sec)	As-tested permeability (millidarcys)	Water jar + water wt. (g)	Saturation (%)	Dry-core permeability (millidarcys)	Relative permeability to nitrogen (ratio)
5.00	0.00	none	No gas flow		NA	0.000		0.01665	0.0933	0.000	0.000	221.21	100	0.919	0.000
10.00	0.00	none	No gas flow		NA	0.000		0.01665	0.2167	0.000	0.000	221.21	100	0.877	0.000
15.00	0.00	none	No gas flow		NA	0.000		0.01665	0.3702	0.000	0.000	221.68	98	0.854	0.000
20.00	0.00	pip	Pipette & stopwatch		NA	0.026		0.01665	0.5538	0.001	0.028	222.02	96	0.831	0.031
25.00	0.00	pip	Pipette & stopwatch		NA	0.078		0.01665	0.7674	0.003	0.055	222.69	92	0.809	0.068
30.00	0.00	pip	Pipette & stopwatch		NA	0.153		0.01665	1.0111	0.005	0.082	223.02	91	0.800	0.103
40.00	0.00	pip	Pipette & stopwatch		NA	0.363		0.01665	1.5889	0.012	0.124	223.43	88	0.785	0.158
50.00	0.00	pip	Pipette & stopwatch		NA	0.702		0.01665	2.2869	0.023	0.167	223.72	87	0.753	0.221
60.00	0.00	pip	Pipette & stopwatch		NA	1.200		0.01665	3.1053	0.039	0.210	224.17	84	0.714	0.293
80.00	0.00	pip	Pipette & stopwatch		NA	2.424		0.01665	5.1030	0.079	0.257	224.81	81	0.671	0.384
100.00	0.00	pip	Pipette & stopwatch		NA	3.736		0.01665	7.5820	0.122	0.267	225.45	78	0.632	0.423
120.00	0.00	pip	Pipette & stopwatch		NA	5.160		0.01665	10.5423	0.168	0.265	226.17	74	0.599	0.443

Equipment used:	Control No.:	Calibration due date:
Mettler PM6100 balance	PTL-2684	3/21/90
Brown & Sharpe Digit-Cal II micrometer	PTL-6786	1/17/90
Omega Model 871 digital thermometer	PTL-6976	3/27/90
Heise digital barometer	PTL-5296	6/19/90
Heise CMM 61186 0-200 psi gauge	PTL-4481	1/10/90
Wallace & Tiernan FA145 0-30 psi gauge	PTL-388	2/24/90
Markson Science #16573 digital stopwatch	S/N 006543	Manufacturer's undated certificate
Corning and Kimble pipettes	None	Not calibrated
SKC soap film flowmeters	None	Not calibrated

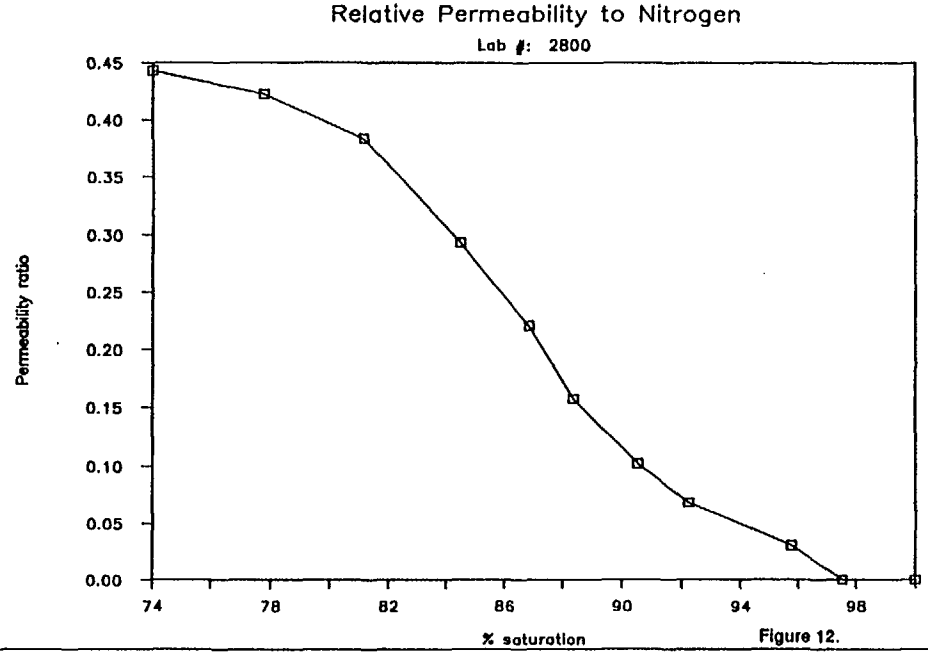

Figure 12.

TABLE 10. NITROGEN GAS PERMEABILITY (API RP27)

Project: YMP Wet & Dry Drilling	Print date: January 10, 1990	663.4	= atmospheric pressure (mm Hg)
Requestor: Dr. Alan L. Flint	Request #: GT-38	6.096	= diameter (cm)
Organization: USGS	H&N ID #: 50036 C	29.186	= cross-sectional area (cm2)
Address: Box 327, M/S 721, Mercury, Nv	WBS #: 1.2.3.3.6.1	3.785	= length (cm)
Phone: 5-5805	WIN #: YMP:NTS:WI:89-006	239.93	= weight (g)
Tested by: J. Moore	SCN: Not established	2.172	= density (g/cc)
Test date: 8/4/89	QA level: III	0.0	= moisture (%)
Checked by:	Lab #: 2818		
Check date:	Hole & depth: U12G.12 WD-2, 22.2-22.6'		

Inlet pressure (psig)	Outlet pressure (psig)	Meter code	Meter type	(For Actual dT/dF	rotameters) Lookup dT/dF	Flow rate (std. cc/sec)	Nitrogen temp (C)	Nitrogen vis-cosity (cp)	(P1^2-P2^2)/2L (atm^2/cm)	(QbPb)/A (cm atm/sec)	1/((P1+P2)/2) (1/atm)	Permeability (millidarcys)
5.00	0.00	pip	Pipette & stopwatch		NA	0.018	22.60	0.01762	0.0938	0.001	0.959	0.117
10.00	0.00	pip	Pipette & stopwatch		NA	0.039	22.60	0.01762	0.2181	0.001	0.824	0.108
15.00	0.00	pip	Pipette & stopwatch		NA	0.062	22.60	0.01762	0.3730	0.002	0.723	0.100
20.00	0.00	pip	Pipette & stopwatch		NA	0.086	22.60	0.01762	0.5585	0.003	0.644	0.093
25.00	0.00	pip	Pipette & stopwatch		NA	0.113	22.60	0.01762	0.7746	0.004	0.580	0.088
30.00	0.00	pip	Pipette & stopwatch		NA	0.143	22.60	0.01762	1.0213	0.005	0.528	0.085
40.00	0.00	pip	Pipette & stopwatch		NA	0.207	22.60	0.01762	1.6064	0.007	0.448	0.078
50.00	0.00	pip	Pipette & stopwatch		NA	0.277	22.60	0.01762	2.3138	0.010	0.388	0.073
60.00	0.00	pip	Pipette & stopwatch		NA	0.356	22.70	0.01763	3.1436	0.012	0.343	0.069
80.00	0.00	pip	Pipette & stopwatch		NA	0.530	22.70	0.01763	5.1701	0.018	0.278	0.062
100.00	0.00	pip	Pipette & stopwatch		NA	0.739	22.70	0.01763	7.6860	0.025	0.234	0.058
120.00	0.00	pip	Pipette & stopwatch		NA	0.969	22.70	0.01763	10.6911	0.033	0.202	0.055

Equipment used:	Control No.:	Calibration due date:
Mettler PM6100 balance	PTL-2684	9/3/89
Brown & Sharpe Digit-Cal II micrometer	PTL-6786	1/17/90
Omega Model 871 digital thermometer	PTL-6976	9/13/89
Heise digital barometer	PTL-5296	6/19/90
Heise CMM 61186 0-200 psi gauge	PTL-4481	8/16/89
Wallace & Tiernan FA145 0-30 psi gauge	PTL-388	8/18/89
Markson Science #16573 digital stopwatch	S/N 006543	Manufacturer's undated certificate
SKC soap film flowmeters	None	Not calibrated

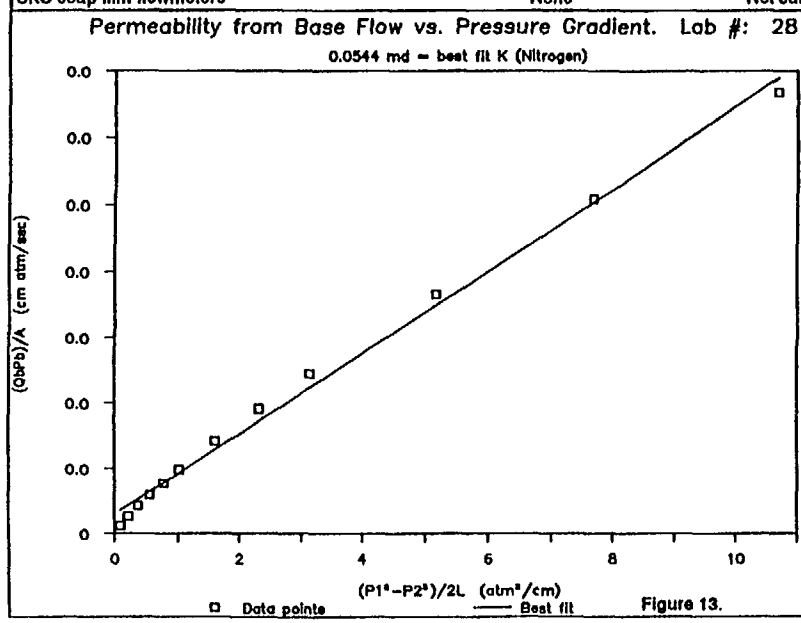

Figure 13.

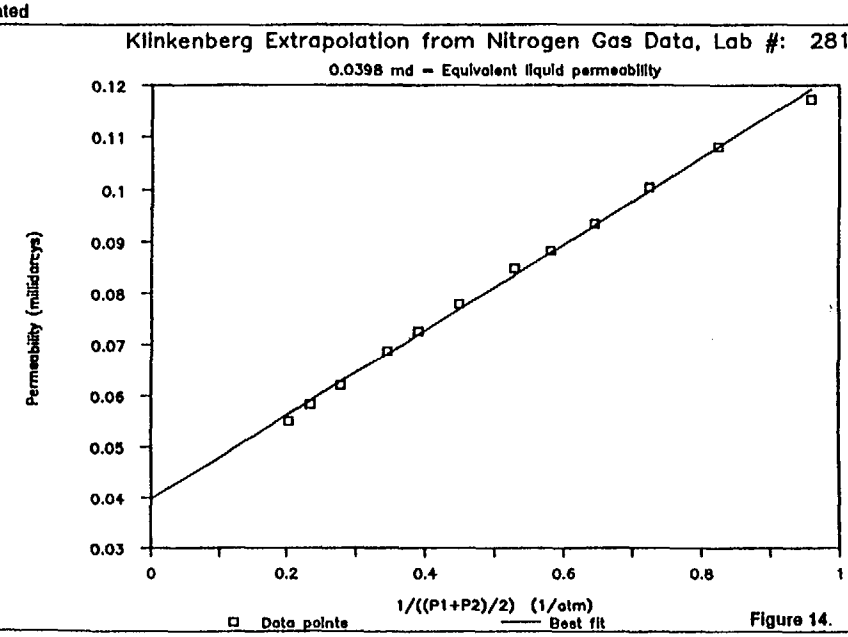

Figure 14.

APPENDIX A6

Summary of variography and
spatial variability analyses

Summary of variography and spatial variability analyses

Experimental variograms were calculated for the nonwelded borehole (Figures A.6a and b) by using a fixed 0.1 m pair spacing and variable pair number with no pair number less than 30. The experimental variograms for bulk density, sorptivity, porosity and saturation provided some insight into the structure of the spatial variability. The undulation or "hole effect" in the variogram for the nonwelded dry drilled borehole (Fig. A.6a and b) is the result of the alternating zeolitic and silicified beds penetrated by the borehole. This effect for porosity is more subtle because it is less sensitive to lithology differences than the other three parameters. The beds alternate at approximately 2 m distance as does the experimental variogram.

A Gaussian model with a nugget was fit to each experimental variogram. A Gaussian model fit better than a spherical model due to small scale continuity that showed up at the sample spacing of 0.1 m but not at larger spacings. The nugget values for porosity and bulk density are relatively small because their physical characteristics are independent of any other variable and should show a greater continuity at the sampling scale. Sorptivity and saturation both depend on porosity but introduce additional variables thus increasing the inherent variability displayed in their higher nugget values. Sorptivity has the highest nugget value due to flow processes being influenced by variables such as tortuosity, clays and zeolites.

The range of each model variogram was 1.12 m. Even though visually the beds repeat at 2 m, the contacts are fairly diffuse when judged using hydrologic properties. The range of 1.12 m indicates that a sample may not be representative of the rock more than a meter away and a minimum of 5 samples would be required to use the model variogram to any advantage to estimate properties at all unmeasured locations. If classical statistics such as mean and standard deviation were to be used instead, it would be calculated that 7 samples would be needed to characterize bulk density, 14 would be needed for porosity, 6 for saturation, and 75 samples would be needed to characterize sorptivity in this 10 m borehole. These sample numbers are for calculating mean values and do not attempt to characterize the spatial structure as does the geostatistical analysis. Using a knowledge of the spatial structure of the flow parameter, sorptivity, is certainly an advantage in limiting the number of measurements needed.

Variograms on were done as above on the core measurements from the welded borehole (Figure A.6c). Linear models were fitted to the sample variograms using regression. There is some evidence of very weak spatial correlation for bulk density and saturation at this scale and sample spacing provided by the small positive slope of the models. The degree of spatial correlation, however, is extremely small, and the application of geostatistics (using a "pure nugget" model, for example) or any other technique utilizing a spatial model may not provide any advantages over classical

statistical methods in estimating mean values, confidence intervals, and minimum sample sizes for the purpose of characterization. Although it is likely that significant spatial correlation for some parameters within the welded unit does exist at some scale, either a closer sample spacing or a larger sample domain (i.e., a longer borehole) is needed before such spatial structure can be identified and correctly modeled. Classical statistics in this case provided estimates of these parameters and was satisfactory for determination of number of samples necessary to describe the properties in the welded unit. It can be calculated that 3 samples would be necessary to characterize bulk density, 5 would be needed for porosity and saturation, but approximately 126 samples would be required to characterize sorptivity. It would be understandably useful, therefore, to be able to define the spatial structure of the welded borehole in order to reduce the number of samples required.

A comparison of sample variograms between the welded and nonwelded samples indicates that the absolute variability for all parameters is less for the welded samples. With the exception of saturation, the overall variability for the welded unit is less than or approximately equivalent to the nugget values of fitted models for the nonwelded unit. It can be concluded that, although the spatial correlation of most parameters in the welded unit is poor relative to the nonwelded unit, the total variablity of measured values is much less throughout the welded borehole.

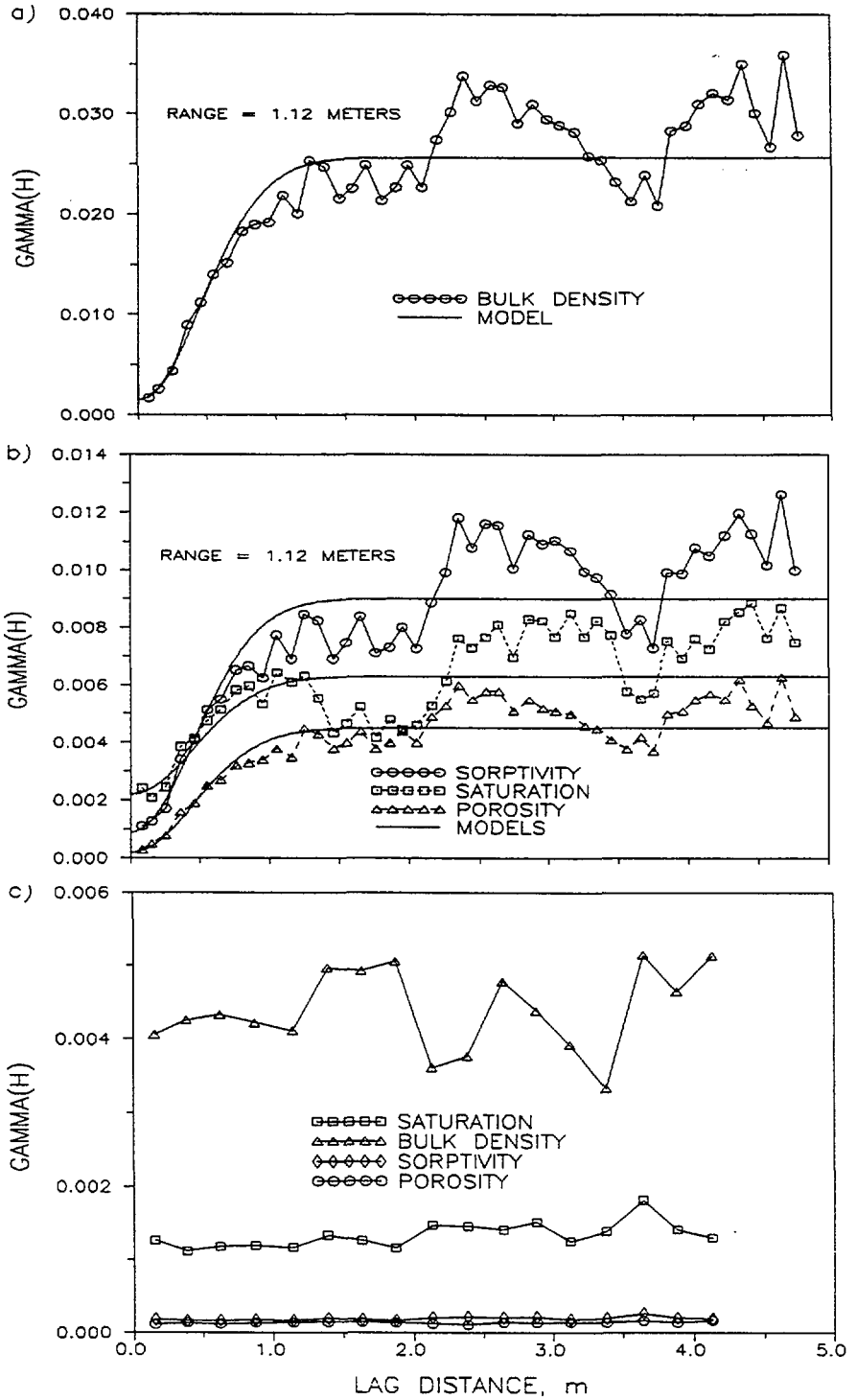

Figures A.6a, b, c. Variograms of a) bulk density, b) sorptivity, relative saturation and porosity all with fitted models in nonwelded borehole, and c) saturation, bulk density, sorptivity and porosity in welded borehole.

APPENDIX A7

Rock temperature measurements during borehole drilling

Rock temperature measurements during borehole drilling.

Borehole rock temperatures were measured using 15 thermocouples inside a borehole immediately after the termination of drilling. Figure A.7a is the temperature 1 minute after drilling stopped. Higher temperatures are evident in the kerf marks where the diamond core bit makes contact. A low temperature area exists below the center of the core. Figure A.7b is the temperature 20 minutes after cessation of drilling and Figure A.7c is the temperature after 1 hour. The ambient rock temperatures were approximately 17.5 C and were reached within 2 hours.

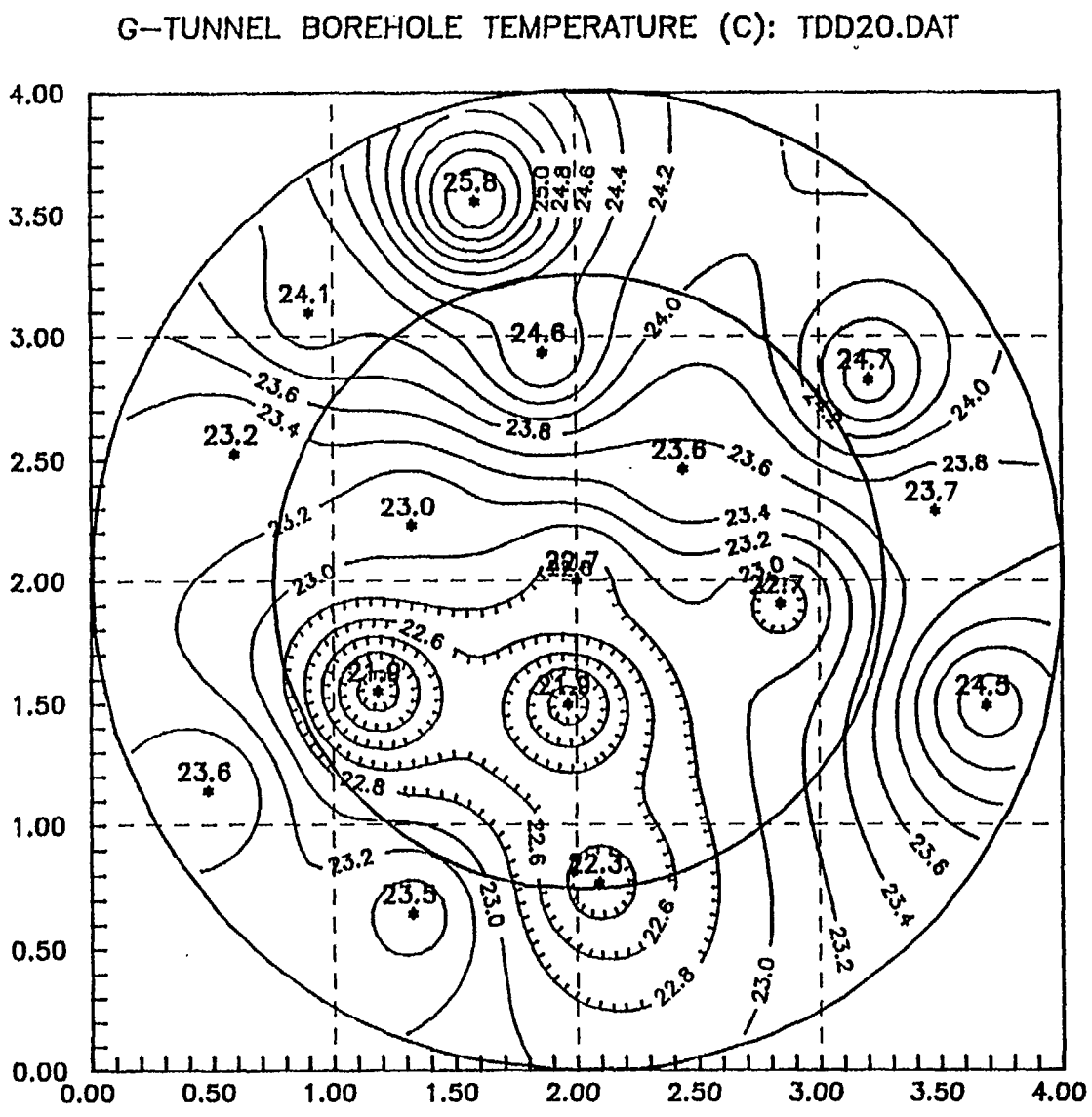

Figure A.7a. Isohyetal representation of rock temperature field in the end of dry drilled welded borehole, DD-2 based on rock temperature measurements with 15 thermocouples, 1 minute following cessation of drilling.

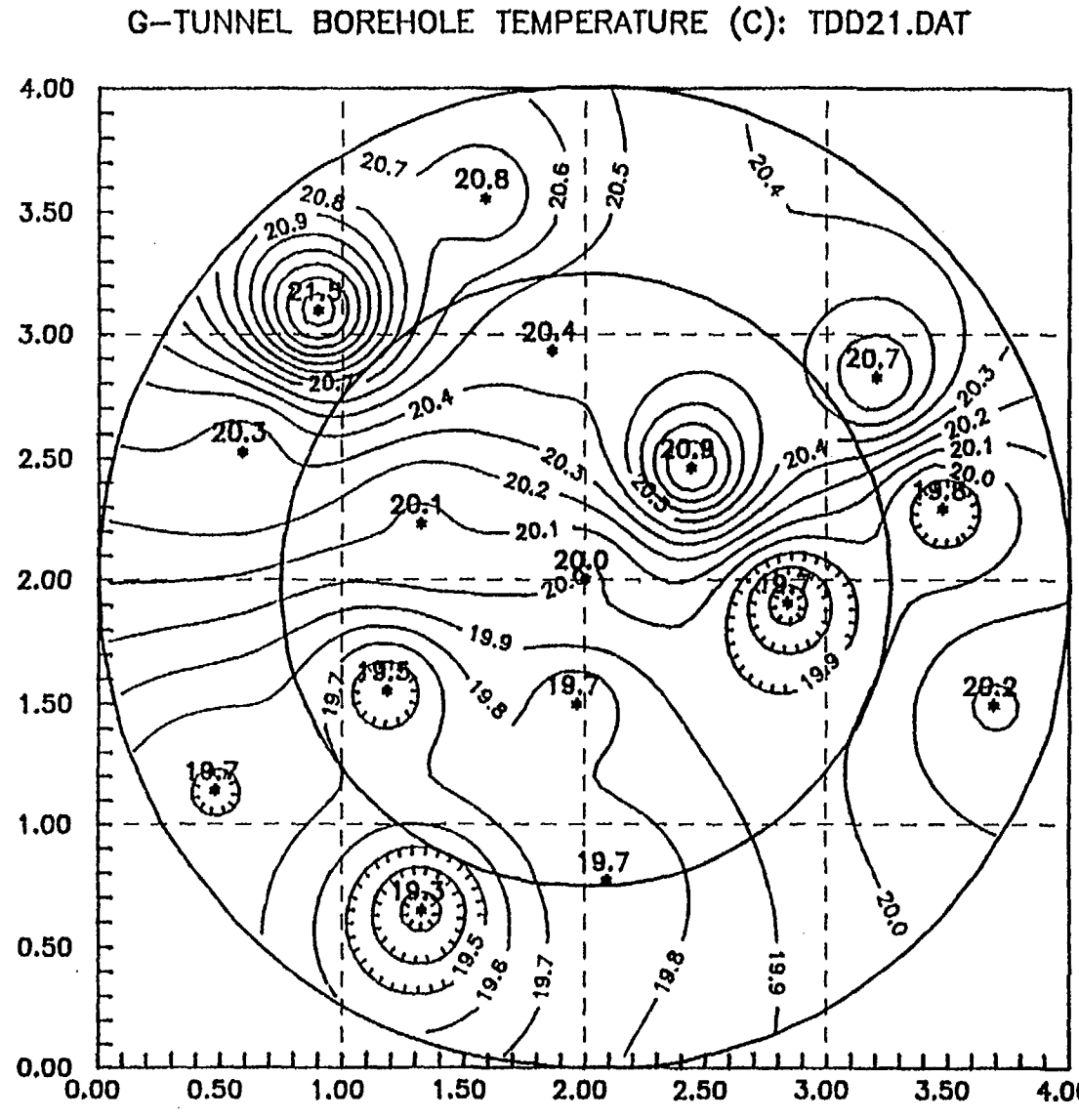

Figure A.7b. Isohyetal representation of rock temperature field in the end of dry drilled welded borehole, DD-2 based on rock temperature measurements with 15 thermocouples, 20 minutes following cessation of drilling.

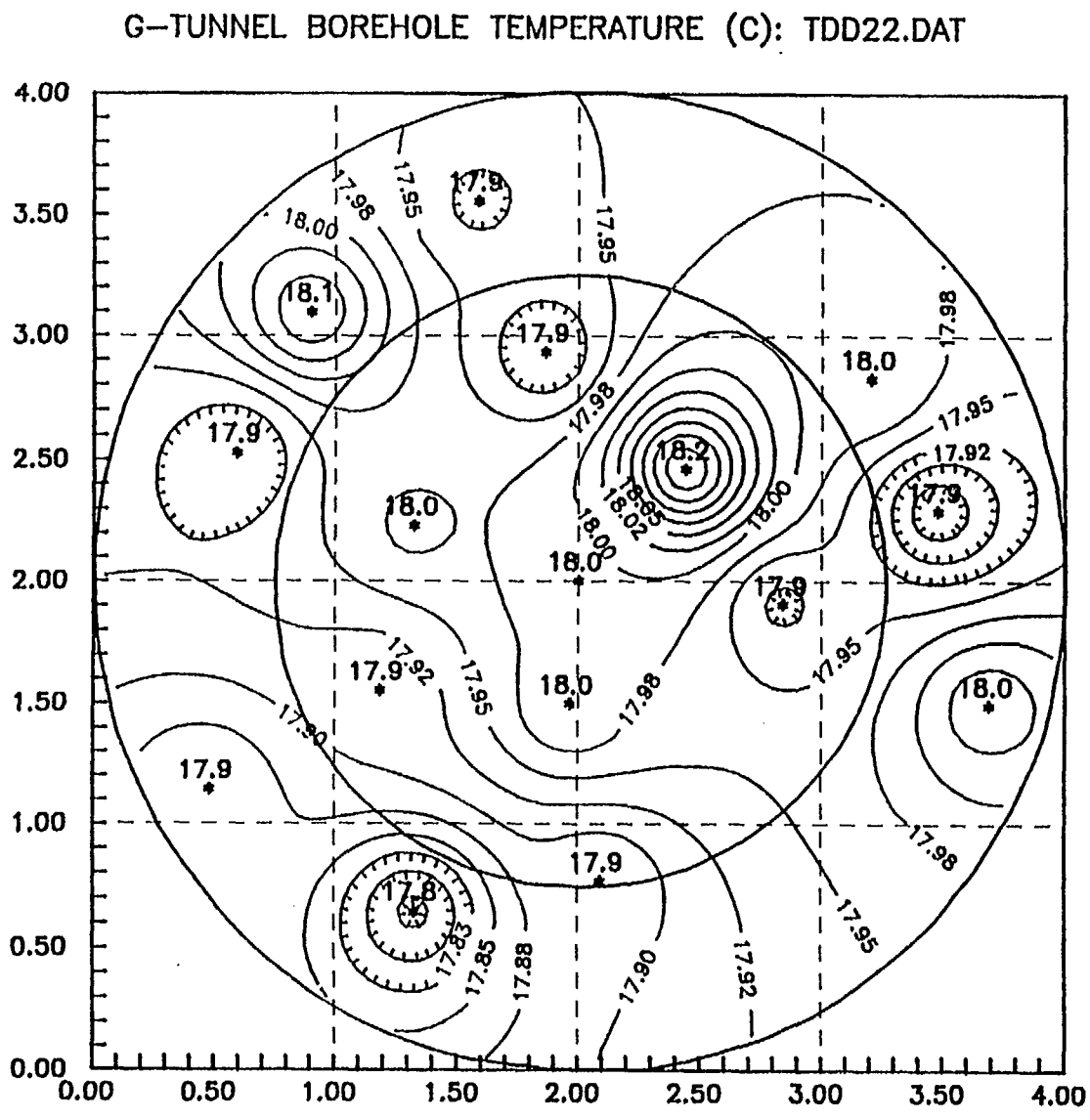

Figure A.7c. Isohyetal representation of rock temperature field in the end of dry drilled welded borehole, DD-2 based on rock temperature measurements with 15 thermocouples, 1 hour following cessation of drilling.

APPENDIX A8

Example data sets

Example data sets.

Example data sets are represented in the following figures corresponding to 1) physical and hydrologic measurements on core samples, (8 figures), 2) neutron logging measurements in 4 boreholes, (4 figures), and 3) in situ measurements of borehole conditions following drilling in 4 boreholes (3 figures).

a)

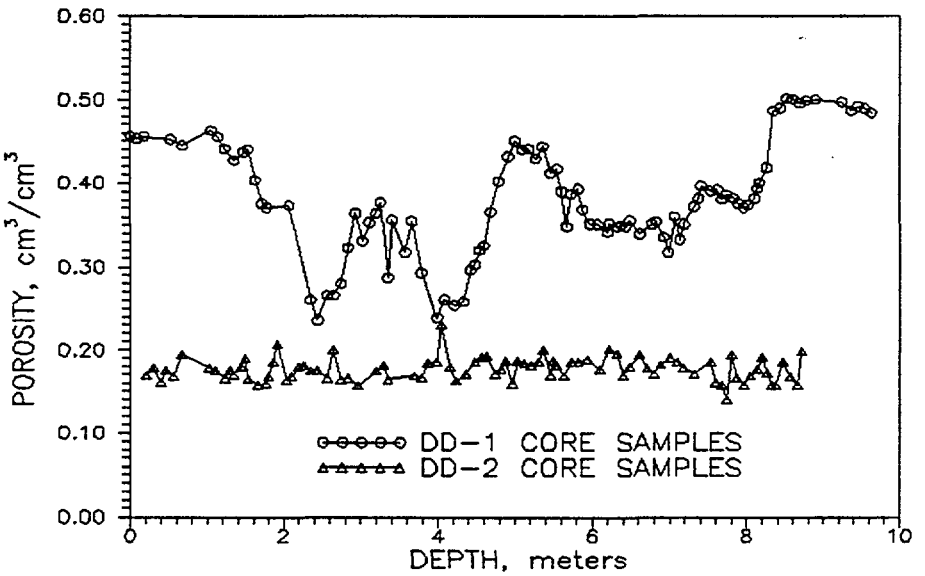

b)

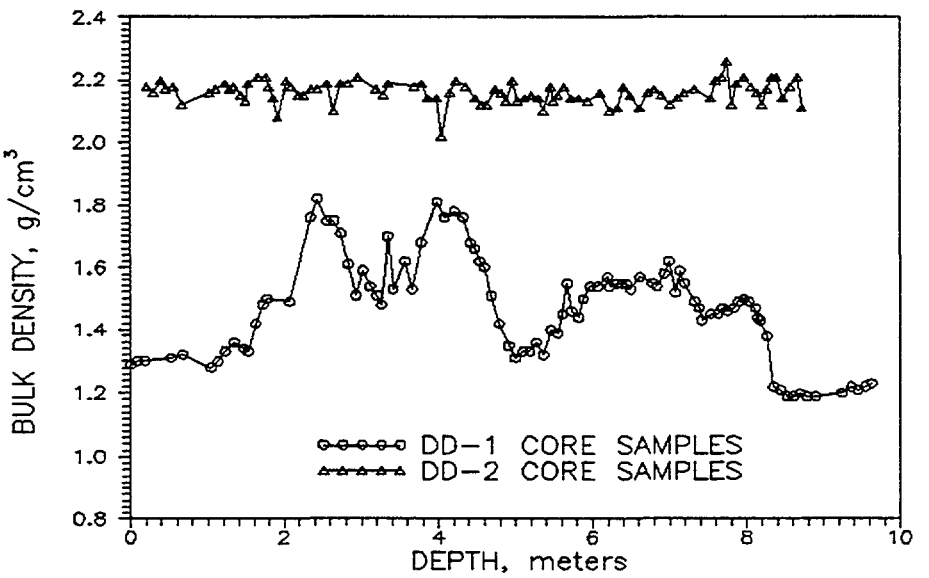

Figure A.8a and b. Measurements of porosity and bulk density on core samples collected from dry drilled nonwelded and welded boreholes. Almost mirror images of each other, porosity and bulk density show a lower variability in physical structure in the welded DD-2 samples, with a much lower porosity and higher bulk density than for the nonwelded DD-1 samples.

c)

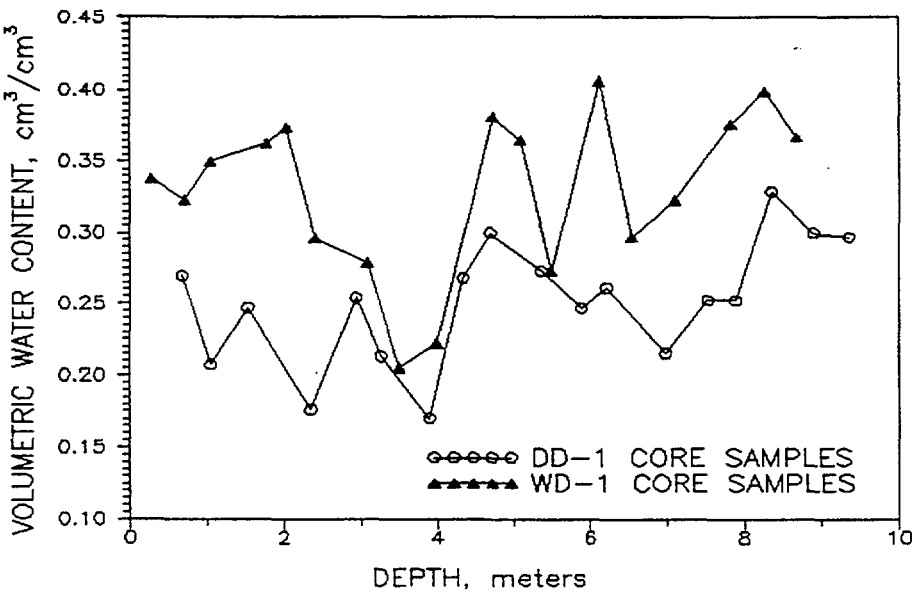

d)

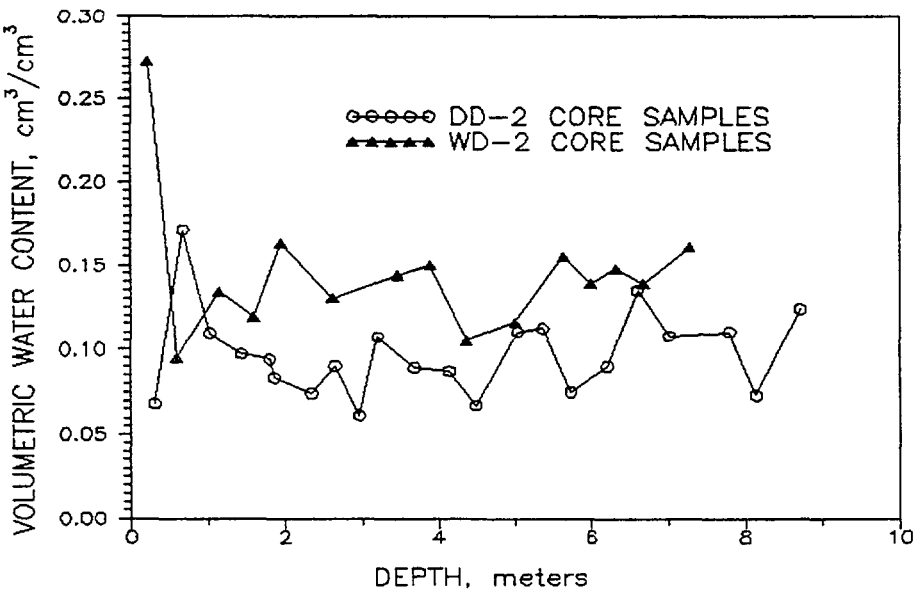

Figure A.8c and d. Volumetric water contents measured on welded and nonwelded core samples obtained from wet and dry drilled boreholes. On average, the welded samples were half as wet as the nonwelded samples, due to their lower porosity. The wet drilled samples were wetter than the dry drilled in both rock units. The samples from the nonwelded boreholes have water contents that reflect the higher porosity in the zeolitized zones (see Figure 2 in section 3.1.1) and lower porosity silicified zones.

e)

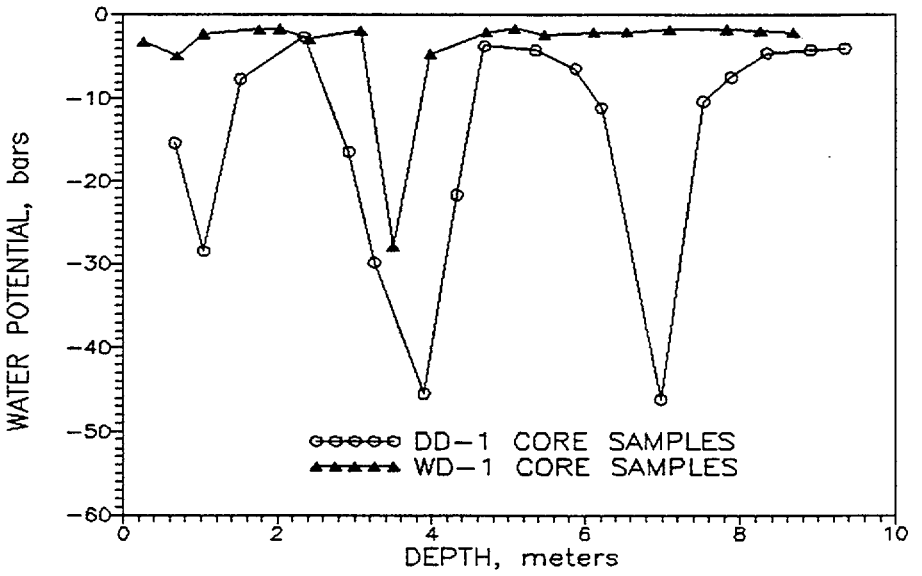

f)

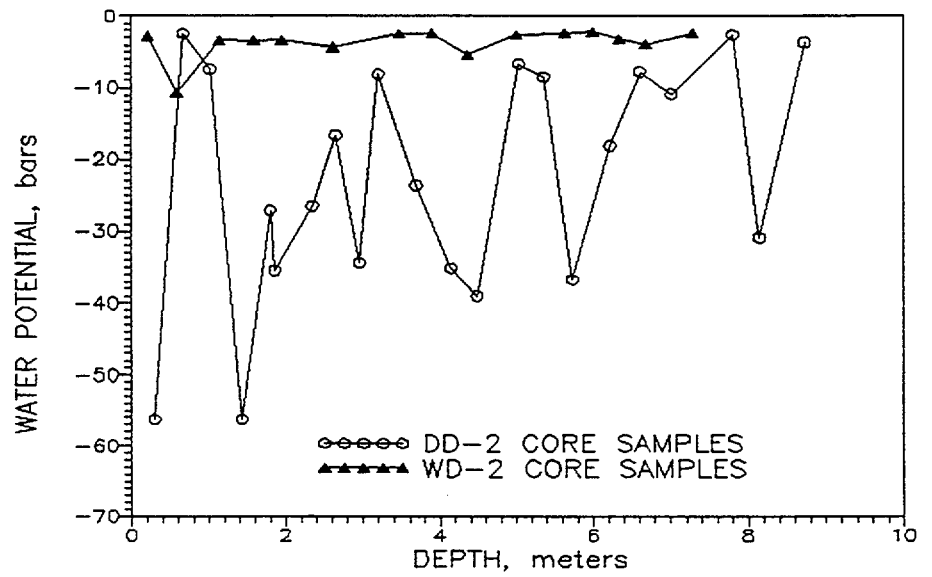

Figure A.8e and f. Water potential measured using a Richards' psychrometer, on chips taken directly adjacent to core samples from 4 boreholes. Welded boreholes show much higher water potentials and less variability than the nonwelded boreholes except in the two locations where lower potentials reflect air flow patterns through a large fracture zone (WD-2) and low porosity in a silicified zone (WD-1). DD-1 shows lower potentials in the silicified zones, while DD-2 shows much variability throughout the highly fractured welded borehole, probably indicating air flow through fractures.

g)

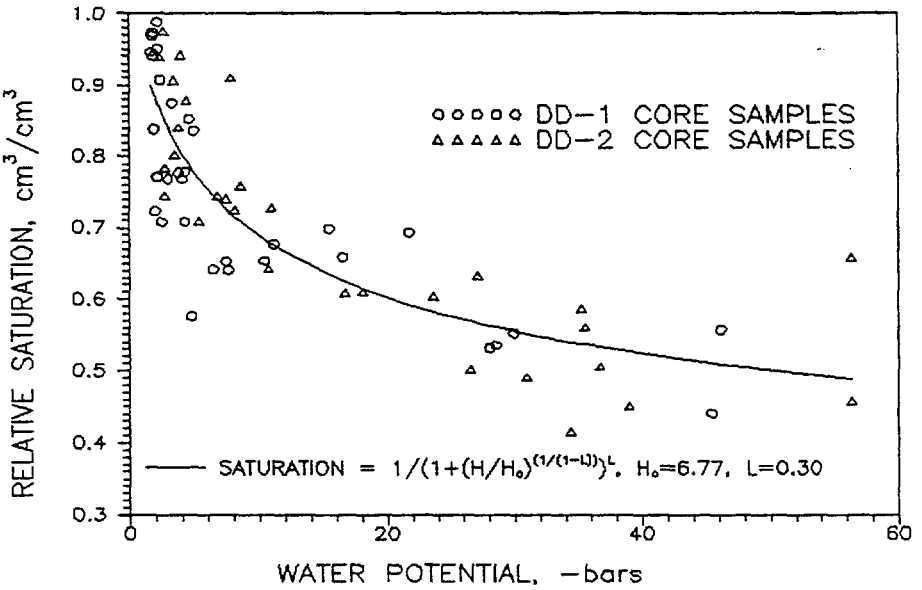

Figure A.8g. Moisture characteristic composite curve assembled by measuring water potential on chips from core samples followed by water content measurements. Curve is fit minimized on saturation. Points reflect <u>in situ</u> moisture characteristic of core, whether in desorption or sorption phase.

h)

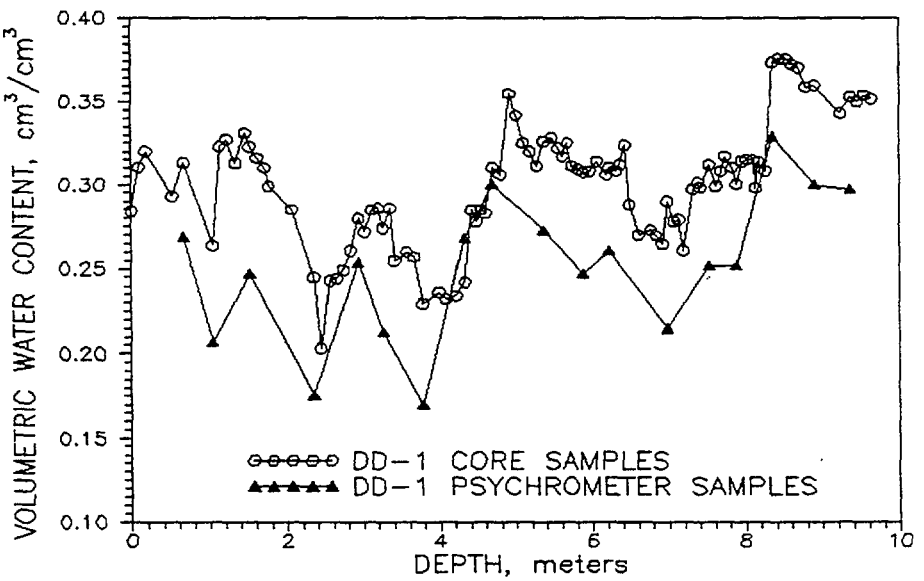

Figure A.8h. Volumetric water content of core samples from DD-1 and corresponding adjacent chips upon which water potential was measured immediately followed by water content measurements. This indicates an error introduced by sample handling during the water potential measurement causing drying of the sample.

i)

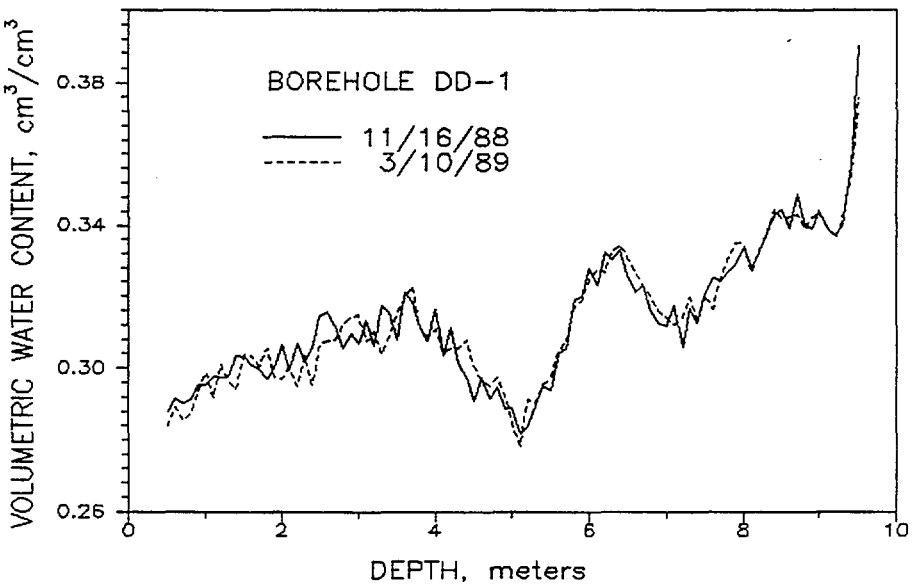

j)

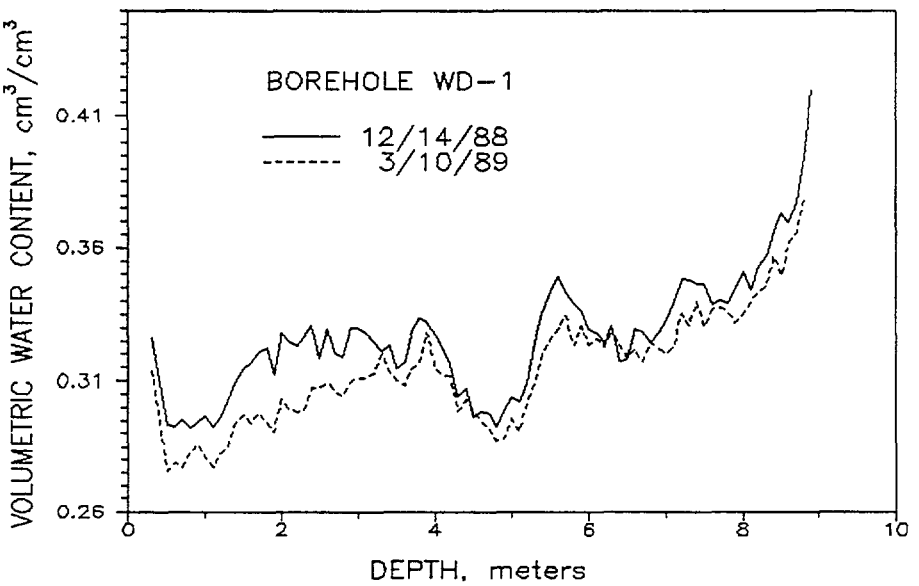

Figure A.8i and j. Volumetric water content determined in nonwelded boreholes using neutron moisture meters. Logs were run immediately following drilling and approximately 3 months later, assuming equilibration to ambient pre-drilling moisture conditions. There was very little change in water content in DD-1, however wet drilling in WD-1 contributed water to the formation throughout the depth of the borehole. This is especially true in the more porous nonwelded rock (See Fig. A.8l).

k)

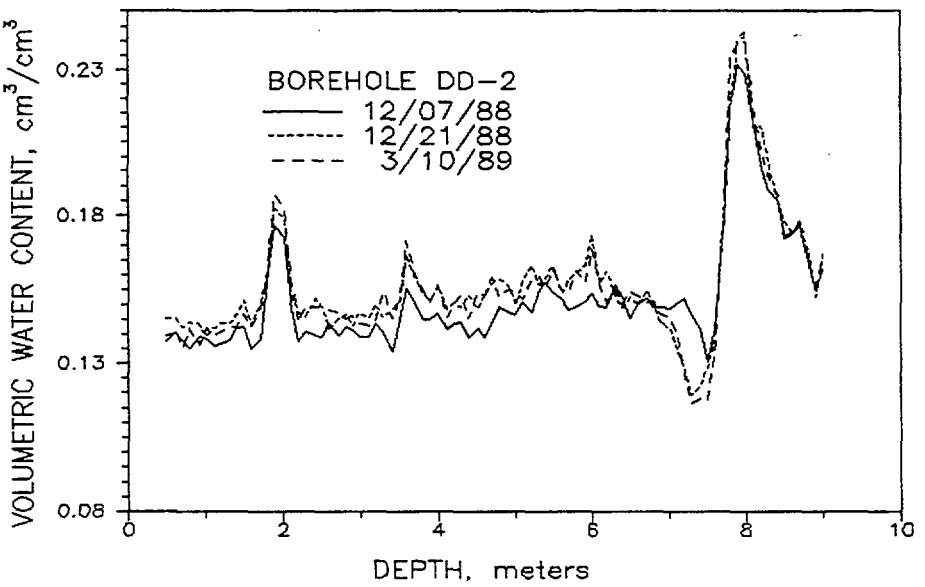

l)

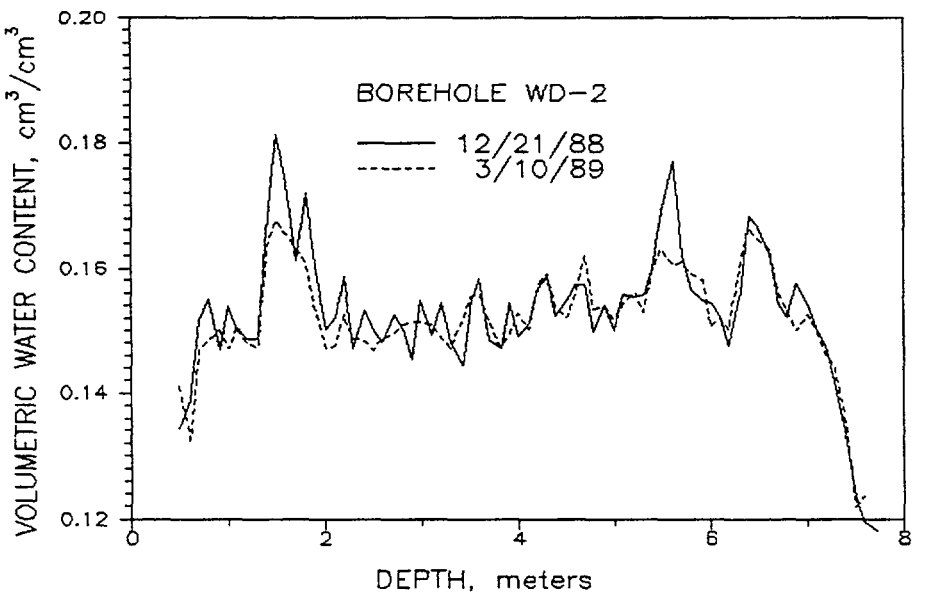

Figures A.8k and l. Volumetric water content determined in welded boreholes using neutron moisture meters. Logs were run immediately following drilling and approximately 3 months later. An additional log was run in DD-2 2 weeks following drilling, which suggests that ambient conditions were reached in 2 weeks in this borehole. The data in DD-2 also suggests there may have been drying effects from the drilling in the welded tuff that weren't seen in DD-1, probably due to higher air flow through the fractured welded system. Water content increases were lower in WD-2 compared to WD-1 but elevated water contents were found in some areas.

m)

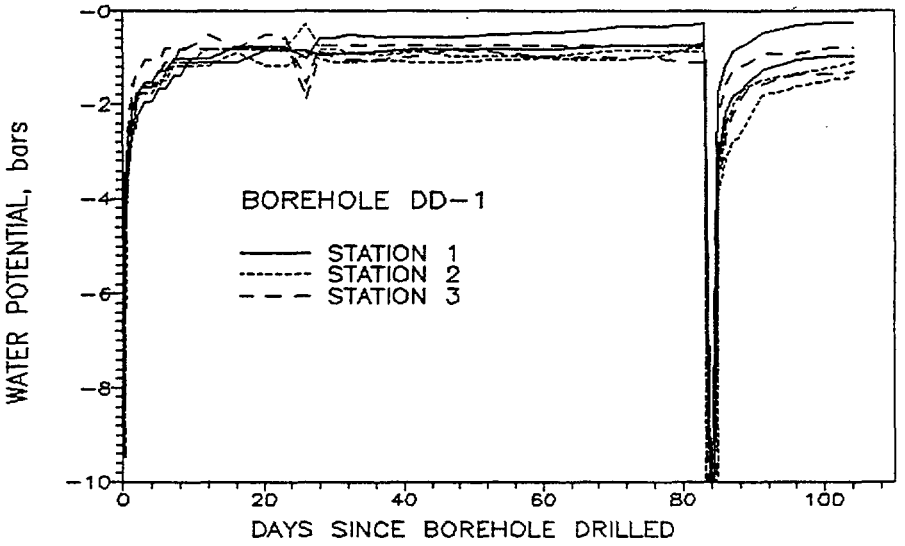

Figure A.8m. Water potential measured at 3 stations separated by inflatable packers using two peltier type thermocouple psychrometers at each station. Station 1 is approximately 1 meter into the borehole, station 2 is in the middle and station 3 is approximately 7.5 m into the borehole. On day 82 the instrument string was removed to determine the effects of instrument equilibration without drilling effects. This suggests that the two weeks it took to equilibrate following drilling were probably only a function of the instruments, rather than the formation.

n)

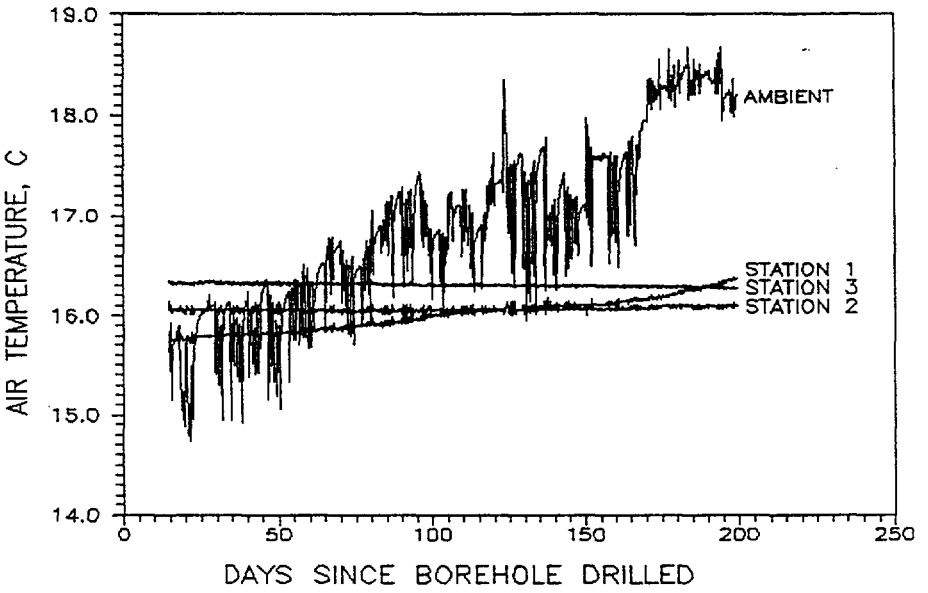

Figure A.8n. Air temperature, C, measured with thermocouples at three stations (described in Figure A.8m) in DD-1 and ambient temperature in the tunnel. All stations within the borehole show very little fluctuations, station 2 and 3 changing very little over the 9 months measured. Station 1 raises in temperature about 3/4 of a degree C as the ambient temperature raises over the season about 3 1/2 C.

o)

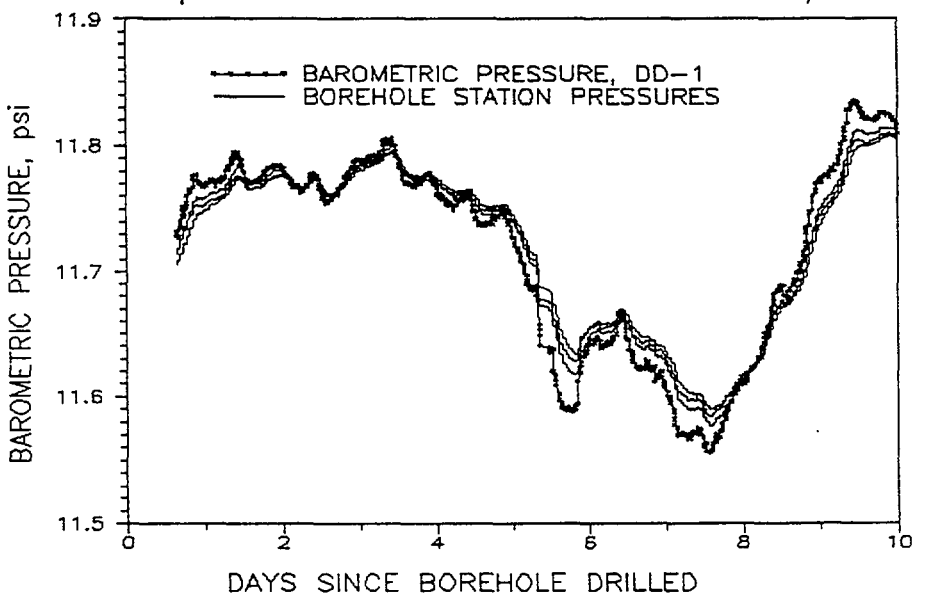

Figure A.8o. Barometric pressure measured in tunnel and air pressure measured at each station in DD-1. Over a 10 day period is shown a lag in station pressures. The station more closely matching barometric pressure is station 3 which is close to a fault, while the next closest line is station 1.

APPENDIX B1

Validation studies for assessing unsaturated flow
and transport through fractured rock

Table of contents

Validation Studies for Assessing Unsaturated Flow and Transport Through Fractured Rock

Todd C. Rasmussen & Daniel D. Evans
Department of Hydrology and Water Resources
College of Engineering and Mines
University of Arizona, Tucson AZ 85721

INTRODUCTION

This document outlines the various experimental stages completed and currently underway related to providing datasets for model validation studies with respect to unsaturated flow and transport in fractured rock. The experimental stages progress from relatively simple laboratory experiments for uncoupled, unfractured processes, to more sophisticated laboratory experiments which include nonisothermal and fracture processes, to complex field experiments under nonisothermal, unsaturated, fractured conditions. The following sections describe the five experimental stages for tests which have been completed, as well as for those which are currently underway.

STAGE 1: Laboratory Core Measurements

Purpose:

The objective of this problem is the characterization of fluid flow, including air and water, thermal energy and solute transport in unfractured, variably saturated tuffaceous rocks at laboratory scales. The data from these measurements will be used in the simplest flow models which do not incorporate fractures or coupled processes. Additional complexity is introduced in subsequent stages.

Background:

The rock matrix excluding fractures is highly heterogeneous with substantial porosity and other material properties changing rapidly over short distances. In order to determine the magnitude and correlation structure of the heterogeneities, as well as to determine the effect of variable fluid saturation on material properties, a large number of measurements on cores obtained at various locations are required. The cores examined in this analysis were removed from borehole cores at three meter intervals from nine boreholes. A total of 105 core locations were examined.

Conceptual Model:

The rock is assumed to be a homogeneous porous medium at the scale of the laboratory measurement. Samples are tested at matric suctions of 0, 10, 25, 50, 100, 300 and 500 kPa and oven-dry conditions, whenever feasible. Physical, hydraulic, pneumatic, and thermal transport parameters are investigated using the core segments.

Measurement Techniques:

Hydraulic:

- Saturated samples maintained at steady state gradient. Flow rate per unit area is measured and divided by gradient to determine saturated hydraulic conductivity.

- Characteristic curves are determined in wet range using pressure extraction vessel maintained at constant pressure. In the dry range, a thermocouple psychrometer is used to measure atmospheric moisture potential surrounding rock maintained at a constant water content.

- Unsaturated conductivity is measured using incremental changes in applied pressure in Tempe Pressure Cell and measuring cumulative outflow.

Pneumatic:

- Unsaturated samples are tested at two pressure gradients in permeameter. Moisture potentials of the rock is prescribed by allowing samples to equilibrate in the pressure extraction vessel prior to insertion in permeameter.

Thermal:

- Two small holes are drilled into the core. A heater coil is placed inside a hole drilled in the center of the core, and a thermistor is used to measure the temperature a short distance away. A constant amperage is prescribed through the heater coil for a finite duration. The experiments are repeated at various moisture potentials prescribed using the pressure extraction vessel.

Available Data Sets:

Rock matrix physical and hydraulic properties, including porosity, bulk density, and moisture characteristic curves are available. Also available are the pneumatic and thermal conductivities as a function of water content.

Sampling Strategy:

- Sampling of rock matrix at three meter intervals in nine boreholes.

- Replication of tests on same sample to determine reproducibility.

STAGE 2: Laboratory Fractured Rock Experiment

Purpose:

The objective of this problem is the characterization of fluid flow and solute transport in variably saturated fractures in tuff rocks at laboratory scales. The data is to complement the Stage I experiments which exclude fracture characterization. The scale of Stage II experiments is designed to allow processes to be examined in the laboratory, and the resultant model used to predict phenomena at field scales, which are to be tested in Stage III experiments.

Background:

Fractures and other macropores provide conduits of high conductivity for flow through saturated rock. Because flow velocities through fractures may be orders of magnitude greater than matrix velocities, the confinement capability of fractured rock may be compromised. Fractures in unsaturated rock may not provide these pathways, however, because large cavities are empty except very near saturation. To investigate the behavior of unsaturated fractured rock, a series of experiments have been and are being performed to characterize the hydraulic properties of fractures and the rock matrix for a range of matric suctions.

To perform the analysis, various rock blocks measuring approximately 60 cm high, 20 cm wide and 20 cm deep have been collected which contains a fracture oriented in the longer plane. Three porous plates are used on both upper and lower rock surfaces to impose negative pressure boundary conditions over a range of suctions from 0.1 to 1.5 kPa. On both the upper and lower surfaces, one plate lies immediately over the fracture, while the other two plates lie beside the fracture plate over the matrix only.

Conceptual Model:

1 A single discrete fracture bisects a tuff rock along the long axis of blocks measuring approximately (20 x 20 x 50 cm).

2 The permeability of the fracture when saturated is much higher than the surrounding matrix, but the relative permeability decreases to near zero at a matric suction between 0 and 1.5 kPa.

3 The rock matrix is initially dry, approximately 50 MPa.

4 Porous plates are positioned above and below the matrix, with separate plates positioned above and below the fracture.

5 At matric suctions greater than 1.5 kPa, the fracture remains unsaturated, while the matrix is saturated.

6 At matric suctions greater than 1.5 kPa, flow is vertically downward due to gravity, and also due to capillary forces when a wetting front is present.

7 At matric suctions of 0 kPa, fluid flow is through both the matrix and the fracture, with some flow from the matrix into the fracture near the porous plates.

8 Solute transport occurs in the fracture and matrix in response to fluid convection, as well as to convection-induced dispersion.

9 Solute transport may also result from diffusion.

10 Preferential flow within the fracture may cause nonuniform advancement of solutes in channels.

Boundary Conditions:

- Top and bottom surfaces of matrix and fractured maintained at a constant suction.

- Sides of block are enclosed within a chamber held at nearly constant temperature and saturated vapor pressure.

- Alternating concentrations between 0.1 and 0.001 M CaCl solutions are applied to the upper surface as steps and pulses.

Initial Conditions:

- Block is initially dry, with a relative saturation between 10 and 20 percent, corresponding to matric suctions about 50 MPa.

Available Data Sets:

Rock matrix physical and hydraulic properties, including porosity, bulk density, and moisture characteristic curves are available. The unsaturated hydraulic conductivity of the rock matrix is available from measurements of flow rates through the rock matrix for constant matric suctions and a constant vertical gravitational gradient. During these tests, the absence of fracture flow can be confirmed using visual evidence of wetting front advance and by comparing flow rates through the plate over the fracture with flow rates through the porous plates over the matrix.

Time series of matric potentials are monitored in a vertical fracture and in the rock matrix surrounding the fracture in response to a step increase in the matric potential at the inflow surface. Flow rates and fluid potentials in the matrix and fracture at the inflow and outflow surfaces are also monitored before and after the step change in matric potential.

Time series of solute concentrations at interior sampling ports and at the outflow surface resulting from a step change in solute concentration at the inflow surface are being monitored. A steady influent concentration of $CaCl_2$ is used until a steady outflow concentration is observed. Once steady outflow concentrations are obtained, a step change in the influent $CaCl_2$ concentration is imposed. The complete data requirements for simulation studies include:

- Matrix/Fracture material properties including fracture aperture distribution, fracture surface characteristics, porosity, matrix and fracture permeabilities, and relative fracture permeability.

- Temperature, relative humidity and matric potential of chamber.

- Initial and time-dependent water contents as a function of depth.

- Initial and time-dependent rock matric potentials as a function of depth and distance from fracture.

- Solute concentrations as a function of time, depth, and distance from fracture.

Sampling Strategies:

- Sampling of fractures and matrix at various horizontal and vertical locations.

- Sampling of outflow from lower porous plates.

STAGE 3: Field Imbibition/Redistribution Experiment

Purpose:

The purpose of this experiment is to evaluate the magnitude and distribution of fluid flow in unsaturated fractured tuff. Results from Stage I experiments conducted on unfractured rock are combined with Stage II experiments conducted on fracture segments in the laboratory in order to form a prediction model for flow through fractured rock under in situ conditions. Results from Phase III activities will be combined with Phase IV experiments in nonisothermal rocks under laboratory conditions for the purpose of designing Phase V experiments in nonisothermal in situ conditions. The dimensions of this experiment are larger than the Stage I and Stage II experiments, with the range of investigation ranging from 1 to perhaps 30 meters.

Background:

When a borehole is flooded with water, fractures may allow the rapid movement of water away from the boreholes. Subsequent movement of the fluid from the fractures into the matrix may result in fingers of saturation along planar discontinuities around the injection region. The fingers may not develop if the matrix intake is large due to low fracture transmissivity, a high matrix hydraulic conductivity, or a high initial water content. Also, if the matrix permeability is practically zero, the fingers will not be observable using the neutron probe due to low water contents over the intervals being monitored. Following the injection phase, the matric suction will decrease, causing a decrease in fracture transmissivity and matrix hydraulic conductivity, with the fracture transmissivity decreasing faster than the matrix hydraulic conductivity. While flow during the injection phase may be dominated by the physical and hydraulic properties of fractures, flow during the redistribution phase may be dominated by matrix properties.

The use of equivalent continuum models is to be tested for describing the processes associated with water infiltration into unsaturated fractured rock and the redistribution of infiltrated water over time. Instead of modeling flow through discrete fractures, the equivalent continuum models assume that an anisotropic tensor can be used to represent the fractured medium. Of particular concern are the potential effects of multiple porosity (i.e., matrix and fracture porosities) on fluid movement during the injection and redistribution phases. The dependency of flow regime on matric suction may or may not be accurately represented using equivalent continuum models.

Conceptual Model:

1 Liquid water will move in response to a gradient of total hydraulic head. The total head is the sum of elevation, pressure, osmotic, thermal, electric, and other heads.

2 The magnitude of liquid water flux is dependent on the product of the total hydraulic head gradient and the hydraulic conductivity of the medium.

3 In unsaturated rock, the hydraulic conductivity and the water content decreases with increasing matric suction (i.e., the negative of pressure head)

4 The fracture 'transmissivity' (i.e., conductivity parallel to the fracture multiplied by the fracture aperture) may decrease to near zero at matric suctions between 0 and 1 kPa.

5 The fracture 'conductance' (i.e., conductivity perpendicular to the fracture divided by the fracture aperture) may decrease less rapidly and at larger matric suctions than fracture transmissivity.

Imbibition Phase:

1 Outward water flow from a flooded borehole will occur through fractures and through the matrix.

2 Near the flooded borehole, fracture flow away from the borehole will be greater than flow through the matrix.

3 Away from the borehole, fracture flow may be attenuated by infiltration into fracture walls.

Redistribution Phase:

1 Water in fractures will be imbibed into fracture walls.

2 Movement of water will be away from the injection borehole through the matrix, with a preference for downward movement.

3 If drained fractures inhibit matrix flow, zones of increased saturation within the matrix on one side of a fracture may develop.

Initial Conditions:

- Ambient water contents of approximately 70 to 80 percent of saturations and ambient matric potentials of approximately 50 to 100 kPa.

Boundary Conditions:

- Upper surface: covered, no flow.

- Sides: no flow at infinity.

- Lower surface: constant total head gradient, or zero pressure head gradient.

Available Data Sets:

Time series of water injection volumes in four boreholes are available. Water was maintained at a constant total head within inclined boreholes for more than three weeks. Injection volumes were measured approximately every 20 hours. Two of the boreholes are 15 m long, while the other two are 30 m long. Final injection rates varied from a low of 1.27 l/hr in a 15 m long borehole, to a high of 34.68 l/hr in a longer borehole.

Rock matrix and fracture hydraulic properties are available at three-meter intervals for 105 locations in nine boreholes, including the four flooded

boreholes. The properties were obtained from oriented cores and single hole testing for bulk density, effective porosity, saturated and relative matrix hydraulic conductivity, moisture characteristic curves, fractured rock saturated hydraulic conductivities, fracture density and fracture orientation. Initial water contents of the rock matrix are also available.

To augment the data sets obtained from the existing boreholes, it is planned to conduct another experiment of longer duration and to monitor the experiment with greater spatial detail. Water contents using the neutron probe will be monitored in the boreholes. The injection phase will maintained for an extended period of time, and then monitored for a year or two after the flooding period. Specific design specifications can be modified as a result of simulation experiments using existing data sets. The complete data requirements for simulation analysis include:

- Rock material properties, including fracture locations, fracture/ matrix permeabilities, and characteristic curves.

- Water contents as a function of space and time.

- Rock matric potentials as a function of space and time.

- Evidence of free water in boreholes.

Solutes will be used during the course of the experiment as tracers to indicate travel rates and paths.

Sampling Strategies:

- Intensive sampling of fractures and fracture zones above and around injection intervals at various distances.

- Intensive sampling of matrix around fractures and fracture zones.

- Moderate sampling of matrix away from fractures.

STAGE 4: Laboratory Tuff Core Heating Experiment

Purpose:

The purpose of this experiment is to evaluate the magnitude and distribution of induced fluid flow and solute transport along a partially saturated tuff core. The complicated influences of fractures will be removed in this experiment so that coupling between fluid, heat, vapor, and solute flows can be separated. Stage 5 experiments using in situ experiments will incorporate results from both isothermal experiments conducted in Stages II and III, as well as nonisothermal matrix flows conducted here. The scale of this experiment is rather small, on the order of 5 to 10 cm.

Background:

The processes affecting the movement of water and entrained solutes near a high-level nuclear waste repository are of interest for predicting the performance of the waste repository. A thermal source in an unsaturated fractured rock can dramatically affect saturation levels, as well as air, vapor, water and solute movement due to the effect of forced convection and the effects of heat on vapor and air density driven free convection. A laboratory experiment is being conducted to provide calibration and validation data sets for thermal, solute, liquid and air transport as a result of a thermal gradient.

The system to be modeled consists of coupled liquid, vapor, solute and thermal transport in nonisothermal, variably saturated rock. The physics of multiple phase fluid flow under conditions of steady heat flux will be tested using laboratory data sets. Also, theories used to predict the migration of a conservative solute in the liquid phase within a closed system will be evaluated for conditions of an equilibrium thermal gradient. Various complexities can be evaluated including: water plus water vapor only; water plus water vapor and air; and water plus water vapor plus air and solutes. Each additional level of complexity incorporates additional parameters.

Conceptual Model - Heating Phase:

1 Liquids around a heat source will vaporize in response to an increase in the vapor pressure deficit, forming a zone of desiccation near the heat source.

2 The vapor will move to zones away from the heat source due to pressure gradients and diffusion.

3 Heat flux away from the source will occur as sensible heat conduction and latent heat transfer in the vapor phase.

4 As the temperature decreases away from the heat source, the vapor will condense at some distance from the heat source, forming a zone of liquid water accumulation.

5 Liquid water will move from the zone of accumulation due to a potential gradient.

6 Solutes will accumulate in the zone of desiccation due to their low vapor pressure.

Cooling Phase:

1 Once the heat source has been removed, rock temperatures will decrease over time due to redistribution along the core.

2 Vaporization of liquid water will decrease and vapor phase transport will diminish, except along the boundary between the zones of desiccation and accumulation where the greatest temperature gradients may be found.

3 Vapor phase redistribution will predominate, with the greatest redistribution occurring between the zones of desiccation and accumulation.

4 Solutes will move toward the heat source due to liquid phase convection and away from the heat source due to concentration gradients.

Initial Conditions:

- Ambient initial water contents will be varied.

- Initial solute concentration profile.

Boundary Conditions:

- No flow hydraulic and pneumatic boundary conditions on all surfaces.

- Constant temperature over time at either end, with thermal insulation along the sides of the core.

Available Data Sets:

The physical, hydraulic, pneumatic and thermal properties of the rock matrix will be measured on the rock sample or on samples next to the core. The parameters include the bulk density, porosity, saturated and relative hydraulic, pneumatic, and thermal conductivities, moisture dependent heat capacity, and moisture characteristic curves. The bulk density and initial, transient and final water content distributions within the core will be determined at one cm intervals along the core using gamma ray attenuation methods.

The distribution of solutes concentrations, temperatures, and water contents within the core during the heating experiment will be measured at one cm intervals during the course of the experiment.

STAGE 5: Field Heating Experiment

Purpose:

The purpose of this experiment is to evaluate the magnitude and distribution of induced fluid flow around a heat source in unsaturated fractured tuff at field scales. Stage III measurements are also conducted at field scales but neglect the effects of a thermal source. Stage IV experiments were conducted incorporating thermal variations, but ignore field scale processes such as fracture flow.

Conceptual Model - Heating Phase:

1 Liquids around a heat source will vaporize in response to an increase in the vapor pressure deficit, forming a zone of desiccation.

2 The vapor will move to zones away from the heat source due to pressure gradients and diffusion.

3 Outward vapor flow will be greater in undrained fractures than in the matrix due to higher pneumatic permeabilities in fractures.

4 Heat flux away from the source will occur as sensible heat conduction and latent heat transfer in the vapor phase.

5 As the temperature decreases away from the heat source, the vapor will condense within fractures and the matrix at some distance from the heat source, forming a zone of liquid water accumulation.

6 Liquid water will move from the zone of accumulation in various directions:

- Radially inward towards the zone of desiccation due to a potential gradient;
- Radially outward, also due to a potential gradient; and
- Downward due to gravitational forces.

7 Below the heat source, the upward flow of liquid water towards the zone of desiccation will be small, with accumulated water draining downward through vertical fractures due to gravitational forces.

8 Within the horizontal plane of the heat source, net liquid water flow will be downward, away from the heat source, carried away by gravity drainage in vertical fractures.

9 Above the heat source, the largest zone of accumulation will be found. Liquid flow will occur back toward the heat source in fractures, and may reach the heat source, depending upon many factors, including the:

- Strength and horizontal extent of the heating source;
- Downward rate of percolation from above;
- Fracture and matrix permeabilities;
- Initial rock water content;

- Rock thermal conductivity; and
- Magnitude of free convection.

Cooling Phase:

1 Once the heat source has been removed, rock temperatures will decrease over time due to conduction and convection outward.

2 Vaporization of liquid water will decrease and vapor phase transport will diminish, except along the boundary between the zones of desiccation and accumulation where the greatest temperature gradients may be found.

3 Vapor phase redistribution will predominate, with the greatest redistribution occurring between the zones of desiccation and accumulation above the heat source.

4 The rate of liquid phase invasion of the zone of desiccation will be greatest from the zone of accumulation above the heat zone.

5 Initial drainage through fractures from the zone of accumulation will occur quickly, while redistribution of rock matrix water contents will occur at a slower rate.

Initial Conditions:

- Ambient water contents of approx. 80 percent of saturation and matric potentials of approx. 100 kPa.

Boundary Conditions:

- Thermal, hydraulic, pneumatic (controlled vs. natural).

Data Requirements:

- Matrix/Fracture material properties including permeabilities, characteristic curves, thermal conductivities, vapor diffusivities.

- Temperatures, relative humidities, water contents, matric potentials.

- Evidence of free water in boreholes.

Sampling Strategies:

- Intensive sampling of fractures and fracture zones above and around heating borehole at various distances.

- Intensive sampling of matrix around fractures and fracture zones.

- Moderate sampling of matrix away from fractures, and lateral and below heating borehole.

APPENDIX B2

Two-phase flow simulations in a
heated tuff drillcore

KEMAKTA AR 90-10

TWO-PHASE FLOW SIMULATIONS IN A HEATED TUFF DRILLCORE

INTRAVAL Case 11

Maria Lindgren
Anders Rasmuson

Kemakta Consultants Co
Stockholm, Sweden
September 1990

ABSTRACT

This study include simulations of an experiment on a heated tuff drillcore performed at the Apache Leap Tuff Site near Arizona, USA. The water transport in both liquid and vapor phase in the drillcore have been simulated with the Integrated Finite Difference Code, TOUGH. Tracer transport was calculated in a second step, with the results from the water transport simulations, using the Integrated Finite Difference Code, TRUMP.

The TOUGH calculation includes flow of both liquid and gaseous phases due to pressure, viscous and gravity forces according to Darcy's law, with interference between the phases represented by means of relative permeability functions. In addition, vapor transport by diffusion is accounted for. A number of calculations have been made, varying the saturated hydraulic permeability, thermal conductivity and van Genuchten parameters.

Tracer transport was modelled using the unsaturated version of the convection-dispersion equation. The dispersion coefficient dependence on temperature and water content are considered, but the dependence on water flow rate is not.

The simulations give qualitatively expected saturation, temperature and concentration profiles. However, even varying the input parameters within "resonable" bounds still give significant deviations from the experimental curves. This may be due to material heterogeneities or measurement errors.

Table of contents

1 TEST CASE DESCRIPTION

The experiments on the tuff drillcore is one part in a series of experiments performed at the Apache Leap Tuff Site near Arizona, USA. These laboratory experiments were carried out on a nonfractured, nonwelded tuff core with a diameter of 6.4 cm and a length of 12.99 cm. The aim of the experiments was to study water and tracer movement in tuff under impact of heating.

Before the heating started the bulk density was measured gravimetrically. The core was partly wetted with a potassium iodine solution. The average initial saturation degree was 48% and the average KI concentration was about 870 ppm. Five thermocouple ports were drilled into the core to a depth of 1.5 cm. The core was coated in order to prevent moisture from leaving the core.

The prepared core were placed in the heating apparatus, see Figure 1. The hot end were held at a temperature of 70 °C and the cold end at about 5 °C. The heating was continued for 32 days. During the experiments gamma measurments were made at 1 cm intervals. The saturation degree can be calculated from the intensity of the beam passing through the core compared to the beam passing through air.

After heating the core was sliced into 8 sections and each section was cut into an upper and a lower half. The iodine content in each piece were analyzed with high performance liquid chromatography. The analysis gave no differences between the upper and lower halves.

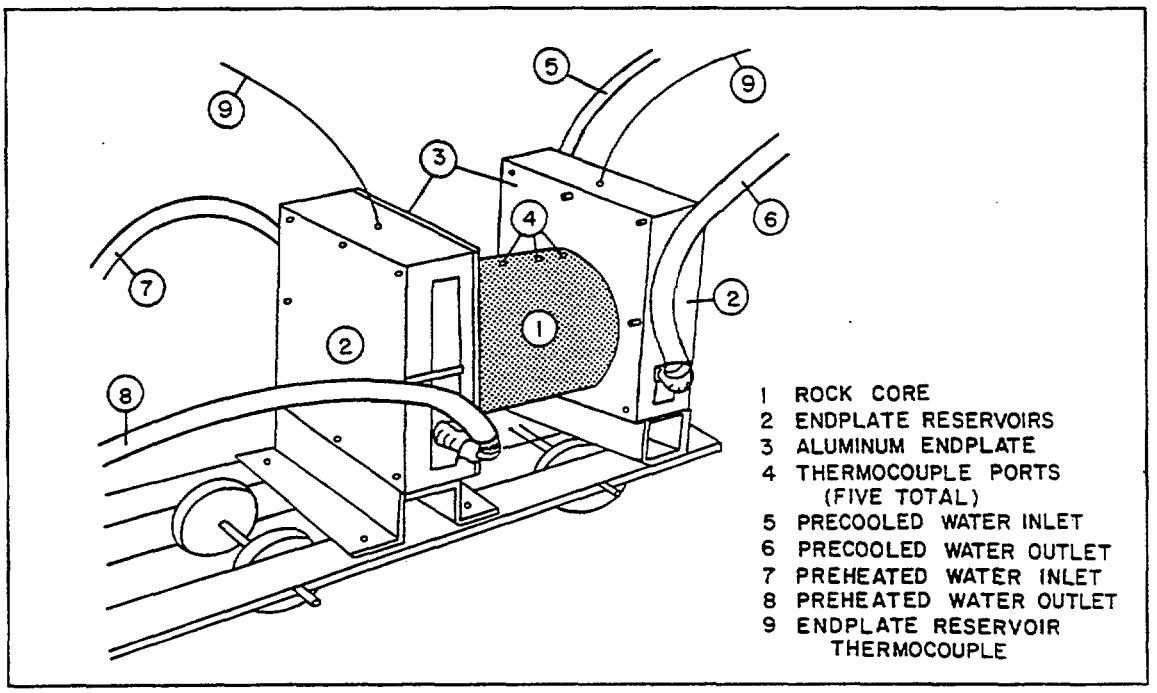

Figure 1 Apparatus used to heat the tuff drillcore (from Davies, 1987).

2 MATHEMATICAL MODEL

2.1 Physicochemical processes

The model is based on the theory of unsaturated flow of liquid, vapor, heat and tracer in porous media. The simulations are carried out in two steps, the first including water and heat transport and the second a tracer calculation using flow, saturation degrees and temperatures from the first step. A one dimensional model representing the length of the core is used.

Water and heat transport

The model used takes into account that fluid flow in both liquid and gaseous phases occurs under pressure, viscous and gravity forces according to Darcy's law, with interference between the phases represented by means of relative permeability functions. Capillary and phase adsorption effects are taken into account for the liquid phase, using capillary pressure (moisture characteristic) curves. In addition binary diffusion in the gas phase is considered, but no allowance is made for vapor pressure lowering. Air is treated as an ideal gas, and additivity of partial pressure is assumed for air/vapor mixtures. Air dissolution in water is represented by Henry's law, excluding the temperature dependence of Henry's constant.

Heat transport occurs by means of conduction, with thermal conductivity dependent on the saturation degree, and convection and binary diffusion, including both sensible and latent heat.

Tracer transport

The tracer transport is modelled as simultaneous convective and diffusive/dispersive transport, where the dispersion is assumed to be diffusion-like and dependent of temperature and saturation degree, but independent of velocity. Preliminary estimates indicate that with the pertinent velocities and grain diameters hydrodynamic dispersion is negligible. The tracers are assumed not to interact with the solid surfaces in the tuff (nonsorbing specie).

2.2 Mathematical formulation

Water and heat transport

The calculations have been carried out using the integrated finite difference code TOUGH, developed at Lawrence Berkeley Laboratories */Pruess, 1983/*. TOUGH is a multi-dimensional numerical model for simulating coupled transport of water, air and heat in porous and fractured media. The code solves an integrated form of the basic mass- and energy-balance equations for an arbitrary flow domain V_n:

$$\frac{d}{dt}\int_{V_n} M^{(\kappa)} dv = \int_{\Gamma_n} F^{(\kappa)} \cdot n \, d\Gamma + \int_{V_n} q^{(\kappa)} \, dv \tag{1}$$

$\kappa = 1$: water
$\kappa = 2$: air
$\kappa = 3$: heat

The mass accumulation terms ($\kappa = 1,2$) are:

$$M^{(\kappa)} = \varepsilon \sum_{\beta=l,g} S_\beta \rho_\beta X_\beta^{(\kappa)} \tag{2}$$

The heat accumulation term contains rock and fluid contributions:

$$M^{(3)} = (1-\varepsilon)\rho_R \, Cp_R \, T + \varepsilon \sum_{\beta=l,g} S_\beta \rho_\beta u_\beta \tag{3}$$

The mass flux terms contain a sum over phases:

$$F^{(\kappa)} = \sum_{\beta=l,g} F_\beta^{(\kappa)} \tag{4}$$

where the flux in each phase is:

$$F_\beta^{(\kappa)} = - k \frac{k_{r\beta}}{\mu_\beta} \rho_\beta X_\beta^{(\kappa)} (\nabla P_\beta - \rho_\beta g) - \delta_{\beta g} D_{va} \rho_\beta \nabla X_\beta^{(\kappa)} \tag{5}$$

This is the usual formulation of Darcy's law for multiphase systems with an additional term accounting for gas phase diffusion. The first term on the right-hand side represents flow due to pressure forces and the second flow due to gravitational forces.

Heat flux contains conductive and convective components (no dispersion):

$$F^{(3)} = - \lambda \nabla T + \sum_{\substack{\beta=l,g \\ \kappa=1,2}} h_\beta^{(\kappa)} F_\beta^{(\kappa)} \tag{6}$$

Henry's law was assumed for solubility of air in liquid water:

$$P_a = K_H X_l^{(air)} \cdot \frac{M_{H_2O}}{M_{air}} \tag{7}$$

The vapor-air diffusion coefficient is written as:

$$D_{va} = \tau \, \phi \, S_g \frac{D_{va}^0}{P} \left(\frac{T + 273.15}{273.15} \right)^\beta \tag{8}$$

Heat conductivity was assumed to be dependent on the square root of the saturation degree:

$$\lambda(S_l) = \lambda(S_l = 0) + \sqrt{S_l} \cdot (\lambda(S_l = 1) - \lambda(S_l = 0)) \quad (9)$$

a linear dependence was also tested:

$$\lambda(S_l) = \lambda(S_l = 0) + S_l \cdot (\lambda(S_l = 1) - \lambda(S_l = 0) \quad (10)$$

Relative permeabilities and capillary pressure were assumed to follow the van Genuchten equations */van Genuchten, 1980/*. A dimensionless saturation degree is defined by:

$$S^{\blacklozenge} = \frac{S_l - S_{lr}}{S_{ls} - S_{lr}} \quad (11)$$

The relative liquid permeability is given by:

$$k_{rl} = \begin{cases} \sqrt{S^{\blacklozenge}} \, (1 - (1 - (S^{\blacklozenge})^{1/m})^m)^2 & \text{if } S_l < S_{ls} \\ 1 & \text{if } S_l \geq S_{ls} \end{cases} \quad (12)$$

and the relative gas permeability by:

$$k_{rg} = 1 - k_{rl} \quad (13)$$

The capillary pressure is given by:

$$P_{cap} = \begin{cases} 0 & \text{if } S_l \geq S_{ls} \\ -\frac{1}{\alpha} \, ((S^{\blacklozenge})^{-1/m} - 1)^{1-m} & \\ -P_{\max} & \text{if } \frac{1}{\alpha}((S^{\blacklozenge})^{-1/m} - 1)^{1-m} \geq P_{\max} \end{cases} \quad (14)$$

Tracer transport

The tracer transport calculations are made with a modified version of the integrated finite difference code TRUMP. This code is originally written for transient heat transport calculations in multi-dimensional heterogeneous media with arbitrary geometry */Edwards, 1972/*.

$$\left(\frac{Q}{c} + \theta\right) \frac{\partial c}{\partial t} = \nabla(D\nabla c) - \nabla(\bar{q}c) + G - \rho Q_a \frac{\partial a}{\partial t} - \rho Q_b \frac{\partial b}{\partial t} \quad (15)$$

accumulation | diffusion/ dispersion | convection | source | chemical reactions

The diffusion coefficient dependence of the temperature can be predicted for an electrolyte at infinite dilution using the equation */Perry, 1973/*:

$$D_0 = 8.931 \cdot 10^{-10}\, T \left(\frac{l_+^0\, l_-^0}{\Lambda^0} \right) \left(\frac{z_+ + z_-}{z_+ z_-} \right) \qquad (16)$$

where the ionic conductance, l^0, is given by:

$$l^0 = l^0_{25°C} + a(t-25) + b(t-25)^2 + c(t-25)^3 \qquad (17)$$

The constants for K^+ and I^- are given in Table 1.

Table 1 Constants for calculating ionic conductance (from Perry, 1973).

Ion	*a*	$b \cdot 10^2$	$c \cdot 10^4$
K^+	1.433	0.406	-0.318
I^-	1.509	0.438	-0.217

3 CALCULATIONS

3.1 Input data

The calculations were performed in one dimension, assuming radial differences to be negligible. The length used in the calculations was 12.99 cm. The length was divided into 40 equal elements. All calculations were performed in a transient mode simulating the processes for 32 days. In all cases except the case with the lowest permeability steady state conditions were obtained. The boundary conditions at the ends were 5 °C and 70 °C respectively. All boundaries were isolated for water transport.

Water and heat transport

The material data needed in the simulations were primarily taken from measurements on the core */Davies, 1987/* and secondary from measurements on 105 small cores taken from the same area */Rasmussen et al, 1989/*. The porosity was 0.19 and the initial saturation degree was 48%. The specific heat used was 770 J/kg,°C. The heat conductivity was varied between 1.0 and 1.8 W/m,°C. The permeability was varied between $4 \cdot 10^{-15}$ and $4 \cdot 10^{-18}$ m^2 and the van Genuchten parameter α between 0.046 and 0.01 and n between 1.3 and 1.55. The residual water content was set to zero in all cases except case V2 (S_r=0.05). The calculational cases are specified in Table 2 and the capillary pressure and permeabiltiy curves are depicted in Figure 2-3 together with experimental values.

Tracer transport

The tracer calculation was performed for one water and heat transport calculation, case V2 in Table 2. The same material data as in the water and heat transport simulations were used. The diffusion/dispersion coefficient was calculated for each node from the saturation degree and temperature achieved in the heat transport calculations according to:

$$D = D_0(T)\, S_l\, \varepsilon \qquad (18)$$

where D_0 is calculated according to equation (16).

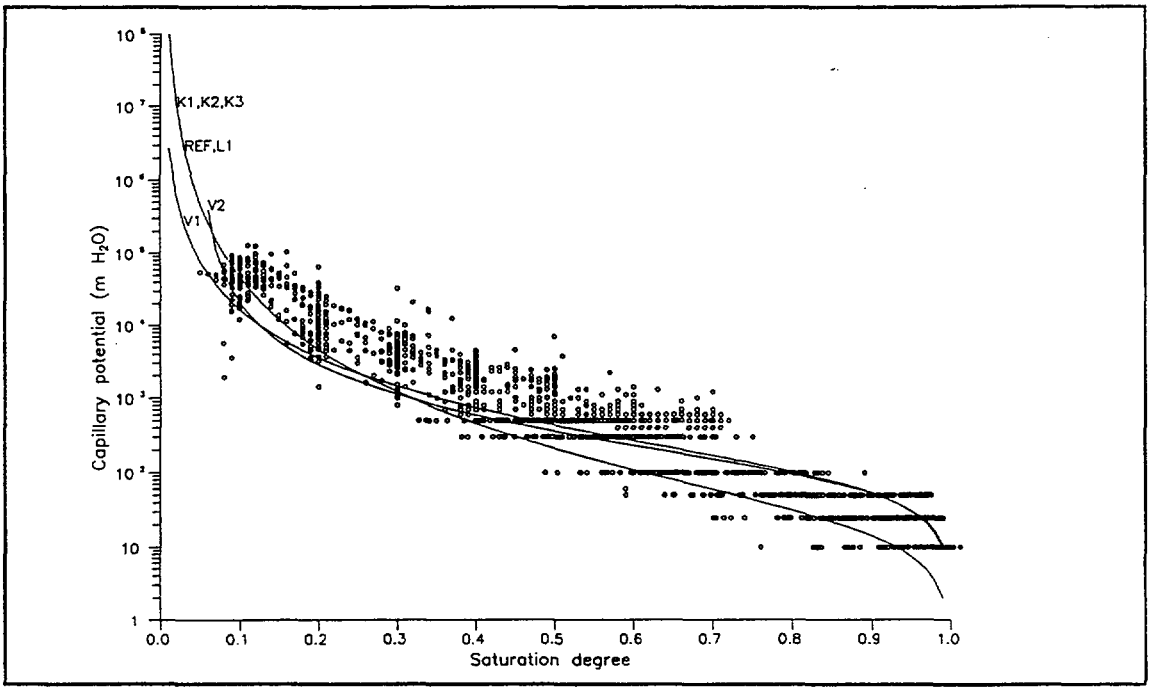

Figure 2 Characteristic curves used in the calculations. Measured values from the 105 small cores are also indicated.

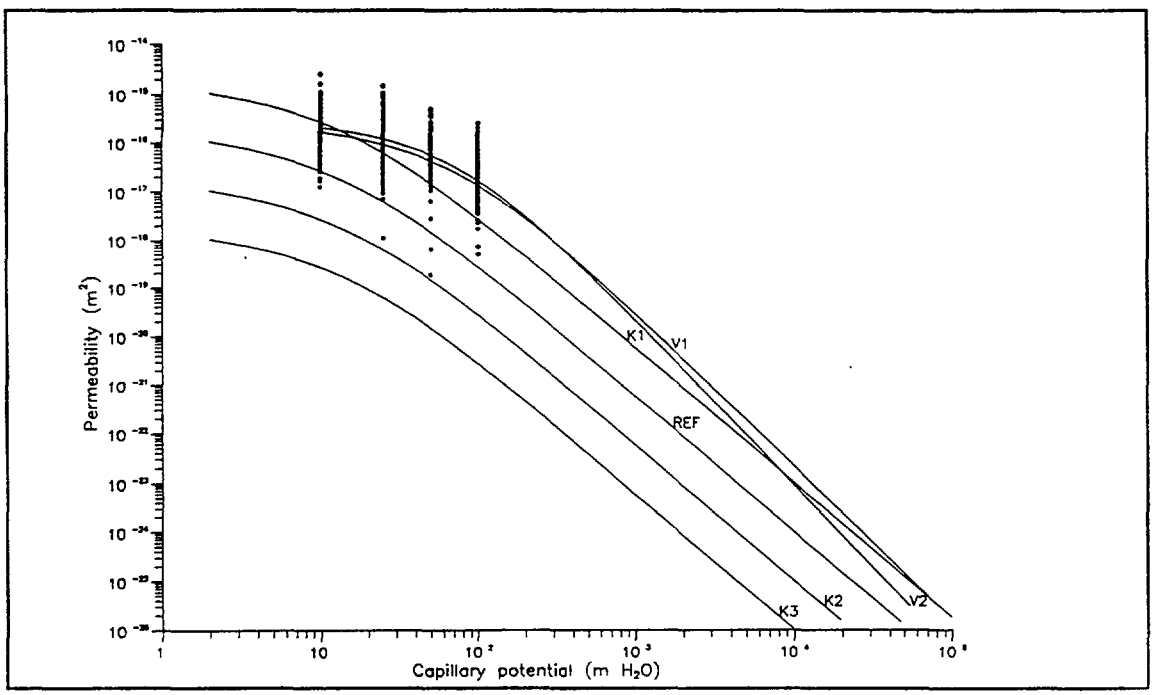

Figure 3 Relative permeability as functions of capillary potential used in the calculations. Experimental data are also indicated.

3.2 Calculation cases

A summarized description of the water and heat transport calculation cases is presented in Table 2.

Table 2 Calculation cases

	K1	REF	K2	K3	L1	V1	V2
ε	0.19	0.19	0.19	0.19	0.19	0.19	0.19
k_s	$4 \cdot 10^{-15}$	$4 \cdot 10^{-16}$	$4 \cdot 10^{-17}$	$4 \cdot 10^{-18}$	$4 \cdot 10^{-16}$	$4 \cdot 10^{-16}$	$4 \cdot 10^{-16}$
α	0.046	0.046	0.046	0.046	0.046	0.01	0.01
n ‡	1.3	1.3	1.3	1.3	1.3	1.45	1.55
S_r	0	0	0	0	0	0	0.05
Cp	770	770	770	770	770	770	770
λ(S=0)	1.3	1.3	1.3	1.3	1.0	1.3	1.3
λ(S=1)	1.8	1.8	1.8	1.8	1.8	1.8	1.8

‡ n=1/(1-m)

4 RESULTS

Water and heat transport

The saturation degree as a function of the length for the different calculation cases in comparison with the experimental data are shown in Figure 4. The variation in temperature in the calculations compared to the experimental data is depicted in Figure 5. Some cases (K1, V1, V2) have been excluded, they are all more linear than those shown in the figure. The results, theoretical and experimental, are given after an elapsed time of 32 days. This also represent steady state conditions except for case K3.

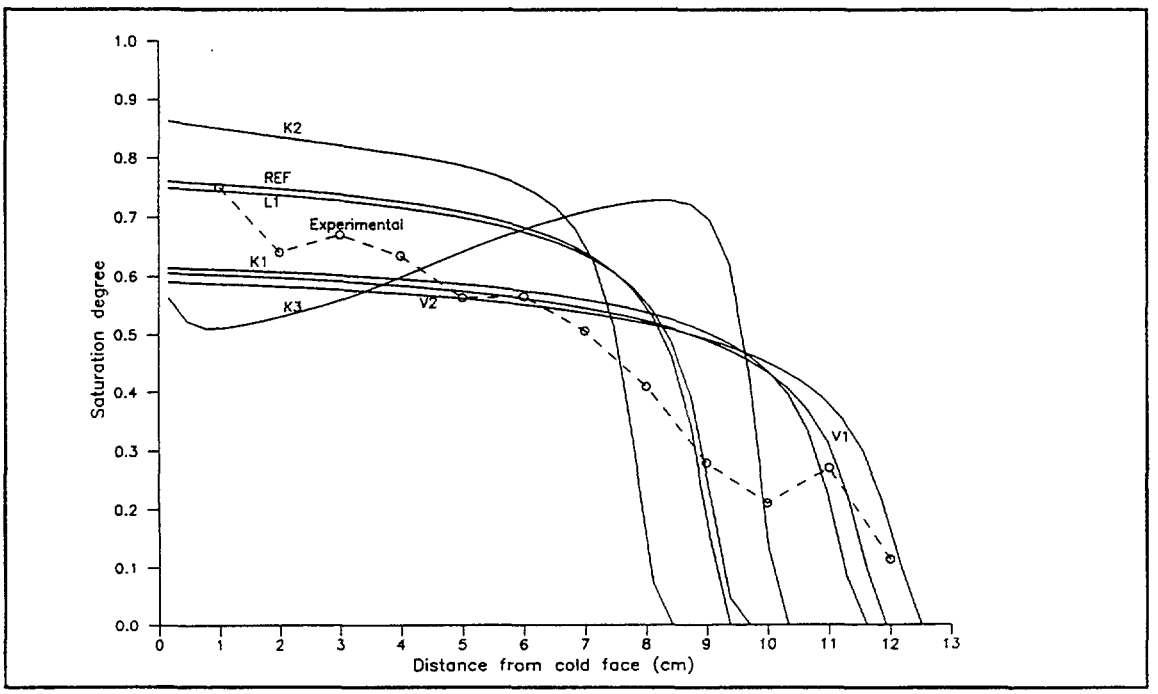

Figure 4 Saturation degree along the core, simulations compared to experiments.

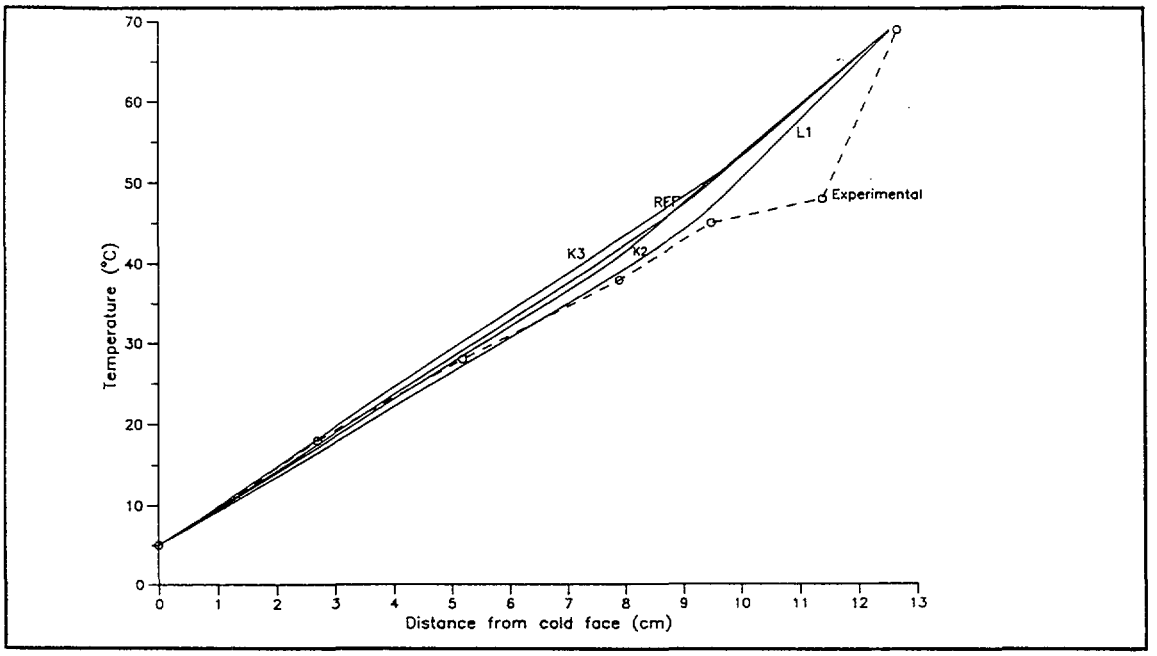

Figure 5 Variation in temperature along the core, simulations compared to experiments.

Tracer transport

The concentration from the calculation compared to the experimental data is shown in Figure 6.

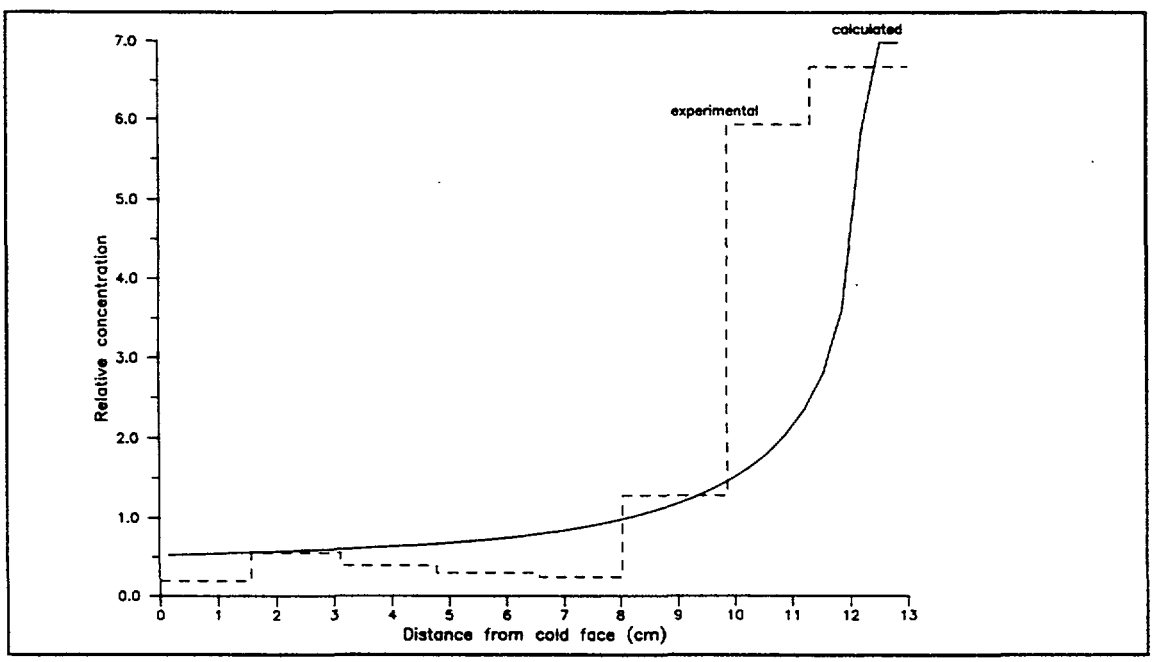

Figure 6 Relative iodine concentrations along the core, simulations compared to experiments.

5 DISCUSSION

As indicated in Figure 4, the measured saturation degree shows a rather erratic behavior with a gradual decrease towards the hot end of the core. In contrast, all the simulated results indicate that a steep gradient (front) in the saturation degree should occur with almost complete dryness at the hot end. The anomalous result for case K3 is caused by the very low permeability and still after 32 days instationary conditions prevails. All other cases show the same general shape during the instationary period. Even when the hydraulic parameters are varied within the large bounds as given in Table 2 it is impossible to get a good agreement between experimental and simulated saturation degrees. One explanation might be that the core is heterogeneous with cracks providing faster transport of water.

As depicted in Figure 5 the experimental temperature profile indicates a significant dip quite close to the hot end. In the simulations there is also a dip in temperature but not so significant and not so close to the hot end. The simulated dip follows rather closely the sharp change in saturation as shown in Figure 4. A dip in temperature is expected since at the saturation front heat is taken from the liquid water for the evaporation. This energy, however, may be supplied from the hot end if the heat conductivity and moisture content is high enough. In this case less lowering of the temperature occurs. The largest deviation from linear temperature profile is obtained for case L1, where the heat conductivity is lowered. It should be noted that the large dip in the experimental temperature profile originates mostly from one measuring point. If this point is in error the profile may change substantially.

As indicated in Figure 6 a fairly good agreement is obtained between experimental and calculated tracer concentration profiles. However, since the agreement between experimental and calculated saturation degrees is not very good it is not possible to assert too much significance to this result.

6 CONCLUSIONS

Simulating transport of water and heat in the tuff drillcore using the computer code TOUGH works generally well and the saturation and temperature profiles obtained show, qualitatively, the expected behavior. However, the agreement with the experimental results is less good and significant deviations occur. One reason for this are due to uncertainties in material data, mainly because they are not measured on the used core. However, even varying the input parameters within "reasonable" bounds still give significant deviations from the experimental results. This may be caused by heterogeneities or measurement errors.

Simulations of tracer transport with TRUMP using water flow data from the TOUGH calculations also works well. In this case a fairly good agreement with the experiments is obtained.

ACKNOWLEDGEMENTS

This work was funded by the Swedish Nuclear Power Inspectorate (SKI).

NOTATION

a	Constant for calculation of ionic conductance
b	Constant "
c	Constant "
c	Tracer concentration (units/m^3 water)
Cp	Specific heat (J/kg,°C)
D	Diffusion coefficient (m^2/s)
D_{va}^{0}	Air/Vapor diffusivity at standard conditions (P=1 bar, T=0°C)
F	Flux
G	Source or sink
g	Gravitational acceleration (m/s^2)
h	Specific enthalpy (J/kg)
K_H	Henry's constant (N/m^2)
k	Permeability (m^2)
l^0	Ionic conductance at infinite dilution (mhos/equivalent)
M	Accumulation term
M	Molar weight (g/mol)
m	van Genuchten parameter (m=1-1/n)
n	van Genuchten parameter (n=1/(1-m))
P	Pressure (N/m^2)
P_a	Solubility of air in liquid (N/m^2)
P_{cap}	Capillary pressure (N/m^2)
Q	Amount of sorberd tracers (units/m^3 bed)
q	Fluid flux (m^3/m^2,s)
S	Saturation degree (m^3 H_2O/m^3 void)

T	Temperature (K)
t	Temperature (°C)
V	Volume (m^3)
X	Mass fraction
z	Absolute valence of ion (-)

Greek letters

α	van Genuchten parameter
β	Material constant
Γ	Boundary surface of an element (m^2)
ε	Porosity (m^3/m^3)
θ	Water content (m^3 H_2O/m^3 total)
Λ^0	Electrolyte conductance at infinite dilution (mhos/equivalent)
λ	Heat conductivity (W/m,°C)
μ	Dynamic viscosity (Ns/m^2)
ρ	Density (kg/m^3)
τ	Tortuosity factor
ϕ	Total potential (m H_2O)

Subscripts

a	air
g	gas phase
l	liquid phase
R	rock
r	relative or residual
s	saturated

v	vapor
+	cationic
-	anionic
β	State of aggregation

Supscripts

κ	$\kappa=1 \Leftrightarrow$ water : $\kappa=2 \Leftrightarrow$ air : $\kappa=3 \Leftrightarrow$ heat
$\blacklozenge$	Dimensionless

Mathematical operations

∇	"Nabla" operator, the gradient of a scalar

REFERENCES

Davies, B.E., "Water Movement in Nonisothermal Tuff", Thesis for M.Sc, University of Arizona, USA, 1987.

Edwards, A.L., "TRUMP: A computer program for transient and steady state temperature distributions in multidimensional systems", National Technical Information Service, National Bureau of Standards, Springfield, Va, 1972.

van Genuchten, M.T., "A Closed-form Equation for Predicting the Hydraulic Conductivity of Unsaturated Soils", Soil Sci. Soc. Am. J., vol.44, p.892-898, 1980.

Perry, R.H., Chilton C.H., "Chemical Engineers' Handbook", McGraw-Hill Book Company, 5th ed., 1973.

Pruess, K. "Development of the General Purpose Simulator MULKOM, Annual Report 1982", Earth Science Division, Report LBL-15500, Lawrence Berkeley Laboratory, 1983.

Pruess, K., "TOUGH user's guide", Earth Science Division, Report LBL-20700, Lawrence Berkeley Laboratory, 1987.

Rasmussen, T.C., Evans, D.D., Sheets, P.J., Blanford, J.H., "Unsaturated Fractured Rock Characterization Methods and Data Sets at the Appache Leap Tuff Site", Department of Hydrology and Water Resources, University of Arizona, USA, 1989.

APPENDIX B3

Large block modeling exercise

Table of contents

LARGE BLOCK MODELING EXERCISE[1]

by

William Ford, Jeffrey Pohle, Richard Codell, and Timothy McCartin

U.S. Nuclear Regulatory Commission
Washington, D. C.

ABSTRACT

This report describes computer simulations of water flow through a block of unsaturated fractured rock. These simulations were performed to help design future experiments and to assess the ability of an existing code to simulate this type of ground water flow. While the simulations did mimic the concept of a fracture acting as a barrier to moisture flow it is not clear that the experimental design or the equivalent porous media approach used in the simulations is the correct way to test this concept. It is also unclear how to obtain, either experimentally or theoretically, equivalent porous media properties for a fracture.

INTRODUCTION

The University of Arizona is conducting field and laboratory investigations of flow and transport phenomena in unsaturated rock. Using rock matrix laboratory data from some of these investigations, exercises modeling a hypothetical block of tuff with a single fracture were conducted. These exercises provided the opportunity to evaluate the usefulness of the preliminary experimental design to the INTRAVAL program and to test current fractured rock unsaturated ground water flow and transport concepts using a two dimensional equivalent porous media code.

UNSATURATED FRACTURED ROCK FLOW CONCEPTS

Concepts of ground water flow in unsaturated fractured rock have evolved from theories of unsaturated ground water flow through soil. Conceptualizations of unsaturated flow in a fractured-porous medium are "based on capillary bundle theory {e.g., Wang and Narasimhan (1985)} which states that there is a relationship between pore size and equilibrium pressure head. Thus, the saturation of a material containing pores of many different sizes is related to the equilibrium pressure head in the material..." (Klavetter, 1986a, p. 6). Because of the higher capillary suction (tension) forces exerted by small pores; as water is added to a rock or soil; water will fill small pores in preference to large pores. For the same reason, when a rock matrix is at low saturation, a fracture with a larger average aperture than the average matrix pore diameter

---

[1]This paper was prepared by an employee of the United States Nuclear Regulatory Commission. It presents information that does not correctly represent an agreed-upon staff position. The Nuclear Regulatory Commission has neither approved nor disapproved its technical content.

will be essentially dry. Under these conditions, water flow will be confined to the matrix with little or no flow across or down fractures.

For most fractures, it is assumed that the pore spaces caused by matrix grain to grain contacts across the fracture (asperities) are smaller across the fracture than longitudinally within the fracture. Therefore, as saturation increases and the water occupies larger pore spaces, water movement across a fracture will tend to occur, with little or no water flowing down the fracture. At slightly higher saturations, fracture conductivity in the plane of the fracture should become nonzero allowing water to flow longitudinally in sinuous channels in the fracture. Finally, when the matrix and the fracture are almost completely saturated the fractures become efficient contributors to water flow (Klavetter, 1986).

This concept indicates that in unsaturated rock, fracture flow is a function of saturation and aperture size. This implies that, because fractures are generally irregular in shape and have irregular apertures it is possible to have water flow in regions of the fracture with small aperture and not have flow in other areas of the fracture with larger apertures (Klavetter, 1986). Similarly, it is also possible to have water flow in fractures with small average apertures while little or no flow is occurring in fractures with larger average apertures. When a rock is completely saturated, the situation is reversed. "The majority of the flow in the fracture occurs in those regions where the fracture aperture is large, with little flow occurring where the fracture aperture is small because the flow rate is proportional to the cube of the aperture" (Klavetter, 1986, p. 13).

To summarize this concept, "the average fracture conductivity for water movement in the plane of the fracture is a highly nonlinear function of fracture saturation or pressure head. If the flux is less than the saturated conductivity of the matrix, then the water will tend to flow only in the matrix as it moves downward. If the flux is greater than the saturated conductivity of the matrix, then the matrix will saturate, and the fractures will carry water also" (Klavetter, 1986, p. 15).

EQUIVALENT POROUS MEDIA APPROACH

An equivalent porous media approach was used in the simulations. In the equivalent porous media approach, unsaturated zone hydrologic properties are represented by characteristic curves which describe moisture content and conductivity as a function of pressure head. This approach is commonly used to represent the hydrologic properties of the rock matrix. However, the equivalent porous media approach also assumes that, like the rock matrix, flow in the fractures can also be modeled as an equivalent porous medium. Therefore, under unsaturated flow conditions, the hydrologic properties of the fracture can be represented by characteristic curves which describe moisture content and conductivity as a function of pressure head. However, at this time, while moisture characteristic curves for rock matrix have been generated from experimental data, this has yet to be done for a fracture.

DESCRIPTION OF BLOCK EXPERIMENTS

To obtain experimental data on flow and transport processes in fractured rock, the U.S. Nuclear Commission has a contract with the University of Arizona to conduct unsaturated flow tests on blocks of tuff. These studies have been undertaken because the hydraulic properties of partially saturated fractures are poorly understood and because flow through fractures may result in

accelerated ground water flow velocities from a high level nuclear waste repository located in unsaturated fracture rock. To develop an experimental design preliminary laboratory tests have been performed on two blocks of tuff containing natural fractures. These blocks measure approximately (20 x 20 x 50 cm) and (20 x 20 x 70 cm) respectively. Both blocks contained a natural fracture oriented vertically near the center of the block. Each block was enclosed within a chamber to prevent evaporation during the experiments. Ceramic porous plates placed on the upper surface of the rock controlled water flow through the blocks. Details of these experiments have been published in Chuang (1990).

SIMULATIONS

All simulations used the computer code VAM2D (Huyakorn, 1989), a proprietary code developed by Hydrogeologic, Inc. with the help of funding from the U.S. Nuclear Regulatory Commission. VAM2D is a two-dimensional, finite element code that simulates moisture movement and solute transport in variably saturated porous media. Material heterogeneities and anisotropy are handled using quadrilateral finite elements. Further information on VAM2D can be obtained from Huyakorn (1989).

SIMULATION PARAMETERS

Effective porosity data for the rock matrix were obtained from laboratory tests of small cores taken from the blocks (Table 3.10 of Chuang, 1990, p. 91). A saturated hydraulic conductivity was obtained for the rock matrix by averaging the saturated hydraulic conductivities derived from Block Number One core (Chuang, 1990, Table 3.9). A rock matrix moisture release curve was derived from Block Number One core (Chuang, 1990, Table B.22) by treating the core data if they had all been obtained from a single sample. A computer program (El-Kadi, 1987) was then used to estimate a best fit van Gneuchten characteristic curve to simulate the hydrologic properties of the matrix.

The fracture effective porosity was arbitrarily set at almost 100 % (0.97). A van Gneuchten characteristic-curve for the fracture was obtained from Table 2 of Dudley (1988). This table contains assumed properties of unsaturated zone, hydrologic units at the proposed high-level waste repository at Yucca Mountain, Nevada. Properties of Topopah Springs Unit fractures were chosen for use in the simulations, since it was felt that this unit might be closer to the actual properties in the experimental blocks than other geologic units in the table.

Both fracture and matrix hydrologic properties used in the block simulations were isotropic. The following table contains the matrix and fracture properties used in the simulations.

TABLE 1: MATRIX AND FRACTURE PROPERTIES

MATRIX PROPERTIES	
HORIZ. K SAT.	0.00253 cm/hr
VERT. K SAT.	0.00253 cm/hr
SAT. H2O CONT.(POR)	0.189
VAN GENUCHTEN	
ALPHA	0.001214 /cm
BETA	1.953
RESIDUAL SAT.	0.027
FRACTURE PROPERTIES	
HORIZ. K SAT.	6.12 cm/hr
VERT. K SAT.	6.12 cm/hr
SAT. H2O CONT.(POR)	0.97
VAN GENUCHTEN	
ALPHA	0.0128 /cm
BETA	4.23
RESIDUAL SAT.	0.005

SIMULATION GRID

The block was modeled in two dimensions having a width of 20 cm and a length of 60 cm. A grid spacing of 0.2 cm was used in the vertical direction (y axis), whereas a variable grid spacing ranging from 0.005 cm to 1.5 cm was used along the x axis. The variable x axis grid spacing allowed for detailed definition of the simulated fracture. For VAM2D this resulted 1122 nodes and 1056 elements (33 elements in the y direction and 32 elements in the x direction). In an attempt to explicitly model a vertical fracture in the center of the block, fracture hydrologic properties were assigned to those cells between 9.995 cm and 10.025 cm in the x direction and from 0.0 cm to 60 cm in the y direction. This simulated a fracture aperture of 0.01 cm. The fracture was simulated by 33 elements in the Y direction and 2 elements in the X direction.

SIMULATIONS 1 AND 2

The initial simulations modeled a block of tuff where all sides of the block were no flow boundaries with the exception of the block bottom and the top left 1/4 boundary. The top left 1/4 boundary was defined as a constant potential boundary of -1000 cm, while the bottom of the block was designated a constant potential boundary of -1500 cm. Initial matric potentials for both matrix and fracture elements were set at -1500 cm over the rest of the block. This combination of initial and boundary conditions caused water to flow in the 2 dimensional model from the upper left corner of the block towards the bottom. A maximum of 30 days were simulated. The objective of this hypothetical experiment was to observe how the flow field changed as water from the top left corner of the block encountered the fracture. To observe the effect of the fracture, two simulations were done; one simulation without a fracture (Simulation 1) and one simulation with a fracture (Simulation 2). The matric potentials at the end of 10 hours and 30 days from these two simulations are plotted in Figures 1, 2, 3, and 4. In Simulation 2, the

fracture performed as a barrier to flow, because fracture hydraulic conductivities were always very small because of the low moisture contents.

SIMULATION 3

Simulation 3 is similar to Simulation 2, with the exception that dryer initial conditions and a wetter top boundary were simulated. It was hoped the increased contrast between the wet and dry matrix properties would create a sharper wetting front and that water saturations would increase enough to allow water to cross over the fracture. As in the previous simulations, all boundaries were defined as no-flow boundaries with the exception of the block bottom and the top left 1/4 boundary. The top left 1/4 boundary was designated a constant potential boundary of 0 cm, while the block bottom was defined as a constant potential boundary of -4000 cm. Initial matric potentials were set at -4000 cm over the rest of the block. Again this combination of initial and boundary conditions caused water to flow from the upper left corner of the block towards the bottom. The model simulated a maximum of 35 hours. As can be seen in the matric potential plots of this simulation (Figures 5, 6, 7, 8, 9, and 10) the contrast between the initial conditions and the upper boundary condition produced a sharp wetting front. Further, the fracture acted as a lateral flow barrier until at 5 hours, water contents in the fracture were high enough that water could cross the fracture. For all later time periods the fracture acted as a barrier to lateral flow where water contents were low and matric potentials high (large negative values) and less of a barrier where water contents were high and matrix potentials low (small negative values).

While water saturations were high enough to allow significant water flow laterally across the fracture, they were not high enough to generate significant flow vertically down the fracture. It was anticipated that significant vertical flow would occur when the matric potentials were almost zero in the matrix. Computer requirements from the previous simulations indicated that it would take too long to simulate this aspect of the problem.

To better assess the results of this simulation, matric potential and hydraulic conductivity profiles were prepared (Figure 11) of the 35 hour simulation. In these profiles the fracture is approximately located at 10 cm. width. Profile A (Figure 12) was constructed across an area where the infiltrating water had not yet reached. Therefore, it essentially represents the initial conditions in the block. From this profile it can be seen that the matric potential is the same in the fracture and the matrix, but the hydraulic conductivity of the fracture is dramatically lower than the matrix. Profile B (Figure 12) was constructed across an area where the fracture is acting as a barrier to flow. From this profile it can be observed that matrix potentials reflect wetter conditions on the left side of the fracture, but on the right side of the fracture conditions have not changed from their initial values. Also the hydraulic conductivity on the left side of the fracture has increased along with the hydraulic conductivity of the fracture, but the fracture hydraulic conductivity is still much lower than matrix values. Profile C was constructed across an area where water has just begun to flow across the fracture and Profile D was constructed in an area where a larger volume of water has crossed the fracture (Figure 13). In both profiles matric potentials reflect wetter conditions on both sides of the fracture. However, while the hydraulic conductivity of the fracture has significantly increased, it is still lower than the matrix. This is why flow vertically and horizontally is always faster in the matrix than the fracture.

SIMULATION 4

A laboratory imbibition experiment has been conducted on test Block Number Two, for about 30 days (Chuang, 1990). In this test the visual wetting front was observed (Chuang, 1990) as the water moved down the block. Matric potentials and water contents were not known before, during, or after the test, however, it was observed that after 28 days the visual wetting front had moved to an elevation of about 37 cm. While it is not known how visual wetting fronts compare with water contents or matric potentials, a one dimensional model was built to see how close the matrix wetting front of Simulation 5 approximated the visual wetting front of the imbibition experiment. At the end of 23.52 hours the wetting front in the simulation had penetrated about 22 cm into the block. This compares rather poorly with the visual wetting front which had moved approximately 5 cm into the block (Figure 14). If the visual wetting front observed in the experiment correlates with the steep matric potential front generated by the model, then the simulated wetting front moved faster than the visual wetting front.

DISCUSSION AND OBSERVATIONS

The simulations were an attempt to assist the development of experiments to test the hypotheses of unsaturated fracture matrix flow. According to these hypothesis, significant fracture flow would not occur until the flux of water through the rock approaches the saturated conductivity of the matrix. One of the design concerns of this type of experiment is that instrumentation is not available to measure fracture hydrologic parameters or flow. However, it was felt that the hydrologic conditions on either side of the fracture could be monitored, allowing flow across a fracture to be detected. Therefore, the simulations were configured to allow flow both horizontally and vertically from one side of the fractured block to the other. The objective of a laboratory experiment would be to see if conceptual models could acceptably predict when water would cross the fracture.

While the model did mimic the concept of a fracture acting as a barrier until moisture saturations increased sufficiently in the rock matrix, it is not clear that this is the correct experimental design to test the concept of unsaturated fracture matrix flow. In the simulations the fracture aperture was considered to be uniform over the length of the block, whereas in reality the aperture of the fracture is expected to be nonuniform. Therefore, theory would predict that as moisture increased in the matrix, water would cross the fracture in those areas where the aperture is smallest. Since, it is unlikely that detailed fracture aperture data can be obtained it may be very difficult to predict when water would cross the fracture. At this time the final experimental design of the block experiments have yet to be determined.

The model may have been too simple to simulate fully the hypothesis of unsaturated ground water flow through fractured rock. In the simulations it was assumed that fracture hydrologic properties were isotropic with respect to direction. However, present theory would predict that fracture apertures should be larger parallel to the direction of the fracture and smaller transverse to the fracture. For a two dimensional porous equivalent porous media code to mimic this phenomena the moisture characteristic curves would have be anisotropic. At this time the authors are not aware of any two dimensional codes that can mimic this concept.

Obtaining realistic equivalent porous media parameters for the fracture was another problem encountered in the simulations. The fracture parameters obtained from the literature were actually not estimates for individual fractures, but were estimates for large numbers of fractures (calculated as fracture aperture times 1 square meter times the number of fractures per cubic meter) (Klavetter, 1986a, page 21). Further, the characteristic curves for these fractures appear to have not been developed to mimic flow across the fracture, but rather flow down the fracture. Unfortunately, the literature contains few if any data on equivalent porous media properties within or across the fractures. Equivalent porous media approaches assume that like the rock matrix, flow in fractures can be represented by characteristic curves that describe moisture content and conductivity as a function of pressure head. However, it is not presently known how these curves can be experimentally determined or what is the appropriate theoretical method to derive them for use in models.

The use of the equivalent porous media approach to model a single fracture assumes that there is enough porous material that a representative elementary volume concept is valid. A representative elementary volume is a volume above which average properties can be used to describe fluid flow through a rock. Below this volume average properties can no longer be used to describe the flow of fluid through a rock and the complex distribution of pore channels at the microscopic level must be considered. For Darcy's law a representative elementary volume is a size corresponding to a large number of pores. However, the small size of fractures may mean that a single fracture may not contain a enough pore volume for average values to be used. Furthermore, the shape of fractures may mean that this could be more of a problem in modeling flow across a fracture rather than within the fracture. If a single fracture cannot be described using the average values of a representative elementary volume concept; the porous media approach to modeling a single fracture may not be applicable. At this time the viability of using a porous media approach to modeling a single fracture is unknown.

REFERENCES CITED

Chuang, Y., et al, 1990, Laboratory Analysis of Fluid Flow and Solute Transport Through a Variably Saturated Fracture Embedded in Porous Tuff, Dept. of Hydrology and Water Resources University of Arizona, Prepared for U.S. Nuclear Regulatory Commission, NUREG/CR-4582.

Dudley, A.L., et al., 1988, Total System Performance Assessment Code (TOSPAC) Volume 1: Physical and Mathematical Bases, SAND85-0002, Sandia National Laboratories, Albuquerque, New Mexico.

El-Kadi, A.I., Estimating the Parameters of Soil Hydraulic Properties, SOIL, Microcomputer Interactive Version, IGWMC-BAS14, International Ground Water Modeling Center, Holcomb Research Institute, Butler University, Indianapolis, Indiana.

Huyakorn, P., et al, 1989, VAM2D - Variably Saturated Analysis Model in Two Dimensions, Version 5.0 With Hysteresis and Chained Decay Transport, Documentation and User's Guide, Hydrogeologic Inc., Prepared for U.S. Nuclear Regulatory Commission, NUREG/CR-5352.

Klaveter, E.A. and Peters, R.P., 1986, Estimation of Hydrologic Properties of An Unsaturated, Fractured Rock Mass, SAND84-2642, Sandia National Laboratories, Albuquerque, NM.

Klavetter, E.A. and Peters, R.P., 1986a, Fluid Flow in a Fractured Rock Mass, Sandia Report, SAND85-0855, Sandia National Laboratories, Albuquerque, NM.

van Genuchten, R., 1980, A Closed-Form Equation for Predicting the Hydraulic Conductivity of Unsaturated Soils, Soil Science Society of America Journal, Vol. 44, No. 4, pp. 892-898.

Wang, J.S.Y., and Narasimhan, T.N., 1985, "Hydrologic Mechanisms Governing Fluid Flow in Partially Saturated, Fractured, Porous Tuff at Yucca Mountain", SAND84-7202, Sandia National Laboratories, Albuquerque, NM.

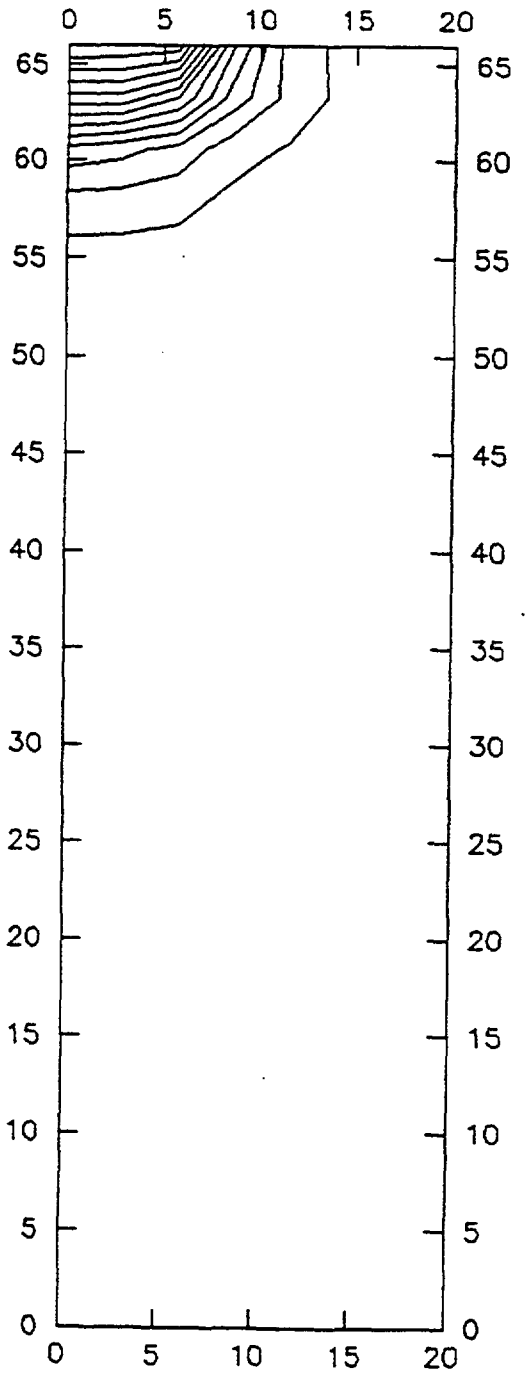

Block Height = 20 cm.
Block Width = 66 cm.
Contour Interval = 40 cm.
Maximum Matric Potential = -1000 cm.
Minimum Matric Potential = -1500 cm.

Boundary Conditions
  Sides = No Flow
  Top Left 1/4 = Constant Matric
    Potential of -1000 cm.
  Top Right 3/4 = No Flow
  Bottom = Constant Matric
    Potential of -1500 cm.
Initial Matric Potentials = -1500 cm.

Length of Simulation = 10 Hours

Figure 1: Simulation 3, 2-D Matric Potential Plot After 10 Hrs., Simulated Block With No Fracture

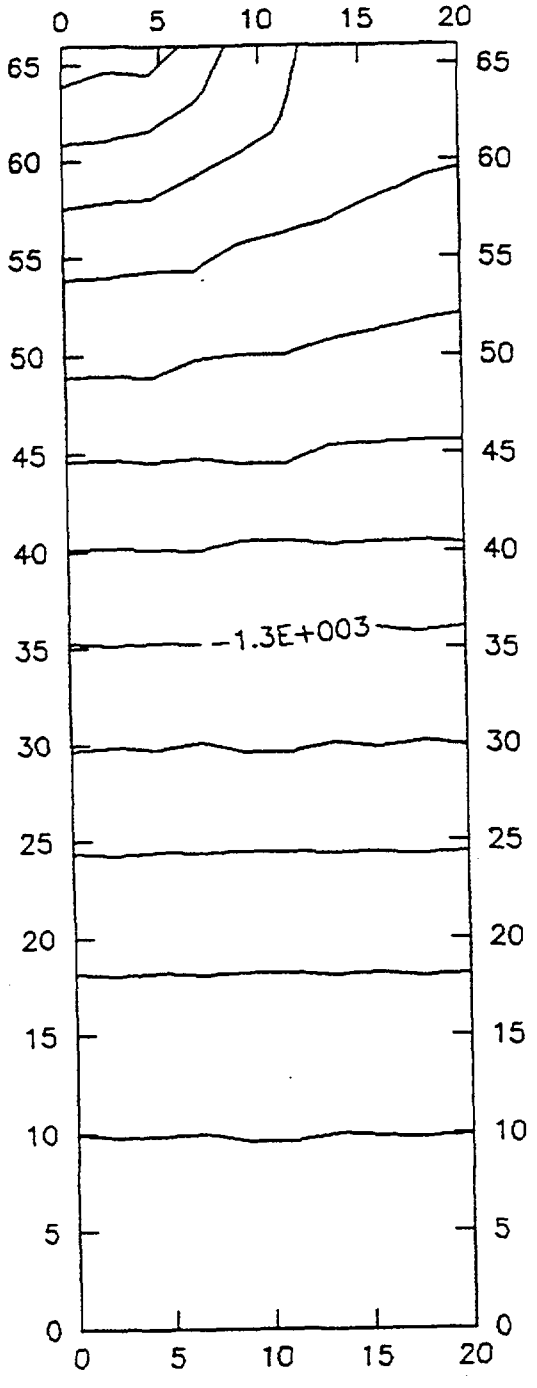

Block Height = 20 cm.
Block Width = 66 cm.
Contour Interval = 40 cm.
Maximum Matric Potential = -1000 cm.
Minimum Matric Potential = -1500 cm.

Boundary Conditions
  Sides = No Flow
  Top Left 1/4 = Constant Matric
      Potential of -1000 cm.
  Top Right 3/4 = No Flow
  Bottom = Constant Matric
      Potential of -1500 cm.
Initial Matric Potentials = -1500 cm.

Length of Simulation = 30 Days

Figure 2: Simulation 3, 2-D Matric Potential Plot After 30 Days, Simulated Block With No Fracture

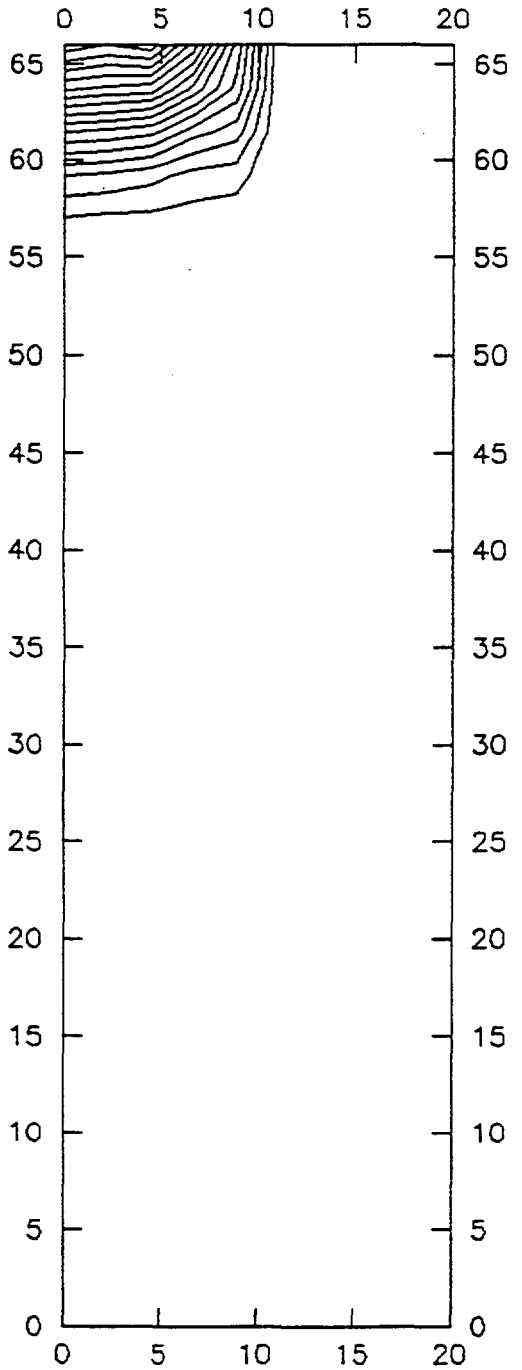

Block Height = 20 cm.
Block Width = 66 cm.
Contour Interval = 40 cm.
Maximum Matric Potential = -1000 cm.
Minimum Matric Potential = -1500 cm.

Boundary Conditions
Sides = No Flow
Top Left 1/4 = Constant Matric Potential of -1000 cm.
Top Right 3/4 = No Flow
Bottom = Constant Matric Potential of -1500 cm.
Initial Matric Potentials = -1500 cm.

Length of Simulation = 10 Hours

Figure 3: Simulation 4, 2-D Matric Potential Plot After 10 Hrs., Simulated Block With Fracture

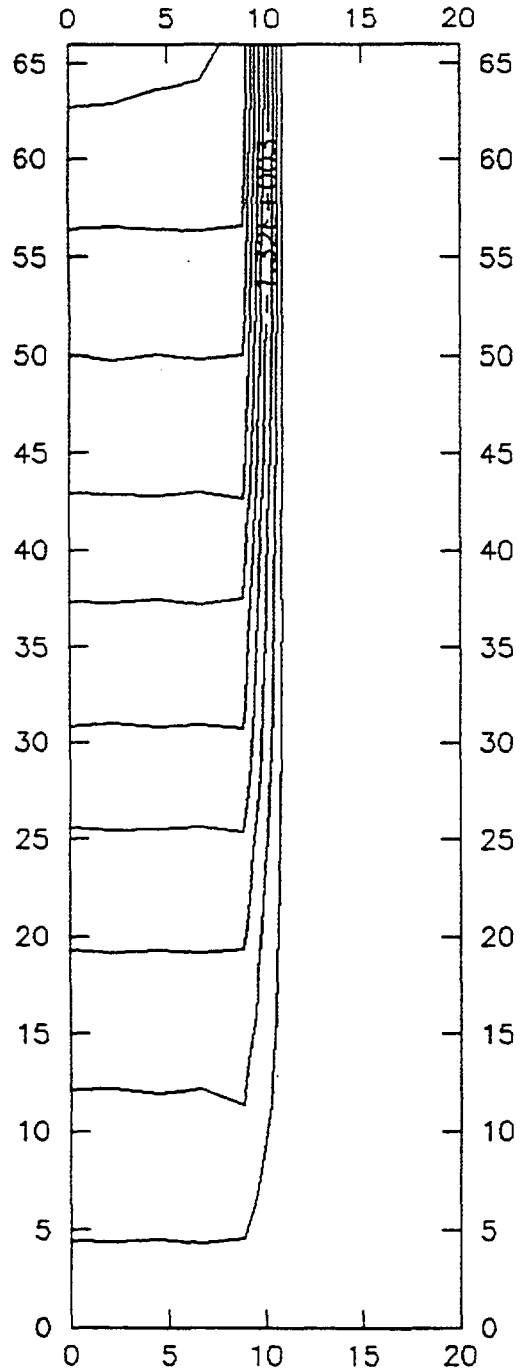

Block Height = 20 cm.
Block Width = 66 cm.
Contour Interval = 40 cm.
Maximum Matric Potential = -1000 cm.
Minimum Matric Potential = -1500 cm.

Boundary Conditions
- Sides = No Flow
- Top Left 1/4 = Constant Matric Potential of -1000 cm.
- Top Right 3/4 = No Flow
- Bottom = Constant Matric Potential of -1500 cm.

Initial Matric Potentials = -1500 cm.

Length of Simulation = 30 Days

Figure 4: Simulation 4, 2-D Matric Potential Plot After 30 Days, Simulated Block With Fracture

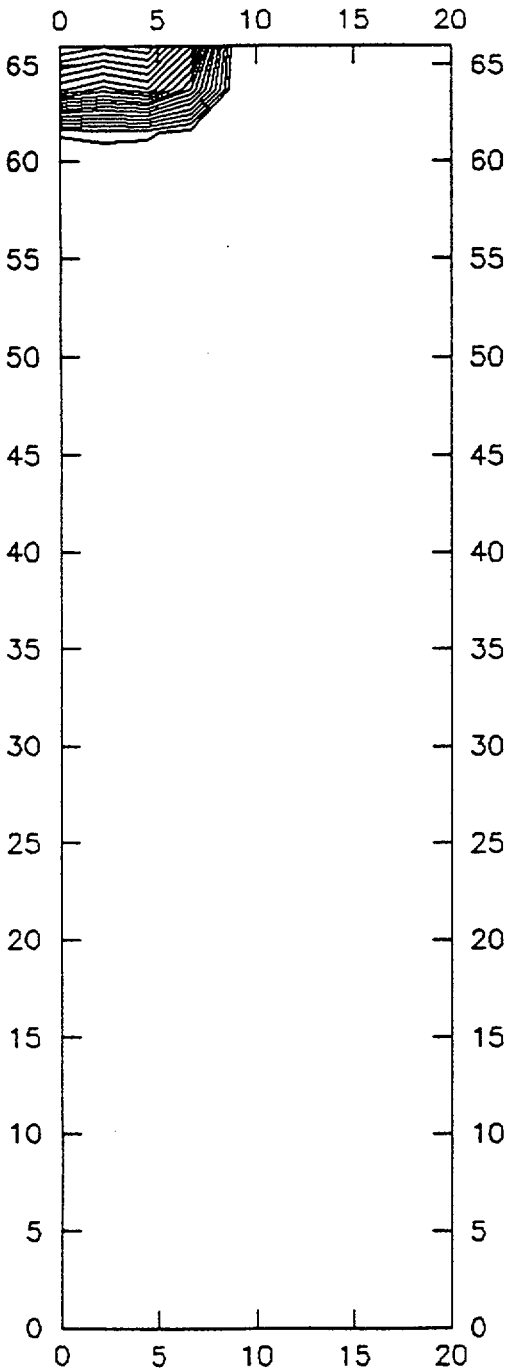

Block Height = 20 cm.
Block Width = 66 cm.
Contour Interval = 200 cm.
Maximum Matric Potential = 0.0 cm.
Minimum Matric Potential = -4000 cm.

Boundary Conditions
  Sides = No Flow
  Top Left 1/4 = Constant Matric
      Potential of 0.0 cm.
  Top Right 3/4 = No Flow
  Bottom = Constant Matric
      Potential of -4000 cm.
Initial Matric Potentials = -4000 cm.

Length of Simulation = 0.1 Hours

Figure 5: Simulation 5, 2-D Matric Potential Plot After 0.1 Hrs., Simulated Block With Fracture

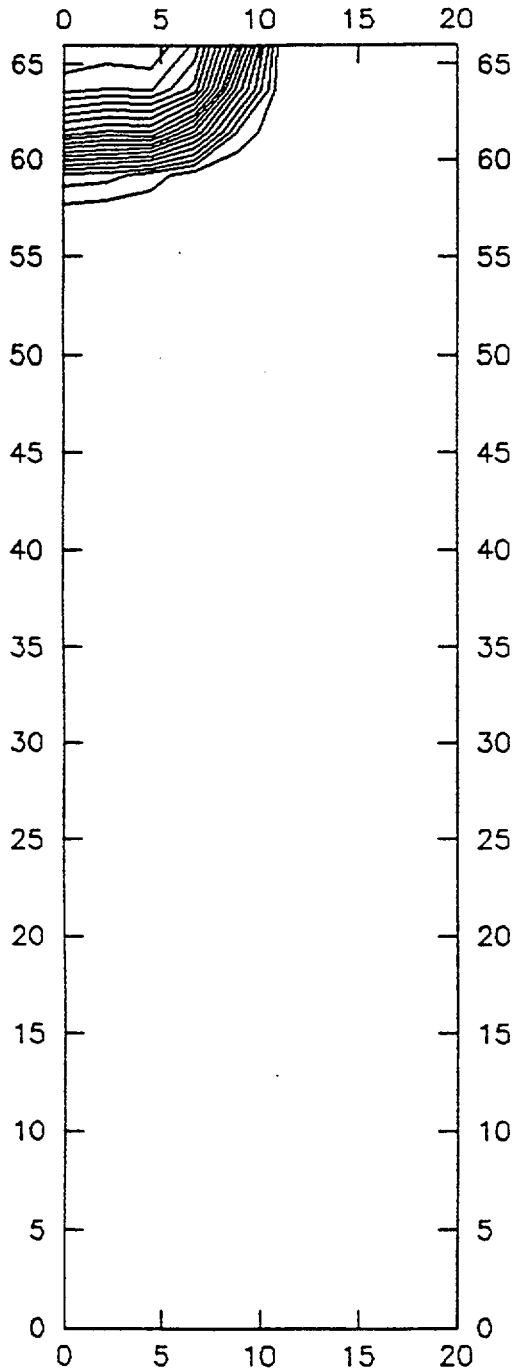

Block Height = 20 cm.
Block Width = 66 cm.
Contour Interval = 200 cm.
Maximum Matric Potential = 0.0 cm.
Minimum Matric Potential = -4000 cm.

Boundary Conditions
  Sides = No Flow
  Top Left 1/4 = Constant Matric
      Potential of 0.0 cm.
  Top Right 3/4 = No Flow
  Bottom = Constant Matric
      Potential of -4000 cm.
Initial Matric Potentials = -4000 cm.

Length of Simulation = 1.0 Hours

Figure 6: Simulation 5, 2-D Matric Potential Plot After 1.0 Hrs., Simulated Block With Fracture

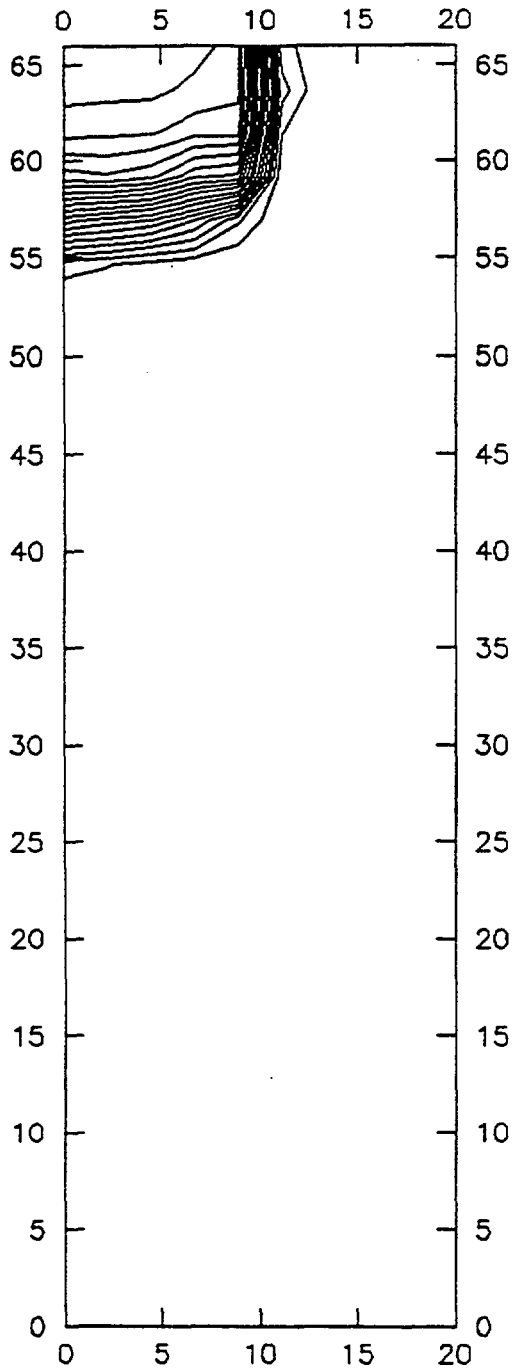

Block Height = 20 cm.
Block Width = 66 cm.
Contour Interval = 200 cm.
Maximum Matric Potential = 0.0 cm.
Minimum Matric Potential = -4000 cm.

Boundary Conditions
  Sides = No Flow
  Top Left 1/4 = Constant Matric
      Potential of 0.0 cm.
  Top Right 3/4 = No Flow
  Bottom = Constant Matric
      Potential of -4000 cm.
Initial Matric Potentials = -4000 cm.

Length of Simulation = 5.0 Hours

Figure 7: Simulation 5, 2-D Matric Potential Plot After 5.0 Hrs., Simulated Block With Fracture

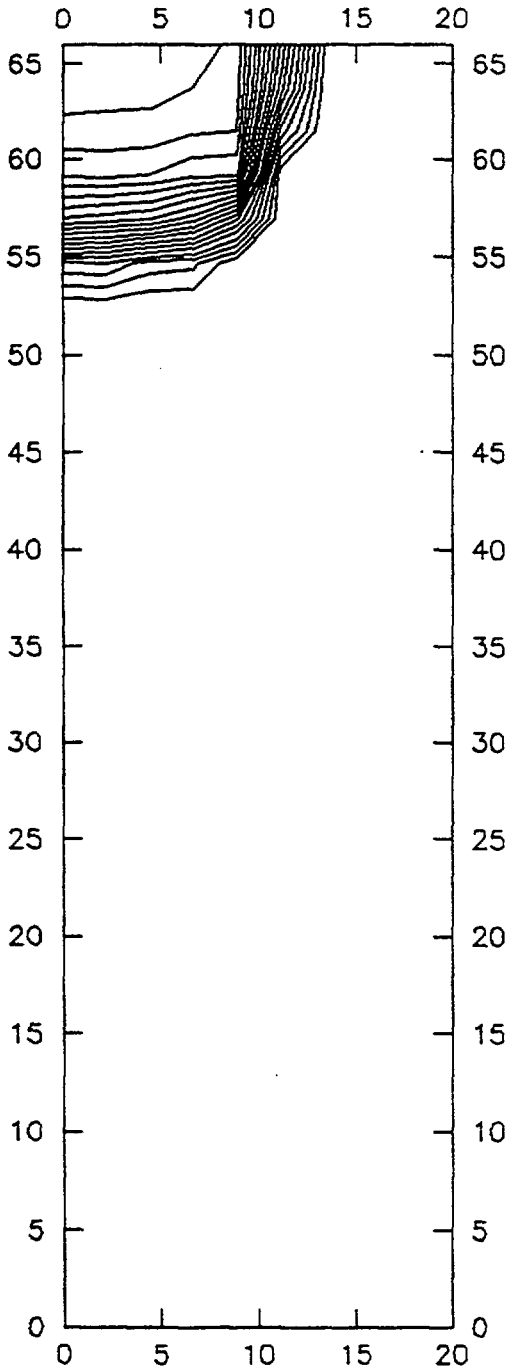

Block Height = 20 cm.
Block Width = 66 cm.
Contour Interval = 200 cm.
Maximum Matric Potential = 0.0 cm.
Minimum Matric Potential = -4000 cm.

Boundary Conditions
Sides = No Flow
Top Left 1/4 = Constant Matric Potential of 0.0 cm.
Top Right 3/4 = No Flow
Bottom = Constant Matric Potential of -4000 cm.
Initial Matric Potentials = -4000 cm.

Length of Simulation = 7.0 Hours

Figure 8: Simulation 5, 2-D Matric Potential Plot After 7.0 Hrs., Simulated Block With Fracture

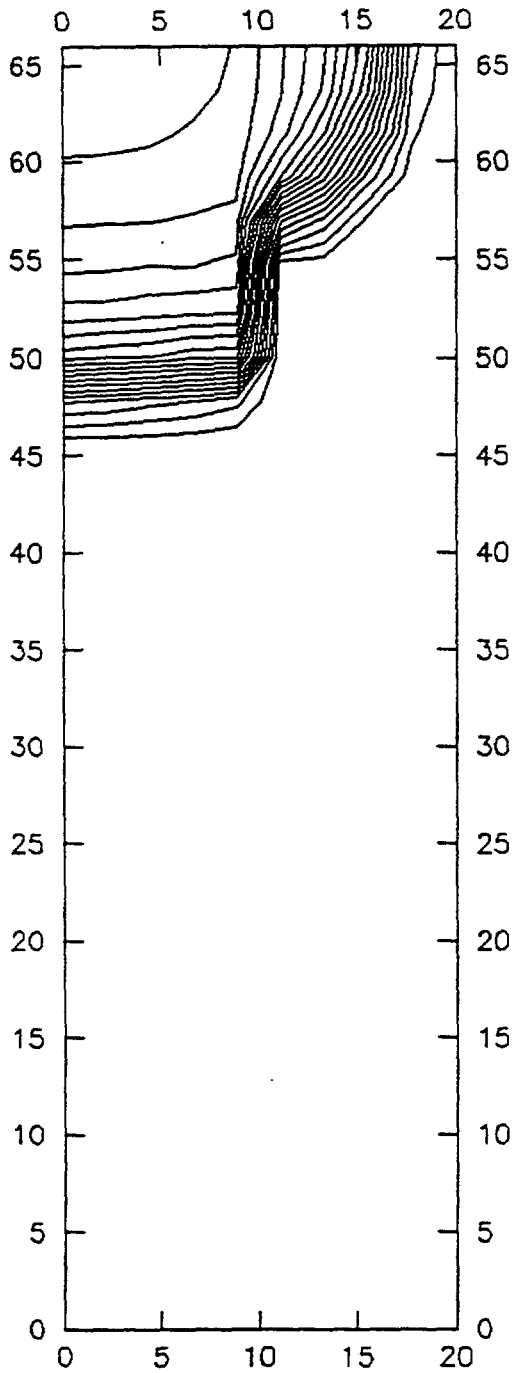

Block Height = 20 cm.
Block Width = 66 cm.
Contour Interval = 200 cm.
Maximum Matric Potential = 0.0 cm.
Minimum Matric Potential = -4000 cm.

Boundary Conditions
Sides = No Flow
Top Left 1/4 = Constant Matric Potential of 0.0 cm.
Top Right 3/4 = No Flow
Bottom = Constant Matric Potential of -4000 cm.
Initial Matric Potentials = -4000 cm.

Length of Simulation = 22.0 Hours

Figure 9: Simulation 5, 2-D Matric Potential Plot After 22 Hrs., Simulated Block With Fracture

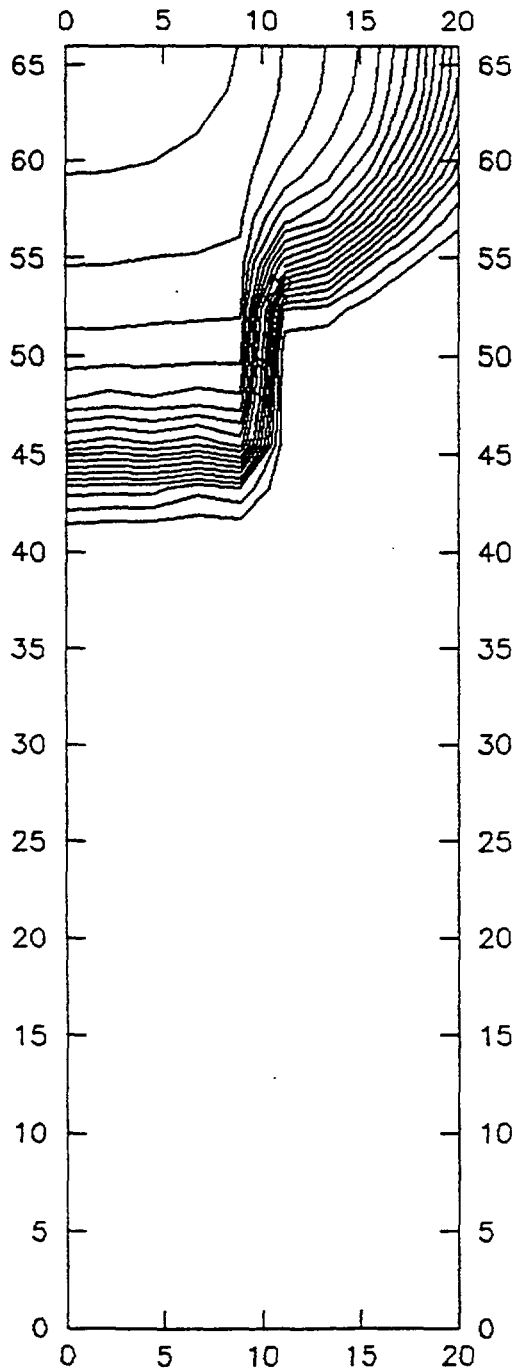

Block Height = 20 cm.
Block Width = 66 cm.
Contour Interval = 200 cm.
Maximum Matric Potential = 0.0 cm.
Minimum Matric Potential = -4000 cm.

Boundary Conditions
  Sides = No Flow
  Top Left 1/4 = Constant Matric
      Potential of 0.0 cm.
  Top Right 3/4 = No Flow
  Bottom = Constant Matric
      Potential of -4000 cm.
Initial Matric Potentials = -4000 cm.

Length of Simulation = 35.0 Hours

Figure 10: Simulation 5, 2-D Matric Potential Plot After 35 Hrs., Simulated Block With Fracture

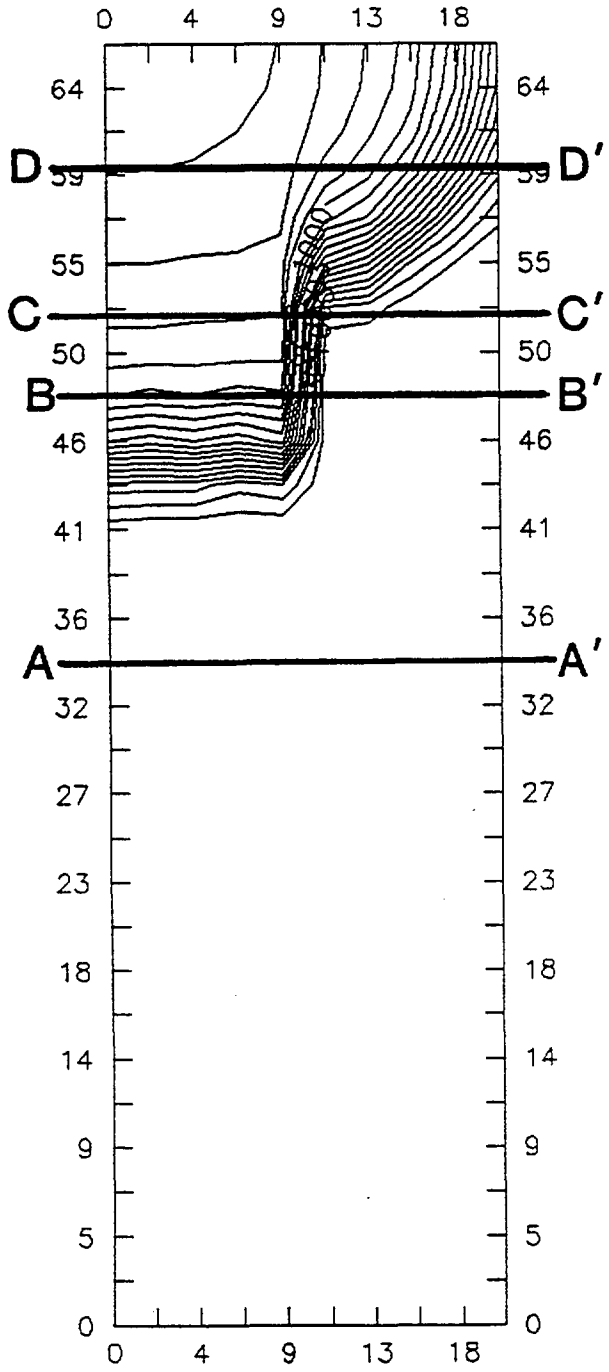

Figure 11: Simulation 5, 2-D Matric Potential Plot After 35 Hrs. With Profile Locations

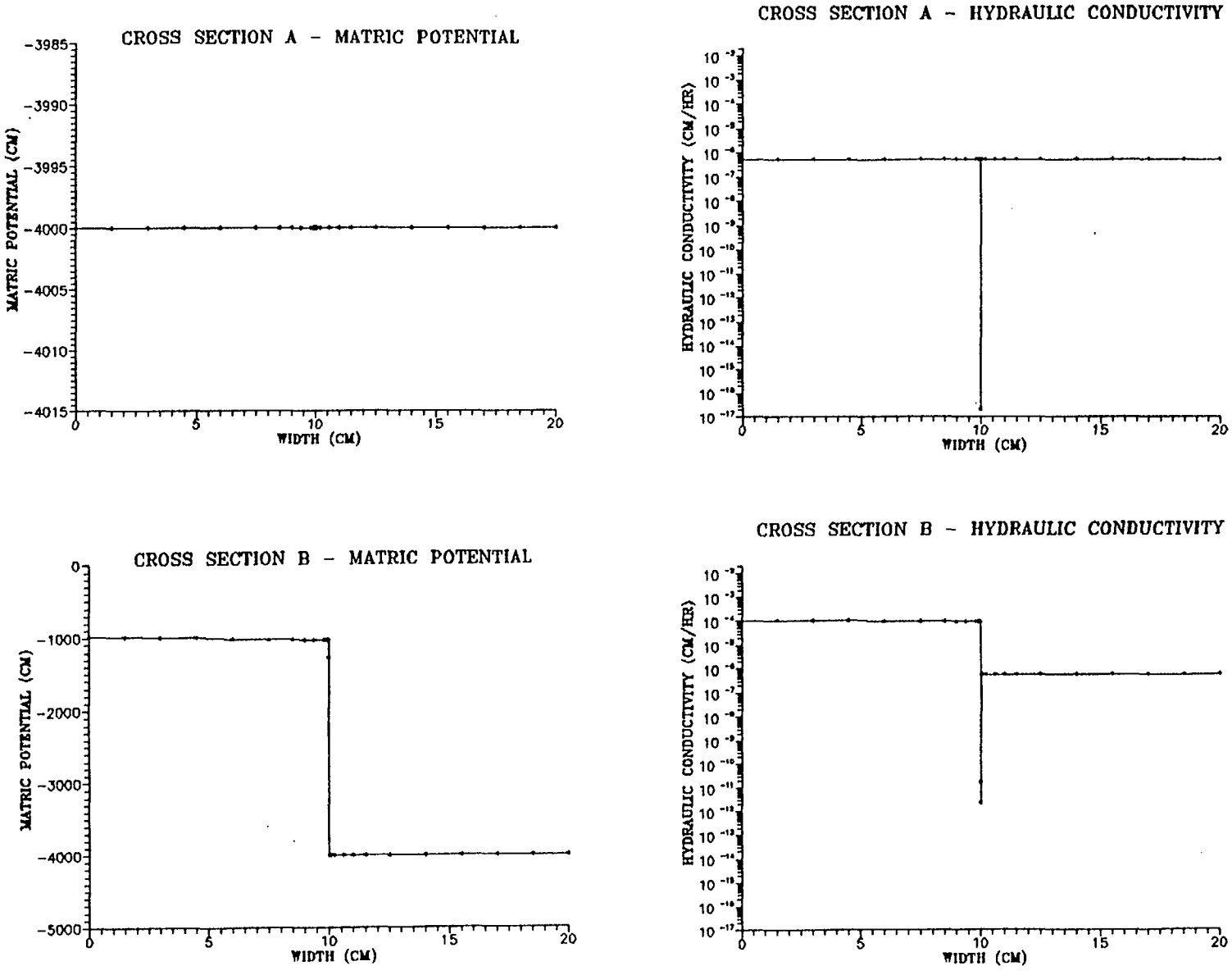

Figure 12: Simulation 5, Matric Potential And Hydraulic Conductivity Profiles A and B

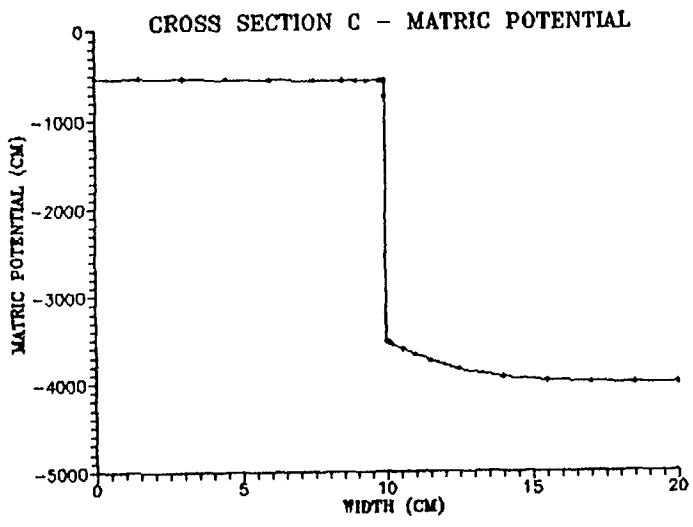

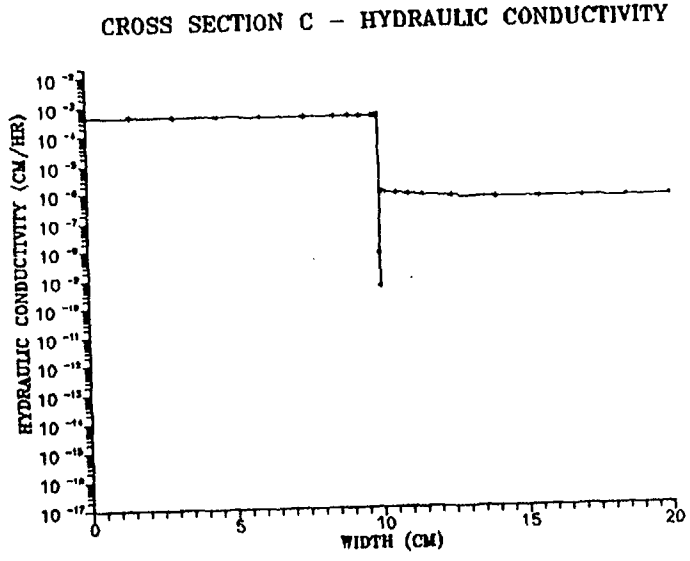

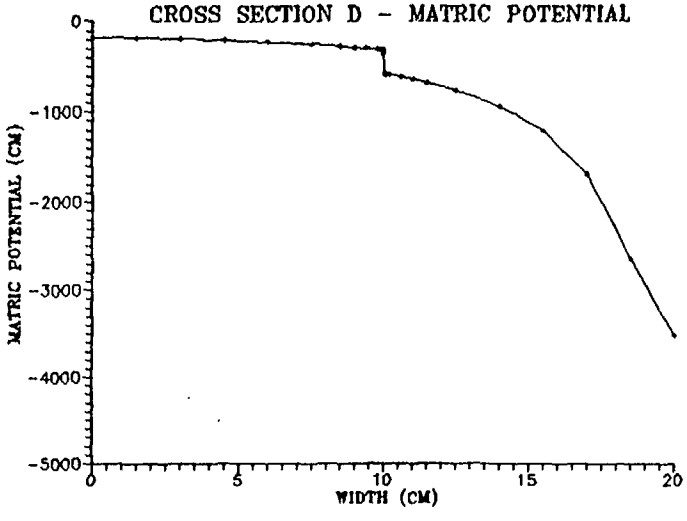

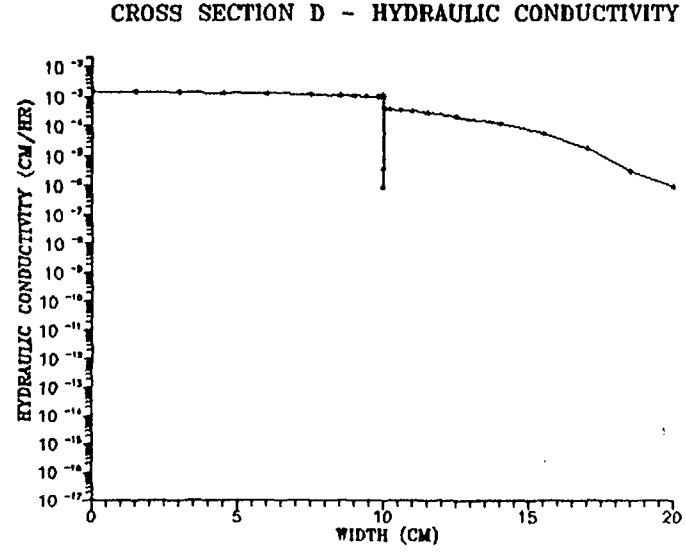

Figure 13: Simulation 5, Matric Potential And Hydraulic Conductivity Profiles C and D

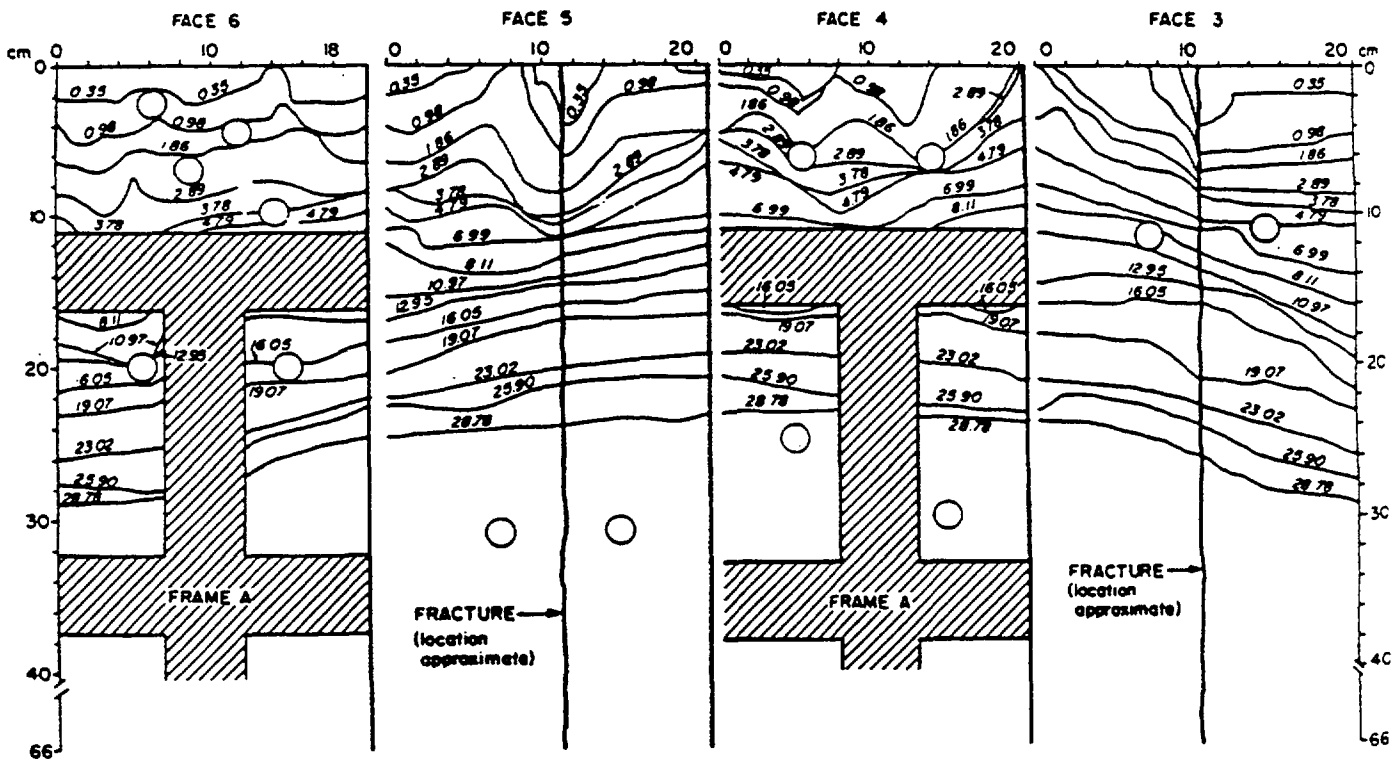

Figure 14: Wetting Front Advancement During Test Block Number 2 Imbibition Test. Numbers Indicate Days From Beginning of Test (Chuang, 1990).

APPENDIX C1

INTRAVAL experiments at the
Las Cruces Trench Site

Table of contents

List of Figures

INTRAVAL Experiments at the Las Cruces Trench Site

by

P. J. Wierenga[1]
R. G. Hills[2]
D. B. Hudson[1]

[1]Department of Soil and Water Science, University of Arizona, Tucson, AZ 85721

[2]Mechanical Engineering Department, New Mexico State University, Las Cruces, NM 88003

ABSTRACT

In order to examine conceptual models of partially saturated flow and transport through heterogeneous porous media, a series of experiments was performed at the Las Cruces Trench Site. The site was characterized extensively using in-situ measurements, and core and disturbed soil samples. Observations of water content, tension, and solute movement from a series of large-scale field infiltration and transport experiments were made and are available in database format.

1.0 INTRODUCTION

1.1 Experimental Group Identification

The experimental group was comprised of the U.S. Nuclear Regulatory Commission (USNRC) Waste Management Branch, Washington, DC (Group Leader); Massachusetts Institute of Technology (MIT), Cambridge, MA; New Mexico State University (NMSU), Las Cruces, NM; Pacific Northwest Laboratory (PNL), Richland, WA; and the University of Arizona (UA), Tucson, AZ.

1.2 Purpose and Overview of the Phase I Experiments

The purpose of the INTRAVAL Phase I Las Cruces Trench experiments was to test stochastic flow theories by comparing model predictions with observed water flow and transport. To accomplish this objective, a set of characterization experiments and two infiltration/redistribution experiments were completed during Phase I of INTRAVAL.

Approximately 600 core and 600 disturbed soil samples were collected for the characterization experiments. The soil-water retention characteristics and saturated hydraulic conductivities were estimated using these samples. In addition, the saturated hydraulic conductivities were determined in-situ through borehole permeameter tests at a similar number of locations.

The purpose of the Plot 1 experiment was to test the feasibility of using tensiometers and solute samplers in very dry soils, to develop and test the data acquisition methods used in later experiments, and to provide long term infiltration and redistribution data. Water was applied at a rate of 1.82 cm/day for 86 days to an area adjacent to the south side of the trench (Figure 1). Tritium was applied with the water during the first 10 days of irrigation. Tritium movement and tension were monitored through solute samplers and tensiometers inserted through the south wall of the trench during infiltration (Figure 2). Water content was monitored through neutron probe readings along several vertical plans during infiltration and redistribution. The data analysis for the Plot 1 experiment is complete and is presently available in the Las Cruces Database.

The experience gained during the Plot 1 experiment was used to design and run the Plot 2a experiment. During this experiment, water was applied at 0.43 cm/day to an area north of the trench for 75.5 days (Figure 1). Tritium and bromide were applied with the first 11.5 days of water application. The movement of tritium and bromide was monitored through approximately 50 solute samplers inserted through the north wall of the trench during both infiltration and redistribution (Figure 3). The movement of water was monitored through approximately 50 tensiometers inserted through the north wall of the trench and through neutron probe readings taken at approximately 1000 locations and depths (Figure 1). The data analysis for the Plot 2a experiment is complete and is presently available in the Las Cruces Database.

2. EXPERIMENTAL DESIGN

2.1 Experimental Location

The experiment is located at the New Mexico State University College Ranch, 40 km northeast of Las Cruces, NM, USA. The field site is on a basin slope of Mount Summerford, which is at the north end of the Dona Ana Mountains. The Dona Ana Mountains form a domal uplift complex of younger rhyolitic and older andesitic volcanics intruded by monzonite (Gile, Hawley and Crossman (1970)). The sediments on the mid-piedmont have young soils (6500 to 4000 years B.C.) of the Dona Ana and Onite series (coarse-loamy Typic Haplargids). Sediments on the lower-piedmont slopes are older soils (mid-late Pleistocene) dominated by the Berino series (fine-loamy Typic Haplargids). The geologic features, Geomorphic surfaces, soil series and vegetation types found in the area around the field test area are typical of many areas of southern New Mexico and are similar to arid and semiarid areas of the southwestern United States.

The climate in the region is characterized by an abundance of sunshine, low relative humidity, and an average Class A pan evaporation of 239 cm/yr. Average annual precipitation is 23 cm with 52% of the rainfall occurring between July 1 and September 30. The average monthly maximum air temperature is highest in June at 36 C and lowest in January at 13 C.

2.2 Details of the Trench and Irrigation System

A trench 26.4 m long, 4.8 m wide and 6.0 m deep was dug in the undisturbed soil to provide soil samples and to provide horizontal access to the irrigated area through the trench face. The walls of the trench were excavated vertically and reinforced to prevent cave-in. The trench and

adjacent irrigated area were covered to prevent surface runoff and infiltration due to rainfall and to minimize evaporation.

A 4 m by 9 m irrigated area was located on the south side of the trench for the Plot 1 experiment. The drip irrigation system consisted of 60 irrigation lines placed parallel to the trench face with each irrigation line containing 13 drippers. Laboratory and field uniformity tests of the drip irrigation system prior to the Plot 1 experiment indicated extremely small non uniformities and a random distribution of the non uniformities.

A 1.2 m by 12 m irrigated area was located on the north side of the trench for the Plot 2a experiment. The drip irrigation system consisted of 40 irrigation lines placed parallel to the trench face with each irrigation line containing 4 drippers. The applied water was metered onto the plot to allow for water balance calculations. Laboratory and field uniformity tests of the drip irrigation system prior to the Plot 2a experiment indicated extremely small non uniformities and a random distribution of the non uniformities.

Additional details of the experimental configurations are given in Wierenga et al. (1986), in Nicholson et al. (1987), Wierenga et al. (1990a, 1990b), and in Hills et al. (1990).

2.3 Parameters Measured

Key measurements include the following:

1. Saturated hydraulic conductivity (both in-situ and laboratory measurements) and $\theta(h)$ data were determined for approximately 600 locations in a vertical plane along the north face of the trench.

2. Measurements of θ_r and θ_s and estimates of the van Genuchten water retention parameters α and n were determined for each of the 600 locations. Specific water capacity, C, can be estimated from the resulting van Genuchten curves.

3. Moisture content or moisture profiles as a function of time were monitored using neutron probes.

4. Tension data obtained from tensiometers placed on two dimensional grids on the north and south trench walls were monitored as a function of time.

5. Concentrations of the tracers were sampled through the trench wall on two dimensional grids as a function of time.

2.4 Sampling Strategy

Two sampling strategies were used:

Scheme 1: HYDROLOGIC PARAMETER CHARACTERIZATION.

Soil samples were collected from each of 9 horizontal morphological soil layers to a depth of 6 m. The horizontal spacing between samples in each layer was 0.5 m. In addition, samples were collected from 3 vertical transects down to 6 m with a vertical spacing of 0.13 m. Measurements of field saturated hydraulic conductivity were made in-situ with a saturated-borehole technique (borehole permeameter). Cores collected adjacent to these boreholes were taken to the laboratory for analysis of a) water retention characteristics, b) particle-size analysis, c) bulk density, and d) soil chemical properties (e.g., $CaCO_3$ content, soil paste pH and soluble cations and anions). Over 600 measurements of field saturated hydraulic conductivity were made. Similar numbers of water retention curves, particle-size analysis, bulk densities, and chemical properties were measured in the laboratory from the core samples.

Scheme 2: INFILTRATION AND REDISTRIBUTION TESTING OF WATER AND SOLUTE MOVEMENT

The face of the experimental trench was monitored intensively with solution samplers and tensiometers (Figures 2 and 3). The solution samplers were tensiometer cups connected to a vacuum line (sometimes called suction lysimeters). These units collected small (2-10 ml) quantities of soil solution as the water infiltrated into the soil profile. Tracer pulses were analyzed by periodic collection of samples. A 10 day pulse of tritium was used to trace the transport of water during the Plot 1 experiment. The Plot 1 experimental results indicated that the use of solution samplers is a viable technique for monitoring solute transport in unsaturated soils, particularly when tensions are less than 150 cm. At higher suctions, the water transmission rate is too low to obtain sufficient quantities of sample. These samplers were also used during the Plot 2a experiment. Tensiometers placed adjacent to suction samplers were used to monitor tensions and operated reasonably well after the wetting front had passed. These units do not work in dry soil. Water tensions in dry soil are inferred from the water retention characteristics described in Scheme 1. Neutron probes were used to monitor water contents in several planes located parallel and perpendicular to the trench face (Figure 1). The neutron probe monitoring, solute sampling, and tensiometer reading was done on the order of days during initial infiltration and on the order of weeks during the later stages of redistribution.

2.5 Independence Between Data Sets

The soil samples for hydraulic characterization were taken during the excavation of the trench from an area adjacent to the Plot 1 and 2a infiltration and redistribution experiments. The results from the Plot 1 and 2a experiments were not used to calibrate or redefine the characterization data. The characterization data were thus independent of the Plot 1 and 2a data. The Plot 1 and Plot 2a data were also independent in that they were taken from opposite sides of the trench for experiments with different infiltration rates. Water flow in the soil was monitored with both tensiometers and neutron probes. Since these methods are different, the corresponding data are independent.

2.6 Biases Inherent in the Design

The soil retention characteristics determined in the laboratory may not truly represent water release characteristic in the field. Sampling and measurement techniques are not developed to the point where the entire (wet to dry) range of the water retention curve can be measured in the field by a single instrument. Hence, laboratory measurements are used to supplement field observations. Also, pressure plate techniques may tend to over estimate water contents at high tensions (1.0 to 1.5 MPa values).

Since tensiometers only operate in the wet range, the useful tension data is in the wet soil range where tensions are not too large (< 150 cm H_2O). This biases the data toward wetter environments than occur naturally in arid regions. In contrast, neutron probes can measure very small water contents. However, neutron probes cannot define sharp wetting fronts due to the relatively large effective area of the probe measurement. Sharp wetting fronts tend to be smoothed.

The unsaturated conductivity functions determined from pore-size models and water retention data may inadequately describe the actual unsaturated conductivity values in the field. This data should be checked against laboratory measurements of unsaturated conductivity and possibly using the instantaneous profile method with fixed data.

2.7 Complementary Experiments

A suite of experiments have been performed to evaluate model capabilities. The large lysimeter tests (described in Wierenga et al. (1986), Wierenga and van Genuchten (1989), and Hills et al. (1989)) as well as laboratory column tests were used to estimate transport parameters (i.e., Peclet number, dispersion coefficients, etc.). These parameters are used to understand field transport in soils of similar physical and chemical characteristics. The experiments consisted of infiltration and redistribution tests in uniform and layered soils under flow conditions similar to those of the field tests. The lysimeter tests are complete.

Plot 2b and Plot 3 experiments are planned for the near future. The Plot 2b experiment will use the Plot 2a experimental set-up. Different water application rates and tracers will be used. The Plot 3 experiment will be at a different location on the north side of the trench and will extend over a larger scale. Information gained during the Plot 2b experiment and suggestions from the INTRAVAL participants will be carefully considered during the Plot 3 experimental design.

3.0 AVAILABLE EXPERIMENTAL RESULTS

3.1 Raw Data

The Las Cruces Database (discussed below) contains water retention data, density profiles, particle-size data, and saturated hydraulic conductivities measured through both laboratory and in-situ techniques during the characterization experiments; and water content data, tensiometer data, tritium and bromide concentrations, and water applications rates measured during the Plot 1 and Plot 2a experiments. In addition, morphological mapping of the trench face, drip irrigation

distribution tests, and outflow and inflow measurements from large and small column-support tests are on file at NMSU and at UA.

3.2 Processed Data

The processed data are reported in two annual reports (NMSU to NRC 1985, 1986), in Wierenga et al. (1986), in Nicholson et al. (1987), and in Wierenga et al. (1989). The processed data for the Plot 1 experiment consist of moisture profiles determined from neutron probes, tensions, tritium breakthrough curves, and wetting front observations obtained through visual mapping. The processed data for the Plot 2a experiment consist of moisture profiles determined from neutron probes, tensions, and tritium and bromide breakthrough curves. In addition, the van Genuchten water retention parameters α and n for each of the 600 core sample locations and the parameters for uniform and layered soil models are included (Wierenga et al. (1989)).

3.3 Data Storage

Data are stored at Las Cruces in laboratory notebooks, on IBM (5 1/4" floppy) disks, and on 10 MByte Bernoulli disks. Redundant copies of the digital data are stored in Tucson, Arizona on 20 MByte Bernoulli disks and in the Las Cruces Database.

3.4 The Las Cruces Database

The Las Cruces Database is installed on a Digital VAX and is backed up regularly by computer center personnel. The database consists of 27 files in ASCII format and is accessible at no cost through the international computer networks using FTP. The database is updated on a regular basis. The database is divided into three subsets of data files: 1) Soil Property Data Files, 2) Plot 1 Data Files, and 3) Plot 2 Data Files. The Soil Property Data Files contain the soil property characterization data from the Las Cruces Trench Site. These data include laboratory and in-situ saturated hydraulic conductivities, soil particle size distribution data, measured water retention data, and estimates of the van Genuchten parameters. The Plot 1 Data Files contains water and solute application rate information, and measurements of volumetric water contents, tensions, and relative tritium concentrations for the first trench experiment. The Plot 2 Data Files contain water and solute application rate information, and measurements of volumetric water contents, tensions, and relative tritium and bromide concentrations for the second trench experiment.

All files have the same general tabulated structure. The fields (i.e. columns) are tab delimitated and carriage returns are used to denote end of records (i.e. lines). The records have variable lengths. The maximum record length is 87 bytes (or 87 ASCII characters). The first line of each file contains the column titles. The value -999 is used to denote missing data. All character strings are surrounded by single quotes. The maximum number of characters in a field is 15 (17 including quotes). The use of quotes simplifies the FORTRAN code when reading the data files.

4.0 EXPERIMENTAL RESULTS

The experimental results, numerical simulation, and the database are documented in Hills et al. (1989), Wierenga et al. (1989), Wierenga et al. (1990a, 1990b), and Hills et al. (1990). Experimental and numerical results for water flow and solute transport are also presented in the following appendices.

5.0 REFERENCES

Gile, L. U., J. H. Hawley, and R. B. Grossman, "Distribution and Genesis of Soils and Geomorphic Surfaces in a Desert Region of Southwestern New Mexico, Guidebook," pp. 156. Soil Sciences Society of America and New Mexico State University, Las Cruces, (1970).

Hills, R.G., D.B. Hudson, I. Porro, and P.J. Wierenga, "Modelling One-Dimensional Infiltration Into Very Dry Soils - Part 2: Estimation of the Soil-Water Parameters and Model Predictions," Water Resources Research, Vol. 25, No. 6, pp. 1271-1282, (1989).

Hills, R.G., P.J. Wierenga, D.B. Hudson, M.R. Kirkland, "Site Description, Experimental Results, and Two-Dimensional Flow Predictions for the Las Cruces Trench Experiment 2," submittal to Water Resource Research, (1990).

Nicholson, T. J., and others, "Validation of Stochastic Flow and Transport Models for Unsaturated Soils: A Comprehensive Field Study, "Proceedings of USDOE-AECL Symposium on Geostatistical Sensitivity and Uncertainty Methods for Groundwater Flow and Radionuclide Transport Modeling, San Francisco, CA, (1987).

Wierenga, P. J., and others, "Validation of Stochastic Flow and Transport Models for Unsaturated Soils: A Comprehensive Field Study," NUREG/CR-4622, U.S. Nuclear Regulatory Commission, Washington, DC, (1986).

Wierenga, P.J., and M. Th. van Genuchten, "Solute Transport through Small and Large Unsaturated Soil Columns," Groundwater, Vol. 27, No. 1, pp.35-42, (1989).

Wierenga, P. J., A. Toorman, D. Hudson, J. Vinson, M. Nash, and R.G. Hills, "Soil Physical Properties at the Las Cruces Trench Site," NUREG/CR-5441, U. S. Nuclear Regulatory Commission, Washington, DC, (1989).

Wierenga, P.J., R.G. Hills, and D.B. Hudson, "Site Description, Experimental Results, and One-Dimensional Flow Predictions for the Las Cruces Trench Experiment 1," submittal to Water Resource Research, (1990a).

Wierenga, P.J., D.B. Hudson, R.G. Hills, I. Porro, M.R. Kirkland, "Experiments 1 and 2 at the Las Cruces Trench Site, U.S. Nuclear Regulatory Commission NUREG report, in preparation (1990b).

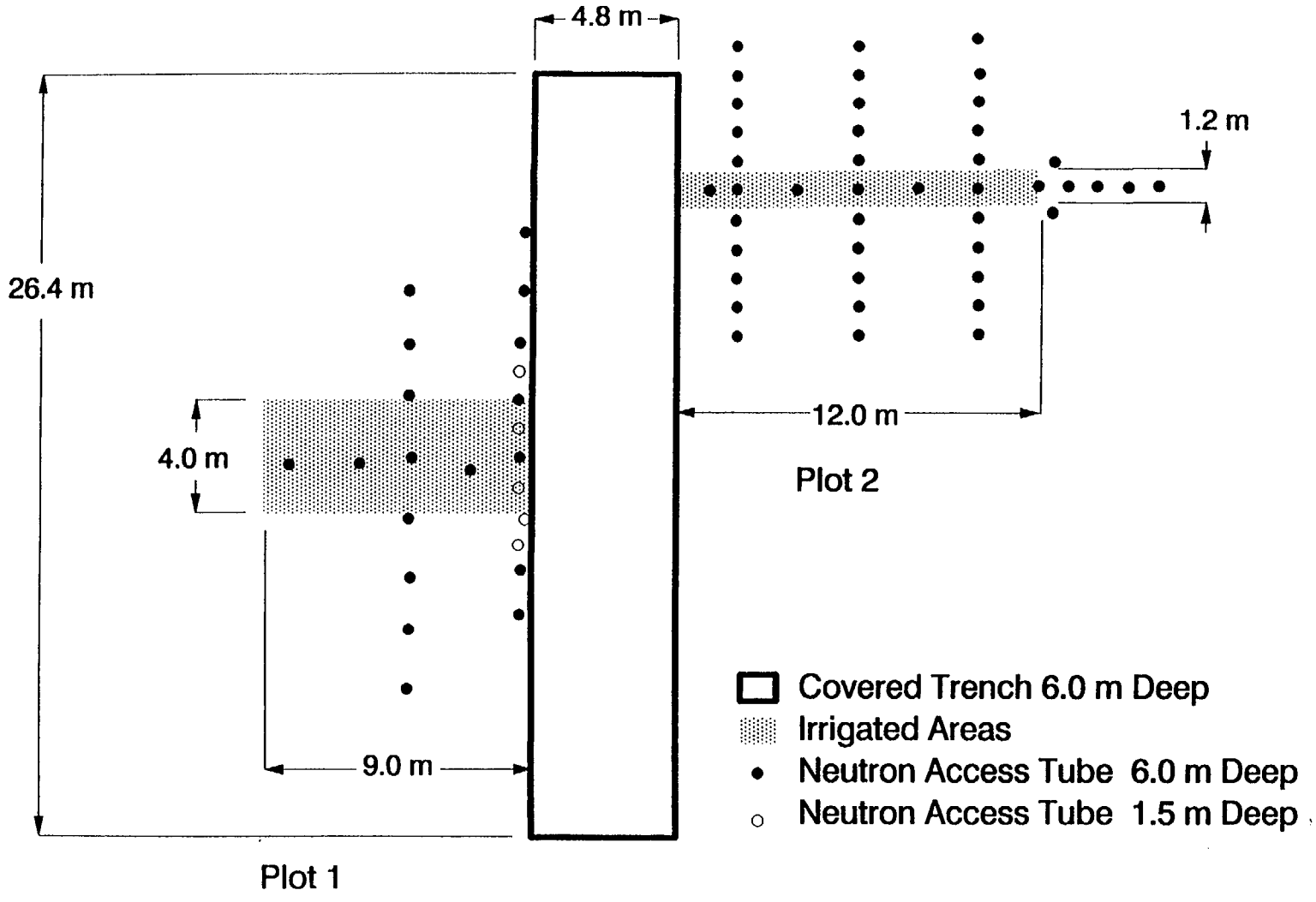

Figure 1: Plan view of the Plot 1 and 2 experiments

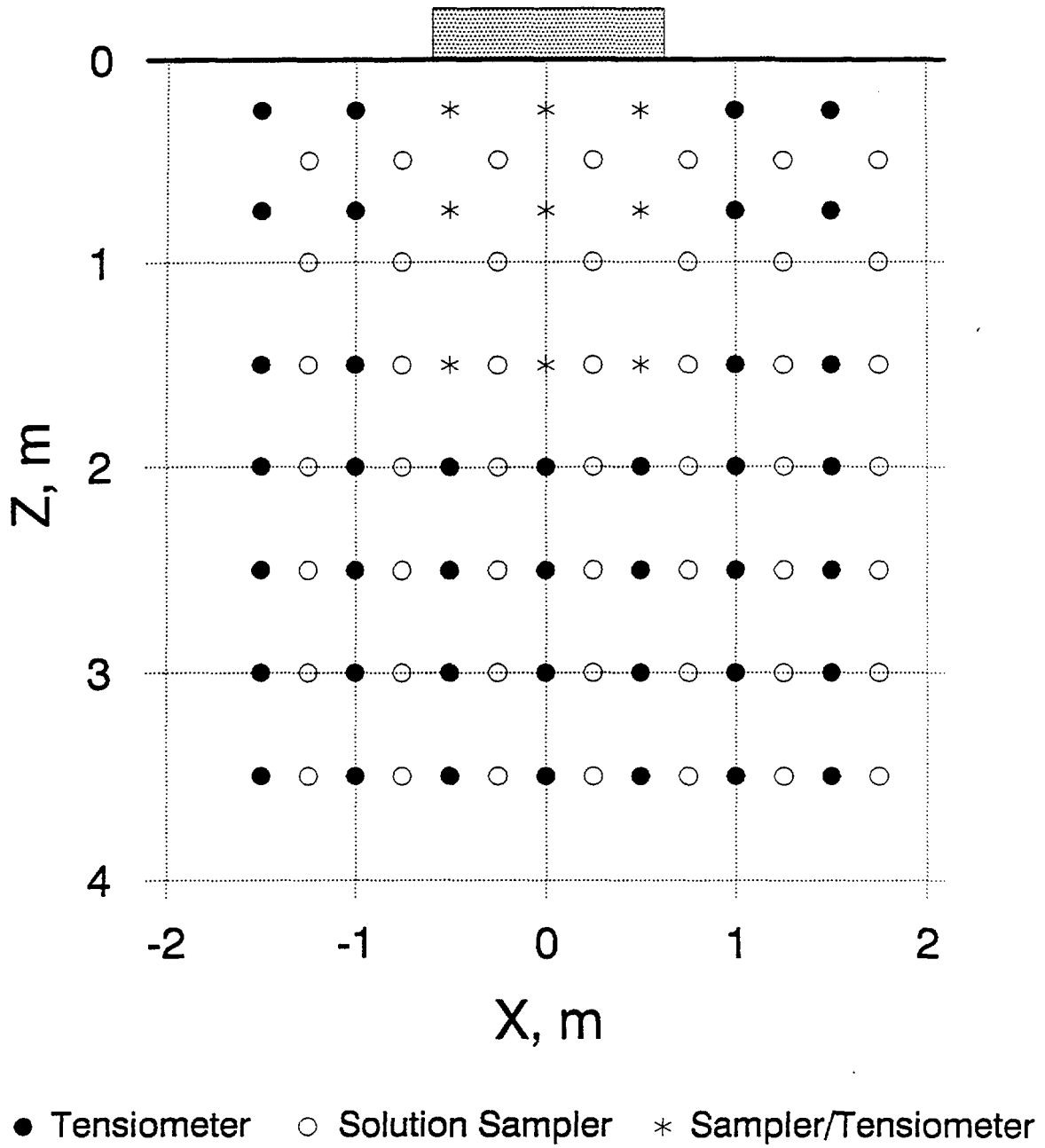

Figure 2: Location of solute samplers and tensiometers for the Plot 1 experiment

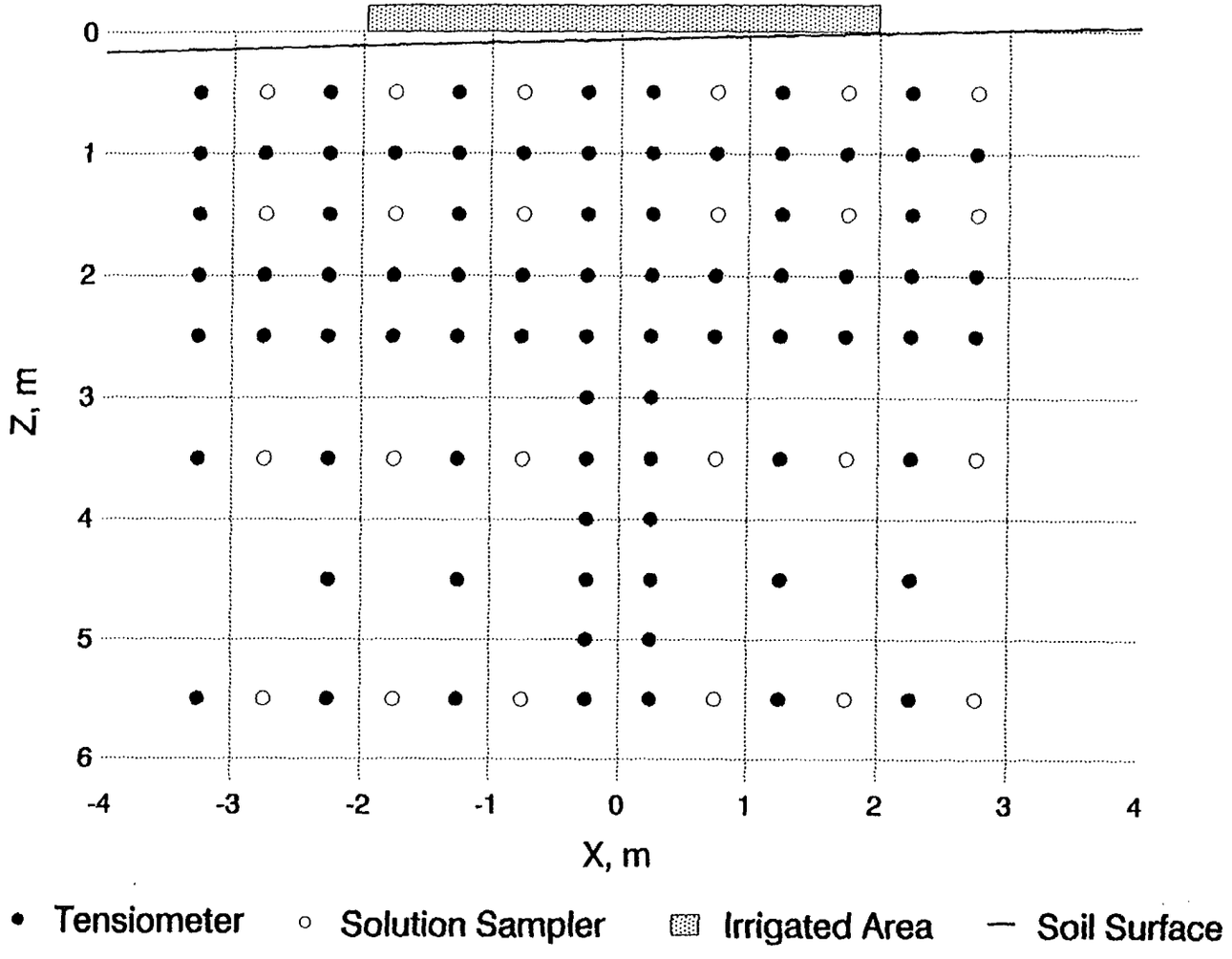

Figure 3: Location of solute samplers and tensiometers for the Plot 2 experiment

APPENDIX C2

High-resolution modeling of strip source infiltration:
three-dimensional synthetic experiment
analogous to Las Cruces Trench experiment

Table of contents

High-Resolution Modeling of Strip Source Infiltration: Three-Dimensional Synthetic Experiment Analogous to Las Cruces Trench Experiment

by

Rachid Ababou
Center For Nuclear Waste Regulatory Analyses
Southwest Research Institute
San Antonio, Texas 78228-0510

ABSTRACT

A high-resolution, three-dimensional finite difference model based on a mixed variable formulation of partially saturated or unsaturated flow is used to model strip source infiltration and natural drainage in a randomly heterogeneous and imperfectly stratified soil. The flow regime, soil properties, and boundary conditions are analogous to those of the first Las Cruces strip source experiment, albeit with some differences. The nonlinear behavior and statistical properties of the unsaturated soil are inferred, in part, from preliminary hydrodynamic data collected at the trench site. A 15 m x 15 m x 5 m computational domain is discretized into 300,000 finite difference cells or grid points. The parameters of the unsaturated conductivity curve are assumed to be single realizations of spatially correlated random fields. Each finite difference cell possesses its own, distinct conductivity function. The detailed simulation captures the complex three-dimensional heterogeneity of the transient moisture plume, and provides direct evidence of horizontal spreading and moisture-dependent anisotropy due to imperfect, spatially variable stratification.

1.0 INTRODUCTION

1.1 Modeling Group Identification

The numerical model and simulation results described here were previously generated and partially analyzed by the M.I.T. group [Ababou 1988; Ababou and Gelhar 1988]. The Center for Nuclear Waste Regulatory Analyses is currently exploiting these results and developing new simulations toward model validation [Ababou, 1990].

1.2 Purpose and Overview

The simulations to be described below were developed with two distinct objectives in mind. The first objective was to test the linearized analytical theory of stochastic flow [Mantoglou and Gelhar, 1987 a,b,c], and particularly the moisture-dependent anisotropy of effective flow behavior, under more realistic conditions of nonlinearity, randomness, and flow geometry than allowed for in theory. The second objective was, given the constraints of the first theoretical objective, to mimic as closely as possible the conditions of the first Las Cruces strip-source experiment.

2.0 NUMERICAL EXPERIMENT SET-UP

2.1 Input Data

The problem set-up, described below, involves a strip-source geometry and discharge rate similar to those of the first Las Cruces strip-source experiment. However, the initial soil moisture ($\Theta \approx 0.15$, or $\Psi \approx 150$ cm) used in the model was higher than that observed at the field site in order to avoid an excessive conductivity contrast near the wetting front. Note that relatively low rate infiltration in moderately dry soil can produce large conductivity contrasts, owing to the very sharp decrease of conductivity with increasing suction for the exponential conductivity model adopted here.

One of the main reasons for selecting the exponential conductivity model was its convenience for developing analytical solutions of the stochastic flow equations [Mantoglou and Gelhar, a,b,c]. The exponential relationship is not adequate for modeling the very dry range of unsaturated flow. Recognizing this restriction, we studied the discrepancy between exponential and other conductivity models (Mualem-Van Genuchten) for the field site data. The discrepancy was found to be relatively minor in the suction range 50 cm $\leq \Psi \leq$ 150 cm. This is illustrated in *Figure 1* from Ababou [1988, Chap. 7, Fig. 7.10].

Besides being highly nonlinear, the two-parameter exponential conductivity curve $K(h,\underline{x}) = Ksat(\underline{x}) \exp(\alpha(\underline{x})h)$ was highly variable in space as well. The parameters $Ksat(\underline{x})$ and $\alpha(\underline{x})$ were assumed to be spatially correlated replicates of two log-normally distributed, independent random fields. Furthermore, the three-dimensional correlation structure was taken to be anisotropic, with a vertical-to-horizontal anisotropy ratio of 1/4 in terms of the directional correlation scales.

A summary of input data is given in *Table 1*, from Ababou [1988, Chap. 7, Table 7.2]. Note that the coefficients of variation of Ksat and α are 67% and 22%, respectively. Single-point and two-point statistics were inferred more or less directly from in-situ field observations such as those reported in Wierenga et al.[1989]. During infiltration, the top boundary condition was a fixed flux of 2 cm/day imposed on the 4 m wide strip source, and zero flux elsewhere. The lateral boundary conditions were zero flux. The bottom boundary condition was gravity drainage (zero pressure gradient). The gravity drainage condition was quite successful in allowing moisture plumes to migrate downward, through the bottom boundary, with minimal disturbance. For more details on problem set-up, see Ababou [1988, Section 7.3.1]. For random field generation by the Turning Band method, see also Tompson et al. [1989].

2.2 Simulation and Output Data

The numerical code "BIGFLO", previously developed at MIT [Ababou, 1988], was used to generate the results discussed here. The BIGFLO code is a fully three-dimensional finite difference simulator for saturated or partially saturated flow in highly heterogeneous porous media. The algorithms are described in detail in Ababou [1988, Chap. 5]. Summaries of solution algorithms and model problems can be found in Ababou and Gelhar [1988] for the case of unsaturated flow, and Ababou et al. [1989] for the case of saturated flow.

The strip source simulation comprised two phases, an infiltration phase (q=2 cm/day) and a natural drainage phase (q=0). Given the depth of the computational domain (5 m) and the particular choice of initial conditions discussed earlier, infiltration was turned off after a relatively short time (10 days) and natural drainage was simulated for 10 more days. The simulation outputs were expressed mainly in terms of three-dimensional pressure fields. Output times of interest here are t=5 days and t=10 days (infiltration phase), and t=15 days (drainage phase).

A preliminary visualization of the results was obtained by contouring the pressure fields along selected slices [Ababou, 1988, Chap. 7.3]. More recently, the fully three-dimensional pressure fields have been visualized using 3D color graphics techniques such as perspective views of solid, color-coded iso-surfaces in 3D space [Ababou, 1990]. Each frame represents a snapshot of the moisture plume at a fixed, pre-selected output time.

3.0 ANALYSIS OF SIMULATION RESULTS

Some of the heterogeneous suctions obtained for three vertical slices are shown in *Figure 2* (t=5days), *Figure 3* (t=10 days), and *Figure* 4 (t=15 days). We recall from the previous section that the infiltration phase ended at t=10 days. Also, note that the heterogeneous moisture content distribution follows the same pattern as pressure, due to the fact that a single one-to-one relation $\Theta=\Theta(\Psi)$ was assumed, regardless of spatial location.

The detailed moisture patterns at any time differ considerably from section to section, reflecting the three-dimensional nature of the local flow process. If the soil was uniformly layered, rather than randomly stratified as here, the moisture patterns in any vertical cross-section would be nearly the same everywhere except near the free edge of the finite length strip source.

It is interesting to analyze the vertical versus horizontal extent of the moisture movement as seen in these figures. Let us define the moisture plume by $\Theta \geq \Theta_F$, where Θ_F is a relatively dry moisture content, e.g. close to the initial value. The contours shown in *Figures* 2, 3, 4 reveal significant lateral spread of the moisture plume. A number of localized wet lenses appear to be hanging over drier regions, reflecting the statistical anisotropy, or imperfect stratification, of the synthetic soil. This feature can be observed near the geometric center of the x_2=9.8 m cross-section (around depth x_1=2.5m and abscissa x_3=0). Another, more subtle phenomenon is the relatively larger spread of the relatively dry margins of the moisture plume (light gray tones), compared to the wet core of the plume (dark gray tones). This behavior is consistent with the moisture-dependent anisotropy predicted by Mantoglou and Gelhar [1987 a,b,c].

The above-mentioned features appear more clearly in full three-dimensional representation. The attached black-and-white reproductions of color plates, *Figure 5* and *Figure 6*, show three-dimensional views of the moisture plume after 10 days of infiltration. The amount of detail in this simulation helps capture the heterogeneity of the moisture pattern over a wide range of scale. The horizontal spread due to random stratification is clearly far from uniform. Layers have "holes". Horizontal "fingers" and wet lenses tend to remain suspended over dryer lenses of soil.

These results are encouraging, and suggest the feasibility of similar simulations under conditions more closely related to the Las Cruces Trench experiment. This may involve, for instance, using

both probabilistic and site-specific deterministic input data, combined through stochastic conditioning techniques (work in progress).

4.0 REFERENCES

Ababou R., Three-Dimensional Flow in Random Porous Media, *PhD Thesis*, Department of Civil Engineering, Massachusetts Institute of Technology, Cambridge, Massachusetts, 2 Volumes, 833 pp., Jan. 1988.

Ababou R., High-Resolution Modeling of Three-Dimensional Flow Fields, 4th INTRAVAL Workshop, Las Vegas, Nevada, Feb. 5-10, 1990.

Ababou R. and Gelhar L. W., A High-Resolution Finite Difference Simulator for 3D Unsaturated Flow in Heterogeneous Media, in *Computational Methods in Water Resources*, Elsevier and Computational Mechanics Publications, Vol. 1, 173-178, June 1988.

Ababou R., McLaughlin D., Gelhar L. W., Tompson A. F., "Numerical Simulation of Three-Dimensional Saturated Flow in Randomly Heterogeneous Porous Media", *Transport in Porous Media*, 4, 549-565, 1989.

Mantoglou A. and Gelhar L. W., (1987a), "Stochastic Modeling of Large-Scale Transient Unsaturated Flow Systems", *Water Resour. Res.*, 23(1), 37-46.

Mantoglou A. and Gelhar L. W., (1987b), "Capillary Tension Head Variance, Mean Soil Moisture Content, and Effective Specific Soil Moisture Capacity of Transient Unsaturated Flow in Stratified Soils", *Water Resour. Res.*, 23(1), 57-67.

Mantoglou A. and Gelhar L. W., (1987c), "Effective Hydraulic Conductivities of Transient Unsaturated Flow in Stratified Soils", *Water Resour. Res.*, 23(1), 57-67.

Tompson A. F., Ababou R., and Gelhar L. W., Implementation of the Three-Dimensional Turning Bands Random Field Generator, *Water Resour. Res.*, 25(10), 2227-2243, 1989.

Wierenga P. J., Gelhar L. W., Simmons C. S., Gee G.W., and Nicholson T.J., "Validation of Stochastic Flow and Transport Models for Unsaturated Soils: A Comprehensive Field Study", Report NUREG/CR-4622, U. S. Nuclear Regulatory Commission, Washington, D.C., 1986.

Wierenga P. J., Toorman A., Hudson D., Vinson J., Nash M., and Hills R. G., "Soil Physical Properties at the Las Cruces Trench Site," NUREG/CR-5541, U. S. Nuclear Regulatory Commission, Washington, DC, (1989).

TABLE 1

SUMMARY OF INPUT DATA FOR THE SINGLE-REALIZATION SIMULATION OF STRIP-SOURCE INFILTRATION IN A STATISTICALLY ANISOTROPIC SOIL ("TRENCH EXPERIMENT")

Type of Data	Description	Value
Domain Geometry, Boundary Conditions, and Initial Conditions	Vertical domain size	L_1 = 5.0 m
	Transverse horizontal domain size	L_2 =15.0 m
	Transverse longitudinal domain size	L_3 =15.0 m
	Strip source width	W_s = 4.0 m
	Strip source length	L_s = 9.9 m
	Flux at the surface of the strip	$q_0 \equiv$ 2 cm/day
	Condition at the bottom boundary	q_1 = - K(h)
	Initial pressure head	h_{in} = - 150 cm
Space-Time Discretization	Time step	Variable
	Mesh size Δx_i (i=1,2,3)	Δx_i= 0.10,0.20,0.20 m
	Unidirectional number of nodes n_i	n_i= 52, 76, 76
	Total number of nodes of 3D grid	N = 300352
Exponential Conductivity Curve (Random)	Geometric mean saturated conductivity	K_G = 100 cm/d
	Standard deviation of $\ell n\ K_s$	σ_f = 0.6083
	Geometric mean of the ℓn K-slope	α_G = 0.0494 cm^{-1}
	Standard deviation of $\ell n\ \alpha$	σ_a = 0.2202
	Anisotropic correlation scales λ_i	λ_i = 0.25,1.0,1.0 m
Van-Genuchten Retention Curve (Deterministic)	Saturated moisture content	θ_s = 0.368
	Residual moisture content	θ_r = 0.102
	Scaling parameter	β = 0.0334 cm^{-1}
	Shape factor (real number)	n = 1.982

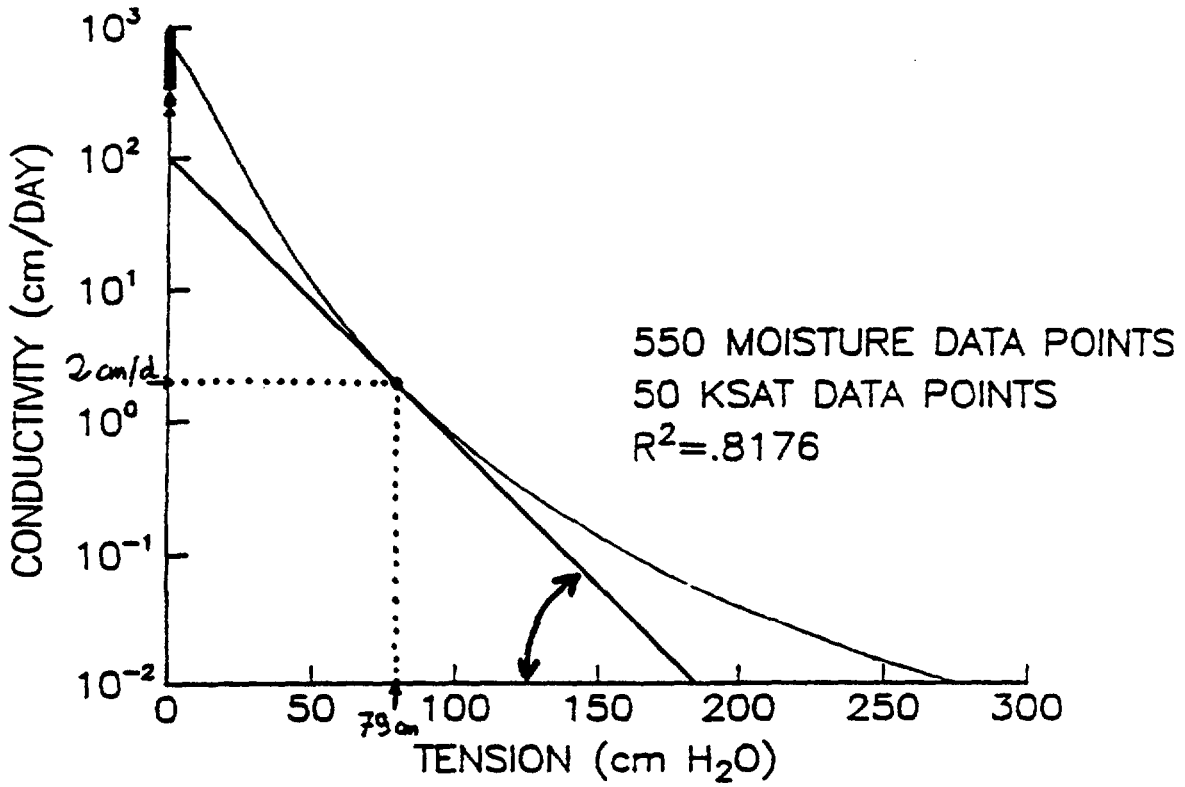

Figure 1. Mean unsaturated conductivity curve K(h) for the soil of the strip-source "trench experiment": the straight line corresponds to the exponential model actually used in the numerical simulation; the other curve is the Mualem-Van Genuchten model indirectly fitted to field data by Wierenga et. al., 1986.

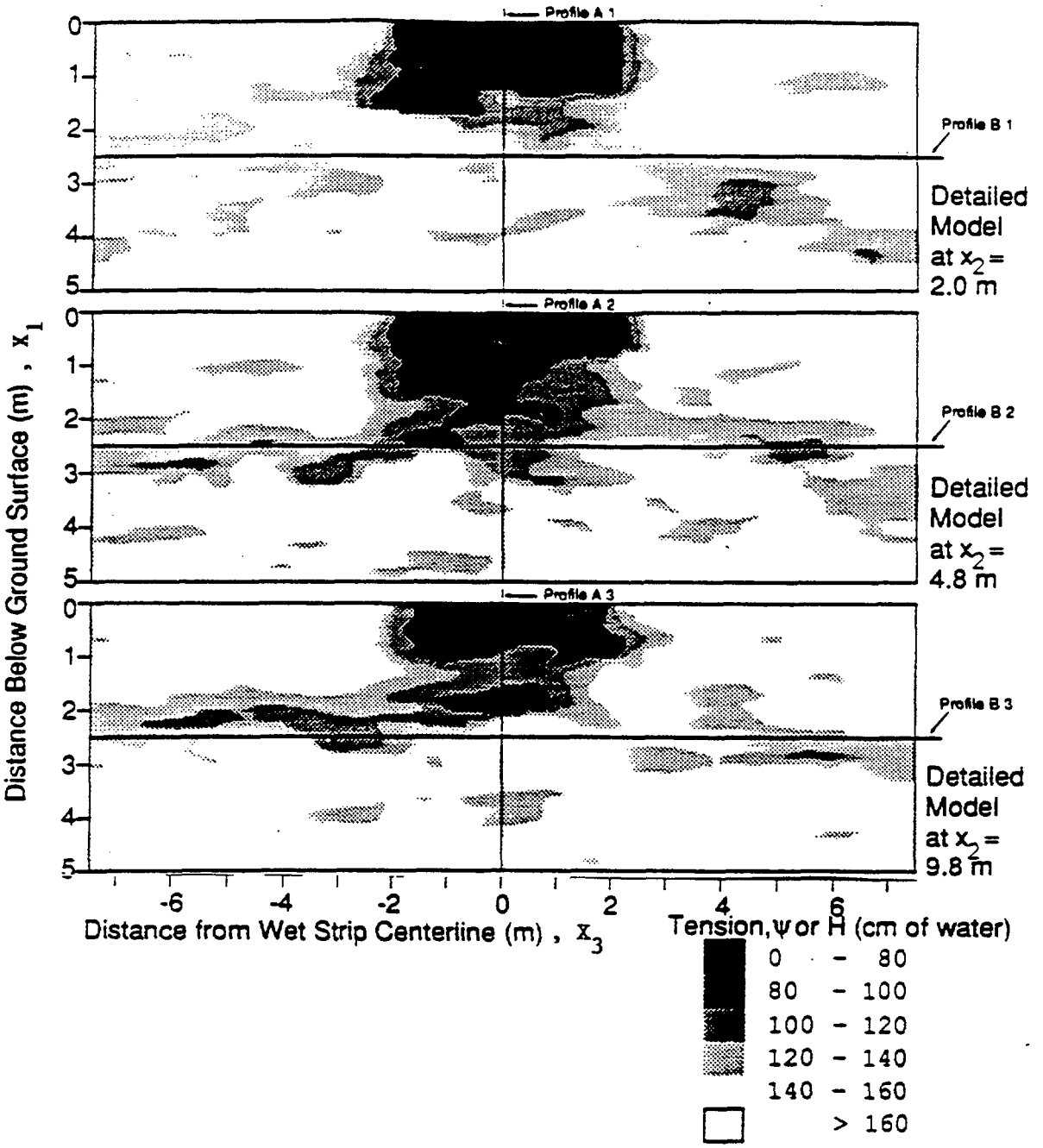

Figure 2. Infiltration (t=5 days)

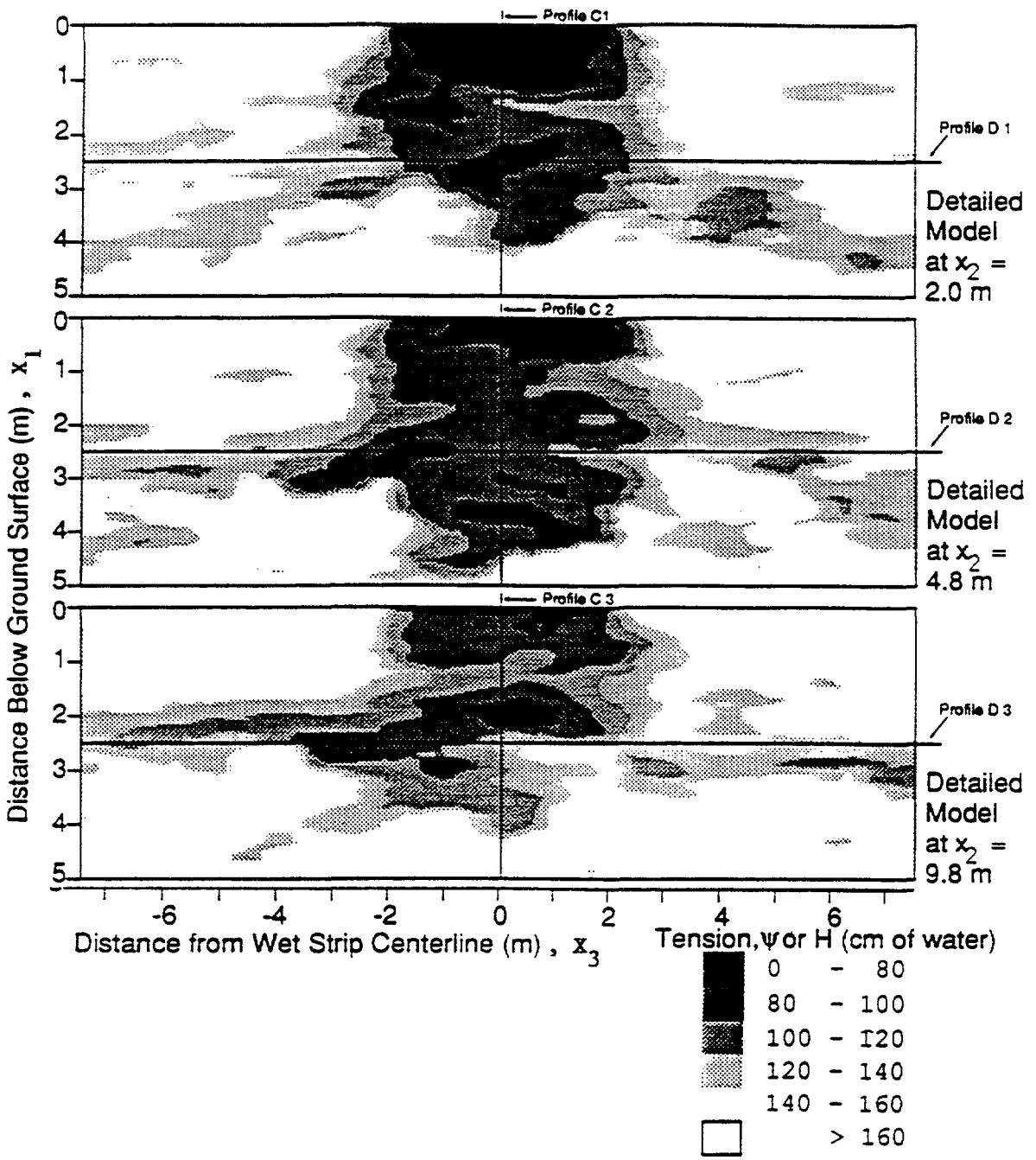

Figure 3. Infiltration (t=10 days)

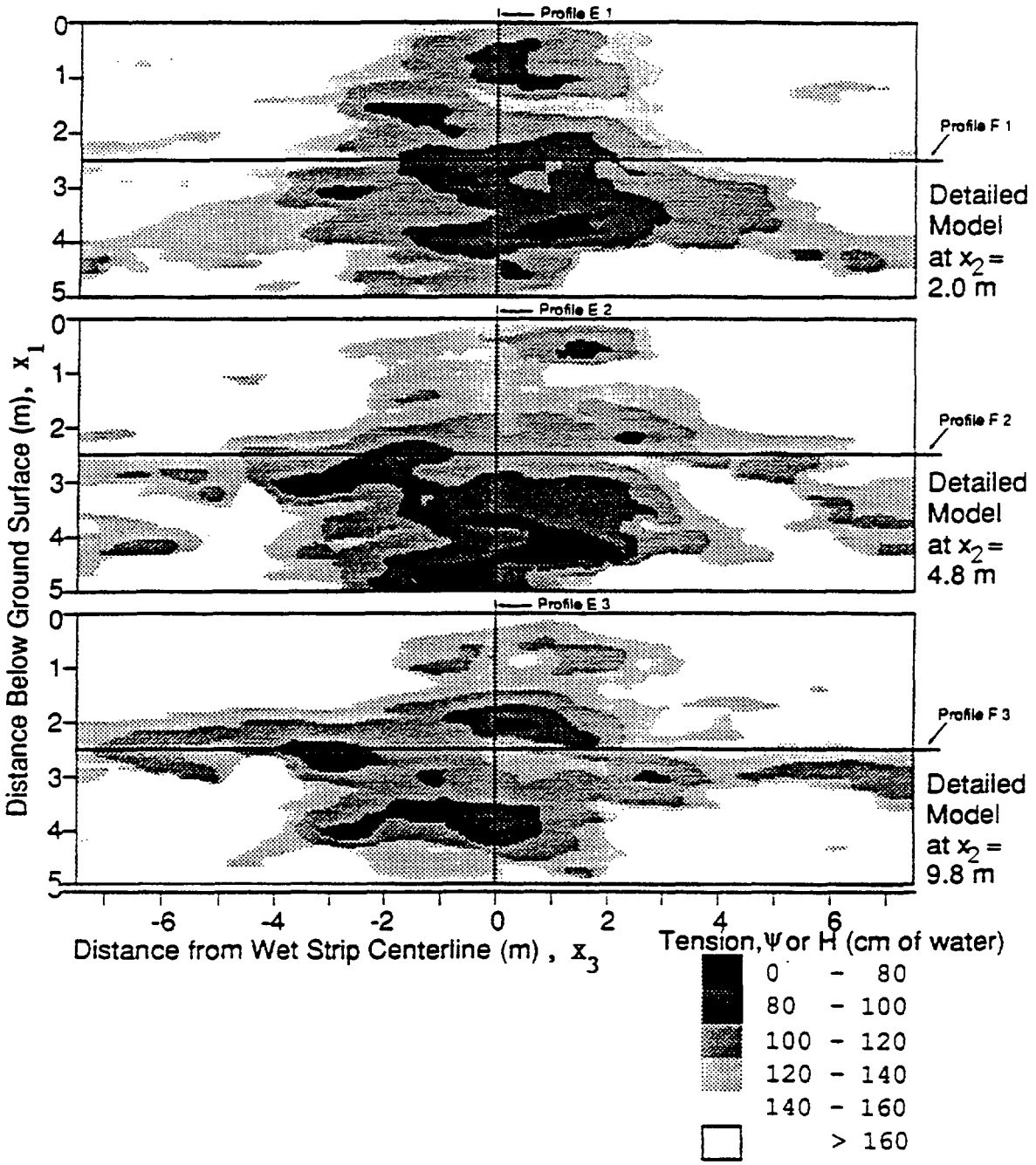

Figure 4. Drainage (t=15 days)

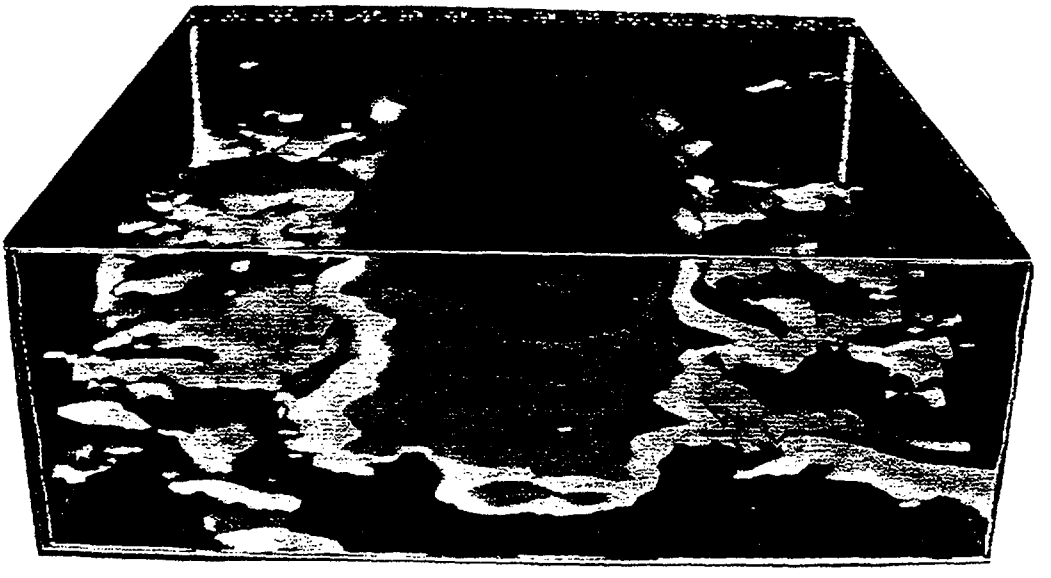

Figure 5 Front View of Three-Dimensional Moisture Plume, from Stochastic Flow Simulations of Ababou (1988).

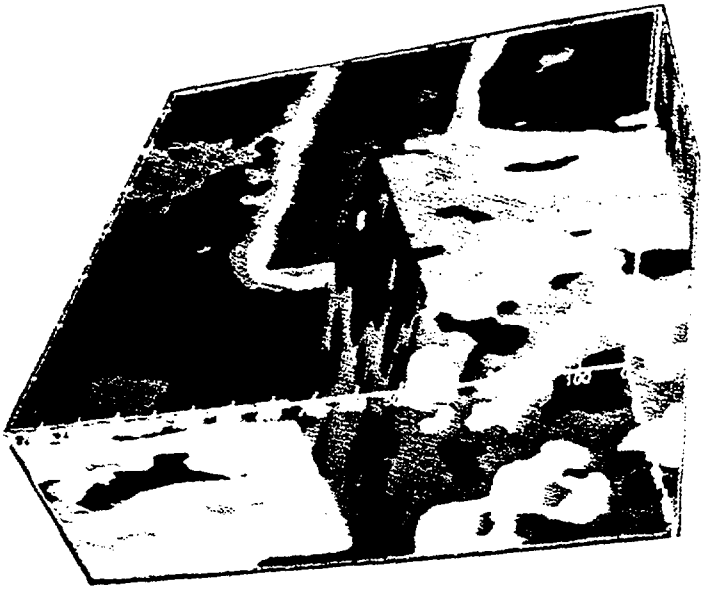

Figure 6 Back View of Three-Dimensional Moisture Pattern, with Moisture Plume Visible in Purple and Blue (Simulations from Ababou, 1988).

APPENDIX C3

Stochastic modelling of the first
Las Cruces Trench experiment

Table of contents

Stochastic Modelling Of The First Las Cruces Trench Experiment

Jacob Bensabat, Lynn W. Gelhar and Dennis B. Mc Laughlin
R.M. Parsons Laboratory
Massachussets Institute Of Technology
Cambridge, MA, 02139

1 Introduction

The aim of this study is to demonstrate a model validation approach for the first Las Cruces trench experiment, based on the stochastic methodology developed by Mantoglou and Gelhar (1987).

The proposed model uses the effective mass balance equation developed by Mantoglou and Gelhar (1987), which incorporates the information on the spatial variability of the soil unsaturated properties and the effective soil parameters developed by Polmann (1989), which allow extrapolation of the parameters values far beyond the water content ranges for which data on the unsaturated soil properties is available. The resulting mathematical model is a highly non–linear one which is solved using a Galerkin Finite–Element procedure and a Modified Picard iterative scheme developed by Bouloutas and Celia (1989). This numerical model allows a high degree of flexibility in the determination of the initial and boundary conditions, while converging relatively fast.

Preliminary simulations, based on parameters for a synthetic soil, show that, for this experiment, a deterministic model is unable to reproduce, even qualitatively, the experimental results especially for large time scales.

The results of the simulations show qualitative and quantitative differences between a deterministic approach and the proposed stochastic one, which seems to show better qualitative agreement with the experimental results.

2 Objectives and Methods

The objective of this study is to test the stochastic modelling methodology of Mantoglou and Gelhar (1987), using the the field data from the first Las Cruces trench experiment.

The first experiment is uniquely appropriate for this purpose because of its long duration (3 years) and its resulting large spatial extent. The purpose here is to summarize the results of some preliminary simulations which have been developed using synthetic soil properties input based on the Maddock soil data (Carvallo et al., 1976). The synthetic input was necessary since unsaturated hydraulic conductivity data is not currently available at the site. It is expected that unsaturated conductivity data will be available in the near future and consequently a more definitive evaluation can be expected as part of the INTRAVAL phase 2. The proposed model uses:

- The effective mass balance equation developed by Mantoglou and Gelhar (1987), which incorporates the information on the spatial variability of the soil unsaturated properties.
- The effective soil parameters developed by Polmann (1989), which allow extrapolation of the parameter values far beyond the the water content ranges for which data on the unsaturated soil properties is available.
- The resulting mathematical model is a highly non–linear one, which is solved using a Galerkin Finite–Element Procedure and a Modified

Picard iterative scheme developed by Bouloutas and Celia (1989). This numerical model allows a high degree of flexibility in the determination of the intial and boundary conditions, while converging relatively fast.

3 Mathematical Model

3.1 Model Assumptions

1. The soils are assumed to be locally isotropic and homogeneous.

2. At large scales, the soil properties are assumed to behave as stationary stochastic processes.

3. the local unsaturated hydraulic conductivity is assumed to be a random variable log–normally distributed, i.e.,

$$Ln(K) = y = \overline{y} + y' \tag{1}$$

4. The local water content is assumed to be a random variable normally distributed, i.e.,

$$\theta = \Theta + \Theta' \tag{2}$$

where $\Theta = E[\theta]$ and Θ' is a zero mean normally distributed variable. Θ is also a non–linear function of the tension.

5. The local tension, ψ, is assumed to be the sum of a mean term, Ψ, and of a zero mean normally distributed random perturbation h,

$$\psi = \Psi + h \tag{3}$$

3.2 Balance Equation

The effective mass balance equation can be found in Mantoglou and Gelhar (1987), and takes the form of Richard's equation.

$$\frac{\partial\left(\Psi, \nabla\Psi, \frac{\partial\Psi}{\partial t}\right)}{\partial t} = \nabla \cdot \left[\hat{K}\left(\Psi, \nabla\Psi, \frac{\partial\Psi}{\partial t}\right)\nabla(\Psi + z)\right) \tag{4}$$

where Θ ($[\Theta] = cm^3/cm^3$), Ψ ($[\Psi] = cm$) and $\hat{K}$ ($[\hat{K}] = cm/hr$) are the effective water content, tension and conductivity tensor, respectively. In general, Θ and $\hat{K}$ are functions of the mean time derivative, gradient and tension. Since this dependence of the parameters on the time and spatial derivatives may modify the parabolic nature of the mass balance equation, it has been decided, as a preliminary step, to impose zero mean gradient and and steady state conditions in the evaluation of the parameters.

The hydraulic conductivity tensor is diagonal one with components,

$$\hat{K}_{xx} = \hat{K}_{yy} = exp\left[\overline{y} + \frac{\sigma^2_{y'}}{2} + \frac{E[y'\frac{\partial h}{\partial z}]}{\frac{\partial\Psi}{\partial z} + 1}\right] \tag{5}$$

$$\hat{K}_{zz} = exp\left[\overline{y} + \frac{\sigma^2_{y'}}{2}\right] \tag{6}$$

4 Parameters

Even at scales of a few meters, soil properties show usually show a high degree of variability, both under saturated and unsaturated conditions. Therefore, we consider these properties as random ones. The parameters used in this study are the ones developed by Polmann (1989), and represent a combination of the data available from the Las Cruces site (water retention curves and the saturated conductivities) and from the information on the Maddock soil unsaturated conductivities as reported in Carvallo et al. (1976).

5 Numerical Simulations

The flow domain is A 2-d strip, 10 m. in the vertical and 20 m. in the horizontal (Fig. 1). At the top of the left corner, we imposed a flux of 2 cm/day during the first 82 days then the system was relaxed. Simulated moisture distributions for the times 32, 57, 82, 177 and 365 days, 2, 3 and 4 years are shown for a deterministic (homogeneous) soil (Figs. 2 and 3) and the stochastic model (Figs. 4 and 5). The stochastic simulations clearly show more lateral spreading, this feature is also evident in the field observations shown in Figs. 6 and 7.

For the same times, moisture transects at $x = 0.0$, $x = 6.0$ and $z = 7.0$ m. are displayed in Figs. 8 to 10. These transects show the simulated mean moisture content with bands corresponding to 1 standard deviation, and the observed moiture distributions based on neutron probes measurements at these locations. Generally the stochastic model seems to capture the overall trend and variability of the observations.

6 Conclusions

Even for an assumed behaviour of the soil parameters, it has been shown that the stochastic approach reproduces with better accuracy the experiment results, at least qualitatively. However, it is our feeling that there is a crucial need for having information on the unsaturated soil properties at the site itself.

The next phase in this study will be to relax the conditions under which the effective parameters are evaluated (steady state and zero mean gradients).

7 References

Bouloutas, E.T. and M.A. Celia, " Efficient Finite Element Methods for Modeling Fluid Flow in Partially Saturated Porous Media," to appear in the Proceedings of the Fifth International Symposium on Numerical Methods in Engineering, Gruber et al. (eds.), Springer Verlag, pp. 673–678, 1989.

Carvallo, H.O., D.K. Cassel, J. Hammomd and A. Bauer, " Spatial Variability of In Situ Unsaturated Conductivity of Maddock Sandy Loam, Soil Science, 12 (1), 1–8, 1976.

Mantoglou, A. and L.W. Gelhar, " Effective Hydraulic Conductivities of Transient Unsaturated Flow in Stratified Soils," Water Resources Research, Vol. 23, N_o 1, pp. 57–67, January 1987.

Polmann, D.J.P., " Application of Stochastic Models to Transient Flow and Transport in Heterogeneous Unsaturated Soils," Ph. D. Thesis, Dept. of Civil Eng., MIT, Cambridge, MA (1990), 476 pages.

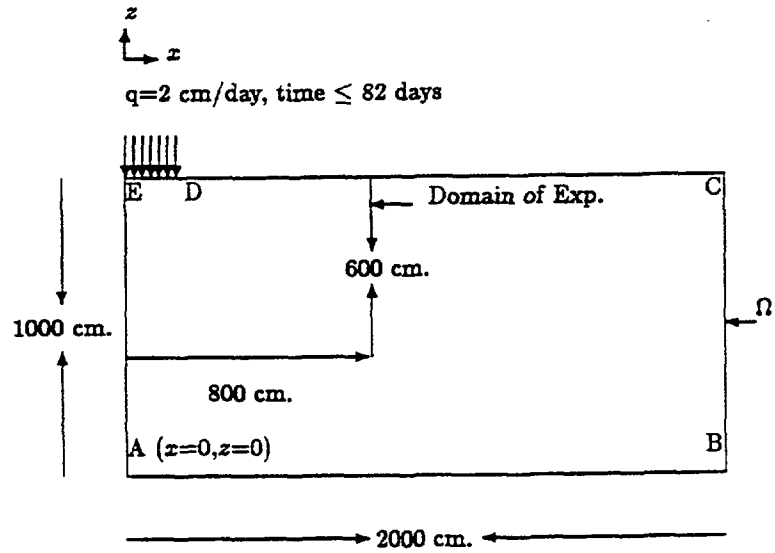

21 points in the X direction ($\Delta x = 100.0$ cm.)
51 points in the Z direction ($\Delta z = 20.0$ cm.)

Initial Conditions

$$\Psi = -50000.0cm. \qquad \forall\,(x,z) \in \Omega$$

Boundary Conditions

$$\left[K_z\left(\frac{\partial \Psi}{\partial z} + 1\right)\right] = 2cm/day \qquad \text{Along DE}$$

$$\left[K_z\left(\frac{\partial \Psi}{\partial z} + 1\right)\right] = 0 \qquad \text{Along CD}$$

$$\Psi = -50000.0cm \qquad \text{Along AB}$$

$$K_z\frac{\partial \Psi}{\partial x} = 0 \qquad \text{Along AE and BC}$$

Figure 1: Illustration of the flow Domain and initial and boundary conditions.

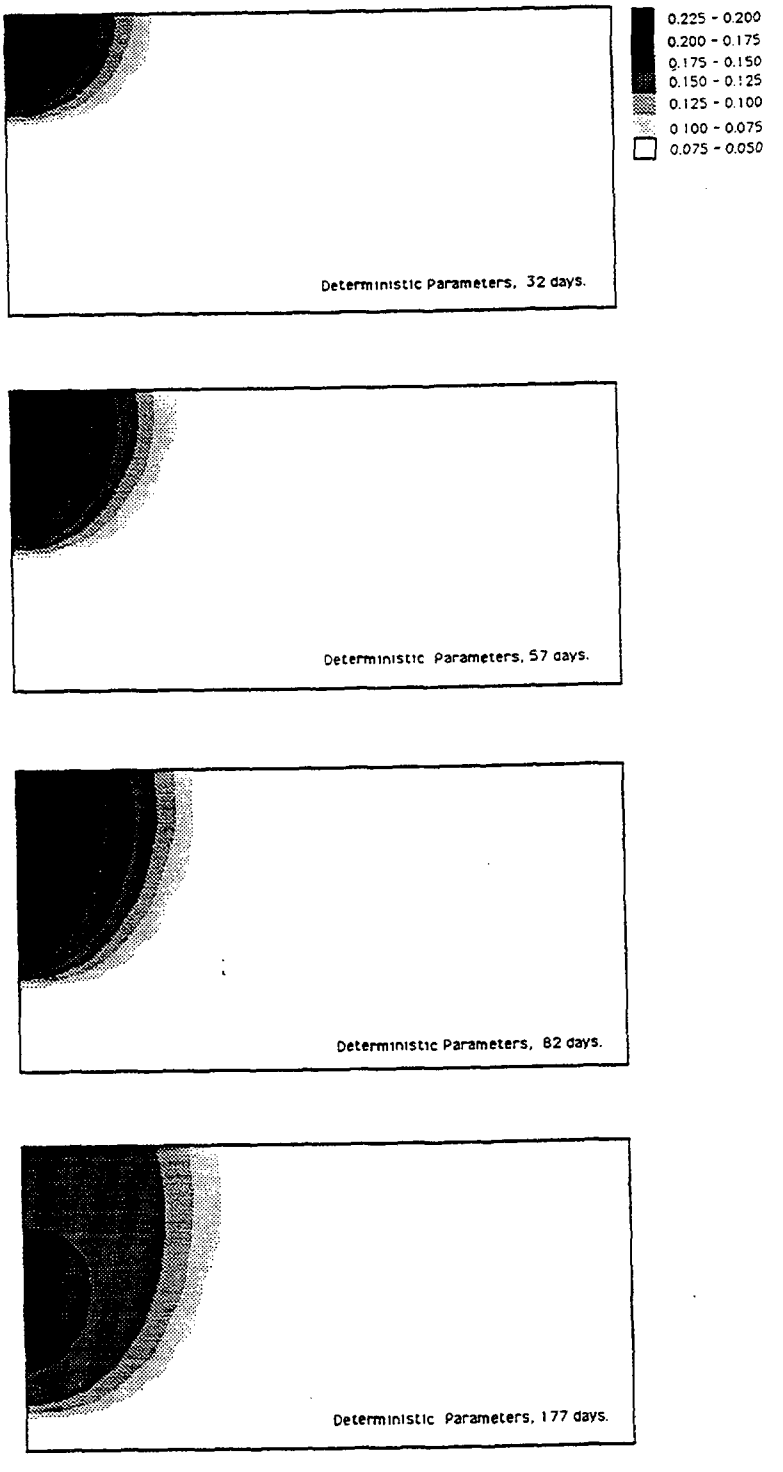

Figure 2: Water content distributions for the deterministic simulations, days 32–177.

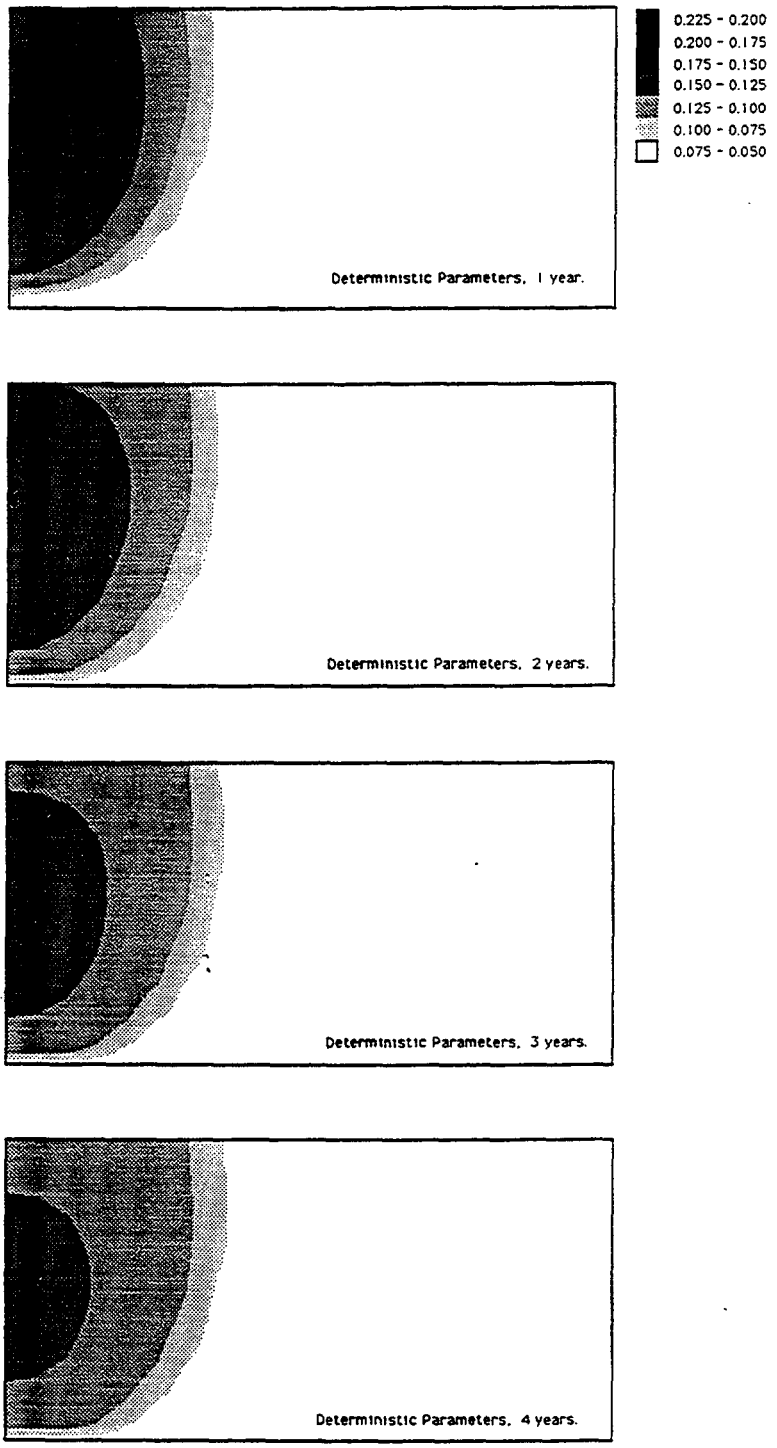

Figure 3: Water content distributions for the deterministic simulations, years 1 – 4.

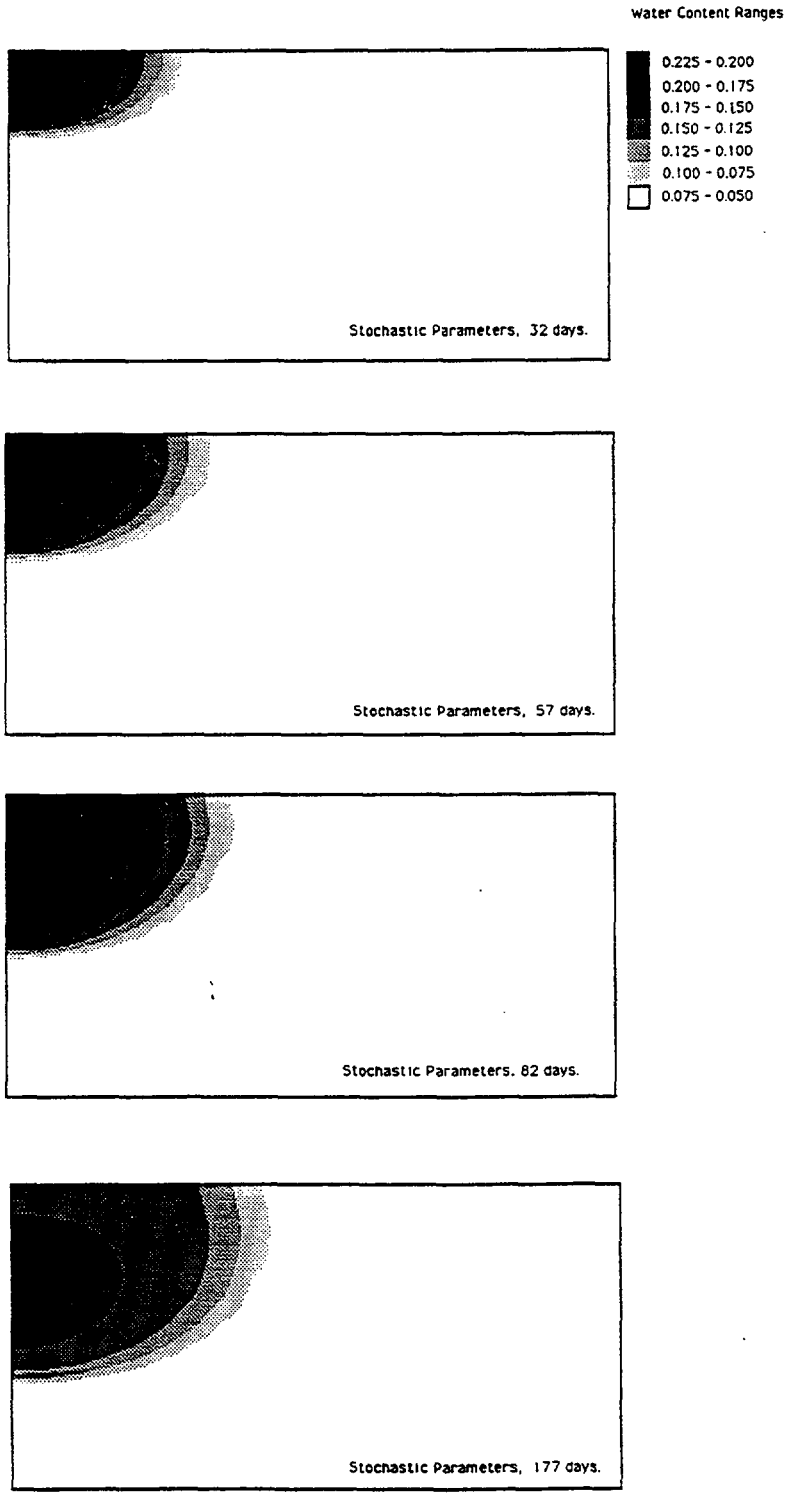

Figure 4: Water content distributions for the stochastic simulations, days 32 – 177.

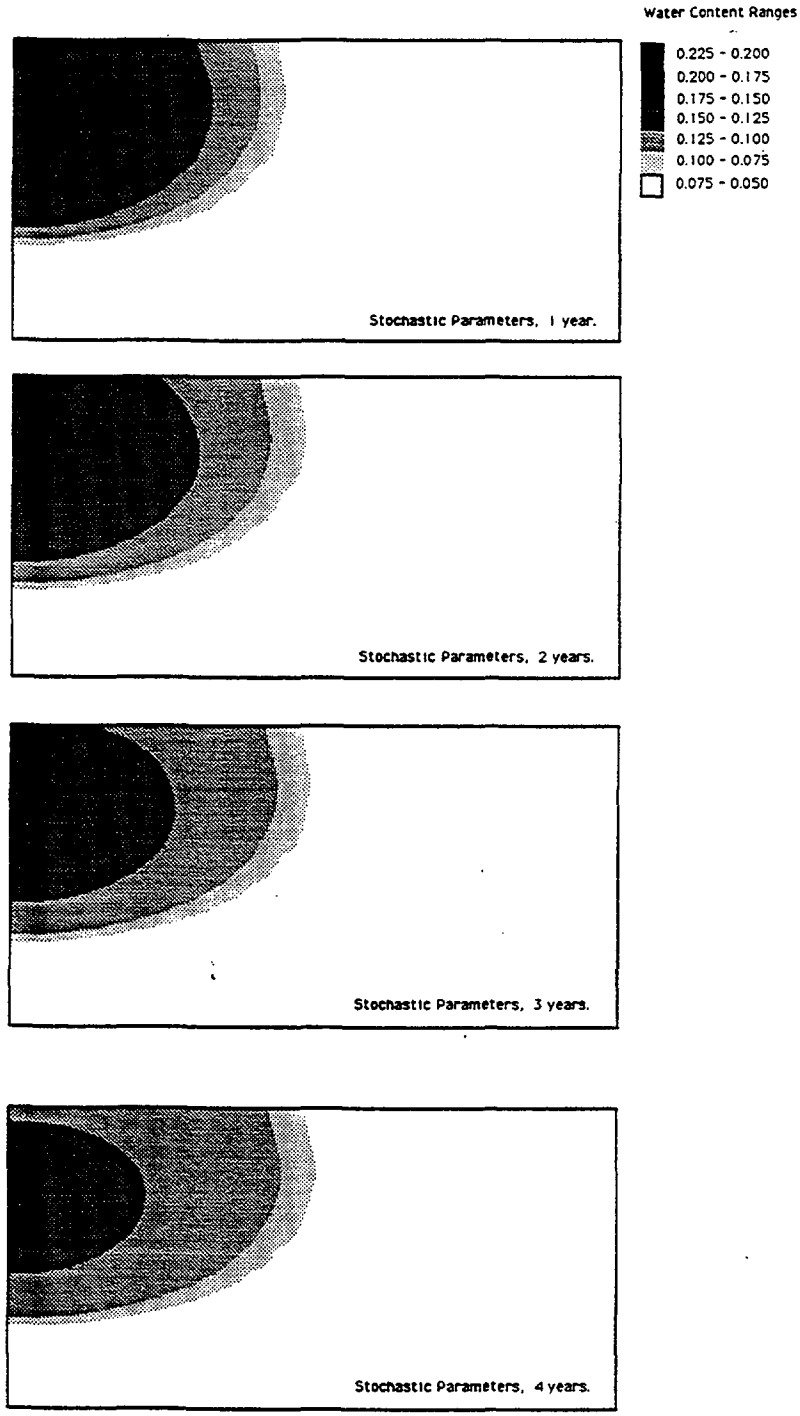

Figure 5: Water Content distributions for the stochastic simulations, years 1–4.

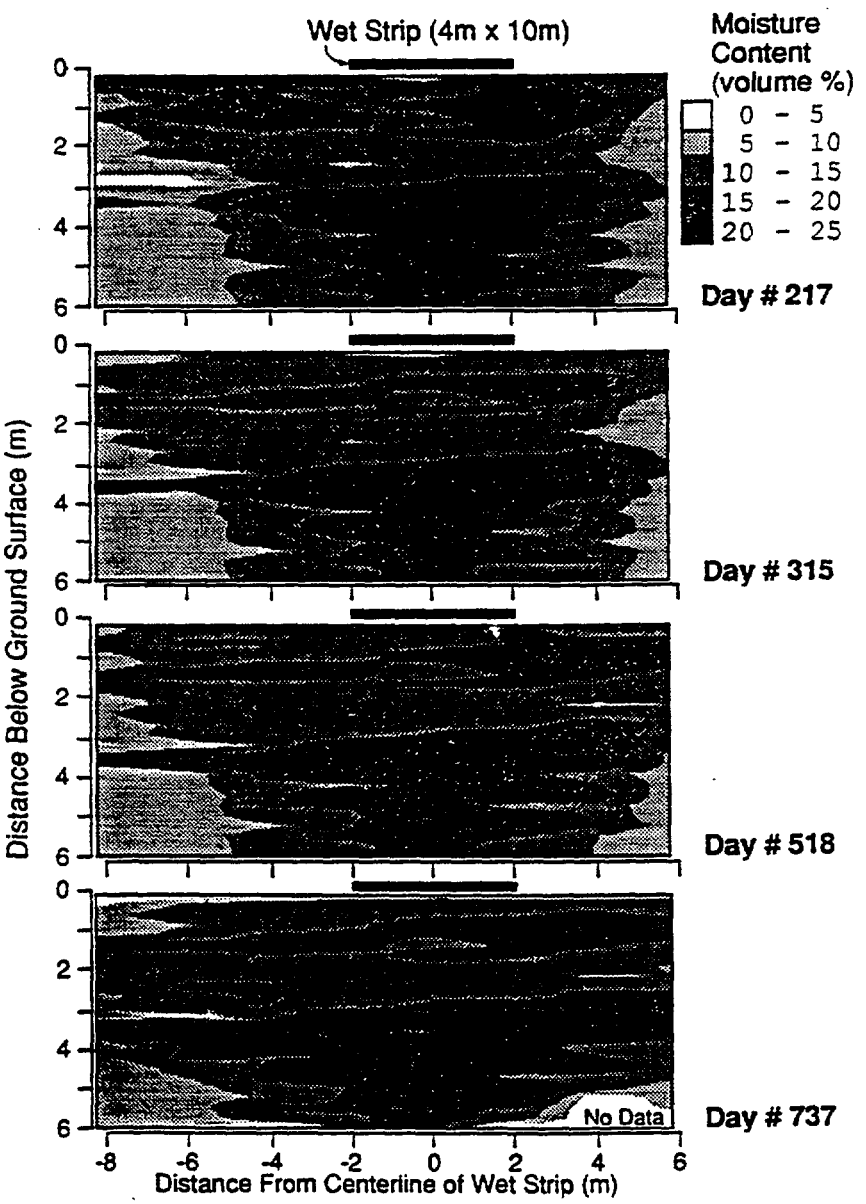

Figure 6: Cross–section Profile of water content, from neutron probe readings, during experiment # 1 at Jornada site; days 10 – 117.

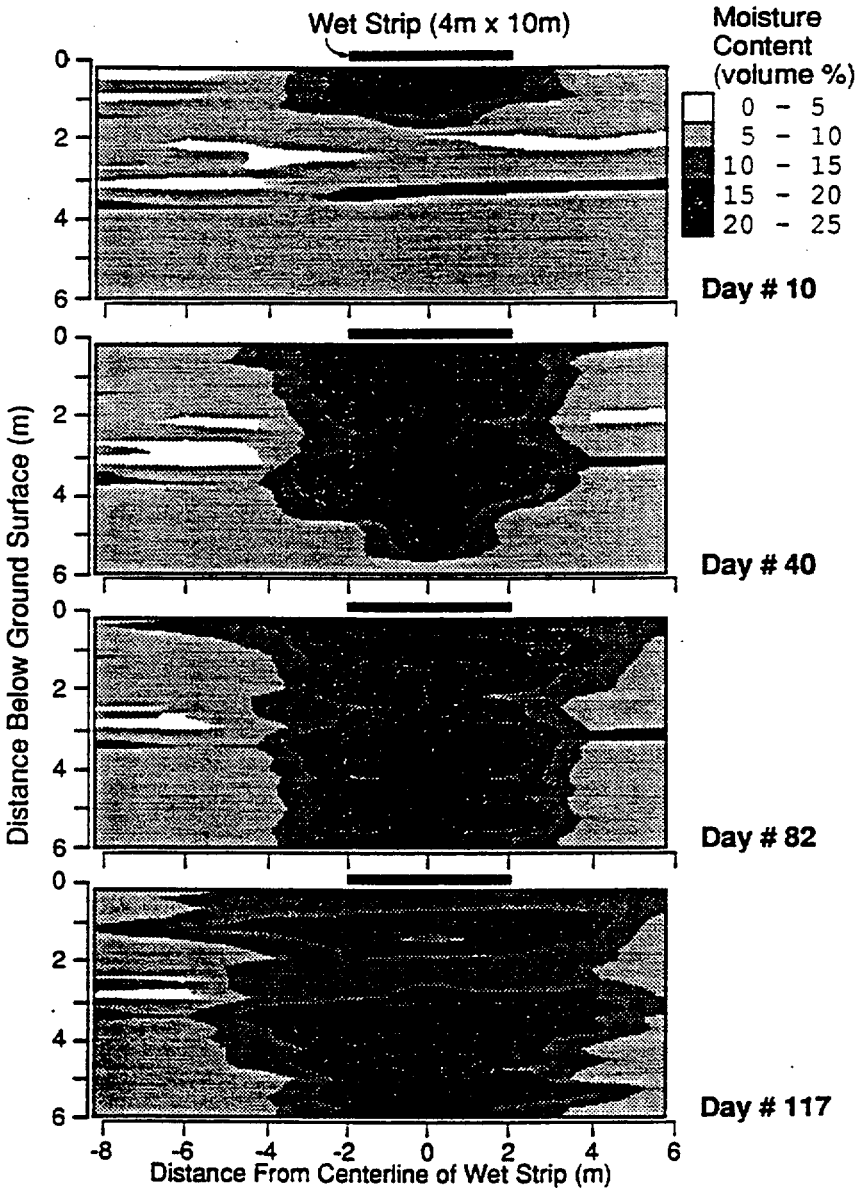

Figure 7: Cross–section Profile of water content, from neutron probe readings, during experiment # 1 at Jornada site; days 217 – 737.

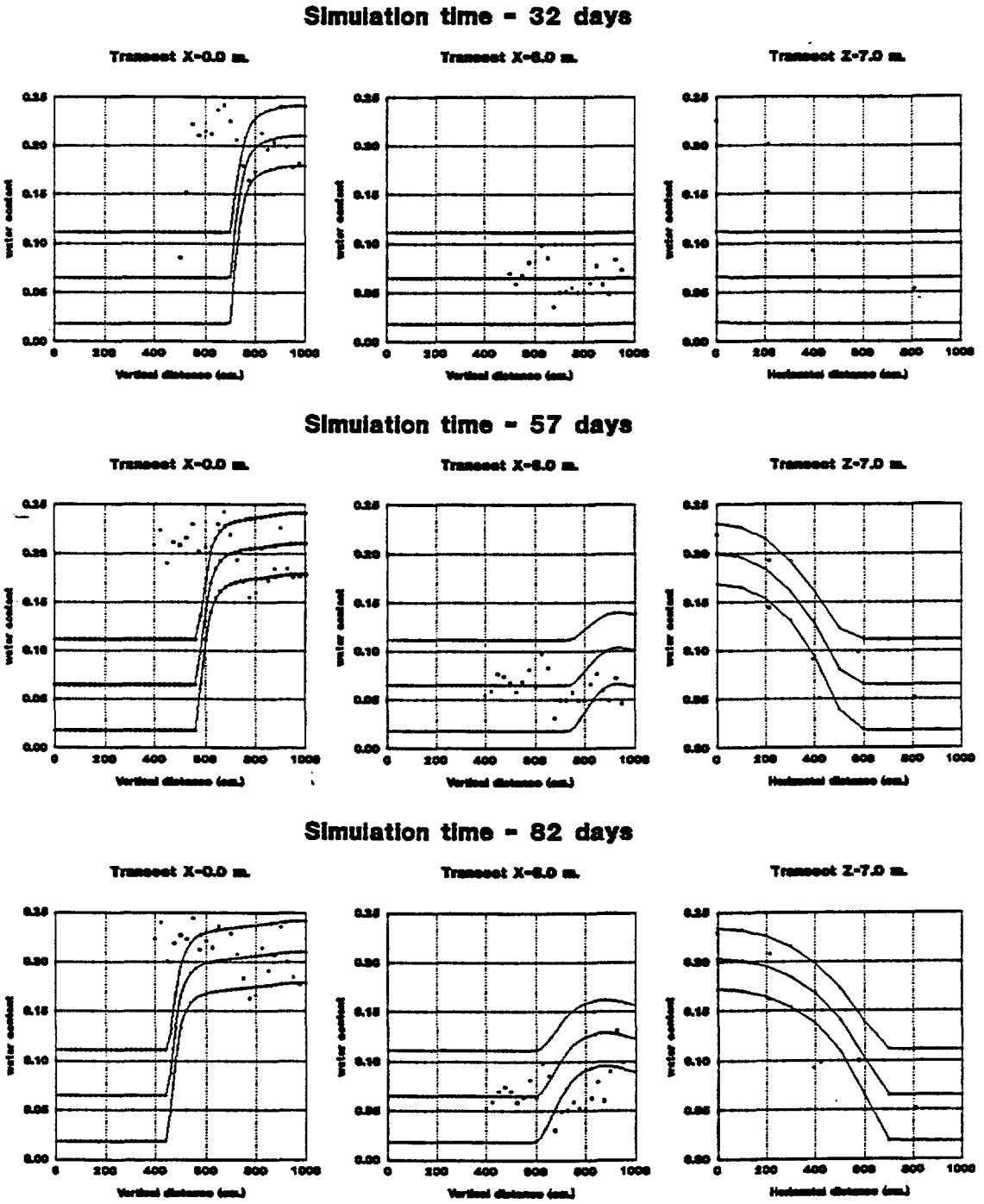

Figure 8: Measured and simulated mean water content distributions with bands corresponding to 1 standard deviation, transects x=0.0 m., x=6.0 m. and z=7.0 m., days 32–82.

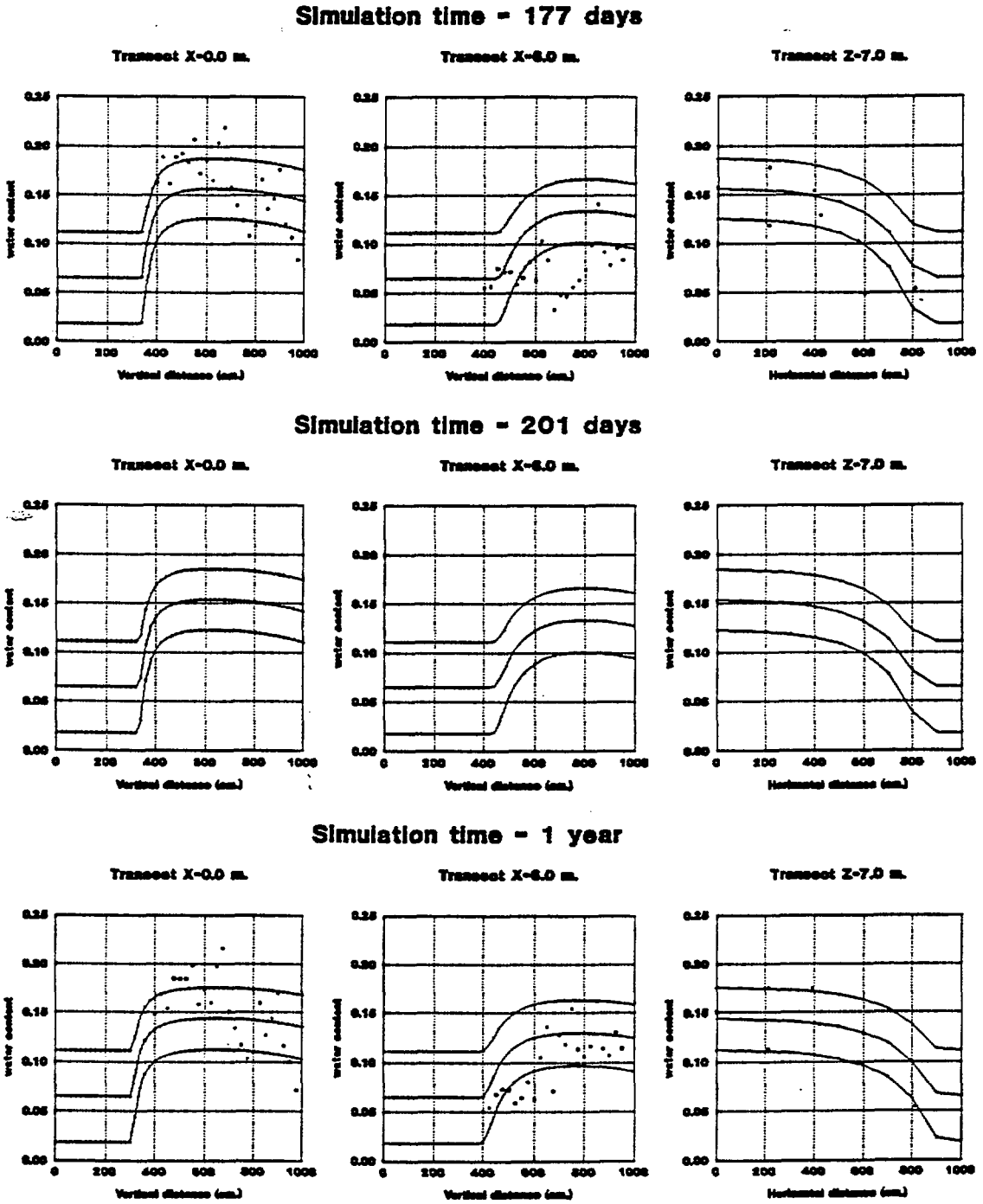

Figure 9: Measured and simulated mean water content distributions with bands corresponding to 1 standard deviation, transects x=0.0 m., x=6.0 m. and z=7.0 m., days 177 to 1 year.

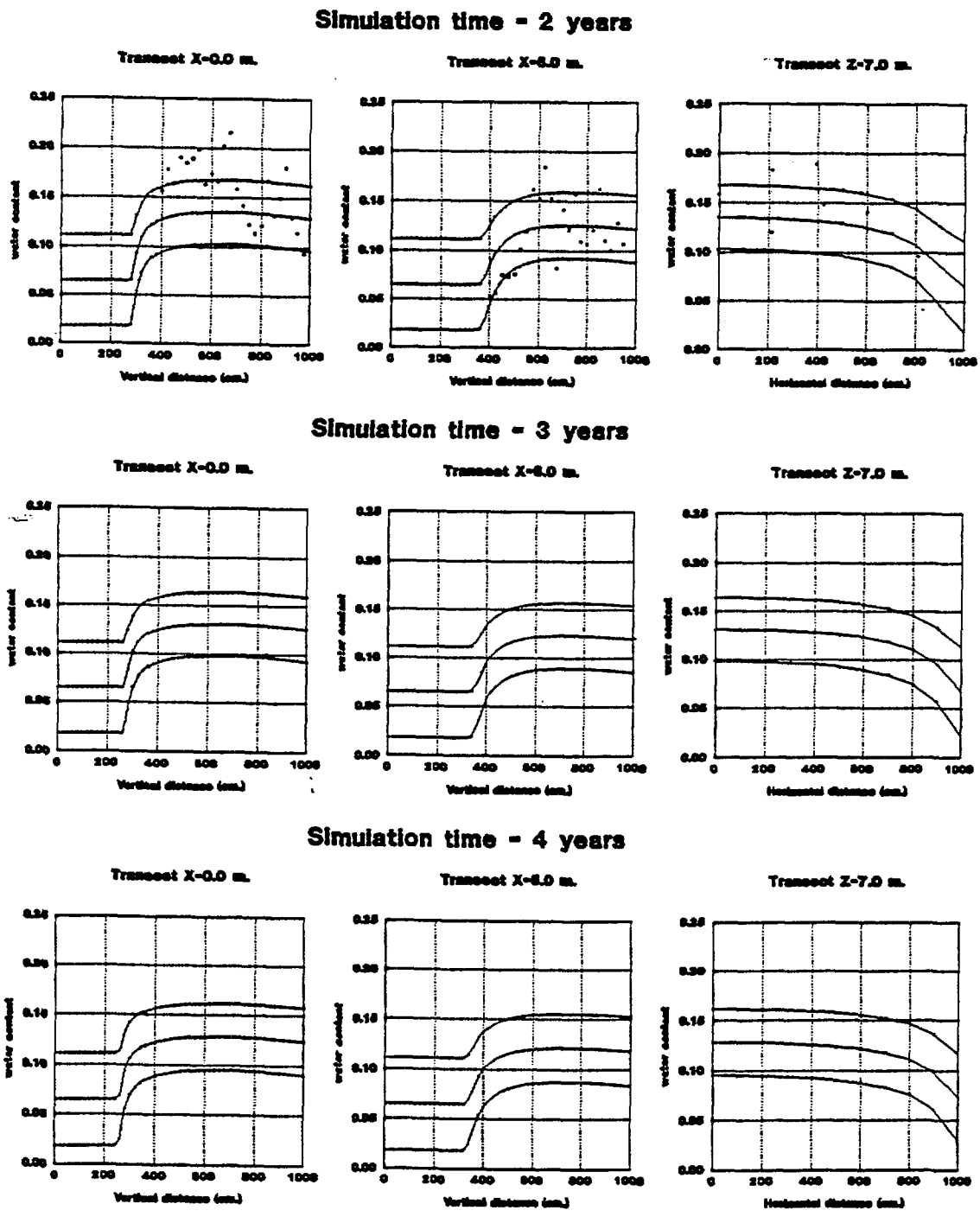

Figure 10: Measured and simulated mean water content distributions with bands corresponding to 1 standard deviation, transects x=0.0 m., x=6.0 m. and z=7.0 m., years 2–4.

APPENDIX C4

Two-dimensional flow and transport predictions
for the Las Cruces Trench experiment 2

Table of contents

List of Figures

Two-Dimensional Flow and Transport Predictions for the Las Cruces Trench Experiment 2

by

R. G. Hills[1]
P. J. Wierenga[2]
M. R. Kirkland[1]

[1]Mechanical Engineering Department, New Mexico State University, Las Cruces, NM 88003

[2]Department of Soil and Water Science, University of Arizona, Tucson, AZ 85721

ABSTRACT

As part of a comprehensive field study designed to provide data to test stochastic and deterministic models of water flow and transport in the vadose zone, several trench infiltration experiments were performed in the semi-arid region of southern New Mexico. In one of the experiments, a 1.2 m wide by 12 m long area on the north side and perpendicular to a 4.8 m wide by 26.4 m long by 6 m deep trench was irrigated with water containing tracers using a carefully controlled drip irrigation system. Water containing tritium and bromide was applied during the first 11.5 days of the study. Thereafter, water was applied without tracers for an additional 64 days. Both water and tracer movement were monitored in the subsoil during infiltration and redistribution.

Models for water flow and transport were tested by simulating the experiment using finite difference deterministic models assuming a uniform soil. Comparisons between measurements and predictions made with a two-dimensional model show qualitative agreement for two of the three water content measurement planes. Model predictions of tritium and bromide transport were not as satisfactory. Measurements of both tritium and bromide show localized areas of high relative concentrations and a large downward motion of bromide relative to tritium during redistribution. While the simple deterministic model does show larger downward motions for bromide than for tritium during redistribution, it does not predict the high concentrations of solute observed during infiltration, nor does it predict the heterogeneous behavior observed for tritium during infiltration and for bromide during redistribution.

1.0 INTRODUCTION

Prediction of water flow and chemical transport from disposal areas generally requires the use of computer models. While there are many numerical models available, the validity of these models for dry soils on the field scale has not been adequately tested. Field studies insoil science and hydrology conducted during the past decade have demonstrated extensive variability in saturated and unsaturated hydraulic conductivities and water retention properties. Such studies cast doubt on the validity of deterministic models on the field scale. This has ledto the development of stochastic models for the prediction of water flow and chemical transport through soils and groundwater. However, before such models find widespread use for prediction

purposes, the advantage of stochastic models over simpler deterministic models must be tested with field data.

This study is restricted to a simple deterministic model for water flow and transport of bromide and tritium for the Las Cruces Plot 2 experiment. This simple model provides a reference for more sophisticated models that are currently being tested. Water flow and transport is assumed to be two-dimensional and time dependent. The model domain is a vertical plane parallel to the north trench wall. The soil is assumed to behave as a uniform isotropic media without hysteresis. A description of the trench and experimental configuration is provided in an earlier appendix and in Wierenga et al. (1989, 1990a, 1990b) and Hills et al. (1990).

2.0 GOVERNING EQUATIONS

2.1 Water Flow

Richards equation for two-dimensional water flow with isotropic hydraulic conductivity is given by:

$$\frac{\partial \theta}{\partial t} + \frac{\partial}{\partial x}\left(K \frac{\partial h}{\partial x}\right) + \frac{\partial}{\partial z}\left(K + K \frac{\partial h}{\partial z}\right) = 0 \qquad (1)$$

θ is the volumetric water content, K is the hydraulic conductivity, h is the tension, t is time, x is the horizontal position, and z is the vertical position measured downward. Writing Eq.(1) in terms of water content gives

$$\frac{\partial \theta}{\partial t} - \frac{\partial}{\partial x}\left(D \frac{\partial \theta}{\partial x}\right) - \frac{\partial}{\partial z}\left(D \frac{\partial \theta}{\partial z} - K\right) = 0 \qquad (2)$$

where D is defined by

$$D \equiv - \frac{K}{\frac{d\theta}{dh}} \qquad (3)$$

While Eq.(2) is not valid across soil layer interfaces, it can be applied to a uniform soil. Here we use a two-dimensional extension of the one-dimensional algorithm developed by Hills, et al. (1989). This extension is based on the alternating direction implicit method and is used to model water flow in a uniform soil.

The initial and boundary conditions on water content are

$$\theta(x,z,0) = \theta_{init}(z) = \theta(h_{init}(z)) \qquad (4a)$$

$$\left(K - D \frac{\partial \theta}{\partial z}\right)_{z=0} = \begin{cases} 0.43\ cm/day, & -0.61\ m \geq x \geq 0.61\ m;\ t \leq 75.5\ days \\ 0, & otherwise \end{cases} \qquad (4b)$$

$$\left(K - D \frac{\partial \theta}{\partial z} \right)_{z=b} = 0.0 \tag{4c}$$

$$D \frac{\partial \theta}{\partial x} \Big)_{x=-a} = 0.0 \tag{4d}$$

$$D \frac{\partial \theta}{\partial x} \Big)_{x=a} = 0.0 \tag{4e}$$

where a and b are sufficiently large, and the initial water contents sufficiently small so that significant water movement does not occur normal to these boundaries during the simulation. Values of a = 5.0 m and b = 6.0 m are adequate for 300 days of simulation.

The van Genuchten models (1980) for water retention and unsaturated hydraulic conductivity are used.

$$S_e = \frac{\theta - \theta_r}{\theta_s - \theta_r} = \frac{1}{[1 + (\alpha h)^n]^m} \tag{5}$$

$$m = 1 - \frac{1}{n} \tag{6}$$

where θ, θ_r, and θ_s are the volumetric water content, residual water content, and saturated water content, respectively, α and n are parameters that affect the shape of the retention curve, and h is tension. Given estimates of the parameters in Eq. (5) and the uniform soil value for the saturated hydraulic conductivity K_s, the unsaturated hydraulic conductivity is modeled by

$$K = K_s S_e^{1/2} [1 - (1 - S_e^{1/m})^m]^2 \tag{7}$$

2.2 Solute Transport

To model the transport of tritium and bromide, the convection/dispersion equation is used with the assumption that the dispersivity is homogeneous and isotropic and that the solute is non reactive and non decaying. Neglecting the radioactive decay of tritium results in only a 1% error in concentration on day 71 and a 4% error on day 277 due to tritium's half life of 12.26 years. The governing partial differential equation is given by

$$\frac{\partial}{\partial t}(R\theta c) = \frac{\partial}{\partial x}\left(\theta D_s \frac{\partial c}{\partial x} - q_x c \right) + \frac{\partial}{\partial z}\left(\theta D_s \frac{\partial c}{\partial z} - q_z c \right) \tag{8}$$

where R is the retardation factor, D_s is the dispersion coefficient, and q_x and q_z are the Darcian fluxes and x and z are coordinate directions. A normalized or relative concentration is used for c where the normalization constant is the average concentration applied during the first 11.5 days of the experiment. Thus, the normalized or relative concentration for the solute applied at the surface is unity. The x and z components of the Darcian fluxes are given by

$$q_x = K\frac{\partial h}{\partial x} = -D\frac{\partial \theta}{\partial x} \tag{9a}$$

$$q_z = K + K\frac{\partial h}{\partial z} = K - D\frac{\partial \theta}{\partial z} \tag{9b}$$

where h represents tension. The dispersion coefficient, D_s (the subscript s is used to distinguish the dispersion coefficient from the hydraulic diffusivity, D), is given by

$$\theta D_s = \theta D_m + \varepsilon\,|\bar{q}| \tag{10}$$

where D_m is the molecular dispersion coefficient, ε is the dispersivity, and $|\bar{q}|$ is the magnitude of the Darcian flux.

A zero initial concentration was used. Zero fluxes on the lateral and lower boundaries and a constant flux on the upper boundary were specified. The initial and boundary conditions for the relative concentration $c(x,z,t)$ are:

$$c(x,z,0) = 0.0 \tag{11a}$$

$$\left(q_z c - \theta D_s \frac{\partial c}{\partial z}\right)_{z=0} = \begin{cases} 0.43\ cm/day, & -0.61\ m \geq x \geq 0.61\ m;\ t \leq 11.5\ day \\ 0, & otherwise \end{cases} \tag{11b}$$

$$\left(q_z c - \theta D_s \frac{\partial c}{\partial z}\right)_{z=b} = 0.0 \tag{11c}$$

$$\left(q_x c - \theta D_s \frac{\partial c}{\partial x}\right)_{x=-a} = 0.0 \tag{11d}$$

$$\left(q_x c - \theta D_s \frac{\partial c}{\partial x}\right)_{x=a} = 0.0 \tag{11e}$$

Again, the a and b must be taken to be sufficiently large so that the wetting and solute fronts do not interact with the boundaries during the numerical simulation. Note that the normalized concentration of the solute applied to the surface is unity and dimensionless. Thus the right hand side of Eq. (11b) has the units of cm/day.

3.0 THE NUMERICAL ALGORITHMS

The solutions to the proceeding equations were approximated using alternating direction implicit finite difference algorithms. The convective terms were handled explicitly with central differences. The grid size was sufficiently small so that the convective terms did not lead to instability. During each time step, Richards equation was solved, the water contents and Darcian fluxes were evaluated, and then the transport equation was solved. Details of the finite difference algorithms are provided in Hills et al. (1990)

The water flow and transport algorithms were implemented in VAX FORTRAN using double precision arithmetic. The water flow algorithm was validated by comparing algorithm predictions

against those obtained from other one-dimensional water content and head based water flow algorithms (Hills et al., 1989). Separate horizontal and vertical water flow numerical experiments were performed to validate the two-dimensional algorithm along both coordinate directions. Mass balance errors were also calculated and found to be within machine precision.

The transport algorithm was validated against one-dimensional analytical solutions of the transport equation (in both directions) using various boundary and initial conditions. The solute mass balance errors were calculated and also found to be within machine precision.

A 6 m deep by 10.1666 m wide model domain was used. Symmetry was assumed along the vertical centerline of the irrigated area to reduce the computational domain to a 6 m deep by 5.0833 m wide area. The grid and time step size used for all numerical simulations were Δx = 0.050833 m, Δy = 0.05 m and Δt = 0.5 days. A value of 0.050833 for Δx was used to insure that the irrigation width (1.22 m) could be represented by an integer number of Δx's. To check convergence and the effect of numerical diffusion, contour plots of water flow and solute transport on days 71 and 277 were compared to those obtained when the time and spatial step sizes were halved. The differences between the fine grid and coarse grid contours were very small.

Here we use contour plots to compare model predictions to field observations. Since the resulting contours can be very sensitive to the density of the sampling grid used to generate the contours, model predictions were sampled on a grid with the same density as the corresponding field observations. This grid is much coarser than the finite difference grid (the full finite difference grid was used to check convergence). For example, the model predictions were sampled on a grid with a horizontal increment of 1 m and a vertical increment of 0.25 m. This is the same sampling grid as was used for the neutron probe measurements. A 0.25 m by 0.25 m contour grid was used for the solute predictions. Due to the irregular nature of the measurement sampling grid, weighted averages of all measurements made within two grid cells of a grid node were used to estimate the nodal value of concentration. Inverse distance-squared weighting was used. The axis tick marks shown in the figures represent the intersection of the contour grid with the vertical and horizontal axes. Once the nodal values for water content and relative concentration were determined, WingZ (Informix Software, Inc., 1988) was used to generate the contour plots. WingZ is a Macintosh based spreadsheet and uses B-splines to generate smooth contour surfaces.

4.0 MODEL SELECTION CRITERIA

The water content based finite difference algorithm for Richard's equation was selected because it can be applied to unsaturated flow into homogeneous but very dry soils without the need for fine grid or time step sizes (Hills et al. (1989)). This results in large savings in CPU time. The transport equation was also modeled using finite differences with explicit center differences used for the convective terms. The center difference approximation is adequate as long as the grid Peclet and Courant numbers are sufficiently small to insure stability.

5.0 MODEL CALIBRATION

The initial water content $\theta_{init}(z)$ for the model was determined from the uniform soil water retention model and observed initial tensions reported in the Las Cruces Database (Wierenga et al. (1990b)). The upper 1.5 m of the soil was initially wet enough to be in the tensiometer range ($h < 500$ cm). These high near-surface water contents were due to heavy rainfall in the weeks prior to covering the experimental plot. To obtain a depth dependent model for initial tension, averages of all the tensions obtained from tensiometers at similar depths down to 1.5 m were taken. The tensions from tensiometers installed through the trench face and from tensiometers installed vertically through the surface of the irrigated area were used to obtain the averages. Specifically, the readings from 8 tensiometers at 0.25 m, 5 tensiometers at 0.75 m, 4 tensiometers at 1.0 m, and 6 tensiometers at 1.5 m depth were averaged. Since only two good readings were obtained at a depth of 0.5 m, an average value for this depth was not included in the initial tension model. These measurements were taken on day 1 which was the first day that readings were available after the plot was fully covered. The initial tensions were too high to be in the tensiometer range for depths greater than 1.5 m. Initial field tensions for depths greater than 1.5 m were obtained from soil samples using a thermocouple psychrometer. Seven samples were taken from each of 7 depths (ranging from 2.1 to 6.6 m) and the resulting initial tensions averaged. These samples were collected during the installation of access tubes along the centerline of the irrigated area. The resulting average tension versus depth data are shown in Table 1. For simulation purposes, an initial tension of 143.9 cm H_2O was used for depths less than 25 cm. Linear interpolation was used to estimate the initial tensions at intermediate depths.

Equation (5) was used to model the water retention characteristics and Eq. (7) was used to model the unsaturated hydraulic conductivity. The parameter values used for these equations are taken from Wierenga, et al. (1989, 1990a) and are summarized in Table 2.

Field values for dispersivity typically range up to 10 cm or more (Nielsen et al. 1986). Since the dispersivity has not been determined for the trench experiment, $\varepsilon = 5$ cm was arbitrarily chosen. The molecular diffusion is $D_m = 1.0$ cm^2/day. The relatively low value for

Table 1: Initial Tensions used for the Numerical Simulation. For $z \leq 1.5$ m, tensiometers measurements were used; for $z > 1.5$ m, psychrometer measurements were used.

Depth	h
(cm)	(cm H_2O)
25	143.9
75	170.2
100	249.3
150	215.5
210	28860
285	36980
360	47090
435	48020
510	53300
585	56330
660	64940

Table 2: van Genuchten Parameters for the Las Cruces Test Site: Uniform Soil Model.

θ_s	θ_r	α	n	K_s
(cm^3 cm^{-3})	(cm^3 cm^{-3})	(cm^{-1})	(-)	(cm/day)
0.3209	0.0828	0.0550 1	1.5093	270.1

ε is typical of the soils at the Las Cruces Trench Site and results in transport that is dominated by convection rather than dispersion. Retardation factors of 1.0 for tritium and 0.84 for bromide were used. The low retardation factor for bromide is based on studies with laboratory columns and field lysimeters filled with top soil removed from the area surrounding the trench site. No attempt was made to "calibrate" the model by choosing other values for the dispersivity or the retardation factor.

6.0 RESULTS

Figures 1 and 2 show the water contents as measured in vertical planes 2 m, 6 m, and 10 m from the trench wall on day 1. These date were taken from the Las Cruces Database (Wierenga et al. (1989, 1990b)). The vertical axis in each contour plot represents depth in meters and the horizontal axis represents horizontal distance in meters from the irrigation area centerline. Contours were not shown for depths less than 0.25 m since no measurements were made at these depths. To facilitate the comparison, the initial water contents for the model are presented together with the observed water contents for the y = 2 m plane. The y = 2 m plane is closest to the plane of solute samplers (y = 0.5 m) and to the plane from which the soil samples were taken for characterization (y = -0.5 m). Day 1 represents the first day that measurements were taken after the plot was covered. As a result of significant rainfall and the lack of a cover on previous days, the day 1 observations represent the best estimate of the initial conditions that existed prior to the controlled application of the water and solute. As Figures 1 and 2 illustrate, there is some spatial variability in the observed water contents and strong indications of layering. The day 1 volumetric water contents range from less than 0.04 cm^3/cm^3 to greater than 0.16 cm^3/cm^3 with wetter conditions occurring near the surface at y = 6 m. In contrast, the initial water content distribution for the finite difference simulation (see Figure 1), which is based on a simple depth dependent tension model (Table 1), shows no variation in the y direction. Also, the high initial water contents (>0.08 cm^3/cm^3 throughout and >0.16 cm^3/cm^3 near the surface) suggests that the uniform soil retention model over predicts the water contents at the initial tensions used, especially at intermediate depths where the observed initial water contents range from 0.04 to 0.08 cm^3/cm^3.

Comparisons between observed and the predicted changes in water contents on day 71 for the y = 2 m plane are presented in Figure 3. The observed changes in water content are the differences between the water contents measured on day 71 and those measured on day 1. The predicted changes in water content are the differences between the predicted water contents on day 71 and the initial water contents for the model. The change in water contents are plotted

because they illustrate movement of water better than absolute water contents. Also, the observed changes show less effect of spatial variability and are somewhat easier to interpret. The water content changes for the observation planes at y = 6 m and 10 m are shown in Figure 4. As Figures 3 and 4 illustrate, the water moves in a fairly uniform fashion for all three planes during the first 71 days of infiltration. More spreading occurs in the y = 6 m plane than in the other planes. After 71 days of water application, the contours suggest that the leading edge of the wetting front has generally moved downward to a depth of 2 to 2.5 m while it has moved laterally from each edge of the irrigated zone by 1 to 2 meters. Overall, the changes in predicted water contents show lateral spreading and vertical movement that agree qualitatively with the observations made in the three planes. The large degree of lateral spreading demonstrated in the numerical predictions (Figure 3) suggests that the tension gradient rather than gravity is the dominant driving force at the low flow rates present. There is little movement of water during the first 71 days at depths greater than 3 m. However, very small differences in the measured water contents can result in negative changes in the water contents at these depths. These small changes may be due to water movement or simply due to random error in the neutron probe measurements. Most of the spatial variation in the change in water contents shown below the wetting front in Figures 3 and 4 is a result of these very small differences.

The observed and predicted relative tritium and bromide concentrations on day 71 in the y = 0.5 m plane are shown in Figures 5 and 6. The tritium and bromide fronts lag far behind the water front (note that different scales are used for Figures 3 and 5). Displacement of the initial water in the soil profile causes this lag. Also, the predicted bromide front moves slightly faster than the predicted tritium front (Figures 5 and 6) because of the lower retardation factor due to anion exclusion for bromide. In contrast to the day 71 model predictions, this effect is not readily apparent in the day 71 observations. The 0.05 contours for the model predictions and the field observations for both tritium and bromide tend to show qualitatively similar downward and lateral motions of the solute front. However, the observed relative peak concentration of tritium is much higher than the predicted peak concentrations at 1 m depth and 0.5 m to the right of the centerline. The observed day 71 relative bromide concentrations are also higher than model predictions at 1 m depth but do not show as much net horizontal motion.

Figures 7 and 8 show the observed and predicted changes in water contents for day 276. Water application stopped on day 75.5, so the day 276 results represents 200.5 days of redistribution. The observations show an overall downward movement in water with a net increase in water content to the right for the y = 2 plane. This increase in water content is greater after 200 days of redistribution for the y = 2 m plane than after the 71 days of infiltration. The observations show that the model under predicts the maximum depth of the wetting front (defined here as the 0.02 contour) for the y = 2 m case and over predicts the wetting front location for the y = 10 m case for day 276. The comparison improves for the y = 6 m case. However, it is clear that the deterministic model used here cannot accurately predict point values for water content due to spatial variation in field hydraulic properties because this variation is not accounted for in the model.

The relative tritium and bromide concentration profiles for day 277 (no solute samples were taken on day 276) are shown in Figures 9 and 10. Comparing Figures 5 and 6 with Figures 9 and 10 suggests that tritium moves little during the 201.5 days of redistribution. In contrast, the bromide shows significant downward and rightward movement during the same period. A

possible explanation for this contrasting behavior is anion exclusion forces the bromide closer to the leading edge of the water front where most of the redistribution occurs. As a result, bromide movement appears to be correlated to the higher day 276 water content changes and the lower day 1 water contents which exist toward the right as illustrated in Figures 7 and 1. The model predictions show a downward motion of tritium during redistribution. This suggests an over prediction of water movement due to gravity at depths around 1 m. Comparisons between model predictions and the measured relative bromide concentrations show similar depths of penetration for the tracer fronts but significant differences in lateral motion. Bromide shows a larger net movement to the right than does tritium after 201.5 days of redistribution. This is in contrast to the day 71 results. However, it should be noted that Figure 10 is somewhat incomplete in that many solution samplers failed to operate to the left of $x = 0.5$ m because the soil was too dry.

Considering the simplistic nature of the water flow model, the model was surprisingly good at predicting water flow during the 75 days infiltration for all three planes and during the subsequent 200 days on redistribution for two of the three neutron probe measurement planes. However, there were large discrepancies between predictions and observations for the $y = 2$ m plane during redistribution due to lateral heterogeneities in the soil. These heterogeneities were apparent in both the day 1 and day 276 observations.

Bromide showed a similar non homogeneous behavior during redistribution. This is not surprising considering that the solute sampling plane ($y = 0.5$ m) is close to the $y = 2$ m neutron probe plane. The significant differences in the observed motion of tritium and bromide is surprising. Although they were applied together, tritium showed a stronger non homogeneous motion during infiltration but little motion during redistribution. In contrast, bromide showed a fairly homogeneous motion during infiltration but a highly non homogeneous motion during redistribution. The simple uniform soil transport model can not predict this heterogeneous behavior.

7.0 VALIDATION

Comparisons between the predicted and measured changes in water content show qualitative agreement after 71 days of infiltration for all three neutron probe planes. After 200 days of redistribution, fair agreement was demonstrated in the $y = 6$ m and $y = 10$ m planes but poor agreement was shown in the $y = 2$ m plane. Comparisons between the predicted and observed behavior of tritium and bromide show less satisfactory results. Model predictions of bromide transport were better during the initial 71 days of infiltration than they were after 200 days of redistribution. Model predictions for the motion of tritium were generally poor. The increased effect of the spatial variability near the trench face during redistribution appears to be the primary reason for the larger discrepancies between predicted and observed solute movement.

The results presented here provide qualitative validation (or invalidation) at best. One conclusion that can be reached is that modeling water flow during infiltration gives better results than modeling water flow and transport during redistribution for the Plot 2 experiment. The effect of spatial variability on water flow appears to be more important during redistribution. In addition, the differences between the observed transport of tritium and bromide through the soil profile during redistribution cannot be accounted for using the simple non reactive homogeneous model tested here.

8.0 UNRESOLVED ISSUES

The uniform soil water flow and transport models presented are the simplest two-dimensional models being used for the Plot 2 experiment. Comparisons between prediction and observation clearly indicate that point values for water content and solute concentration cannot be estimated using such models due to the spatial variability of the soil at the trench site. Whether the use of heterogeneous models will improve predictions of point values of water content and concentration for the Plot 2 experiment is not clear.

Comparisons between predicted and observed mean behavior of water flow and solute transport were not made. Indicators of such behavior include the motion of the center of mass of the water and solute pulses through the soil profile, and the cumulative mass of water and solute transported through a horizontal plane as a function of time. Of primary interest is whether stochastic models will provide significantly better estimates of these mean quantities than the simpler deterministic models for the Las Cruces Trench Site.

Simple comparisons of model predictions of point and mean behavior with field observations and predictions from other models can be misleading in the presence of spatially variable soils. While one model may appear to provide better predictions, the improvements may not be statistically significant. Quantitative validation methodology must be developed to account for the random nature of spatially variable soils, and the uncertainties associated with measurement error.

9.0 REFERENCES

Hills, R.G., I. Porro, D.B. Hudson and P.J. Wierenga. 1989. Modelling One-Dimensional Infiltration into Very Dry Soils - Part 1: Model Development and Evaluation. Water Resour. Res. 25(6): 1259-1269.

Hills, R.G., P.J. Wierenga, D. B. Hudson, and M. R. Kirkland. 1990. Site description, experimental results, and two dimensional flow predictions for the Las Cruces Trench Experiment 2. Submitted to Water Resour. Res.

Informix Software, Inc., 1988, 16011 College Boulevard, Lenexa, Kansas.

Nielsen, D.R., M. Th. van Genuchten, and J.W. Bigger. 1986. Water flow and solute transport processes in the unsaturated zone. Water Resour. Res. 22: 895-1085.

van Genuchten, M. Th. 1980. Calculating the unsaturated hydraulic conductivity with a new closed-form analytical model. Report 78-WR-08. Dept. of Civil Engineering, Princeton University.

Wierenga, P.J., A.F. Toorman, D.B. Hudson, J. Vinson, M. Nash, and R.G. Hills. 1989. Soil physical properties at the Las Cruces Trench Site. NUREG/CR-5441, U.S. Nuclear Regulatory Commission, Washington, D.C.

Wierenga, P. J., R. G. Hills, and D. B. Hudson. 1990a. Site description, experimental results, and one dimensional flow predictions for the Las Cruces Trench Experiment 1. Submitted to Water Resour. Res.

Wierenga, P.J., D.B. Hudson, R.G. Hills, I. Porro, M.R. Kirkland. 1990b "Experiments 1 and 2 at the Las Cruces Trench Site, U.S. Nuclear Regulatory Commission NUREG report, in preparation.

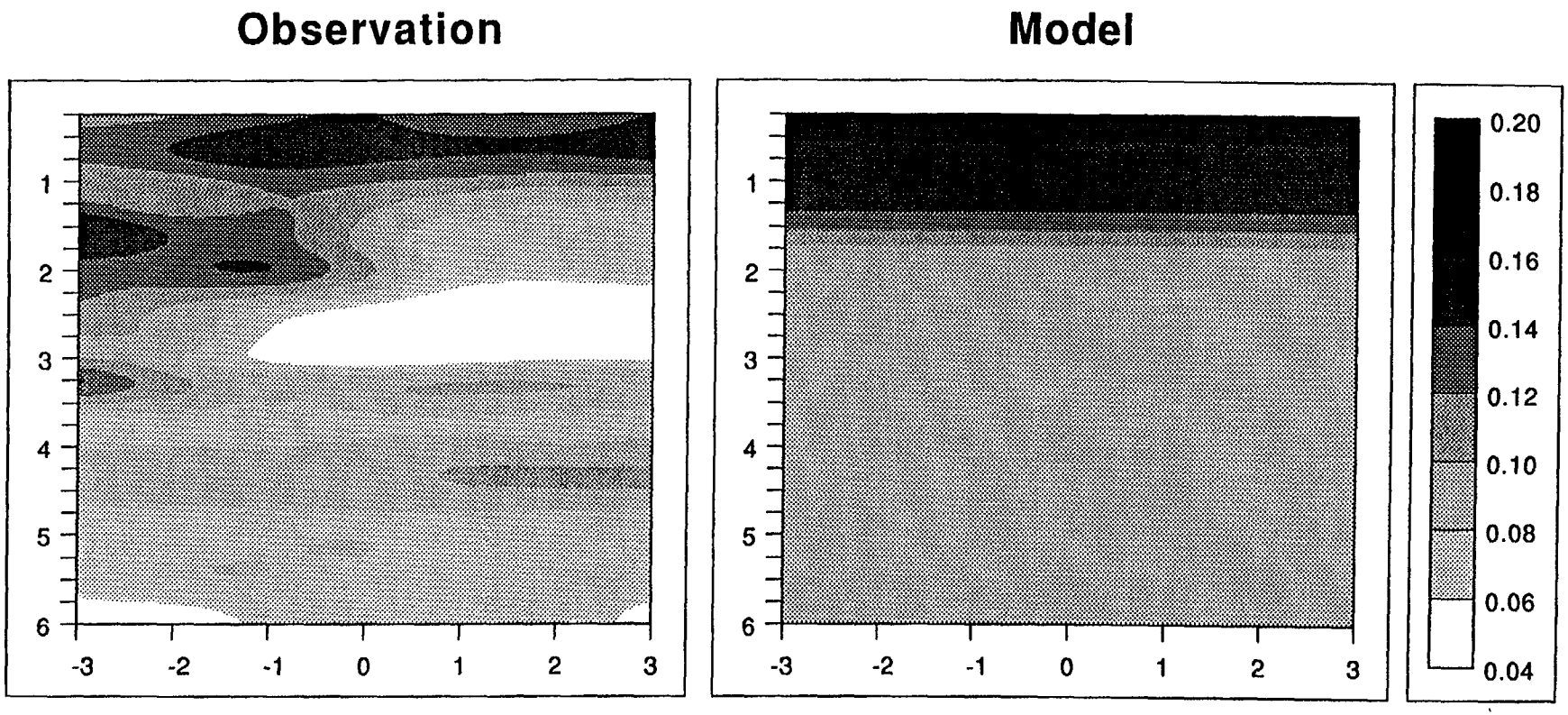

Figure 1. Observed and modeled initial water contents: y = 2 m

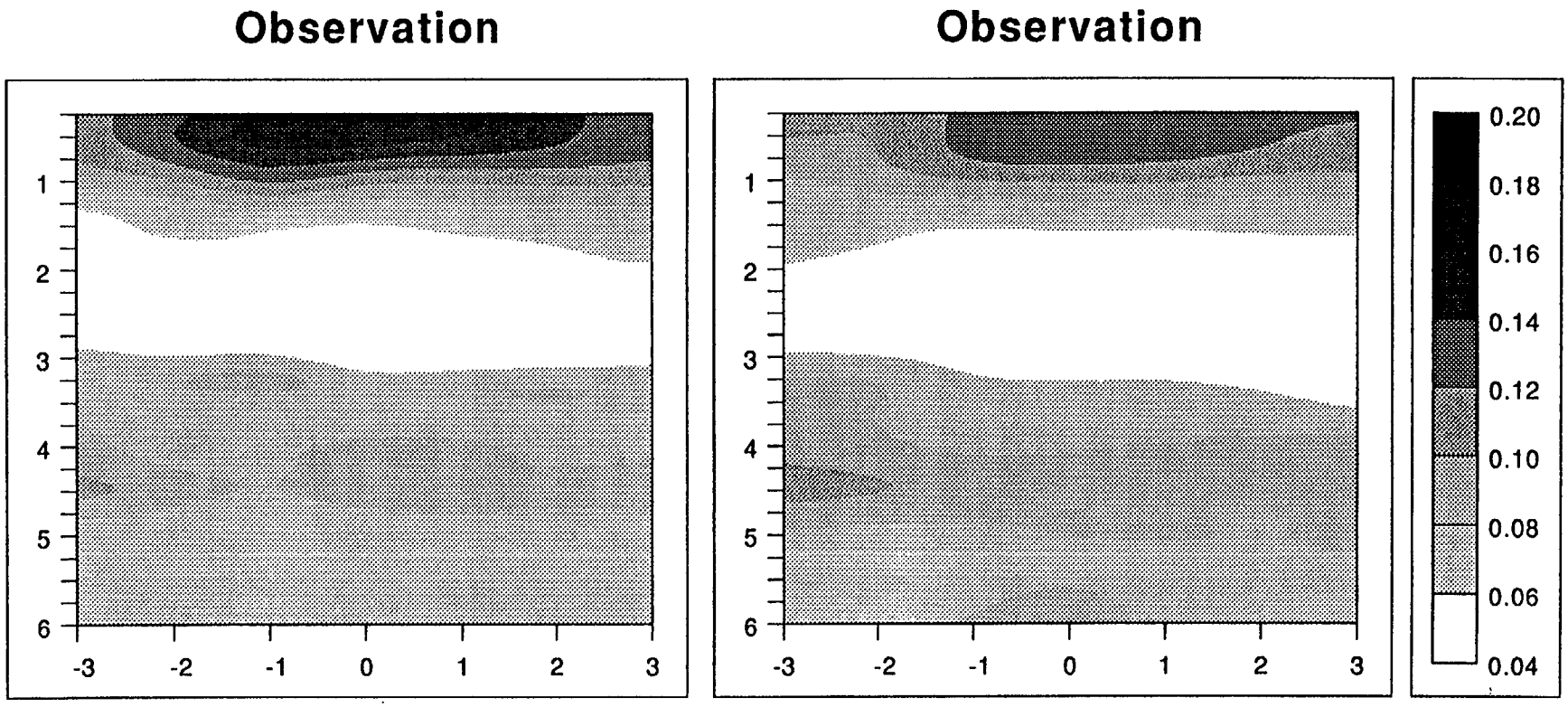

Figure 2. Observed initial water contents: y = 6 m and 10 m respectively.

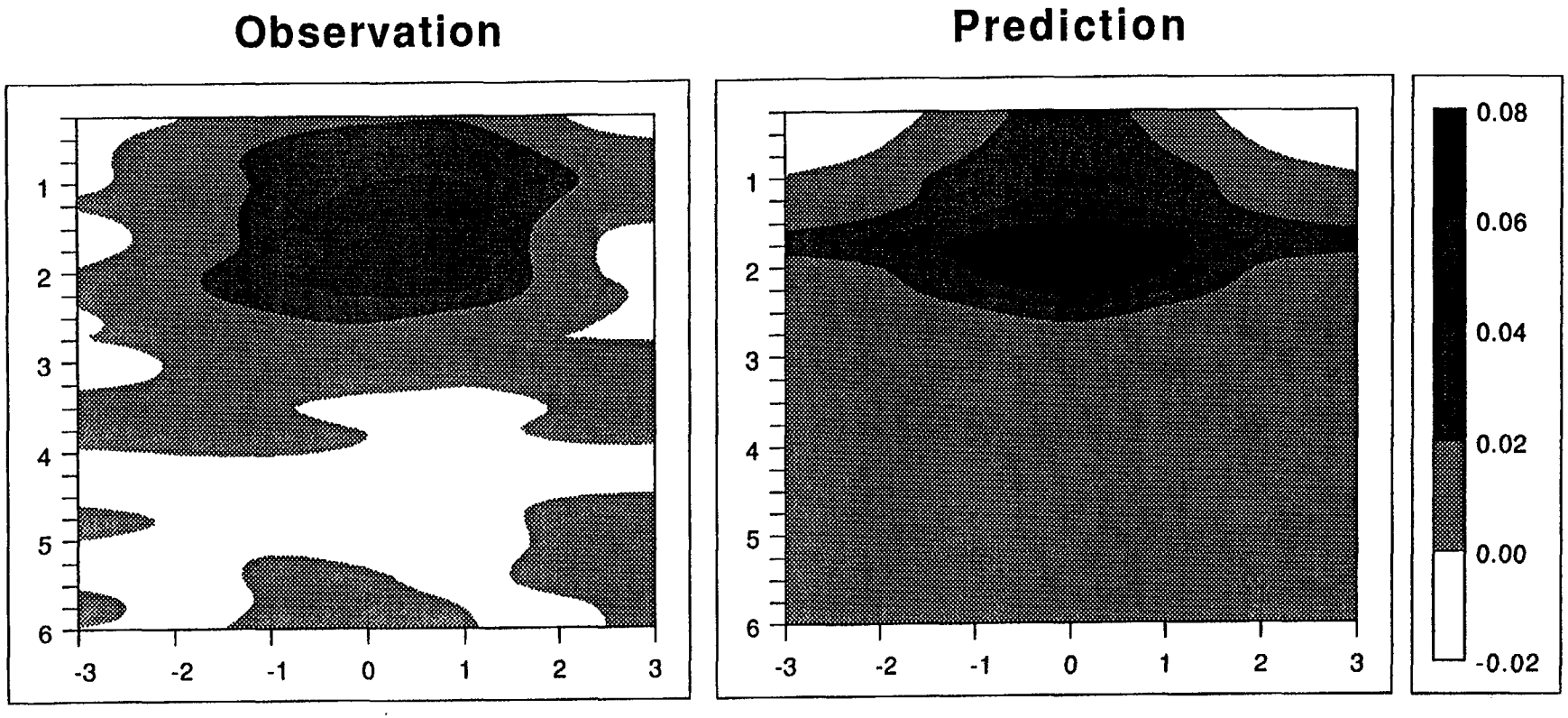

Figure 3. Changes in observed and predicted water contents on day 71: y = 2 m.

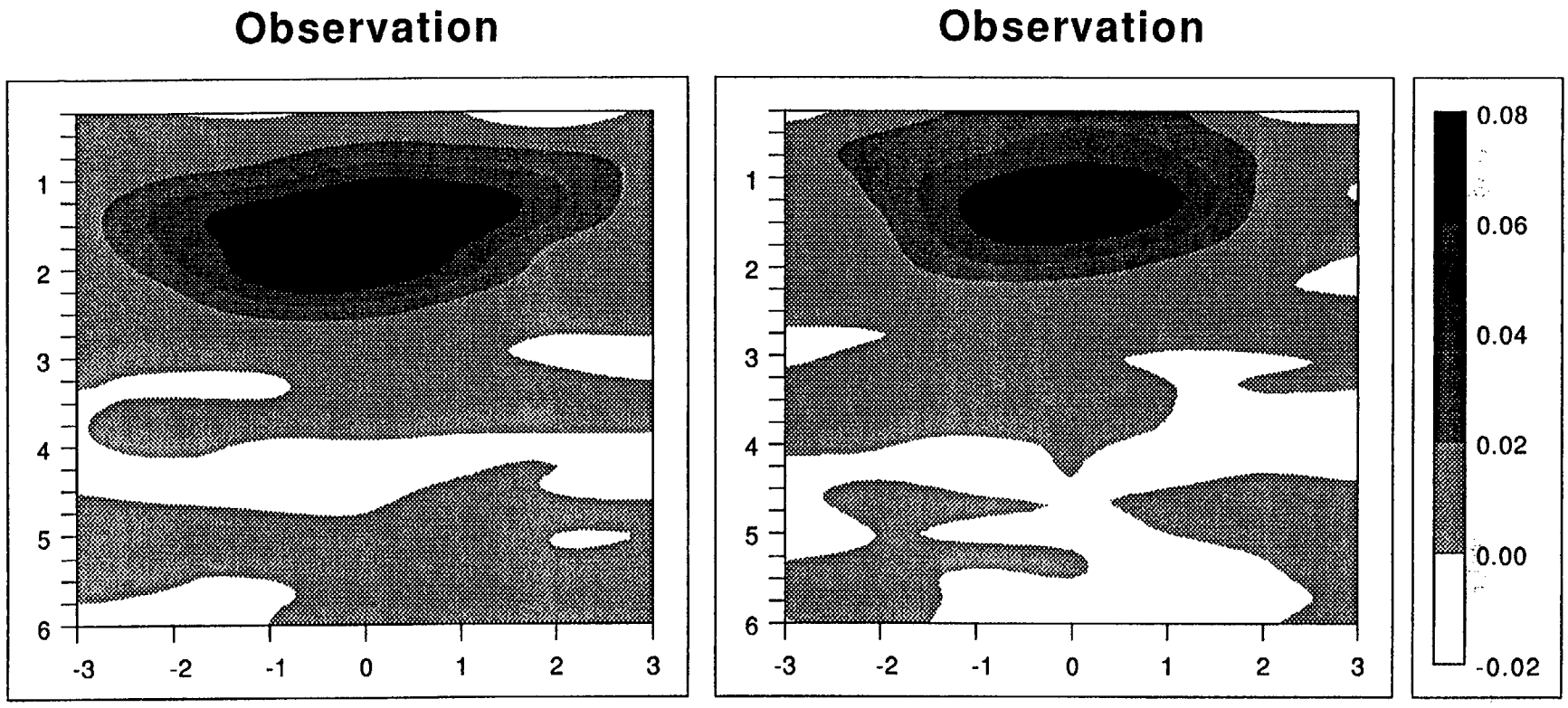

Figure 4. Changes in observed water contents on day 71: y = 6 m and 10 m respectively.

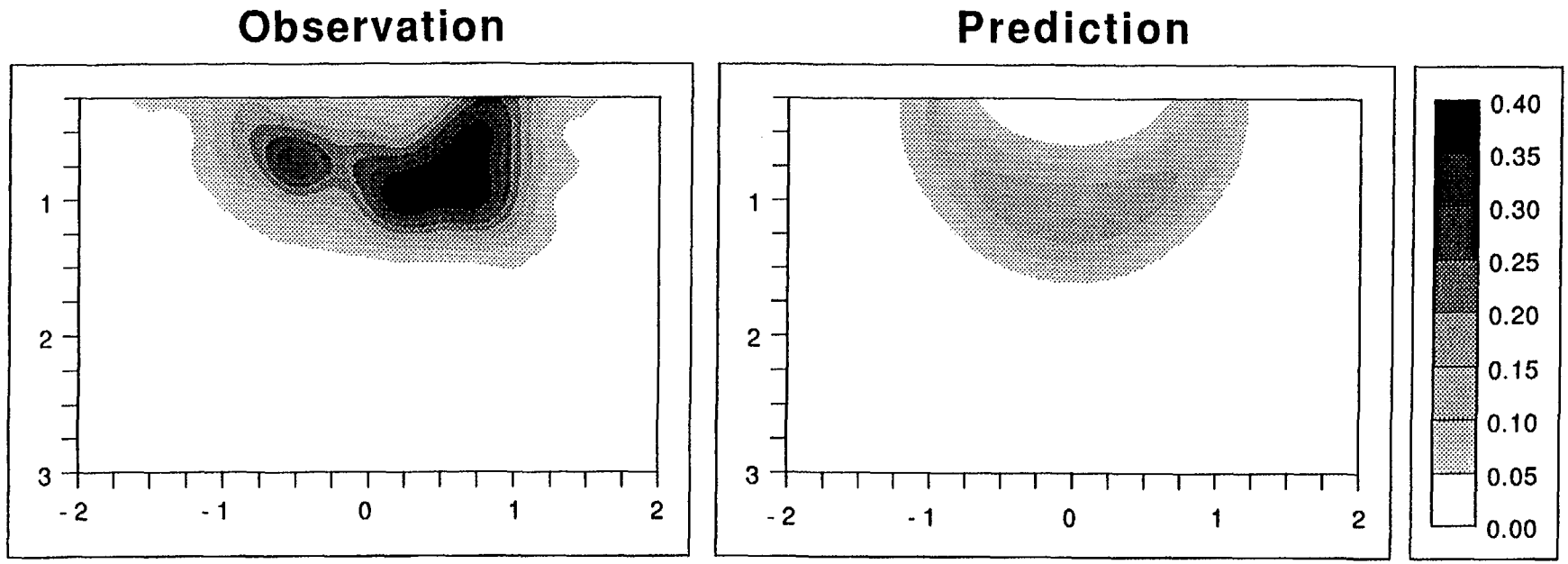

Figure 5. Observed and predicted relative tritium concentrations on day 71: y = 0.5 m.

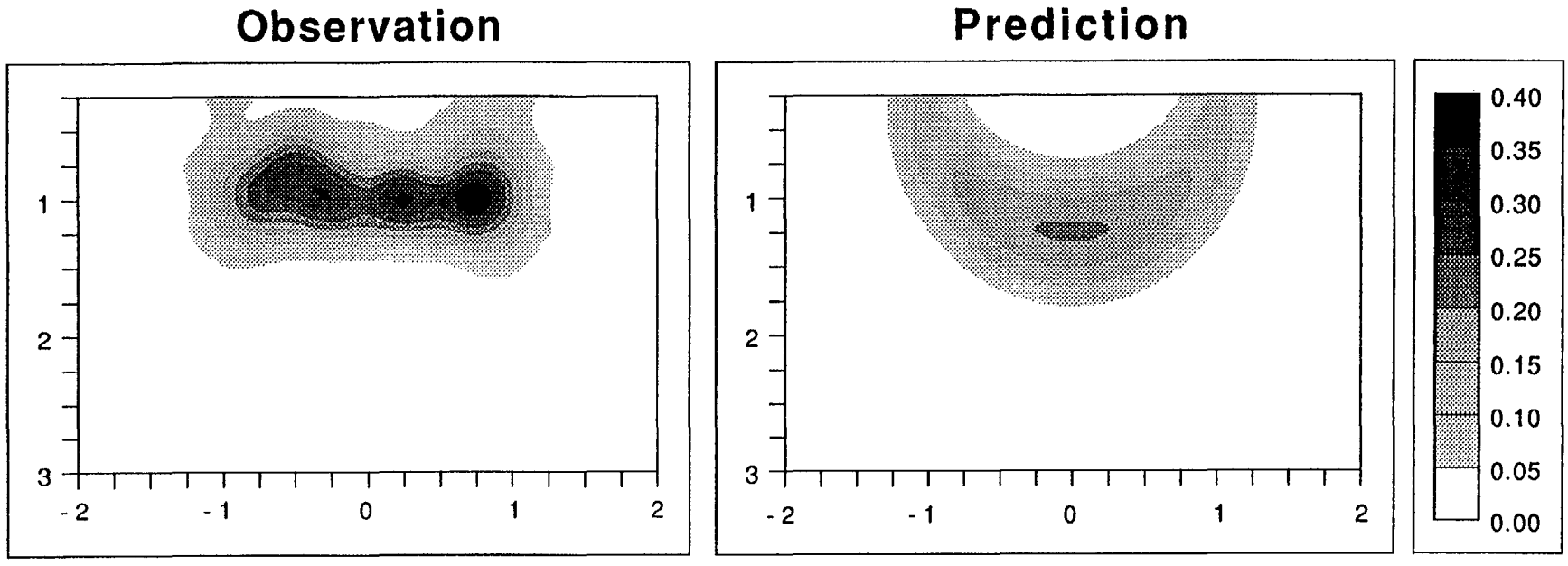

Figure 6. Observed and predicted relative bromide concentrations on day 71: y = 0.5 m

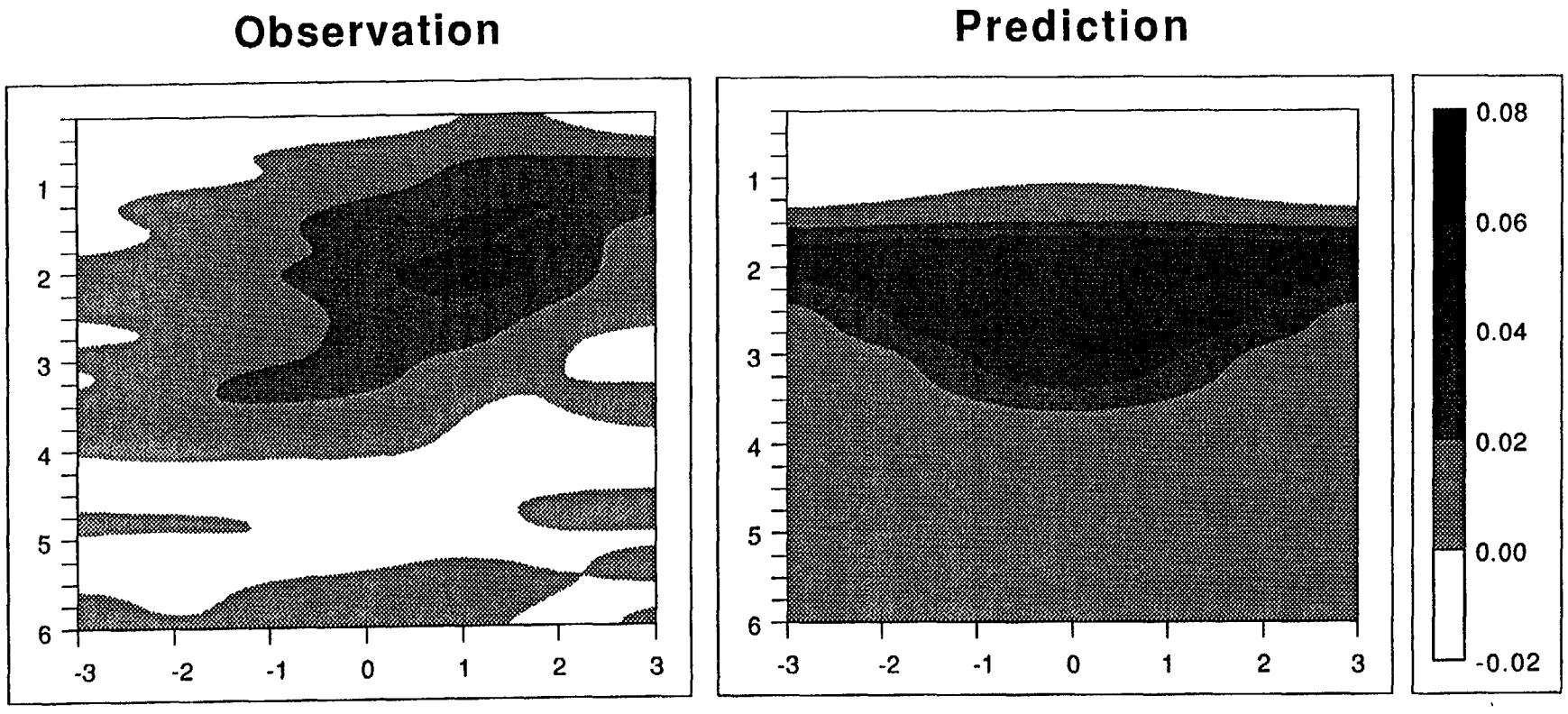

Figure 7. Changes in observed and predicted water contents on day 276: y = 2 m.

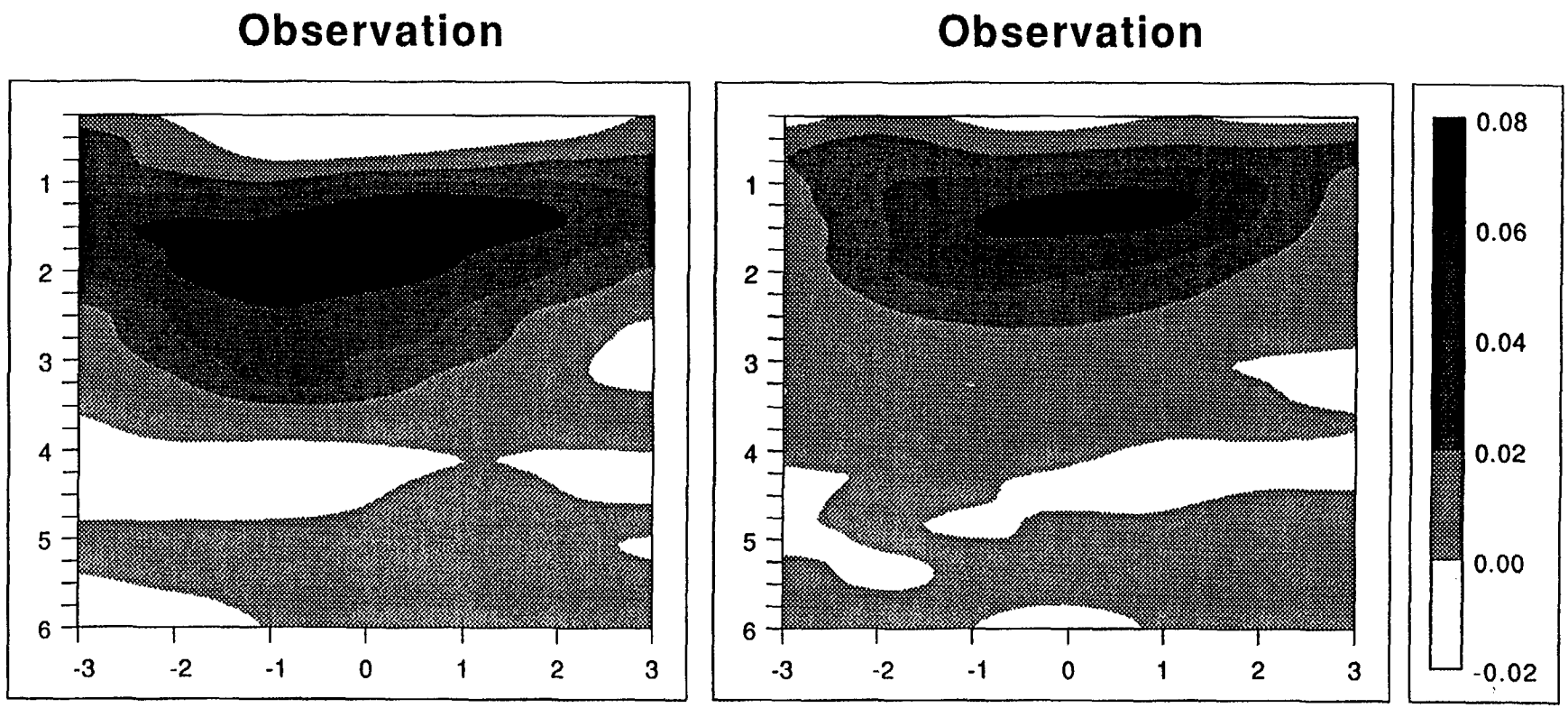

Figure 8. Changes in observed water contents on day 276: y = 6 m and 10 m respectively.

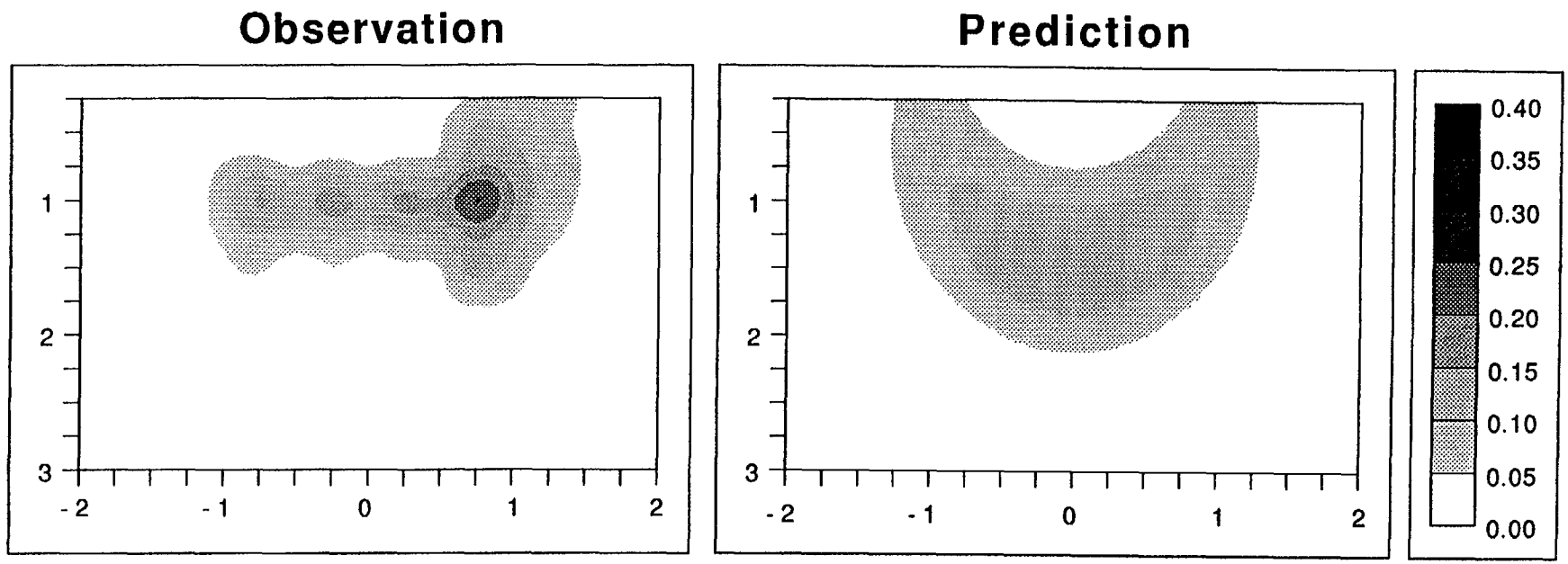

Figure 9. Observed and predicted relative tritium concentrations on day 277: y = 0.5 m.

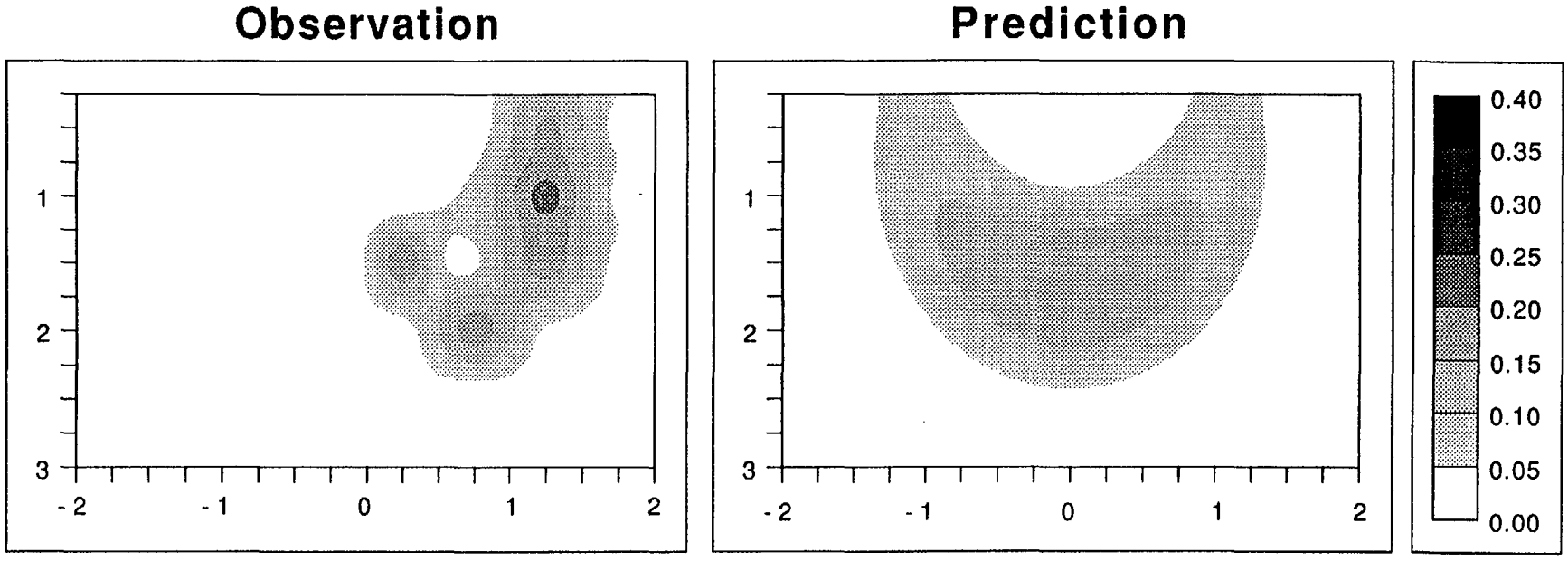

Figure 10. Observed and predicted relative bromide concentrations on day 277: y = 0.5 m.

APPENDIX C5

Application of the VAM2D code to the second
Las Cruces Trench experiment

APPLICATION OF THE VAM2D CODE TO THE SECOND LAS CRUCES TRENCH EXPERIMENT

J.B. Kool

HydroGeoLogic, Inc.
1165 Herndon Parkway
Suite 900
Herndon, VA 22070

May, 1991

SUMMARY

The second Las Cruces Trench infiltration experiment was simulated using the VAM2D variably saturated flow and transport code (Huyakorn et al., 1989). The field experiment involves infiltration and redistribution of water and non-reactive tracers in an initially dry, heterogeneous field soil. Intense site characterization and monitoring has been conducted at the Las Cruces field site resulting in a detailed database for calibration and validation of unsaturated flow and transport models. In this study the level of detail in the flow and transport model required to reproduce key features as well as the significance of hysteresis and saturation dependent anisotropy of the observed water and solute plumes were evaluated. In all cases it was assumed that flow and transport were described by the Richard's and advection-dispersion equation, respectively. However, effects of soil heterogeneity were accounted for in different ways. Four different simulation scenarios were evaluated, i.e.: I) uniform, isotropic soil with literature derived unsaturated hydraulic parameters, IIa) uniform, isotropic soil with unsaturated hydraulic parameters determined by averaging individual sample values, IIb) uniform, but anisotropic soil with unsaturated hydraulic parameters determined in a manner analogous to scenario IIa but different averaging procedure, and III) non-uniform but isotropic soil with different soil material properties assigned to each element in the computational grid in order to represent as closely as possible the heterogeneity observed in the field. The possible effects of hysteresis in the soil moisture characteristic on water movement were evaluated as a variant of scenario IIa.

The field experiment simulated involved infiltration and redistribution of a 75.5 day duration irrigation pulse with conservative tracers (bromide, tritium) supplied during the first 11.5 days. The irrigation was applied at a low rate resulting in unsaturated conditions throughout the experiment. Two-dimensional, cross-sectional simulations were performed using the VAM2D computer code. Even though the experiment was designed to maintain a two-dimensional flow regime, the field data showed significant migration in three-dimensions. In order to be able to compare model and field results, the field data were averaged in the third dimension. Salient features of the field moisture content distribution were the irregular water content contours and lateral spreading of the applied water. These features were reproduced quite well in modeling scenario III. Scenario IIb reproduced the horizontal spread of the moisture plume reasonably well, but not the irregular moisture level contours. The simulated effect of hysteresis was the opposite of observed field flow behavior, indicating that capillary hysteresis is not a significant factor in the field experiment. Overall, the results suggest that the observed pattern of water movement at the second Las Cruces trench experiment may be explained either as resulting from local heterogeneities in an isotropic soil, or as resulting from a macroscopic anisotropy in a locally uniform soil. These apparently contradictory results agree qualitatively with the stochastic unsaturated flow theory developed at the Massachusetts Institute of Technology (MIT) by Dr. Lynn Gelhar and coworkers. The latter theory predicts among others, that local soil heterogeneities may manifest themselves in transient unsaturated flow as an apparent large scale anisotropy. It was attempted to model the trench experiment using a pressure head dependent anisotropy factor calculated from the stochastic flow theory. This resulted however in a severe overprediction of the degree of anisotropy of hydraulic conductivity, and a poor prediction of water movement patterns.

In addition to unsaturated transient flow, the movement of the tritium tracer which was applied during the first part of the experiment was also simulated with VAM2D, using the four different conceptual flow models discussed above. In contrast to the unsaturated flow results, none of the three modeling scenarios showed good agreement with field concentration data. Maximum observed concentration levels were several times higher than simulated and the bromide plume shape was also not well reproduced. However, field solute monitoring data is much less detailed than available moisture data. It was therefore not possible to resolve whether discrepancies between model transport predictions and field observations are due to deficiencies in the modeling or due to a lack of sufficiently detailed data on three-dimensional solute movement.

Table of contents

LIST OF FIGURES

LIST OF TABLES

1. INTRODUCTION

During the last several years, the U.S. Nuclear Regulatory Commission (U.S. NRC) has sponsored detailed field experiments conducted at the University of New Mexico's facility near Las Cruces New Mexico (Wierenga et al., 1986, 1989, 1990). These experiments were designed to study the movement of water containing chemical tracers through an initially dry, spatially variable soil. The series of experiments that have been conducted at this site have involved a very detailed soil characterization and monitoring effort, with the objective of developing a database for testing deterministic as well as stochastic unsaturated flow and transport models. The work described herein presents modeling of the second Las Cruces trench experiment using the VAM2D computer code (Huyakorn, et al., 1989, 1991). VAM2D is a two-dimensional, variably saturated flow and transport code. The flow solution is based on the pressure head form of the Richard's equation, while the transport solution is based on the conventional advection-dispersion equation. One objective of this study was to test the applicability and numerical accuracy of the code for the difficult Las Cruces trench simulation problem. A second objective was to gain more insight in the factors and mechanisms controlling flow and transport in the field experiment. This objective was approached by analyzing a number of different modeling scenarios which differed in the processes that were accounted for in the transient flow simulation. The emphasis in this study is on unsaturated flow modeling on the notion that accurate description of water movement is the first and essential step in assessment of the migration of dissolved chemicals which in many instances will be of ultimate environmental concern.

2. MATERIALS AND METHODS

2.1 FIELD EXPERIMENT

A series of unsaturated zone flow and transport field experiments have been conducted at the New Mexico State University's Jornada experimental site near Las Cruces, New Mexico. Detailed descriptions of the site conditions, design of the experiments and experimental data are provided by Wierenga et al. (1986, 1989, 1990). The following is a summary of site and experimental conditions.

The experimental site is located 40 km north-east of Las Cruces, New Mexico. The field site is on a basin slope of Mount Summerford, which is part of the Dona Ana mountain range. Climatic conditions, geologic features, geomorphic surfaces, soil types and vegetation in the area are typical of many areas of southern New Mexico and are similar to arid and semi-arid areas of the Southwestern United States. The average annual precipitation is 23 cm/year while the Class A pan evaporation averages 239 cm/year. The soil profile at the site shows several buried horizons, indicating a cyclic pattern of sediment accumulation and erosion. Within each of the four main deposits that have been distinguished in the upper 6m of the soil, several morphologically different soil horizons have been identified. The sequence of soil layers is depicted in Figure 1. The soil texture in the various horizons shown in Figure 1 is generally loamy sand or sandy loam.

The present study involves the second trench infiltration experiment conducted at the site. A plan view of the field experiment is shown in Figure 2. The central feature of the experiment is a large trench, 26.5 m long by 4.8 m wide by 6.0 m deep which has been dug in the undisturbed soil. The actual experiment was conducted in the area labeled as Plot #2 in Figure 2. The trench itself is not part of the experimental plot, but it provides access to subsurface monitoring instruments. During trench excavation soil cores and soil samples were taken along the length of the trench at 0.5 m horizontal intervals. At each sampling location, soil cores were collected at each of the nine sampling depths indicated in Figure 1 to a depth of 5.8 m. A total

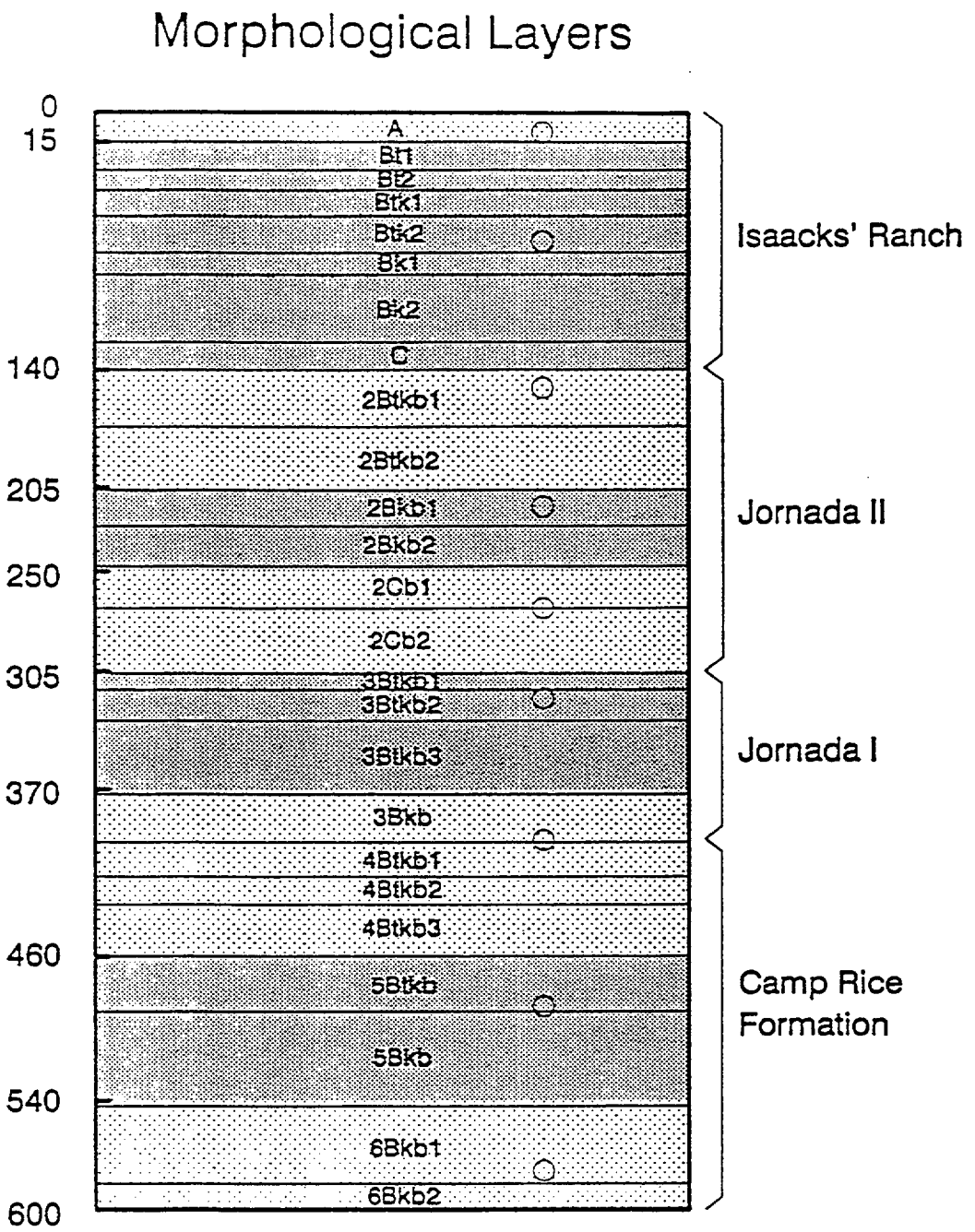

Figure 1. Deposits and soil horizons present in upper 6m of the soil at the Jornada experimental site. Circles indicate the depths from which samples were taken (from Wierenga et al., 1989).

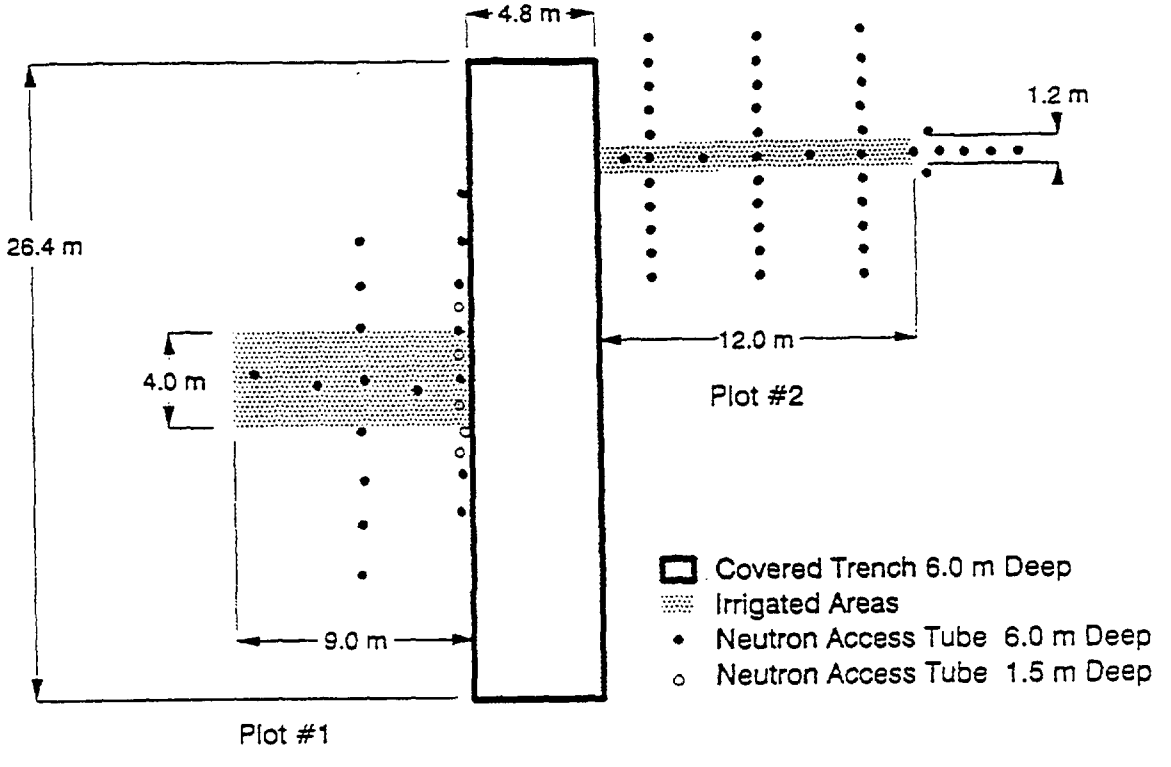

Figure 2. Plan view of the Las Cruces trench site (from Wierenga et al., 1989).

of 50 cores and samples were collected in this way from each sampling depth. Additional cores were collected at three locations along the trench, using an approximately 20 cm depth interval, to further resolve vertical soil variation. A total of 640 soil cores and samples were analyzed for determination of bulk density, particle size distribution, saturated hydraulic conductivity and the soil-water retention characteristic.

In addition to the laboratory analyses, saturated hydraulic conductivities were determined in-situ using the bore hole permeameter method. The in-situ hydraulic conductivity measurements were performed for all nine soil layers from which laboratory samples were collected. From each layer, 50 equally spaced measurements along the length of the trench were obtained adjacent to the locations from which samples were collected.

The infiltration experiment conducted in Plot #2 on the north side of the trench involved controlled application of water and solute tracers over a 1.22 m wide by 12 m long irrigation area, as indicated by shading in Figure 2. Water was applied through a grid of drip emitters, involving a total of 40 parallel irrigation lines. Water was applied twice daily resulting in an average flux density of 0.43 cm/day over the irrigated area. The application was started on August 8, 1988 and continued for 75.5 days. Tritium and bromide tracers were mixed in with the water during the first 11.5 days. Tritium was added in a concentration of 0.1 mCi/L; the bromide concentration was 0.799 gr/L. The irrigation and surrounding area were covered with a plastic liner throughout the irrigation and subsequent redistribution period, to eliminate both evaporation and infiltration of rain water.

Water flow and solute movement have been monitored during and following the irrigation event using tensiometers, neutron logging and solution samplers. A total of 43 neutron probe access tubes were installed to a depth of 6m in the Plot #2 area. The location of each access tube is shown in Figure 2. Neutron probe readings were taken at 0.25 m depth increments with a frequency as high as every 4 to 5 days during the irrigation period and decreasing frequency during the distribution period. It may be noted that moisture movement could be monitored in three dimensions (x, y, z) using neutron logging. The tensiometers were installed underneath the center of the irrigation area, through the trench face at an angle of 10^{o} from horizontal, such that the sensing cups were located in a two-dimensional (x, z) plane located 50 cm away from the trench face in the y-direction. The coordinate convention used here is that the x-axis represents the horizontal direction parallel to the long axis of the trench, the y-axis represents the perpendicular horizontal direction, i.e., parallel to the long axis of the irrigation plot, and the z-axis represents the vertical direction. Soil solution samplers were installed from the trench face in a manner similar to the tensiometers. The location of tensiometers and solute samplers underneath the experimental plot is shown in Figure 3. Tensiometers and solution samplers were thus installed in a two-dimensional x-z plane and thus do not provide information on pressure head and concentration variations in the y-direction.

2.2 FLOW AND TRANSPORT MODEL

2.2.1 Governing Equations

The flow solution in the VAM2D computer code is based on the two-dimensional Richard's equation for isothermal flow in a rigid porous medium

$$\frac{\partial}{\partial x}\left[K_{xx}\,k_r\,\frac{\partial \psi}{\partial x}\right] + \frac{\partial}{\partial z}\left[K_{zz}\,k_r\,(\frac{\partial \psi}{\partial z} + 1)\right] = \frac{d\theta}{d\psi}\,\frac{\partial \psi}{\partial t} \qquad (1)$$

where ψ is pressure head (L), θ is the volumetric water content, K_{xx} and K_{zz} are the components of saturated conductivity (L/T) in the x- and z- direction, respectively, k_r is the relative permeability, x and z are cartesian coordinates (L) and t is time (T). We use the convention that the z- coordinate points upward. Constitutive relations used in the flow modeling are taken to be of the form (van Genuchten, 1980)

$$\theta = \begin{cases} \theta_s & \psi \geq 0 \\ \theta_r + (\theta_s - \theta_r)\,[\,1 + (-\alpha\psi)^{\beta}]^{\gamma} & \psi < 0 \end{cases} \qquad (2)$$

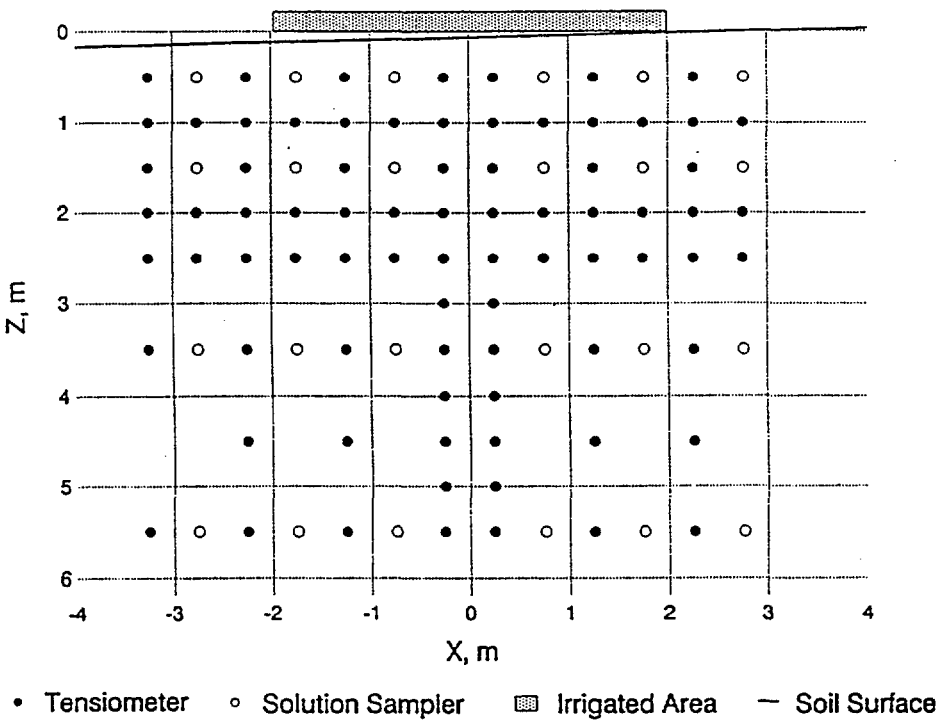

Figure 3. Cross-sectional view showing location of tensiometers and solute samplers underneath the irrigation plot (from Wierenga et al., 1990).

$$k_r = S_e^{1/2} \left[1 - (1-S_e^{1/\gamma})^{\gamma}\right]^2 \tag{3}$$

where θ_s is the saturated water content, θ_r is a residual water content, and α, β and γ are shape parameters with γ=1-1/β. S_e is the effective saturation defined as $S_e=(\theta-\theta_r)/(\theta_s-\theta_r)$.

Transport simulations were based on the advection-dispersion equation for a conservative solute

$$\frac{\partial}{\partial x}\left(D_{xx}\frac{\partial c}{\partial x}\right) + \frac{\partial}{\partial z}\left(D_{zz}\frac{\partial c}{\partial z}\right) + \frac{\partial}{\partial x}\left(D_{xz}\frac{\partial c}{\partial z}\right) + \frac{\partial}{\partial z}\left(D_{zx}\frac{\partial c}{\partial x}\right) - V_x\frac{\partial c}{\partial x} - V_z\frac{\partial c}{\partial z} = \theta\frac{\partial c}{\partial t} \tag{4}$$

where c is solute concentration (M/L^3), D_{xx}, D_{zz}, D_{xz} and D_{zx} are dispersion coefficients (L^2/T) and V_x and V_z are the x- and z- components of the Darcy velocity tensor (L/T). The dispersion coefficients incorporate the effects of hydrodynamic mixing and molecular diffusion and are determined as

$$D_{xx} = \alpha_L \frac{V_x^2}{|V|} + \alpha_v \frac{V_Z^2}{|V|} + \tau D^o \tag{5a}$$

$$D_{zz} = \alpha_v \frac{V_x^2}{|V|} + \alpha_L \frac{V_Z^2}{|V|} + \tau D^o \tag{5b}$$

$$D_{zx} = D_{xz} = (\alpha_L - \alpha_v)\frac{V_x V_z}{|v|} \tag{5c}$$

where α_L and α_v are the longitudinal and vertical dispersivity (L), respectively, D^o is the bulk solution coefficient of molecular diffusion (L^2/T) and τ is a water content dependent tortuosity coefficient given by (Millington and Quirk, 1959)

$$\tau = \theta^{10/3}\theta_s^{-2} \tag{6}$$

Using the tortuosity factor given by (6) has the effect of reducing molecular diffusion as the water content decreases. It was found necessary to introduce this tortuosity factor after initial simulations with a constant effective diffusion coefficient indicated a significant over-prediction of diffusion.

The flow equation is solved in VAM2D using the Galerkin finite element technique with either Picard or Newton-Raphson iteration methods. The transport equation is treated using the upstream-weighted finite element method. The transport solution in VAM2D can account for linear equilibrium sorption as well as (chained) decay reactions. However, these processes were ignored in the present analysis. For both flow and transport problems, spatial discretization is performed using simple rectangular elements or orthogonal curvilinear elements, allowing element matrices to be computed using highly efficient influence coefficient matrix formulas. The numerical schemes used are well documented (Huyakorn and Pinder, 1983; Huyakorn et al., 1984, 1985, 1989) and are not repeated here. Various aspects of the computational procedure that are related specifically to mass balance accuracy and convergence of the transient, variably saturated flow solution are discussed in the next section.

2.2.2 Numerical Procedures for Efficient Flow and Transport Simulation

Simulation of transient water and solute movement in very dry soils represents a numerically challenging problems. Experience with pressure head based solutions of the Richards equation has shown that it may be difficult to obtain a solution with accurate mass balance, unless very fine space and time discretizations are employed (e.g. Hills et al., 1989). Typically it is found that mass is "lost" in the simulation and that computed infiltration depths are less than they should be. Mass balance errors in numerical solutions of (1) are usually related to the manner in which the storage terms in the governing equation are treated. Although effective ways to treat this problem have been known for some time (e.g. Cooley, 1983, Hornung and Messing, 1984) difficulties that have been encountered in modeling of the Las Cruces trench experiments have caused renewed interest in the mass balance problem in unsaturated flow modeling (Hills et al., 1989; Celia et al., 1990).

Milly (1985) has discussed several alternative ways to evaluate the moisture capacity $C = d\theta/d\psi$ in finite element solutions of (1) that can be used to achieve an accurate moisture mass balance. The usual definition of the moisture capacity as the tangential approximation of $d\theta/d\psi$ will result in an exact mass balance only for infinitely small space and time discretizations. For more practical grid sizes and time steps, substantial mass balance errors may occur when sharp moisture fronts are present. In order to obtain a mass conservative result, Milly (1985) pointed out that the moisture capacity should be defined in such a way that the following holds at the element level

$$\int_e \bar{C}(\psi^{t+\Delta t} - \psi^t)\, de = \int_e (\theta^{t+\Delta t} - \theta^t)\, de \tag{7}$$

in which $\bar{C}$ is the effective soil water capacity expressed in terms of the finite element interpolation functions within the element and where integration is performed on an element by element basis. The resulting expression for the nodal values of C depend on how the finite element storage matrix is formed, i.e., whether or not a diagonalized (lumped) matrix is used. The simplest scheme results when mass-lumping is applied so that the element storage matrix is the same as in finite difference schemes, i.e., a diagonal matrix given by

$$[C]^e = \frac{\Delta_x \cdot \Delta_y}{4\Delta t} \begin{bmatrix} C_1 & & 0 \\ & \ddots & \\ 0 & & C_4 \end{bmatrix} \tag{8}$$

where Δ_x and Δ_y are the element dimensions. In this case the nodal values of C_i are given simply by

$$C_i^{t+\Delta t} = \frac{\theta_i^{t+\Delta t} - \theta_i^t}{\psi_i^{t+\Delta t} - \psi_i^t} \tag{9}$$

The same result has been presented by Horning and Messing (1984). Celia et al. (1990) have recently reviewed an alternative approach, based on the mixed form of the Richards equation which yields an equivalent result. In the VAM2D simulations a mass-lumped flow solution was used with a backward difference time approximation and with nodal moisture capacities evaluated using (9). The average cumulative mass balance errors expressed as a fraction of the total added amount of water was 1.2% for all flow simulations. In contrast, initial simulations which used a non-mass conserving way to evaluate moisture capacities showed mass balance errors as high as 20%. The mass balance error could presumably be reduced further by using a finer finite element grid and smaller time steps. However, it was felt that the level of accuracy achieved in the flow simulations was commensurate with the level of detail in available field data.

While mass balance accuracy of a numerical unsaturated flow solution can be quite sensitive to the manner in which storage terms are calculated, the mass balance error in solute transport solutions can be similarly sensitive to the way in which the velocity components (V_x, V_z) are computed. When saturation and hydraulic conductivity values vary drastically across an element, it is intuitively clear that transport solutions can be sensitive to the nodal averaging procedures used to calculate elemental velocity values. Velocities are obtained by local application of Darcy's Law which requires knowledge of the effective elemental hydraulic conductivity. The computationally most expedient way to calculate these is to evaluate element water content and relative conductivities after averaging nodal pressure head values, i.e.,

$$\langle \psi \rangle = \frac{1}{n} \sum_{j=1}^{n} \psi_j \tag{10a}$$

$$\langle \theta \rangle = \theta(\langle \psi \rangle) \tag{10b}$$

$$\langle k_r \rangle = k_r(\langle \theta \rangle) \tag{10c}$$

where < > denotes elemental value, k_r is the relative permeability and n is the number of nodes associated with the element. In this case the constitutive relations $\theta(\psi)$ and $k_r(\theta)$ need to be evaluated only once for each element. However, in the transport simulations of the trench experiment, the above scheme resulted in solute mass balance errors as high as 10%, even though very good mass balance was obtained in the flow solution itself. It was found that solute mass balance errors could effectively be eliminated by performing the averaging over the nodal values of θ and K_r themselves as

$$\langle \theta \rangle = \frac{1}{n} \sum_{j=1}^{n} \theta(\psi_j) \tag{11a}$$

and

$$\langle k_r \rangle = \frac{1}{n} \sum_{j=1}^{n} k_r(\theta_j) \tag{11b}$$

In the flow and transport simulations, the bulk of the computational effort is taken up by the nonlinear flow solution, and a considerable savings can be achieved by using efficient time stepping procedures in conjunction with techniques to enhance convergence of the iterative solution scheme. VAM2D incorporates several of these features and the trench simulations provided a good test for their effectiveness. The features in VAM2D are not entirely new, rather they are based on techniques that have been found to be effective elsewhere (e.g. Cooley, 1983; van Genuchten, 1982; Huyakorn et al., 1984). Mass-lumping and use of a fully implicit time approximation are well known to reduce oscillations and thus improve convergence (e.g. Milly, 1985; Celia et al., 1990). Use of a Newton-Raphson iteration procedure will also improve convergence compared to the Picard scheme. However, the Newton-Raphson procedure itself requires approximately twice the effort per iteration that the Picard scheme does, so the trade-off between Picard and Newton-Raphson iteration is not always clear. In the VAM2D trench simulations, Picard iteration was used in conjunction with an under-relaxation scheme for updating nodal pressure head values between iterations, based on a procedure proposed by Cooley (1983). This combination was found to be quite competitive in speed of convergence with Newton-

Raphson iteration while requiring less computational effort. Another aspect of the computational scheme is the selection of optimal time step size during the transient simulation. Aside from the effect that time step size has on the simulation accuracy, there will be a large effect on CPU time. An overly small timestep may slow the simulation down, even though the solution will probably converge rapidly at each time step. On the other hand, convergence may be very slow or fail at all if a too large timestep is used, necessitating cutbacks in time step size and/or a large number of iterations per time step. VAM2D incorporates a simple automatic time step adjustment scheme, adopted from van Genuchten (1982), which has proven very effective. In this scheme an initial, minimum and maximum time step size are specified as input parameters. The simulation is started using the initial time step size. At the beginning of each new time step, the step size is adjusted depending on the number of iterations required during the just completed time step. If convergence was rapid, the time step size is increased by a preset fraction until the maximum allowable stepsize is reached, otherwise the step size is kept constant or, if convergence was slow, decreased. The minimum time step value guards against excessively long simulation times if convergence is slow. The maximum step size is set to control errors in the numerical approximation. In the Las Cruces trench simulations the initial time step was set to Δt_{in} = 1 day and the maximum time step was set to Δt_{max} = 7 days. All simulations discussed in this report covered a 277 day time period; between 90 and 130 time steps were required for the transient simulations.

A final consideration is the selection of an appropriate pressure head convergence tolerance. In the relatively wet parts of the modeled domain, a small convergence tolerance should be used, since water contents and conductivities will be sensitive to relatively small pressure head changes. On the other hand, in the dry parts of the domain, the water contents approach residual values and are quite insensitive to pressure head changes. Consequently, a much larger convergence tolerance can be used here. In order to accommodate both considerations, we used a combination of absolute and relative tolerances. The nodal convergence tolerance, τ_i, is then determined from

$$\tau_i = \tau_a + \tau_r |\psi_i| \tag{12}$$

where τ_a and τ_r are the absolute and relative tolerances and where τ_r typically ranges from 0.01 to 0.001.

All simulations reported here were performed on a 25 MHz 80386 personal computer equipped with a 80387 FPU and 8 megabytes of RAM memory. The flow and transport simulations required between 4 (Scenario I and II) and 7 (Scenario III) hours of computer time. While these simulation times are by no means trivial, they compare quite favorably with results reported by Hills et al. (1989) which demonstrates the effectiveness of the computational schemes employed in the VAM2D computer code.

2.2.3 Model Domain and Boundary Conditions

Flow and transport were modeled in a two-dimensional vertical (x-z plane) cross-section. Flow and transport in the y-direction were not considered. Restricting the modeling to two dimensions is dictated by the selection of the 2-D VAM2D computer code. However, considering the relatively large dimension of the irrigation area in the y-direction (Figure 2) and the uniform

water and tracer applications, this assumption was deemed reasonable for most of the actual plot, with possible exception of the ends of the plot. The modeled domain and assigned boundary conditions are depicted in Figure 4. This figure also shows the spatial coordinate convention used in the modeling. The x-coordinate origin is taken to be directly underneath the center of the experimental plot. The modeled region extends 600 cm to both the left and right. The vertical (z-) coordinate is taken to be positive upwards. The soil surface is thus located at an elevation of 500 cm. The dimensions of the modeled region were chosen large enough that boundary effects on flow and transport would be negligible. As shown in Figure 4, the left and right side boundaries are assigned no-flux conditions for flow and transport. The upper boundary which corresponds to the soil surface is also assigned a no-flux condition, except for the zone that corresponds to the irrigation area. This boundary section was

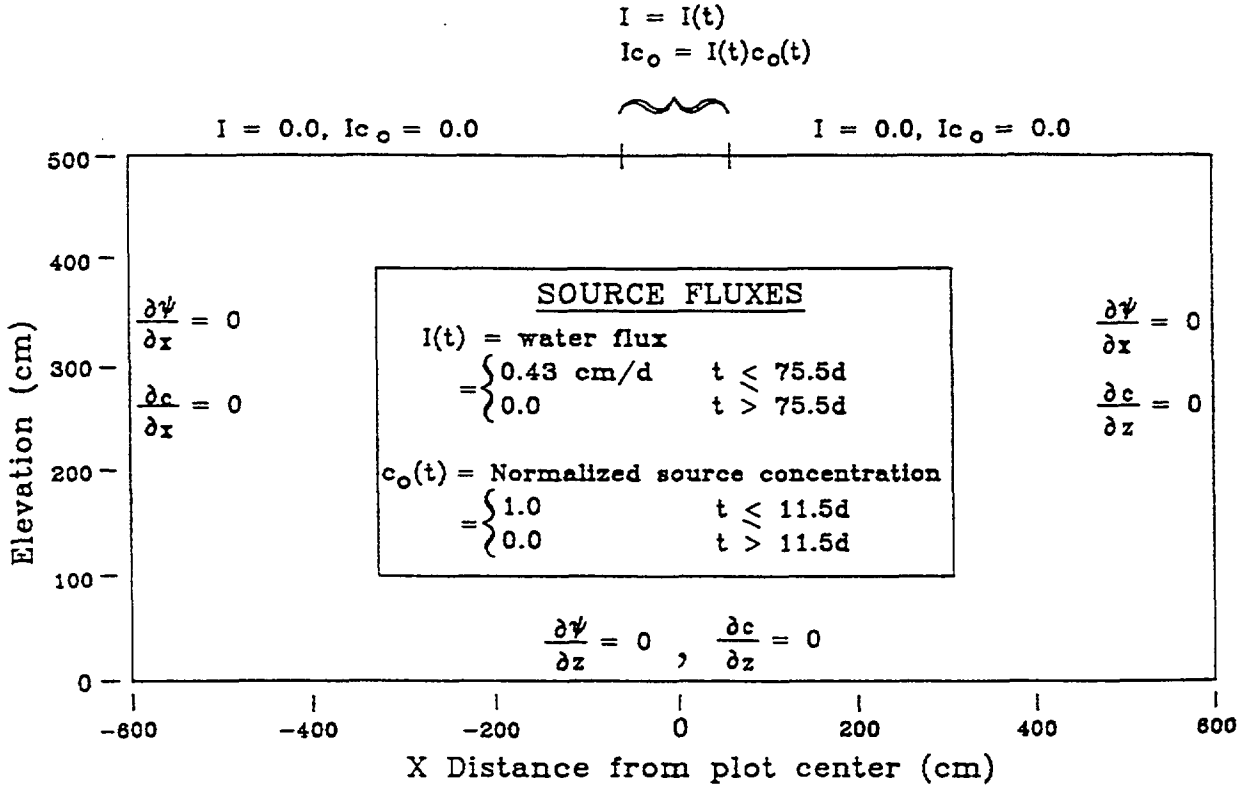

Figure 4. Schematic view of the modeled two-dimensional cross-section and assignment of boundary conditions.

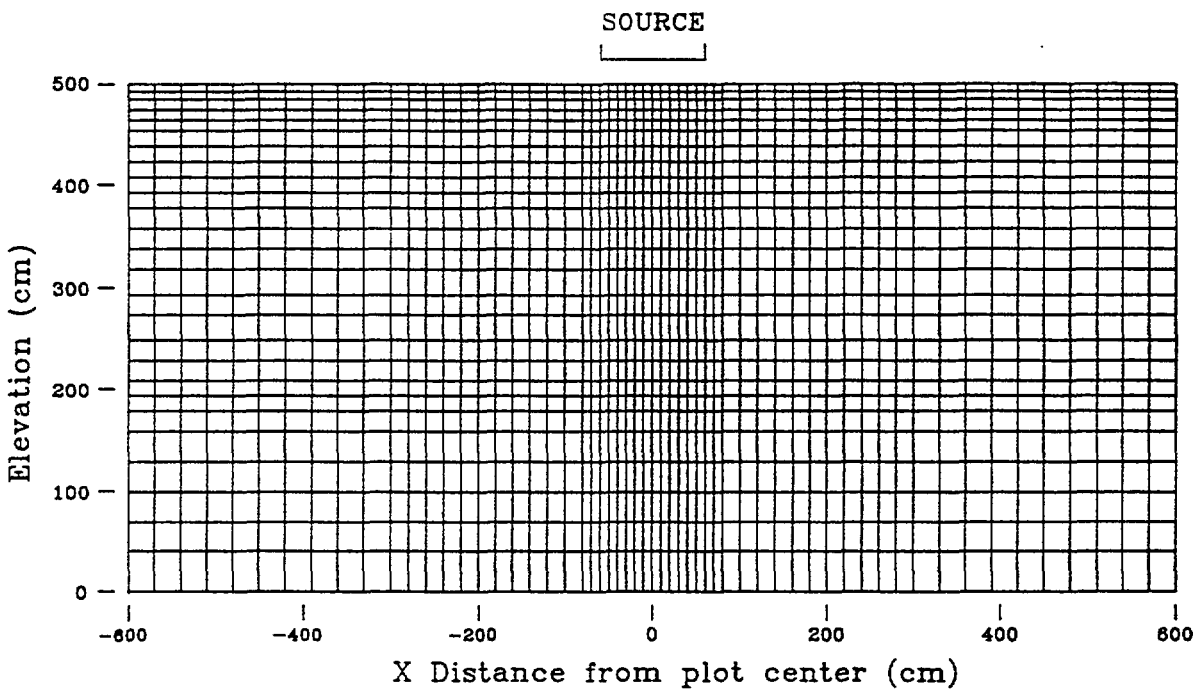

Figure 5. Finite element discretization used in VAM2D flow and transport simulations.

assigned time-dependent water and solute flux conditions corresponding to the water and solute applications in the field experiment. The lower boundary was assigned a zero pressure head gradient and zero concentration gradient condition. These conditions will allow the free-exit of water and solute through the boundary, and are a reasonable representation of physical conditions in a deep, well-drained soil.

The finite element discretization of the model domain is shown in Figure 5. A total of 1508 rectangular elements was used, with the element size varying from 10 x 10cm underneath the source to 30 x 30cm near the side and lower boundaries. The chosen discretization provided sufficient resolution in the flow and transport simulations without requiring excessive computational effort. Initial conditions and assignment of material zones were different for the various simulation scenarios considered, and are discussed below.

2.2.4 Flow and Transport Modeling Scenarios

An important aspect of the conceptualization underlying the flow and transport modeling was that soil hydraulic properties and their spatial distribution have a pronounced influence on flow and solute transport behavior. We therefore evaluated different simulation scenarios that employed varying amounts and detail of site specific hydraulic data for model calibration. Alternatively, these different simulation scenarios may be thought of as representing different conceptual models of the key factors controlling flow and solute transport of the trench site.

The different simulation scenarios/conceptual models were:

I. Uniform, isotropic soil with hydraulic properties of a typical sandy loam soil. This scenario used no site specific data for flow calibration.

IIa. Uniform isotropic soil with hydraulic properties given by averages obtained from trench soil core data.

IIb. Uniform, but anisotropic soil with soil hydraulic properties determined as in Scenario IIa, with exception of saturated hydraulic conductivity which was allowed to be anisotropic and calculated assuming a lognormal distribution of local K values.

IIc. As Scenario IIa, except that the effect of hysteresis in the moisture retention characteristic is accounted for in the computer simulation.

III. Non-uniform, isotropic soil with spatial variation of hydraulic properties and initial conditions reflecting as close as possible that obtained from soil core samples and neutron logging, respectively.

In each of the above scenarios, the initial condition for the flow simulations was defined in terms of moisture content(s) as measured at the site prior to the experiment. In order to convert these to initial pressure head(s) which are required for the VAM2D computer code, the inverse of (2) was used with appropriate values of the parameters θ_s, θ_r, α and β. It should be noted that

the individual soil core values of θ_r, α and β used for Scenarios II and III are different from the values given in the Las Cruces trench database (Wierenga et al., 1989). For a number of the soil cores, the θ_r values given in the database are larger than actual water contents measured in the field at the same x- and z- locations, prior to the initiation of water and solute application. This would imply that the initial pressure head at these locations was undefined. In reality the soil cores, which were collected inside the trench, and neutron probe measurements represent data from spatially different locations, i.e., different y-coordinate (see Figure 2) and the conflict between θ_r values in the database and actual measurements of water contents may be an artifact of modeling the site as a two-dimensional cross-section in which soil variations in the y-direction are ignored. On the other hand, the parameter θ_r in (2) is essentially a curve-fitting parameter and there is no physical objection to imposing certain constraints in the parameter estimation. A new set of values of θ_r, α and β was therefore determined for each soil core using the following procedure: The soil layer from which each core was collected was determined. An upper bound for θ_r was determined for each of the nine identified soil layers as slightly less than the minimum observed water content for that layer. θ_r, α and β were subsequently fitted again to the experimental θ (ψ) curves under this constraint. The resulting van Genuchten parameters for each core sample used in the VAM2D modeling are listed in Appendix A. The rationale and input parameter selection for each of the modeling scenarios are discussed below.

2.2.4.1 Scenario I

In this scenario it was assumed that very little site specific data was available for model calibration. This case corresponds to the situation, in practice not at all uncommon, where computer modeling is performed while little or no site characterization data is available and one has to estimate key model parameters. Since for the Las Cruces site there actually is quite a large amount of data available, it is possible to assess the accuracy of model predictions obtained with estimated parameters. This scenario represents a base case for evaluating the gain in accuracy obtained with the other modeling scenarios which do use site specific information. The soil in Scenario I was assumed to be uniform and isotropic. The only site specific information used was the soil textural classification (sandy loam) and an estimate of the initial water content. Estimated van Genuchten soil parameters for the sandy loam soil were obtained from the literature (Carsel and Parrish, 1988; see Table 1). The initial water content distribution was taken to be uniform and assigned a value of θ_i (x,z) = 0.10, which corresponds approximately to the actual average water content in the soil at the initiation of irrigation.

Table 1. Flow and Transport Parameter Values Used in VAM2D Simulations

	Modeling Scenario				
	I	IIa	IIb	IIc	III
Hydraulic Parameters					
K_{xx}; K_{zz}(cm/d)	106; 106	270; 270	1310; 655	270; 270	}
θ_s	0.410	0.320	0.320	0.320	} individually
θ_r	0.065	0.025	0.025	0.025	} assigned to
α (cm^{-1})	0.075	0.112	0.112	0.112; 0.224	} every element
β					}
Transport Parameters					
α_L (cm)	5.0	5.0	5.0	-	5.0
α_T (cm)	5.0	5.0	5.0	-	5.0
D^o (cm^2/d)	1.0	1.0	1.0	-	1.0

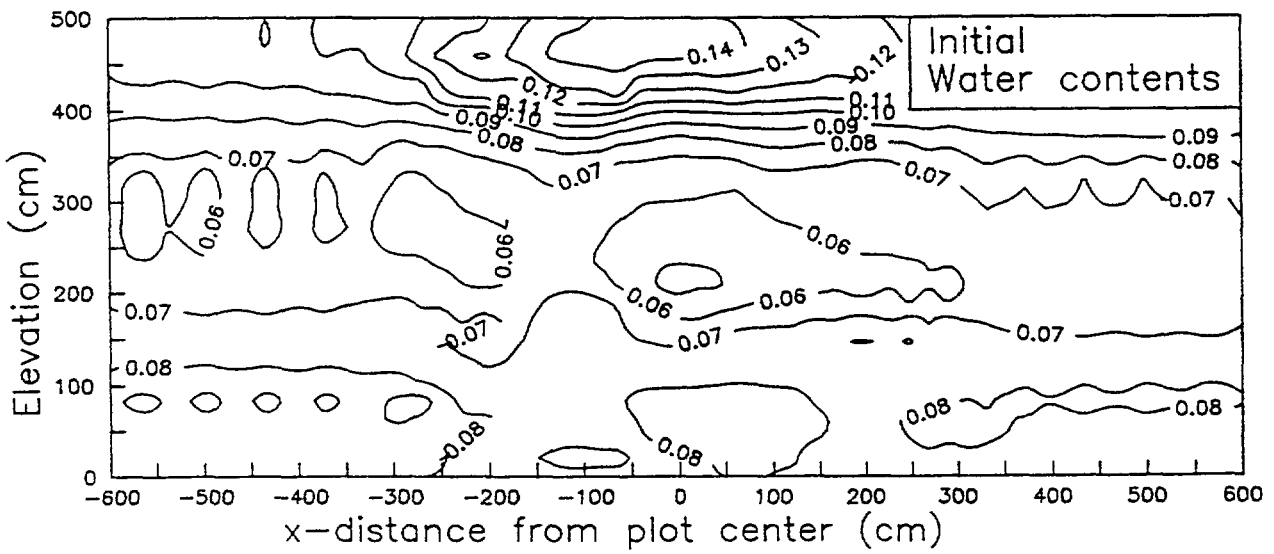

Figure 6. Initial water content distribution measured in central neutron probe row.

2.2.4.2 Scenario IIa

In this scenario, the soil was again taken to be uniform, but it was assumed that sufficient site characterization data were available to accurately define average values of the van Genuchten parameters. The values (Table 1) used are the averages of the parameters for the individual soil cores. This modeling scenario tests the assumptioin that any effects of local soil heterogeneity are averaged out at the scale of the field experiment, and that the experiment can thus be reproduced using averaged soil properties. The average values of parameters θ_r, θ_s, and α and β were calculated as arithmetic means of individual soil core values, while saturated conductivity was calculated as a geometric mean of individual soil core values (Wierenga et al., 1989). The initial water content distribution in Scenario IIa was obtained from field neutron probe readings taken just prior to the water and solute application. Data from the central row of neutron probe access tubes (Figure 2) were used. The field data (Figure 6) show a distinct variation of water content with depth, but more or less uniform water contents in the x-direction. The vertical variation of water contents was retained in the simulation, but a uniform water content in the x-direction was used, resulting in the modeled initial water content vertical distribution shown in Figure 7.

2.2.4.3 Scenario IIb

Scenario IIb is a variant of IIa; it was included in the simulation following evaluation of Scenario IIa, in order to improve the agreement between the VAM2D simulation and observed water content distributions following infiltration and redistribution. Scenario IIb differs from IIa in the way saturated hydraulic conductivity is evaluated. In Scenario IIb, the average hydraulic conductivity was computed assuming a lognormal distribution of individual K-values, i.e.,

$$\langle K \rangle = \exp(\mu_{ln} + 1/2\sigma^2_{ln}) \tag{13}$$

where μ_{ln} and σ_{ln} are the mean and standard deviation, respectively, of the log transformed K values of individual soil cores and angular brackets denote mean value. Additionally, the saturated hydraulic conductivity in this scenario was taken to be anisotropic with

$$\langle K_{xx} \rangle = 2 \langle K_{zz} \rangle \tag{14}$$

Since all soil cores were taken vertically downward, measured K-values represent vertical conductivities; the mean conductivity calculated from (7) thus estimates K_{zz}. The horizontal conductivity in Scenario IIb was simply assigned a value twice as large as the vertical value. Values of the hydraulic parameters used in this scenario are listed in Table 1.

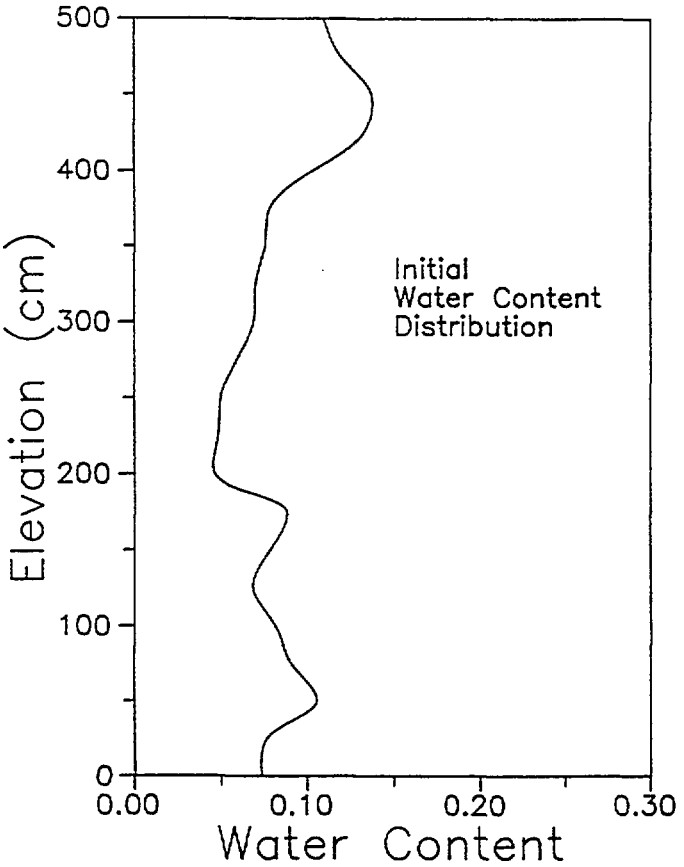

Figure 7. Depth variation of initial water content for Scenario IIa, IIb, and IIc.

2.2.4.4 Scenario IIc

This simulation was another variant of the second modeling scenario, designed to evaluate the possible influence of soil moisture hysteresis on infiltration and distribution of water. The VAM2D computer code has the ability to model hysteresis in the $\theta(\psi)$ relation, using the procedure described by Kool and Parker (1987). The general procedure for modeling hysteresis requires that soil moisture parameters describing both the drying and wetting branches of the soil moisture characteristic are specified. The code then keeps track of the state, either wetting or drying, as well as the appropriate $\theta(\psi)$ scanning curve of each element in the computational grid during the simulation, and evaluates the hydraulic properties accordingly. No actual data on soil moisture hysteresis are available for the trench site. Measured $\theta(\psi)$ relations all correspond to the main drying branch of the moisture characteristic. Lacking data on the wetting characteristic, the same average moisture parameter values were used for both wetting and drying branches, except that the α parameter for the wetting branch was assigned a value of twice the drying branch value, as recommended by Kool and Parker (1987). The resulting hysteretic moisture retention characteristic is shown graphically in Figure 8. It can be seen that the assumed ratio of $\alpha^w : \alpha^d = 2.0$, imposes only a modest degree of hysteresis. However, the ratio used is typical of undisturbed field soils (Kool and Parker, 1987).

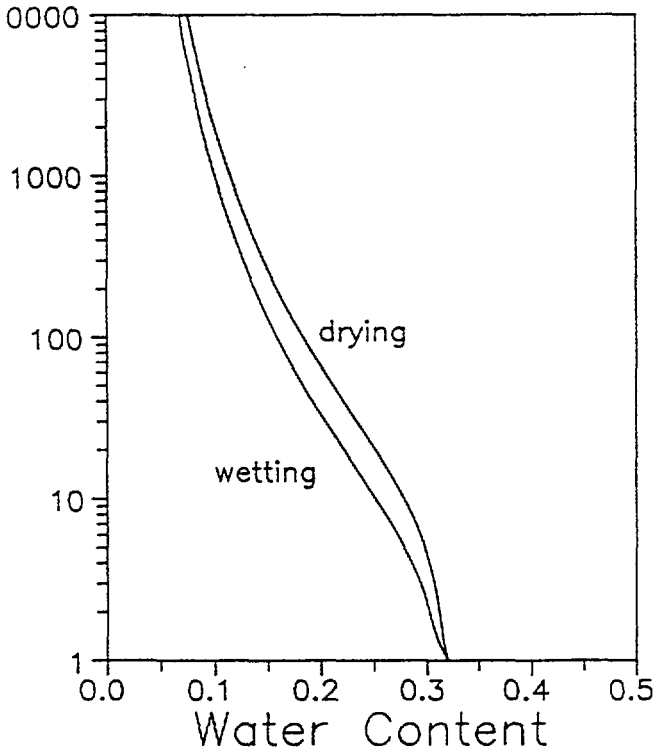

Figure 8. Wetting and drying moisture characteristic curves used in the hysteretic flow simulation (Scenario IIc).

2.2.4.5 Scenario III

In the final simulation scenario, all available data were utilized to determine spatially variable soil hydraulic properties and initial water contents. Material properties and initial water contents were allowed to vary from element to element. The van Genuchten parameter values describing hydraulic relationships at element centroids of the finite element grid were determined by spatially interpolating values from soil cores collected in a two-dimensional (x-z) grid inside the trench. Initial water contents were determined similarly from field neutron probe readings taken just prior to the field experiment. Measurements from the middle neutron probe row were used. Spatial interpolation was achieved by kriging. In the case of saturated hydraulic conductivity, the interpolation was performed on ln-transformed values. The resulting distribution of saturated conductivity is shown as an illustrative example in Figure 9. Although different material properties were assigned to each element in the computational grid, these hydraulic parameter values were determined from samples taken several meters away from the location of the actual infiltration experiment. It can thus not be expected that the elemental soil properties result in good point-wise correspondence with actual soil properties. However, invoking the assumption of ergodicity (Dagan, 1990), it is expected that the spatial variability of soil properties is reproduced in Scenario III, allowing a direct evaluation of the effects of local soil heterogeneity on simulated flow and transport behavior.

2.2.4.6 Solute Transport Parameters

Tritium and bromide were added as tracers during the first part of the irrigation experiment. Both tracers would be expected to behave as ideal, non-reactive tracers. Field concentration monitoring data however showed noticeable divergence of the tritium and bromide plumes. The probable cause is the influence of anion exclusion on bromide migration (Wierenga et al., 1990). For this reason, the transport simulations of a generic, non-reactive solute were compared against the tritium field data only. Radioactive decay of tritium during the simulation period was ignored. The error due to ignoring tritium decay is on the order of 4% at the end

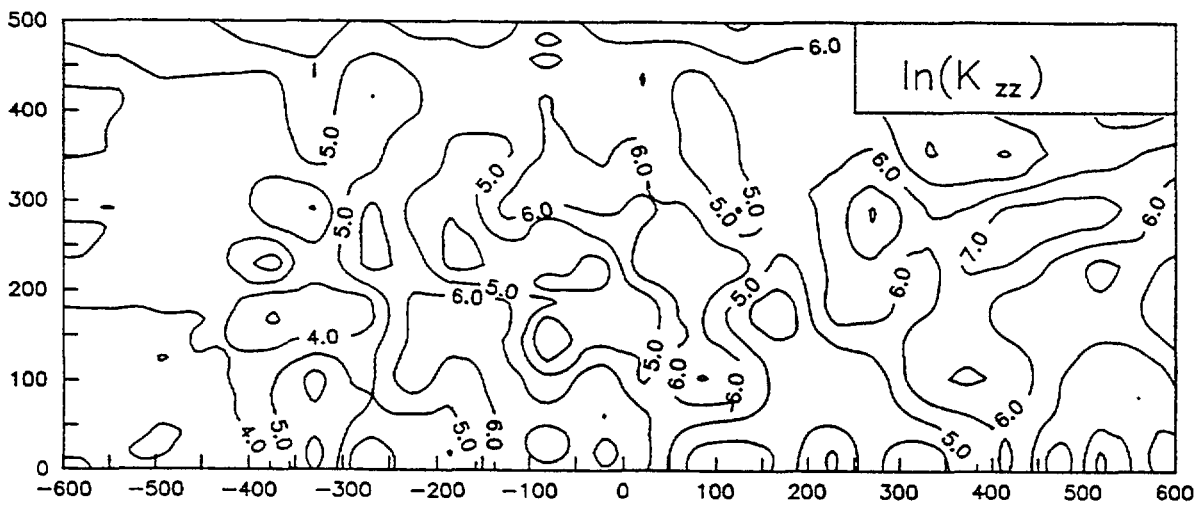

Figure 9. Spatial variation of ln K (cm/d) for Scenario III.

of the 277 day simulation period (Wierenga et al., 1990). The only additional parameters necessary for the transport simulations were therefore the longitudinal and transverse dispersivities, α_L and α_T, and the molecular diffusion coefficient, D°. In contrast to the detailed data on soil hydraulic properties, there is little data available on transport parameters for the Las Cruces trench. The following dispersion parameters were assumed for all simulations: $\alpha_L = \alpha_L = 5.0$ cm; $D^\circ = 1$ cm^2/d (Table 1). These values are the same as used by Wierenga et al. (1990) in their flow and transport simulations and thus facilitate comparison of their transport predictions with the VAM2D results. Since the value assigned to the dispersivity in the advection-dispersion transport model represents the uncertainty about local variations in pore water velocity, an argument can be made that larger dispersivity values should be used in the simulation with averaged hydraulic parameters (I, II), and a smaller dispersivity in the case of Scenario III. In the latter case the variation in hydraulic properties was described in detail, and thus a more accurate representation of local pore water velocity fluctuations would presumably be obtained in this case. The effect of varying dispersivity values was however not explored in this study.

2.3 MODEL EVALUATION CRITERIA

To evaluate flow and transport results for the different simulation scenarios, predicted water content and solute distributions at t=277 days after the start of irrigation were compared against field results. To accommodate the fact that different initial water content distributions were used, we follow the convention of Wierenga et al. (1990) to evaluate the flow simulations on the basis of water content changes, Θ, rather than actual water contents, where

$$\Theta(x,z,t) = \theta(x,z,t) - \theta(x,z,t=0) \qquad (15)$$

Two dimensional (x-z) field water content distributions were available from the three neutron probe rows installed parallel to the trench. If the actual flow regime in the field would have been two-dimensional, then the total water content increase measured along each individual neutron probe row should have been the same with differences only in the spatial distribution due to local soil heterogeneity. In reality, there were significant differences between the three sets of neutron probe data (Figure 10), indicating that appreciable three-dimensional flow occurred in the field. The observed water contents for the three sets of neutron probe tubes shown in Figure 10 show that the water content increase at y = 2 m distance from the trench is substantially less than expected assuming uniform application and true 2-D flow. Measurements at the center (y = 6 m) row of neutron probe tubes indicate an excess of moisture at this distance, while a mass-balance of the water contents at y = 10 m indicates that at this distance the water content increase agrees fairly well with the amount of applied water under 2-D flow conditions. Deviations from strictly 2-D flow were probably caused by the spatial variation of soil hydraulic properties and initial water content distribution. Non-uniformity in the water application during the irrigation period is expected to have contributed only little to the observed soil moisture distribution. To minimize the influence of three-dimensional flow in comparisons with the two-dimensional simulations, the water content data from the three neutron probe rows were averaged in the third dimension, i.e., along the y-axis. Tritium concentration data for transport modeling evaluation were available from a single two-dimensional grid of solution samplers, all of which were installed at a distance of 50 cm away from the trench face. The significance of lateral (y-direction) solute migration on measured concentration data could thus not be evaluated directly.

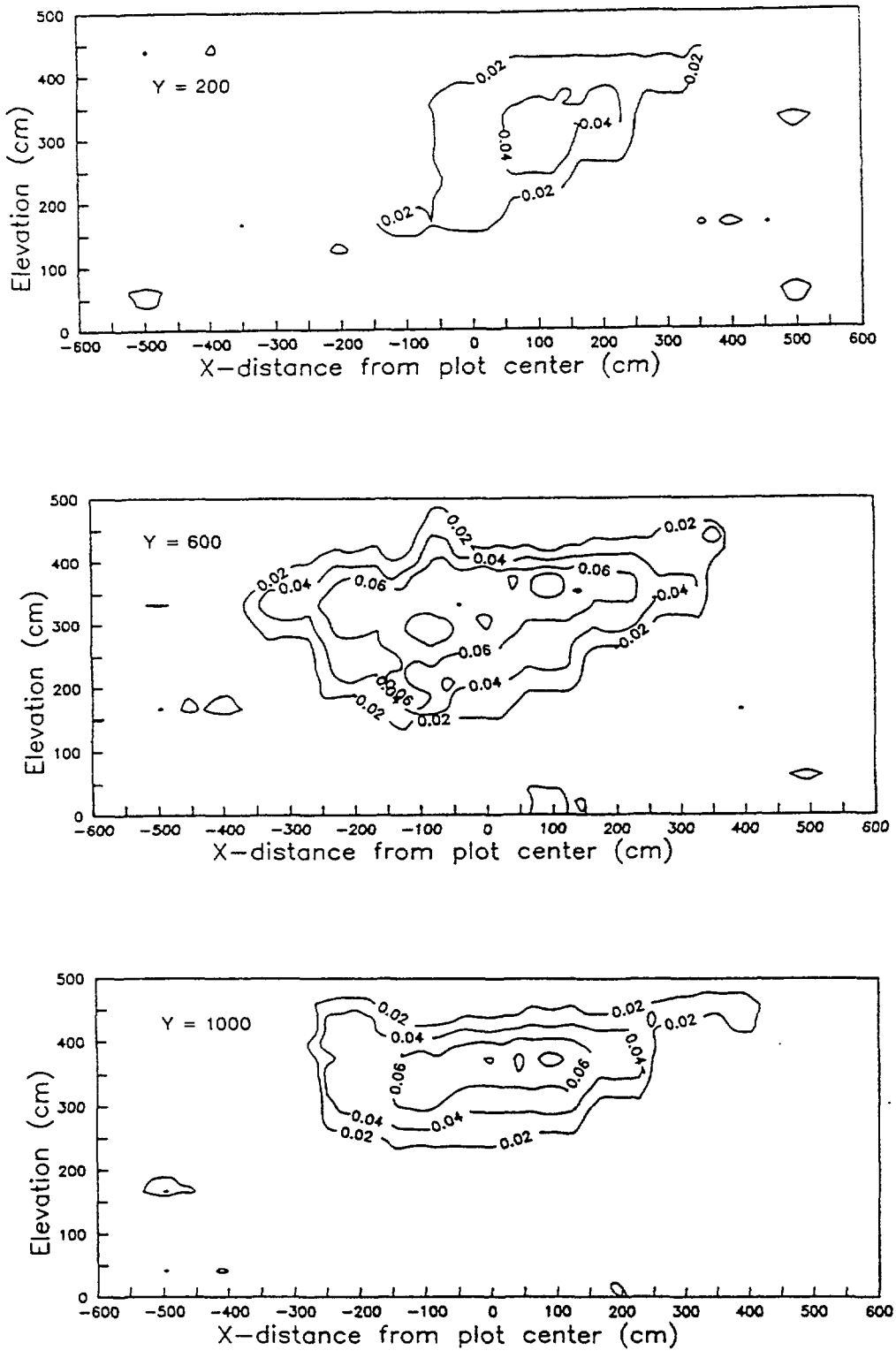

Figure 10. Water content increases at 276 days measured in three neutron probe rows; y-value indicates distance from trench face (cm).

In addition to visual comparisons of contour plots of field data and simulated results, spatial moments of water content and solute distributions were computed and compared. This provides a quantitative measure of the goodness of model predictions. The ij-th spatial moment of the water content change, $M^{\Theta}_{ij}(t)$, is defined as (Freyberg, 1986)

$$M_{ij}^{\Theta}(t) = \int_{-\infty}^{\infty} \int_{-\infty}^{\infty} \Theta(x,z,t)\, x^{i} z^{j} dx dz \tag{16}$$

Analogously, the ij-th moment of the solute mass distribution, $M^{c}_{ij}(t)$ is defined as

$$M_{ij}^{c}(t) = \int_{-\infty}^{\infty} \int_{-\infty}^{\infty} \theta(x,z,t)\, c\,(x,z,t)\, x^{i} z^{i} dx dz \tag{17}$$

Of most interest are the lower-order moments, i.e., the zero, first and second moments (i+j = 0, 1 or 2, respectively). The zero-th moment is equal to the total mass present in the system.

The first moments, normalized by total mass, define the location of the center of mass (Freyberg, 1986), in the x- and z- directions

$$x_c = M_{10}/M_{00} \tag{18a}$$

$$z_c = M_{01}/M_{00} \tag{18b}$$

The second normalized moment determines a spatial covariance tensor:

$$\sigma = \begin{bmatrix} \sigma_{xx} & \sigma_{xz} \\ \sigma_{zx} & \sigma_{zz} \end{bmatrix} \tag{19}$$

with

$$\sigma_{xx} = M_{20}/M_{00} - x_c^2 \,;\, \sigma_{zz} = M_{02}/M_{00} - z_c^2 \,;\, \sigma_{xz} = \sigma_{zx} = M_{11}/M_{00} - x_c z_c$$

The components of this covariance tensor provide a measure of the spread of the water and solute plumes about their center of mass. Since the zero-th moment (mass added) was the same in all modeling scenarios considered we used first and second moments to evaluate the model simulations.

3. RESULTS AND DISCUSSION

In this section, modeling results are presented and evaluated against field observations. Flow modeling is discussed first, followed by transport modeling.

3.1 FLOW MODELING

Results of the Scenario I, IIa and III simulations, as well as field results are presented in Figure 11. In all cases, contour plots of water content increases at the end of the simulation (t=277 days) are shown. The field results correspond to measurements at t=276 days. During the redistribution phase moisture movement was very slow, so that the 1 day time difference between simulation results and field data has negligible influence on the comparison. The field data represent averages from the three rows of neutron probes. By averaging the field data in the y-direction, most of the effects of three-dimensional flow could be removed. It should be noted however that the amount of water present in the averaged field results (Figure 10), is approximately 15% higher than it should be based on strictly 2-D flow. As a consequence, the field results appear somewhat "wetter" than any of the simulations. The field results show a distinct horizontal spreading of the moisture plume and rather irregular water content contours. The degree of horizontal spreading is not an artifact of the averaging applied to the field data, but was also exhibited by water content distributions measured along individual neutron probe rows (see Figure 10). The predicted moisture plumes for the four different modeling scenarios reproduced the observed results to varying degrees. The uniform soil Scenarios I and IIa predicted moisture plumes which are smooth and symmetric about the x=0 axis. Differences between Scenarios I and IIa are primarily due to differences in the assigned soil moisture retention curves (Figure 12). The curve obtained from the literature for Scenario I is a typical curve for a light textured (sandy loam) soil, with a rather abrupt decrease in water content at pressure heads below a few tens of centimeters. In contrast, the curve for Scenario II, which is a composite of individual soil core measurements shows a much more gradual change of water content with pressure head. As a result, Scenario I over-predicted the downward movement of water, while the applied irrigation was retained as shallower depths in Scenario IIa, which agrees better with observed results. The horizontal spread of the plume between 350 and 400 cm elevation in Scenario IIa reflects the influence of depth-varying initial water contents. Scenario III resulted in quite good visual agreement with field observations. Although this heterogeneous soil scenario did not necessarily result in accurate point-wise prediction of field results, it did reproduce the observed non-symmetric plume shape and irregular water content contours. Upon closer inspection it can be seen that the horizontal spreading in the simulation occurs mostly around the edges of the water plume. The contours in the wetter center of the plume indicate more dominantly downward flow. In contrast, the field data show distinct horizontal spreading at all contour levels. This was exhibited both by the average result as well as by data from the individual neutron probe rows.

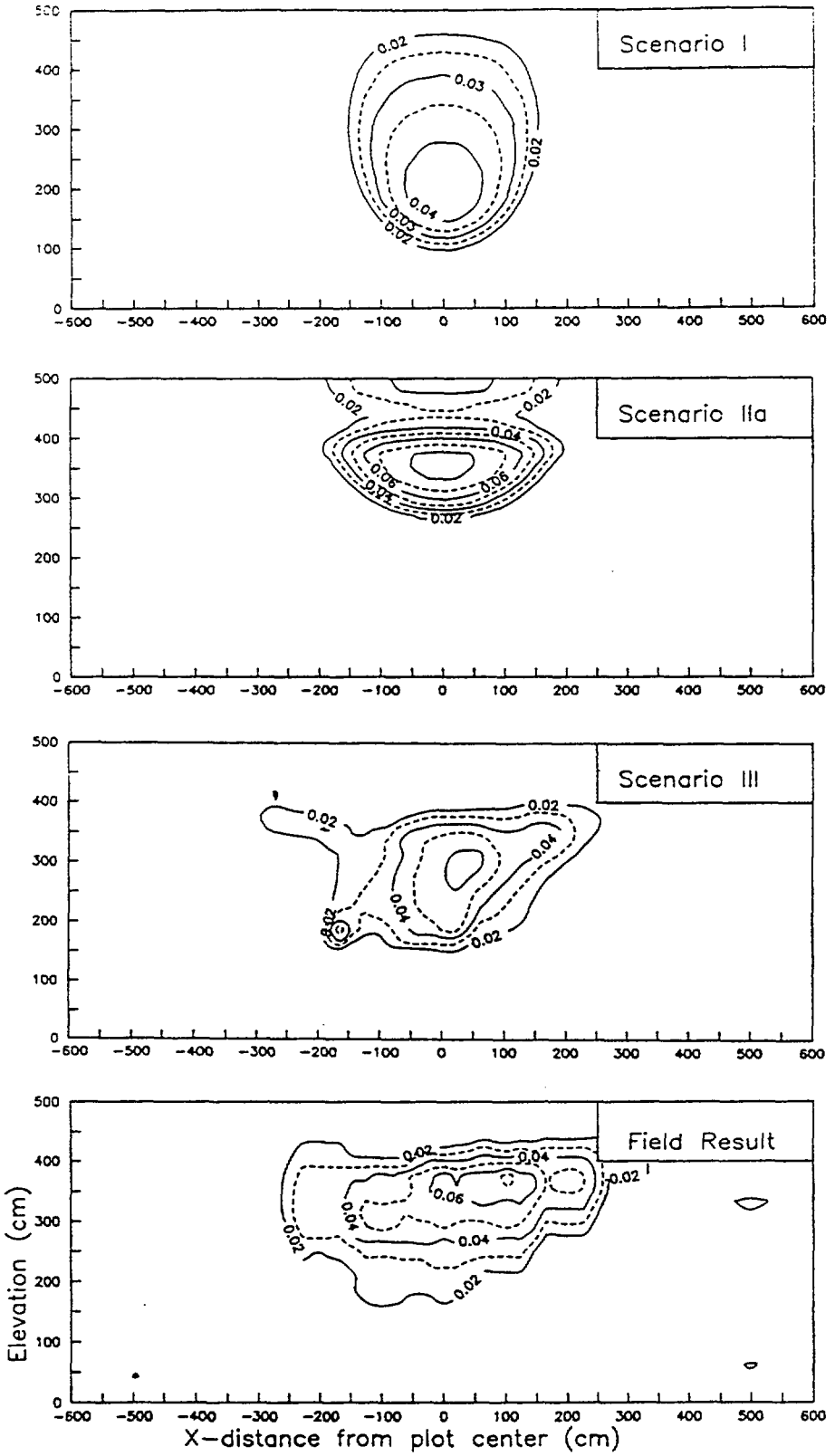

Figure 11. Comparison of predicted water plumes at t=277 days for Scenarios I, IIa, and III with field results.

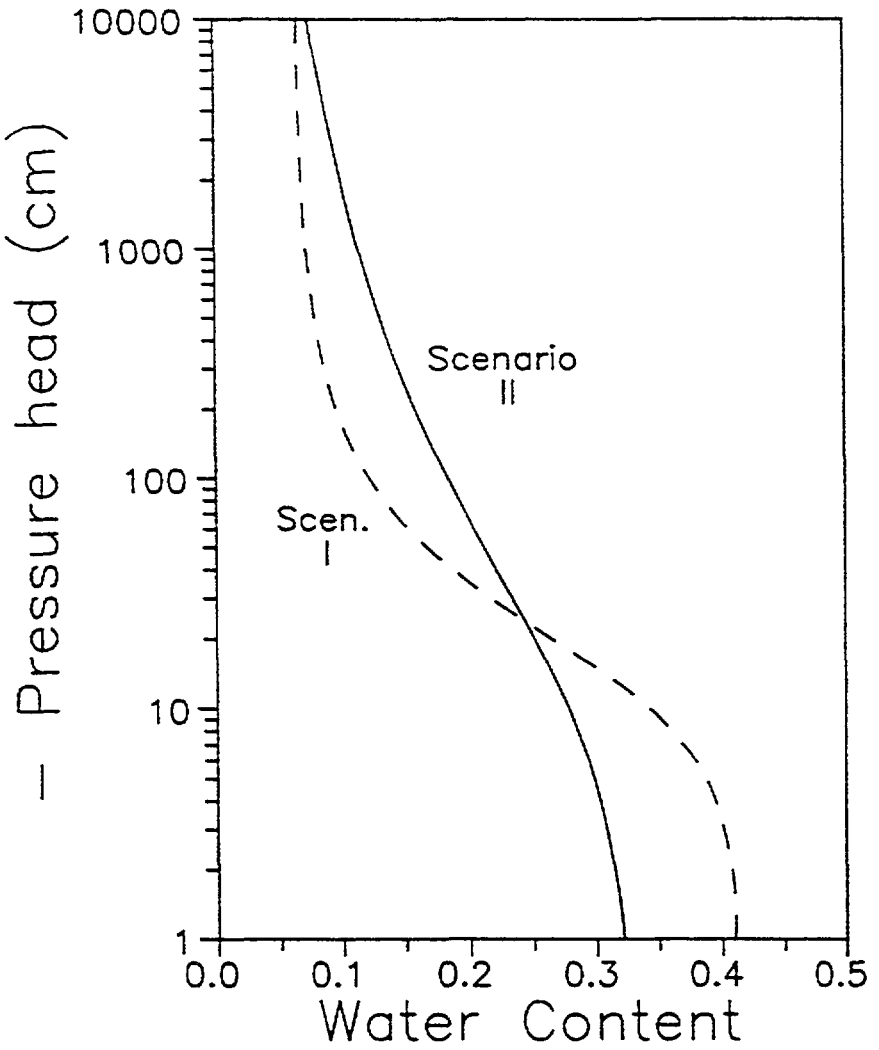

Figure 12. Soil water retention curves used in the Scenario I and II flow modeling.

Comparison of Scenario IIa and III results indicates that explicit consideration of soil variability, as opposed to using averaged soil properties, results in better agreement with field observations. One of the features of both the field data and Scenario III modeling results is the distinct horizontal spreading of the moisture plume. The horizontal spreading was not reproduced at all in the uniform soil scenario I. Some spreading can be seen in the result for scenario IIa. The spreading in the plume reflects the vertically non-uniform initial condition used in this model scenario. The degree of horizontal spreading was however much less than observed in the field. The observed spreading resembles the effect of anisotropy in soil hydraulic properties. It is unknown to what extent the actual soil at the trench site is anisotropic (see below). All soil cores were taken vertically downward, and parameters measured from these cores, especially saturated conductivity, thus represent vertical values. In the case of the Scenario III simulation, the apparent anisotropy was strictly a result of the local variability of soil properties, since isotropy was assumed in the modeling.

In order to evaluate the effect of anisotropy on modeling results, a variant of Scenario IIa was included in the modeling as Scenario IIb. The purpose of Scenario IIb was to see to what extent field results could be reproduced by assuming anisotropy in an otherwise uniform soil. In Scenario IIb, the average value of hydraulic conductivity, i.e., $\langle K_{zz} \rangle$, was recalculated assuming a lognormal distribution of conductivity values. The horizontal conductivity was then assigned a value of twice the mean vertical conductivity to produce the desired anisotropic effect. Flow results for Scenario IIb are compared with field results and with results from Scenario III in Figure 13. It can be seen that a 2:1 anisotropy ratio induced horizontal spreading similar to that observed in the field. The vertical spread of the Scenario IIb plume however, was less than either that observed in the field or predicted by Scenario III. The mean conductivity in Scenario IIb was calculated from a lognormal distribution, rather than as a geometric mean as in Scenario IIa. The former value is about 2.5 times greater than the geometric mean value. The main motivation for using the larger value in Scenario IIb was to obtain sufficient vertical plume movement in the simulation. Using the geometric mean value in the anisotropic simulation resulted in a much too low predicted plume depth after 277 days. Lognormal probability distributions of saturated hydraulic conductivity have quite often been observed in hydrologic studies (e.g., Peck, 1983; Sudicky, 1986) and this lends some justification to the procedure for calculating $\langle K \rangle$. Interestingly though, the actual probability distribution of saturated conductivity of core samples from the Las Cruces trench does not appear to follow a lognormal distribution. The experimental data could not be described well with either a normal, lognormal or exponential distribution (Goodrich and Davis, 1989). Comparison of soil core and in-site conductivity measurements does suggest higher K-values in the horizontal than vertical direction. However, conclusive data does not exist on the actual existence and magnitude of hydraulic conductivity anisotropy at the site. The *a priori* justification for selecting the hydraulic conductivity values in Scenario IIb is thus rather slim. Nevertheless, the simulation demonstrates that the infiltration of water in heterogeneous soil could be reproduced reasonably well by assuming anisotropy in an otherwise uniform soil.

Other factors that could influence the degree of horizontal spreading of the moisture plume are the presence of layers with different hydraulic properties and the influence of hysteresis in the soil moisture characteristic. Quite possibly, the observed result may reflect the influence of a combination of factors. Nine different soil layers have been identified in the upper 6 m of the soil profile at the site (Wierenga et al., 1989). The different layers have been

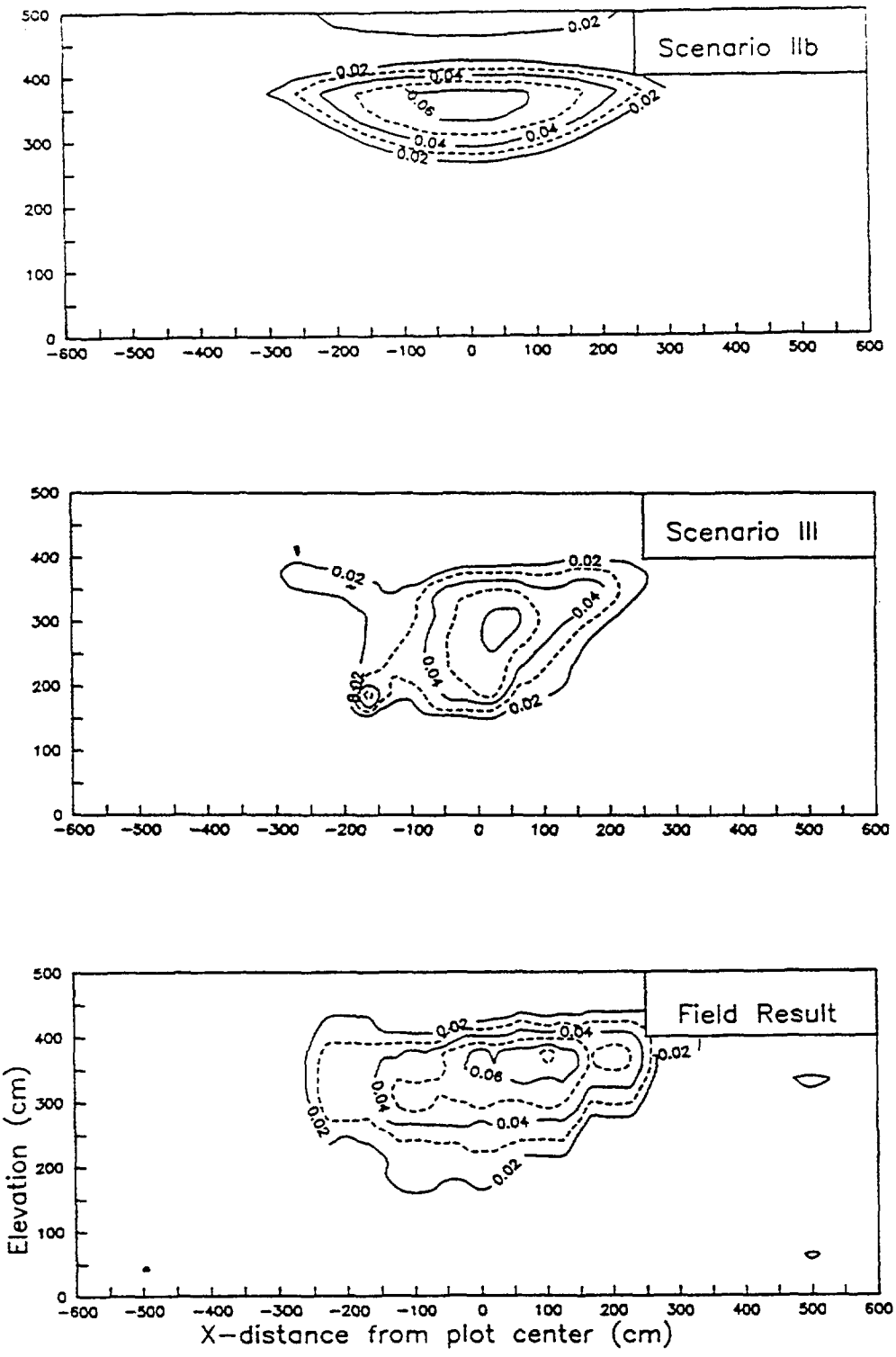

Figure 13. Comparison of predicted water plumes at t=277 days for Scenarios IIb and III with field results.

distinguished based on visual criteria which may or may not correlate with differences in hydraulic properties. Average values of the van Genuchten parameters for each of the morphological soil layers have been calculated also (Wierenga et al., 1989). These values indeed show differences between layers. A statistical analysis of saturated hydraulic conductivity values has been conducted by Sandia National Laboratories (Goodrich, 1990). This analysis suggested that three, rather than nine, layers with significantly different saturated hydraulic conductivity exist. The analysis did not consider hydraulic parameters other than the saturated conductivity. Unsaturated flow behavior though, will depend on interactions between the entire set of parameters defining the hydraulic constitutive relations. Since this is a complex interrelationship, it is not straight-forward to relate flow responses to differences in individual model parameters. Collin et al. (1990) have directly evaluated the impact of vertical soil variations on unsaturated flow modeling by simulating the trench experiment using a layered model with layer boundaries and properties taken from Wierenga et al. (1989). Their layered model thus falls in between the Scenarios IIa and III considered here. It was found that the layered model resulted in better agreement with experimental data especially in terms of lateral spreading than did a uniform soil model. This suggests that the presence of hydraulically contrasting, although individually uniform and isotropic soil layers may have contributed to the apparent anisotropic flow behavior observed in the field.

Another possible explanation for the observed flow behavior is that the lateral spreading reflects the influence of hysteresis in the soil moisture retention characteristic. The expected effect of hysteresis on moisture movement would be to enhance water movement during the wetting phase and retard movement during the redistribution phase. The moisture retention characteristic of porous media is well known to be hysteretic, although the effect on unsaturated flow, particularly in heterogeneous and imperfectly known field soils is less clear. This is a result of both a paucity of data and a lack of modeling tools that have capability to account for hysteresis. VAM2D is one of the few multi-dimensional computer codes that have this capability. In the absence of data on capillary hysteresis, a number of additional assumptions were made for the hysteretic flow simulation (Scenario IIc). The experimental moisture retention data for the trench site all represent primary drainage curves. As a first approximation, soil wetting and drying moisture characteristics can often be described with the same set of van Genuchten parameters, with the value of parameter α for the wetting curve set to twice the value of the drying curve (Kool and Parker, 1987). To verify the possible significance of hysteresis, a variant of the scenario IIa incorporating hysteresis with $\alpha^w = 2\ \alpha^d$ (See Figure 8) was simulated.

In a hysteretic simulation it must also be specified whether the initial condition corresponds to a wetting or drying condition. The upper meter of the soil at the field site was probably in a wetting condition as a result of rainfall in the weeks prior to covering the soil. The initial condition in the lower part of the soil is uncertain. However, since this part of the profile was quite dry, assuming either wetting or drying conditions leads to the same result since the wetting and drying retention curves converge at the prevailing low pressure heads. For simplicity therefore, the entire profile was assigned an initial wetting condition in the simulations. Other than allowing for hysteresis, this simulation was identical to Scenario IIa. Results for the hysteretic case are depicted in Figure 14. To facilitate comparison, the original simulation results for Scenario IIa are shown also. It can be seen that accounting for hysteresis does indeed lead to different flow predictions. However, the effect of hysteresis is to reduce, rather than enhance lateral spreading. The results presented in Figure 14 show that in the hysteretic simulation the

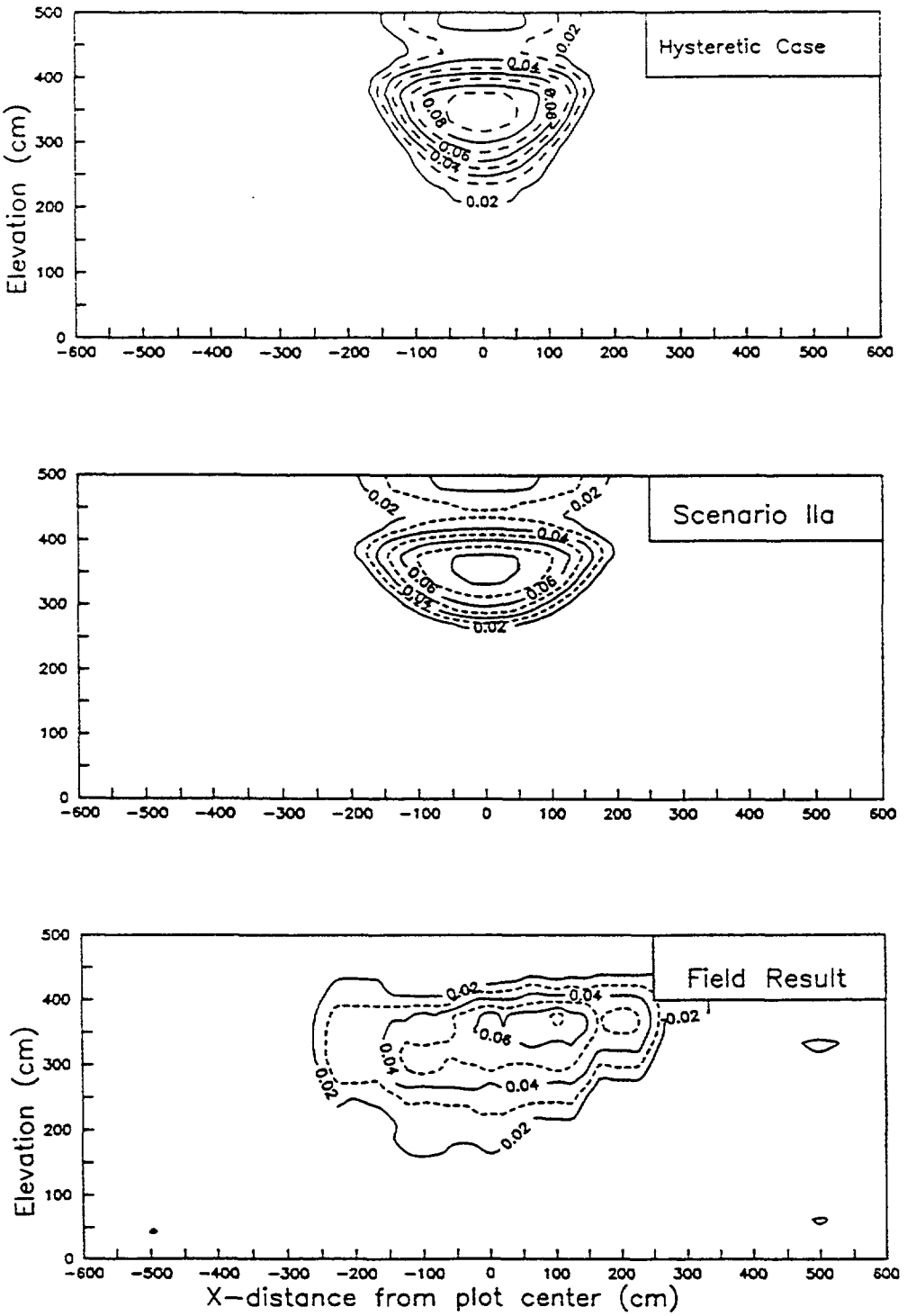

Figure 14. Predicted moisture plume at t = 277 days for hysteretic case (Scenario IIc) compared with the non-hysteretic simulation (Scenario IIa) and field result.

vertical plume penetration depth after 277 days is greater, while the lateral plume extent is less, than the original simulation of Scenario IIa. The reason for this behavior is that the field experiment represents a wetting event, and water movement is determined primarily by the wetting branch of the moisture retention characteristic. The shape of the wetting $\theta(\psi)$ curve in the hysteretic simulation is similar to the $\theta(\psi)$ curve used in modeling scenario I, and the moisture distribution simulated by scenario IIc approximates the result of scenario I. This results in greater downward movement and less lateral spreading of the moisture plume at the end of the 277 day period compared to the simulation based on the drying branch of the moisture retention characteristic used in the original Case IIa scenario. The effect of hysteresis in the simulation is completely the opposite of the observed field behavior. This suggests that capillary hysteresis either does not have a significant effect on water movement, or if hysteresis is present, its influence is masked by other, opposing processes.

First and second values of the plume moments (Table 2) confirm conclusions from the visual plume comparisons. Since the effect of hysteresis in the field experiment was apparently not significant, the Scenario IIc was omitted from the moment analysis. All modeling scenarios predict essentially vertical downward movement of the plume center-of-mass, i.e., a negligible value for M_{10}. In contrast, the field results show a distinct sideways movement of the moisture plume. The extent of downward movement of the plume center-of-mass (M_{01}) is overpredicted in Scenarios I and III, but underpredicted in Scenarios IIa and IIb. The amount of under- and overprediction, respectively, in Scenarios IIb and III, is about the same. The plume second moments clearly illustrate the horizontal spreading of the moisture plume observed in the field. The spread of the plume is approximated most closely in Scenario III, while it can be seen again that Scenario I results in a poor prediction of the plume shape; this scenario predicts a vertically, rather than horizontally, elongated plume.

Table 2. Normalized Spatial Moments of Simulated and Observed Water Plumes

Moments		Scenario I	IIa	IIb	III	Field
M_{10}	(cm)	-0.4	0.3	0.4	7.3	60.5
M_{01} [1)]	(cm)	287.2	376.4	366.3	274.4	318.9
M_{20}	(cm^2)	8272.4	28984.9	43978.8	52826.4	60109.5
M_{02}	(cm^2)	11086.4	6650.0	6676.3	7112.7	8859.1

1) Reflects z-coordinate convention used in modeling, i.e., z is positive upwards with soil surface at z=500 cm.

In summarizing the results of the VAM2D flow simulations, it is clear that the most accurate result is obtained with the Scenario III simulation which accounts on closely as possible for local scale soil heterogeneity. A key feature of the observed field behavior, namely the lateral spreading of the moisture plume, can be reproduced by allowing for anisotropy in the saturated conductivity. Since no data on directional hydraulic conductivities are available, it is not possible to determine how significant local anisotropy actually is, or whether the apparent anistropy results solely from local soil heterogeneities. The good results obtained with simulation Scenario III suggest that the latter explanation may be the most appropriate.

The notion that the effect of local heterogeneities may manifest itself as an apparent large scale anisotropy is supported theoretically by stochastic unsaturated flow models developed by L.W. Gelhar and co-workers at MIT. One conclusion from this work is that the anisotropy of effective conductivity in unsaturated media is dependent on the mean pressure head. Yeh et al. (1985) have presented the following expression for the apparent anisotropy of hydraulic conductivity under unit gradient flow with soil layering parallel to the x-axis:

$$\frac{\hat{k}_{xx}}{\hat{k}_{zz}} = \exp\left[\frac{\sigma_f^2 + \sigma_a^2\psi^2}{1 + A\lambda}\right] \qquad (20)$$

where ^ denotes effective value and A, λ, σ_f and σ_a are soil dependent parameters related to the mean, isotropic, hydraulic conductivity and its spatial covariance function. Specifically, σ_f^2 is the variance of the log saturated conductivity (ln [K_s]), $A = d\ln k_r/d\psi$ is the mean value of the slope of the ln k_r (ψ) relation, σ_a^2 is the variance of A, and λ is the correlation length in the direction perpendicular to the soil layering. The stochastic flow theory as represented by (20) suggests that soils which behave as uniform media under relatively wet conditions will exhibit increasing effects of heterogeneity as they become drier. Inspection of (20) shows that it predicts that the apparent anisotropy will vary as the exponential of pressure head squared. Equation (20) can be incorporated in a numerical flow solution in a straight-forward manner, and provided the necessary statistical parameters are known, it allows evaluation of this aspect of the stochastic unsaturated flow theory in an otherwise deterministic flow simulation. McCord et al. (1988) have used (20) in numerical simulations of subsurface water and solute movement along a hillslope and have obtained good qualitative agreement between simulations and observed data. The implementation of (20) in VAM2D is discussed by Huyakorn et al. (1989), following in part suggestions of Polmann et al. (1988). Polmann et al. (1988) also provide values of the parameters in (20) for the Las Cruces site, and which are summarized in Table 3. First of all, it may be noted that (20) provides an expression for the anisotropy ratio, but not for the actual, directional relative permeabilities themselves. In order to obtain the desired, monotonically decreasing $\hat{k}_{xx}$ (ψ) and $\hat{k}_{zz}(\psi)$ relations, an empirical logarithmic interpolation procedure was developed which ensures that both $\hat{k}_{xx}$ and $\hat{k}_{zz}$ decrease with decreasing pressure head while maintaining the correct anisotropy ratio for any ψ value.

Table 3. Statistical parameters describing the anisotropic k_r (ψ) relation. Parameter values from Polmann et al. (1988).

Parameter	Value
A (cm^{-1})	0.117
σ_a^2 (cm^{-2})	0.0007
σ_f^2	0.36
λ (cm)	25.0

In implementing the algorithm in the VAM2D code, it was found that the predicted anisotropy ratio is quite sensitive to the chosen values of A and σ_a^2. The stochastic theory is based on an exponential relationship between relative permeability and pressure head

$$k_r = e^{\alpha\psi} \tag{21}$$

where

$$\alpha = A + a \tag{22}$$

and a is the local variation of A, with zero mean and variance σ_a^2. In the original theory, A is constant, independent of ψ. When a different relative permeability relation, such as the van Genuchten relation (3) is employed, A is no longer a constant but becomes a function of ψ. With the van Genuchten $k_r(\psi)$ relation, the corresponding value of A will decrease as the pressure head ψ becomes more negative. For instance, using the van Genuchten $k_r(\psi)$ relation for the Las Cruces trench soil, with parameters from the averaged $\theta(\psi)$ data (Scenario II), the value of the slope of ln k_r decreases from A = 0.57 near saturation to A = 10^{-3} at ψ = -2500 cm. Using a variable A therefore tends to considerably magnify the predicted degree of anisotropy. Recognizing this, Polmann et al. (1988) suggested that it would be reasonable to assume a constant coefficient of variation for A, i.e., a fixed ratio of σ_a/A. However, in this case σ_a^2 will vary as A squared which in turn will tend to reduce the predicted anisotropy. To illustrate these different effects, the predicted anisotropy ratio for the Las Cruces trench soil is plotted in Figure 15 using (20) with different ways of calculating A and σ_a^2. When these parameters are fixed at their nominal value (Table 3), the predicted anisotropy ratio increases quickly with decreasing pressure head, up to 7 orders of magnitude at ψ = 300 cm. When A is treated as a variable and computed from the van Genuchten $k_r(\psi)$ relation with constant σ_a^2 = 0.0007, the computed anisotropy ratio becomes even more extreme. On the other hand, when σ_a^2 and A are both treated as variables with a fixed ratio σ_a/A, the anisotropy is effectively suppressed. In this latter case, the predicted anisotropy remains less than 1.5 over the entire range of pressure heads. The extreme sensitivity of predicted anisotropy to different, plausible ways of evaluating model parameters is clearly a problematic aspect of incorporating the algorithm into a general purpose simulator like VAM2D. This aspect of the stochastic theory is not explored further. Rather, in subsequent analyses, the parameters A and σ_a were both treated as constants with values as given

in Table 3, i.e., the modeled anisotropy ratio for the Las Cruces trench site is represented by the solid curve in Figure 15. The applicability of (20) for the trench experiment was evaluated through additional flow simulations. The Scenario IIa average hydraulic parameters were used together with (20). The result of this simulation is shown in Figure 16. As in the previous figures, the results are shown in terms of the increase in water contents after 277 days. The simulation predicts a large degree of horizontal spreading of the applied irrigation water and relatively little vertical penetration of the plume. Compared to the field result, the apparent anisotropy is significantly overpredicted by the model. The computed anisotropy ratio in the simulation is around 7:1 or 8:1 in the center of the plume and reaches much higher values at the drier fringes of the plume. As shown in the simulation of

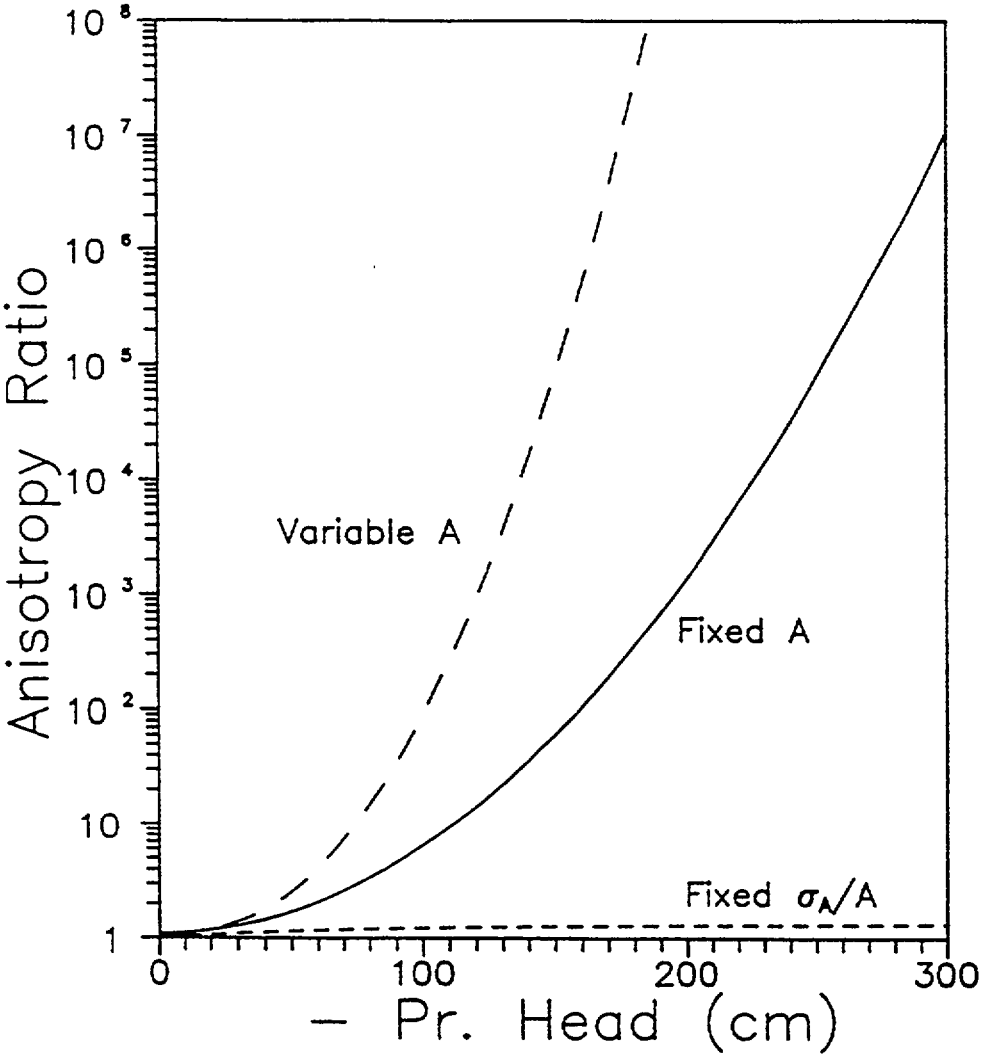

Figure 15. Anisotropy ratio as a function of pressure head, ψ, predicted from (20) with parameters for the Las Cruces trench site from Polmann et al. (1988) and different ways of evaluating A and σ_a.

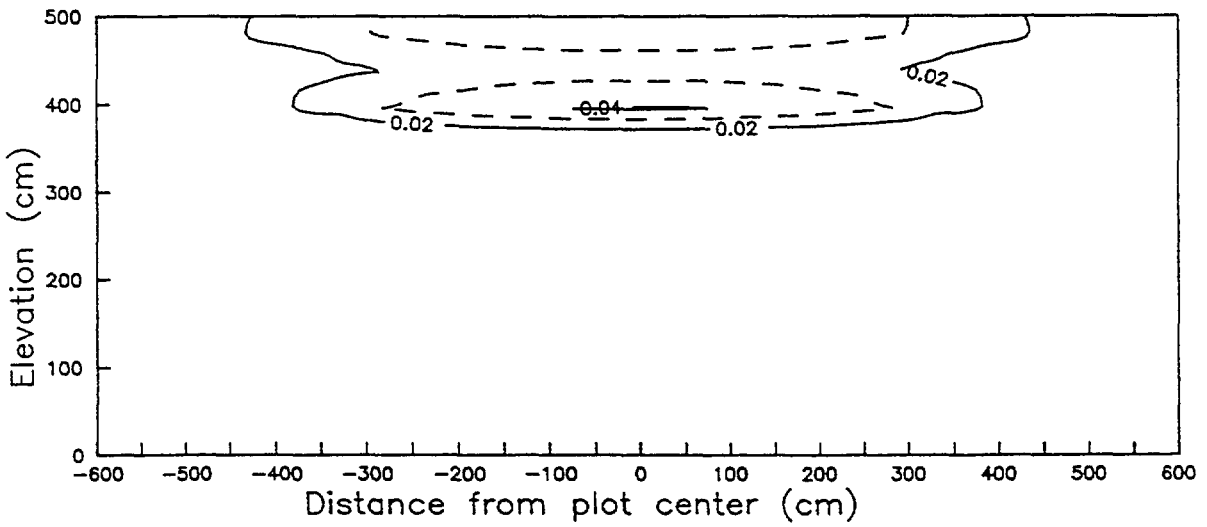

Figure 16. Moisture plume at t = 277 predicted using pressure head dependent anisotropy of the relative permeability.

scenario IIb, the apparent anisotropy ratio in the field result is approximately 2:1. Estimating the effective anisotropy factor from the stochastic flow theory via (20) results in a poor prediction of the field experiment. As mentioned, McCord et al., (1988) have reported good qualitative agreement between field observations of solute transport in unsaturated soil and simulations employing (20). A possible explanation for the poor results obtained here, compared to the findings of McCord et al., is the drier conditions of the trench experiment. It may well be that while the assumptions and simplifications embodied in (20) hold in relatively wet soils, they failed under the much drier conditions of the second Las Cruces Trench experiment.

3.2 SOLUTE TRANSPORT MODELING

Tritium transport was simulated for the four Scenarios I, IIa, IIb, and III; Scenario IIc involving hysteresis was not considered in the transport analysis. As mentioned, the same dispersion parameters were used in all cases; differences in transport predictions thus reflect differences in flow simulations. Predicted tritium profiles were compared with data from in-situ solution samplers. As only one set of solution samplers was installed, there is no spatial averaging of concentration data as was done for the field water content data. Nor is it possible to directly evaluate the extent of three-dimensional solute migration. Predicted concentration contours for the four modeling scenarios are compared with field tritium data in Figure 17. First and second spatial moments of the solute mass distribution are given in Table 4.

Table 4. Normalized Spatial Moments of Simulated and Observed Tritium Plumes

Moments		Scenario I	IIa	IIb	III	Field[1)]
M_{10}	(cm)	0.0	0.0	0.0	17.8	-10.9
M_{01}[2)]	(cm)	361.8	405.5	418.3	367.5	423.7
M_{20}	(cm^2)	4338.0	5578.9	9019.8	7379.1	9967.9
M_{02}	(cm^2)	4623.0	2608.9	2165.2	5757.1	2352.9

1) Computed using water content data from nearest neutron probes at y=200 cm.

2) Reflects z-coordinate convention used in modeling, i.e., z is positive upwards with soil surface at z=500 cm.

In calculating the field moments, water content measurements from the neutron probe row at y=200 cm (i.e., nearest the solution samples) were used in (17). As expected, the predicted tritium plume for each scenario follows the flow results shown in Figures (11) and (13). Compared to the flow results in Figures 11 and 13, it can be seen that the solute front in all cases lags behind the water front. This is due to a "snowplow" effect in the flow modeling, in which displaced antecedent water is pushed ahead of the infiltrating water and solute front. The predicted depth of tritium penetration is significantly greater for Scenarios I and III than observed in the field. The overall plume shape for Scenarios IIa and IIb shows better agreement with the field result. Upon closer inspection it is seen however, that the concentration values observed in the field are substantially larger than maximum values in any of the four simulation scenarios. The highest measured relative concentration value at t=277 days was about 0.45, while none of the predicted concentrations was higher than 0.17. A partial reason for this discrepancy may have been overestimation of dispersivities and thus greater spreading in the modelled results. However, this cannot explain the apparently much larger solute mass measured in the field than was present in the simulation results. As mentioned, the solute mass present in the simulations was equal to the applied mass to within about 2%. The recovered field solute mass cannot be directly calculated since there were no coincidental water content and concentration measurements. The high concentration measurements in the field may in fact reflect much lower actual than predicted water contents at the solution sampler locations. Water content data from the nearest neutron probe row at y=200 cm from the trench show indeed much lower than average water contents (Figure 10). However, even if these water contents are combined with measured tritium concentration data, the resulting solute mass as estimated by the zero-th moment of the field tritium distribution is still approximately 80% higher than the actually applied amount based on uniform application and two-dimensional transport. Lacking more spatially detailed solute data, it can only be surmised that the high concentration values observed in the field represent a solute and/or water content distribution that is highly uneven in the y-direction. Since the discrepancy with simulated results is so large, the field observations cannot really be used to judge the

individual simulations. Still, it is of some interest to note that Scenario III, which resulted in the best flow predictions, does not result in the closest transport predictions. Based on the first and second spatial moments (i.e., plume shape); Scenario IIb results in the best approximation of the field solute distribution.

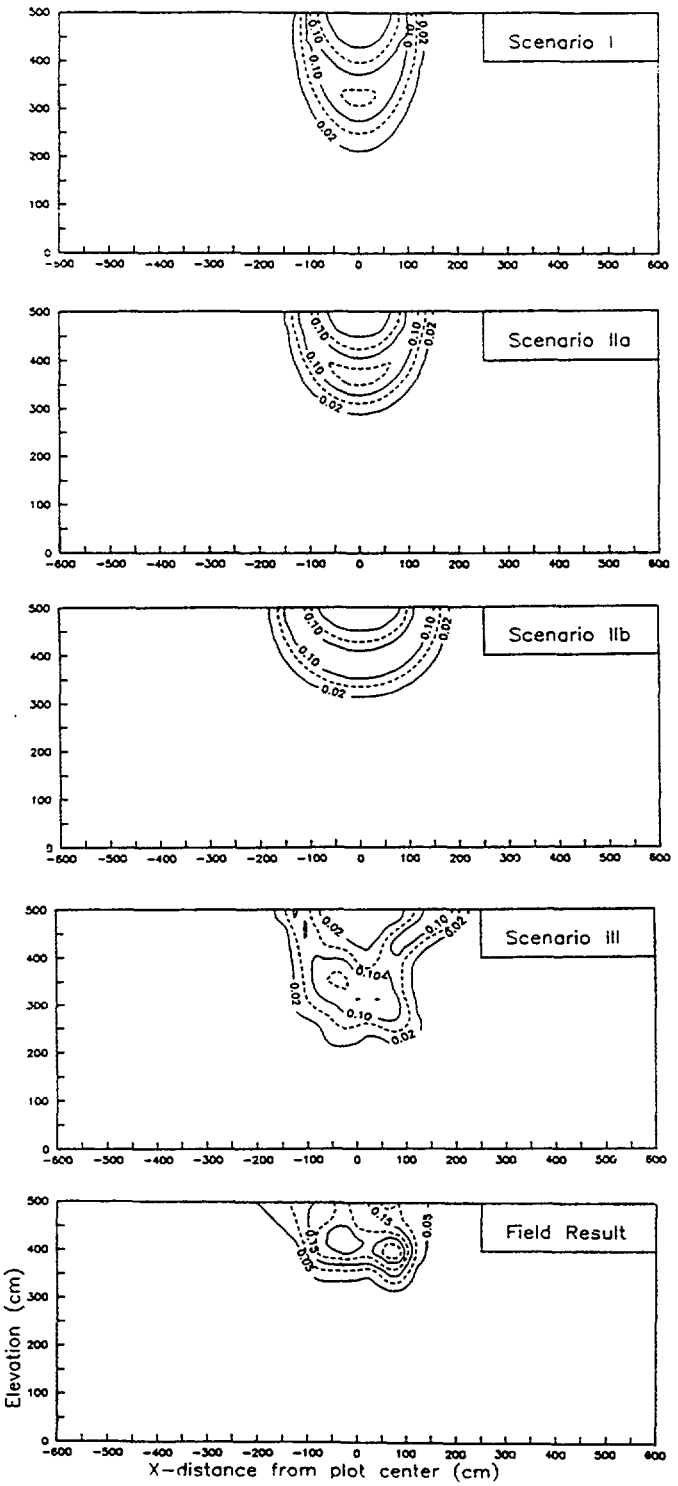

Figure 17. Predicted concentration distributions at t=277 days for four modeling scenarios and field results.

4. CONCLUSIONS

The first observation in evaluating modeling results of the second trench experiment against field flow and transport data, is the significant influence of three-dimensional flow and transport in the field. Even though the field experiment was designed to produce two-dimensional flow and transport, as much as 40% of the applied water may have moved in the lateral y-direction (INTRAVAL 1989 Progress Report). Water content data from three rows of neutron probes access tubes are available. By averaging data in the third dimension (y-direction) it was possible to minimize the 3-D flow effects and obtain a set of field results that can be used to evaluate the two-dimensional modeling results. Only one set of measured concentration data is available. Coupled with the lack of coincidental water content measurements, the available concentration data are too limited to provide a basis for rigorously evaluating the transport modeling results.

The flow simulations indicate the strong influence of soil heterogeneity on water infiltration and redistribution. In evaluating the flow simulations, we observe that in two cases, Scenario IIb and III, good agreement with field data was obtained. The use of non-site specific model calibration data in Scenario I on the other hand resulted in poor predictions. Results of the Scenario IIc suggest that hysteresis is not a significant factor in this experiment. It should be noted that no parameter adjustment was performed in Scenario III in order to match the field results. Scenario IIb on the other hand, was included as one of the modeling scenarios following evaluation of Scenario IIa. Hydraulic parameters for IIb were deliberately chosen to reproduce the observed horizontal plume spread.

We did not obtain very good agreement between observed and simulated tritium transport. The ability to quantitatively evaluate the solute transport simulations is limited due to the lack of coincident water content and concentration data and the lack of spatial resolution in the solution sampler data, especially with respect to three-dimensional solute migration. There was significant water movement in the third (y-) dimension and presumably the same applies to solute movement in the experiment. Based on predicted and observed tritium plume shapes, the uniform but anisotropic soil model (Scenario IIb) yielded results at least as good as the simulation based on the more complex, heterogeneous soil model (Scenario III). It would probably be wrong to conclude from this that the Scenario IIa represents a more accurate description of the actual field site than Scenario III. However, this fact does illustrate that when the conceptualization of important processes is incomplete (e.g., ignoring 3D migration) and/or when sufficient data for model calibration and validation are lacking, a more complex model may not provide any more reliable results than a simpler model.

These results suggest the desirability of incorporating as much information as possible about soil heterogeneity in a computational model. In the absence of detailed data, it may be possible to account for the effects of soil variability as an apparent large scale anisotropic effect. It is less clear, however, how to a priori determine the effective anisotropy or even, as illustrated in the case of calculating the effective mean saturated hydraulic conductivity, how to average variable soil properties to obtain a meaningful effective value. The finding that local soil heterogeneity may manifest itself as an apparent large scale anisotropy, agrees qualitatively with conclusions from stochastic flow theories developed at MIT. In this case, however, we were not successful in using the stochastic theory to predict the large scale hydraulic conductivity. This may reflect a deficiency in the underlying theory, or alternatively, the hazards of using an isolated

result from this theory, i.e., Equation (20), outside of the context of the stochastic theory of which it is a part.

Finally, referring back to the first objective of this study, the simulations of the Las Cruces trench experiment have proven to be a very valuable test for the computational routines employed in VAM2D. Difficulties encountered in initial simulations have led to further improvements to the numerical schemes used in VAM2D. Simulations reported here used the various procedures discussed in Section 2.2.2 to achieve an accurate and numerical solution. Our results show that it is indeed feasible to obtain accurate and mass-conservative solutions to the variably saturated flow and transport equations, even when sharp saturation fronts are present, provided the numerical schemes are internally consistent and coefficients are evaluated in a consistent and appropriate manner.

Celia, M.A., and E.T. Bouloutas, and R.L. Zarba, 1990. A general mass-conservative numerical solution for the unsaturated flow equation. Wat. Resour. Res., 26: 1483-1496.

Collin, M., M. Lindgren, and A. Rasmuson, 1990. Flow and transport simulations of the second Las Cruces trench experiment, INTRAVAL Case 10, Report No. KEMAKTA AR 90-04, KEMAKTA Consultants Co., Sweden (DRAFT).

Cooley, R.L., 1983. Some new procedures for numerical solution of variably saturated flow problems, Water Resour. Res., v. 19, 1271-1285.

Dagan, G., 1989. flow and transport in porous formations. Springer-Verlag, Berlin Heidelberg, 465 pp.

Freyberg, D.L., 1986. A natural gradient experiment on solute transport in a sand aquifer 2. Spatial moments and the advection and dispersion of non-reactive tracers. Wat. Resour., Res., 13:2031-2046.

Goodrich, M.T., and P.A. Davis, 1989. A statistical analysis of the Las Cruces trench hydraulic data. INTRAVAL workshop, Helsinki, Finland.

Hills, R.G., I. Porro, D.B. Hutson, and P.J. Wierenga, 1989. Modeling one-dimensional infiltration into very dry soils, 1. Model development and evaluation. Wat. Resour. Res., 25:1259-1269.

Hornung, U., and Messing, W., 1984. Poröse Medien - Methoden und Simulation. Verlag Beiträge zur Hydrologie, Kirchzarten, F.R.G.

Huyakorn, P.S., J.B. Kool, and J.B. Robertson, 1989. VAM2D - Variably saturated analysis model in two dimensions. Report No. NUREG/CR-5352, U.S. Nuclear Regulatory Commission, Washington, D.C.

Huyakorn, P.S., J.W. Mercer, and D.S. Ward, 1985. Finite element matrix and mass balance computational schemes for transport in variably saturated porous media, Water Resour. Res., v. 21: 346-358.

Huyakorn, P.S., S.D. Thomas, and B.M. Thompson, 1984. Techniques for making finite elements competitive in modeling flow in variably saturated porous media, Water Resour. Res., v. 20: 1099-1115.

Huyakorn, P.S., S.D. Thomas, and B.M. Thompson, 1984. Techniques for making finite elements competitive in modeling flow in variably saturated porous media. Wat. Resour. Res., 20:1099-1115.

Huyakorn, P.S., and G.F. Pinder, 1983. Computational Methods in Subsurface Flow, Academic Press, Orlando, Florida, 474 pp.

Kool, J.B., and J.C. Parker, 1987. Development and evaluation of closed-form expressions for hysteretic soil hydraulic properties, Water Resour. Res., v. 23: 105-114.

McCord, J.T., D.B. Stephens, and J.W. Wilson, 1988. Field experiments and numerical simulations of unsaturated flow and transport: The roles of hysteresis and state-dependent anisotropy. Proceedings Nato Advanced Study Institute on Recent Advances in Modeling Hydrologic Systems, Sintra, Portugal, July 9-23.

Millington, R.J., and J.M. Quirk, 1961. Permeability of porous solids. Trans. Faraday Society, 57: 1200-1207.

Milly, P.C.D., 1985. A mass-conservative procedure for time-stepping in models of unsaturated flow. Adv. Wat. Resour., 8:32-36.

Peck, A.J., 1983. Field variability of soil physical properties. In: Advances in Irrigation, Vol. 2. Academic Press, Inc.

Polmann, D.M., E.G. Vomvoris, D. McLaughlin, E.M. Hammick, and L.W. Gelhar, 1988. Application of stochastic methods to the simulation of large-scale unsaturated flow and transport. Report No. NUREG/CR-5094, U.S. Nuclear Regulatory Commission, Washington, D.C.

Robertson, J.B., 1984. Geologic problems at low-level radioactive waste sites; cn: Groundwater Contamination, National Research Council, National Academy Press, p. 104-109.

Russo, D., and G. Dagan, 1991. On solute transport in heterogeneous porous formation under saturated and unsaturated water flows. Wat. Resour. Res., 27:285-292.

Shipers, L.R., and C.P. Harlan, 1989. Background information for the development of a low-level waste performance assessment methodology. Volume 2: Assessment of relative significance of migration and exposure pathways. Report No. NUREG/CR-5453, U.S. Nuclear Regulatory Commission, Washington, D.C.

Sudicky, E.A., 1986. A natural gradient experiment on solute transport in a sand aquifer: Spatial variability of hydraulic conductivity and its role in the dispersion process. Wat. Resour. Res., 22:2069-2082.

van Genuchten, M. Th., 1982. A numerical model for water and solute movement in and below the rootzone. Research Report No. 121, USDA-ARS, U.S. Salinity Laboratory, Riverside, CA (DRAFT).

van Genuchten, 1980. A closed-form equation for predicting the hydraulic conductivity of unsaturated soils. Soil Sci. Soc. Am. J., 44:892-898.

Wierenga, P.J., D.B. Hudson, R.G. Hills, I. Porro, M.R. Kirkland, and J. Vinson, 1990. Flow and transport at the Las Cruces trench site, Experiments 1 and 2. Report No. NUREG/CR-5607, U.S. Nuclear Regulatory Commission, Washington, D.C.

Wierenga, P.J., A.F. Toormann, D.B. Hudson, J. Vinson, M. Nash, and R.G. Hills, 1989. Soil Physical properties at the Las Cruces trench site, Report No. NUREG/CR-5441, U.S. Nuclear Regulatory Commission, Washington, D.C.

Wierenga, P.J., 1988. Validation of flow and transport models at the Jornada test facility. In: P.J. Wierenga & D. Bachelet (Eds.), Validation of Flow and Transport Models for the Unsaturated Zone: Conference Proceedings. Research Report 88-55-04, New Mexico State University.

Wierenga, P.J., L.W. Gelhar, C.S. Simmons, G.W. Gee, and T.J. Nicholson, 1986. Validation of stochastic flow and transport models for unsaturated soils: A comprehensive field study. Report No. NUREG/CR-4622, U.S. Nuclear Regulatory Commission, Washington, D.C.

Yeh, T.-C. J., L.W. Gelhar, and A.L. Gutjahr, 1985. Stochastic analysis of unsaturated flow in heterogenous soils 2. Statistically anisotropic media with variable α. Wat. Resour. Res., 21:457-464.

APPENDIX

Values of van Genuchten
Soil Parameters for Individual
Soil Cores Used in the
VAM2D Simulations

This Appendix contains the values of the van Genuchten hydraulic parameters for each of the individual soil cores collected from the trench. The values that are given here are the ones used in simulation scenarios IIa-c and III. These values are different from the ones given in the Las Cruces trench database since an upper limit was set for the parameter θ_r (WCR) in the fitting procedure, based on the minimum observed water content for each soil layer in the field. Imposing constraints on θ_r affects the fitted values of parameters α and β also. The following information is provided:

Sample ID number	SAMPLE
x-coordinate of sample location (m)	x
y-coordinate of sample location (m)	y
z-coordinate of sample location (m)	z
Saturated water content	WCS
Residual water content	WCR
Parameter α (cm^{-1})	ALPHA
Parameter β	BETA

The sample ID number is the same as used in the Las Cruces trench database (Wierenga et al., 1989). The sample location is given using the convention used throughout this report; the origin for the x-coordinate axis is the center of irrigation plot #2, the origin for the y-axis trench face with positive y-values away from the trench, and the origin for the z-axis is at 5 m below the soil surface, with positive z-values going upward. The y-coordinate for all samples was constant, i.e. all samples were collected from transects parallel to the long axis of the trench and inside the trench at a distance of 60 cm from the trench face (y=-0.6 m). Missing parameters are assigned a numerical value of -999.

SAMPLE	X	Y	Z	WCS	WCR	ALPHA	BETA
1-1	-3.78	-0.60	4.94	0.345	0.0350	0.05966	1.5512
1-2	-3.28	-0.60	4.94	0.352	0.0350	0.06320	1.5273
1-3	-2.78	-0.60	4.94	0.323	0.0350	0.05445	1.4862
1-4	-2.28	-0.60	4.94	0.311	0.0350	0.05449	1.5824
1-5	-1.78	-0.60	4.94	0.329	0.0350	0.05279	1.4984
1-6	-1.28	-0.60	4.94	0.301	0.0350	0.04776	1.6520
1-7	-0.78	-0.60	4.94	0.288	0.0350	0.04801	1.5453
1-8	-0.28	-0.60	4.94	0.300	0.0350	0.04473	1.6543
1-9	0.22	-0.60	4.94	0.315	0.0350	0.04642	1.5491
1-10	0.72	-0.60	4.94	0.381	0.0350	0.03894	1.8007
1-11	1.22	-0.60	4.94	0.335	0.0350	0.04089	1.5313
1-12	1.72	-0.60	4.94	0.345	0.0350	0.05017	1.5496
1-13	2.22	-0.60	4.94	0.364	0.0350	0.04995	1.4942
1-14	2.72	-0.60	4.94	0.343	0.0350	0.05296	1.5021
1-15	3.22	-0.60	4.94	0.342	0.0350	0.04992	1.6663
1-16	3.72	-0.60	4.94	0.309	0.0350	0.04614	1.5663
1-17	4.22	-0.60	4.94	0.318	0.0350	0.04582	1.4875
1-18	4.72	-0.60	4.94	0.333	0.0350	0.03867	1.5751
1-19	5.22	-0.60	4.94	0.347	0.0350	0.03984	1.6613
1-20	5.72	-0.60	4.94	0.341	0.0350	0.03810	1.5817
1-21	6.22	-0.60	4.94	0.341	0.0350	0.02804	1.6524
1-22	6.72	-0.60	4.94	0.384	0.0350	0.03866	1.6471
1-23	7.22	-0.60	4.94	0.343	0.0350	0.03501	1.5037
1-24	7.72	-0.60	4.94	0.364	0.0350	0.03583	1.5236
1-25	8.22	-0.60	4.94	0.351	0.0350	0.03150	1.5693
1-26	8.72	-0.60	4.94	0.342	0.0350	0.03865	1.4851
1-27	9.22	-0.60	4.94	0.312	0.0350	0.03974	1.4770
1-28	9.72	-0.60	4.94	0.364	0.0350	0.03726	1.5925
1-29	10.22	-0.60	4.94	0.360	0.0350	0.05774	1.5650
1-30	10.72	-0.60	4.94	0.334	0.0350	0.05403	1.4410
1-31	11.22	-0.60	4.94	0.322	0.0350	0.03133	1.4715
1-32	11.72	-0.60	4.94	0.376	0.0350	0.04706	1.5334
1-33	12.22	-0.60	4.94	0.320	0.0350	0.03194	1.4852
1-34	12.72	-0.60	4.94	0.335	0.0350	0.03631	1.5652
1-35	13.22	-0.60	4.94	0.327	0.0350	0.03008	1.6256
1-36	13.72	-0.60	4.94	0.339	0.0350	0.03524	1.6003
1-37	14.22	-0.60	4.94	0.334	0.0350	0.03176	1.5801
1-38	14.72	-0.60	4.94	0.336	0.0350	0.03852	1.4842
1-39	15.22	-0.60	4.94	0.341	0.0350	0.03053	1.5847
1-40	15.72	-0.60	4.94	0.369	0.0350	0.03960	1.5264
1-41	16.22	-0.60	4.94	0.397	0.0350	0.04616	1.5933
1-42	16.72	-0.60	4.94	0.373	0.0350	0.05281	1.5808
1-43	17.22	-0.60	4.94	0.357	0.0350	0.04259	1.5727
1-44	17.72	-0.60	4.94	0.342	0.0350	0.04324	1.5082
1-45	18.22	-0.60	4.94	0.381	0.0350	0.04256	1.5934
1-46	18.72	-0.60	4.94	0.359	0.0350	0.03193	1.6296
1-47	19.22	-0.60	4.94	0.332	0.0350	0.03521	1.5424
1-48	19.72	-0.60	4.94	0.338	0.0350	0.04241	1.4720
1-49	20.22	-0.60	4.94	0.342	0.0350	0.04496	1.5219
1-50	20.72	-0.60	4.94	0.366	0.0350	0.04944	1.5214
2-1	-3.78	-0.60	4.29	0.285	0.0350	0.08740	1.3351
2-2	-3.28	-0.60	4.29	0.277	0.0350	0.08741	1.3621
2-3	-2.78	-0.60	4.29	0.291	0.0350	0.06872	1.3242
2-4	-2.28	-0.60	4.29	0.270	0.0350	0.07109	1.3718
2-5	-1.78	-0.60	4.29	0.312	0.0350	0.11595	1.4226
2-6	-1.28	-0.60	4.29	0.293	0.0350	0.14284	1.4310
2-7	-0.78	-0.60	4.29	0.286	0.0350	0.09702	1.4118

SAMPLE	X	Y	Z	WCS	WCR	ALPHA	BETA
2-8	-0.28	-0.60	4.29	0.297	0.0350	0.10246	1.3407
2-9	0.22	-0.60	4.29	0.280	0.0350	0.07352	1.4248
2-10	0.72	-0.60	4.29	0.288	0.0350	0.08009	1.3238
2-11	1.22	-0.60	4.29	0.351	0.0350	0.12479	1.3488
2-12	1.72	-0.60	4.29	0.338	0.0350	0.09980	1.3552
2-13	2.22	-0.60	4.29	0.357	0.0350	0.06086	1.3438
2-14	2.72	-0.60	4.29	0.356	0.0350	0.08459	1.3269
2-15	3.22	-0.60	4.29	0.348	0.0350	0.07686	1.3032
2-16	3.72	-0.60	4.29	0.385	0.0350	0.07555	1.3717
2-17	4.22	-0.60	4.29	0.305	0.0350	0.05054	1.3811
2-18	4.72	-0.60	4.29	0.369	0.0350	0.03730	1.2742
2-19	5.22	-0.60	4.29	0.371	0.0000	0.06875	1.1997
2-20	5.72	-0.60	4.29	0.314	0.0350	0.04153	1.3094
2-21	6.22	-0.60	4.29	0.298	0.0350	0.03079	1.4943
2-22	6.72	-0.60	4.29	0.309	0.0350	0.04127	1.4286
2-23	7.22	-0.60	4.29	0.360	0.0350	0.04886	1.4245
2-24	7.72	-0.60	4.29	0.325	0.0350	0.04489	1.3546
2-25	8.22	-0.60	4.29	0.353	0.0350	0.02586	1.3781
2-26	8.72	-0.60	4.29	0.339	0.0350	0.04517	1.2872
2-27	9.22	-0.60	4.29	0.375	0.0350	0.06221	1.3241
2-28	9.72	-0.60	4.29	0.351	0.0350	0.02552	1.3845
2-29	10.22	-0.60	4.29	0.324	0.0350	0.04700	1.5254
2-30	10.72	-0.60	4.29	0.303	0.0350	0.02367	1.4925
2-31	11.22	-0.60	4.29	0.337	0.0350	0.04153	1.4783
2-32	11.72	-0.60	4.29	-999	-999	-999	-999 -999
2-33	12.22	-0.60	4.29	0.399	0.0350	0.12280	1.3761
2-34	12.72	-0.60	4.29	0.370	0.0350	0.04514	1.4876
2-35	13.22	-0.60	4.29	0.388	0.0350	0.05476	1.3473
2-36	13.72	-0.60	4.29	0.366	0.0350	0.05793	1.3784
2-37	14.22	-0.60	4.29	0.370	0.0350	0.03876	1.4126
2-38	14.72	-0.60	4.29	0.375	0.0350	0.11809	1.3409
2-39	15.22	-0.60	4.29	0.394	0.0350	0.04857	1.3572
2-40	15.72	-0.60	4.29	0.388	0.0350	0.29827	1.1655
2-41	16.22	-0.60	4.29	0.353	0.0350	0.04776	1.5674
2-42	16.72	-0.60	4.29	0.375	0.0350	0.10598	1.3015
2-43	17.22	-0.60	4.29	0.380	0.0350	0.05836	1.3218
2-44	17.72	-0.60	4.29	0.338	0.0350	0.06175	1.5231
2-45	18.22	-0.60	4.29	0.371	0.0350	0.05409	1.4769
2-46	18.72	-0.60	4.29	0.370	0.0350	0.05215	1.5047
2-47	19.22	-0.60	4.29	-999	-999	-999	-999 -999
2-48	19.72	-0.60	4.29	0.330	0.0350	0.05747	1.4733
2-49	20.22	-0.60	4.29	0.376	0.0350	0.04632	1.3903
2-50	20.72	-0.60	4.29	0.312	0.0350	0.07378	1.5037
3-1	-3.78	-0.60	3.49	0.372	0.0350	0.10682	1.1804
3-2	-3.28	-0.60	3.49	0.395	0.0000	0.03227	1.2904
3-3	-2.78	-0.60	3.49	0.369	0.0000	0.05586	1.2377
3-4	-2.28	-0.60	3.49	0.355	0.0000	0.07678	1.2577
3-5	-1.78	-0.60	3.49	0.360	0.0179	0.10793	1.2713
3-6	-1.28	-0.60	3.49	0.320	0.0350	0.03373	1.5167
3-7	-0.78	-0.60	3.49	0.337	0.0350	0.04937	1.3894
3-8	-0.28	-0.60	3.49	0.350	0.0350	0.05254	1.3826
3-9	0.22	-0.60	3.49	0.354	0.0350	0.02918	1.4399
3-10	0.72	-0.60	3.49	0.354	0.0350	0.04420	1.4084
3-11	1.22	-0.60	3.49	-999	-999	-999	-999 -999
3-12	1.72	-0.60	3.49	0.366	0.0350	0.05272	1.2761
3-13	2.22	-0.60	3.49	0.326	0.0350	0.05787	1.3837
3-14	2.72	-0.60	3.49	0.347	0.0350	0.07287	1.3492

SAMPLE	X	Y	Z	WCS	WCR	ALPHA	BETA
3-15	3.22	-0.60	3.49	0.321	0.0350	0.05334	1.3029
3-16	3.72	-0.60	3.49	0.318	0.0350	0.06299	1.3500
3-17	4.22	-0.60	3.49	0.369	0.0350	0.16539	1.2658
3-18	4.72	-0.60	3.49	0.262	0.0350	0.05776	1.4145
3-19	5.22	-0.60	3.49	0.350	0.0350	0.04465	1.4883
3-20	5.72	-0.60	3.49	0.328	0.0350	0.06748	1.4372
3-21	6.22	-0.60	3.49	0.309	0.0350	0.04294	1.5486
3-22	6.72	-0.60	3.49	-999	-999	-999	-999 -999
3-23	7.22	-0.60	3.49	0.332	0.0350	0.15239	1.4936
3-24	7.72	-0.60	3.49	0.305	0.0350	0.11893	1.4160
3-25	8.22	-0.60	3.49	0.353	0.0350	0.06531	1.4480
3-26	8.72	-0.60	3.49	0.305	0.0350	0.09027	1.4064
3-27	9.22	-0.60	3.49	0.302	0.0350	0.07655	1.3774
3-28	9.72	-0.60	3.49	0.314	0.0350	0.06277	1.5139
3-29	10.22	-0.60	3.49	0.302	0.0350	0.03267	1.7437
3-30	10.72	-0.60	3.49	0.323	0.0350	0.20674	1.3469
3-31	11.22	-0.60	3.49	0.310	0.0350	0.06524	1.4893
3-32	11.72	-0.60	3.49	0.333	0.0350	0.07886	1.5705
3-33	12.22	-0.60	3.49	0.319	0.0350	0.09408	1.4733
3-34	12.72	-0.60	3.49	0.337	0.0350	0.10217	1.5730
3-35	13.22	-0.60	3.49	0.357	0.0350	0.09415	1.6320
3-36	13.72	-0.60	3.49	0.312	0.0350	0.09905	1.5552
3-37	14.22	-0.60	3.49	0.344	0.0350	0.07955	1.7063
3-38	14.72	-0.60	3.49	0.312	0.0350	0.08506	1.6141
3-39	15.22	-0.60	3.49	0.330	0.0350	0.06758	1.6289
3-40	15.72	-0.60	3.49	0.334	0.0350	0.07827	1.6134
3-41	16.22	-0.60	3.49	0.306	0.0350	0.02683	1.6158
3-42	16.72	-0.60	3.49	0.347	0.0350	0.04637	1.4010
3-43	17.22	-0.60	3.49	0.361	0.0350	0.02477	1.3775
3-44	17.72	-0.60	3.49	0.361	0.0350	0.01742	1.5212
3-45	18.22	-0.60	3.49	0.329	0.0350	0.02608	1.5253
3-46	18.72	-0.60	3.49	0.352	0.0350	0.05597	1.3126
3-47	19.22	-0.60	3.49	0.321	0.0350	0.03020	1.3798
3-48	19.72	-0.60	3.49	0.361	0.0350	0.03730	1.4206
3-49	20.22	-0.60	3.49	0.347	0.0350	0.03740	1.3564
3-50	20.72	-0.60	3.49	0.316	0.0350	0.02789	1.3198
4-1	-3.78	-0.60	2.84	0.293	0.0000	0.01215	1.4692
4-2	-3.28	-0.60	2.84	0.305	0.0000	0.04678	1.1746
4-3	-2.78	-0.60	2.84	0.283	0.0250	0.03348	1.6832
4-4	-2.28	-0.60	2.84	0.287	0.0250	0.03785	1.5882
4-5	-1.78	-0.60	2.84	0.297	0.0250	0.02325	1.5715
4-6	-1.28	-0.60	2.84	0.307	0.0250	0.03367	1.5439
4-7	-0.78	-0.60	2.84	0.309	0.0000	0.02475	1.4011
4-8	-0.28	-0.60	2.84	0.291	0.0250	0.01951	1.4064
4-9	0.22	-0.60	2.84	0.267	0.0000	0.06225	1.1364
4-10	0.72	-0.60	2.84	0.343	0.0250	0.01968	1.3904
4-11	1.22	-0.60	2.84	0.306	0.0250	0.04108	1.3612
4-12	1.72	-0.60	2.84	0.303	0.0250	0.04694	1.3935
4-13	2.22	-0.60	2.84	0.301	0.0250	0.04966	1.3666
4-14	2.72	-0.60	2.84	0.378	0.0250	1.31299	1.3288
4-15	3.22	-0.60	2.84	0.351	0.0250	0.12961	1.6250
4-16	3.72	-0.60	2.84	-999	-999	-999	-999 -999
4-17	4.22	-0.60	2.84	-999	-999	-999	-999 -999
4-18	4.72	-0.60	2.84	0.364	0.0250	5.31402	1.3080
4-19	5.22	-0.60	2.84	0.322	0.0250	0.19272	1.5632
4-20	5.72	-0.60	2.84	0.294	0.0250	0.13313	1.1871

SAMPLE	X	Y	Z	WCS	WCR	ALPHA	BETA
4-21	6.22	-0.60	2.84	0.290	0.0000	0.03778	1.2737
4-22	6.72	-0.60	2.84	0.361	0.0061	0.05257	1.3144
4-23	7.22	-0.60	2.84	0.263	0.0000	0.04187	1.2492
4-24	7.72	-0.60	2.84	0.349	0.0000	0.07569	1.3311
4-25	8.22	-0.60	2.84	0.315	0.0250	0.04542	1.4223
4-26	8.72	-0.60	2.84	0.292	0.0250	0.02927	1.3835
4-27	9.22	-0.60	2.84	0.294	0.0250	0.03867	1.4133
4-28	9.72	-0.60	2.84	0.307	0.0250	0.07259	1.4154
4-29	10.22	-0.60	2.84	-999	-999	-999 -999	-999
4-30	10.72	-0.60	2.84	0.348	0.0250	0.07540	1.4246
4-31	11.22	-0.60	2.84	0.312	0.0250	0.04938	1.4329
4-32	11.72	-0.60	2.84	0.326	0.0250	0.12628	1.4806
4-33	12.22	-0.60	2.84	0.342	0.0000	0.03840	1.3562
4-34	12.72	-0.60	2.84	0.346	0.0250	0.06393	1.4940
4-35	13.22	-0.60	2.84	0.305	0.0250	0.07566	1.5796
4-36	13.72	-0.60	2.84	0.294	0.0250	0.04428	1.6457
4-37	14.22	-0.60	2.84	0.308	0.0250	0.10927	1.5301
4-38	14.72	-0.60	2.84	0.334	0.0250	0.67592	1.4033
4-39	15.22	-0.60	2.84	0.317	0.0250	0.15022	1.6424
4-40	15.72	-0.60	2.84	0.349	0.0250	0.84037	1.3922
4-41	16.22	-0.60	2.84	0.276	0.0250	0.06243	1.5612
4-42	16.72	-0.60	2.84	0.296	0.0250	0.08345	1.4580
4-43	17.22	-0.60	2.84	0.291	0.0250	0.02760	1.5478
4-44	17.72	-0.60	2.84	0.325	0.0250	0.05697	1.3535
4-45	18.22	-0.60	2.84	0.371	0.0250	0.02357	1.3827
4-46	18.72	-0.60	2.84	0.307	0.0250	0.02775	1.5833
4-47	19.22	-0.60	2.84	0.303	0.0250	0.03912	1.4617
4-48	19.72	-0.60	2.84	0.281	0.0250	0.02082	1.5449
4-49	20.22	-0.60	2.84	0.281	0.0250	0.03113	1.5184
4-50	20.72	-0.60	2.84	0.316	0.0000	0.05763	1.3841
5-1	-3.78	-0.60	2.84	0.299	0.0250	0.05288	1.4455
5-2	-3.28	-0.60	2.84	0.288	0.0000	0.04653	1.3190
5-3	-2.78	-0.60	2.84	0.331	0.0000	0.02953	1.4134
5-4	-2.28	-0.60	2.84	0.310	0.0250	0.03715	1.4356
5-5	-1.78	-0.60	2.84	0.306	0.0000	0.08504	1.2240
5-6	-1.28	-0.60	2.84	0.312	0.0000	0.04767	1.3018
5-7	-0.78	-0.60	2.84	0.269	0.0000	0.02704	1.3593
5-8	-0.28	-0.60	2.84	0.318	0.0000	0.01091	1.5090
5-9	0.22	-0.60	2.84	0.328	0.0000	0.04053	1.2790
5-10	0.72	-0.60	2.84	0.314	0.0250	0.04113	1.5503
5-11	1.22	-0.60	2.84	0.272	0.0250	0.04004	1.5504
5-12	1.72	-0.60	2.84	0.286	0.0250	0.02684	1.5899
5-13	2.22	-0.60	2.84	0.327	0.0250	0.07158	1.3078
5-14	2.72	-0.60	2.84	0.252	0.0250	0.03436	1.4388
5-15	3.22	-0.60	2.84	0.297	0.0138	0.19335	1.3076
5-16	3.72	-0.60	2.84	0.312	0.0250	0.06933	1.4137
5-17	4.22	-0.60	2.84	0.355	0.0250	0.09316	1.4584
5-18	4.72	-0.60	2.84	0.327	0.0250	0.06955	1.5566
5-19	5.22	-0.60	2.84	0.318	0.0250	0.05323	1.4640
5-20	5.72	-0.60	2.84	0.319	0.0250	0.07631	1.5048
5-21	6.22	-0.60	2.84	0.282	0.0250	0.02632	1.5041
5-22	6.72	-0.60	2.84	0.319	0.0000	0.17129	1.3162
5-23	7.22	-0.60	2.84	0.305	0.0250	0.05894	1.3933
5-24	7.72	-0.60	2.84	0.306	0.0141	0.06349	1.3421
5-25	8.22	-0.60	2.84	0.290	0.0250	0.04053	1.5044
5-26	8.72	-0.60	2.84	0.287	0.0205	0.04436	1.3674
5-27	9.22	-0.60	2.84	0.278	0.0250	0.02535	1.3129

SAMPLE	X	Y	Z	WCS	WCR	ALPHA	BETA
5-28	9.72	-0.60	2.84	0.309	0.0250	0.04561	1.3035
5-29	10.22	-0.60	2.84	0.274	0.0000	0.06907	1.1966
5-30	10.72	-0.60	2.84	-999	-999	-999 -999	-999
5-31	11.22	-0.60	2.84	0.297	0.0250	0.08127	1.3784
5-32	11.72	-0.60	2.84	0.297	0.0250	0.03758	1.4749
5-33	12.22	-0.60	2.84	0.276	0.0000	0.03612	1.3418
5-34	12.72	-0.60	2.84	0.305	0.0250	0.10007	1.2688
5-35	13.22	-0.60	2.84	0.362	0.0250	0.01690	1.3170
5-36	13.72	-0.60	2.84	0.304	0.0250	0.02767	1.4413
5-37	14.22	-0.60	2.84	0.302	0.0250	0.03737	1.4573
5-38	14.72	-0.60	2.84	0.311	0.0250	0.04177	1.4525
5-39	15.22	-0.60	2.84	0.327	0.0000	0.04790	1.3127
5-40	15.72	-0.60	2.84	-999	-999	-999 -999	-999
5-41	16.22	-0.60	2.84	0.328	0.0250	0.01710	1.4991
5-42	16.72	-0.60	2.84	0.308	0.0250	0.01608	1.5428
5-43	17.22	-0.60	2.84	0.284	0.0250	0.01715	1.4959
5-44	17.72	-0.60	2.84	0.287	0.0250	0.01625	1.5344
5-45	18.22	-0.60	2.84	0.296	0.0250	0.01301	1.6336
5-46	18.72	-0.60	2.84	0.320	0.0250	0.02446	1.4967
5-47	19.22	-0.60	2.84	0.338	0.0000	0.04497	1.2965
5-48	19.72	-0.60	2.84	0.325	0.0250	0.05281	1.4034
5-49	20.22	-0.60	2.84	0.320	0.0214	0.13728	1.4008
5-50	20.72	-0.60	2.84	0.338	0.0250	0.08509	1.3334
6-1	-3.78	-0.60	1.79	0.324	0.0350	0.06359	1.1956
6-2	-3.28	-0.60	1.79	0.353	0.0000	0.09345	1.1421
6-3	-2.78	-0.60	1.79	0.345	0.0350	0.03787	1.2330
6-4	-2.28	-0.60	1.79	0.277	0.0000	0.02695	1.3199
6-5	-1.78	-0.60	1.79	0.434	0.0000	0.07620	1.1029
6-6	-1.28	-0.60	1.79	-999	-999	-999 -999	-999
6-7	-0.78	-0.60	1.79	0.280	0.0350	0.02881	1.4280
6-8	-0.28	-0.60	1.79	0.290	0.0350	0.02970	1.4817
6-9	0.22	-0.60	1.79	0.314	0.0350	0.06355	1.2882
6-10	0.72	-0.60	1.79	0.235	0.0350	0.03388	1.5130
6-11	1.22	-0.60	1.79	0.315	0.0350	0.08242	1.2772
6-12	1.72	-0.60	1.79	0.323	0.0350	0.12489	1.2127
6-13	2.22	-0.60	1.79	0.306	0.0350	0.07565	1.2778
6-14	2.72	-0.60	1.79	0.312	0.0350	0.10439	1.5025
6-15	3.22	-0.60	1.79	0.283	0.0350	0.07358	1.5873
6-16	3.72	-0.60	1.79	0.286	0.0350	0.15413	1.4667
6-17	4.22	-0.60	1.79	0.293	0.0350	0.05865	1.5615
6-18	4.72	-0.60	1.79	0.283	0.0350	0.05317	1.4344
6-19	5.22	-0.60	1.79	0.287	0.0350	0.06649	1.5564
6-20	5.72	-0.60	1.79	0.288	0.0350	0.11094	1.7106
6-21	6.22	-0.60	1.79	0.240	0.0350	0.09622	1.7199
6-22	6.72	-0.60	1.79	0.305	0.0350	0.14162	1.5667
6-23	7.22	-0.60	1.79	0.296	0.0350	0.06432	1.5613
6-24	7.72	-0.60	1.79	0.314	0.0350	0.04939	1.9278
6-25	8.22	-0.60	1.79	0.335	0.0350	0.08258	1.5643
6-26	8.72	-0.60	1.79	0.315	0.0350	9.22314	1.2420
6-27	9.22	-0.60	1.79	0.305	0.0350	0.06872	1.5492
6-28	9.72	-0.60	1.79	0.303	0.0350	0.56168	1.5534
6-29	10.22	-0.60	1.79	0.310	0.0350	0.60731	1.7995
6-30	10.72	-0.60	1.79	0.286	0.0350	0.05516	1.7304
6-31	11.22	-0.60	1.79	0.278	0.0350	0.03787	1.6971
6-32	11.72	-0.60	1.79	0.297	0.0350	0.04496	1.8078
6-33	12.22	-0.60	1.79	0.301	0.0350	0.04888	1.3357
6-34	12.72	-0.60	1.79	0.282	0.0350	0.04470	1.8342

SAMPLE	X	Y	Z	WCS	WCR	ALPHA	BETA
6-35	13.22	-0.60	1.79	0.297	0.0000	0.05068	1.4114
6-36	13.72	-0.60	1.79	0.245	0.0267	0.04041	1.7488
6-37	14.22	-0.60	1.79	0.274	0.0350	0.11881	1.7211
6-38	14.72	-0.60	1.79	0.281	0.0350	0.06384	1.9254
6-39	15.22	-0.60	1.79	0.291	0.0341	0.04342	1.7414
6-40	15.72	-0.60	1.79	0.287	0.0350	0.04579	1.8836
6-41	16.22	-0.60	1.79	0.300	0.0350	0.03631	1.6288
6-42	16.72	-0.60	1.79	0.218	0.0350	0.02562	1.6163
6-43	17.22	-0.60	1.79	0.287	0.0350	0.06589	1.4778
6-44	17.72	-0.60	1.79	0.260	0.0300	0.09048	1.5269
6-45	18.22	-0.60	1.79	0.289	0.0350	0.05824	1.5601
6-46	18.72	-0.60	1.79	0.287	0.0000	0.05224	1.3436
6-47	19.22	-0.60	1.79	0.280	0.0350	0.03663	1.4934
6-48	19.72	-0.60	1.79	0.307	0.0350	0.06903	1.5100
6-49	20.22	-0.60	1.79	0.273	0.0350	0.07438	1.8061
6-50	20.72	-0.60	1.79	0.329	0.0319	0.08314	1.5154
7-1	-3.78	-0.60	1.02	0.340	0.0000	0.15335	1.1944
7-2	-3.28	-0.60	1.02	0.320	0.0000	0.03772	1.2225
7-3	-2.78	-0.60	1.02	0.343	0.0000	0.05522	1.2444
7-4	-2.28	-0.60	1.02	0.339	0.0000	0.06051	1.3191
7-5	-1.78	-0.60	1.02	0.348	0.0000	0.01452	1.4770
7-6	-1.28	-0.60	1.02	0.323	0.0450	0.01133	1.6878
7-7	-0.78	-0.60	1.02	0.331	0.0000	0.05406	1.3031
7-8	-0.28	-0.60	1.02	0.350	0.0000	0.27426	1.1144
7-9	0.22	-0.60	1.02	0.356	0.0000	0.04934	1.2169
7-10	0.72	-0.60	1.02	0.333	0.0000	0.16264	1.1000
7-11	1.22	-0.60	1.02	0.299	0.0450	0.03203	1.3455
7-12	1.72	-0.60	1.02	0.332	0.0000	0.09616	1.1511
7-13	2.22	-0.60	1.02	0.311	0.0450	0.00768	1.6163
7-14	2.72	-0.60	1.02	0.327	0.0000	0.03755	1.2282
7-15	3.22	-0.60	1.02	0.310	0.0450	0.02909	1.3688
7-16	3.72	-0.60	1.02	0.296	0.0000	0.01348	1.4197
7-17	4.22	-0.60	1.02	0.307	0.0000	0.03405	1.2374
7-18	4.72	-0.60	1.02	0.316	0.0000	0.14227	1.1331
7-19	5.22	-0.60	1.02	0.331	0.0000	0.14257	1.1195
7-20	5.72	-0.60	1.02	0.351	0.0000	0.15798	1.1124
7-21	6.22	-0.60	1.02	0.322	0.0000	0.12351	1.1079
7-22	6.72	-0.60	1.02	0.326	0.0000	0.02959	1.2664
7-23	7.22	-0.60	1.02	0.301	0.0000	0.04823	1.1735
7-24	7.72	-0.60	1.02	0.322	0.0000	0.03859	1.3137
7-25	8.22	-0.60	1.02	0.309	0.0450	0.01759	1.4440
7-26	8.72	-0.60	1.02	0.323	0.0450	0.01992	1.4069
7-27	9.22	-0.60	1.02	0.393	0.0000	0.06239	1.1731
7-28	9.72	-0.60	1.02	0.355	0.0450	0.03237	1.3222
7-29	10.22	-0.60	1.02	0.296	0.0000	0.05088	1.2009
7-30	10.72	-0.60	1.02	0.308	0.0000	0.05488	1.2066
7-31	11.22	-0.60	1.02	0.322	0.0000	0.04081	1.2684
7-32	11.72	-0.60	1.02	-999	-999	-999	-999 -999
7-33	12.22	-0.60	1.02	0.324	0.0000	0.03561	1.2530
7-34	12.72	-0.60	1.02	-999	-999	-999	-999 -999
7-35	13.22	-0.60	1.02	0.329	0.0450	0.04452	1.3668
7-36	13.72	-0.60	1.02	0.304	0.0000	0.04136	1.2214
7-37	14.22	-0.60	1.02	0.308	0.0000	0.05647	1.1908
7-38	14.72	-0.60	1.02	0.295	0.0450	0.05906	1.2184
7-39	15.22	-0.60	1.02	0.300	0.0000	0.02026	1.2946
7-40	15.72	-0.60	1.02	0.319	0.0450	0.02651	1.3073

SAMPLE	X	Y	Z	WCS	WCR	ALPHA	BETA
7-41	16.22	-0.60	1.02	0.346	0.0450	0.02232	1.4406
7-42	16.72	-0.60	1.02	0.317	0.0000	0.05606	1.1901
7-43	17.22	-0.60	1.02	0.305	0.0000	0.08768	1.1326
7-44	17.72	-0.60	1.02	0.293	0.0450	0.05893	1.3721
7-45	18.22	-0.60	1.02	0.334	0.0000	0.02688	1.4089
7-46	18.72	-0.60	1.02	0.287	0.0450	0.08904	1.4906
7-47	19.22	-0.60	1.02	0.283	0.0000	0.03362	1.3541
7-48	19.72	-0.60	1.02	0.279	0.0000	0.05301	1.3169
7-49	20.22	-0.60	1.02	0.275	0.0450	0.02642	1.3943
7-50	20.72	-0.60	1.02	0.285	0.0311	0.06524	1.4800
8-1	-3.78	-0.60	0.11	0.335	0.0000	0.07698	1.2018
8-2	-3.28	-0.60	0.11	0.312	0.0000	0.03946	1.2126
8-3	-2.78	-0.60	0.11	0.325	0.0450	0.05413	1.2298
8-4	-2.28	-0.60	0.11	0.282	0.0450	0.07070	1.2004
8-5	-1.78	-0.60	0.11	0.336	0.0450	0.03433	1.3559
8-6	-1.28	-0.60	0.11	0.308	0.0000	0.03576	1.3983
8-7	-0.78	-0.60	0.11	0.352	0.0450	0.06153	1.2721
8-8	-0.28	-0.60	0.11	0.337	0.0000	0.05318	1.2561
8-9	0.22	-0.60	0.11	0.306	0.0000	0.04905	1.2123
8-10	0.72	-0.60	0.11	0.305	0.0000	0.05355	1.2155
8-11	1.22	-0.60	0.11	0.295	0.0000	0.03311	1.2671
8-12	1.72	-0.60	0.11	0.338	0.0450	0.03136	1.4523
8-13	2.22	-0.60	0.11	0.355	0.0000	0.05834	1.2574
8-14	2.72	-0.60	0.11	0.309	0.0000	0.04188	1.2767
8-15	3.22	-0.60	0.11	0.301	0.0450	0.08091	1.1959
8-16	3.72	-0.60	0.11	-999	-999	-999	-999 -999
8-17	4.22	-0.60	0.11	0.351	0.0000	0.05752	1.1983
8-18	4.72	-0.60	0.11	0.324	0.0450	0.06216	1.1773
8-19	5.22	-0.60	0.11	0.337	0.0000	0.05758	1.1895
8-20	5.72	-0.60	0.11	0.337	0.0000	0.04625	1.1829
8-21	6.22	-0.60	0.11	0.326	0.0000	0.05443	1.2024
8-22	6.72	-0.60	0.11	0.359	0.0000	0.05672	1.2531
8-23	7.22	-0.60	0.11	0.295	0.0450	0.02527	1.4072
8-24	7.72	-0.60	0.11	0.310	0.0000	0.05617	1.1552
8-25	8.22	-0.60	0.11	0.271	0.0149	0.06879	1.1000
8-26	8.72	-0.60	0.11	0.282	0.0000	0.07960	1.1056
8-27	9.22	-0.60	0.11	0.349	0.0000	0.04870	1.2033
8-28	9.72	-0.60	0.11	0.351	0.0000	0.02851	1.2601
8-29	10.22	-0.60	0.11	0.334	0.0000	0.04398	1.1949
8-30	10.72	-0.60	0.11	0.332	0.0450	0.03199	1.2700
8-31	11.22	-0.60	0.11	0.345	0.0000	0.05733	1.1848
8-32	11.72	-0.60	0.11	0.366	0.0000	0.09011	1.1973
8-33	12.22	-0.60	0.11	0.316	0.0000	0.05640	1.2424
8-34	12.72	-0.60	0.11	0.321	0.0000	0.03894	1.3425
8-35	13.22	-0.60	0.11	0.337	0.0450	0.06862	1.2534
8-36	13.72	-0.60	0.11	0.326	0.0000	0.31292	1.1408
8-37	14.22	-0.60	0.11	0.399	0.0000	0.06472	1.2918
8-38	14.72	-0.60	0.11	0.344	0.0450	0.03715	1.3887
8-39	15.22	-0.60	0.11	0.330	0.0450	0.01764	1.5120
8-40	15.72	-0.60	0.11	0.332	0.0000	0.05466	1.2720
8-41	16.22	-0.60	0.11	0.373	0.0000	0.04332	1.2470
8-42	16.72	-0.60	0.11	0.345	0.0000	0.03941	1.1840
8-43	17.22	-0.60	0.11	0.359	0.0450	0.02181	1.4635
8-44	17.72	-0.60	0.11	0.362	0.0450	0.03547	1.5460
8-45	18.22	-0.60	0.11	0.313	0.0450	0.02969	1.4529
8-46	18.72	-0.60	0.11	0.349	0.0450	0.01905	1.4682

SAMPLE	X	Y	Z	WCS	WCR	ALPHA	BETA
8-47	19.22	-0.60	0.11	0.358	0.0000	0.11636	1.2786
8-48	19.72	-0.60	0.11	0.334	0.0000	0.15403	1.2982
8-49	20.22	-0.60	0.11	0.332	0.0450	0.10218	1.4419
8-50	20.72	-0.60	0.11	0.280	0.0450	0.05096	1.4527
9-1	-3.78	-0.60	-0.79	0.356	0.0450	0.01705	1.5738
9-2	-3.28	-0.60	-0.79	0.363	0.0000	0.01309	1.6162
9-3	-2.78	-0.60	-0.79	0.263	0.0450	0.01687	1.5463
9-4	-2.28	-0.60	-0.79	0.289	0.0000	0.04198	1.2053
9-5	-1.78	-0.60	-0.79	0.270	0.0262	0.04477	1.4447
9-6	-1.28	-0.60	-0.79	0.330	0.0000	0.02811	1.3440
9-7	-0.78	-0.60	-0.79	0.322	0.0450	0.03409	1.7116
9-8	-0.28	-0.60	-0.79	0.294	0.0408	0.05198	1.5290
9-9	0.22	-0.60	-0.79	0.310	0.0000	0.03789	1.2858
9-10	0.72	-0.60	-0.79	0.285	0.0450	0.01860	1.4954
9-11	1.22	-0.60	-0.79	0.280	0.0000	0.03841	1.3039
9-12	1.72	-0.60	-0.79	0.334	0.0000	0.06312	1.3427
9-13	2.22	-0.60	-0.79	-999	-999	-999	-999 -999
9-14	2.72	-0.60	-0.79	0.293	0.0000	0.05591	1.2289
9-15	3.22	-0.60	-0.79	0.307	0.0000	0.05472	1.2973
9-16	3.72	-0.60	-0.79	0.281	0.0419	0.02404	1.4590
9-17	4.22	-0.60	-0.79	0.317	0.0450	0.03590	1.5351
9-18	4.72	-0.60	-0.79	0.224	0.0000	0.05302	1.2103
9-19	5.22	-0.60	-0.79	0.275	0.0000	0.05688	1.3220
9-20	5.72	-0.60	-0.79	0.276	0.0000	0.14881	1.1182
9-21	6.22	-0.60	-0.79	0.356	0.0000	0.04943	1.3048
9-22	6.72	-0.60	-0.79	0.329	0.0000	0.04888	1.1929
9-23	7.22	-0.60	-0.79	0.268	0.0000	0.03917	1.2563
9-24	7.72	-0.60	-0.79	0.257	0.0185	0.05336	1.5082
9-25	8.22	-0.60	-0.79	0.247	0.0000	0.05149	1.2695
9-26	8.72	-0.60	-0.79	0.322	0.0000	0.04907	1.2715
9-27	9.22	-0.60	-0.79	0.283	0.0000	0.02446	1.3304
9-28	9.72	-0.60	-0.79	0.315	0.0000	0.05882	1.1744
9-29	10.22	-0.60	-0.79	-999	-999	-999	-999 -999
9-30	10.72	-0.60	-0.79	0.320	0.0000	0.01921	1.4523
9-31	11.22	-0.60	-0.79	0.326	0.0000	0.05168	1.2709
9-32	11.72	-0.60	-0.79	0.292	0.0000	0.05462	1.2181
9-33	12.22	-0.60	-0.79	0.311	0.0000	0.03728	1.3465
9-34	12.72	-0.60	-0.79	0.304	0.0000	0.03433	1.3366
9-35	13.22	-0.60	-0.79	0.300	0.0000	0.05688	1.3110
9-36	13.72	-0.60	-0.79	0.267	0.0000	0.07091	1.2302
9-37	14.22	-0.60	-0.79	0.321	0.0000	0.09065	1.1548
9-38	14.72	-0.60	-0.79	0.301	0.0000	0.53732	1.1011
9-39	15.22	-0.60	-0.79	0.279	0.0450	0.11277	1.4635
9-40	15.72	-0.60	-0.79	0.350	0.0000	0.33724	1.2758
9-41	16.22	-0.60	-0.79	0.367	0.0000	0.62708	1.2232
9-42	16.72	-0.60	-0.79	0.337	0.0450	0.11368	1.2400
9-43	17.22	-0.60	-0.79	0.529	0.0000	0.27160	1.1315
9-44	17.72	-0.60	-0.79	0.352	0.0450	0.09061	1.2524
9-45	18.22	-0.60	-0.79	0.327	0.0000	1.06125	1.1044
9-46	18.72	-0.60	-0.79	0.338	0.0450	0.12384	1.3424
9-47	19.22	-0.60	-0.79	0.323	0.0450	0.10534	1.3273
9-48	19.72	-0.60	-0.79	0.287	0.0000	0.05966	1.3267
9-49	20.22	-0.60	-0.79	0.374	0.0000	0.05615	1.2142
9-50	20.72	-0.60	-0.79	0.412	0.0000	0.06479	1.2871

APPENDIX C6

Data analysis and deterministic modelling of
the Las Cruces Trench infiltration experiments

INTRAVAL Case 10

DATA ANALYSIS AND DETERMINISTIC MODELLING OF THE LAS CRUCES TRENCH INFILTRATION EXPERIMENTS

INTRAVAL Phase I Unsaturated Test Cases' Summary[1]

M.T. Goodrich[2], J.T. McCord, and C.D. Updegraff[2]

Sandia National Laboratories
Albuquerque, NM 87185
Operated by
Sandia Corporation
for the
U.S. Department of Energy

April 1991

Prepared for
Waste Management Branch
Division of Engineering
Office of Nuclear Regulatory Research
U.S. Nuclear Regulatory Commission
Washington, DC 20555
NRC FIN No. A1266 and L1153

1. Work performed under Sandia contract Nos. 40-4331
2. GRAM Inc., Albuquerque, NM

Table of contents

LIST OF FIGURES

Fig. 15. Experiment #2 2D Monte Carlo simulation results: overall average as well as layer 1-3 average moisture content breakthrough curves. Field observations (average of 4 points) are also presented as × for comparison, as well as the limits on the field measurements.

Fig. 16. Moisture diffusivities for LCT soils computed using (1) van Genuchten characteristic parameters given in the database (median D along with 90% confidence limits), and (2) inverse solution of Philip (1990) (experiment #1 yielded the higher of the 2 inverse-solution D values).

INTRODUCTION

Sandia National Laboratories (SNL) is part of the U.S. NRC INTRAVAL team. The purpose of this document is to summarize progress to date on modeling the Las Cruces trench (LCT) experiments (INTRAVAL Phase I, Case 10). The experimental setup and soil physical characteristics are discussed in detail in Wierenga et al. [1989] and will not be reiterated here.

This report is separated into two areas: analysis of soil hydraulic properties and flow modeling. The hydraulic data analysis consists primarily with a comparison of saturated hydraulic conductivity measurements obtained by field and laboratory methods. The modeling includes simulations using both a one-dimensional analytical solution to the flow equation and a two-dimensional model of fluid flow. Several conceptual models have been proposed: homogeneous, layered, and fully heterogeneous. This report focuses on two possible ways of simulating unsaturated flow through an acknowledged heterogeneous media profile using a homogeneous medium representation. Since the purpose of INTRAVAL is model validation, this report attempts to follow the spirit of the validation strategy proposed by Davis and Goodrich [1990]. Their strategy argues that model validation per se is a site-specific process and unachievable. Hence, for a given set of boundary and physical conditions, one can declare a model "invalid" or "not invalid" for use within a specified context.

A difficult part of the model validation process is deciding on the acceptance criteria. For the purposes of this study, model results are considered to be not invalid if they fall within the experimental error band. Model results falling outside this band will be considered invalid.

COMPARISON OF FIELD AND LAB K_{sat} MEASUREMENTS

A detailed analysis of the saturated hydraulic conductivity (K_{sat}) data from the Las Cruces trench experiment was conducted. Data were collected at the experimental site in two ways [Wierenga et al., 1989]. First, cores were removed from the site and taken back to the laboratory. The vertically-oriented cores were taken at a 50 cm horizontal separation distance from a 1 m wide ledge along the trench face for all of the 9 soil horizons that have been identified at the site. Since the trench is 25 m long, this resulted in 50 samples per layer and 450 samples total. Saturated hydraulic conductivity was determined in the laboratory using a constant head permeameter. Field estimates of saturated hydraulic conductivity were made using a Guelph permeameter and analyzed using the method of Reynolds and Elrick [1985]. The boreholes for the in-situ tests were separated from the original lab sample core holes by about 20 cm in a direction perpendicular to the trench face. The same number of samples per layer were taken, again resulting in about 450 samples total. Three questions were posed regarding the two K_{sat} data sets (hereafter referred to as "lab" and "field"):

1) Are the two data sets statistically different?
2) If so, why are they different?
3) Which data set is appropriate to use for modeling?

The next three sections will address each of the above questions.

Are the K_{sat} Data Sets Statistically Different?

To answer this first question, two tests were performed. The first was the Mann-Whitney test, a non-parametric method of testing whether the means of two independent, random, sets of data are significantly different at a specified confidence level [Davis, 1986]. The results of this analysis showed that the means are statistically different at the 90% confidence level. The second was the Lilliefors test [Lilliefors, 1967; Lilliefors, 1969; Iman, 1982], to determine whether the distributions of the data are different. This test showed, again at a 90% confidence level, that the field data are lognormally distributed (Figure 1). The lab data, however, were not lognormally distributed (Figure 2). The lab data also were tested for normal and exponential distributions, but did not fit these distributions either. This was somewhat disconcerting since the literature is replete with references attesting to the fact that hydraulic conductivity is lognormally distributed [for example, Freeze, 1975; Hoeksema and Kitanidis, 1985; Freeze et al., 1987]. The point is, however, that the distributions for the two data sets are not the same. Therefore, based on the results of the Mann-Whitney and Lilliefors tests, it was concluded that the field data and the lab data are statistically different at the 90% confidence level.

As an additional comparison of the two data sets, variograms of the $\ln K_{sat}$ of the two data sets were computed to estimate the horizontal correlation length. The field data (Figure 3) can be fit to an exponential variogram model with a nugget effect of 0.35 and a correlation length of 1.6 m. The lab data (Figure 3) were also fit to an exponential variogram but the nugget is 0.9 and the correlation length is 2 m. The sill (variance) for the field data is about 1.1, and about 1.25 for the lab data. Nicholson et al. [1987] report similar results for the field data using an exponential model except the correlation length was estimated to be 2 m. The lab data are more difficult to interpret because of the large scatter in the range less than 3 m and the large apparent nugget effect.

We also investigated the statistical characteristics of the 9 soil layers identified in Wierenga et al. [1989]. While there probably are 9 different soil horizons from a pedological perspective, a contour plot of the K_{sat} field does not reveal 9 obvious hydraulic layers (Figure 4). The Mann-Whitney test was again employed to decide if layer 1 is different from layer 2, and if layer 2 is different from layer 3, and if layer 3 is different from layer 4, and so on. This was done for both the lab and field data; the results indicate that some of the layers could be combined:

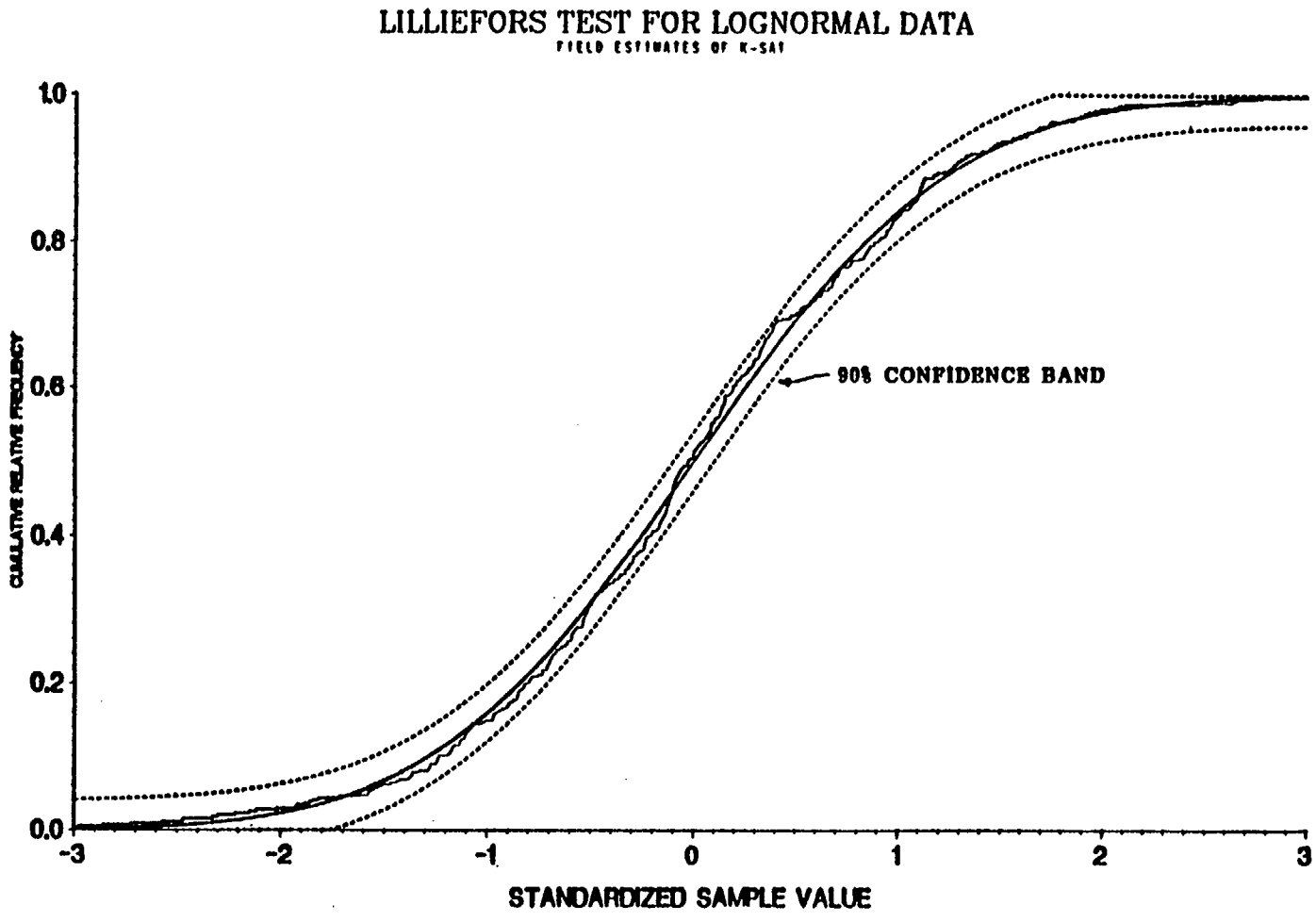

Fig. 1. Lilliefors statistical test of the lognormality of the field K_{sat} values.

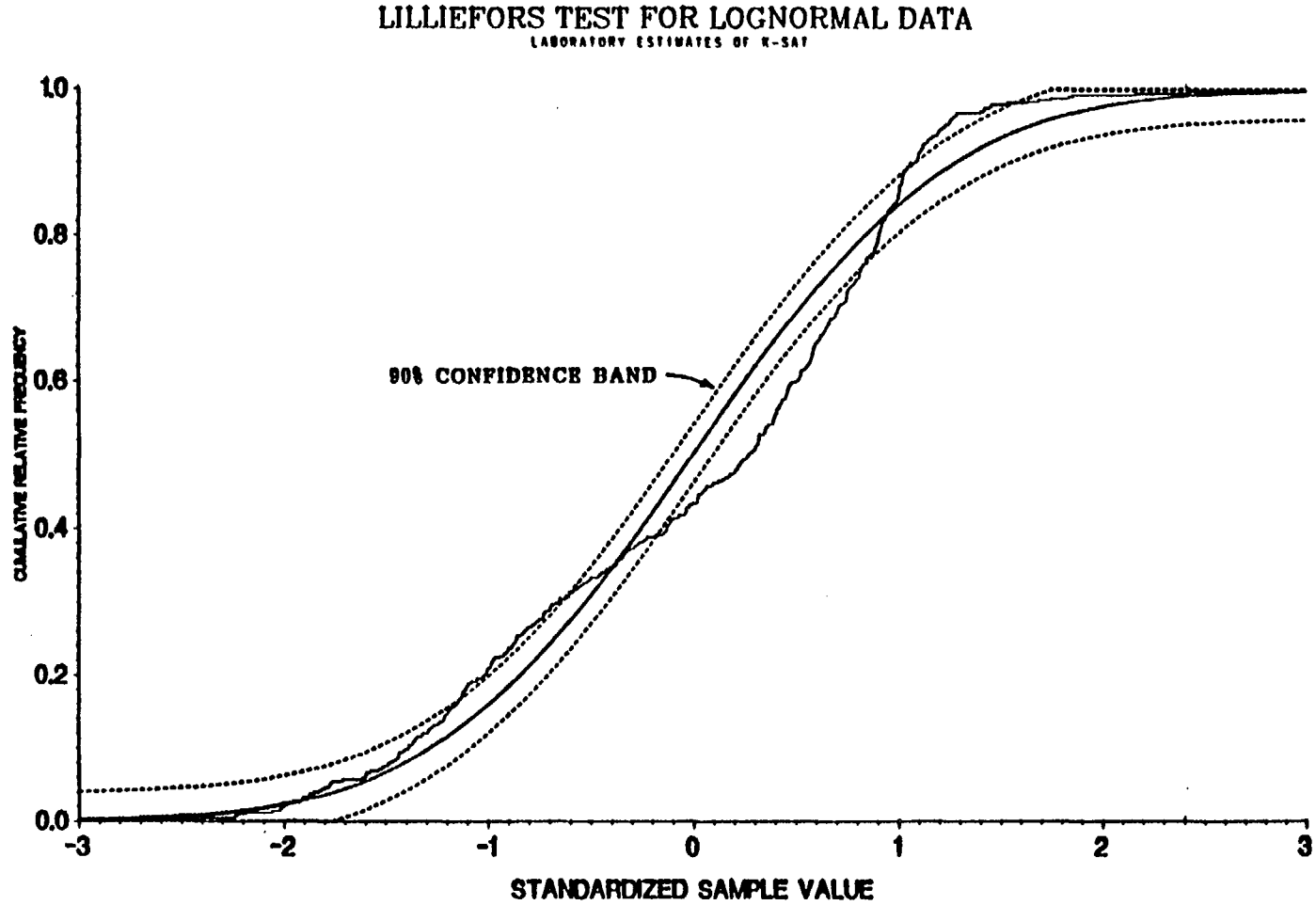

Fig. 2. Lilliefors statistical test of the lognormality of the lab K_{sat} values.

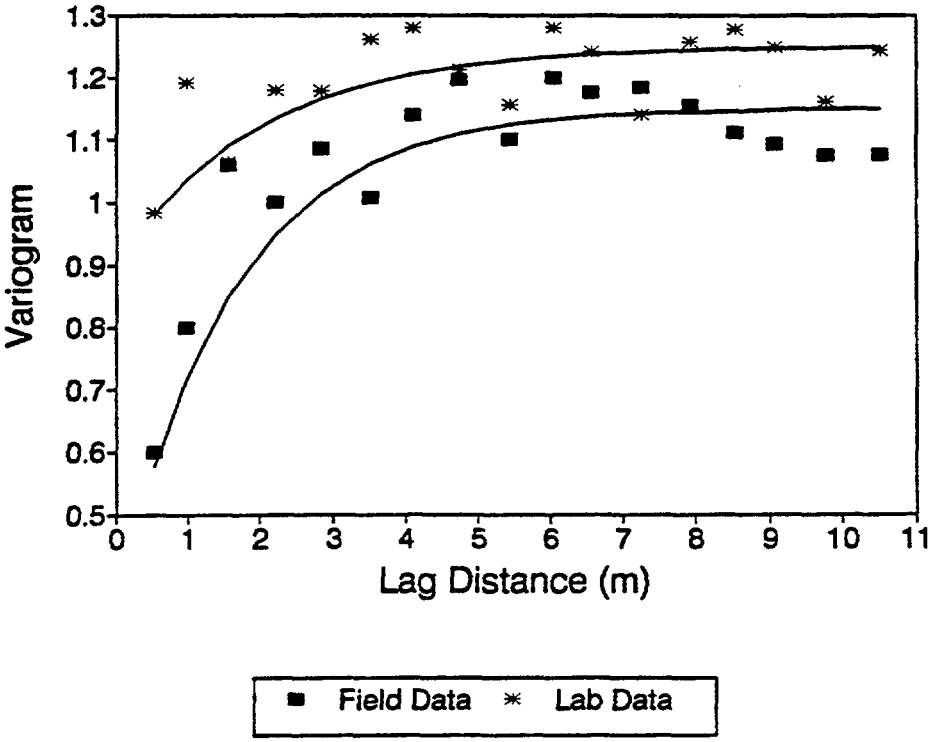

Fig. 3. Variograms of the field and lab K_{sat} values.

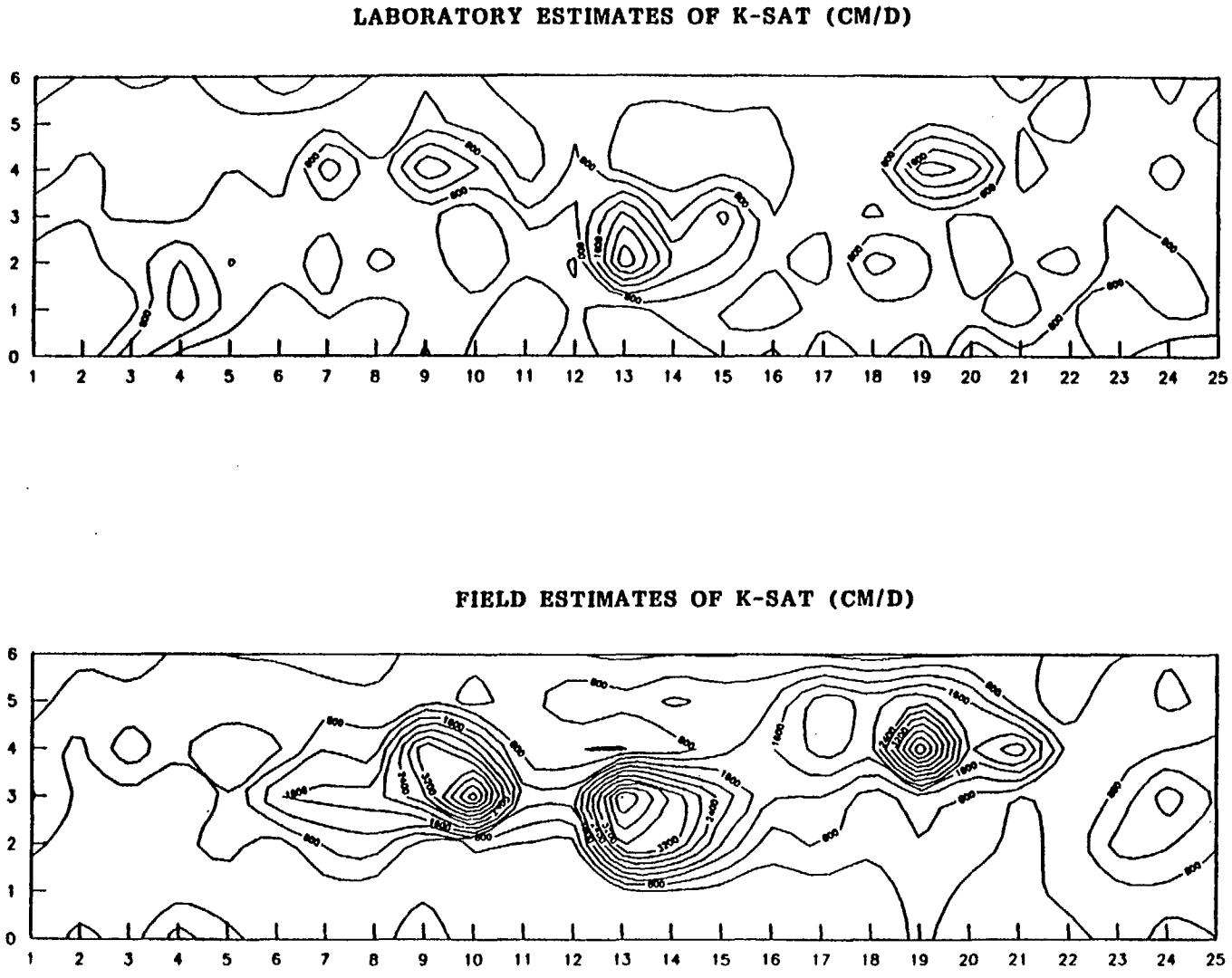

Fig.4. Contour plots of vertical spatial distribution of the field and lab K_{sat} values.

	Lab	Field
New layer 1:	layer 1	layer 1
New layer 2:	layer 2,3,4,5	layer 2,3,4,5,6
New layer 3:	layer 6,7,8,9	layer 7,8,9

Hence, for the purposes of modeling flow, this 9-layer system could probably be treated as a 3-layer system. However, since the means and variances of some of the layers are different, the principal of stationarity is violated and both data sets should be considered statistically non-homogeneous. The variogram of the lab data would confirm this if, as suspected, it is truly nugget. However, it is not clear what this means with regard to the field data since that variogram appears reasonable. Nicholson et al. [1987] made a similar observation about the stationarity of the data and de-trended the data to account for it. A similar approach should be taken for this data and three new variograms, representing each of the three new layers identified above, constructed.

Why are the Data Sets Different?

The second question is more difficult to answer. Some possible reasons for the differences are discussed below.

1. Random Error. This is not possible if the means are statistically different (as was shown with the Mann-Whitney test).

2. Systematic Error. An example of systematic error would be if the person doing the tests always reads high or low; another example would be if the holes left by removal of the lab cores were having an effect on the Guelph permeameter test. A systematic error can be tested for by looking at the correlation between the two data sets; if the differences in the two sets were only due to some systematic shift, then one would expect to obtain a good correlation. Four equations were tested and the associated coefficients of determination are:

y = a + bx (linear)	r^2 = 0.25
y = a exp(bx) (exponential)	r^2 = 0.08
y = a + b log(x) (logarithmic)	r^2 = 0.07
y = a x**b (power)	r^2 = 0.07

Clearly, these results indicate no correlation between the two data sets; thus it can be concluded that the differences are not due to systematic error.

3. Horizontal Conductivity vs. Vertical Conductivity. The lab core is encased in an aluminum ring during the lab tests. One net result is that water is only allowed to flow vertically through the core. On the other hand, the field test actually

measured a value that was averaged over some larger volume. In addition, the literature on the Guelph permeameter states that it is primarily a measure of horizontal conductivity [Reynolds and Elrick, 1986]. So, perhaps the differences are due to the fact that two different parameters were measured, vertical conductivity in the lab and horizontal conductivity in the field. This can be tested by comparing the ratio of the average values of the two data sets (field:lab). If the two data sets are approximately equal, then the average ratio should be about 1:1. In fact, the average ratio is 4.8:1; a t-test was performed and indicated that 4.8 is statistically different from 1.0 at the 90% confidence level. Therefore, we cannot, at this time, rule out the possibility that the differences are due to the fact that one test is measuring vertical conductivity and one test is measuring a volume-averaged primarily horizontal conductivity.

4. Spatial Variability. All of the data that have been collected at the site indicate that the media is very heterogeneous. It is possible that the differences in the data sets are due to this heterogeneity. The lab test measured only one core volume. Each field test measured an average of several core volumes (approximately 10) and is strongly influenced by those core volumes with the highest hydraulic conductivity. This could make the average field value greater than the average core value. In addition, this would cause the field variance to be smaller than the lab variance. This could explain both the difference in means and the slight variance reduction for the field measurements.

In conclusion, it cannot be said with complete certainty what is causing the lab data to be different from the field data. The differences may be due to the fact that two different directional conductivities are being measured, spatial variability, a combination of the two, or something else that was not considered in this analysis.

Which Data Set is Appropriate to Use for Modeling?

The third and final question cannot be answered conclusively at this time. Based on the results of the Lilliefors test and the variogram analysis, one might be tempted to conclude that the field data are the best. However, as was mentioned above, the two tests might be measuring vertical vs. horizontal conductivity, and that they are testing different sample volumes, so it would be incorrect to discard the lab data. Although we are probably not dealing with your classical "apple and orange" comparison, we perhaps have a "peach and nectarine" case, and thus conformity should not be expected.

With respect to the subsequent modeling study discussed here, we used the lab values of K_{sat} since the unsaturated characteristics employed in the modeling were obtained from the laboratory samples. Other possible options would have included using field K_{sat} in conjunction with the lab θ-ψ data, or perhaps using the field K_{sat} values for horizontal conductivities and the lab K_{sat} data for vertical conductivities. However, for consistency we felt that we should use the laboratory K_{sat} data set.

ONE-DIMENSIONAL SIMULATIONS

The first modeling effort involved determining whether a one-dimensional (1D) analytical solution to the moisture content-based Richards equation could accurately simulate movement of the wetting front. To achieve this goal the constant-rate rainfall infiltration solution of Broadbridge and White [1988; henceforth referred to as B&W] was implemented in a computer code and applied to the LCT experiments. The performance measure used for comparing the experimental observations to the model predictions was the change in moisture content versus time at the 1.5 m depth. We selected this performance measure because it can be related easily to groundwater travel time.

Mathematical Model

The B&W infiltration equation is obtained by solving the nonlinear Fokker-Planck diffusion-convection equation commonly used to describe one-dimensional flow in uniform soils:

$$\frac{\partial \theta}{\partial t} = \frac{\partial}{\partial z}\left[D(\theta)\frac{\partial \theta}{\partial z}\right] - K'\frac{\partial \theta}{\partial z} \qquad (1)$$

where θ is the volumetric water content, t is time, $K(\theta)$ is the hydraulic conductivity, $K' = \partial K/\partial \theta$, $D(\theta) = K(\theta)[\partial \psi/\partial \theta]$ is the moisture diffusivity with ψ being the capillary pressure head, z is the vertical space variable (positive downward). This partial differential equation is solved subject to the constant rainfall rate surface boundary condition:

$$K(\theta) - D(\theta)\frac{\partial \theta}{\partial z} = R(z=0) \qquad (2)$$

where R is the specified constant surficial flux rate, and the uniform water content initial condition:

$$\theta(z>0, t=0) = \theta_i \qquad (3)$$

In the soil physics literature, equation (1) is often referred to as the one-dimensional water content-based Richards equation.

Model Input - Soil Hydraulic Properties

For input the B&W solution requires both the moisture content-capillary pressure head (θ-ψ) and the unsaturated conductivity-moisture content (K-θ) relationships for the site soils. The θ-ψ relationships were measured on 445 "undisturbed" ring samples (obtained from the field site) in the laboratory using the hanging column and pressure cell techniques [Wierenga et al., 1988]. Saturated conductivity

measurements were performed on the same samples in a constant head permeameter. The unsaturated conductivities given in the LCT database were obtained by calculating a relative permeability curve from the water retention curve for each sample using the van Genuchten [1978] fit to Mualem's [1976] model, and using the saturated conductivity for the conductivity match point. Although it would be more desireable to have conductivity *measurements* over the entire range of saturations of interest, this approach (of computing the unsaturated conductivity based on the moisture retention data) is often taken in practice.

To obtain an analytical solution to (1), B&W assumed a particular form for the soil moisture characteristic functions (θ-ψ, $K(\theta)$, and $D(\theta)$). The functional form selected by B&W relies on only a single shape parameter, which they term C, and the saturated and residual water contents (θ_{sat} and θ_r, respectively) to describe the θ-ψ curve. The unsaturated conductivity is completely determined by C, the saturated conductivity K_{sat}, and the sorptivity S. The saturated and residual water contents, as well as the saturated conductivity measurements are reported in the LCT database [Wierenga et al., 1989], and the sorptivity (as a function of initial and final water contents) could be estimated from the infiltration experiments for the "gravity-free" early time [B&W, eqn. 47]. Thus the only unknown parameter is C. The shape parameter C was determined by minimizing the sum of the squared residuals between the B&W curve and the van Genuchten curves for layers 1-4 (top 2 meters of the media profile) given in the LCT database. Figure 5 presents the van Genuchten curves given in the database for layers 1-4 and the "best fit" B&W θ-ψ characteristic (C = 1.026). In addition, the upper and lower bounds on water contents measured in the laboratory for each applied pressure head are also shown. Clearly, the B&W characteristic curve has a significantly more non-linear shape than the van Genuchten curves for layers 1-4, but it lies well within the limits of the laboratory measurements.

1D Model Results

These soil characteristic curves were used as input to the B&W infiltration model to predict the time series of change in water content at the 1.5 m depth for experiments 1 and 2. The experiment #1 results are shown in Figure 6. The results obtained using the B&W characteristics fit to the van Genuchten θ-ψ curves given in the database significantly underpredicts the change in moisture content. Slight changes in the C parameter resulted in large differences in the model results. We obtained a visual "best fit" between the experiment #1 observations and model predictions using C = 1.012. The predicted moisture content time series differed little whether we used the mean K_{sat} (520 cm/day) or the median K_{sat} (380 cm/day) from the database. To further test the 1D analytical solution, we simulated LCT experiment #2. Figure 7 shows that the 1D model poorly predicted the experiment #2 moisture content time series in all cases, whether we used the C value which best predicted experiment #1 or the C value obtained by fitting the B&W characteristic model to the θ-ψ characteristics given in the LCT database. While the 1D B&W model did a good job at predicting experiment #1, in which the

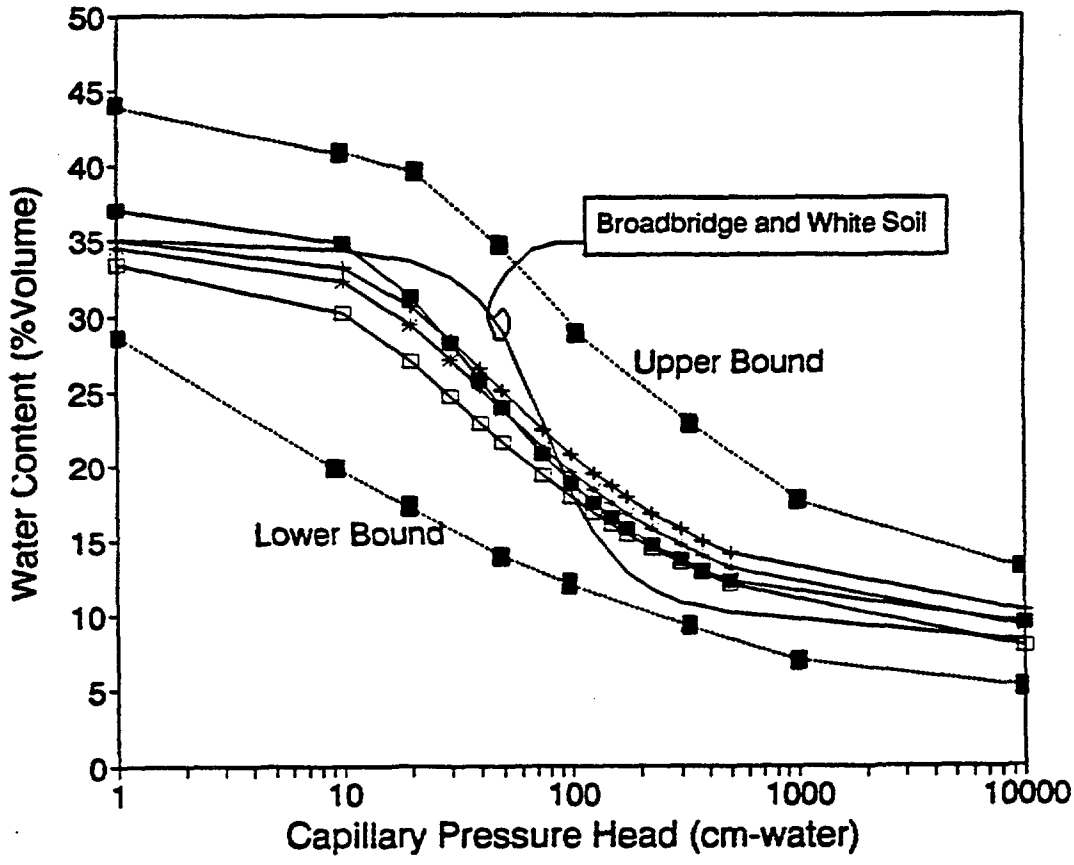

Fig. 5. van Genuchten θ-ψ curves for layers 1-4 and best fit B&W curve, and the lower and upper bounds on moisture contents at each applied pressure as reported in the LCT database.

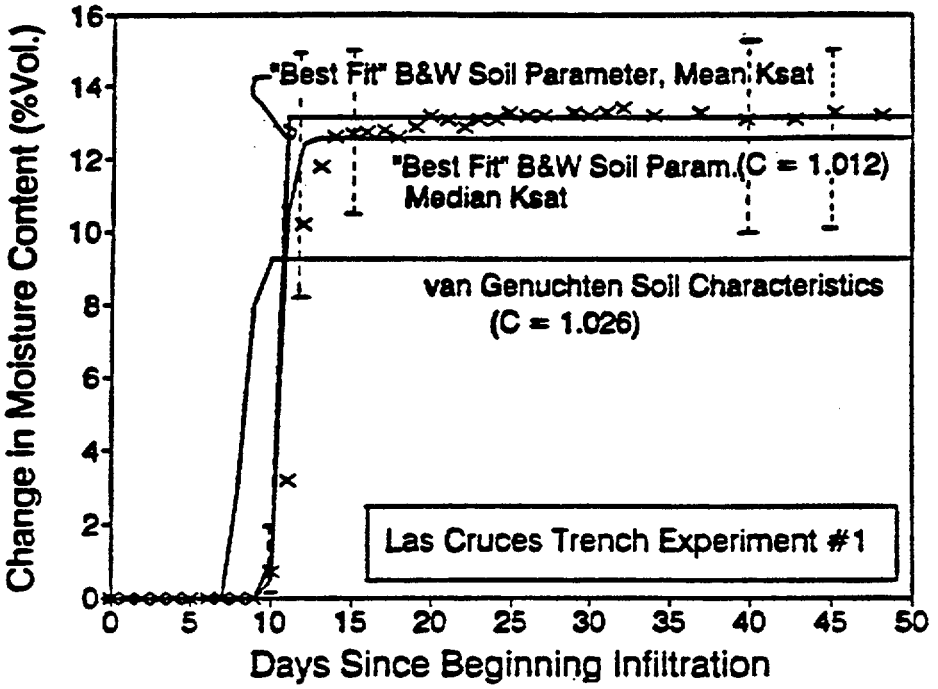

Fig. 6. Experiment #1 B&W 1D analytical solution prediction of moisture content breakthrough at 1.5 m depth. Input characteristic curves used include both best fit to LCT database characteristic curves (see Fig. 4) as well as best fit to experimental observations. Field observations (average of 4 points) are also presented as × for comparison, as well as the limits on the field measurements.

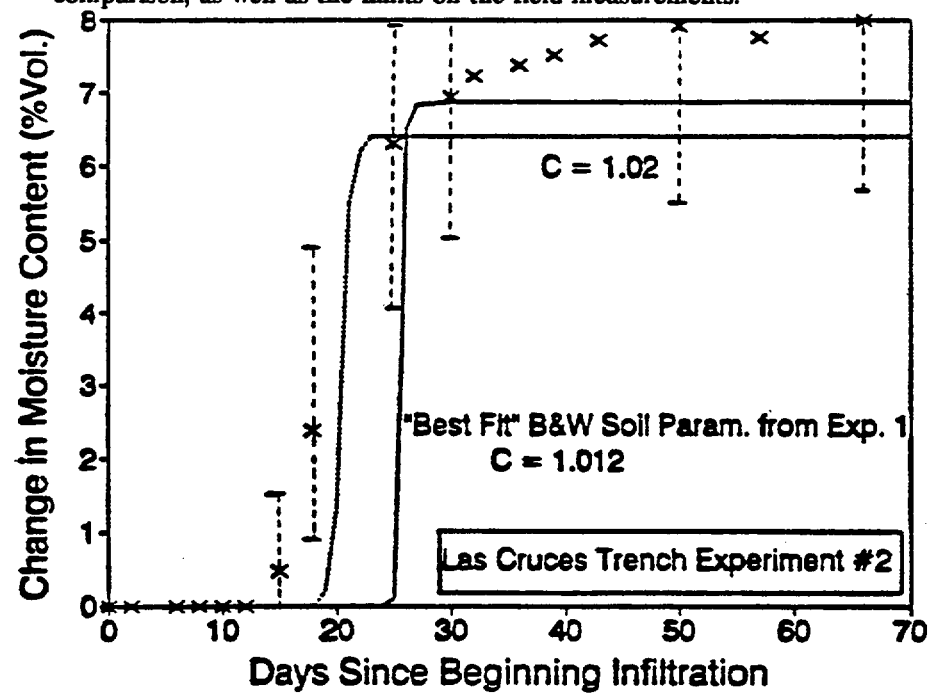

Fig. 7. Experiment #2 B&W 1D analytical solution prediction of moisture content breakthrough at 1.5 m depth. Input characteristic curves used include both best fit to LCT database characteristic curves (see Fig. 4) as well as best fit to Experiment #1 observations (see Fig. 5). Field observations (average of 4 points) are also presented as × for comparison, as well as the limits on the field measurements.

higher surface flux rate (1.9 cm/day) resulted in a Green-Ampt type sharp wetting front; it could not accurately simulate the diffuse wetting front observed in experiment #2 (applied flux = 0.5 cm/day). Perhaps this is unsurprising given that the B&W θ-ψ curve has a step-function shape (Fig. 5) which typically predicts a sharp wetting front. This may suggest that the B&W constant-rate infiltration model may be applicable for only a limited set of soil types, in particular those with Green-Ampt type characteristics.

In summary, the 1D analytical solution of B&W yielded somewhat dissappointing results. The observed moisture content time series could not be simulated accurately using the B&W characteristic curve obtained by best fit to the laboratory moisture retention measurements. However, it was possible to adequately calibrate the model to the experiment #1 results. Unfortunately, using the B&W characteristics obtained by inverse calibration to experiment #1, we could not accurately simulate the moisture content time series for experiment #2. Clearly, if one were interested in predicting average changes in water content versus time beneath the center of the irrigated strip, the one-dimensional model of flow through homogeneous media developed by B&W may be appropriate for only a limited range of soil types.

And finally, using the model acceptance criteria stated in the introduction, we would declare the 1D B&W model invalid (for the performance measure) since the experiment #2 model predictions (Fig.7) lie outside the range of experimental observations.

TWO-DIMENSIONAL SIMULATIONS

The second modeling effort involved application of a two-dimensional (2D) Richards equation model to simulate the flow field. Several other INTRAVAL modeling teams also applied 2D Richards equation models to the LCT experiments. Hills [1990] employed a moisture content-based Richards equation model to simulate flow and transport through a 2D homogeneous media profile, while KEMAKTA Consultants employed a pressure head-based Richards equation model to simulate the same problem, as well as a 2D layered profile. Gelhar and his colleagues from MIT applied their effective large-scale Richards equation model in a 2D implementation [Bensabat and Gelhar, 1990]. Kool et al. [1990] performed 2D simulations through both homogeneous and heterogeneous (with the heterogeneities exactly conditioned on field and laboratory measurments) media profiles using the mixed-formulation Richards equation implemented in the code VAM2D. And finally, Ababou [1990] simulated three-dimensional (3D) flow through a heterogeneous media profile sythetically generated based on the measured spatial statistics of the LCT soils. Our approach was to perform Monte Carlo simulations through a 2D homogeneous media profile.

Although the soil characterization data clearly indicates that the LCT media profile

is highly heterogeneous, we wanted to test the question of whether one can assume that a simple homogeneous model is appropriate for predicting flow behavior through a heterogeneous system. Other INTRAVAL modeling teams also were testing this question, but they used different procedures to obtain "average" properties for model input (from simple direct averaging of measured values [Hills, 1990] to large-scale effective properties developed through spectral stochastic analysis of the governing equations [Bensbat and Gelhar, 1990]). In addition, the other INTRAVAL teams typically employed rather vague subjective performance measures (e.g., the simulated change in moisture content field "looked like" the observed change in moisture content field). The HydroGeoLogic Inc. team [Kool et al., 1990] employed a more rigorous performance measure: comparing the second moment of the simulated moisture content field to that of the experimentally observed field. To provide a direct comparison to the 1D analytical solution results, and to use a performance measure with more direct application to the high level radioactive waste performance standards, we again selected the change in moisture content at the 1.5 m depth as our performance measure.

Mathematical Model

In our Monte Carlo analysis we employed the finite element code VAM2D. VAM2D solves the Richards equation in two dimensions:

$$\nabla[K(S_e)\nabla(\psi+z)]=\frac{\partial S_e}{\partial t} \tag{4}$$

where $S_e=(\theta-\theta_r)/(\theta_{sat}-\theta_{sat})$ is the effective saturation and the other variables are as defined above. Details on features, solution procedures, and algorithms employed in VAM2D can be found in Huyakorn et al. [1989].

Boundary conditions for the model are shown graphically in Figure 8. The irrigated zone was treated as a flux boundary condition (with the flux assigned to be 1.9 cm/d for experiment #1 and 0.5 cm/day for experiment #2) for the duration of the experiment. The bottom boundary was treated as a freely draining boundary, while all other boundaries were assumed to be impermeable. The initial condition pressure head was assigned a value of -10,000 cm-water.

Model Input

The first step in performing such a Monte Carlo analysis was statistically characterizing the media properties reported in the LCT database. Given that this analysis focused on homogeneous media profiles, our interest is only on cross-correlations between the parameters and not on the spatial correlation structure. The LCT database contains measurments and/or calculated values for five parameters which describe the hydraulic characteristics of the soils (and are required input for

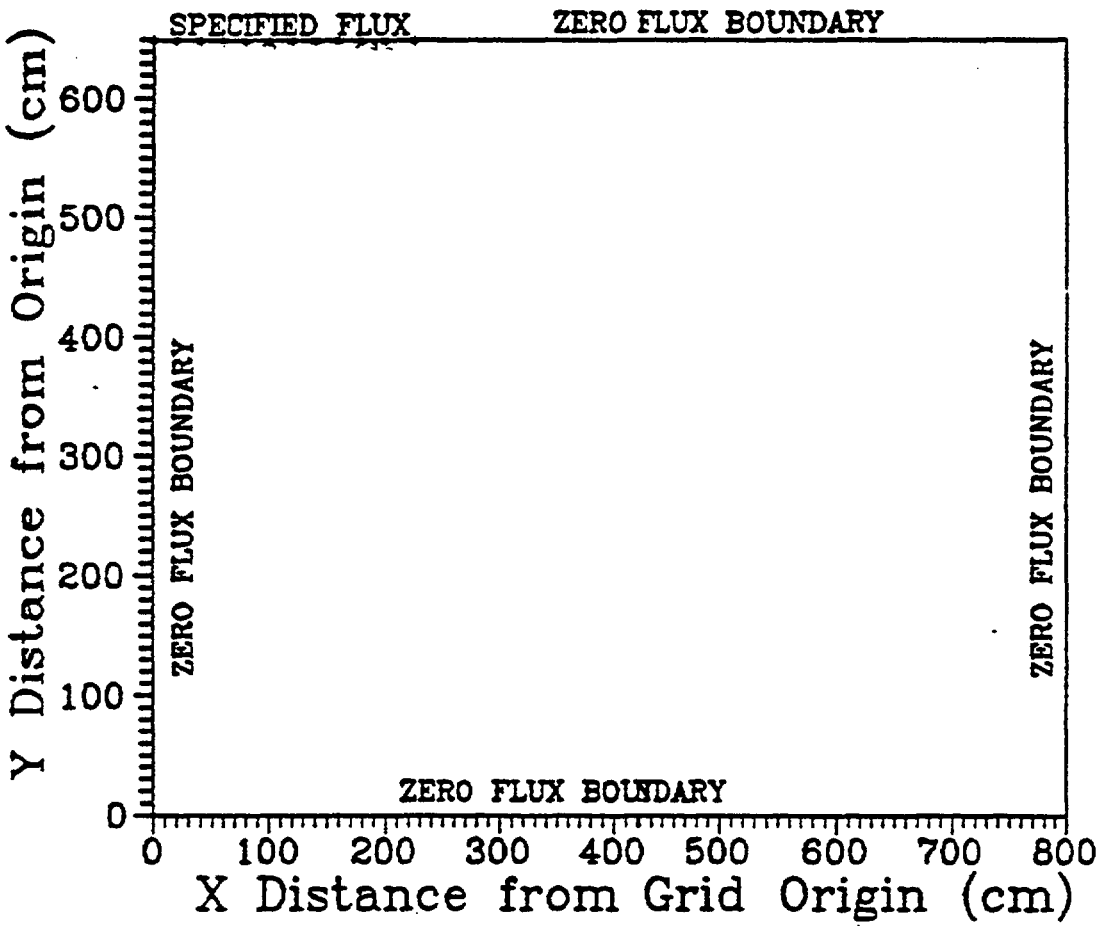

Fig. 8. Conceptual model for 2D Monte Carlo simulation; specified flux was 1.9 cm/day for experiment #1 and 0.49 cm/day for experiment #2.

required input for VAM2D). Those parameters are θ_r, θ_{sat}, K_{sat}[1], and the van Genuchten characteristic curve descriptors α and n. These parameters are employed to calculate the moisture content, θ, from the pressure head, ψ:

$$\theta=\theta_r+(\theta_s-\theta_r)[1+\alpha|\psi|^n]^m \quad (5)$$

and the unsaturated conductivity as a function of effective saturation:

$$K(S_e)=K_{sat}S_e^{1/2}\left[1-\left(1-S_e^{1/m}\right)^m\right]^2 \quad (6)$$

In fitting the laboratory measured data to (5), the m parameter is constrained to $m=1-1/n$. In any rigorous Monte Carlo analysis one would need to vary each of these 5 parameters over the range of their distribution. This would clearly result in a very large number of simulations. Given the significant computer time required to solve the highly non-linear Richards equation (4), we were interested in determining if any significant correlations existed between any of the parameters to help cut down on the number of simulations. To assess cross-correlations we used scatter plots between every pair of the parameters. These scatter plots are shown in Figures 9-11. These plots suggest no obvious cross-correlations, but they do show that each of the parameters vary over a fairly significant range.

Considering the results of the scatter plots (Fig.9-11), the most direct (brute force) Monte Carlo approach would result in several hundred model runs (by stratifying each parameter distribution into equal cumulative probability ranges and then directly sampling from each stratification range for all possible permutations). Besides the unacceptable amount of computer time involved, it is possible that this approach could yield a parameter set (θ_r, θ_{sat}, K_{sat}, α, and n) realization which is not representative of the field data. To avoid these problems, we instead decided to simply assign an index number to each soil sample obtained from the field site, and then randomly select 10 samples from each of the top three layers (top 1.5 m). Thus we ended up with a total number of 30 parameter sets which were assumed to be representative of each of the top three layers (through which the infiltrated water must pass to reach the 1.5 m depth).

2D Modeling Results

Experiment #1 results are depicted in Figures 12 and 13, while the results for experiment #2 are shown in Figure 14 and 15. Figures 12 and 14 shows the results

---

[1]The saturated conductivity K_{sat} was measured both in the laboratory on samples obtained from the field and in situ at the site. The first section of this paper details a comparative analysis of the two K_{sat} data sets. Since the unsaturated hydraulic properties were collected on the same samples used in the lab K_{sat} testing, the lab K_{sat} values were used in the Monte Carlo analysis.

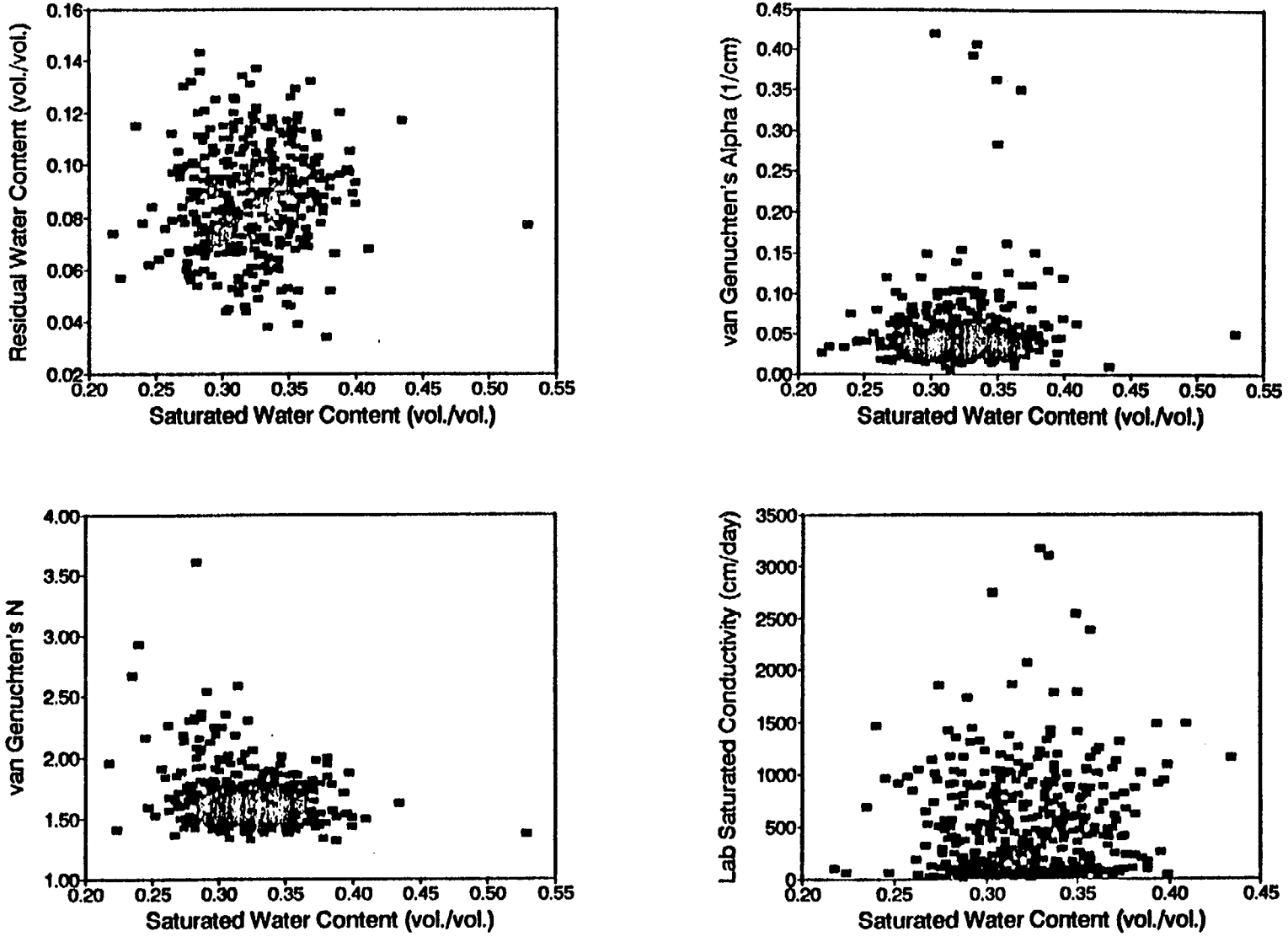

Fig. 9. Scatter plots of θr, the van Genuchten parameters α and n, and K_{sat} versus θ_{sat} for soils

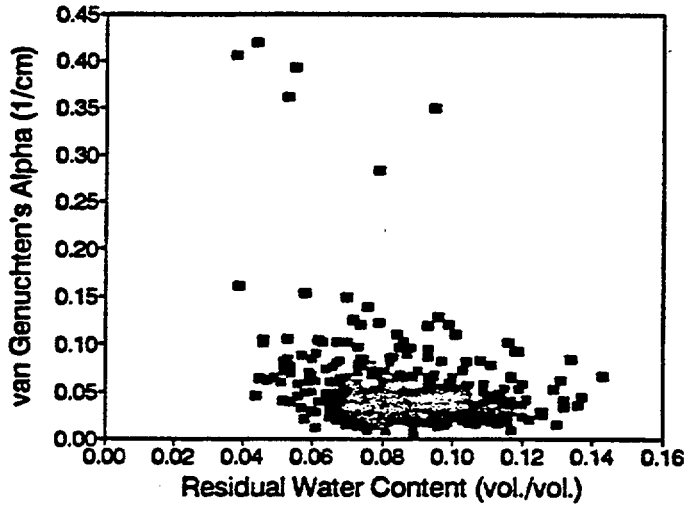

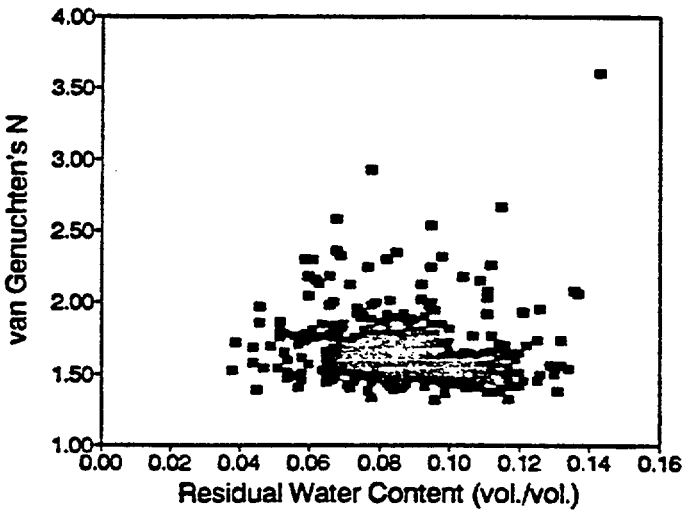

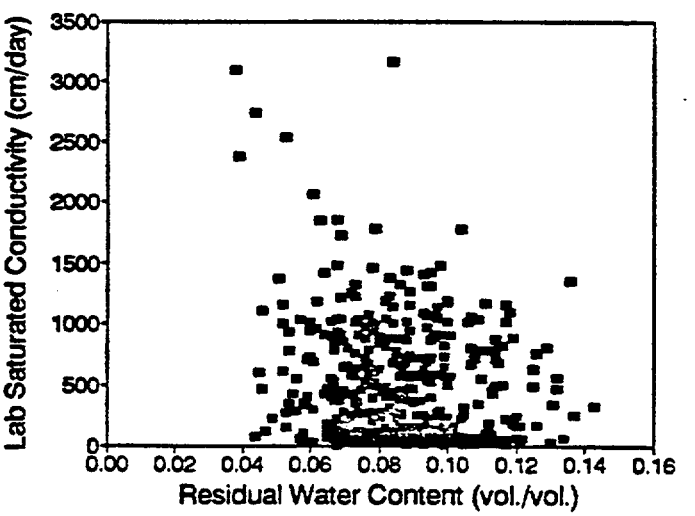

Fig. 10. Scatter plots of the van Genuchten parameters α and n, and K_{sat} versus θ_r for soils reported in the Las Cruces Trench database.

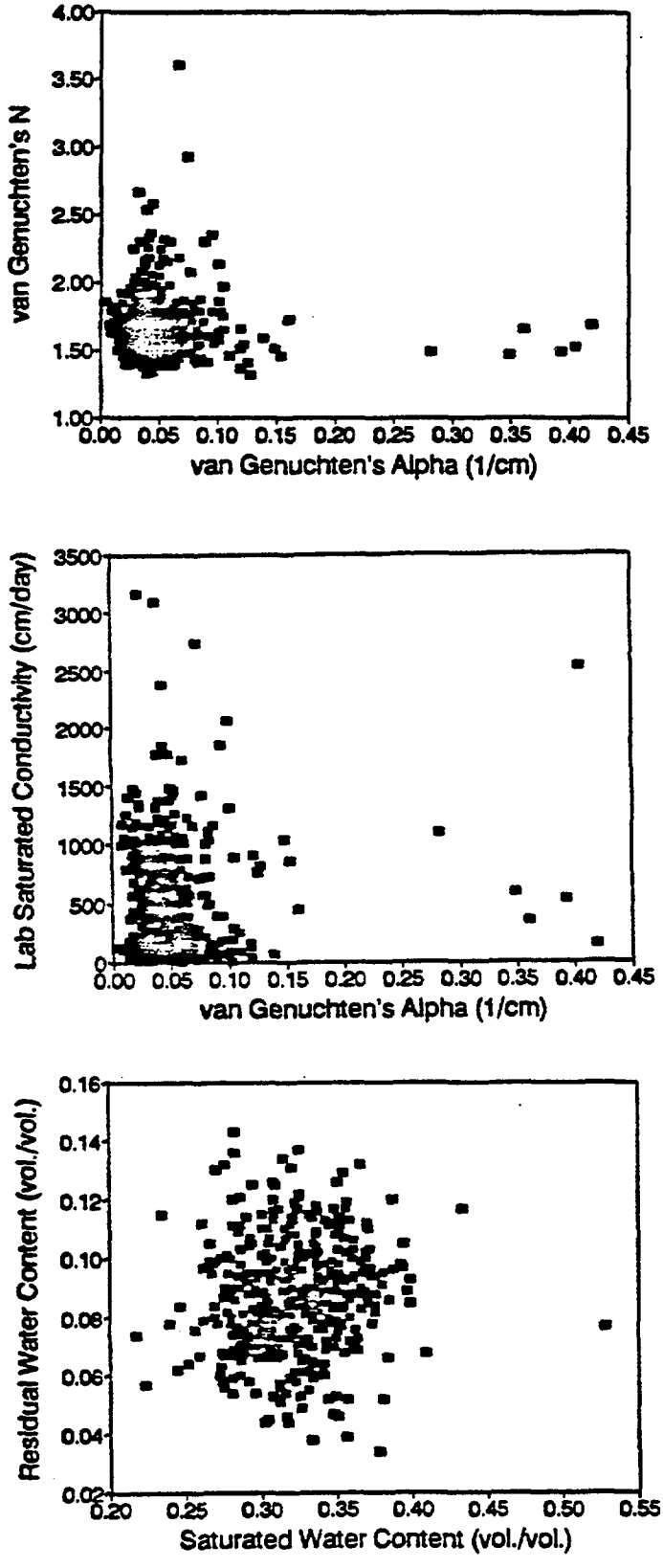

Fig. 11. Scatter plots of n and K_{sat} versus the van Genuchten parameter α, and θ_{sat} versus θr for soils reported in the Las Cruces Trench database.

from each Monte Carlo run, and Figures 13 and 15 summarizes the results by comparing the overall average moisture content breakthrough as well as the individual layer averages to the experimentally observed moisture content breakthrough. These results suggest a number of conclusions and raise several questions. One obvious conclusion is there is an extremely wide range of possible outcomes depending on the model input (Fig. 12). Another is that the layer 1 soils are signicantly different from layers 2 and 3 (Fig. 13). This same conclusion was reached concerning K_{sat} (see section 2). It is also notable that neither the overall average nor the individual layer-average breakthroughs exhibit as sharp of a wetting front as that observed in the field. Additionally, the average layer 1 asymptotic change in moisture content is significantly below the field value.

WHY ARE THE 1D AND 2D RESULTS SO DIFFERENT?

To determine possible causes for the differences between the observed and simulated water content time series, we revisited the diffusion form of the water flow equation (see Eqn. 1 above). Given that the 2D Monte Carlo analysis focused on flow through a homogeneous media, the diffusion model (1) is essentially equivalent to (4) aside from the dimensionality. However, since we were looking at the wetting front breakthrough beneath the center of a relatively wide irrigated plot the 1D and 2D models should yield comparable results. But comparing the 1D predictions (Fig. 2) to the 2D predictions (Figs. 13 and 15), we see that solution of essentially the same partial differential equation subject to the same boundary conditions yields quite different results. The only differences are in the functional forms of the soil properties parameterizing the equations. Figure 5 graphically demonstrates the differences between the θ-ψ curves input to the two different solutions. Looking at (1) and recalling the development of the diffusion form of the flow equation [Kirkham and Powers, 1972] we see that the rate of water flow can be computed as:

$$v_i = D(\theta)\frac{\partial \theta}{\partial x_i} \qquad (7)$$

where v_i is the Darcy velocity and D is the moisture diffusivity as defined for (1). In words, the Darcy flux is simply the moisture diffusivity times the moisture gradient.

The diffusivity, D, can be calculated using the van Genuchten parameters given in the LCT database, or it can be directly obtained from the LCT infiltration experiments using the inverse procedure of Philip (1990). Diffusivities calculated by both of these methods are presented in Figure 14. Note that the D computed using the Broadbridge and White [1988] soil used in the 1D analysis (Fig. 1) lies slightly below the lower of the two diffusivity curves obtained by the Philip (1990) solution. Figure 14 shows that although the median D calculated from the LCT database soil characteristics lies near the inverse-solution D, the distribution of diffusivities was highly skewed and a large fraction of them are extremely large. Thus, in a Monte Carlo analysis which randomly samples from individual soil

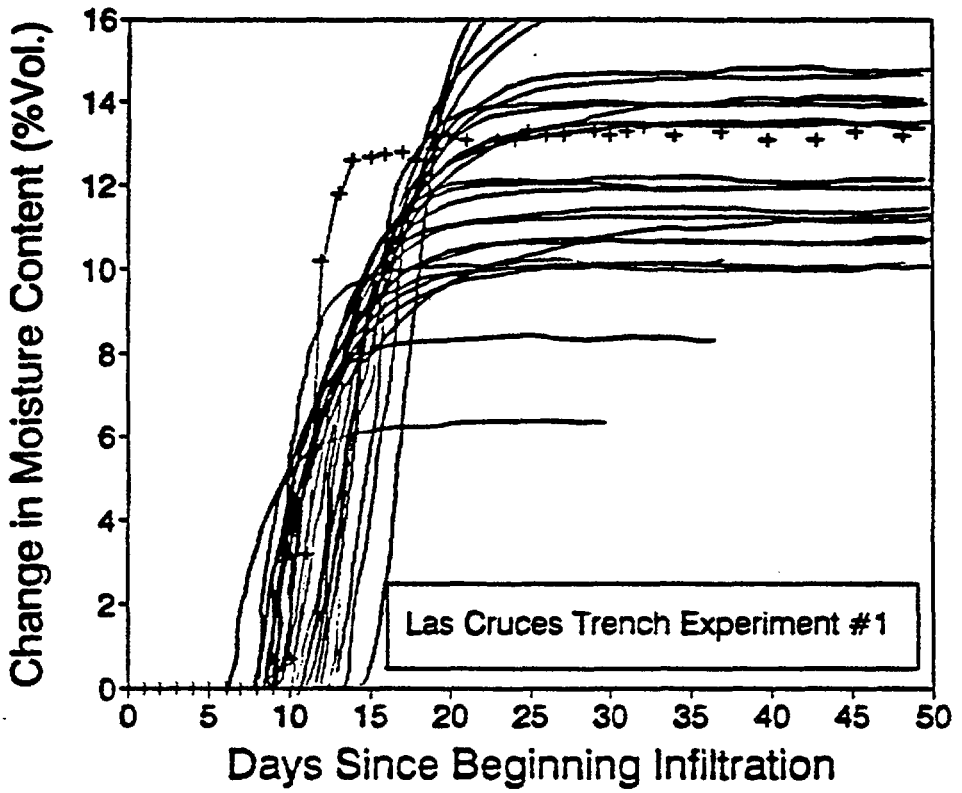

Fig. 12. Experiment #1 2D Monte Carlo simulation results: moisture content breakthrough at 1.5 m depth for each realization. Field observations (average of 4 points) are presented as + for comparison.

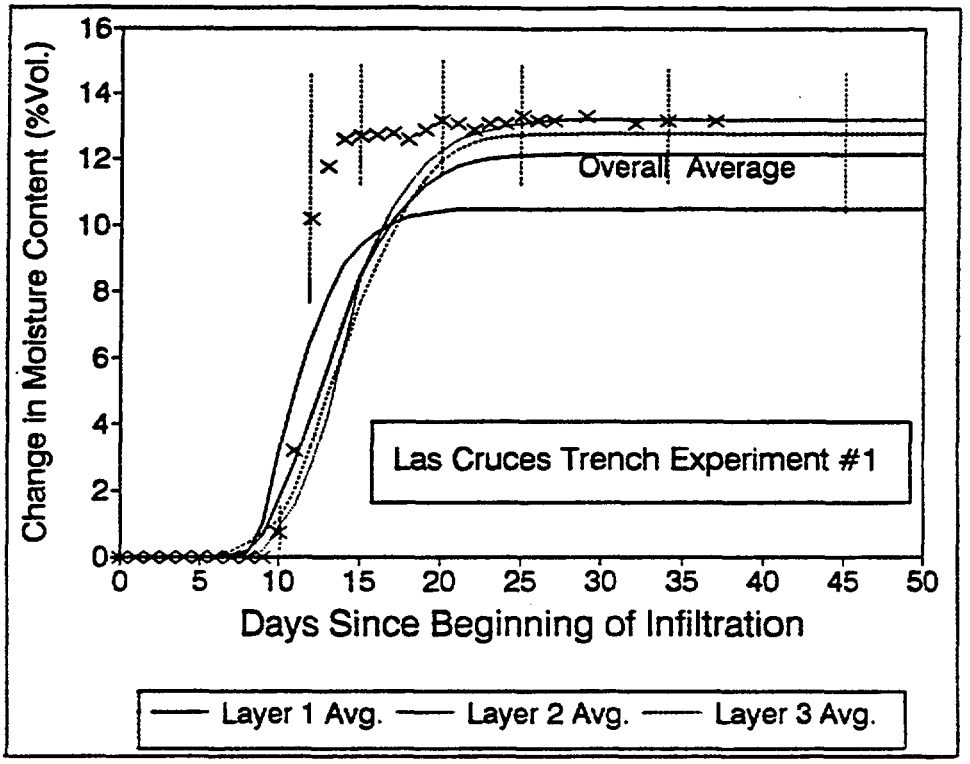

Fig. 13. Experiment #1 2D Monte Carlo simulation results: overall average as well as layer 1-3 average moisture content breakthrough curves. Field observations (average of 4 points) are also presented as × for comparison, as well as the limits on the field measurements.

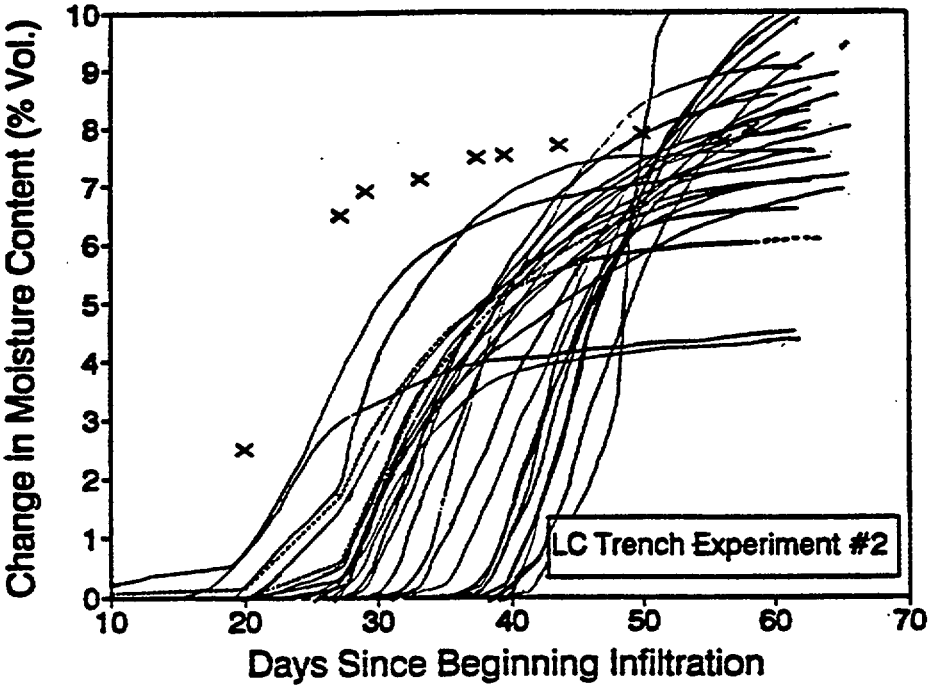

Fig. 14. Experiment #2 2D Monte Carlo simulation results: moisture content breakthrough at 1.5 m depth for each realization. Field observations (average of 4 points) are presented as + for comparison.

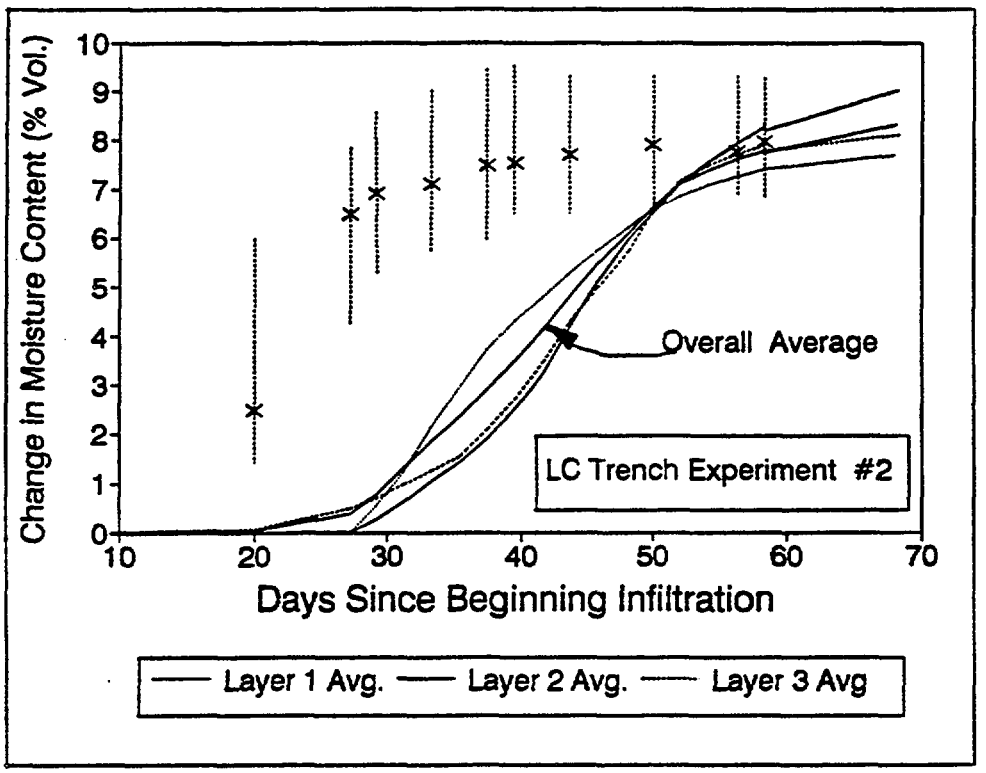

Fig. 15. Experiment #2 2D Monte Carlo simulation results: overall average as well as layer 1-3 average moisture content breakthrough curves. Field observations (average of 4 points) are also presented as × for comparison, as well as the limits on the field measurements.

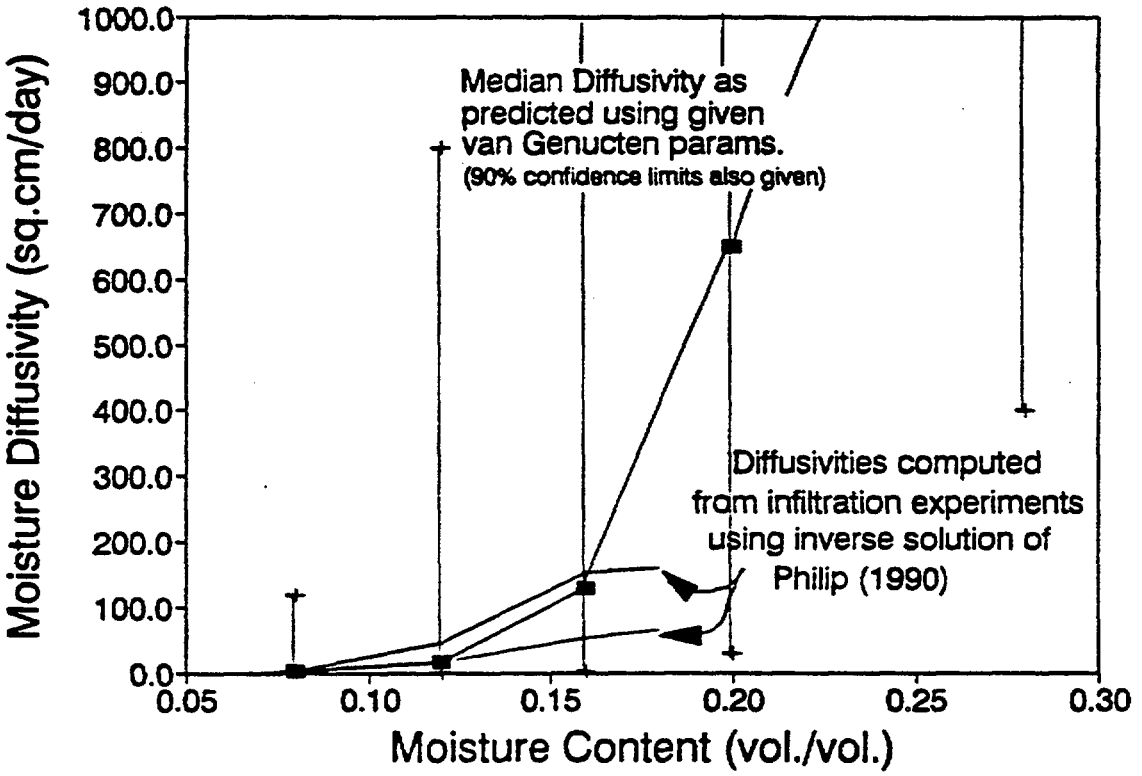

Fig. 16. Moisture diffusivities for LCT soils computed using (1) van Genuchten characteristic parameters given in the database (median D along with 90% confidence limits), and (2) inverse solution of Philip (1990) (experiment #1 yielded the higher of the 2 inverse-solution D values).

properties from the LCT database, one would expect that a significant fraction of the diffusivities would be much larger than effective diffusivities exhibited in the actual infiltration experiments. With the higher D, it would require lower moisture gradients to obtain comparable fluxes. This may offer one explanation for the differences between the 2D predictions and the field observations: the van Genuchten characteristics given in the database simply are not representative of the true bulk hydraulic characteristics of the *in situ* media.

Another possible explanation for the relatively more diffuse wetting front predicted by the model is capillary hysteresis. The laboratory measurements of moisture retention characteristics were made by saturating the core and then draining it under different tensions. Hence, the resulting θ-ψ characteristic represents a drying curve. The experiment, however, would represent a wetting curve since water was applied to a system that was very dry initially. VAM2D has the ability to simulate hysteresis; further studies will be required examine this problem. Since data are only available for the drying curve, the wetting curve characteristics would have to be approximated. Kool and Parker [1987] suggest that van Genuchten's alpha for the wetting curve is about 1.5-2.5 times alpha for the drying curve.

Finally, using the model acceptance criteria stated in the introduction, we would declare the 2D Monte Carlo model invalid (for the performance measure) since the model predictions (Figs. 13 and 15) lie outside the range of experimental observations.

SUMMARY OF CONCLUSIONS FROM PHASE I ANALYSIS OF LAS CRUCES TRENCH EXPERIMENTS

Strictly applying our stated model acceptance criteria we conclude that in both cases, the 1D analytical model and the 2D homogeneous profile Monte Carlo analysis, the models are invalid for predicting the moisture content time series at the 1.5 m depth. Using a different acceptance criteria and/or a different performance measure it is entirely possible that a different conclusion may have been reached.

Perhaps the more interesting issue is why the models failed to meet the declared standards. In both cases it seems that inadequate characterization of the soil hydraulic properties led to the poor model predictions. In applying the 1D Broadbridge and White [1988] analytical solution it appeared that the moisture content-capillary pressure model was not flexible enough to allow accurate prediction for the range of applied infiltration rates. And in the case of the 2D numerical simulations, it also appeared that the soil hydraulic properties given in the LCT database do not accurately reflect the true bulk *in situ* properties. These results confirm (and underline) a well-known problem in unsaturated flow experimentation and modeling: accurately characterizing the soil hydraulic properties over a broad range of spatial scales and hydraulic states is not trivial.

It is clear that more work needs to be done to experimentally measure the soil properties, and to investigate whether current modeling approaches incorporate all of the important processes controlling flow through unsaturated porous materials. These results presented here also tend to confirm the notion already held by many practitioners: the current generation of models can be invaluable in helping us study natural processes in a generic sense, but they fall somewhat short in providing us with tools for accurately predicting the future. When using these models in a forecasting mode, it is vital that parameter uncertainty (and perhaps conceptual model uncertainty) be recognised and accounted for in a clear and defensible manner.

REFERENCES

Ababou, R., 1990. High-resolution three-dimensional simulations of flow in unsaturated soils, *INTRAVAL Phase 1 Meeting*, Las Vegas, Nevada.

Bansabat, J., and L.W. Gelhar, 1990. Stochastic simulation of the second Las Cruces Trench experiment, *INTRAVAL Phase 1 Meeting*, Las Vegas, Nevada.

Davis, J.C., 1986. *Statistics and Data Analysis in Geology*, 2nd. Edition, John Wiley and Sons, Inc., 646 pp.

Davis, P.A., and M.T. Goodrich, 1990. A Proposed Strategy for the Validation of Ground-Water Flow and Solute Transport Models, *Proceedings of the GEOVAL-90 Conference*, May 14-17, 1990, Stockholm, Sweden.

Freeze, R.A., 1975. A Stochastic-Conceptual Analysis of One-Dimensional Groundwater Flow in Nonuniform Homogeneous Media, *Water Resour. Res.*, Vol. 11, No. 5, pp. 725-741.

Freeze, R.A., G. De Marsily, L. Smith, and J. Massmann, 1987. Some Uncertainties About Uncertainty, *Proceedings of the Conference on Geostatistical, Sensitivity, and Uncertainty Methods for Ground-Water Flow and Radionuclide Transport Modelling*, Sept. 15-17, 1987, San Francisco, CA, CONF-870971, Battelle Press.

Hills, R.G., 1990. Simulation of flow and transport in the Las Cruces Trench experiments, *INTRAVAL Phase 1 Meeting*, Las Vegas, Nevada.

Hoeksema, R.J., and P.K. Kitanidis, 1985. Analysis of the Spatial Structure of Properties of Selected Aquifers, *Water Resour. Res.*, Vol. 21, No. 4, pp. 563-572.

Huyakorn, P.S., J.B. Kool, and J.B. Robertson, 1989. *Documentation and User's Guide: VAM2D - Variably Saturated Analysis Model in Two Dimensions (Version 5.0 with Hystersis and Chained Decay Transport)*, NUREG/CR-5352, HGL/89-01, HydroGeoLogic, Inc., Herndon, VA.

Iman, R.L., 1982. Graphs for Use with the Lilliefors Test for Normal and Exponential Distributions, *The Am. Statistician*, Vol. 36, No. 2, pp. 109-112.

Kool, J.B. and J.C. Parker, 1987. Development and Application of Closed-Form Expressions for Hysteretic Soil Hydraulic Properties, *Water*

Resources Research, Vol. 23(1), pp. 105-114.

Kool, J.B., P.S. Huyakorn, and P.J. Wierenga, 1990. Model calibration and simulation of flow in heterogeneous soil, *Proceedings of MODELCARE 90*, International Conf. on Calibration and Reliability in Groundwater Modelling, The Hague, Netherlands, Sept. 3-6, 1990.

Lilliefors, H.W., 1967. On the Kolmogorov-Smirnov Test for Normality with Mean and Variance Unknown, *Am. Stat. Assoc. Jour.*, Vol. 62, pp. 399-402.

Lilliefors, H.W., 1969. On the Kolmogorov-Smirnov Test for The Exponential Distribution with Mean and Variance Unknown, *Am. Stat. Assoc. Jour.*, Vol. 64, pp. 387-389.

Nicholson, T.J., P.J. Wierenga, G.W. Gee, E.A. Jacobson, D.J. Polmann, D.B. McLaughlin, and L.W. Gelhar, 1987. Validation of Stochastic Flow and Transport Models for Unsaturated Soils: Field Study and Preliminary Results, *Proceedings of the Conference on Geostatistical, Sensitivity, and Uncertainty Methods for Ground-Water Flow and Radionuclide Transport Modelling*, Sept. 15-17, 1987, San Francisco, CA, CONF-870971, Battelle Press.

Reynolds, W.D. and D.E. Elrick, 1985. In Situ Measurement of Field-Saturated Hydraulic Conductivity, Sorptivity, and the Alpha Parameter Using the Guelph Permeameter, *Soil Sci.*, Vol. 140, pp. 292-302.

Reynolds, W.D. and D.E. Elrick, 1986. A Method for Simultaneous In Situ Measurement in the Vadose Zone of Field-Saturated Hydraulic Conductivity, Sorptivity, and the Conductivity-Pressure Head Relationship, *Ground Water Monitoring Review*, Vol. 6, pp. 84-95.

van Genuchten, M.Th., 1980. A Closed-Form Equation for Predicting the Hydraulic Conductivity of Unsaturated Soils, *Soil Sci. Soc. Am. J.*, Vol. 44, pp. 892-898.

Wierenga, P.J., A.F. Toorman, D.B. Hudson, J. Vinson, M. Nash, and R.G. Hills, 1989. *Soil Physical Properties at the Las Cruces Trench Site*, NUREG/CR-5441, University of Arizona, Tucson, AZ.

APPENDIX C7

Flow and transport simulations of the
second Las Cruces Trench experiment

KEMAKTA AR 90-04

FLOW AND TRANSPORT SIMULATIONS OF THE SECOND LAS CRUCES TRENCH EXPERIMENT

INTRAVAL Case 10

Marie Collin
Maria Lindgren
Anders Rasmuson

KEMAKTA Consultants Co
Stockholm, Sweden

March 27 1990

ABSTRACT

Water and tracer transport in the second Las Cruces Trench experiment have been simulated with the deterministic Integrated Finite Difference codes TRUST + TRUMP.

Unsaturated water flow is modelled using the "classical" Richard's equation. Three different calculations were performed. In the first, average hydraulic data, where the soil is treated as homogeneous, are used. In the second, a discrepancy between residual water contents obtained on laboratory samples and substantially lower water contents observed in the field is resolved by extrapolation. In the third simulation the layered soil structure is accounted for (but original residual water contents are used). It was found that the layered model gave the best agreement with experimental data especially in terms of lateral spreading.

Tracer transport is modelled using the unsaturated version of the convection-dispersion equation. In the general case, the dispersion coefficient depends on both the water flow rate and the water content. At present, however, only the water-content dependence is considered. Two different values of the dispersion coefficienct, D_0, $2 \cdot 10^{-8}$ and $5 \cdot 10^{-9}$ m^2/s, are used in the calculations. For $D_0 = 2 \cdot 10^{-8}$ m^2/s the peak concentrations are far too low and the spreading far too large in comparison with the experimentally observed concentration plume. For $D_0 = 5 \cdot 10^{-9}$ m^2/s a better agreement is obtained but it is still not good, indicating that even lower dispersion coefficients should be used in the calculations.

Table of contents

TEST CASE DESCRIPTION

The field site is on a basin slope of Mount Summerford, which is at the north end of the Dona Ana Mountains in New Mexico, USA.

The climate in the region is characterized by an abundance of sunshine, low relative humidity and an average class A pan evaporation of 239 cm/yr. Average annual precipitation is 23 cm with 52% of the rainfall occurring between July 1 and September 30. The average monthly maximum air temperature is highest in June at 36°C and lowest in January at 13°C.

Two trench experiments have been carried out, in this study the second has been studied. In Figure 1 a top view of the trench, with the second trench experiment shown on the right side (north) of the trench. The trench is 12 m long, 5 m wide and 6.0 m deep. Tensiometers for measuring the water content are located at planes 1, 2 and 3 (see Figure 1). Solute samplers are located at plane 0 only.

Water was supplied at a rate of 0.43 cm/day for 75 days over a 1.2 m by 12 m area. After 75 days, irrigation was stopped and redistribution was monitored. Water content as function of time and depth was measured with neutron probes.

During the first 11.5 days of water application, 0.01 N $NaBr{\cdot}2H_2O$ (800 ppm) and 0.1 μCi/ml tritium were used as tracers. After 11.5 days, the application of bromide and tritium stopped. Soil solution was collected through the solution samplers and the concentrations of tritium and bromide in the solution samples were measured in the laboratory.

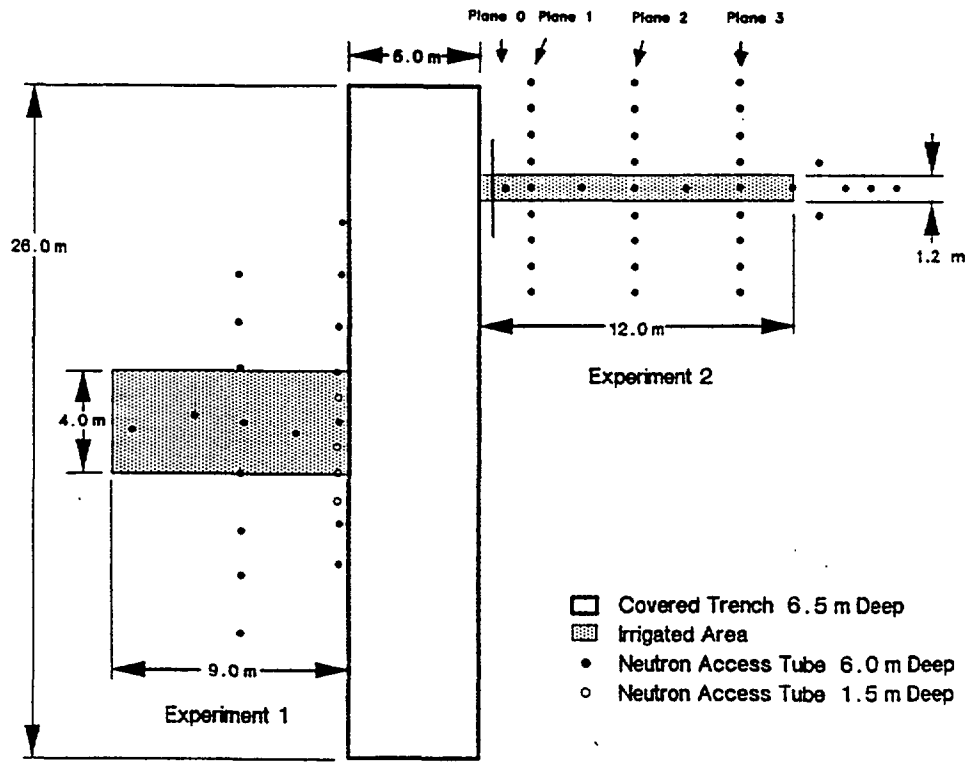

Figure 1 Top view of the experimental trench.

DESCRIPTION OF THE CONCEPTUAL MODEL

The model is based on the theory of unsaturated flow and transport in porous media. The calculations are carried out in two steps, the first being a water flow calculation. Secondly, a tracer transport calculation was made using water flow and distribution data from the water flow calculation. A two-dimensional model is used. The modelled domain is shown in Figure 2. The soil in the modelled domaine may be built up from different layers.

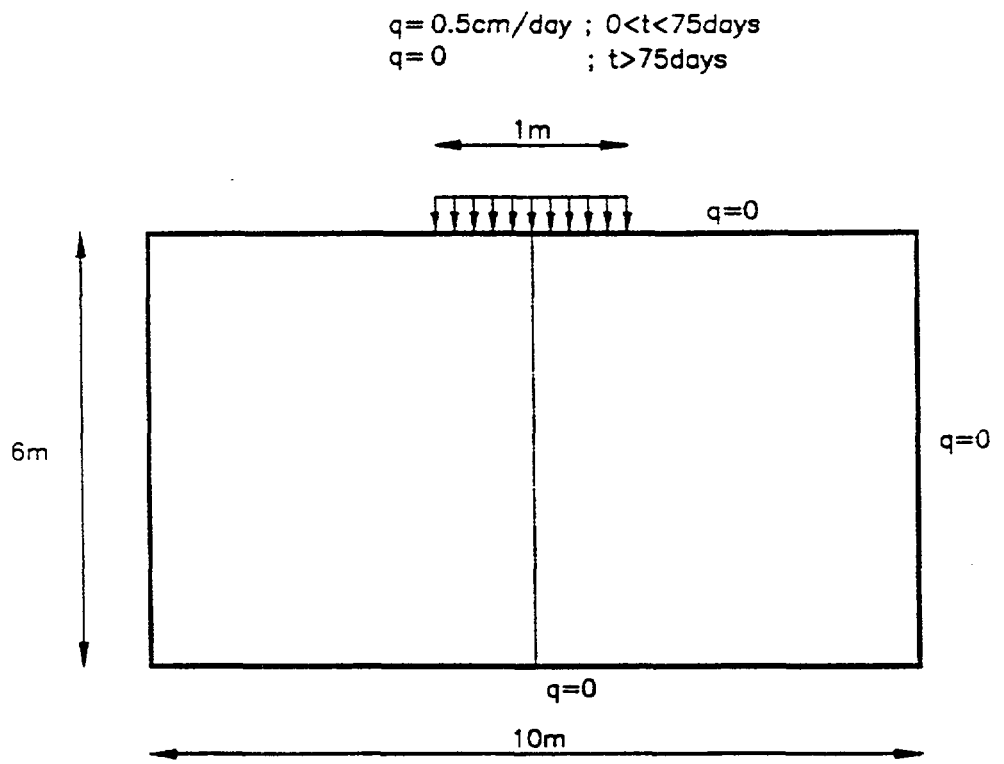

Figure 2 The modelled domaine.

Water flow model

The water flow in the unsaturated soil is modelled by using Richard's equation for unsaturated porous media. The water infiltration at the irrigated area is modelled as constant flux over the boundary during the infiltration period and no flux thereafter. Evaporation from the soil surface is not considered.

Tracer transport model

The tracer transport is modelled as simultaneous convective and diffusive/dispersive transport, where the dispersion is assumed to be diffusion-like and proportional to the water content (but independent of velocity at this stage). The tracers are assumed not to interact with the solid surfaces in the soil (nonsorbing species). The supply of tracers at the irrigated area is modelled as constant flux over the boundary during infiltration of tracer contaminated water, and no flux over the boundary during infiltration of pure water and for the case of no water infiltration.

MATHEMATICAL FORMULATION OF THE MODEL

Water flow model

The Darcy equation for flow in unsaturated porous media may be written as:

$$\overline{q} = - K(\theta)\ \nabla\Phi = - K(\theta)\ \nabla(\psi+z)$$

Generally, the hydraulic conductivity K is a tensor depending on both direction and water content. For a homogeneous and isotropic medium however, K reduces to a simple function of the water content.

The equation of conservation of mass (Richard's equation) in unsaturated incompressible porous media may be written:

$$\frac{\partial\theta}{\partial t} = - \nabla \cdot \overline{q} = \nabla \cdot [K(\theta)\ \nabla\psi]$$

accumulation — capillary flow + gravitational flow

Since $\psi=\psi(\theta)$ this equation can, alternatively, be formulated with the capillary potential as the independent variable:

$$\frac{d\theta}{d\psi}\frac{\partial\psi}{\partial t} = \nabla\ [K(\psi)\ \nabla\psi] + \frac{dK}{d\psi}\frac{\partial\psi}{\partial z}$$

accumulation — capillary flow — gravitational flow

The calculations have been carried out using the integrated finite difference code TRUST, developed at Lawrence Berkeley Laboratories (Narasimhan, 1975). Saturated and unsaturated water flow in up to three dimensions may be calculated with this code. The code solves an integrated version of the equation above over a small sub-volume:

$$\int_{\Gamma} \rho_w \frac{k_w \rho_w g}{\mu_w} \nabla(\psi+z) \cdot \bar{n}\, d\Gamma + G = M_c \frac{D\psi}{Dt}$$

capillary+gravitational flow	source	accumulation

The fluid mass capacity, M_c, is given by:

$$M_c = V_s \rho_w \left[S e \rho_{w0} \beta_w g + S \rho_w g \chi' a_v + e \frac{dS}{d\psi} \right]$$

water compressibility	deformation of soil	desaturation of pores

In the present case only the last term, desaturation of pores, is accounted for.

Tracer transport model

The flux equation for transport of tracer in porous media may be written as:

$$\bar{q}_t = \bar{q}c - D \nabla c$$

where c is the tracer concentration in the water.

The equation of conservation of mass is:

$$\frac{\partial(Q+\theta c)}{\partial t} = -\nabla \cdot \bar{q}_t = \nabla \cdot (D \nabla c) - \nabla \cdot (\bar{q}c)$$

accumulation	diffusion dispersion	convection

Note that the tracer may be accumulated in the system both sorbed on particle surfaces (Q) and dissolved in the water (θc).

The tracer transport calculations are made with a modified version of the integrated finite difference code TRUMP. This code is originally written for transient heat transport calculations in multi-dimensional heterogeneous media with arbitrary geometry (Edwards, 1972). The present version solves the following equation:

$$\left[\frac{Q}{c}+\theta\right]\frac{\partial c}{\partial t} = \nabla \cdot (D\ \nabla c) - \nabla \cdot (\bar{q}c) + G - \rho\ Q_a \frac{\partial a}{\partial t} - \rho\ Q_b \frac{\partial b}{\partial t}$$

accumulation	diffusion dispersion	convection	source	chemical reactions

The procedure for using the TRUST and TRUMP codes for these types of calculations is further described by Collin and Rasmuson (1990).

Generally, the dispersion coefficient depends on both the water flow rate and the water content.

$$D = D(q,\theta)$$

Presently, however, only the water-content dependence is considered.

INPUT DATA

Water flow calculations

Data used for the water flow calculation originate from a copy of a letter from Dr Richard Hill to Dr Tom Nicholson dated February 7 1989. According to this letter, water was applied at a rate of 0.5 cm/day for 75 days over a 1 m by 12 m area. These data are not completely in accordance with data given later (Wierenga et al 1989) where application rate and area were slightly modified to 0.43 cm/day and 1.2 m by 12 m, respectively. The cumulative amount of water applied during the irrigation period is 4500 l and 4721 l, respectively.

Material data for the soil are taken from a Table 2 "van Genuchten parameters for the Las Cruces Test site: Layered soil model". The water retention data are then calculated from:

$$S_e = \frac{\theta - \theta_r}{\theta_s - \theta_r} = \frac{1}{[1 + (\alpha(-\psi))^n]^m}$$

where

$$m = 1 - \frac{1}{n}$$

The unsaturated hydraulic conductivity is calculated from:

$$K = K_s \cdot S_e^{\frac{1}{2}} \left[1 - (1 - S_e^{\frac{1}{m}})^m \right]^2$$

Parameters for both an average for the material in the whole site and for nine layers in a layered model are shown in Table 1.

Table 1 Parameters for the materials used in the calculations

Layer (cm/day)	Depth (cm)	θ_s	θ_r	α (1/m)	n	K_s
1	0-20	0.3483	0.0950	4.189	1.9040	539.2
2	20-120	0.3433	0.0913	6.233	1.5271	250.0
3	120-180	0.3359	0.0848	5.963	1.5738	266.9
4	180-250	0.3129	0.0731	6.758	1.5444	299.8
5	250-290	0.3021	0.0716	4.034	1.5499	250.0
6	290-350	0.2942	0.0889	7.017	1.7085	357.5
7	350-450	0.3100	0.0769	2.694	1.4320	215.8
8	450-530	0.3247	0.0843	4.115	1.3843	171.5
9	530-600	0.3050	0.0822	4.548	1.4549	223.2
Aver.	0-600	0.3207	0.0837	5.472	1.5149	271.3

In Figure 3 the experimental initial water content in the different planes are shown. The different planes show great variations but some observations can be made: the top meter of soil is much wetter than the bottom 5 meters. In Figure 4 the initial conditions measured at plane 2 is shown together with the initial conditions used in the calculation cases A and B.

The experimental data describing the materials are limited by the residual water content achieved, depicted with S_r in Figure 3. The value of the residual water content in these experiments were rather high about 25-30% of the saturated water content. Since the test site is located in a very dry area the initial water content was found to be less than θ_r in most part of the soil. In order to describe the situation better the material data have been recalculated. In Figure 5 the water retention curves for the average material both in original and modified shape are shown. A linear extrapolation is made from S_r to 0. In Figure 6 the corresponding curves on the hydraulic conductivity as function of saturation degree are shown.

The following water flow calculations have been carried out:

Case A: Homogeneous soil with the original material data for the average material. The initial condition is fitted to the observation data at plane 2, with the limitation that the saturation degree must be higher than the residual water content, see Figure 4.

Case B: Homogeneous soil with the modified material data for the average material. The change in material data makes it possible to have saturation degrees below the residual water content. The initial water content used in this case is lower in the bottom 5 meters. For the top meter the same initial conditions as in case A is used (see Figure 4).

Case C: Layered soil structure with the original material data for the layers. The same initial water content in the top meter as in the two other cases was used. For the bottom 5 meters the same capillary potential as in case A was used.

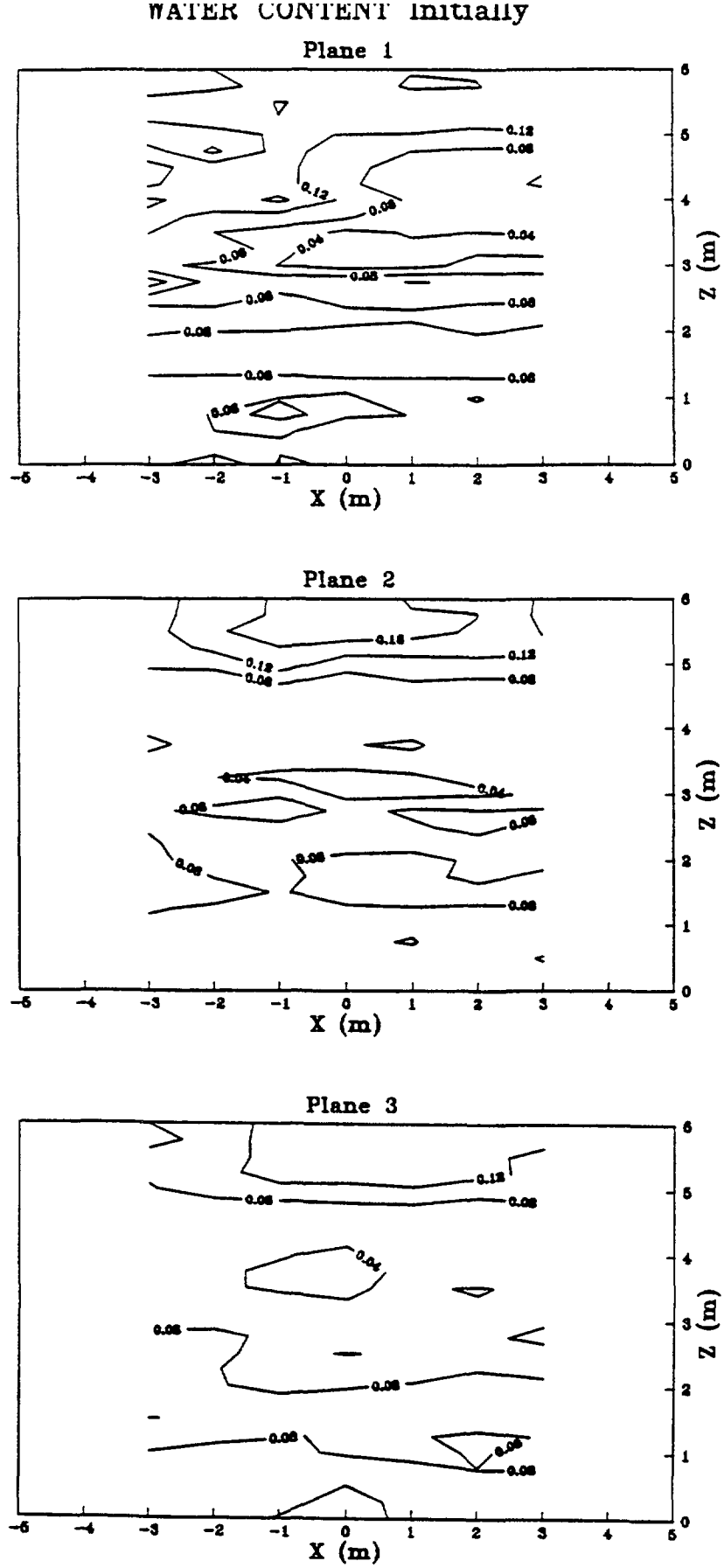

Figure 3 Experimental initial water content (θ) at plane 1, 2 and 3.

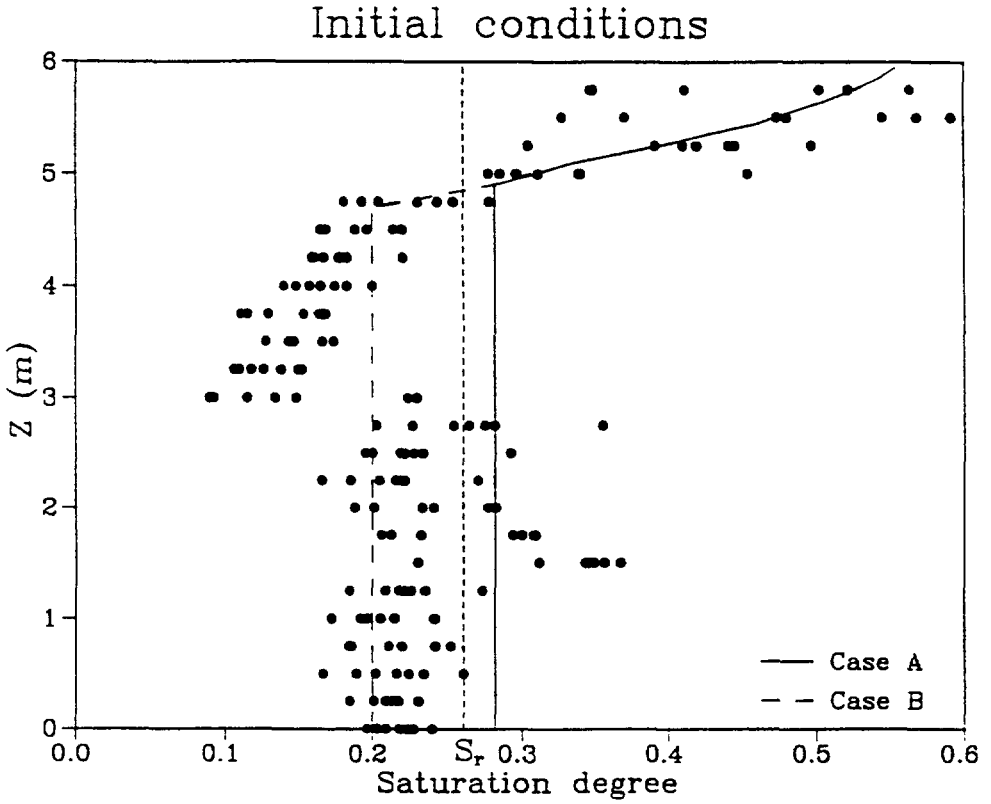

Figure 4 Initial conditions measured at plane 2. Initial conditions used in calculation case A and B.

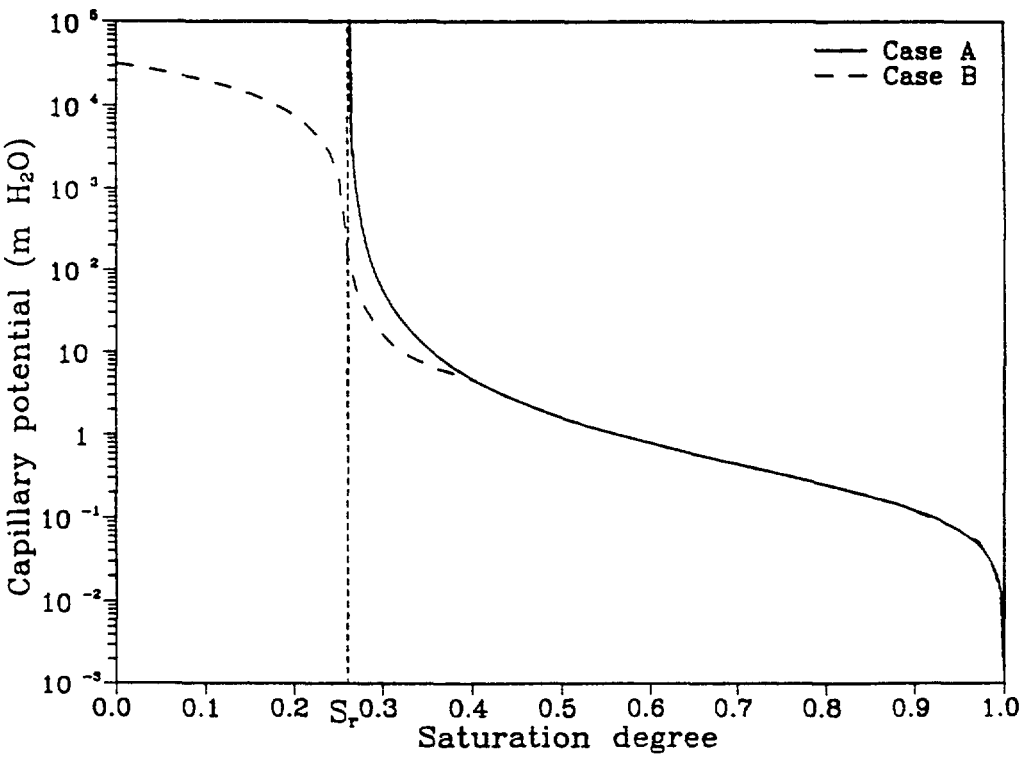

Figure 5 Water retention curves for the average material: original and modified form.

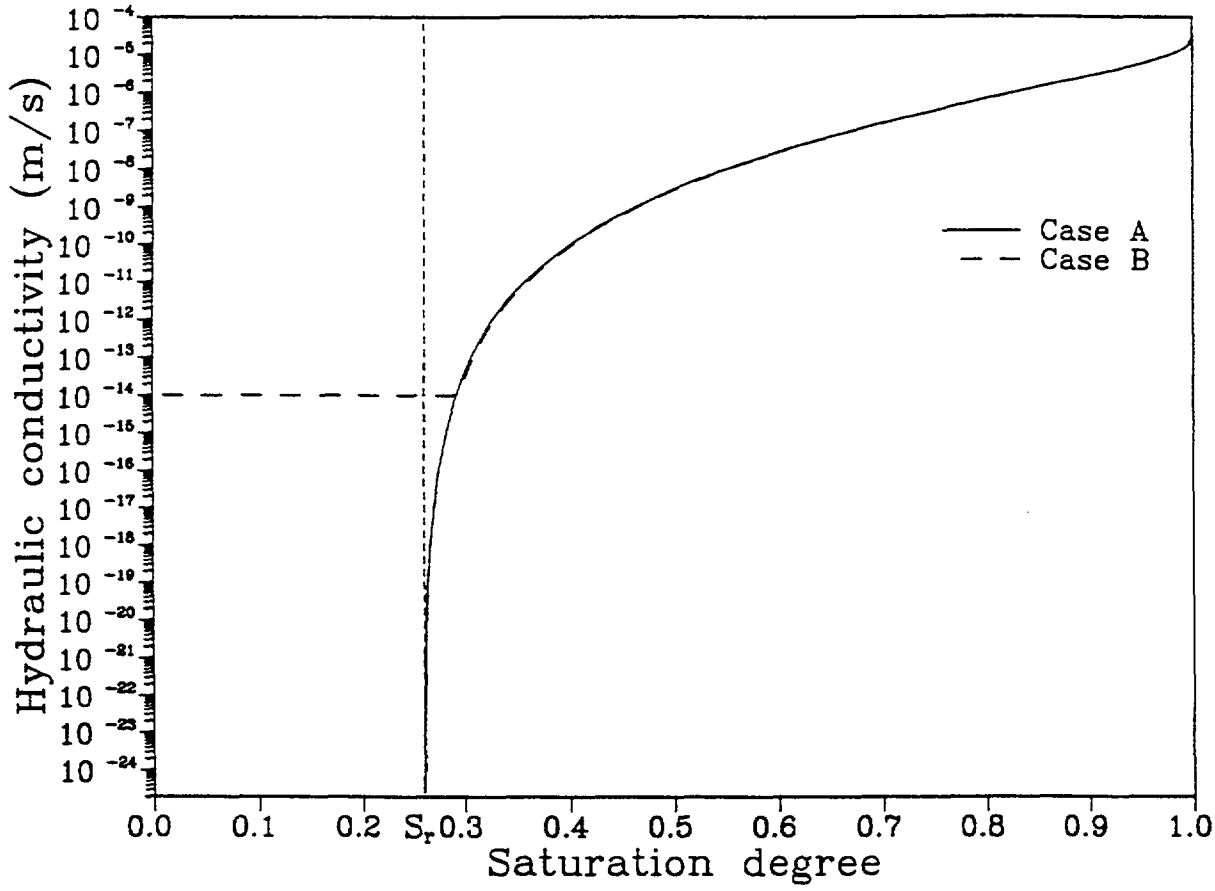

Figure 6 Hydraulic conductivity as function of saturation degree for the average material: original and modified form.

Tracer transport calculations

As mentioned above water flow and distribution from the water flow calculation is used for the tracer transport calculations. The dispersion is modelled to be proportional to the water content:

$$D = D_0 \cdot \theta$$

where D_0 is a constant.

Different values of the dispersion coefficient at saturation D_0 has been tested.

The tracer is applied into the system as a constant flux over the boundary corresponding to the irrigated surface during the first 11.5 days. The calculations are made in dimensionless concentration units corresponding to concentration = 1 in the applied water. This corresponds to a total supply of 552 g Bromide and 69 000 µCi Tritium. According to Wierenga et al (1989) 575 g Bromide and 71 953 µCi Tritium were applied during the experiment. The differences are caused by the difference in amount of water applied. The initial concentrations of tracers in the soil is zero.

SIMULATION RESULTS

Water flow calculations

The predicted water content distribution at 70 and 90 days for the three different cases: A, B and C together with the observations at plane 1, 2 and 3 are shown in Figure 7 and 8.

Case A, uniform soil model - since the initial conditions is much wetter than observed at the trench, the predicted water content are higher during all times. The wetting front seems to go deeper but is not so broad as the trench observations.

Case B, uniform soil model, initially dryer - a modification of case A. The water content variations are in better agreement with the observations. However, the wetting front have the same tendency as in case A, moving more downwards and less to the sides than the observed movement. Due to the steep wetting front numerical problems were encountered and the simulation was made only for the infiltration period.

Case C, 9 layered soil model. The domain was divided into 9 layers with different material data. This calculation seems to be in the best agreement with the experimental water content profiles. In particular, the observed lateral water movement is better encountered for. The agreement between observations at plane 2 and the calculation is rather good. Comparison with experimentally determined water contents at the plane where the solute samples are taken, however, show a poorer agreement. Since this plane is situated close to the end of the irrigated strip one may expect that the water content is affected by the boundary at the trench. The water flow is probably not truly two-dimensional but three-dimensional.

An additional calculation with layered structure and dryer initial conditions seems to be a natural next step.

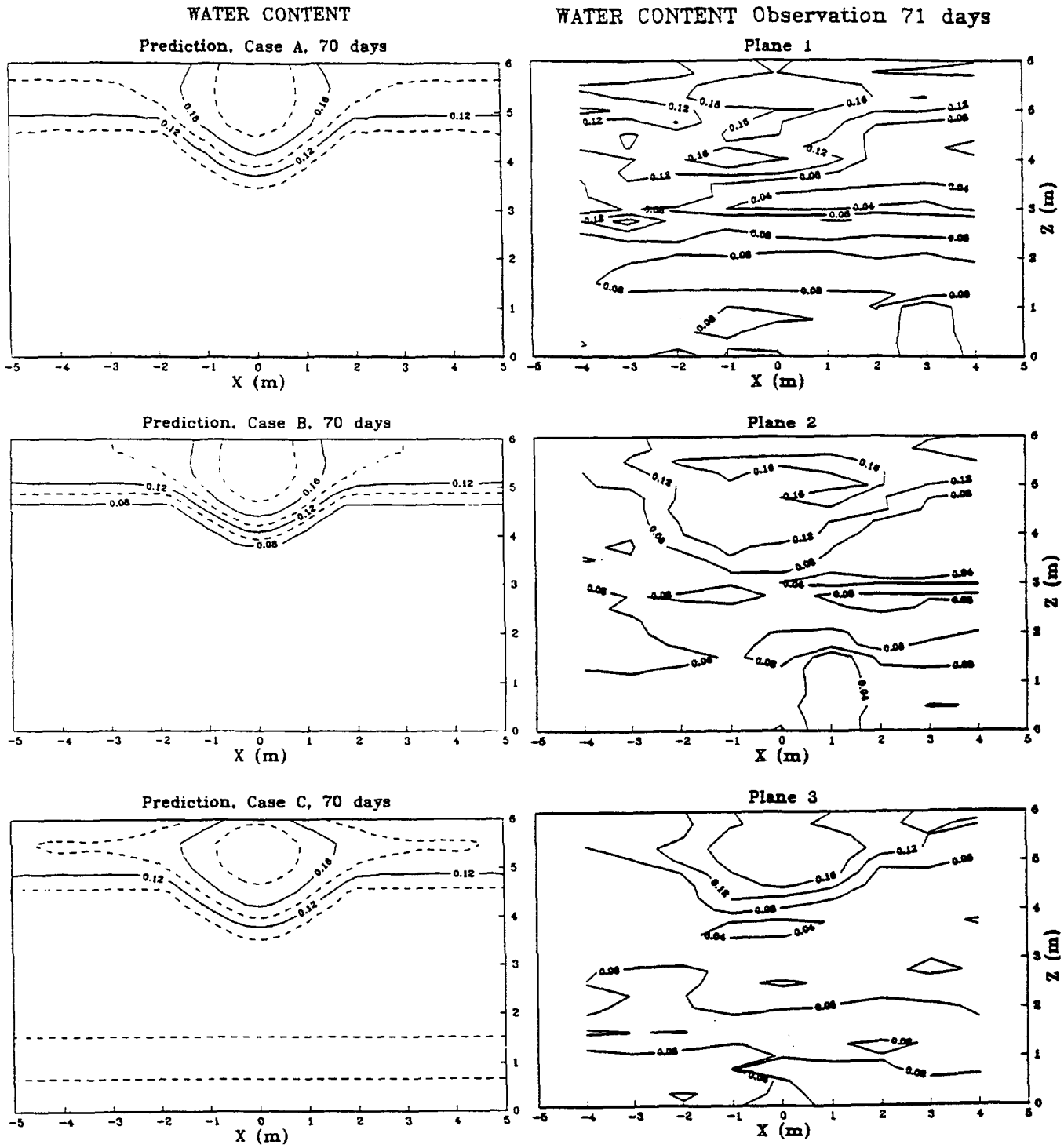

Figure 7 Predicted and observed water content distribution at 70 (71) days.

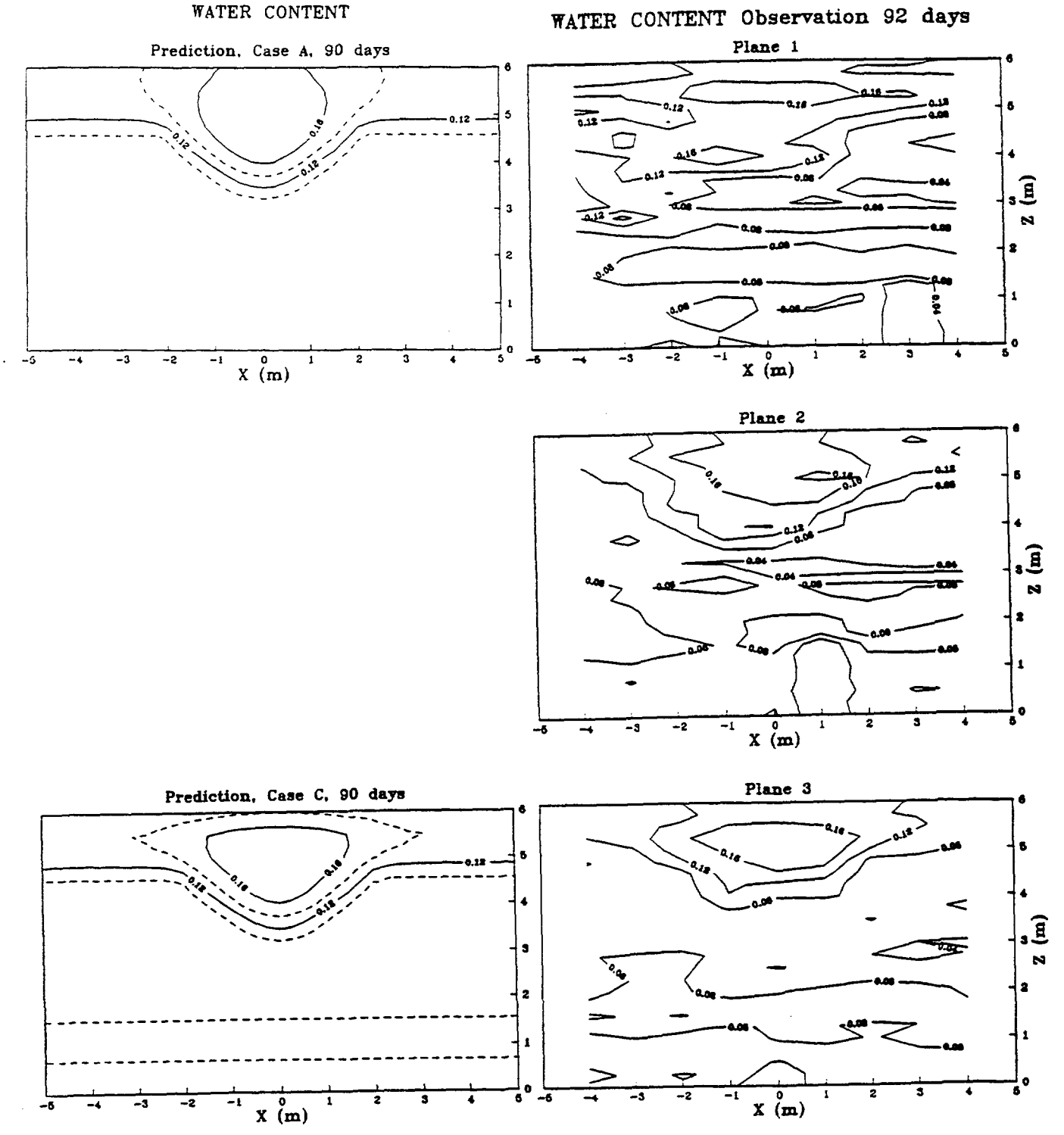

Figure 8 Predicted and observed water content distribution at 90 (92) days.

Tracer transport calculations

Calculations were made for two values of D_0, $2 \cdot 10^{-8}$ (and $5 \cdot 10^{-9}$) m^2/s.

Two-dimensional plots of the concentration distribution for the calculation with low dispersion constant in comparison with observations are shown in Figures 9, 10 and 11. In addition, a series of three one-dimensional plots is given in Figure 12. The first two plots in Figure 12 show the predicted concentration in the middle of the irrigated area (x = 0.125 m) for the calculations with high and low dispersion coefficient respectively. The last plot gives average experimental concentrations for the sampling points at x = $\pm$0.25 and x = 0.

The maximum calculated concentration is much lower than the highest experimental concentration for $D_0 = 2 \cdot 10^{-8}$ m^2/s. For $D_0 = 5 \cdot 10^{-9}$ m^2/s the maximum concentration is higher, but it is still considerably lower than the highest experimental concentration. According to Fried and Combarnous (1971) (Figure 31, page 226) the longitudinal dispersion for flow under saturated conditions is about the same as the molecular diffusion for these very low flow velocities. The molecular diffusion coefficient for Bromide is about $1 \cdot 10^{-9}$ m^2/s. This indicates that an even lower dispersion coefficient should be used in the calculations. Such calculations, however, requires extensive computer time and memory due to the high Peclet-numbers involved.

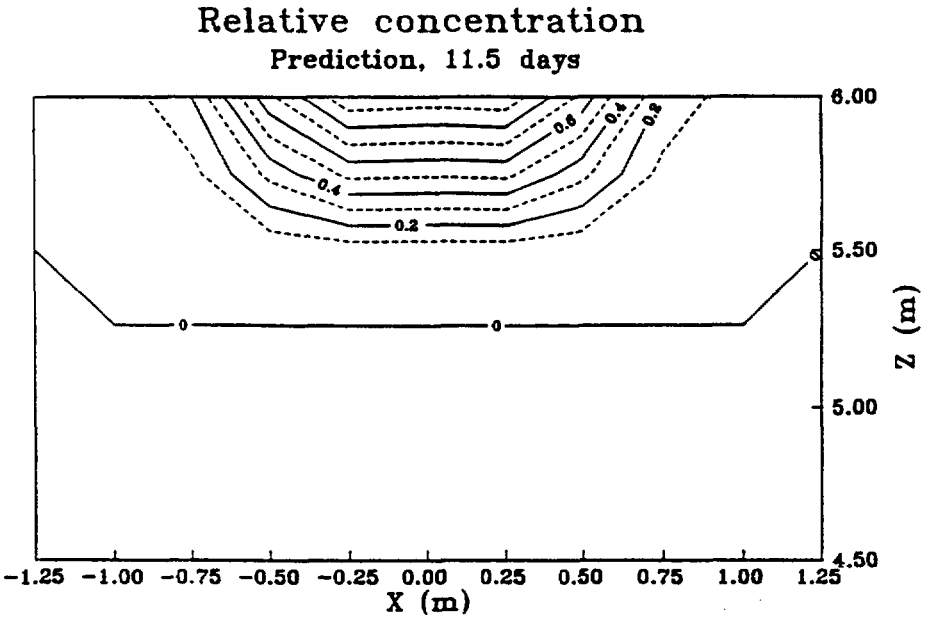

Figure 9 Prediction of tracer distribution at 11.5 days ($D_0 = 5 \cdot 10^{-9}$ m^2/s).

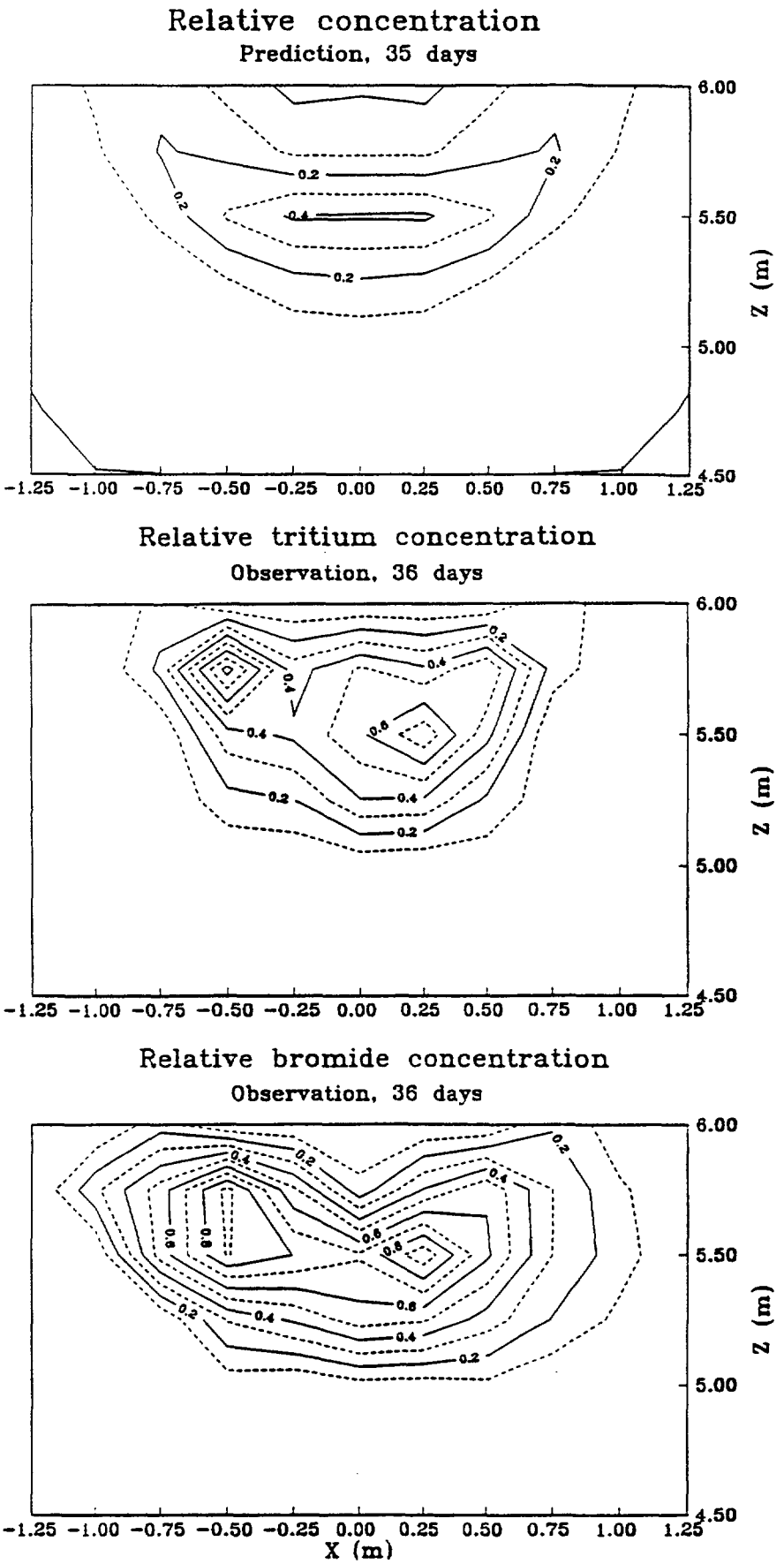

Figure 10 Prediction and observation of tracer distribution at 35 (36) days (D_0 = 5·10-9 m^2/s).

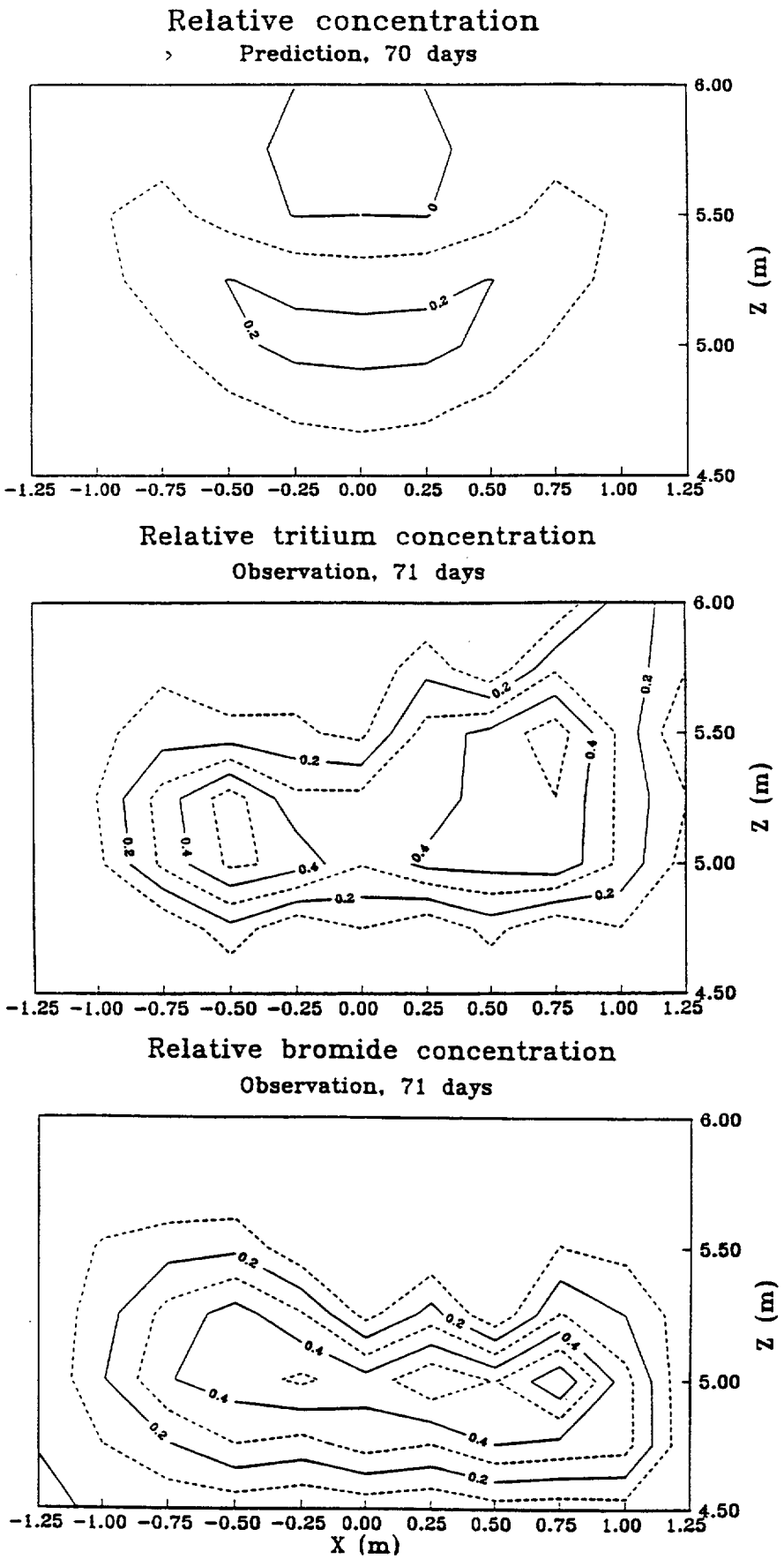

Figure 11 Prediction and observation of tracer distribution at 70 (71) days ($D_0 = 5 \cdot 10^{-9}$ m^2/s).

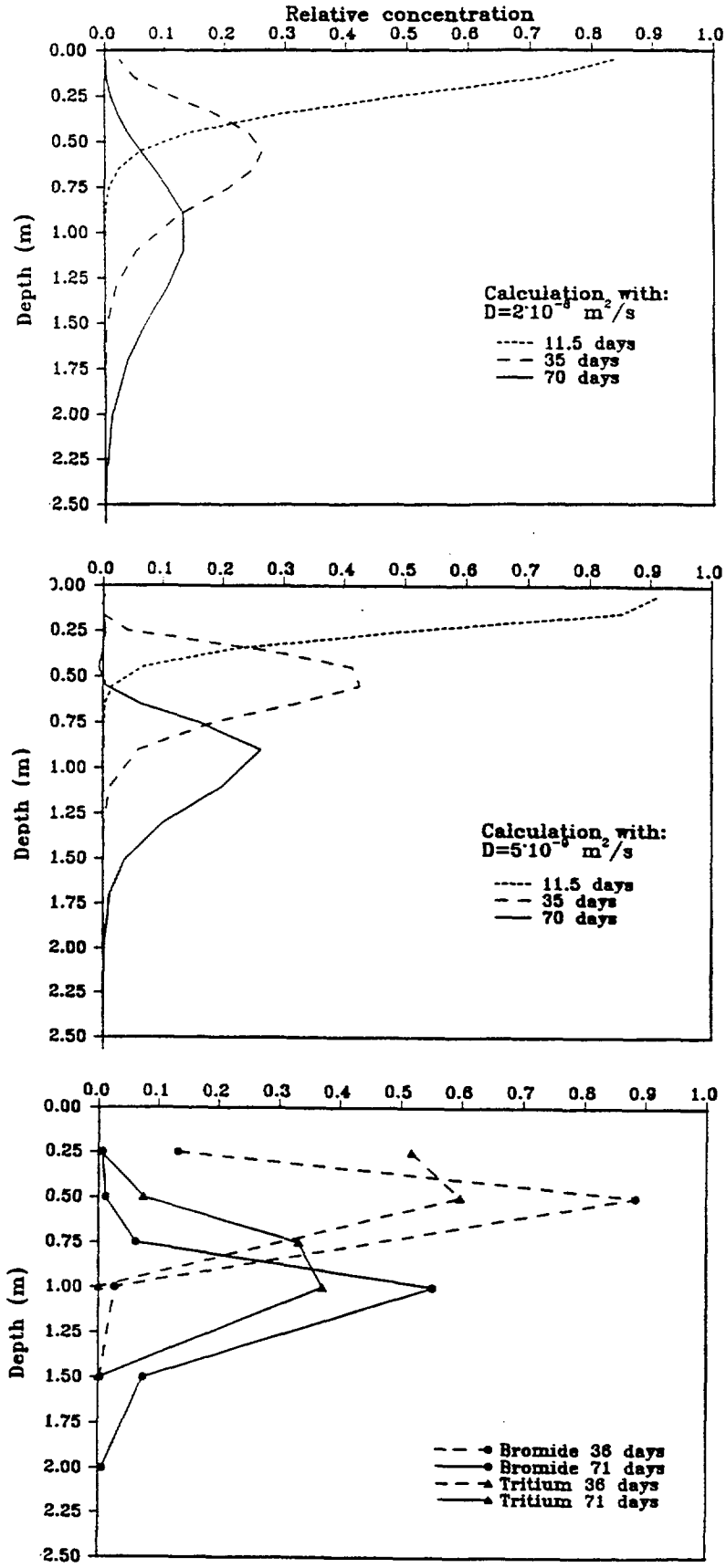

Figure 12 Prediction and observation of tracer concentration in the middle part (low and high dispersion coefficient).

CONCLUSIONS

Water and tracer transport in the second Las Cruces Trench experiment have been simulated with the deterministic Integrated Finite Difference codes TRUST + TRUMP. The calculations show, in general, a semi-quantitative agreement with the observations. The following points should, however, be noted.

1. The experimental initial water contents, except for the top part, are lower than the residual water content used in the fitted $\psi(\theta)$ and $K(\theta)$ relations. Extrapolations had to be made lower water contents. A better agreement was then obtained between simulations and measurements.

2. The experimental data show a large scatter both in water content and tracer concentration. This scatter is due to local heterogeneties which are not encountered for in the deterministic models where smooth profiles are obtained.

3. Using the layered description of the soil gave a better agreement with experimental data in particular regarding the lateral spreading of water. These results should be compared with stochastic modelling results.

4. The calculations performed for the tracer transport so far give too high spreading of the concentration plume. Apparently even lower dispersion coefficients ($< 5 \cdot 10^{-9}$ m^2/s) must be used.

5. The experimental Br^--pulse travels faster than T^3. This is probably due to anion-exclusion effects which are not encountered for in the numerical model.

6. As expected numerical problems were encountered in the well-known situations of initially very dry material for the water flow calculations and for low dispersivities in the tracer calculations.

ACKNOWLEDGEMENTS

This work was funded by the Swedish Nuclear Power Inspectorate (SKI).

NOTATION

a_v compressibility coefficient for the soil skeleton (m s^2/kg)

c tracer concentration (units/m^3 water)

D diffusion or dispersion coefficient (m^2/s)

D_0 diffusion or dispersion coefficient at saturation (m^2/s)

e void ratio (m^3 void/m^3 solid)

G source or sink

g gravitational acceleration (m/s^2)

k_w permeability (m^2)

K hydraulic conductivity (m/s)

K_s saturated hydraulic conductivity (m/s)

m van Genuchten parameter (-) $m = (1 - \frac{1}{n})$

M_c fluid mass capacity (kg/m)

n van Genuchten parameter (-)

$\bar{n}$ unit outwardly directed normal vector

Q amount of sorbed tracers (units/m^3 bed)

q fluid flux (m^3/m^2,s)

q_t tracer flux (units/m^2,s)

S degree of saturation (m^3water/m^3 void)

S_e scaled degree of saturation

S_r residual degree of saturation, corresponding to θ_r

t time (s)

V_s volume of solid (m^3)

z elevation, positive upwards (m)

Greek letters

α van Genuchten parameter (1/m)

β_w volume compressibility coefficient (m^2/N)

Γ boundary surface of a volume element (m^2)

θ water content (m^3/m^3 bed)

θ_r residual water content (m^3/m^3 bed)

θ_s water content at saturation i. e. porosity (m^3/m^3 bed)

μ_w viscosity of water (Ns/m^2)

ρ density (kg/m^3)

ρ_w density of water (kg/m^3)

ρ_{w0} reference density of water at atmospheric pressure (kg/m^3)

Φ total potential (m H_2O)

ψ capillary potential or pressure head (m H_2O)

χ' parameter correlating change in effective stress and change in pore pressure

REFERENCES

Collin, M. and Rasmuson, A.; 1990;
TRUST + TRUMP: Coupling the TRUST and TRUMP codes for simulation of simultaneous unsaturated transport of solute and water; Report Kemakta Consultants Co, Stockholm, Sweden, AR 90-07.

Edwards, A.L.; 1972;
TRUMP: A computer program for transient and steady state temperature distributions in multidimensional systems; National Technical Information Service, National Bureau of Standards, Springfield, Va.

Fried, J.J. and Combarnous, M.A.; 1971;
Dispersion in Porous Media; Advances Hydroscience, vol. 7.

Narasimhan, T.N.; 1975;
A unified numerical model for saturated - unsaturated groundwater flow; Ph. D. Thesis. Lawrence Berkeley Laboratory, University of California.

Wierenga, P.J., Hudson, D., Vinson, J. and Hills, R. G.; 1989;
Las Cruces Trench Experiment Database: Experiment 2. Publication in progress.

APPENDIX C8

Tests of UNSAT2 and TRACR3D codes
using Las Cruces Trench data

APPENDIX C

C.8 TESTS OF UNSAT2 AND TRACR3D CODES USING LAS CRUCES TRENCH DATA

J. D. Smyth
S. B. Yabusaki
G. W. Gee
C. T. Kincaid

November 1991

Prepared for
the U.S. Department of Energy
under Contract DE-AC06-76RLO 1830

Pacific Northwest Laboratory
Richland, Washington 99352

Table of contents

Figures **Page**

Tables

1.0 Introduction

Pacific Northwest Laboratory (PNL)[1] has tested several unsaturated-flow codes for performance on a dry soil site. The data used for these simulations are from the Las Cruces trench experiment and represent preliminary data collected prior to the completion of any infiltration tests. In the time elapsed between completion of the simulations and the writing of this report, two reports have appeared on the Las Cruces data and validation. The reader is referred to Wierenga et al. (1989) for a summary of data and to Hills and Wierenga (1991) for a summary of validation efforts.

Other infiltration simulations have also been conducted using the Las Cruces trench data. Polmann et al. (1988) applied a two-dimensional mean-stochastic flow and transport model developed at the Massachusetts Institute of Technology (MIT) to infiltration at the trench. While qualitatively successful at simulating the wetting front movement at the trench, the 1,000-cm tension used as the initial condition is not representative of the actual moisture conditions found at Las Cruces. The MIT mean-model has not been shown in published studies to effectively solve infiltration problems at tensions found under field conditions common to arid climates.

Hills et al. (1989) have developed a water-content-based, finite-difference model that is very efficient under dry conditions (up to 50,000 cm). Although the published model currently considers only one-dimensional flow, the initial application of the two-dimensional version of Hills' model with trench data was successful (personal communication, 1989). Hills' pre-ponded infiltration model neglects evaporation and transpiration, and does not consider the boundary conditions of ponding that could result in runoff or overland flow. However, a water-content-based approach may be acceptable for modeling infiltration into heterogeneous dry soils, because of its computational efficiency. Testing this method under a range of conditions may be required to solve some omissions. For example, the water-content-based model rrently does not handle saturated-flow conditions that may exist in the lower part of an unsaturated profile draining to a water table.

PNL plans to evaluate one- and two-dimensional water-content-based models similar to Hills'. These models will also consider evaporation, plant transpiration, and rainfall of different intensities. Ideally, overland flow components, as well as infiltration through low-level waste (LLW) site covers, will be evaluated. Numerical models of this type are described by Bresler (1973, 1975), Bresler et al. (1969), and Hanks et al. (1969).

A one-dimensional pressure-based model, UNSAT-H (Fayer et al. 1986), has been shown to efficiently simulate water movement in dry conditions. In addition to simulating plant and climatic effects, UNSAT-H allows diffusion of vapor. Although it is not a fully two-phase flow

[1] PNL is operated for the U.S. Department of Energy by Battelle Memorial Institute.

code, UNSAT-H uses vapor diffusion to account for moisture movement under dry conditions. Under dry conditions, movement of moisture may be significant. Accordingly, vapor flow may be an important factor in assessing infiltration through LLW site covers.

This report documents the modeling of infiltration into unsaturated (dry) soil using "off-the-shelf" computer codes. Two computer models, UNSAT2 (Davis and Neuman 1983) and TRACR3D (Travis 1984), are tested using data from the Las Cruces, New Mexico, test site. The computational efficiency, mass balance control, and key operational features of the codes are assessed.

2.0 Numerical Simulation Methods

For the initial infiltration simulation of the Las Cruces site, PNL has used two multidimensional, variably saturated models, UNSAT2 (Davis and Neuman 1983) and TRACR3D (Travis 1984). These models were the first selected for evaluation because of their multidimensional capability, their availability, and PNL's familiarity with them.

2.1 Las Cruces Trench Data

In 1987, New Mexico State University (NMSU) provided PNL with preliminary soils data from the top 145 cm of the trench. The preliminary soil data identified three horizontal layers. NMSU had used the van Genuchten formulation of the Mualem model:

$$\frac{\theta - \theta_r}{\theta_s - \theta_r} = \left(\frac{1}{1 + (\alpha h)^n} \right)^m \qquad (2.1)$$

where
- θ = volumetric water content
- θ_r = residual water content
- θ_s = saturated water content
- α = fitting parameter
- h = tension (or suction) head
- n = fitting parameter
- m = 1 - 1/n

and

$$K_r = \left(\frac{\theta - \theta_r}{\theta_s - \theta_r} \right)^{1/2} \left\{ 1 - \left[1 - \left(\frac{\theta - \theta_r}{\theta_s - \theta_r} \right)^{\frac{1}{m}} \right]^m \right\}^2 \qquad (2.2)$$

where K_r = relative conductivity = K/K_{sat}, K = unsaturated hydraulic conductivity, and K_{sat} = saturated hydraulic conductivity.

The parameters θ_s, θ_r, α, n, and K_{sat} from the preliminary soil data (Table 2.1) were used to develop three infiltration simulation cases. The three simulation cases were 1) a homogeneous-isotropic soil, 2) a horizontally layered heterogeneous system with the three layers from Table 2.1 (Figure 2.1a), and 3) the horizontally layered heterogeneous system with an embedded zone of

high conductivity (relative to the soils present), (Figure 2.1b). The cases were designed to increase the level of heterogeneity being modeled, and therefore the level of difficulty.

Data from the trench experiment (D. B. Hudson, personal communication from NMSU, 1989) indicate that the water contents under field conditions are equivalent to tensions of 10,000 to 15,000 cm. Because of the numerical difficulty expected in modeling tensions of this magnitude, the first simulations were conducted with a lower initial tension of 724 cm. This arbitrarily selected initial tension is related to the synthesized homogeneous-isotropic soil of Case 1. Soil parameters for this case were calculated by arithmetically averaging the soil model parameters given for Case 3. The initial tension of 724 cm was then derived by defining the initial moisture content as 0.024 cm^3/cm^3 higher than the residual moisture content. Soil parameters for Case 2 were derived by adjusting the residual water content for the homogeneous-isotropic soil to allow a tension equivalent of that found in the field (i.e., ~10,000 cm).

Table 2.1 van Genuchten Soil Parameters

Case	Layer	Depth Interval (cm)	θ_s	θ_r	α (1/cm)	n	K_{sat} (cm/d)
1	Homogeneous-Isotropic		0.348	0.096	0.0347	1.729	558.6
2	Homogeneous-Isotropic		0.363	0.0504	0.1364	1.292	459.9
3	1	0-30	0.368	0.1020	0.0334	1.982	790.9
	2	31-60	0.351	0.0985	0.0363	1.632	469.9
	3	61-650	0.325	0.0859	0.0345	1.573	415.0
4	Embedded high K_{sat} zone	(200-300)	0.348	0.096	0.0347	1.729	4150.0

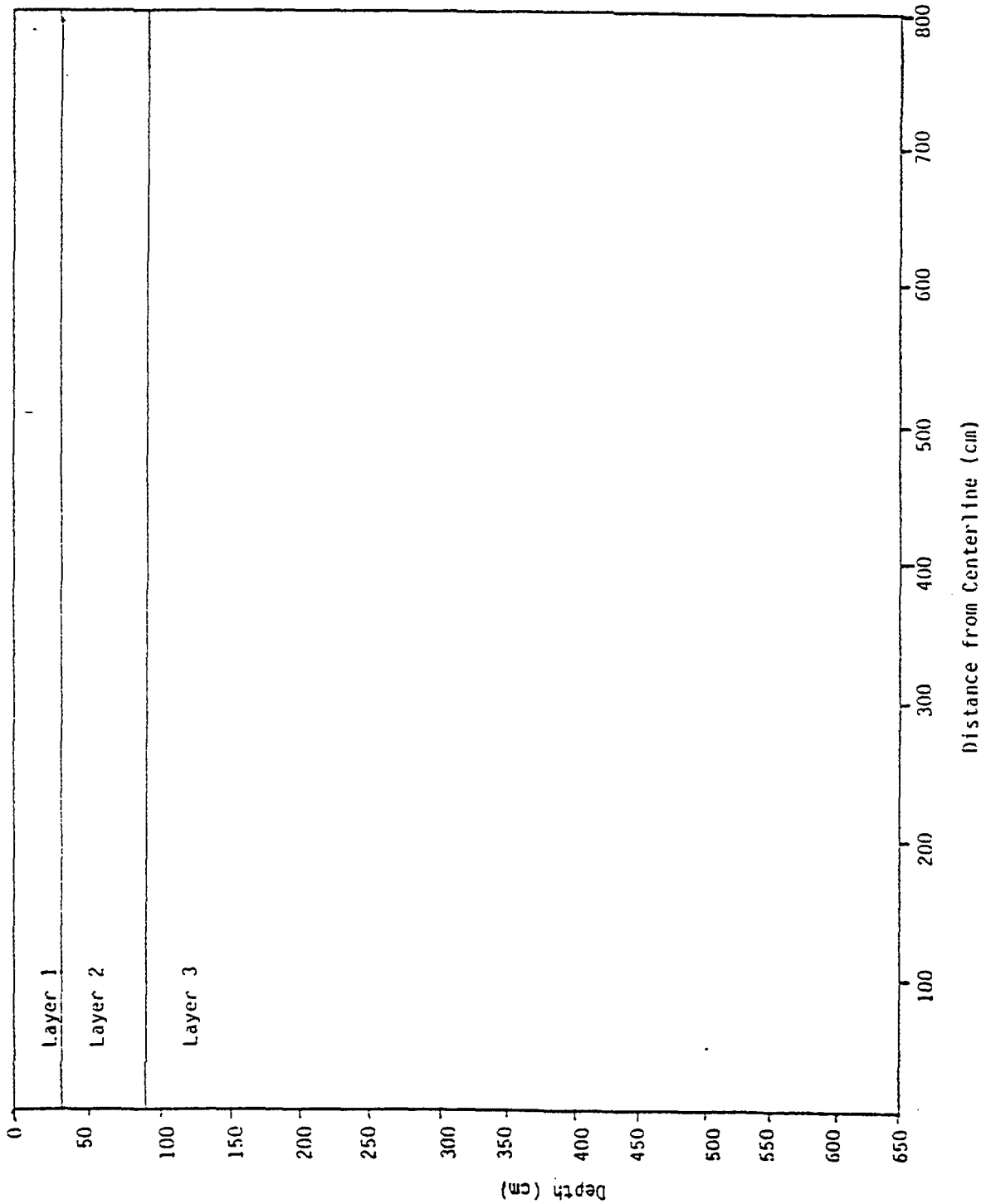

Figure 2.1 Conceptual Model of (a) Case 3 and (b) Case 4

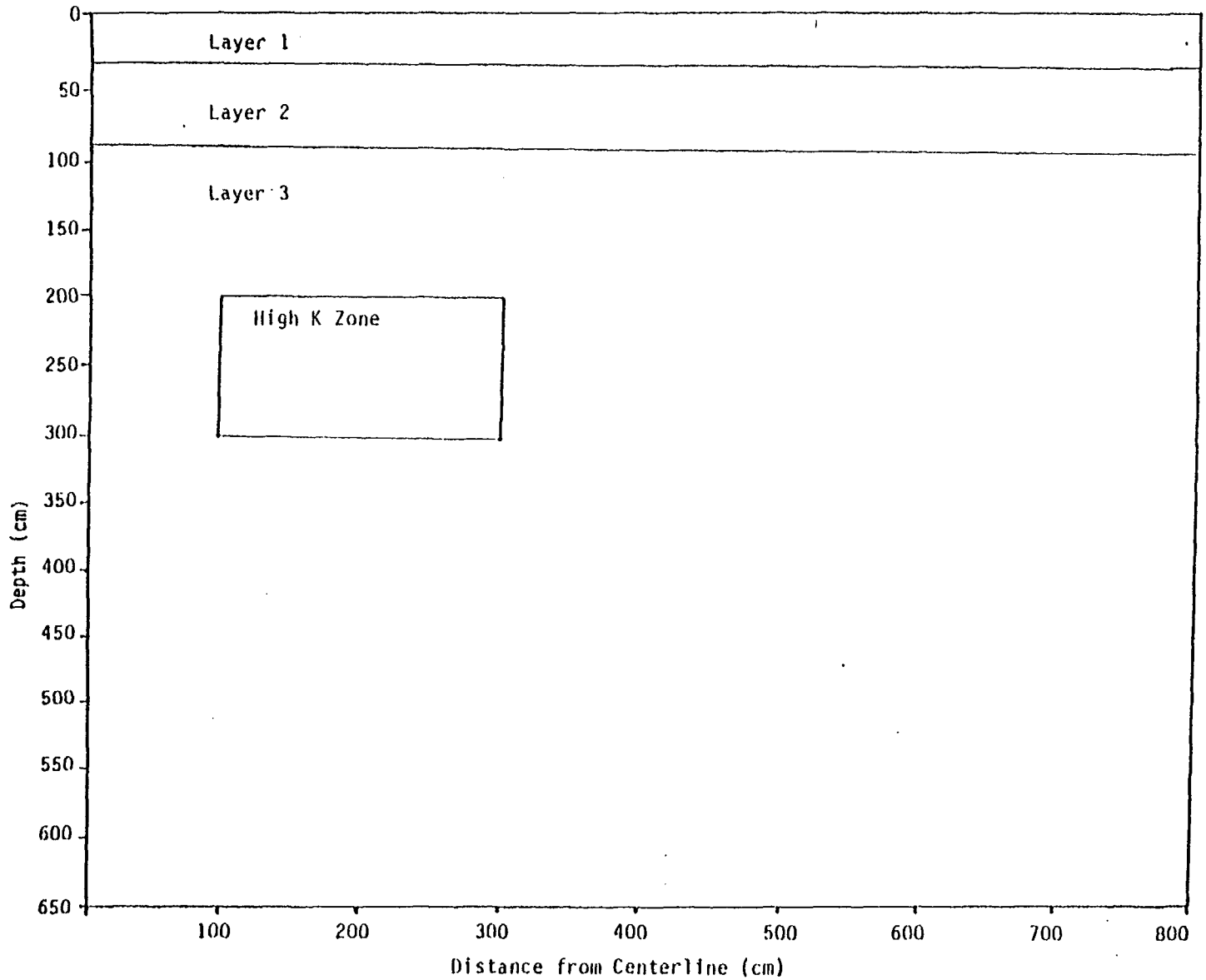

Figure 2.1 (contd)

2.2 Conceptual Model

The geometry of the Las Cruces trench is shown in Figure 2.2. The symmetry of the trench led to the use of a no-flow boundary in the center of the irrigated strip. The right and bottom boundaries were assumed to be unaffected by the flow field and were represented as no-flow boundaries. The top boundary consisted of a specified flux equal to the irrigation rate for 225 cm, with the remainder treated as a no-flow boundary.

Visual observations, neutron probe data, and tensiometer measurements of the wetting front progress during infiltration indicate that the 6.5-m depth of the trench is unaffected for the 30 day simulations PNL conducted. These measurements can be used to compare model results with field data (Figure 2.2). It should be noted the accuracy of results from numerical models is influenced by the discretization of the grid, i.e., grid resolution. Correspondingly, the grid resolution of the numerical model will influence comparisons between field data and model results.

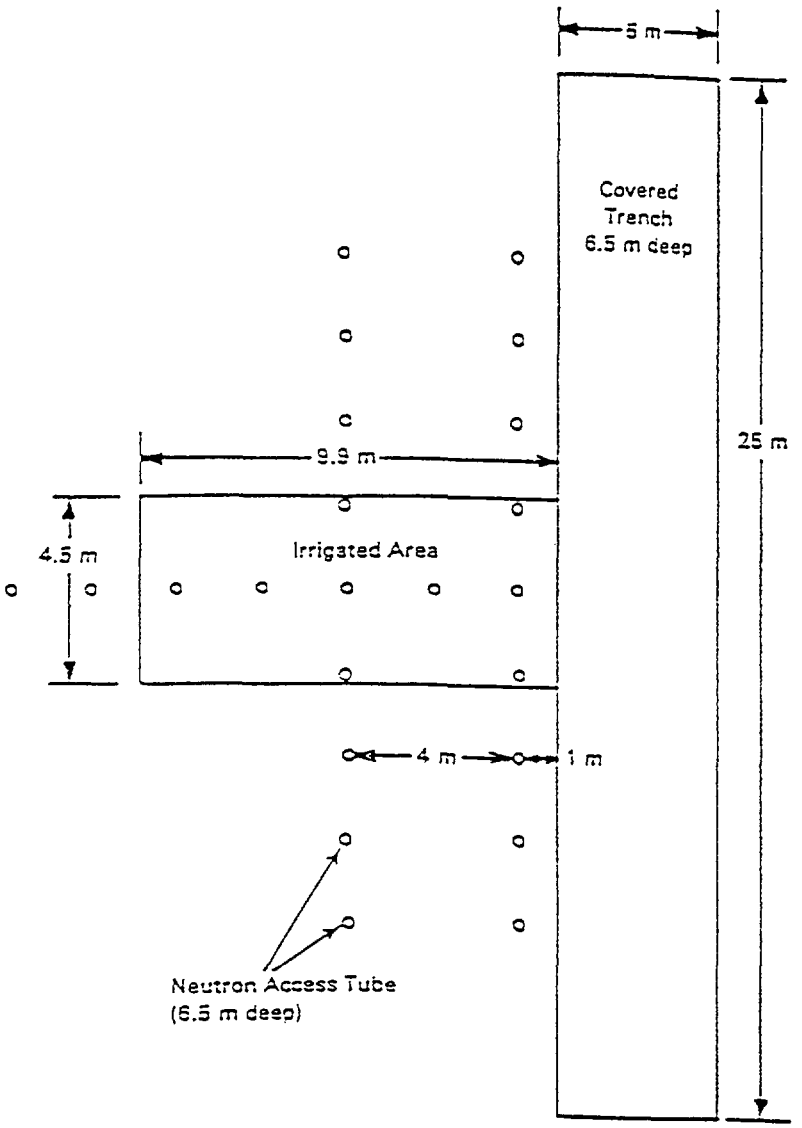

Figure 2.2. Plan View of Trench Experiment (after Wierenga et al. 1986)

3.0 Simulation of Infiltration into Dry Soils using UNSAT2

UNSAT2 is a two-dimensional finite element code that is used to model variably saturated flow. It was developed by Neuman (1973) and enhanced and subsequently documented by Neuman and his colleagues (Feddes et al. 1974, 1975, 1976; Neuman 1975; Neuman et al. 1974; Davis and Neuman 1983). UNSAT2 uses the Galerkin finite-element method on a network of triangular elements with linear basis functions to solve the following flow equation:

$$\frac{\partial}{\partial x_i}\left[K^r(h)\ K_{ij}^s\ \frac{\partial h}{\partial x_j}\right] + \frac{\partial}{\partial x_i}\ K_r(h)\ K_{ij}^s - \left[c(h) + \beta S_s\right]\frac{\partial h}{\partial t} - S = 0 \qquad (3.1)$$

where
- K_r = relative hydraulic conductivity
- h = pressure head
- K_{ij}^s = hydraulic conductivity tensor at saturation
- c = specific moisture capacity
- β = 0 if unsaturated; and 1 if saturated
- S_s = specific storage
- t = time
- S = sink or source term
- X_i = spatial coordinates

The code assumes a single-valued, monotonic relationship between water content and pressure head for which linear interpolation is used to identify values between tabular data points. UNSAT2 is applicable to a two-dimensional flow domain in which bulk flow is always parallel to a vertical cross section.

To run UNSAT2 requires as input data the saturated hydraulic conductivity, specific storage, porosity, relative conductivity versus moisture content data, and pressure head as a function of moisture content. Compressibility effects on moisture storage are negligible in unsaturated soils. Consequently, specific storage was assumed to be zero. All other data requirements were fulfilled by the NMSU data.

3.1 UNSAT2 Simulations

The triangular finite elements in UNSAT2 were formulated with linear basis functions. Consequently, pressure head predictions are constrained to linear variation over each element. Dense grid meshes are necessary in areas where spatial variations of pressure head are locally nonlinear (e.g., 1) along no-flux boundaries, 2) along wetting fronts, and 3) along material

interfaces). These considerations resulted in the formation of the grids for the simulation (Figure 3.1).

UNSAT2 allows the use of central or backward differences for approximating the time derivative. The central difference approximation was selected to attain accuracy. A geometrically increasing time step was used in all simulations.

All UNSAT2 simulations were performed with double-precision real words on a DEC VAX station II. Grid specifications, time-stepping selected, and computational times are summarized in Table 3.1.

Table 3.1 UNSAT2 Simulation Summary

Case	ψ(cm)	Nodes	Elements	Maximum Iterations	Tolerance (cm)	Time Steps (s) Initial	Max	Magnification	Simulation Length (d)	Computation Time (h)
1	724	323	576	50	0.001	360	3600	1.09	7.0	0.167
2	10000	1419	2688	50	0.0001	0.86	3600	1.01	7.0	28
3	724	1794	3420	50	0.0001	360	1080	1.02	30	38
	10000	---	---	--	---	---	---	---	---	---
4	724	1794	3420	50	0.0001	360	1080	1.02	30	38
	10000	---	---	--	---	---	---	---	---	---

3.1.1 Case 1 and Case 2 Results

The grid used for Case 1 consisted of 323 nodes and 576 elements (Figure 3.2). Most of the nodes were concentrated in the top left corner of the model domain, in a dense mesh based on 25-cm grid spacing. After one day (Figure 3.2), the wetting front reached a depth of 0.6 m and extended 0.5 m beyond the surface flux edge. After 7 days (Figure 3.3), the penetration was 1.8 m and the lateral movement away from the flux strip was 2.25 m. The additional mesh revealed more curvature from the right edge of the surface flux down to the deepest penetration of the wetting front. In general, flow directly beneath the flux boundary condition is vertical, as evidenced by the horizontal pressure head contours in this area. Convergence was poorest along the curved portion of the wetting front, where the solution is most sensitive to grid resolution.

Case 2 was used as the test of the low-water-content initial condition in a homogeneous soil. The residual water content in this test is 0.050, as compared to the 0.096 average from the NMSU transects. The extreme initial condition of -10,000 cm pressure head made it necessary to use a very fine grid mesh (nodal spacing as small as 0.1 cm) in conjunction with an initial time step of 1 to perform the 7-day simulation (Figure 3.1b). Furthermore, the 1419 nodes and 2688

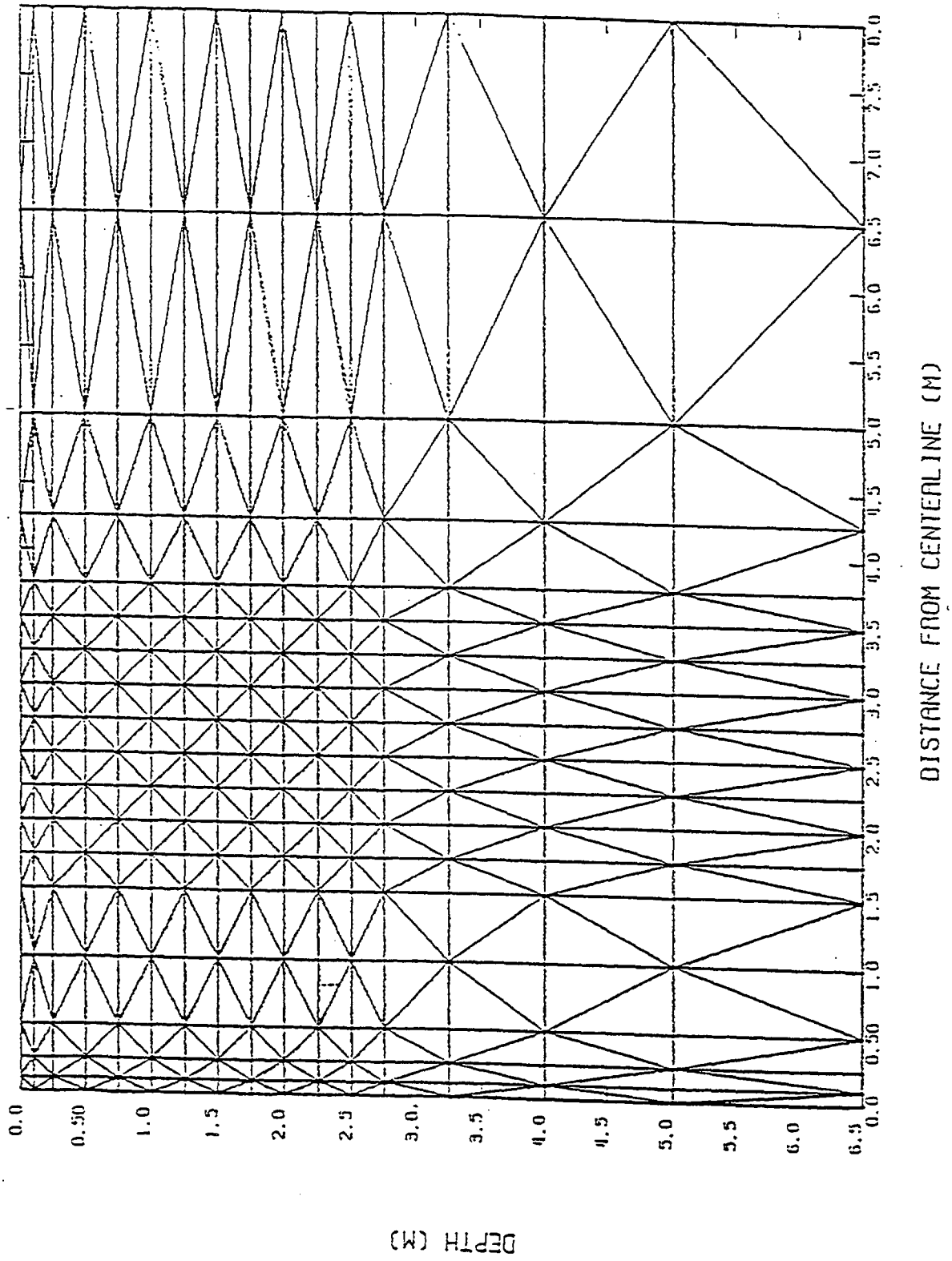

Figure 3.1 Computational Grid for UNSAT

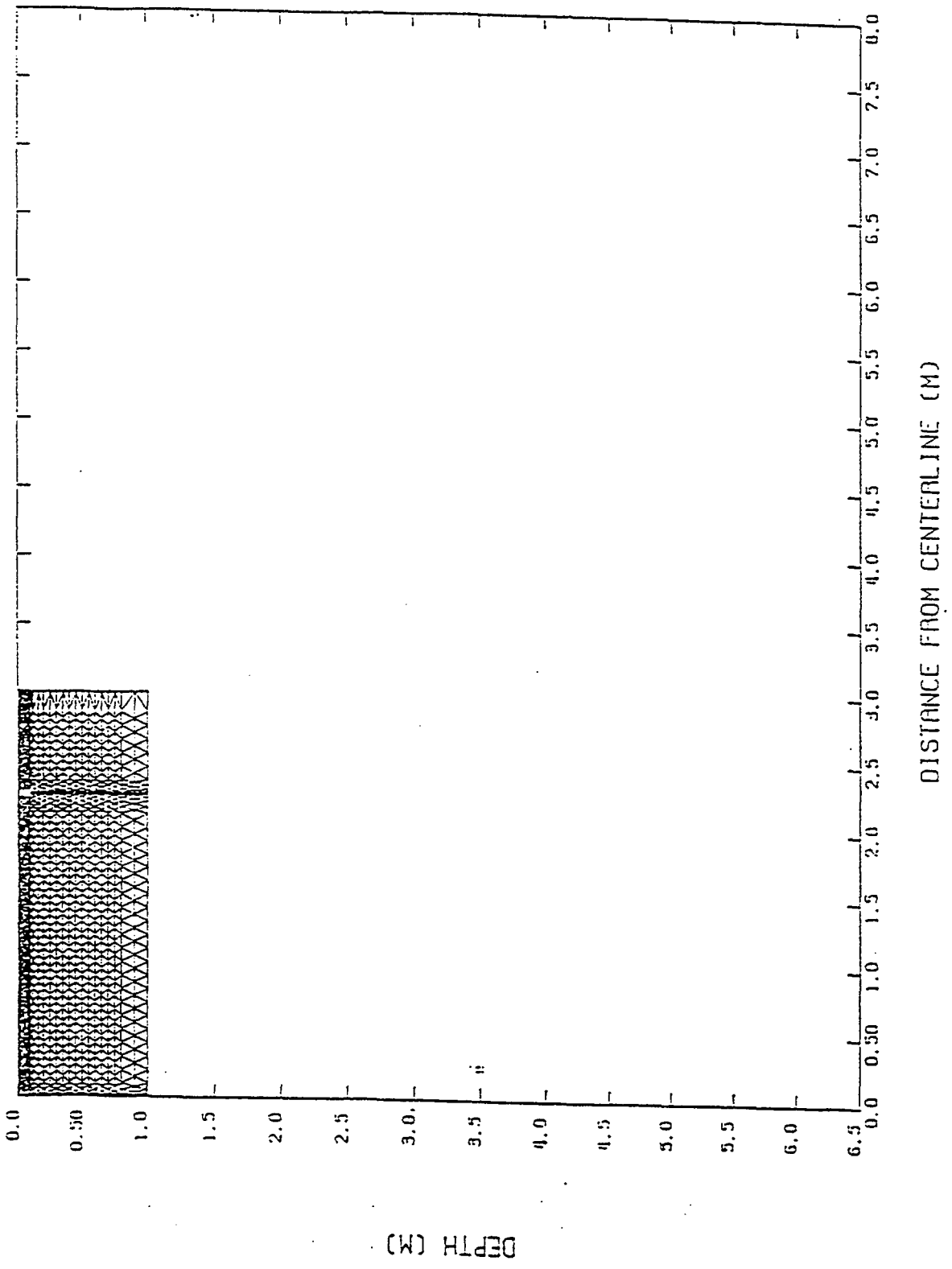

Figure 3.1 (contd)

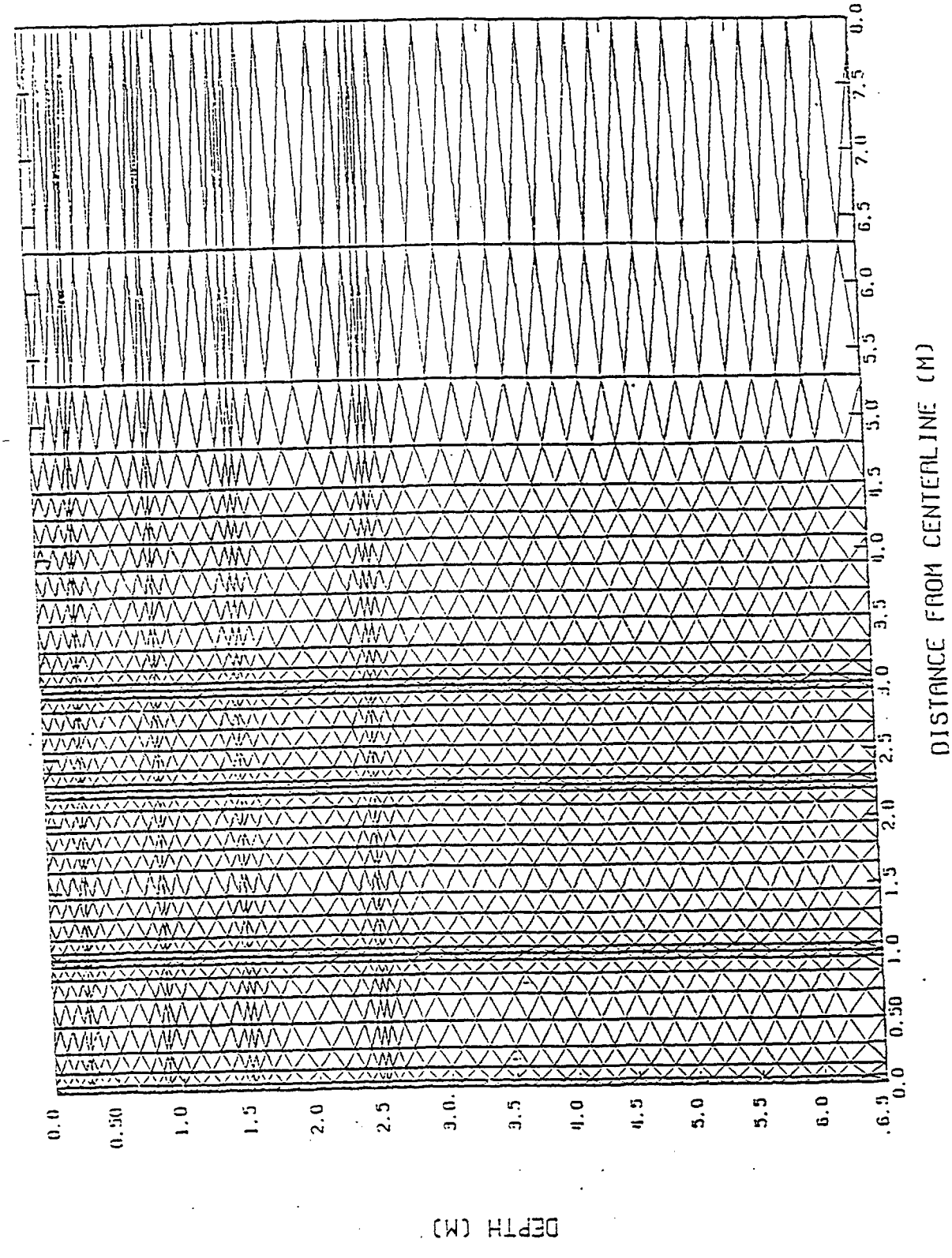

Figure 3.1 (contd)

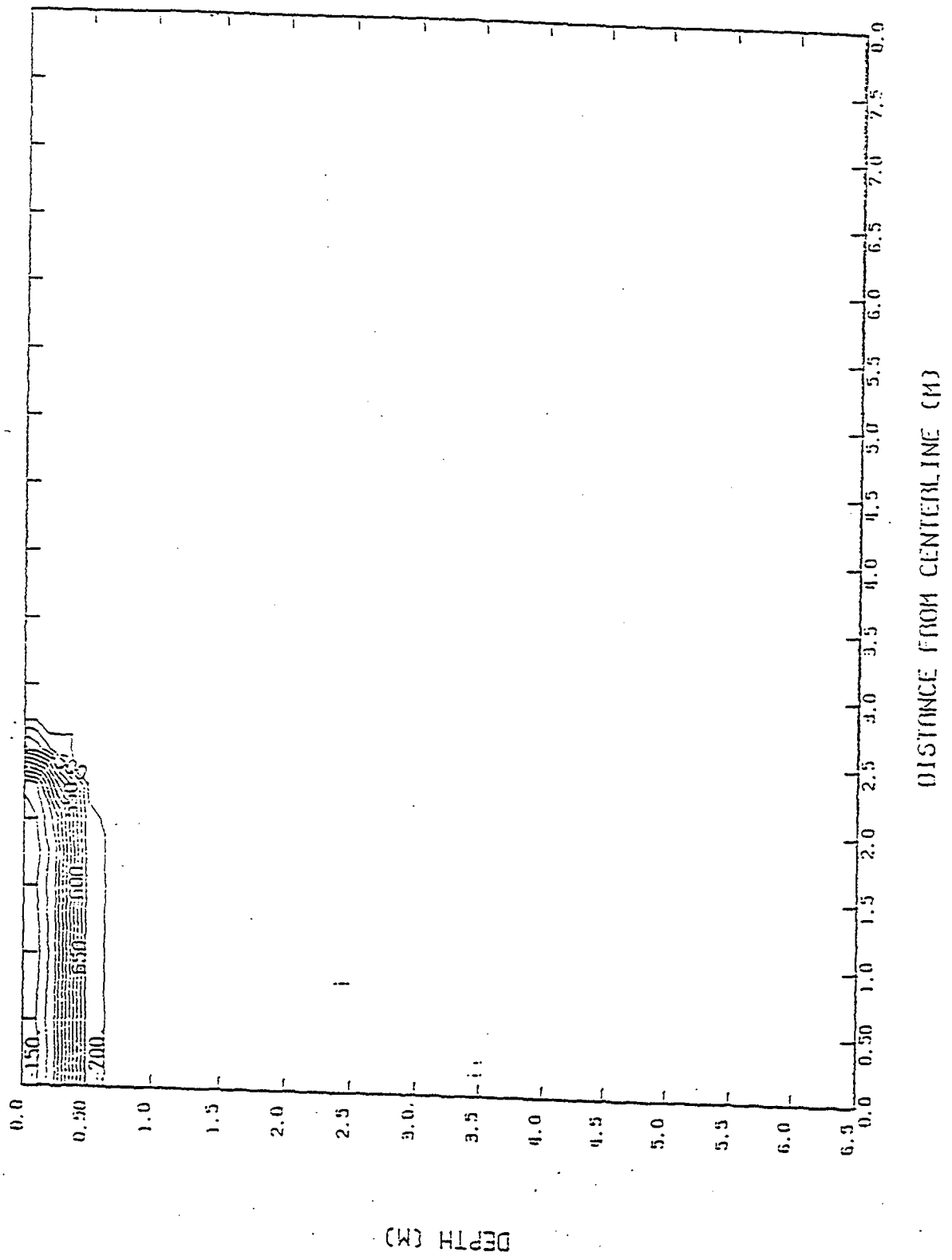

Figure 3.2 UNSAT2 Pressure Head Contours for Case 1 After 1 Day

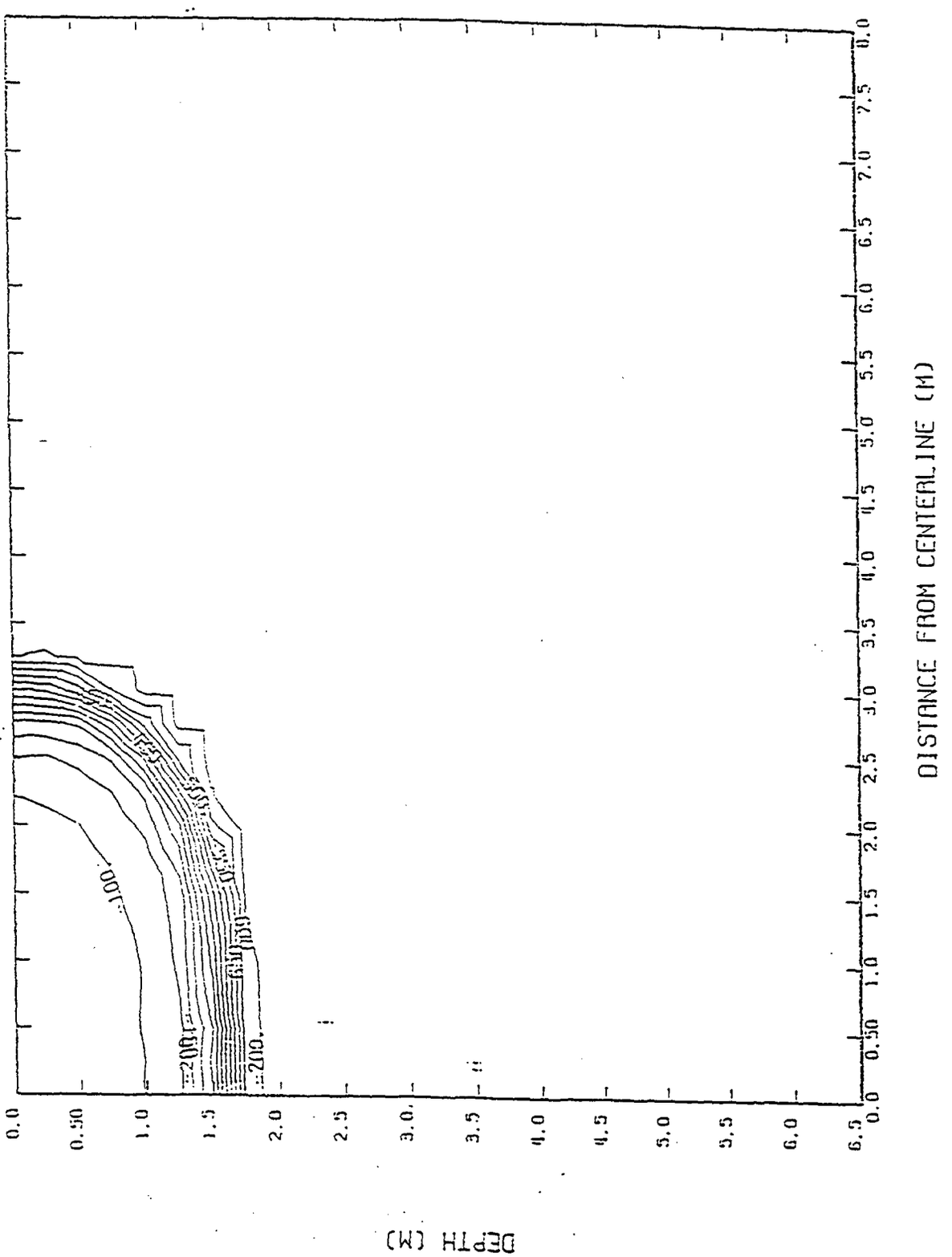

Figure 3.3 UNSAT2 Pressure Head Contours for Case 1 After 7 Days

elements were used to model a subregion, i.e., a block 100 cm deep and 300 cm wide in the top left corner of the problem geometry. Despite these refinements, the predicted solution (Figure 3.4) is probably impractical because of a mass-balance error on the order of 50%. UNSAT2 cannot compute mass balance and that ability should be added before any further testing. The error was detected by comparing the boundary influx to the change in the volume of water stored in the pores.

As another check of the UNSAT2 results, additional simulations on the homogeneous soil column were conducted using the one-dimensional unsaturated flow code, UNSAT-H (Fayer et al. 1986). For the relatively short time that was modeled, UNSAT-H was appropriate to describe the vertical movement of water down the left boundary of the problem. Unlike UNSAT2, which uses an iteration tolerance to determine convergence, UNSAT-H uses a mass balance criterion to select time-step magnitude.

The UNSAT-H modeling used 53 nodes to represent the 650-cm soil column; nodal spacing ranged from 0.1 cm to 50 cm. For the 7-day simulation of Case 1, UNSAT-H reproduced the UNSAT2 prediction of a 1.8-m deep wetting front (Figure 3.5) with a relative mass balance error of 0.02%. For the low-water- content case, UNSAT-H predicted a 7-day wetting front depth of 80 cm (Figure 3.6), which was double the UNSAT2 prediction of 40 cm. Relative mass balance error for UNSAT-H in this case was 0.004%.

Because UNSAT2 could not simulate the homogeneous soil at low water content, the remaining simulations (i.e., Cases 3 and 4) were performed only at the 724-cm tension initial condition.

3.1.2 Case 3 Results

The layered soil model comprised three materials. Layer 1 was confined to the first 30 cm, layer 2 the next 60 cm, and layer 3 the remaining 560 cm of depth (Figure 2.2) The parameters for each material are summarized in Table 3.1.

Refinements to the homogeneous grid were necessary to address the material heterogeneities of the layered soil model and to improve the resolution of the wetting front. For Case 3, the resolution in areas of interest was based on a 20-cm grid spacing. This resulted in a grid with 1794 nodes and 3420 elements (Figure 3.1c). After 30 days, water had moved 550 cm down the left boundary and 440 cm laterally away from the flux boundary near the wetting front where a lack of convergence has caused sawtooth behavior to reappear. These deviations could certainly be minimized by finer grid mesh; however, the tradeoff would be run times on the order of days (Figure 3.7). It is our feeling that the lack of convergence near the wetting front does not detract materially from the accuracy of the result.

Interestingly, drainage effects were seen near the bottom of the modeling domain during this extended simulation. The uniform case in this study was not an equilibrium condition. Without the flux boundary condition and given enough time, water would redistribute to balance the gravitational effect on pore water. This was the case after 30 days, as evidenced by the appearance of a horizontal contour representing -700-cm pressure head near the bottom.

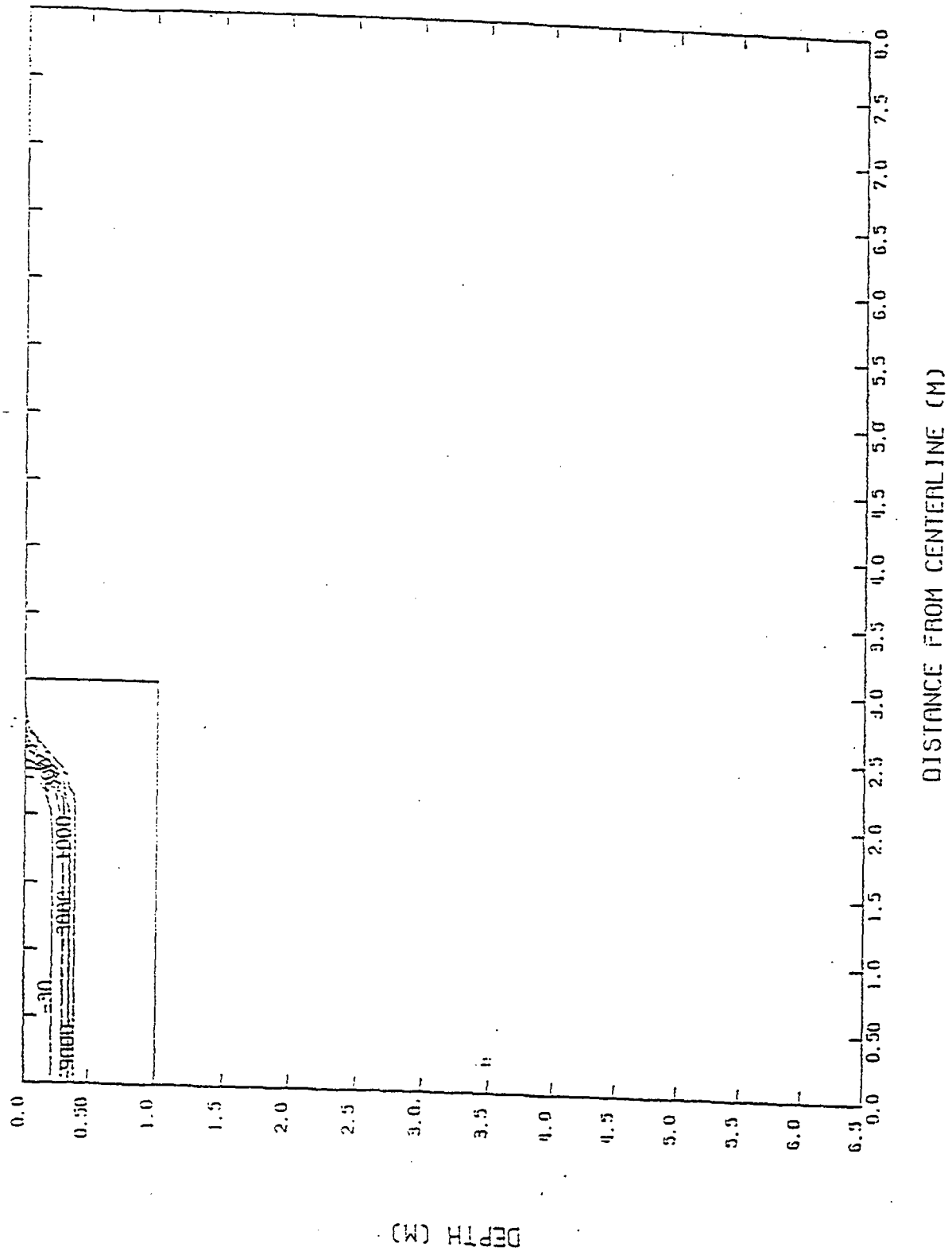

Figure 3.4 UNSAT2 Pressure Head Contours for Case 2 After 7 Days

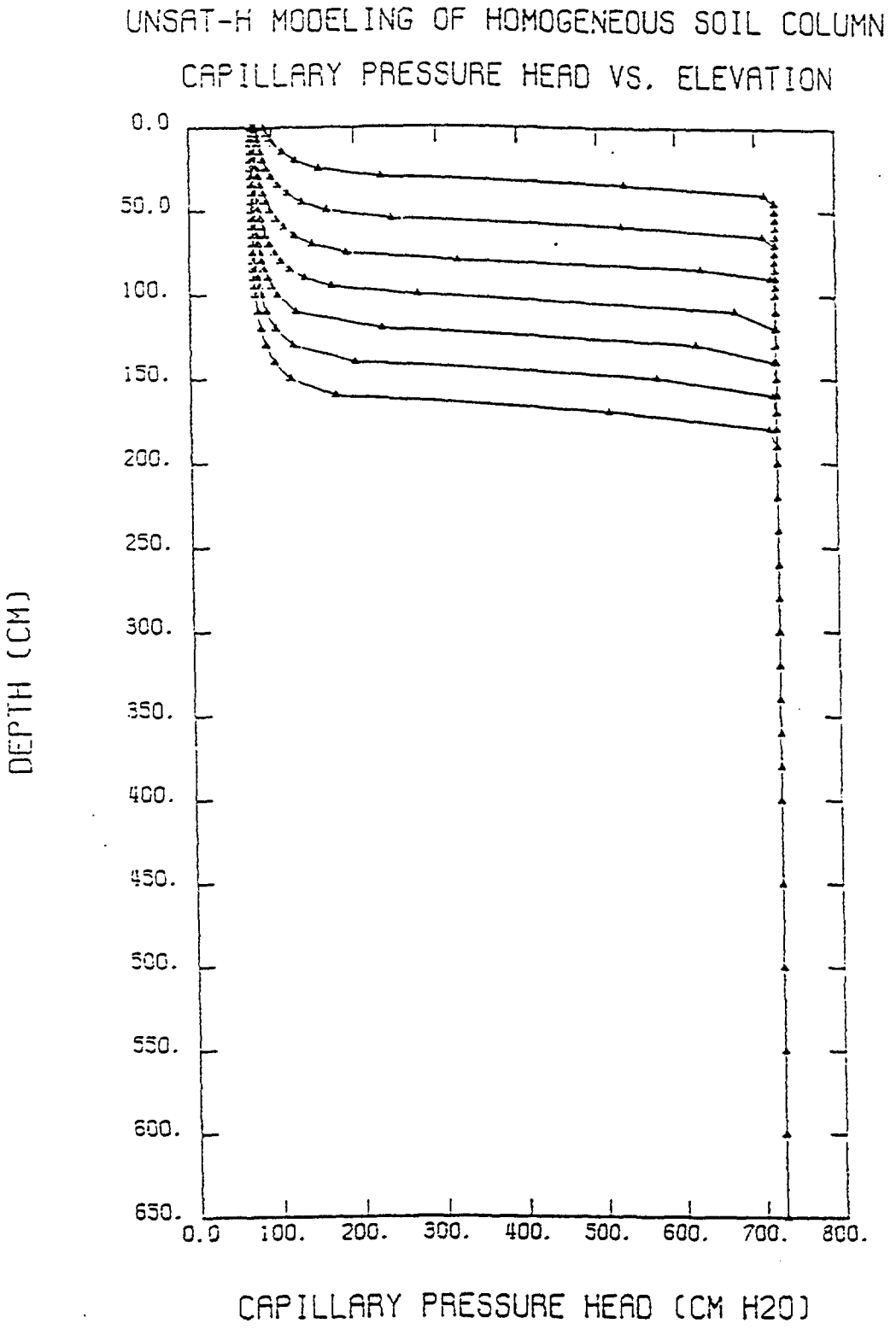

Figure 3.5 UNSAT-H Pressure Head Distribution for Case 1. Results at the end of each day.

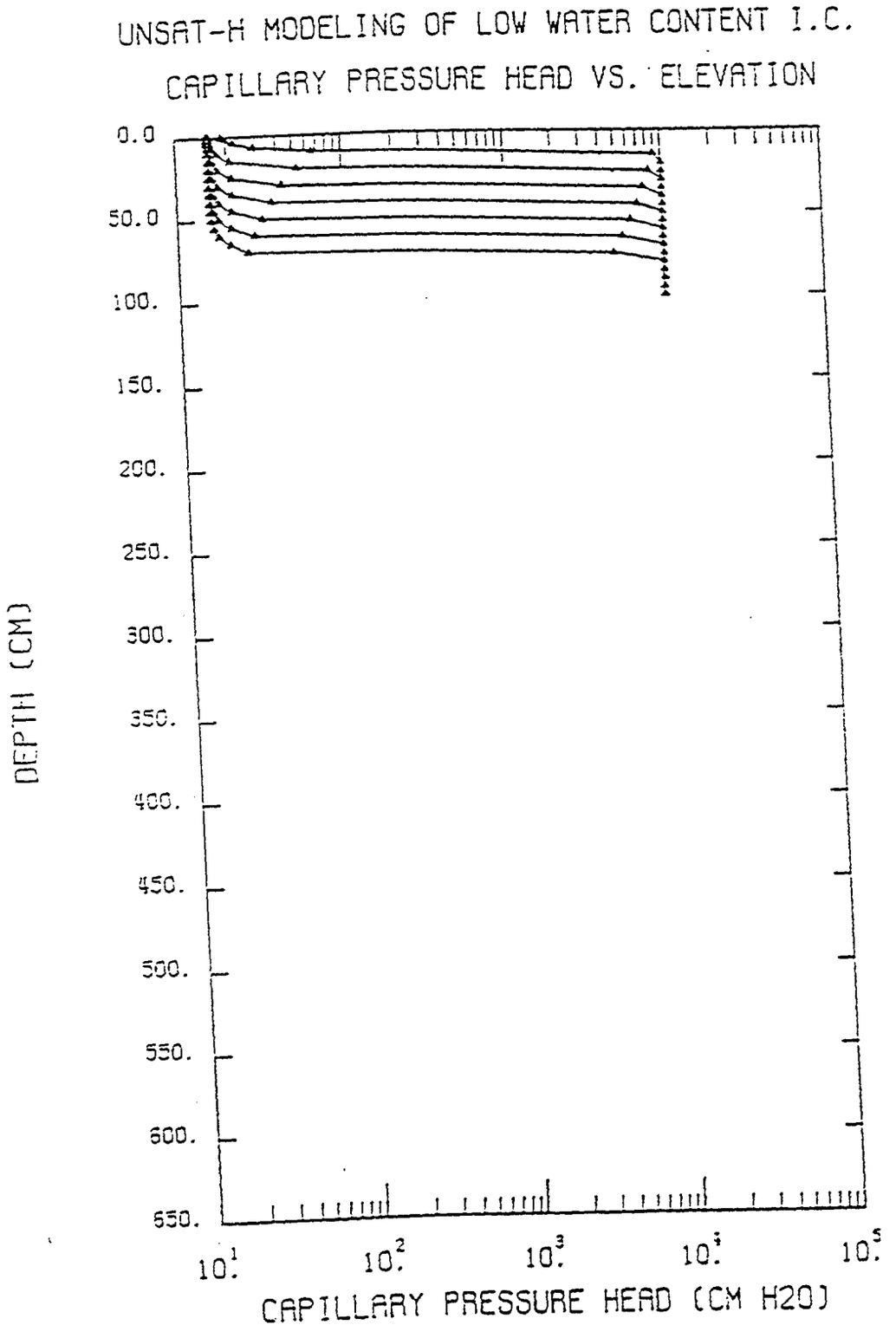

Figure 3.6 UNSAT-H Pressure Head Distribution for Case 2. Results at the end of each day.

3.1.3 Case 4 Results

In this model, the grid and soil representation from the 30-day layered system was repeated, with the addition of a high-conductivity block of soil embedded in the third soil layer (Figure 3.8). The conductivity in this zone was 10 times higher than the conductivity in layer 3. This model was also simulated for a period of 30 days using the same-time step sizes. After 5 days, water had not yet reached the high-conductivity zone and the results were identical to these of the previous layered soil modeling (Figure 3.6).

After 10 days (Figure 3.9), there was a marked effect on the pressure head contours that passed through the high-conductivity zone. As the wetting front moved through the zone, there was less flow resistance; consequently, the distance between pressure head contours widened to reduce the head gradient. The net effect was to almost define the high-conductivity zone by the sudden changes in direction of the contours. Even after 30 days (Figure 3.10), the -100-cm and -150-cm pressure head contours remained disrupted by the high-conductivity zone. The presence of the high-conductivity zone did not significantly change the vertical penetration of the wetting front after 30 days; however, the volume of the soil matrix affected by the constant flux boundary condition was increased.

3.2 Discussions of UNSAT2 Simulations

Converged solutions were obtained using UNSAT2 for each of the three soil models when using a relatively moist initial tension. The most difficult case (from a numerical standpoint) resulted from a high, but realistic, tension head initial condition. Very fine grid mesh and small time steps were necessary for UNSAT2 to model the 7-day simulation period under this initial condition. The simulation required 28 hours of computational time on a VAXstation II and may have uncovered a mass-balance problem in UNSAT2. Over half of the water entering the soil matrix as surface flux could not be accounted for. (UNSAT2 does not monitor mass balance). The error was detected by comparing changes in the soil matrix storage with the boundary flux. The error in mass balance occurred only for the high-tension-head case. The effects of the mass-balance error on the depth and rate of vertical wetting front movement were examined using UNSAT-H. Further refinements to the grid spacing and time step to resolve this error would have led to computational times approaching real time.

From the results of Case 2, it can be concluded that UNSAT2 does not perform well under dry initial conditions. However, when using a initial condition of 724-cm tension, UNSAT2 appeared to do a satisfactory job of simulating wetting front advancement. Although there are no field data that can be used as validation of the simulation under these conditions, the results of the TRACR3D simulations will be used to benchmark the results.

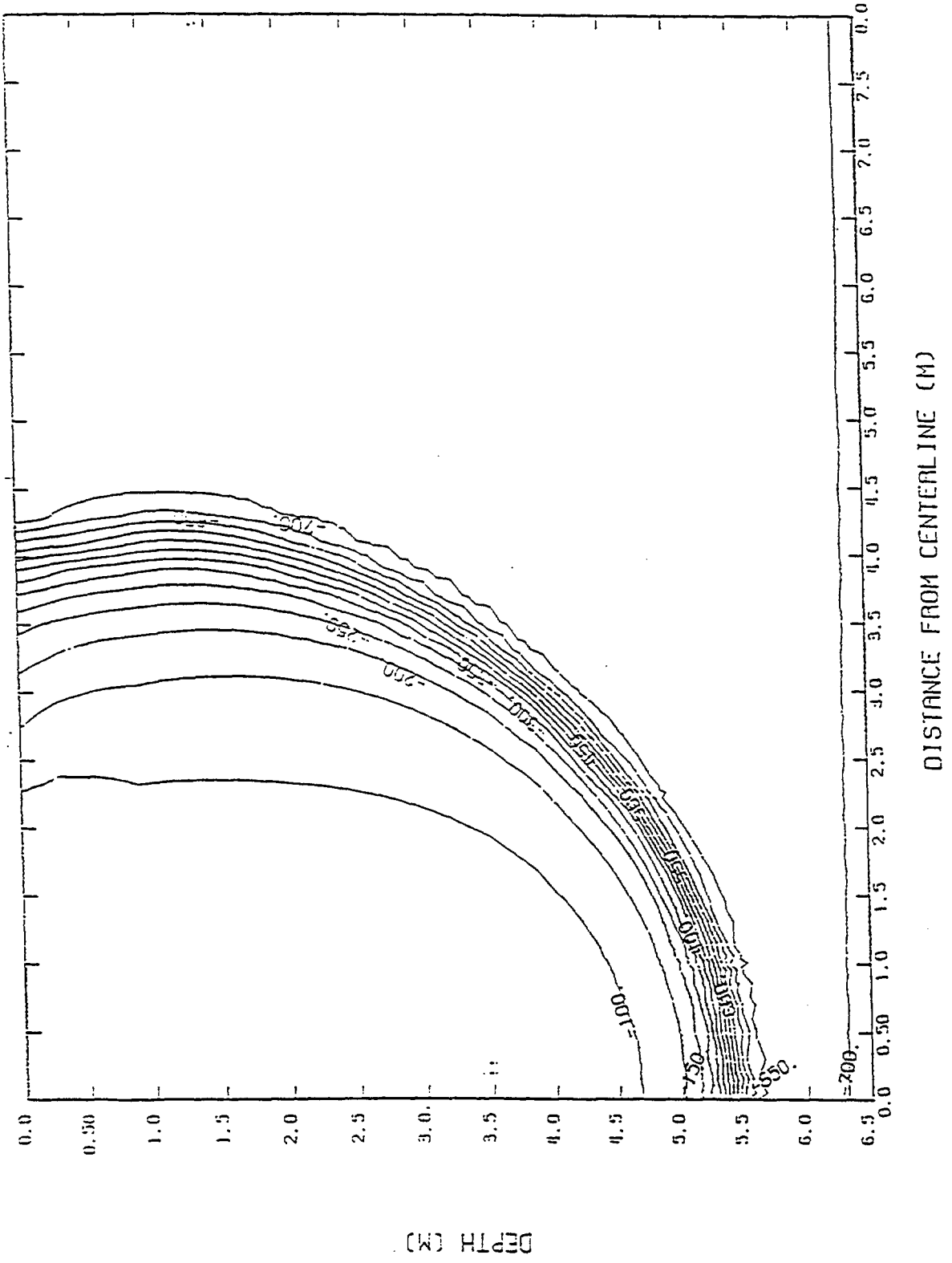

Figure 3.7 UNSAT2 Pressure Head Contours for Case 3 After 30 Days (30 day grid)

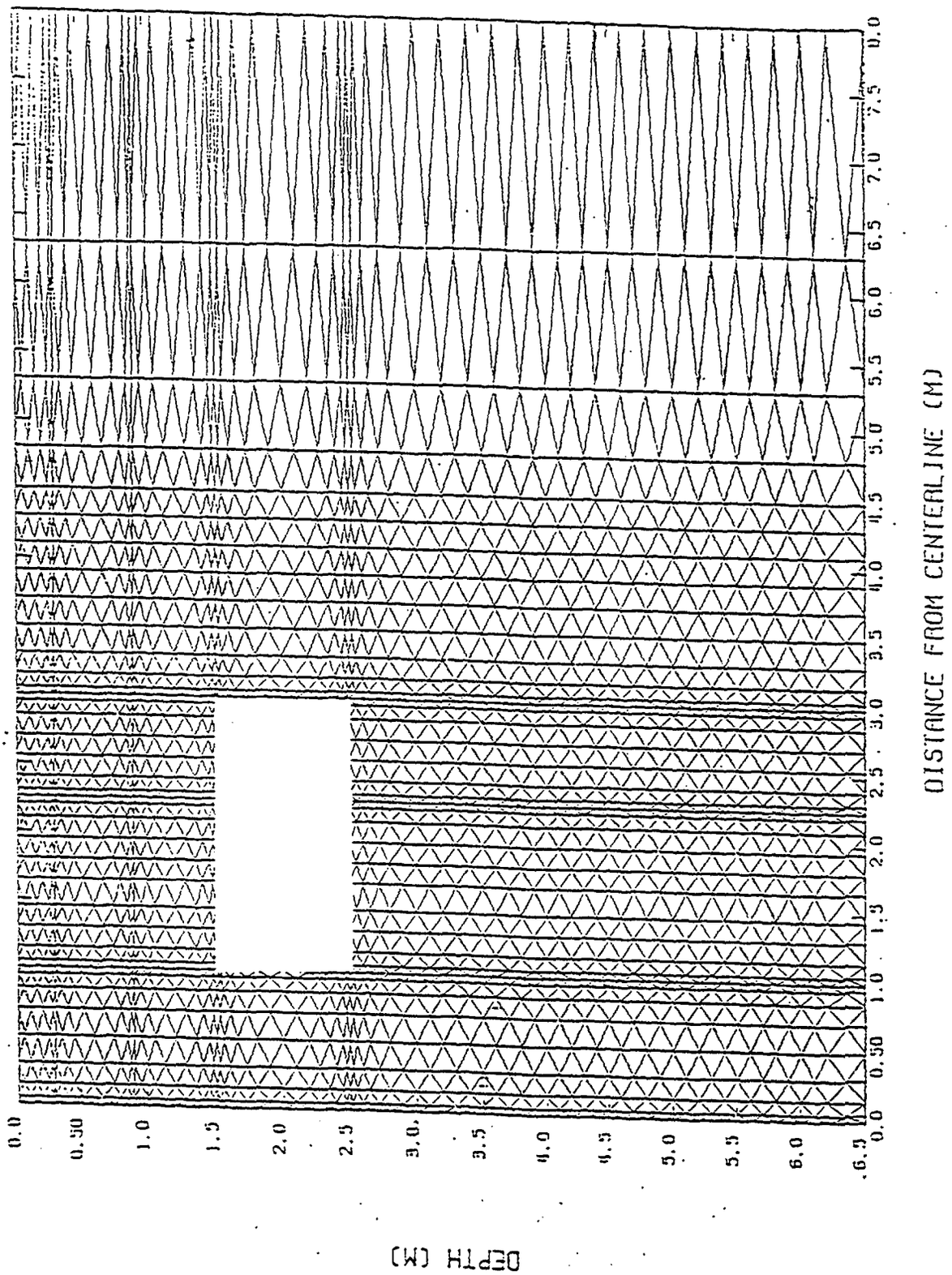

Figure 3.8 Location of High-Hydraulic-Conductivity Zone in Computational Grid

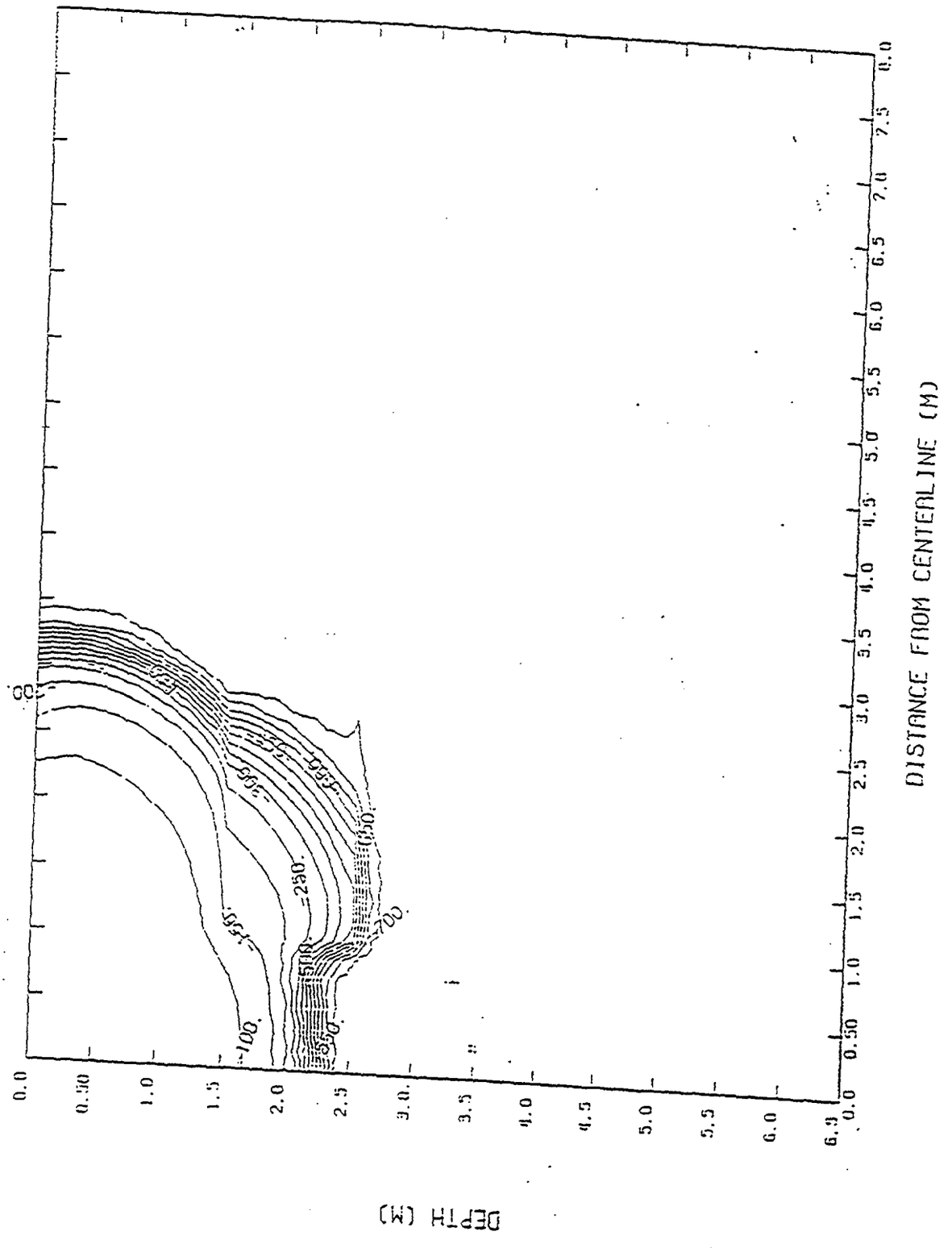

Figure 3.9 UNSAT2 Pressure Head Contours for Case 4 After 10 Days

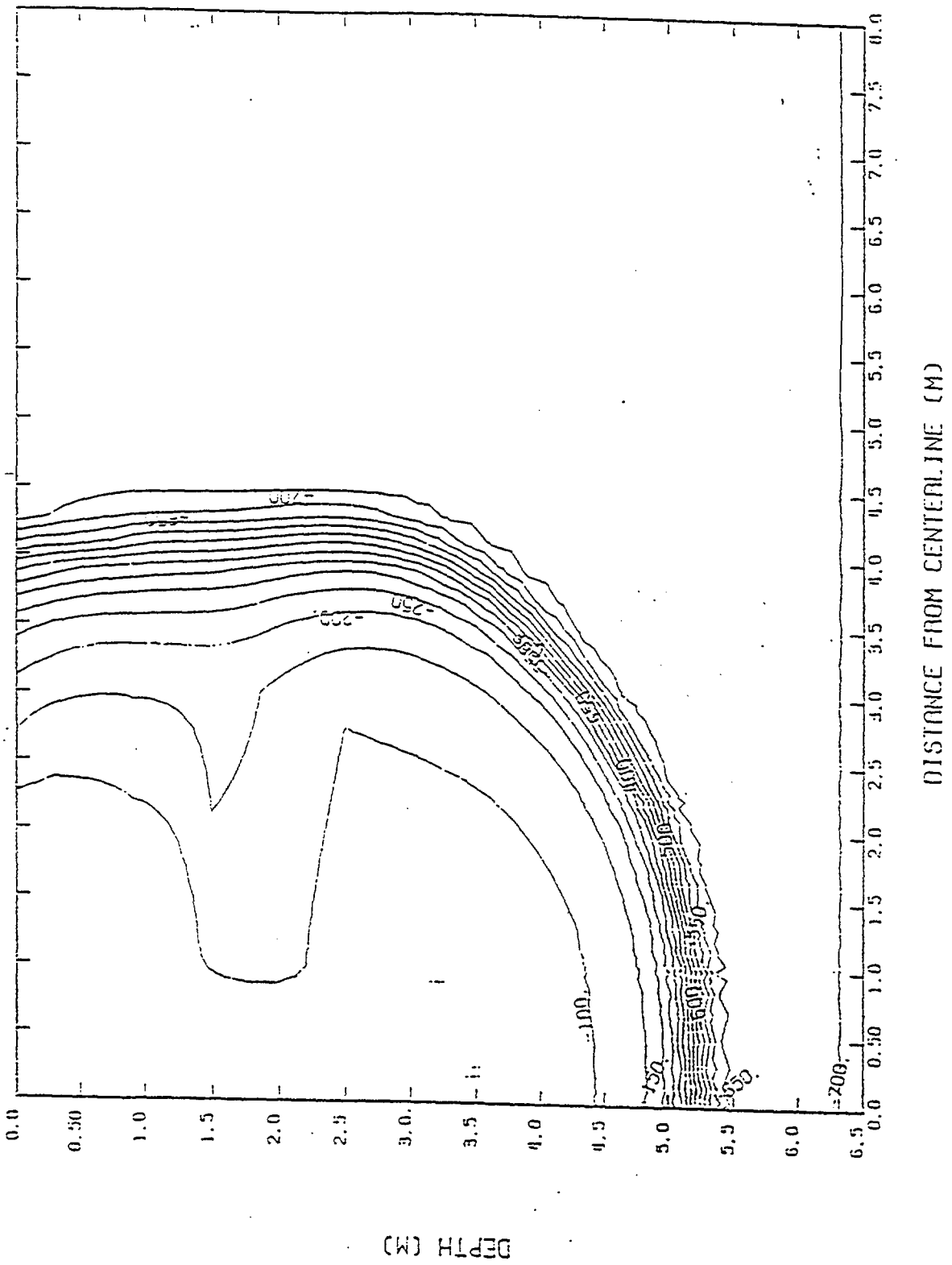

Figure 3.10 UNSAT2 Pressure Head Contours for Case 4 After 30 Days

4.0 Simulation of Infiltration into Dry Soils using TRACR3D

TRACR3D is a transient, multidimensional, variably saturated, two-phase flow and multicomponent transport code for porous media. The code utilizes a finite-difference approximation of the flow equation

$$\frac{\partial}{\partial t}\left(\xi \rho_\ell \sigma_\ell\right) + \nabla \cdot \left(\rho_\ell \vec{u}_\ell\right) = \xi \dot{S}_\ell \tag{4.1}$$

where
- t = time
- ξ = porosity
- ρ_ℓ = liquid density
- σ_ℓ = liquid saturation
- ∇ = the del operator
- $\vec{u}_\ell$ = liquid mass velocity
- $\dot{S}_\ell$ = liquid mass source or sink

An analogous equation is used for gas flow. Forward time-stepping is used for flow calculations. A mass-balance formulation is computed to assess the accuracy of the simulation. Mass transport is determined using either forward or central differencing time-stepping.

TRACR3D is a powerful, flexible, and data-intensive code that can handle a broad range of isothermal flow and transport problems. Previous use by PNL has shown the code to be particularly well-suited to infiltration into strongly heterogeneous, dry soils.

4.1 TRACR3D Simulations

Simulation of infiltration at the Las Cruces trench using TRACR3D required more data than that provided by NMSU. To satisfy TRACR3D's input requirements, the following assumptions were made: water temperature of 15°C and water viscosity of 0.0114 poise. Since TRACR3D does not provide for a specified flux-boundary condition, it was necessary to assume that a specified source in the top layer of the finite-difference grid was equivalent to flux entering the soil (i.e., infiltration).

Although TRACR3D uses finite-difference grids, the attempt was made to approximate the finite-element meshes used in the UNSAT2 modeling as closely as possible. The philosophy of using a fine grid in areas of rapid change was maintained (Figure 4.1). PNL's version of TRACR3D is operated on CRAY X-MP48 computers with CTSS operating system. All simulations were performed in this environment.

Grid specifications, time-stepping, and computational times are summarized in Table 4.1.

Table 4.1 TRACR3D Simulation Summary

Case	Tension (cm)	Nodes	Mass Balance	Time Steps (s) Initial	Maximum	Magnification	Simulation Length (d)	Computation Time (h)
1	724	255	1.000	1200	$2.16 \cdot 10^4$	1.10	7	<0.016
2	10000	4510	1.000	60	$7.20 \cdot 10^3$	1.15	7	0.396
3	724	2376	1.000	1200	$1.08 \cdot 10^4$	1.20	30	0.296
	10000	2376	1.000	60	$2.16 \cdot 10^4$	1.15	30	0.745
4	724	2376	1.000	600	$2.16 \cdot 10^4$	1.30	30	0.164
	10000	2376	1.000	60	$2.16 \cdot 10^4$	1.15	30	0.669

4.1.1 Case 1 and Case 2 Results

Case 1 (724-cm tension, homogeneous soil) was simulated for 7 days using a 255-node grid. The maximum spacings used in the grid were 200.0 and 100.0 cm in the horizontal and vertical directions, respectively. In both the horizontal and vertical directions, 25.0 cm was the minimum spacing used (Figure 4.1a).

After 7 days, the wetting front had moved 125 cm vertically (i.e., progressed to 525 cm above the bottom of the trench) and 100 cm horizontally (i.e., progressed to 325 cm from the left boundary, see Figure 4.2). This movement is also shown in velocity vector plot (Figure 4.3).

As expected, Case 2 (10,000-cm tension, homogeneous soil) took more computational time than Case 1 as a result of the drier initial conditions. The grid used was refined to 4510 nodes. Minimum and maximum spacing were 5.0 and 100.0 cm, respectively, to account for the additional nonlinearity expected in a drier system (Figure 4.1b). Both the vertical and the horizontal movements of the wetting front were less than simulated in Case 1 (Table 4.2).

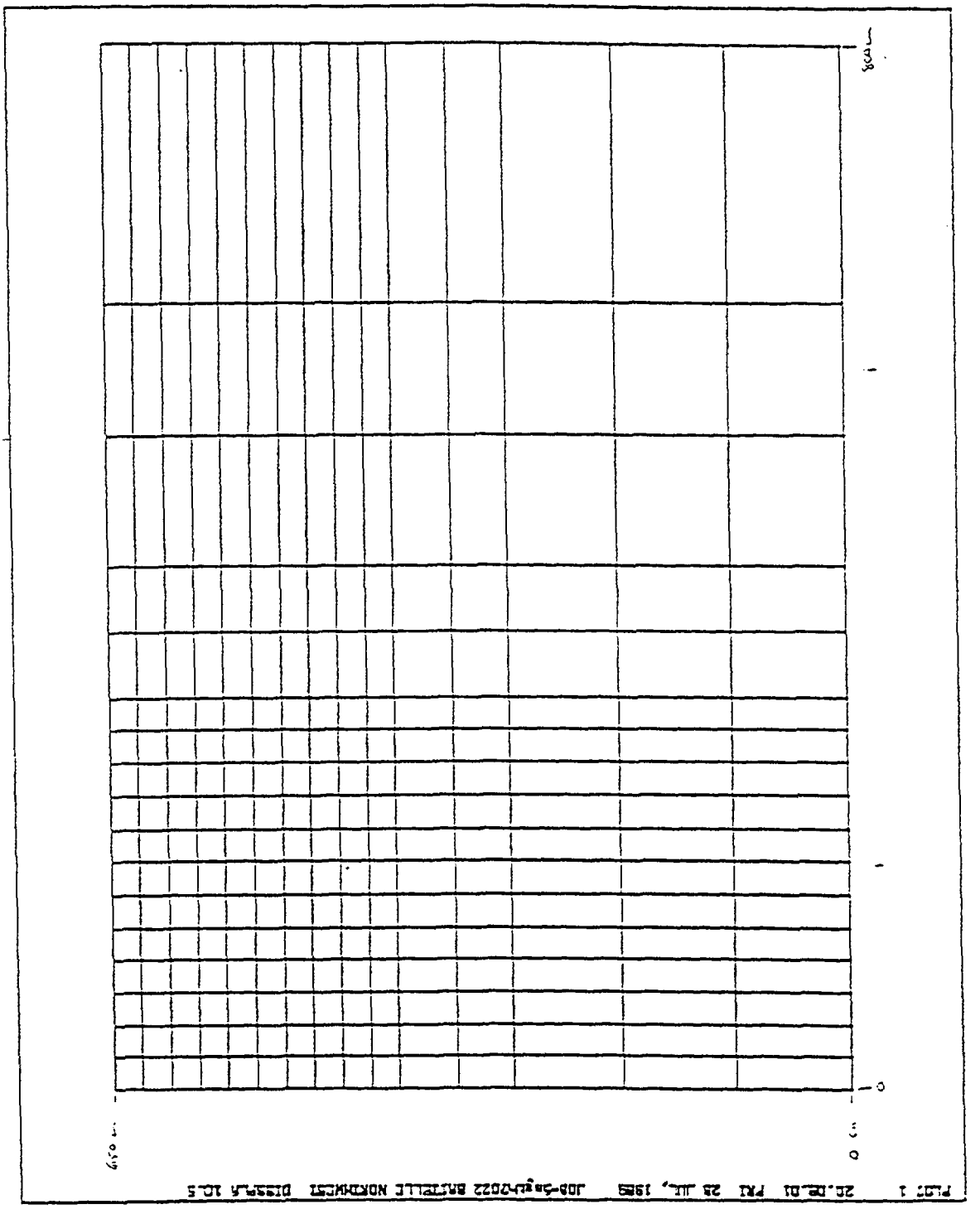

Figure 4.1 Grid Used for TRACR3D Simulations of Case 1, Case 2, Case 3 and Case 4

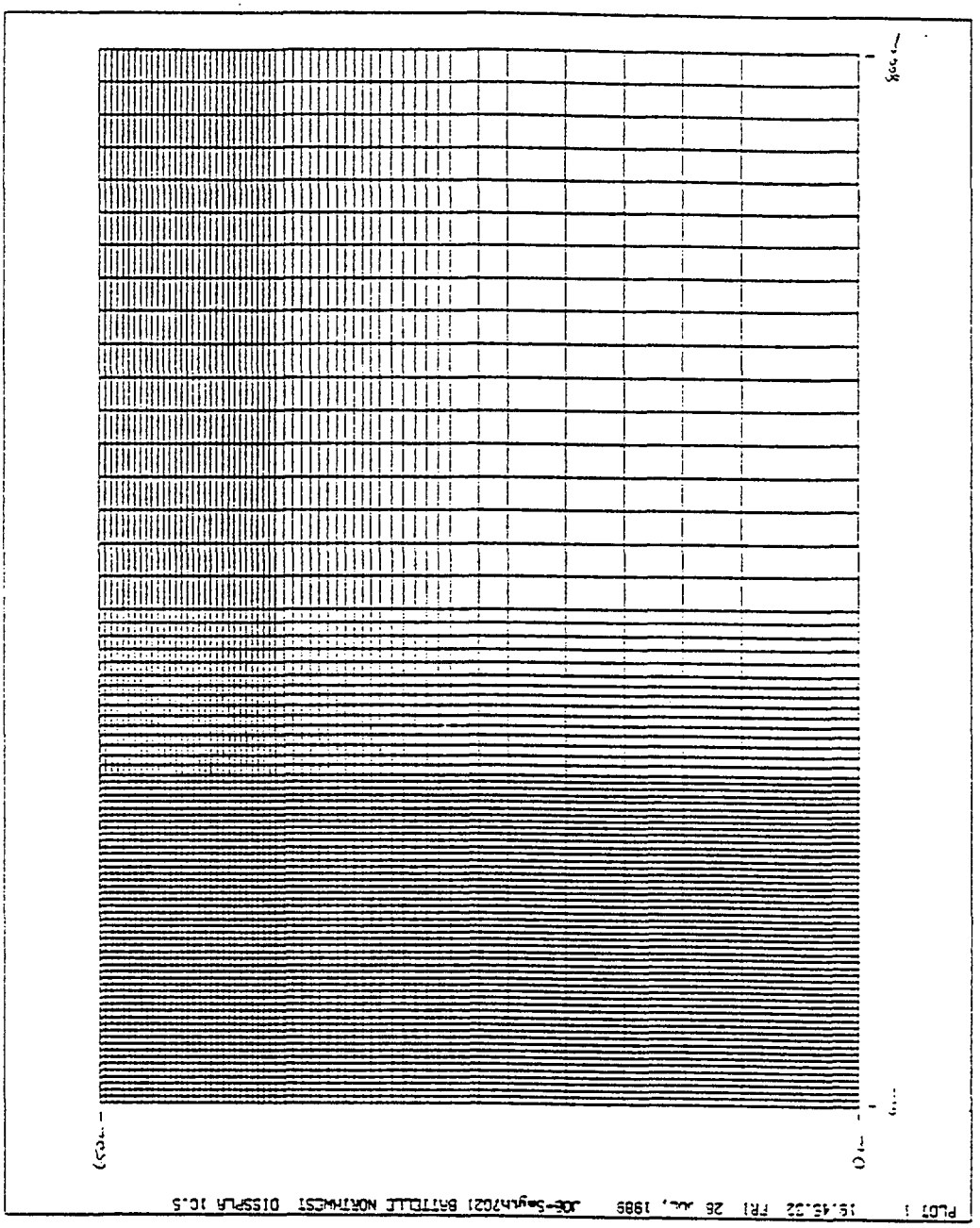

Figure 4.1 (contd)

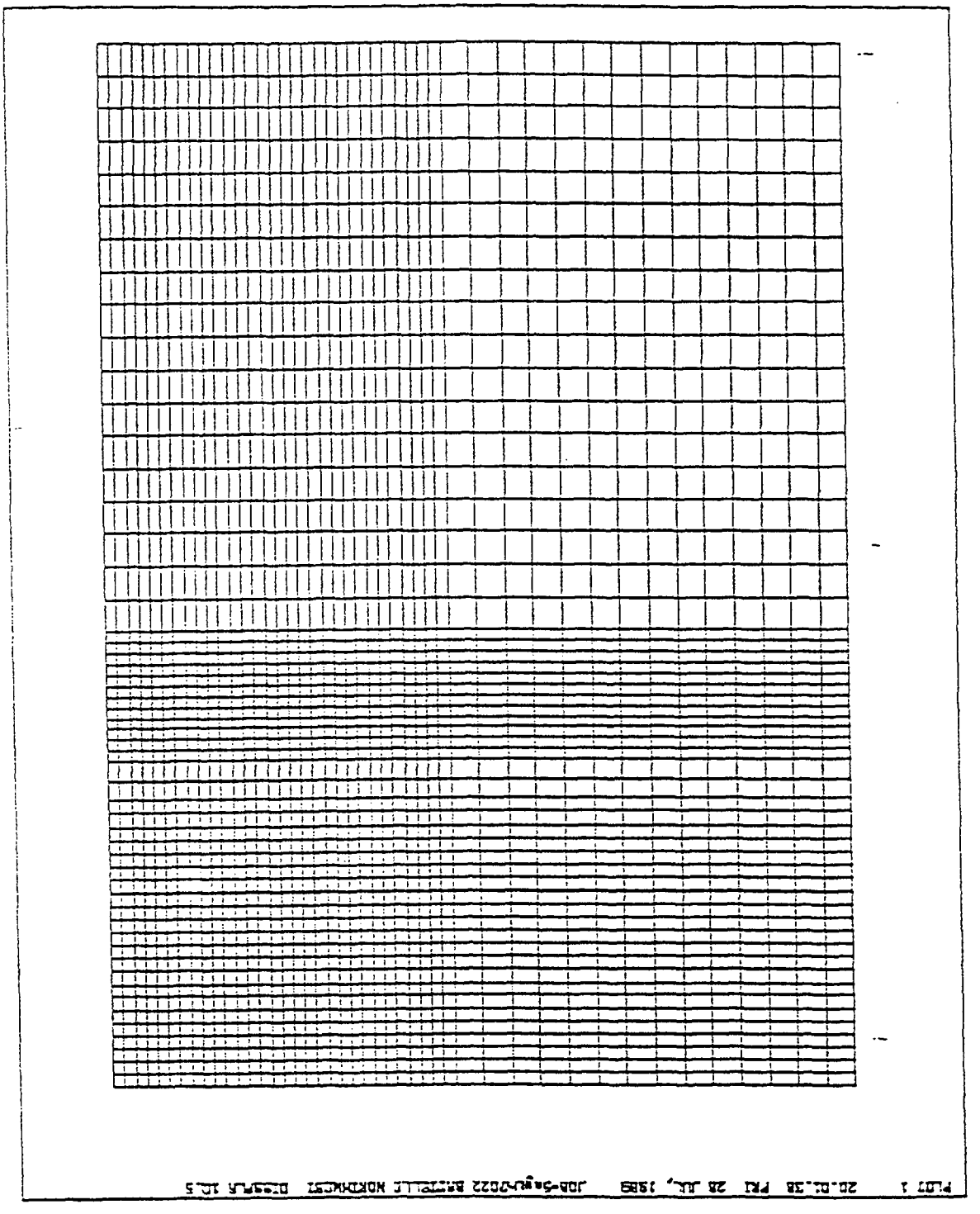

Figure 4.1 (contd)

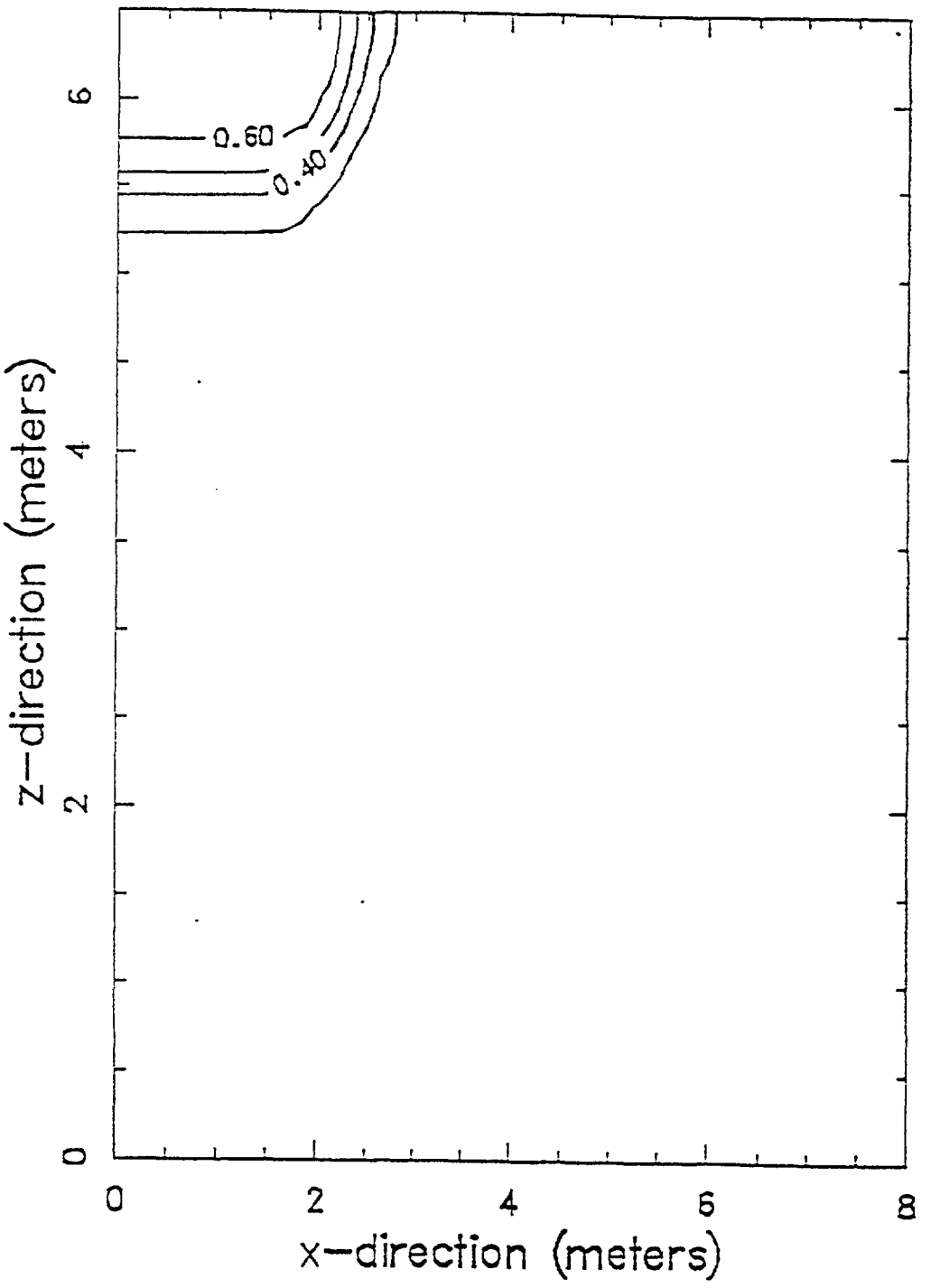

Figure 4.2 TRACR3D, Case 1, Liquid Saturation at 7 Days

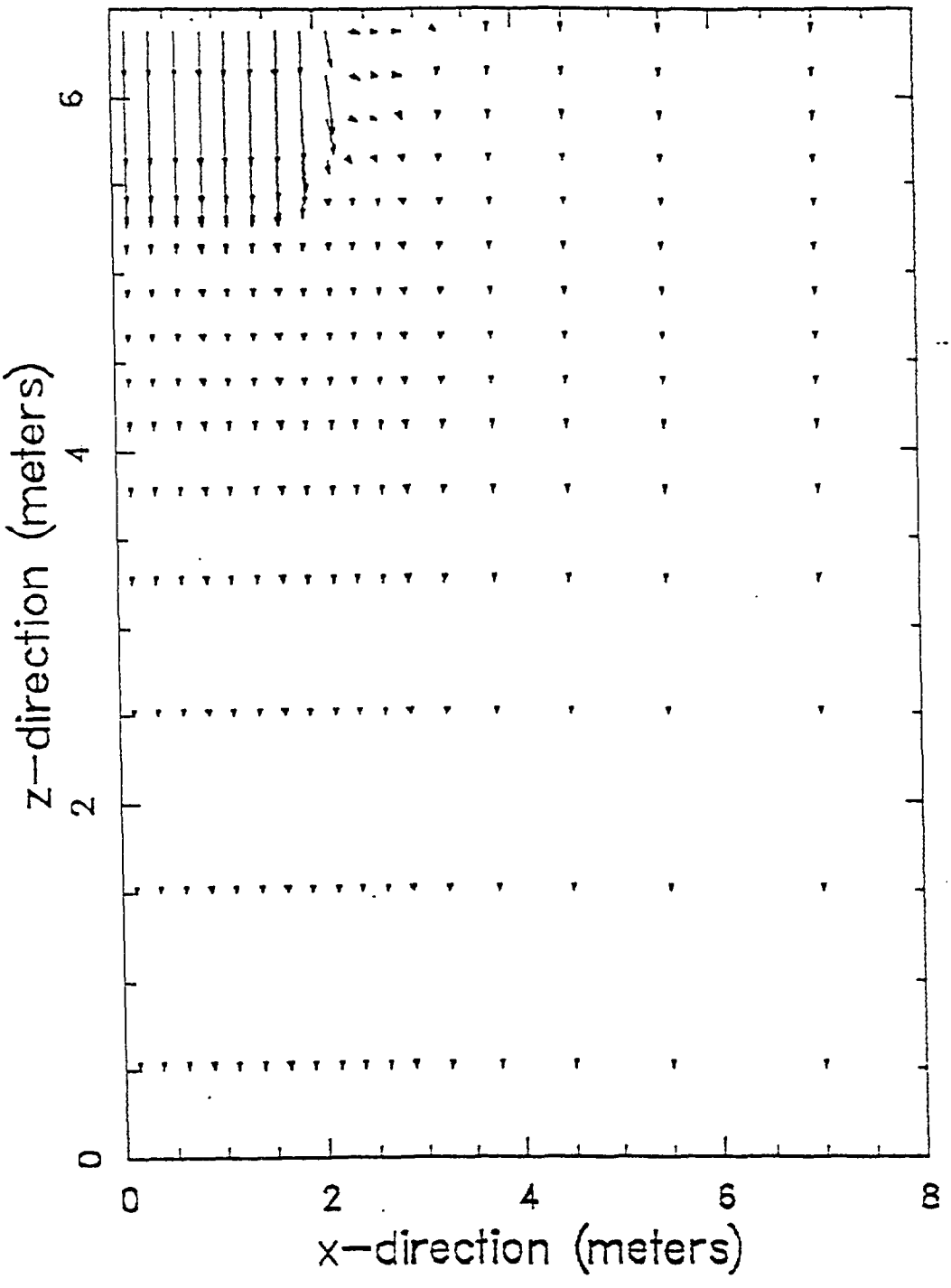

Figure 4.3 TRACR3D, Case 1, Liquid Velocity (cm/s) at 7 Days

Table 4.2 Results of TRACR3D Simulations

Case	Tension (cm)	Total Vertical Movement* (cm)	Total Horizontal Movement** (cm)
1	724	125	325
2	10000	100	250
3	724	650	500
3	10000	480	330
4	724	600	500
4	10000	480	475

* measured from the top boundary
** measured from the left boundary

4.1.2 Case 3 Results

The TRACR3D simulations for Case 3 were conducted successfully for both the 724-cm and the 10,000-cm tension initial condition. The grid used for both simulations consisted of 2376 nodes (Figure 4.1c). Maximum and minimum spacings were 25.0 and 10.0 cm in both the horizontal and vertical directions. The minimum node spacing was increased along the infiltration strip to add more nodes in the center of the horizontal and vertical zones. This was necessary to account for the heterogeneity of the system and to maintain computational efficiency.

The saturation contours (Figure 4.4) show vertical movement of the wetting front to the bottom boundary. This indicates that the assumption that the flow field is not influenced by the bottom no-flow condition is incorrect, at least with the 724-cm tension initial condition. Horizontal movement of the wetting front is 500.0 cm. The velocity plot (Figure 4.5) shows similar results.

Using the 10,000-cm tension initial condition, the movement of the wetting front from the infiltration source after 30 days is considerably less; 480 and 330 cm in the vertical and horizontal directions, respectively. The effect of the heterogeneous layering is evident at both interfaces of soils (30.0 cm and 60.0 cm) for both initial conditions (Figures 4.4 and 4.6). The no-flow boundary condition at the bottom of the grid does not appear to be a problem for the simulation with 10,000-cm tension initial condition.

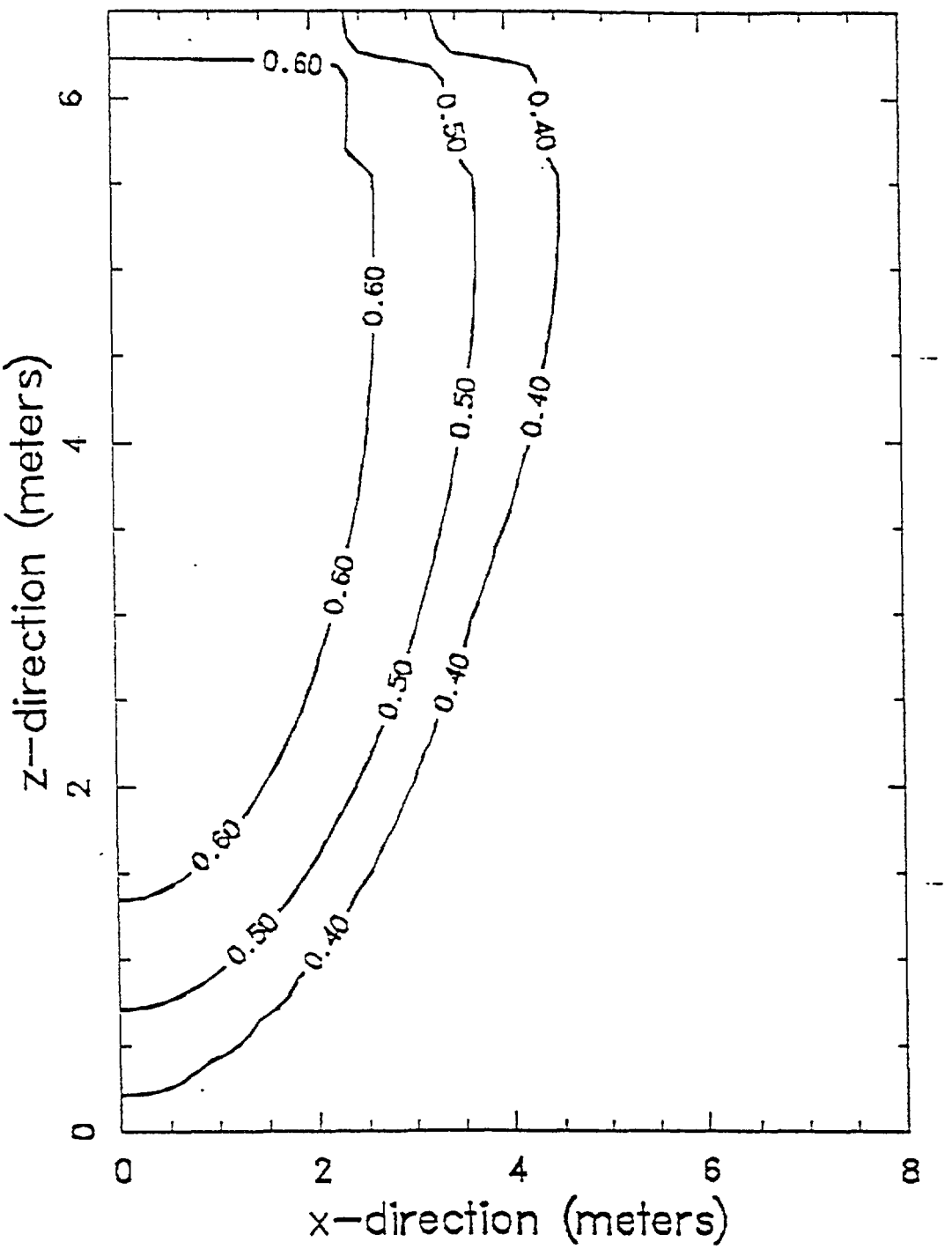

Figure 4.4 Case 3, Liquid Saturation at 7 Days (h = 724 cm)

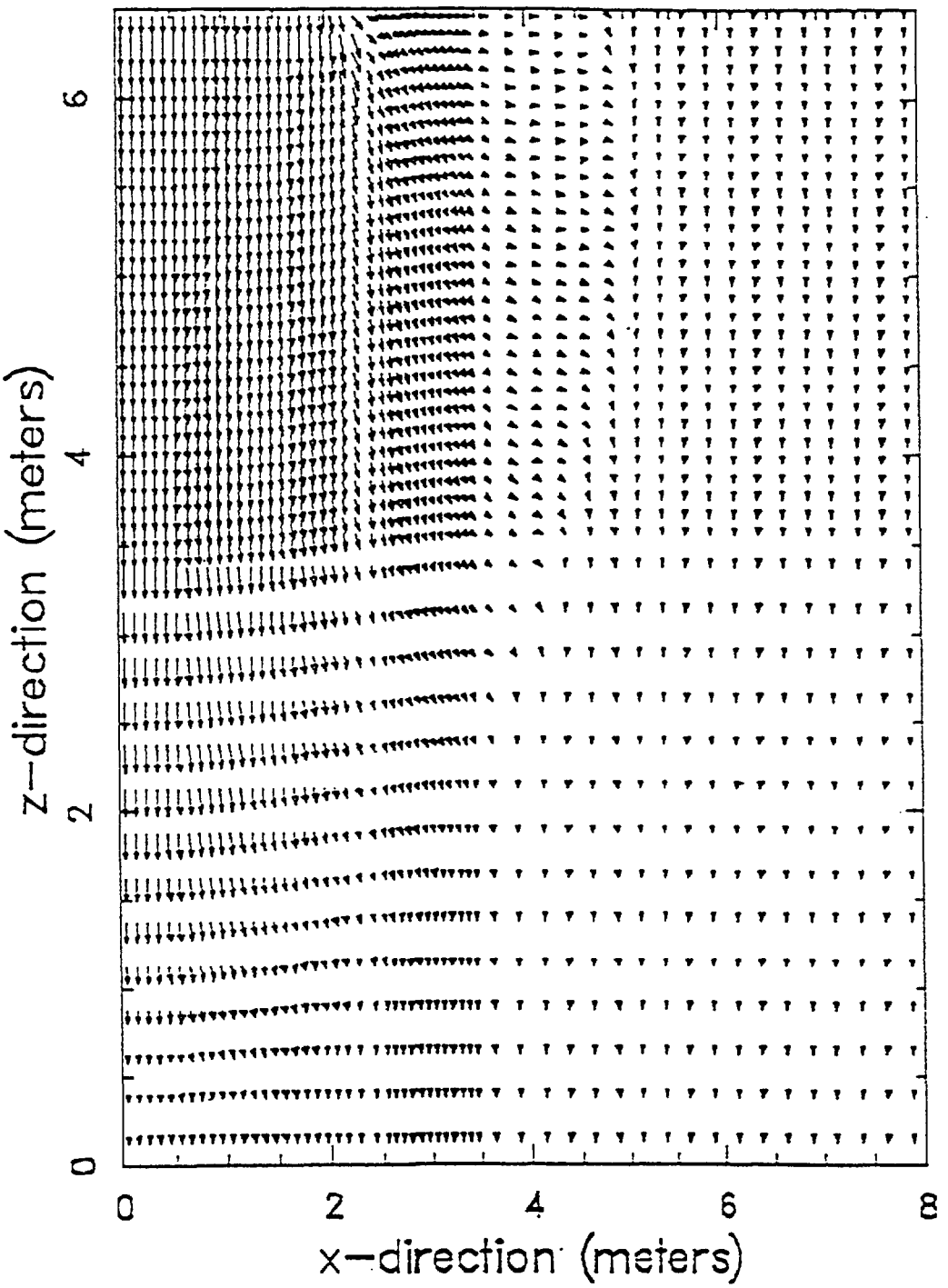

Figure 4.5 Case 3, Liquid Velocity (cm/s) at 30 Days (h = 724 cm)

4.1.3 Case 4 Results

The same grid used in the Case 3 simulations was used for Case 4. When comparing vertical and horizontal movement of the wetting front, the Case 4 results were not significantly different from the Case 3 results for the 724-cm tension initial condition. Although the saturation contours and velocity plot of Case 4 (Figures 4.7 and 4.8) show the effect of the high- conductivity zone, no differences from the Case 3 results are apparent (Figures 4.4 and 4.5). The effect of the high-conductivity zone on horizontal movement of the wetting front could be negligible because of the "wet" initial conditions. The lack of vertical difference in wetting front movement between Case 3 and Case 4 could be a result of using a no-flow boundary at the bottom.

However, when the 10,000-cm tension initial condition is used, the vertical movement of the wetting front is also identical for Cases 3 and 4 (480 cm). The heterogeneity of the system in Case 4 does result in the horizontal movement of the wetting front to 475 cm, 145 cm further than in Case 3 (Figures 4.9 and 4.10). In Figure 4.11, the effect of the high-conductivity zone is shown by velocity vectors. The tenfold higher conductivity of this zone results in the direction of the velocity vectors being more horizontal than in the surrounding soil.

4.2 Discussion of TRACR3D Results

As expected, TRACR3D did not experience any problems with the 10,000-cm tension initial conditions. The mass balance was preserved for all simulations. Computation times were all less than 1 hour of CRAY CTSS time [includes central processing unit (CPU), storage, and input/output (I/O)]. Given that an hour of non-interactive CRAY time costs approximately $140, the simulations ranged from a cost of $2.24 (Case 1) to $104.30 (Case 3, 10,000-cm tension). Although costs will vary with the computer used, it is indicative of the computational intensity necessary to simulate infiltration into dry soils. The trade-off of using a less costly (and hence less powerful) computer would be considerably more computational time.

The results of Cases 3 and 4, using initial tensions of 10,000 cm, are compared with measured data from the Las Cruces trench site in Table 4.3. In the TRACR3D simulations the resolution of wetting front location is ± 25 cm, because of grid spacing. The simulated average pore-water velocity ranges from 15.1 to 16.8 cm/d, resulting in faster average vertical pore-water velocities than were measured. This range could be a result of using preliminary trench soil data. Given the differences in the TRACR3D simulations with different initial moisture conditions, the faster average vertical pore velocities could also be a result of starting with initial conditions wetter than those at the Las Cruces site.

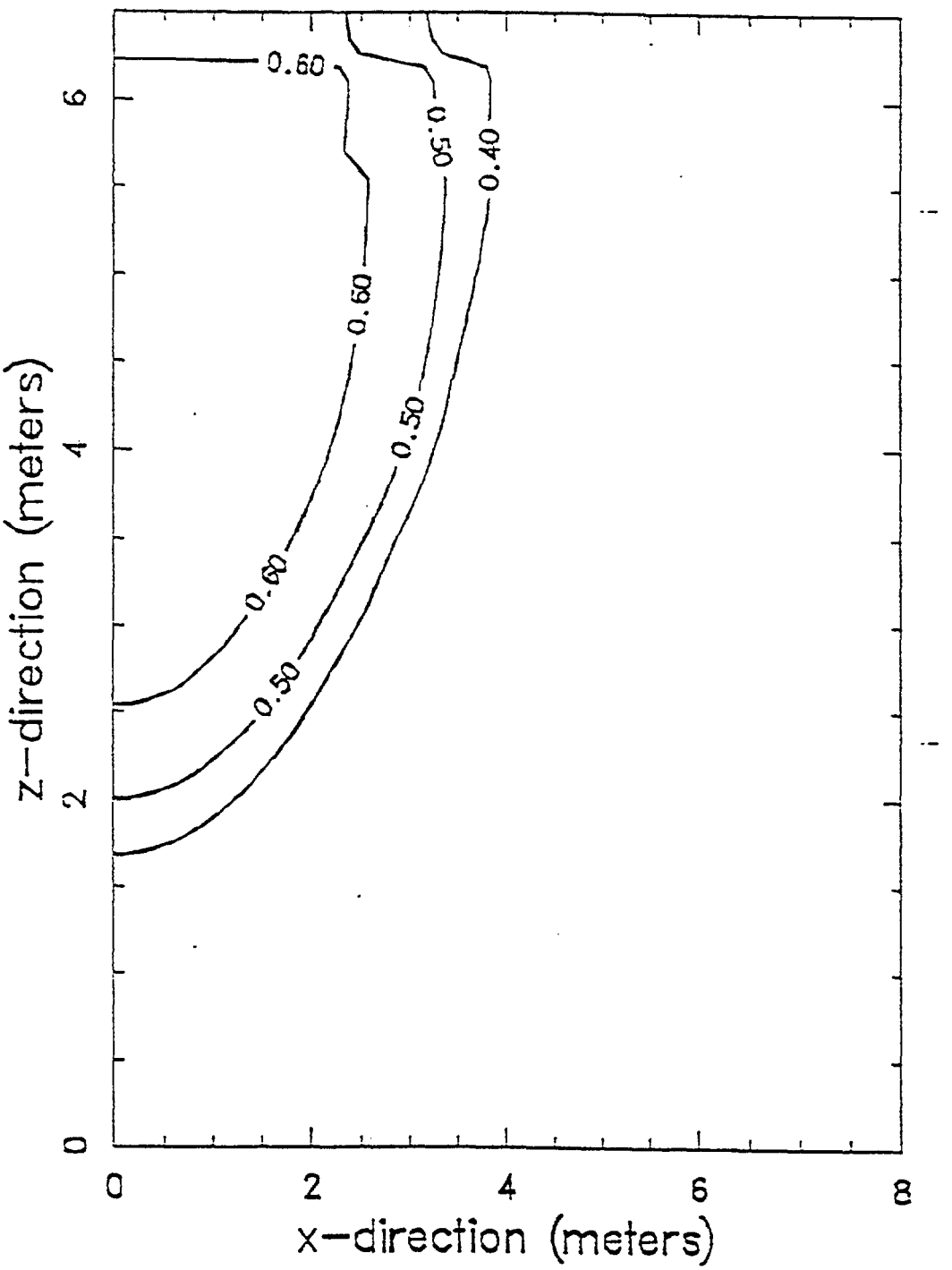

Figure 4.6 Case 3, Liquid Saturation at 30 Days (h = 10,000 cm)

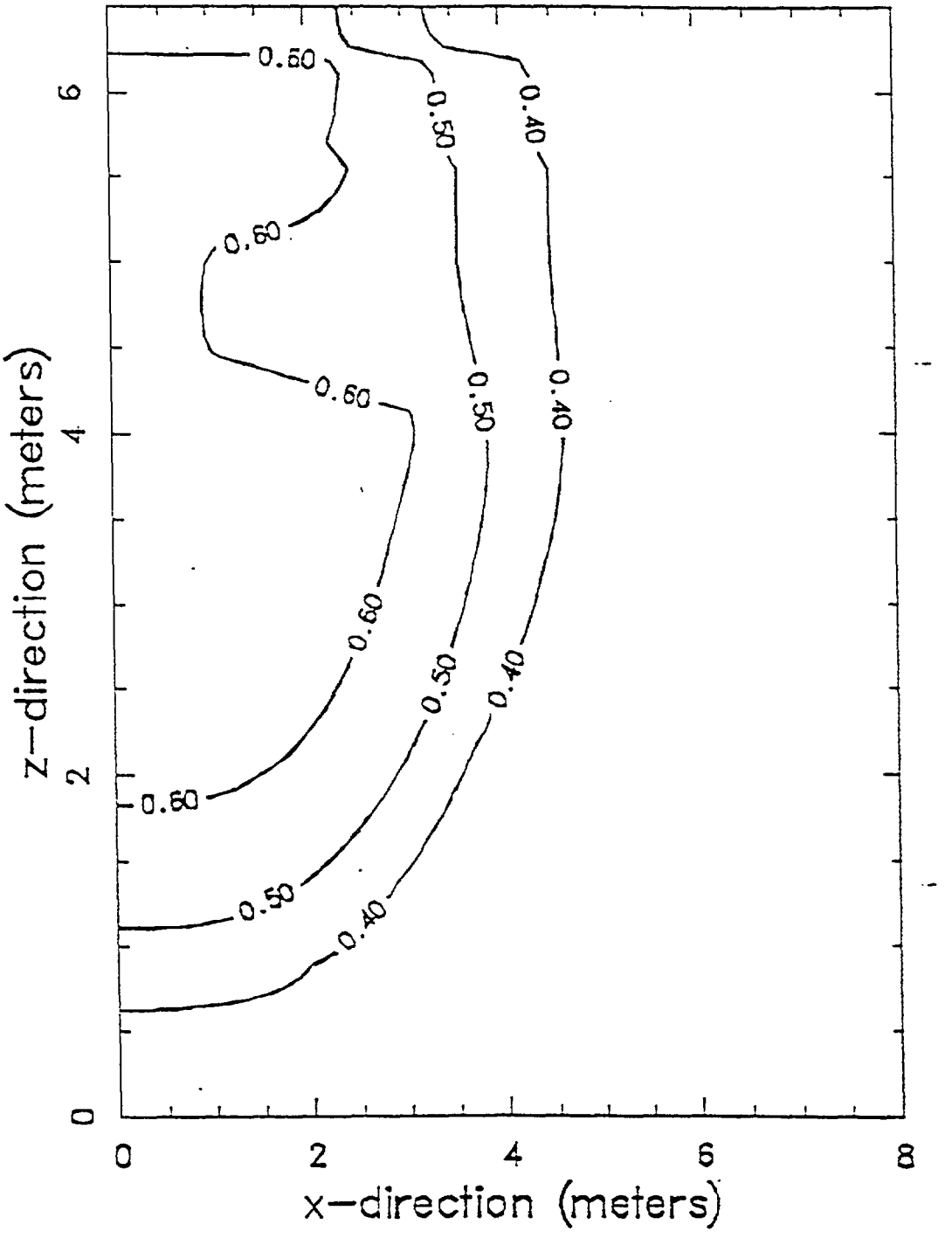

Figure 4.7 Case 4, Liquid Saturation at 30 Days (h = 724 cm)

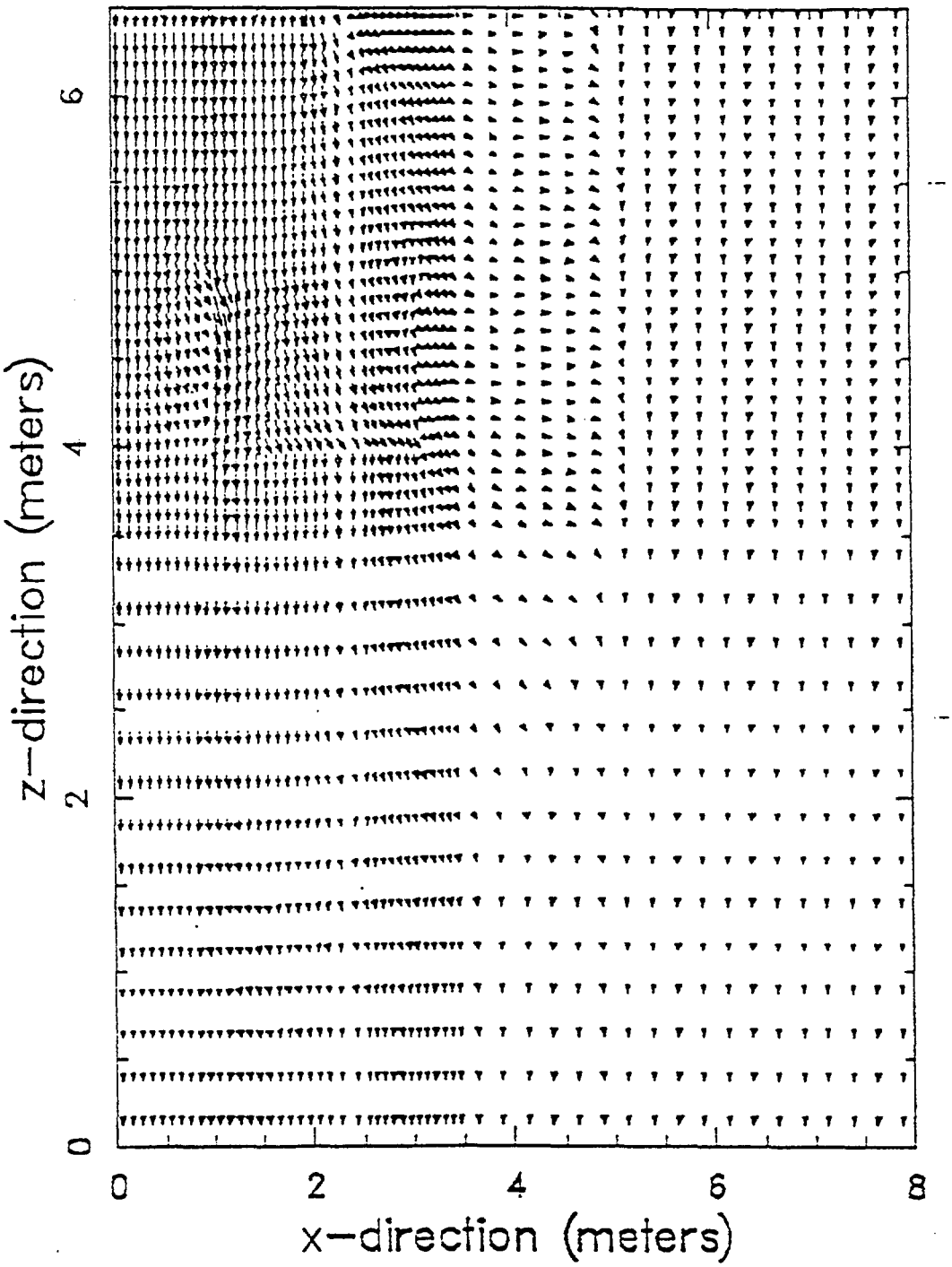

Figure 4.8 Case 4, Liquid Velocity (cm/s) at 30 Days (h = 724 cm)

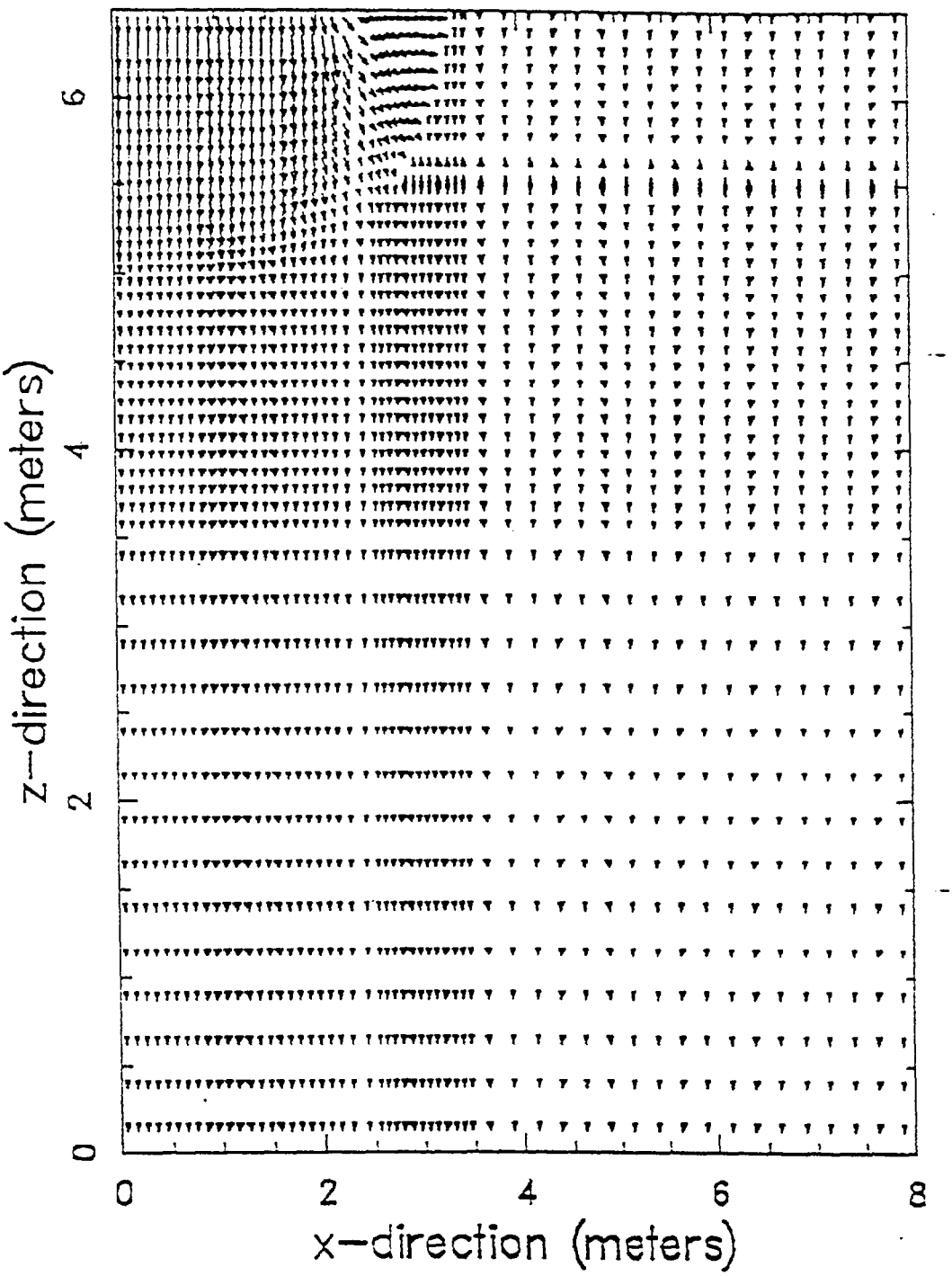

Figure 4.9 Case 3, Liquid Velocity (cm/s) at 7 Days (h = 10,000 cm)

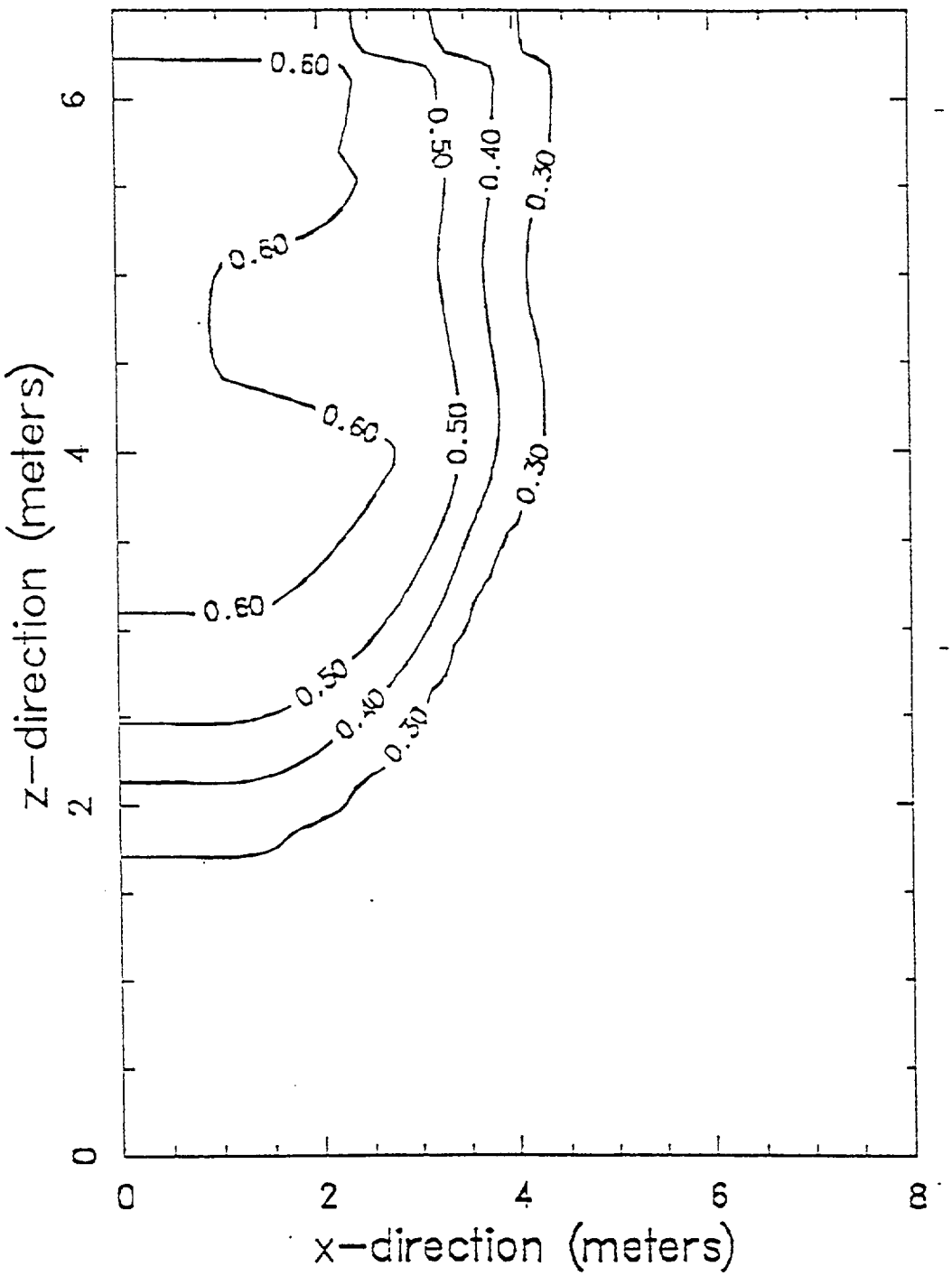

Figure 4.10 Case 4, Liquid Saturation at 30 Days (h = 10,000 cm)

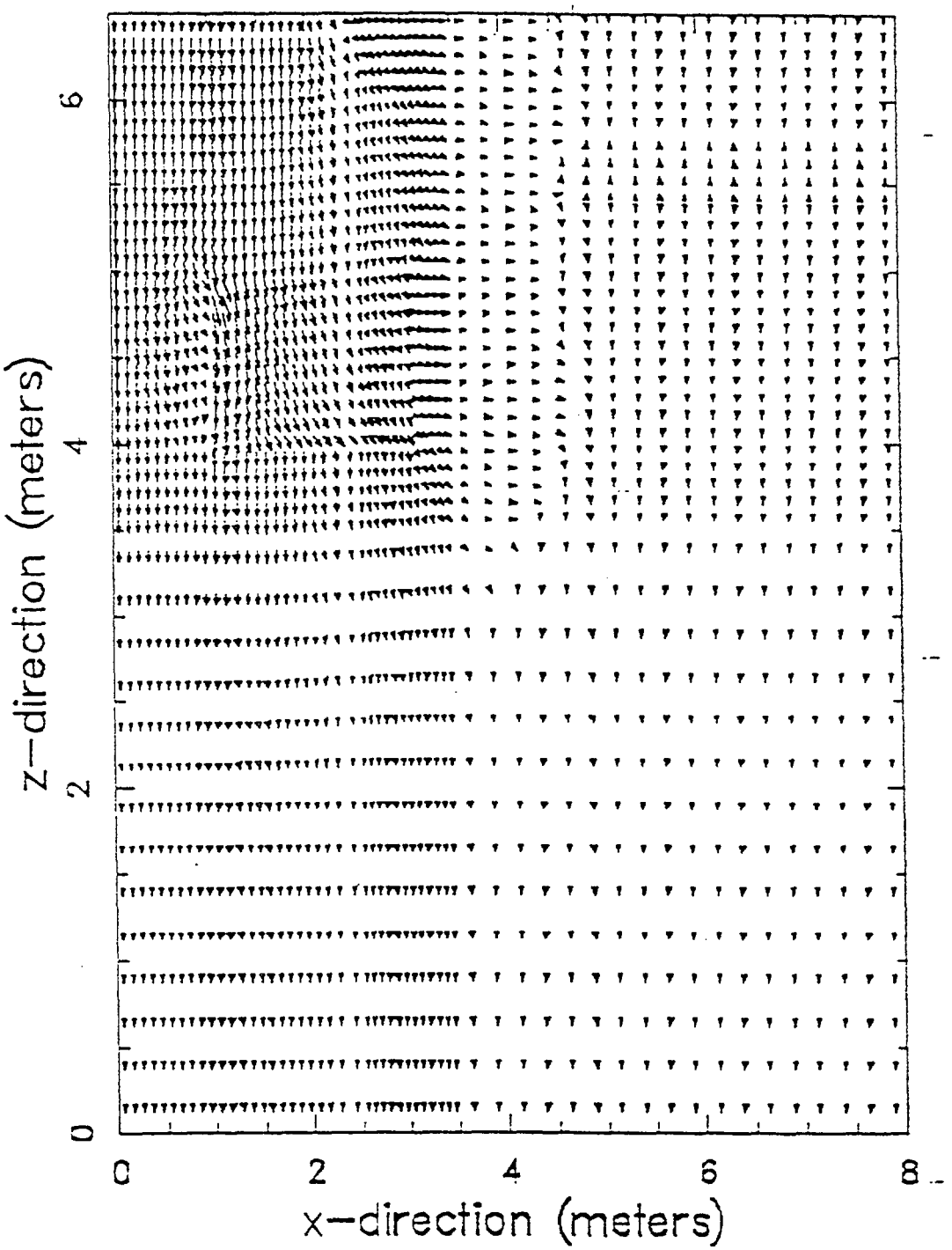

Figure 4.11 Case 4, Liquid Velocity (cm/s) at 30 Days (h = 10,000 cm)

Table 4.3 Comparison of Field Measurements with TRACR3D Results

Source	Time (d)	Average Vertical Pore-Water Velocity (cm/d)
Measurements		
Visual	65	9.8
Tensiometers	50	11.0
Neutron Tube	40	13.7
Average	**51.7**	**12.4**
Simulations		
Case 3 (10,000 cm Tension)	30	15.1 - 16.8
Case 4 (10,000 cm Tension)	30	15.1 - 16.8
Average	**30**	**15.9**

5.0 Summary and Conclusion

Two multidimensional, variably saturated computer codes (UNSAT2 and TRACR3D) were selected and tested on preliminary data from the Las Cruces trench site in New Mexico.

Four test cases with initial conditions of 724-cm tension and 10,000-cm tension were designed to test the ability of the codes to model water infiltration into layered soils. Both codes were able to simulate the wetter initial condition relatively easily (i.e., 724-cm tension). However, UNSAT2 was not able to simulate the more realistic field tension of 10,000 cm. Mass- balance errors on the order of 50% were observed, and prohibitively small grid sizes (1 mm) and time steps would have been required to obtain converged solutions.

TRACR3D successfully simulated wetting front movement with the 10,000 cm initial condition. No mass-balance problems were encountered. The simulations were computationally intensive, however, costing on the order of $100.00 per run for the 10,000 cm tension initial condition on a CRAY X-MP48.

From these initial simulations using UNSAT2 and TRACR3D to model infiltration into dry soils, it can be concluded that UNSAT2 is not well suited for very dry soils. In contrast, TRACR3D performed adequately and did not experience computational difficulties. Thus, TRACR3D appears to be suitable for describing water flow in dry soil. The 30% overprediction of pore-water velocities by TRACR3D is probably a result of the hydraulic property data, the uncertainty of which was at least as large as the prediction error. To increase confidence in using TRACR3D will require additional testing using the complete hydraulic property data set as it becomes available.

6.0 References

Bresler, E. 1973. "Simultaneous Transport of Solutes and Water Under Transient Unsaturated Flow Conditions." Water Resource Research 9:975-986.

Bresler, E. 1975. "Two-Dimensional Transport of Solutes During Non-Steady Infiltration from a Trickle Source." Soil Science Society of America Proceedings 39:604-613.

Bresler, E., W. D. Kemper, and R. J. Hanks. 1969. "Infiltration Redistribution and Subsequent Evaporation of Water from Soil as Affected by Wetting Rate and Hysteresis." Soil Science Society of America Proceedings 33:832-840.

Davis, L. A., and S. P. Neuman. 1983. Documentation and User's Guide: UNSAT2 - Variably Saturated Flow Model. NUREG/CR-3390, U.S. Nuclear Regulatory Commission, Washington, D.C.

Fayer, M. J., G. W. Gee, and T. L. Jones. 1986. UNSAT-H Version 1.0: Unsaturated Flow Code Documentation and Applications for the Hanford Site. PNL-5899, Pacific Northwest Laboratory, Richland, Washington.

Feddes, R. A., E. Bresler, and S. P. Neuman. 1974. "Field Test of a Modified Numerical Model for Water Uptake by Root Systems." Water Resources Research 10(6):1199-1206.

Feddes, R. A., E. Bresler, and S. P. Neuman. 1975. "Finite Element Analysis of Two-Dimensional Flow in Soils Considering Water Uptake by Roots: II. Field Applications." Soil Science Society of America Proceedings 39:231-237.

Feddes, R. A., P. Kowalik, S. P. Neuman, and E. Bresler. 1976. "Finite Difference and Finite Element Simulation of Field Water Uptake by Plants." Hydrology Sciience Bulletin IASH 21(1):81-98.

Hanks, R. J., A. Klute, and E. Bresler. 1969. "A Numeric Method for Estimating Infiltration, Redistribution, Drainage, and Evaporation of Water from Soil." Water Resources Research 5:1054-1069.

Hills, R. G., I. Porro, D. B. Hudson, and P. J. Wierenga. 1989. "Modeling One-Dimensional Infiltration into Very Dry Soils 1. Model Development and Evaluation." Water Resources Research 25:1259-1269.

Hills, R. G., and P. J. Wierenga. 1991. Model Validation at the Las Cruces Trench Site. NUREG/CR-5716, U.S. Nuclear Regulatory Commission, Washington, D.C.

Neuman, S. P. 1973. "Saturated-Unsaturated Seepage by Finite Elements." Journal of the Hydraulics Division, American Society of Civil Engineers. 99(HY12):2233-2250.

Neuman, S. P., R. A. Feddes, and E. Bresler. 1974. Finite Element Simulation of Flow in Saturated-Unsaturated Soils Considering Water Uptake by Plants: Development of Methods, Tools and Solutions for Unsaturated Flow. Third Annual Report, Technion, Haifa, Israel.

Neuman, S. P. 1975. "Galerkin Approach to Saturated-Unsaturated Flow in Porous Media," Chapter 10, In Finite Elements in Fluids, Volume 1: Viscous Flow and Hydrodynamics, edited by R. H. Gallagher, J. T. Oden, C. Taylor, and O. C. Zienkiewicz, John Wiley and Sons, London, pp. 201-217.

Polmann, D. J., E. G. Vomvoris, D. McLaughlin, E. M. Hammick, and L. W. Gelhar. 1988. Application of Stochastic Methods to the Simulation of Large-Scale Unsaturated Flow and Transport. NUREG/CR-5094, U.S. Nuclear Regulatory Commission, Washington, D.C.

Travis, B. J. 1984. TRACR3D: A Model of Flow and Transport in Porous/ Fractured Media. LA-9667-MS, Los Alamos National Laboratory, Los Alamos, New Mexico.

Wierenga, P. J., L. W. Gelhar, C. S. Simmons, E. A. Jacobson, G. W. Gee, and T. J. Nicholson. 1986. Validation of Stochastic Flow and Transport Models for Unsaturated Soils: A Comprehensive Field Study. NUREG/CR-4622, U.S. Nuclear Regulatory Commission, Washington, D.C.

Wierenga, P. J., A. F. Toorman, D. B. Hudson, J. Vinson, M. Nash, and R. G. Hills. 1989. Soil Physical Properties at the Las Cruces Trench Site. NUREG/CR-5441, U.S. Nuclear Regulatory Commission, Washington, D.C.

APPENDIX D1

Variations of hydrological parameters
of tuff and soil

Table of Contents

APPENDIX D: VARIATIONS OF HYDROLOGICAL PARAMETERS OF TUFF AND SOIL

J. S. Y. WANG
Earth Sciences Division
Lawrence Berkeley Laboratory
Berkeley, CA 94720
(510) 486-6753

ABSTRACT

The saturated and unsaturated flow parameters of Yucca Mountain and Apache Leap tuffs and Las Cruces soil are compared. The saturated permeability generally has large variance, spanning over 2 to 4 orders of magnitude within each medium. Among different media, the mean value of saturated permeability are approximately proportional to the square of capillary radius. The capillary radius is determined by the unsaturated characteristic curve. A simple relationship between the variance of saturated permeability and the variance of pore-size distribution index is deduced from these data sets. These relationships could impose constraints on the choice and scaling of hydrological parameters for fractures, faults, or other units with scanty measurements.

INTRODUCTION

To model the flow through a fractured porous medium, we need to specify the parameters characterizing the fractures and the matrix. In this study, we compare parameter distributions of tuff matrix[1,2] with soil data[3]. The constrast in hydrological parameters between tuff matrix and soil may help us to understand the behavior of other heterogeneous systems: the fractured rocks[4] or welded-nonwelded units bounded by faults[5,6]. The soil characteristic parameters have been used for representing fractures[7] and for characterizing nonwelded tuffs[8]. The lack of data in fractures and faults is one of the reasons we study the soil data[9,10].

HYDROLOGICAL PARAMETERS

In addition to saturated permeability k_s and porosity ϕ, we need saturation characteristic curve and relative permeability function to solve most numerical codes for unsaturated flow field. With pore geometry models, the relative permeability can be expressed as a function of saturation[11,12]. We focus on the parameters of the saturation characteristic curve which determine the relative permeability function as well.

The saturation characteristic curve, also known as the moisture retention curve, is the relationship of saturation, S, to the capillary suction pressure head, h. Various empirical analytic functions have been proposed in the literature to quantify saturation characteristics. Two popular functions are the Brooks and Corey model[11] and the van Genuchten model[12].

The Brooks and Corey model[11] is the power function of the form

$$S_e(h) = \begin{cases} 1 & \text{if } |\alpha h| < 1 \\ |\alpha h|^{-\lambda} & \text{if } |\alpha h| \geq 1 \end{cases} \quad (1)$$

and S_e is the effective saturation

$$S_e = \frac{S - S_r}{S_s - S_r} \quad (2)$$

with the subscripts s and r indicating saturated and residual values, respectively. The value of α is positive and the variable h is negative for a unsaturated state. The inverse of the parameter α, $|h_c| = \alpha^{-1}$, is frequently referred to as the air entry value or bubbling pressure head in the soil literature. This is one interpretation for the parameter α or h_c. When suction pressure head h overcomes the air entry pressure h_c ($|h| \geq |h_c|$), air enters the pores and water flows out of the medium to initiate desaturation. This interpretation is based on the cutoff separating the saturated region, $S_e = 1$, from the desaturated region, $S_e = |\alpha h|^{-\lambda}$. Another interpretation for α is to treat it as a scaling parameter. The saturation depends on αh together and not on α and h separately. Characteristic curves with different α, but same λ, can be scaled into one curve. We refer to α as the capillary scaling factor.

If flow channels are represented by capillary tubes, we can define capillary radius by the capillary equation

$$r_c = -\frac{2\sigma\cos\Theta}{\rho g h_c} = \frac{2\sigma\cos\Theta}{\rho g}\,\alpha. \quad (3)$$

In this study, we use surface tension $\sigma = 0.07183\ kg/s^2$, contact angle $\Theta = 0°$, water density $\rho = 1000\ kg/m^3$, and gravitational acceleration $g = 9.80665\ m/s^2$ in calculating r_c from parameter h_c or α. The capillary radius r_c represents the largest pore radius in the medium that is most easily drained in a desaturation process. With σ, ρ, and g as constants, r_c is proportional to α. We can treat the capillary radius r_c as a parameter equivalent to the capillary scaling factor α.

The second parameter λ is an index for pore-size distribution. The value of λ must be positive in Equation 1 to represent the physical situation in which saturation decreases as suction increases (or pressure head becomes more negative). As suction overcomes the air entry cutoff and progressively desaturates the medium, pores with progressively smaller and smaller radii are being drained. If the index λ is large, the saturation decreases rapidly over a narrow range of pressure head. This is equivalent to a narrow pore-size distribution. If the index λ is small, the pore-size distribution is broad. Scaled characteristic curves of effective saturation S_e versus dimensionless pressure head $|\alpha h|$ for different λ are plotted in Figure 1.

For media with broad pore-size distributions, a sharp cutoff at an air entry value may not be well defined. Other empirical functions have been proposed to improve the description of a moisture retention curve near saturation with cutoff-free, continuously differentiable, smooth S-shaped features. The van Genuchten model[12] has been popular in recent years. In its general form:

$$S_e = [1 + (|\alpha h|)^n\ ]^{-m} \quad (4)$$

where α, n, and m are empirical parameters. We use the same symbol α in both Equations 1 and 4 to represent similiar empirical scaling parameters. Even though the van Genuchten model does not have a cutoff at $h = -1/\alpha$, we still use Equation 3 to define an

equivalent capillary radius with the van Genuchten α parameter.

In the range of large suction (large negative pressure head), Equation 4 asymptotically approaches a power function, and is approximately equivalent to Equation 1 with

$$\lambda = mn. \tag{5}$$

In a frequently used special case, van Genuchten reduces the number of empirical parameters by setting

$$m = 1 - \frac{1}{n}. \tag{6}$$

With Equation 6, Equation 5 becomes

$$\lambda = n - 1. \tag{7}$$

Like λ, we also refer to $n - 1$ as a pore-size distribution index. Scaled characteristic curves of Equation 4 with Equation 7 are shown in Figure 1 for different n values. For physical characteristic curves with $S_e \leq 1$, the value of n must be greater than 1. Brooks and Corey curves and van Genuchten curves with equivalent pore-size distribution indices are different in the small suction region near saturation.

PARAMETER CORRELATIONS

The Yucca Mountain[1] and Apache Leap[2] tuff matrix characteristic curves and the Las Cruces[3] soil characteristic curves have been analyzed with the van Genuchten model. In this study, the capillary radius and the pore-size distribution index are plotted against the saturated permeability for each core sample from these three different sites. For the Yucca Mountain data sets, we used different symbols for the following four groups: (1) welded tuff for units in the unsaturated zone, including Tiva Canyon welded unit (TCw) and Topopah Spring welded unit (TSw); (2) nonwelded vitric tuff, including Paintbrush nonwelded unit (PTn), Calico Hill nonwelded vitric unit (CHnv) and Crater Flats Upper nonwelded unit (CFUn); (3) Calico Hill nonwelded zeolitic tuff (CHnz); and (4) welded tuff for units below the water table, including Prow Pass welded unit (PPw) and Bullfrog welded unit (BFw).

There are 26, 16, 17, and 7 core samples for each of the four groups, respectively. The core samples were collected from three deep (up to 700 m) boreholes USW G-1, G-4, and GU-3. For each core sample with saturation characteristic curve measured, saturated permeabilities were determined on one to three subcores or wafers. The corresponding numbers of data points for k_s are 39, 22, 40, and 11 for the four groups, respectively. The Apache Leap tuff set[2] has 105 samples from nine 30-m deep slanted boreholes. The Las Cruces soil set[3] has 594 samples from the face of a 6-m deep trench. For these two data sets, we did not divide the data points into groups.

Figure 2 is the log-log scatter plot of saturated permeability k_s values versus the capillary radius values r_c for the three data sets of Yucca Mountain tuff, Apache Leap tuff, and Las Cruces soil. Excluding the nonwelded vitric tuff data for the moment, the data points for each group or set span 2 to 4 orders of magnitude in the y-axis (saturated permeability k_s) and up to 2 orders of magnitude in the x-axis (capillary radius r_c or capillary scaling factor α). Among very different soil and rock media, the mean value of saturated permeability is approximately proportional to the square of the mean value of capillary radius. The straight line in Figure 2 is the classical Poisseuille equation for a single circular tube.

Figure 3 is the log-log scatter plot of saturated permeability k_s versus the pore-size distribution index λ. We do not expect from physical models and do not observe from experimental data any correlation between the mean values of these two parameters. However, the variance of $\log(k_s)$ is proportional to the variance of $\log(\lambda)$, as shown in Figure 4. A simple equation

$$\sigma_{log\,(k_s)} = 4\,\sigma_{log\,(\lambda)} \tag{8}$$

is proposed. There is no similiar relationship between $\sigma_{log\,(k_s)}$ and $\sigma_{log\,(r_c)}$, even through the mean values are approximately correlated.

DISCUSSION

Although the number of data points are small, we analyze the nonwelded vitric tuff data separately from the welded/zeolitized tuff data. Figure 2 shows that the characteristics of nonwelded vitric tuffs are very different from those of the welded or zeolitized tuff. The nonwelded vitric tuffs have very scattered values for the saturated permeability, covering 6 orders of magnitude for the data of PTn. On the other hand, all these nonwelded vitric tuff samples have similiar values of capillary radius. It is interesting to measure more nonwelded vitric tuff samples to determine statistically meaningful distributions of both the saturated permeability and the unsaturated parameters. If there is a need to further divide the nonwelded units into finer subunits[13], more characterization of these hydrological properties are needed.

The welded tuff and the zeolitized tuff in the unsaturated zone at Yucca Mountain have similiar saturated permeability values and unsaturated parameters. For practical purpose, we could combined these units into one broad class as an approximation. The welded/zeolitized tuff at Yucca Mountain, together with Apache Leap tuff and Las Cruces soil, support very crudely the simple proportionality between saturated permeabilty and capillary radius squared. For stochastic modelings of very heterogeneous systems, we propose to impose this correlation on the mean values of saturated permeability and capillary scaling parameters between domains of very different media. Within a given medium, there is no apparent correlation between these two parameters from the data sets and uncorrelated samplings could adequately represent the data variability.

The Apache Leap tuff[2] and the Las Cruces soil[3] have very similiar variances in saturated permeability and in pore-size distribution index, as shown in Figure 4. Both field field studies systematically collected the core samples in well-defined domains. The near-equality of these variances from two very different media at two different sites leads to the proposition of Equation 8. The variances of welded/zeolitized tuff and nonwelded vitric tuff lend further support for this relationship between the variance of saturated permeability and the variance of pore-size distribution index.

For N samples of a given medium, we have 3N parameters with each sample having one k_s value and two unsaturated characteristic parameters λ and r_c (or α). In the Miller and Miller[14] scaling theory for porous medium, the relative pore structures at different magnifications are assumed to be the same. This is equivalent to the assumption that the pore-size distribution index is a constant for a given medium. Then for N samples, we have 2N+1 parameters with one λ value for all samples. The results presented in this study suggest that the pore-size distribution index does vary within a given medium. It is correlated with the variation of the permeability. Such a correlation between the variances of different parameters are not generally obvious from multi-variance correlation analyses with traditional statistical programs.

Correlations of the mean values and variances between flow and pore-geometry parameters can lead us to better quantification of heterogeneous flow fields and better understanding of the scaling laws of hydrological properties. The simple relationships among the permeability and pore-geometry parameters, in inter-medium mean values and in intra-medium variances, shall motivate more general scaling theories and approaches to quantify hydrological processes through heterogeneous geological formations.

ACKNOWLEDGEMENTS

The critical reviews by K. Pruess and Y. W. Tsang are greatly appreciated. This work was supported by Sandia National Laboratories for the Yucca Mountain Site Characterization Project of the U. S. Department of Energy under Contract No. DE-AC03-76SF00098.

REFERENCES

1. R. R. PETERS, E. A. KLAVETTER, I. J. HALL, S. C. BLAIR, P. R. HELLER, and G. W. GEE, Fracture and Matrix Hydrologic Characteristics of Tuffaceous Materials from Yucca Mountain, Nye County, Nevada, *SAND84-1471*, Sandia National Lab., Albuquerque, NM, 188 p. (1984).
2. T. C. RASMUSSEN, D. D. EVANS, P. J. SHEETS, and J. H. BLANFORD, Unsaturated Fractured Rock Characterization Methods and Data Sets at the Apache Leap Tuff Site, *NUREG/CR-5596*, U. S. Nuc. Reg. Comm., 125 p. (1990).
3. P. J. WIERENGA, D. HUDSON, J. VINSON, M. NASH, A. TOORMAN, and R. G. HILLS, Soil Properties at the Las Cruces Trench Site, *NUREG/CR-5441*, U. S. Nuc. Reg. Comm. (1989).
4. J. S. Y. WANG, and T. N. NARASIMHAN, Hydrologic Mechanisms Governing Fluid Flow in a Partially Saturated, Fractured, Porous Medium, *Water Resour. Res.*, 21(12), pp. 1861-1874 (1985).
5. J. RULON, G. S. BODVARSSON, and P. MONTAZER, Preliminary Numerical Simulations of Groundwater Flow in the Unsaturated Zone, Yucca Mountain, Nevada, *LBL-20553*, Lawrence Berkeley Lab., Berkeley, CA, 91 p. (1986).
6. J. S. Y. WANG, and T. N. NARASIMHAN, Hydrologic Modeling of Vertical and Lateral Movement of Partially Saturated Fluid Flow Near a Fault Zone at Yucca Mountain, *SAND87-7070*, Sandia National Lab., Albuquerque, NM, *LBL-23510*, Lawrence Berkeley Lab., Berkeley, CA, 122 p. (1987).
7. R. R. PETERS, and E. A. KLAVETTER, A Continuum Model for Water Movement in an Unsaturated Fractured Rock Mass, *Water Resour. Res.*, 24(3), pp. 416-430 (1988).
8. P. G. KAPLAN, A Formalism to Generate Probability Distributions for Performance-Assessment Modeling, *Proc. High Level Radioactive Waste Management*, pp. 1487-1490 (1991).
9. H. N. HOLTAN, C. B. ENGLAND, G. P. LAWLESS, and G. A. SCHUMAKER, Moisture-Tension Data for Selected Soils on Experimental Watersheds, *ARS41-144*, Agricultural Research Service, U. S. Department of Agriculture, Beltsville, MD, 609 p. (1968).
10. J. S. Y. WANG, and T. N. NARASIMHAN, Processes, Mechanisms, Parameters, and Modeling Approaches for Partially Saturated Flow in Soil and Rock Media, *SAND88-7054, LBL-26224*, Sandia National Lab., Albuquerque, NM, *LBL-26224*,

Lawrence Berkeley Lab., Berkeley, CA (1991).

11. R. H. BROOKS, and A. T. COREY, Properties of Porous Media Affecting Fluid Flow, *J. Irrigation and Drainage Div., Proc. Am. Soc. Civ. Eng.*, 92, IR2, pp. 61-88 (1966).
12. M. Th. van GENUCHTEN, A Closed-Form Equation for Predicting Hydraulic Conductivity of Unsaturated Soils, *Soil Sci. Soc. Am. J.*, 44, pp. 892-898 (1980).
13. P. G. KAPLAN, and L. YARRINGTON, Modeling the Uncertainties in Parameter Values of a Layered, Variably Saturated Column of Volcanic Tuff Using the Beta Probability Distribution, in *Solving Ground Water Problems with Models,* National Water Well Asso., Columbus, OH (1986).
14. E. E. MILLER, and R. D. MILLER, Physical Theory for Capillary Flow Phenomena, *J. Applied Phys.*, 27(4), 324-332 (1956).

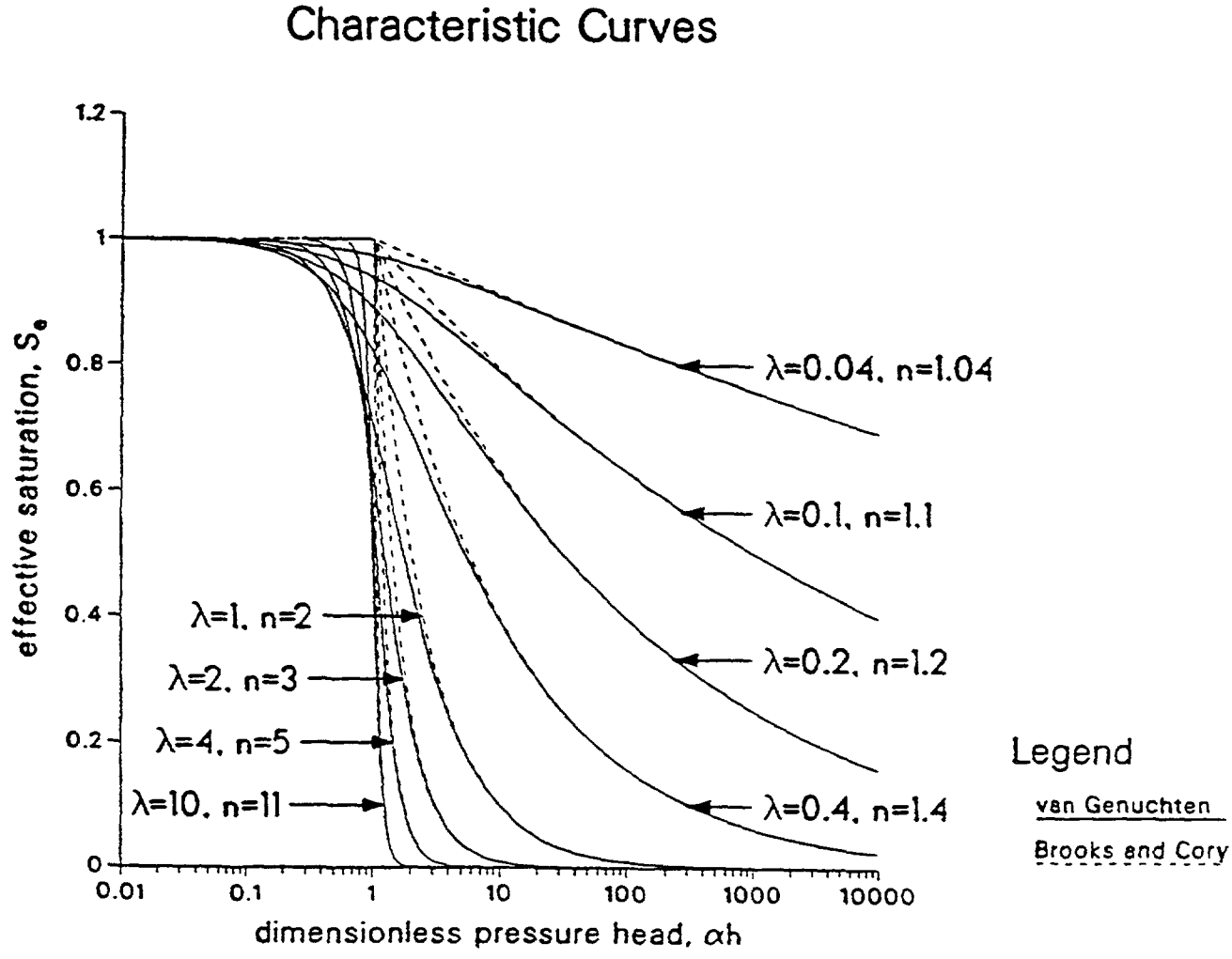

Figure 1. Scaled Characteristic Curves of van Genuchten Model and Brooks and Corey Model.

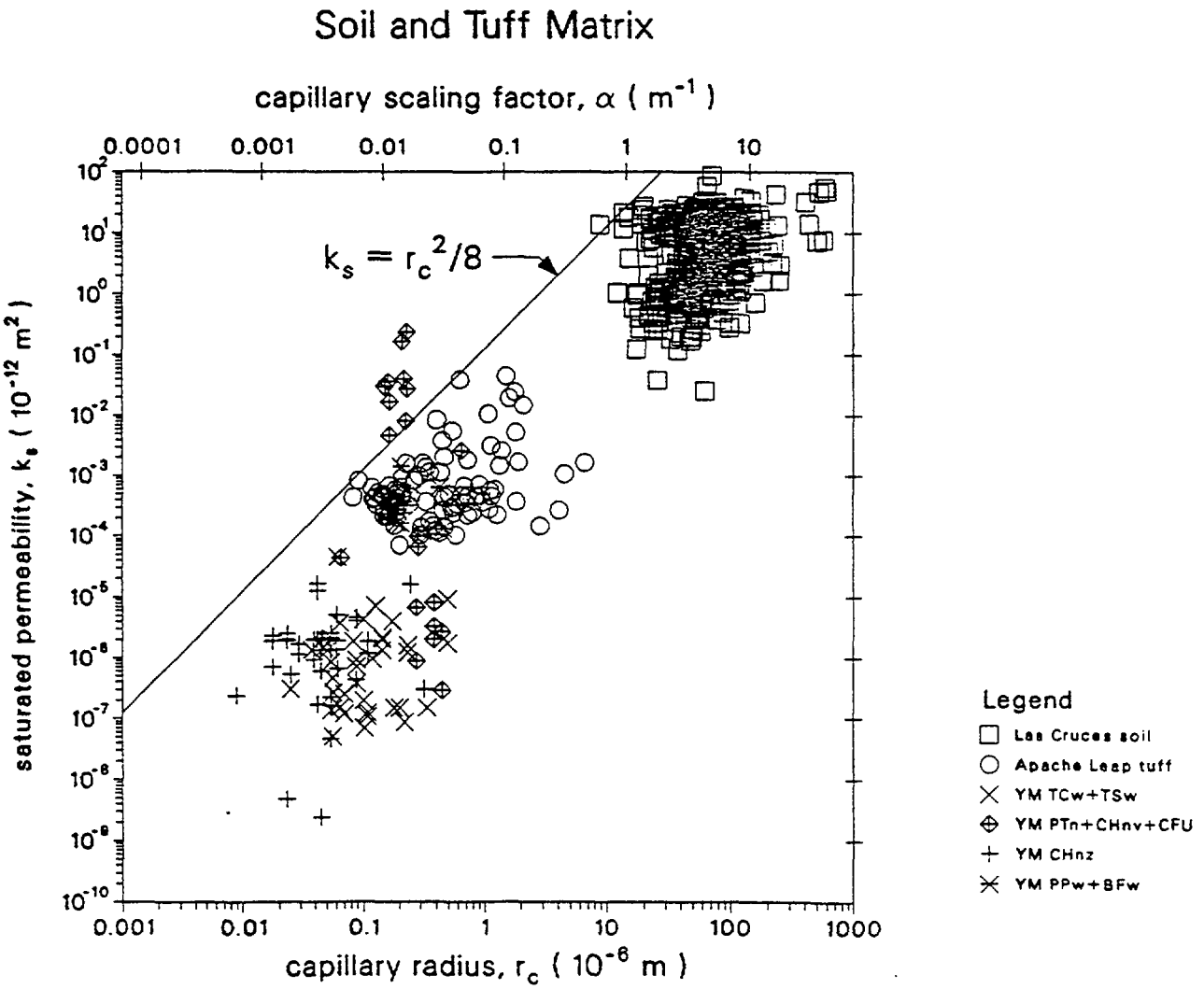

Figure 2. Correlation Between Saturated Permeability and Capillary Radius.

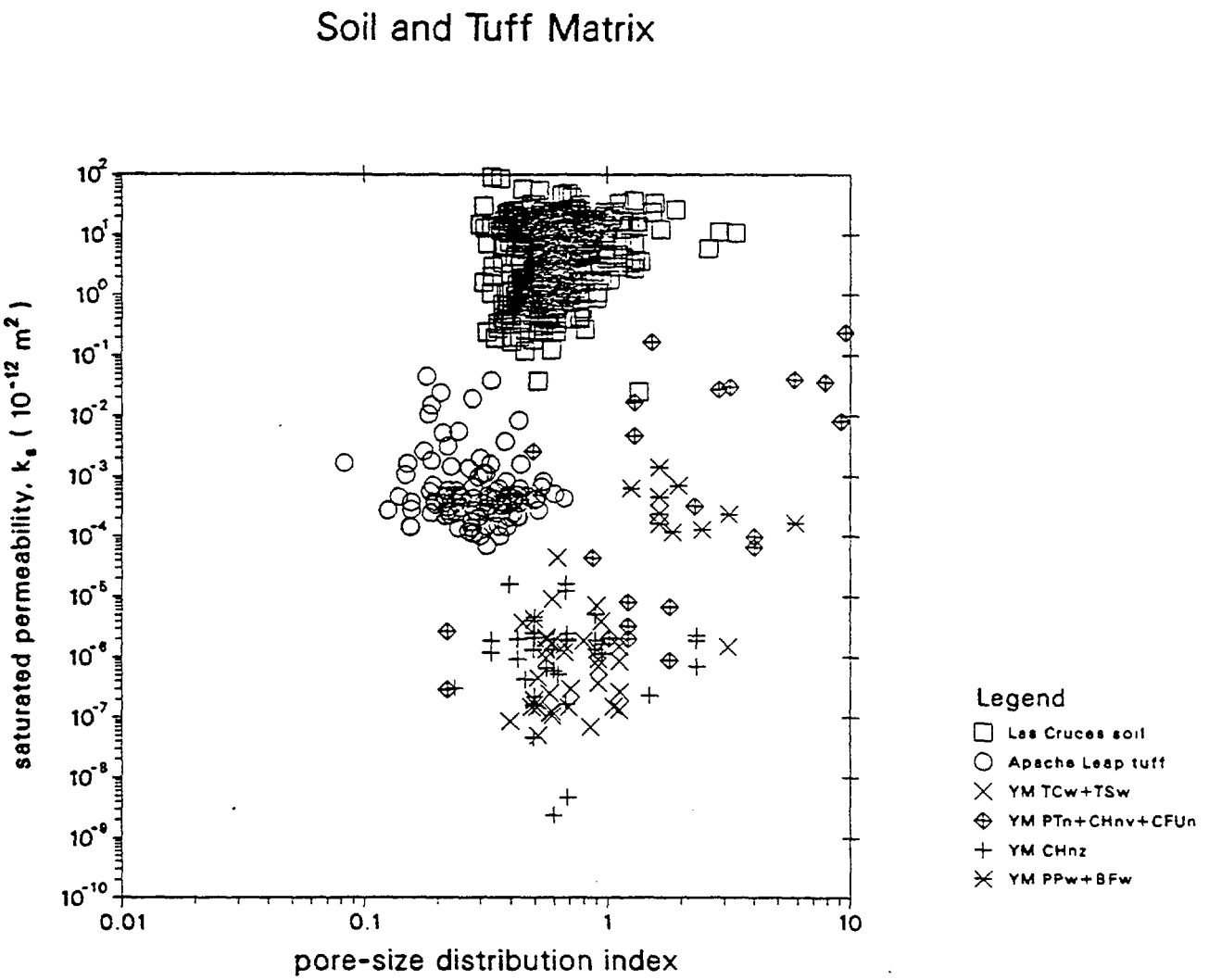

Figure 3. Correlation Between Saturated Permeability and Pore-Size Distribution Index.

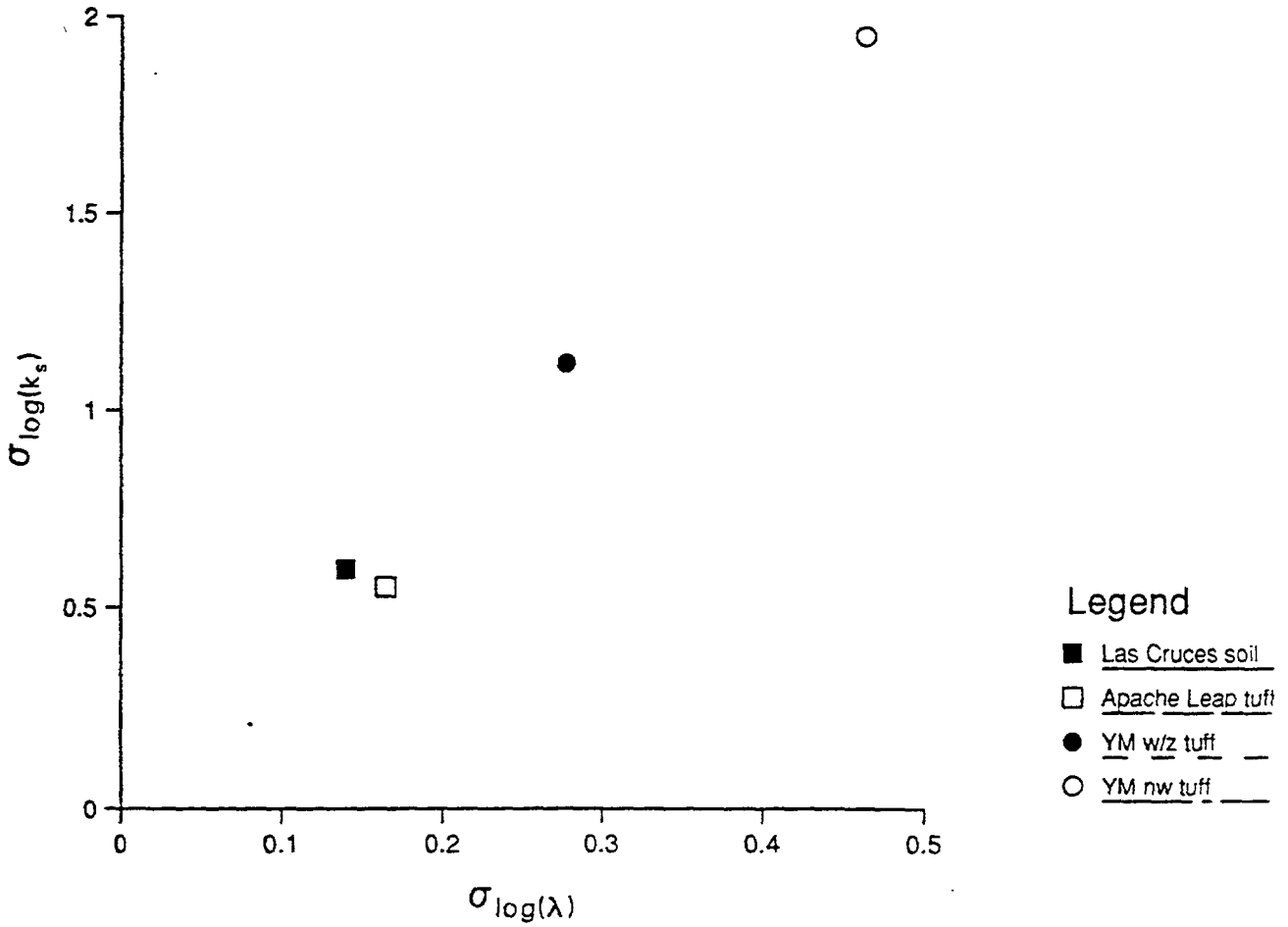

Figure 4. Correlation Between Variance of Log Saturated Permeability and Variance of Log Pore-Size Distribution Index.